ADVANCED TOPICS IN SCIENCE AND TECHNOLOGY IN CHINA

ADVANCED TOPICS IN SCIENCE AND TECHNOLOGY IN CHINA

Zhejiang University is one of the leading universities in China. In Advanced Topics in Science and Technology in China, Zhejiang University Press and Springer jointly publish monographs by Chinese scholars and professors, as well as invited authors and editors from abroad who are outstanding experts and scholars in their fields. This series will be of interest to researchers, lecturers, and graduate students alike.

Advanced Topics in Science and Technology in China aims to present the latest and most cutting-edge theories, techniques, and methodologies in various research areas in China. It covers all disciplines in the fields of natural science and technology, including but not limited to, computer science, materials science, life sciences, engineering, environmental sciences, mathematics, and physics.

Zhi-Zhong Xing
Shun Zhou

Neutrinos in Particle Physics, Astronomy and Cosmology

With 61 figures

ZHEJIANG UNIVERSITY PRESS
浙江大学出版社

Springer

Authors
Prof. Dr. Zhi-Zhong Xing
Institute of High Energy Physics,
Chinese Academy of Sciences,
Beijing 100049, China
E-mail: xingzz@ihep.ac.cn

Dr. Shun Zhou
Institute of High Energy Physics,
Chinese Academy of Sciences,
Beijing 100049, China
E-mail: zhoush@ihep.ac.cn

Max-Planck-Institut für Physik
(Werner-Heisenberg-Institut),
D-80805 München, Germany
E-mail: zhoush@mppmu.mpg.de

ISSN 1995-6819 e-ISSN 1995-6827
Advanced Topics in Science and Technology in China

ISBN 978-7-308-08024-8
Zhejiang University Press, Hangzhou

ISBN 978-3-642-17559-6 e-ISBN 978-3-642-17560-2
Springer Heidelberg Dordrecht London New York

Printed on acid-free paper

Springer is part of Springer Science+Business Media (www.springer.com)

Preface

Neutrinos are a kind of electrically neutral and extremely light spin-1/2 particles which only have weak and gravitational interactions with matter. Their distinctive properties make them become one of Nature's most mysterious messengers. Since the birth of neutrino physics in 1930, when Wolfgang Pauli postulated the existence of neutrinos as a "desperate remedy" for the continuous energy spectrum observed in the beta decay, intriguing puzzles and exciting discoveries have been associated with elusive neutrinos in nuclear physics, particle physics, astronomy and cosmology.

Enrico Fermi took advantage of Pauli's neutrino hypothesis and invented an effective theory of weak interactions in 1933. There were several milestones associated with neutrinos in the subsequent development of particle physics. The discovery of electron antineutrinos from nuclear reactors was made by Clyde Cowan and Frederick Reines in 1956. In the same year Tsung-Dao Lee and Chen Ning Yang published a seminal paper on parity violation in weak interactions, which was soon confirmed by a number of elegant experiments. Motivated by the experimental fact that neutrinos were almost massless and left-handed, Richard Feynman and Murray Gell-Mann proposed the $V-A$ theory of weak interactions in 1958. Leon Lederman, Melvin Schwartz and Jack Steinberger discovered the muon neutrino, a sister of the electron neutrino, by doing the first high-energy accelerator neutrino experiment in 1962. A unified gauge theory of electromagnetic and weak interactions, the so-called standard model (SM), was established by Sheldon Glashow, Steven Weinberg and Abdus Salam in the 1960's. This theory was experimentally verified in 1973, thanks to the discovery of neutral-current interactions via the neutrino-electron and antineutrino-electron scattering. The massive mediators of weak interactions (i.e., $W^{\pm}$ and Z^0 bosons) were finally observed by Carlo Rubbia and Simon van der Meer in 1983.

In this book we start with the SM and elaborate on the intrinsic properties and fundamental interactions of massless neutrinos. Thanks to several compelling neutrino oscillation experiments done in the 1990's and 2000's, we

are now convinced that neutrinos are massive and lepton flavors are mixed. Generally speaking, one has to rely on a specific neutrino mass model when discussing massive neutrinos and their interactions with matter. But our main strategy is to focus on the model-independent properties of elusive neutrinos, such as their electromagnetic dipole moments, flavor mixing, CP violation and oscillations in vacuum and matter. To address the origin of finite neutrino masses, we shall concentrate on various seesaw mechanisms which have currently attracted a lot of interest for model building. By choosing these kinds of topics, we hope to keep us and the readers of our book as close as possible to the true theory of massive neutrinos.

Furthermore, we aim to give an introduction to two newly developed branches of astronomy and cosmology — *neutrino astronomy* and *neutrino cosmology*. The subjects of neutrino astronomy include the studies of relic neutrinos of the Big Bang, stellar neutrinos, supernova neutrinos and high-energy cosmic neutrinos. Such studies may help us to deeply understand the crucial role of neutrinos in the evolution of the Universe, the nuclear burning mechanism of stars in their interiors, the dynamics of supernova explosions, the origin of ultrahigh-energy cosmic rays and gamma rays, and so on. So far solar neutrinos have been well investigated. The deficit of solar neutrinos, which was first observed by Raymond Davis in 1968, provided us with the first experimental evidence for the phenomenon of neutrino oscillations. Another milestone in neutrino astronomy was the observation of a neutrino burst from the Supernova 1987A explosion in the Kamiokande-II experiment led by Masatoshi Koshiba. Davis and Koshiba received the Nobel Prize in Physics in 2002 for their revolutionary contributions to neutrino astronomy. With the development of more advanced experimental technologies, more discoveries and breakthroughs in neutrino astronomy are highly anticipated in the (near) future. In particular, every effort is being made to detect the cosmic neutrino background, supernova neutrinos and ultrahigh-energy cosmic neutrinos.

As an important branch of cosmology, neutrino cosmology describes the most profound interplay between neutrino physics and cosmology. The remarkable success of the standard Big Bang model of cosmology has proved the crucial role of neutrinos in the primordial nucleosynthesis, in the anisotropies of the cosmic microwave background radiation, in the formation of the large-scale structures, and so on. The cosmic neutrino background and neutrino dark matter are also hot topics in cosmology. In addition, the production and decays of heavy Majorana neutrinos in the very early Universe might be responsible for the origin of cosmological matter-antimatter asymmetry via the leptogenesis mechanism. We foresee that more reliable knowledge on the properties of massive neutrinos to be obtained from a variety of new experiments will allow us to understand the role of neutrinos in the evolution of the Universe in a better way and to a better level. On the other hand, the development of neutrino cosmology is likely to provide us with more compelling information about neutrino masses, flavor mixing and CP violation.

The text of this book can be divided into two parts: the first part consists of chapters 1—5 and is devoted to neutrino physics, and the second part is composed of chapters 6—11 and devoted to neutrino astronomy and neutrino cosmology. We admit that it is a big challenge for us to catch up with the rapid developments in neutrino physics, neutrino astronomy and neutrino cosmology, which are partly characterized by the rising number of publications everyday. Although we have tried to cover recent progress in neutrino science, a lot of interesting materials and technical details have to be skipped from this book for a given page limitation. We apologize for missing many useful references for the same reason.

We are deeply indebted to our families for their understanding and support during the writing of this book. We would like to thank many of our collaborators and colleagues who kindly allow us to quote some tables, figures and physical results from their papers. One of us (Z.Z.X.) is grateful to Harald Fritzsch for collaborating on his first scientific paper on neutrino masses in September 1995. One of us (S.Z.) is grateful to Georg G. Raffelt for suggesting the present title of this book and for his encouragement and hospitality at the Max-Planck-Institute in Munich. We would also like to thank the editorial staff of Zhejiang University Press and Springer Verlag for inviting us to write this book and coming to our assistance. This work was supported in part by the National Natural Science Foundation of China under grant No. 10425522 and No. 10875131 (Z.Z.X.), in part by the Ministry of Science and Technology of China under grant No. 2009CB825207 (Z.Z.X.), and in part by the Alexander von Humboldt Foundation of Germany (S.Z.).

Zhi-Zhong Xing
Beijing, August 2010

Shun Zhou
Munich, August 2010

Contents

1

Neutrinos: Past, Present and Future

Elusive neutrinos have been playing a special and important role in nuclear physics, particle physics, astronomy and cosmology. They exist everywhere in the Universe and are Nature's mysterious messengers. In this chapter we shall give a broad but brief overview of the history of neutrino physics and the present situation of neutrino astrophysics. The prospects of neutrino astronomy and neutrino cosmology will also be described.

1.1 Neutrinos in Nuclear and Particle Physics

The history of neutrino physics can be traced back to 4 December 1930, when Wolfgang Pauli wrote his famous letter to the "Dear radioactive ladies and gentlemen" who had gathered in Tübingen [1]. In this letter Pauli conjectured the existence of neutrinos as a desperate remedy for the energy crisis observed in the beta decay because the energy and momentum conservation laws, which had been regarded to be very sacrosanct, were severely challenged by the continuous energy spectrum of the beta ray. Based on the neutrino hypothesis, Enrico Fermi put forward an effective quantum theory of the beta decay in 1933, through which people made the first acquaintance with a new force in nature — the weak interaction. Soon after the experimental discovery of electron antineutrinos in 1956, the space-inversion symmetry (or parity conservation) was found to be maximally violated in a number of processes of weak interactions. Hence neutrinos were assumed to be massless Weyl particles with only two components: left-handed neutrinos and right-handed antineutrinos. They were naturally included into the $V-A$ theory of weak interactions in 1958 and into the standard model (SM) of electroweak interactions in 1967. The latter was experimentally verified in 1974 thanks

[1] See, e.g., Pauli's lecture given in 1957 in Zürich: "Zur älteren und neueren Geschichte des Neutrinos" (i.e., "On the Earlier and More Recent History of the Neutrino"), which was published in 1984 (Pauli, 1984).

to the discovery of neutral-current interactions — a neutrino could interact with another particle and remained to be a neutrino. Although the SM has so far passed almost all experimental tests, it must be incomplete because it does not allow neutrinos to be massive.

Since 1998, a lot of robust experimental evidence has pointed to the fact that neutrinos can oscillate — a pure quantum phenomenon which can take place only if neutrinos have finite masses. This great breakthrough is opening an important window towards new physics beyond the SM. In this section we shall follow the historical line to briefly address the role played by neutrinos in the development of nuclear and particle physics. Some particular attention will be paid to the following three aspects: (1) the background for Pauli to conjecture the existence of neutrinos; (2) the establishment of the $V-A$ theory of weak interactions; and (3) the discovery of neutrinos. An introduction to the experimental and theoretical aspects of neutrino oscillations will be presented in Section 3.1 and Chapter 5.

1.1.1 Pauli's Neutrino Hypothesis

The ultimate goal of particle physics is to explore the fundamental building blocks of matter and the fundamental forces between them, and to discover the basic laws governing how Nature works as it does. In the early stage of the 20th century electrons and protons were commonly regarded as the elementary particles and thus the unique ingredients of atoms, which made up the matter. This picture encountered some serious difficulties, among which the most important two were the "wrong statistics" problem and the continuous energy spectrum of the beta decay.

At that time the nitrogen nucleus ^{14}N was expected to contain 14 protons and 7 electrons. Hence the spin of ^{14}N should be half-integral and obey the Fermi-Dirac statistics. The experiments, however, indicated that ^{14}N actually followed the Bose-Einstein statistics (Kronig, 1928; Heitler and Herzberg, 1929; Rasetti, 1930). This was just the "wrong statistics" problem.

The continuous energy spectrum of the beta decay was first discovered by James Chadwick in 1914 (Chadwick, 1914). After a longtime debate it was finally established. But the final state of the beta decay of an unstable nucleus was assumed to consist of only two particles: the daughter nucleus and the electron. A simple kinematic analysis of this two-body decay mode led to the conclusion that the emitted electron must be monoenergetic. There were two conflicting viewpoints on the observed continuous spectrum at that time: (1) the energy spectrum was originally monochromatic, but it was subsequently broadened due to the energy loss of electrons in nuclei; (2) the electrons from the individual decay modes carried various energies that distributed continuously. In order to verify or falsify either point, one had to measure the energy released in the beta decay as accurately as possible. Such a precision measurement was done by making use of the calorimetry of heat generation, and its result showed that the mean disintegration energy was consistent

with the energy of electrons averaged over the continuous spectrum (Ellis and Wooster, 1927). How to resolve the energy crisis observed in the beta decay became a great challenge to many important theorists in the 1920's. Some exotic ideas emerged, although they sounded unimaginable. In 1929, for instance, Niels Bohr even considered to abandon the conservation laws of energy and momentum in an individual subatomic process.

In December 1930, Pauli postulated that the beta decay might be a three-body decay mode in which an electrically neutral and extremely light particle of spin 1/2 was also emitted from the decaying nucleus. He also conjectured that this new particle should have a small magnetic moment such that it could be bounded in the decaying nucleus. The consequences of Pauli's hypothesis are obvious: (a) in the final state of the beta decay the electron has to share the available energy with the new particle, and hence its energy spectrum must be continuous; (b) because each electron is accompanied by a new particle of spin 1/2, the spin of ^{14}N must be an integer and obeys the Bose-Einstein statistics [2]. In 1932, Chadwick discovered the neutron (Chadwick, 1932) — the counterpart of the proton in a nucleus (Heisenberg, 1932). Then Fermi named Pauli's neutral particle as the "neutrino" and formulated an effective quantum theory of the beta decay (Fermi, 1933).

1.1.2 Weak Interactions and Neutrinos

By combining Pauli's neutrino hypothesis, Dirac's idea about the creation of particles and Heisenberg's isospin concept for neutrons and protons in a coherent way, Fermi proposed the effective Hamiltonian $H_\beta = g(\overline{p}\gamma^\mu n)(\overline{e}\gamma_\mu \nu_e)$ to account for the beta decay $n \to p + e^- + \overline{\nu}_e$, where the vector-current interaction form was analogous to the second-order electromagnetic interaction (Fermi, 1933, 1934). This effective theory allowed Fermi to show the correct energy spectrum of the beta decay. He even suggested that an accurate measurement of the continuous energy spectrum's endpoint be able to pin down the rest mass of the neutrino. However, it turned out that H_β itself was too selective to explain all the beta decays. This unfortunate situation motivated other theorists to postulate different selection rules for the decays of nuclei (Gamow and Teller, 1936). The most general Lorentz-invariant form of the effective Hamiltonian responsible for the beta decay should contain the scalar $\mathbf{1}$ (S), vector γ^μ (V), tensor $\sigma^{\mu\nu}$ (T), pseudoscalar γ_5 (P) and pseudovector $\gamma^\mu\gamma_5$ (A) interactions. Historically, it took a long time for experimentalists to clarify the form of weak interactions (Franklin, 2000).

The breakthrough took place in 1956 and 1957. Questioning the validity of parity conservation in weak interactions, Tsung-Dao Lee and Chen Ning

[2] In 1931, Pauli gave up the idea that his neutral particles were the necessary ingredients of nuclei because it was in conflict with the nuclear mass relations. It was actually the neutron that had later been employed to resolve the "wrong statistics" problem of the nitrogen nucleus.

Yang suggested an experiment to examine the angular distribution of the beta rays emitted from the ^{60}Co nuclei with spins polarized along an external magnetic field (Lee and Yang, 1956) — if parity were conserved, there should be no correlation between the spin and momentum of every electron emitted in the decay [3]. Chien-Shiung Wu and her collaborators did this experiment and found that the electrons were almost always emitted in the direction opposite to the nuclear spins — a signature of *maximal* parity violation (Wu *et al.*, 1957). More evidence for maximal parity non-conservation was later on obtained by other experimental groups in different weak processes (Garwin *et al.*, 1957; Friedman and Telegdi, 1957). Soon after the observation of parity violation, several important theorists independently put forward the idea that neutrinos might simply be massless and could naturally be described in terms of the two-component Weyl spinor (Lee and Yang, 1957; Landau, 1957; Salam, 1957). In such a two-component neutrino theory the helicity of a neutrino must be identical with its handedness or chirality. The aforementioned ^{60}Co experiment indicated that the emitted electron and its accompanying electron antineutrino should have left ($\lambda = -1/2$) and right ($\lambda = +1/2$) helicities, respectively. Direct helicity measurements confirmed $\lambda = -1/2$ for neutrinos and $\lambda = +1/2$ for antineutrinos (Goldhaber *et al.*, 1958; Bardon *et al.*, 1961). That is why neutrinos (antineutrinos) had commonly been accepted to be exactly massless and purely left-handed (right-handed) for several decades before the phenomena of atmospheric and solar neutrino oscillations were firmly established at the end of the 1990's and the beginning of the 2000's.

The discovery of parity non-conservation, together with a coherent analysis of many other experimental data on various weak processes, led to the theoretical observation that weak interactions should have the universal $V-A$ form with maximal parity and charge-conjugation violation (Sudarshan and Marshak, 1958; Feynman and Gell-Mann, 1958). In the $V-A$ theory of weak interactions a four-fermion interaction can be expressed as $g\overline{\psi_1}\gamma^\mu(1-\gamma_5)\psi_2\overline{\psi_3}\gamma_\mu(1-\gamma_5)\psi_4$. Hence it is the effective Hamiltonian $H_\beta = g\overline{p}\gamma^\mu(1-\gamma_5)n\,\overline{e}\gamma_\mu(1-\gamma_5)\nu_e$ that governs the beta decay $n \to p+e^-+\overline{\nu}_e$. Such a current-current interaction picture actually serves for a low-energy approximation of the SM of weak interactions mediated by massive gauge bosons $W^\pm$ and (or) Z^0 (Weinberg, 1967; Salam, 1968).

1.1.3 Discoveries of Neutrinos

Since the beginning of the 1930's, numerous experiments have been done to search for neutrinos and measure their properties. Before the 1950's, however, all of the experiments were designed to observe the energy and momentum carried away by the neutrino in the beta decay. This kind of kinematic measurement was actually realized by detecting the recoil of relevant nuclei and

[3] The correlation between spin and momentum is measured by the average value of the helicity $\lambda \equiv \mathbf{s}\cdot\mathbf{p}/|\mathbf{p}| = \pm 1/2$, which changes sign under a parity inversion and thus must vanish if parity is conserved in a given process.

the emitted electrons (Crane and Halpern, 1939). In 1942, Kan Chang Wang proposed a different idea to kinematically detect neutrinos: since the β^+-radioactive atom could capture a K-shell electron rather than emit a positron, the recoil energy and momentum of the resulting atom would merely depend on the emitted neutrino (Wang, 1942). Taking the element ^{7}Be for example, Wang suggested that one use the process $^7\mathrm{Be} + e_K^- \rightarrow {}^7\mathrm{Li} + \nu_e + (1\ \mathrm{MeV})$ to do the experiment. Such an experiment was soon done by James Allen, who found that the recoil energy of ^{7}Li was well consistent with the expectation from a neutrino emission. So he published the result in a paper entitled "Experimental Evidence for the Existence of a Neutrino" (Allen, 1942).

However, those indirect hints had never been regarded as a real discovery of neutrinos (Crane, 1948). As Hans Bethe and Robert Bacher noted, "It seems practically impossible to detect neutrinos in the free state, i.e., after they have been emitted by the radioactive atom. There is only one process which neutrinos can certainly cause. That is the inverse beta process, consisting of the capture of a neutrino by a nucleus together with the emission of an electron (or positron)" (Bethe and Bacher, 1936). Hence a conclusive experiment to verify Pauli's neutrino hypothesis should detect the inverse beta decay $\overline{\nu}_e + p \rightarrow n + e^+$. In 1952, Clyde Cowan and Frederick Reines realized that a coincidence measurement of the photon signals coming both from the positron annihilation and from the neutron capture on cadmium in the liquid scintillator would greatly reduce the background and provide a convincing signature of the inverse beta decay. They built a detector near the nuclear reactor pile in Hanford in 1953, but their experiment was unsuccessful because it suffered from the intolerable noise induced by cosmic rays. To improve the experiment, Cowan and Reines moved the detector to the Savannah River reactor and placed it underground to reduce the background from cosmic rays. This time they succeeded in observing an unambiguous signature of the inverse beta decay and demonstrated that its cross section was compatible with the theoretical prediction (Cowan *et al.*, 1956) [4]. On 14 June 1956, Reines and Cowan sent a telegram to Pauli: "We are happy to inform you that we have definitely detected neutrinos from fission fragments by observing inverse beta decay of protons. Observed cross section agrees well with expected six times ten to minus forty-four square centimeters". They received no reply from Pauli but learnt later that Pauli and some friends consumed a case of champagne in celebration of this good news (Reines, 1979).

In 1946, Bruno Pontecorvo suggested a radiochemical technique to capture electron neutrinos via the process $^{37}\mathrm{Cl} + \nu_e \rightarrow {}^{37}\mathrm{Ar} + e^-$ (Pontecorvo,

[4]Note that the theoretical prediction that Cowan and Reines quoted in their experiment was based on the parity-conserving formulation of the beta decay. Given maximal parity violation discovered in 1957, the $V-A$ theory of weak interactions predicted that the cross section of the inverse beta decay should be twice as large as that reported previously. Cowan and Reines redid their experiment and arrived at the correct result in 1960 (Reines *et al.*, 1960).

1946). The cross section of this reaction was precisely computable and its energy threshold $E(\nu_e) \geqslant 0.814$ MeV was low enough to make the measurement sensitive to solar ^{8}B neutrinos. It was John Bahcall who carefully calculated the flux of solar neutrinos and the capture rate of ^{8}B neutrinos, demonstrating that Pontecorvo's idea was experimentally feasible (Bahcall, 1964). In the middle of 1960's, Raymond Davis and his team built a 10^5-gallon Chlorine-Argon neutrino detector in the Homestake Gold Mine to detect solar neutrinos (Davis, 1964). The final result of their experiment came out in 1968: the measured flux of solar ^{8}B neutrinos was only about one third of the value predicted by the standard solar model (SSM) (Davis *et al.*, 1968; Bahcall and Shaviv, 1968). This was just the famous solar neutrino problem, which was actually caused by the flavor conversion of solar ν_e neutrinos on their way from the core of the Sun to the detector on the Earth. Davis received the Nobel Prize in Physics in 2002, at the age of 88, for his discovery of solar neutrinos and their deficit.

In the 1960's, another burning question was whether the neutrinos emitted from the primary decay modes of $\pi^{\pm}$ mesons were the same as those from the beta decay. If they were the same particles, the branching ratio of the lepton-flavor-violating decay $\mu \to e+\gamma$ would be of $\mathcal{O}(10^{-5})$, several orders of magnitude larger than the experimental upper bound (Lee and Yang, 1960). If there were only one neutrino species, electrons and muons would be equally produced from the collision between a neutrino beam of several GeV and a nucleon. The situation was clarified by Leon Lederman, Melvin Schwartz and Jack Steinberger, who did the first high-energy accelerator neutrino experiment at the Brookhaven National Accelerator Laboratory in 1962. In their experiment the charged pions were produced by bombarding the metal beryllium target with protons, while the muons emitted from the decaying pions were stopped by ionization loss in the shield. The events of single muon track in the spark chamber were observed, providing the robust evidence for the existence of the muon neutrino ν_μ (Danby *et al.*, 1962). The tau neutrino ν_τ was naturally expected to exist, after the tau lepton was discovered and the missing energy from its decay was observed by Martin Perl and his team in 1975 (Perl *et al.*, 1975). But the ν_τ-induced interactions were not directly observed until the end of 2000 at the Fermilab (Kodama *et al.*, 2001). A picture of three lepton families, including three charged leptons (e, μ, τ) and three neutrinos $(\nu_e, \nu_\mu, \nu_\tau)$, was therefore completed in the SM.

1.2 Neutrinos in Astronomy and Cosmology

Neutrinos were made in astonishing numbers at the time of the Big Bang and took part in the evolution of the Universe from its very beginning. Neutrinos can also be produced in staggering numbers from nuclear burning of stars, violent explosions of supernovae, interactions between the cosmic microwave background (CMB) radiation and ultrahigh-energy cosmic rays, annihilation

of dark matter, and a variety of distant astrophysical sources such as gamma ray bursts and active galactic nuclei. Only the neutrinos emitted from the Sun and Supernova 1987A have been observed. Hence neutrino astronomy is still very much in its infancy, so is neutrino cosmology. We shall give a short account of astrophysical neutrinos in this section. Detailed discussions about hot and important topics of neutrino astronomy and cosmology will be presented in the second part of this book, from Chapter 6 to Chapter 11.

1.2.1 Neutrinos from Stars and Supernovae

In the 1930's, it was unclear whether neutrinos had something to do with why the Sun was shining. Bethe did not include neutrinos into solar nuclear fusion chains when he published his seminal paper on the energy production in stars in 1939 (Bethe, 1939). One year later, George Gamow and Mario Schönberg pointed out that neutrinos would take away a certain part of stellar energies and their role was particularly important in a collapsed star because of the high temperature and density in its interior (Gamow and Schönberg, 1940, 1941). Today we know that solar neutrinos take away a few percent of the total energy of the Sun. Another example is the Supernova 1987A explosion, in which about 99% of the energy was taken away by neutrinos.

The Sun shines as a result of nuclear fusion in its core. The *pp* and CNO chains of hydrogen fusion in the Sun can be expressed as $4p + 2e^- \to {}^4\mathrm{He} + 2\nu_e + (26.7\ \mathrm{MeV})$, so about 98% of the energy radiates in the form of light and only 2% of the energy is taken away by neutrinos. Soon after the $V-A$ theory of weak interactions emerged in 1958, Pontecorvo realized that the bremsstrahlung radiation of neutrinos from the Sun was also possible to take place (Pontecorvo, 1959). But the energy of this kind of solar neutrinos must be very low because it is subject to the Sun's temperature ($T_\odot \sim 10^7\ \mathrm{K} \sim 1$ keV). In comparison, those neutrinos emitted from nuclear reactions inside the Sun are more energetic and their typical energies are of $\mathcal{O}(1)$ MeV.

Solar neutrinos were first observed by Davis in Homestake — the first radiochemical experiment which was sensitive to solar ${}^8\mathrm{B}$ neutrinos (Davis *et al.*, 1968). The subsequent radiochemical experiments, GALLEX/GNO in Gran Sasso (Hampel *et al.*, 1999; Altmann, *et al.*, 2005) and SAGE in Baksan (Abdurashitov *et al.*, 2002), employed the reaction ${}^{71}\mathrm{Ga} + \nu_e \to {}^{71}\mathrm{Ge} + e^-$ to detect solar neutrinos. The energy threshold of this reaction is as low as $E(\nu_e) \geqslant 0.233$ MeV, and hence more than half of the ν_e-induced events in the GALLEX/GNO or SAGE experiment are attributed to solar *pp* neutrinos emitted from the nuclear reaction $p + p \to \mathrm{D} + e^+ + \nu_e$ inside the Sun. The neutrino flux measured in either of these two gallium experiments was only about one half of that predicted by the SSM, implying that the solar neutrino anomaly revealed by the Homestake experiment might be a real problem independent of the uncertainties of the SSM itself. Such an anomaly was also observed in the Kamiokande and Super-Kamiokande (SK) experiments with the help of water Cherenkov detectors, where solar ${}^8\mathrm{B}$ neutrinos (emitted

from the decay $^8\mathrm{B} \rightarrow {}^8\mathrm{Be} + e^+ + \nu_e$) and *hep* neutrinos (emitted from the reaction $^3\mathrm{He} + p \rightarrow {}^4\mathrm{He} + e^+ + \nu_e$) were measured via the elastic neutrino-electron scattering process $\nu_e + e^- \rightarrow \nu_e + e^-$ (Fukuda *et al.*, 1996; Fukuda *et al.*, 2001). The simplest solution to this solar neutrino problem was based on the assumption that solar ν_e neutrinos might have converted into other types of neutrinos which were undetectable in the detectors located on the Earth (Wolfenstein, 1978; Mikheyev and Smirnov, 1986). A decisive experiment was done in 2001 at the Sudbury Neutrino Observatory (SNO), where solar ^{8}B neutrinos were detected via the charged-current process $\nu_e + \mathrm{D} \rightarrow p + p + e^-$, the neutral-current process $\nu_\alpha + \mathrm{D} \rightarrow p + n + \nu_\alpha$ and the elastic scattering process $\nu_\alpha + e^- \rightarrow \nu_\alpha + e^-$ for $\alpha = e,\ \mu$ and τ (Ahmad *et al.*, 2001). The total neutrino flux measured in the SNO experiment was in agreement with that predicted by the SSM. Furthermore, the SNO experiment confirmed the SK result and gave very convincing evidence for $\nu_e \rightarrow \nu_\mu$ and $\nu_e \rightarrow \nu_\tau$ transitions. These important results point to solar neutrino oscillations. The theory of neutrino oscillations will be described in Chapter 5, and the properties of stellar neutrinos will be discussed in Chapter 6.

The observation of neutrinos arising from the Supernova 1987A explosion was another milestone in neutrino astronomy. At 07:35:41 UT on 23 February 1987, the burst of neutrinos from a supernova explosion in the Large Magellanic Cloud at a distance of about 50 kpc was recorded by three neutrino telescopes on the Earth: Kamiokande-II led by Masatoshi Koshiba in Japan (Hirata *et al.*, 1987), IMB in the United States (Bionta *et al.*, 1987) and Baksan in Russia (Alekseev *et al.*, 1987). This burst lasted less than 13 seconds. Totally 24 events of electron antineutrinos were detected in the above observatories (11 at Kamiokande-II, 8 at IMB and 5 at Baksan), and their average energy was around 10 MeV. About 2.5 hours later, the visible light emitted from this supernova explosion reached the Southern Hemisphere and was observed by three independent groups (Arnett *et al.*, 1989). Koshiba won the Nobel Prize in Physics in 2002 for his detection of supernova neutrinos.

The picture of a supernova explosion and the burst of supernova neutrinos can be sketched as follows (Bethe and Wilson, 1985; Bethe, 1990): (a) when the iron core of a star reaches the Chandrasekhar mass limit, the gravitational collapse occurs; (b) after the inner core exceeds the nuclear density, the infalling outer core bounces and a shock forms; (c) the shock wave propagates outward and loses energies by disintegrating the Fe nuclei; (d) the inner core becomes a protoneutron star by releasing the gravitational binding energy of $\mathcal{O}(10^{53})$ erg in the form of neutrinos; (e) neutrinos exchange energies with matter via the reactions $\nu_e + n \rightleftharpoons p + e^-$ and $\overline{\nu}_e + p \rightleftharpoons n + e^+$; and (f) the shock receives energies from these processes and revives to make the final explosion. Although only the Supernova 1987A neutrinos were observed, they have greatly improved our understanding of the stellar evolution and explosion mechanisms. This observation has also been used to constrain neutrino masses, lifetimes and magnetic dipole moments (Raffelt, 1996, 1999).

It is therefore important to study supernova neutrinos so as to probe the dynamics of stars and supernovae and to learn about the intrinsic properties of neutrinos themselves. We shall elaborate these points in Chapter 7.

1.2.2 High-energy Cosmic Neutrinos

The study of high-energy cosmic neutrinos is well motivated because their sources must be associated with the astrophysical sources of high-energy or ultrahigh-energy cosmic rays (Gaisser, 1991; Stanev, 2004). It has been found that the most energetic cosmic ray particles can have kinetic energies up to 10^{21} eV, but where and how they are accelerated remain unknown. Neutrinos are expected to play an important role in searching for cosmic accelerators for two simple reasons: (a) they are electrically neutral and thus their trajectories cannot be bent by interstellar magnetic fields; (b) they do not interact with the CMB and hence they can travel very long distances, from some distant astrophysical sources to the Earth. So high-energy cosmic neutrinos should be a unique cosmic messenger complementary to photons and protons. If there exists an astrophysical object responsible for the production of both cosmic rays and neutrinos, then a successful measurement of the neutrinos (e.g., their direction, energy and flavor distribution) will allow us to probe where this astrophysical source is located and how it accelerates cosmic rays.

There are a number of possible candidates for the sources of high-energy cosmic neutrinos, including active galactic nuclei, gamma ray bursts and supernova remnants (Halzen and Hooper, 2002). In such a violent astrophysical source protons are likely to be accelerated to extremely high energies, leading to high-energy proton-proton (pp) and proton-photon ($p\gamma$) collisions from which vast quantities of pions and kaons can be produced. High-energy neutrinos can subsequently be produced from the primary and secondary decays of $\pi^{\pm}$ and $K^{\pm}$ mesons. Another possible source of high-energy cosmic neutrinos is related to the so-called Greisen-Zatsepin-Kuzmin (GZK) cutoff in the energy spectrum of cosmic rays. Given the existence of the CMB, the cosmic rays with energies higher than $E_{\rm th} = 5 \times 10^{19}$ eV would interact with the background photons via the Δ-resonance process $p+\gamma_{\rm CMB} \to \Delta^+ \to p+\pi^0$ or $n+\pi^+$. This implies that the extragalactic cosmic rays with $E \geqslant E_{\rm th}$ should not travel more than 50 Mpc and thus never reach the Earth (Greisen, 1966; Zatsepin and Kuzmin, 1966). Some recent observational data have indicated that the GZK cutoff seems to exist (Abbasi *et al.*, 2008; Abraham *et al.*, 2008). If such a cutoff is finally verified, it will be a "guaranteed" source of ultrahigh-energy cosmic neutrinos since neutrons and π^+ mesons generated from the Δ^+ decays will definitely produce neutrinos and antineutrinos in their subsequent decays.

The events of high-energy cosmic neutrinos are as rare as those of high-energy cosmic rays, and hence they can only be detected by using extraordinarily large neutrino detectors — the so-called neutrino telescopes. In a given

telescope the neutrino flux is identified by detecting its charged-current interactions with nuclei (i.e., $\nu_\alpha + N \to l_\alpha^- + N'$ and $\overline{\nu}_\alpha + \overline{N} \to l_\alpha^+ + \overline{N}'$ reactions for $\alpha = e, \mu, \tau$). The produced charged leptons move in the detector medium so rapidly that they can emit visible Cherenkov light. An optical Cherenkov neutrino telescope must satisfy the following conditions: (a) large enough that some of the rare galactic or extragalactic neutrinos can interact as they pass by; (b) transparent enough to allow light to travel through a widely-spaced array of optical sensors; (c) dark enough to avoid the interference of natural light; and (d) deep enough below the Earth's surface to avoid the contamination from cosmic rays. Only dark lakes or oceans and deep fields of ice meet all these requirements. The km^3-scale neutrino telescope IceCube is now under construction at the South Pole (Ahrens *et al.*, 2003) and its possible counterpart in the Mediterranean Sea, KM3NeT, has been proposed (Carr *et al.*, 2007). Such a neutrino telescope is expected to be most sensitive to high-energy muon neutrinos, simply because the muon can have a long and clear track in the detector to assure excellent energy and direction resolutions. Needless to say, a measurement of the flavor distribution of high-energy cosmic neutrinos from a distant astrophysical source will be very helpful to probe the production mechanism of cosmic rays and to examine the intrinsic properties of massive neutrinos.

High-energy cosmic neutrinos might also come from the annihilation of dark matter. In addition, the origin of high-energy cosmic neutrinos might be associated with the production of high-energy photons and even gravitational waves at an astrophysical source. Such topics will be discussed in Chapter 8.

1.2.3 Cosmic Neutrino Background

One of the greatest discoveries in the history of cosmology was Edwin Hubble's observation that galaxies were receding from each other at velocities proportional to their distances (Hubble, 1929). This observation, which was consistent with Albert Einstein's prediction for the relationship between velocities and distances (Einstein, 1915), strongly indicated that the Universe was expanding and its dynamics could be correctly described by general relativity. Starting from the present-day data and allowing the equations of general relativity to run backwards in time, one may immediately infer that the Universe should become increasingly hotter and denser until the Big Bang (i.e., the initial singularity or a state of infinite density and temperature) is finally encountered (Lemaitre, 1931). One can then run the clock forward from the Big Bang and construct a time line which orders the evolution of the Universe. Some important events in the evolution of the Universe include cosmological inflation, quark-baryon transition, Big Bang nucleosynthesis (BBN), recombination, large-scale structure formation, and so on.

In the early Universe the energy density was dominated by relativistic leptons, quarks and gauge bosons. Within a few microseconds, the quarks were confined to form protons and neutrons. Within about one second, soon

after neutrinos lose their contact with the thermal bath and decoupled from the rest of matter, the synthesis of primordial nuclei (e.g., D, ^{3}He, ^{4}He and ^{7}Li) began (Alpher *et al.*, 1948). The BBN was completed when the Universe was about several minutes old, but the Universe itself remained too hot for nuclei to capture electrons and form neutral atoms. The epoch of recombination arrived about 3×10^5 years after the Big Bang, when the expanding Universe cooled to a temperature of 0.3 eV, allowing electrons and protons to combine to form neutral hydrogen atoms. This epoch marked the decoupling of matter and electromagnetic radiation. The relic photons finally became the CMB of the Universe, just like the relic neutrinos which formed the cosmic neutrino background (CνB) of the Universe. In 1965, Arno Penzias and Robert Wilson succeeded in detecting the existence of the CMB (Penzias and Wilson, 1965). Their great discovery offered a strong support to the model of hot Big Bang proposed by Alpher, Bethe and Gamow in 1948. The average temperature of the CMB has been measured to an unprecedented accuracy: $T_\gamma = (2.725 \pm 0.001)$ K, and its spectrum fits the blackbody radiation formula very well. The average temperature of the CνB is predicted to be $T_\nu = (4/11)^{1/3} T_\gamma = (1.945 \pm 0.001)$ K in the hot Big Bang model, implying that the kinetic energy of relic neutrinos is only about $E_\nu \sim 1.6 \times 10^{-4}$ eV. How to detect the CνB turns out to be a big challenge in modern neutrino astronomy because the cross section of such a low-energy neutrino flux interacting with matter within a detector is too small, characterized by $(G_{\rm F} E_\nu)^2 \sim 1.4 \times 10^{-63}$ cm^2.

The number density of relic neutrinos can be computed with the Fermi-Dirac statistics at their present-day average temperature. It is found that there are totally about 336 neutrinos and antineutrinos per cubic centimeter in the Universe; i.e., $n_{\nu_\alpha} \approx n_{\overline{\nu}_\alpha} \approx 56$ cm^{-3} for $\alpha = e, \mu$ and τ. In comparison, the cosmic background photons are slightly more numerous and their number density is about $n_\gamma \approx 411$ cm^{-3}. Relic neutrinos are therefore the second most abundant particles in the Universe (Dondelson, 2003; Weinberg, 2008). They must contribute to the total energy density of the Universe, which governs how the Universe evolves. The species of neutrinos must have affected the primordial abundances of light elements during the BBN. In addition, the existence of the CνB can have an impact on the evolution of the CMB anisotropy and the growth of matter perturbations. We shall spell out the crucial roles of neutrinos played in the evolution of the Universe, such as the BBN and the structure formation, in Chapter 9 and Chapter 10.

1.3 Knowledge and Questions on Neutrinos

Neutrinos are very elusive. A neutrino is by Pauli's definition an electrically neutral and extremely light particle of spin 1/2. This section will first outline some fundamental knowledge of neutrinos that we have accumulated in the past eight decades, and then list some important open questions about

the properties of massive neutrinos and their unique roles in the micro- and macro-worlds. The prospects of neutrino physics, neutrino astronomy and neutrino cosmology rely on the extent to which those questions will be answered, and on new discoveries and surprises on the road ahead.

1.3.1 Present Knowledge on Neutrinos

There are three neutrino species (ν_e, ν_μ, ν_τ), consistent with the existence of three families of charged leptons (e, μ, τ), $Q = +2/3$ quarks (u, c, t) and $Q = -1/3$ quarks (d, s, b). The invisible decay width of the gauge boson Z^0 measured in the LEP experiment provides the most stringent constraint on the number of neutrino species: $N_\nu = 2.984 \pm 0.008$ (Nakamura *et al.*, 2010), which is in excellent agreement with the SM expectation $N_\nu = 3$. Note that this constraint is only valid for the active neutrinos that take part in the standard weak interactions and have masses below $M_{Z^0}/2 \approx 45.6$ GeV. Moreover, the observational data on the BBN and CMB set the following consistent but looser bounds on the number of neutrino species: $N_\nu = 3.14^{+0.70}_{-0.65}$ (BBN) at the 68% confidence level (Cyburt *et al.*, 2005) and $N_\nu = 4.4 \pm 1.5$ (CMB) at the same confidence level (Komatsu *et al.*, 2009).

Neutrinos and antineutrinos are electrically neutral fermions of spin 1/2; and they have left ($\lambda = -1/2$) and right ($\lambda = +1/2$) helicities, respectively. Given the electric charge conservation as a fundamental law, one may experimentally constrain the electric charge of an electron antineutrino to be $e_\nu < 3 \times 10^{-21} e$ in the beta decay thanks to the precision measurements of the electric charges of electrons, protons and neutrons (Ignatiev and Joshi, 1995). The astrophysical bounds on the electric charges of neutrinos, such as the one $e_\nu < 2 \times 10^{-14} e$ obtained from the observational data on the globular clusters (Raffelt, 1999), are much looser but they also point to $e_\nu = 0$. Given the angular momentum conservation as a fundamental law, one may consider $\pi^+ \to \mu^+ + \nu_\mu$, $\pi^+ \to e^+ + \nu_e$ and other weak processes to infer that neutrinos must have spin 1/2. In the orbital-electron capture reaction ${}^{152}_{63}\mathrm{Eu} + e^- \to {}^{152}_{62}\mathrm{Sm}^* + \nu_e$ and the decay mode $\pi^- \to \mu^- + \overline{\nu}_\mu$, for example, the helicity of the electron neutrino and that of the muon antineutrino were found to be left (Goldhaber *et al.*, 1958) and right (Bardon *et al.*, 1961), respectively. The ALEPH Collaboration measured the decay mode $\tau^- \to l^-_\alpha + \overline{\nu}_\alpha + \nu_\tau$ (for $\alpha = e$ or μ) and determined the helicity of the tau neutrino to be $\lambda = -0.496 \pm 0.006$ (Heister *et al.*, 2001), consistent with the SM expectation $\lambda = -1/2$. All the available experiments indicate that neutrinos are essentially left-handed while antineutrinos are essentially right-handed, even though their rest masses may not be exactly vanishing.

Neutrinos are actually massive but their rest masses are very tiny, at most of $\mathcal{O}(1)$ eV. Since 1998, the phenomena of neutrino oscillations have convincingly been observed in atmospheric, solar, reactor and accelerator neutrino experiments (Nakamura *et al.*, 2010). The discovery of neutrino oscillations marks a great breakthrough in particle physics, because it implies

that neutrinos have rest masses and the SM itself is incomplete. Current experimental data have revealed the magnitudes of two independent neutrino mass-squared differences: $\Delta m^2_{21} \equiv m^2_2 - m^2_1 \sim 7.7 \times 10^{-5}$ eV^2 and $\Delta m^2_{32} \equiv m^2_3 - m^2_2 = \pm 2.4 \times 10^{-3}$ eV^2. Hence at least two neutrinos must be massive and at least one neutrino mass must be larger than $\sqrt{|\Delta m^2_{32}|} \sim 0.049$ eV. But the absolute scale of neutrino masses cannot be determined from neutrino oscillations. The kinematic measurements of the tritium beta decay $^3\mathrm{H} \to {}^3\mathrm{He} + e^- + \overline{\nu}_e$ and the pion and tau decays have yielded some upper bounds on the effective masses of three neutrinos, but they are looser than those obtained from the neutrinoless double-beta ($0\nu 2\beta$) decay and the cosmological constraints (Fogli *et al.*, 2008). One may conservatively expect that the absolute neutrino mass scale should be of $\mathcal{O}(1)$ eV or smaller.

The neutrino mass eigenstates (ν_1, ν_2, ν_3) do not match the neutrino flavor eigenstates (ν_e, ν_μ, ν_τ), leading to the phenomenon of neutrino flavor mixing which is exactly analogous to that of quark flavor mixing. In the basis where the mass eigenstates of three charged leptons are identified with their flavor eigenstates, the mismatch between mass and flavor eigenstates of three neutrinos can be described by a 3×3 unitary matrix V — the so-called Maki-Nakagawa-Sakata (MNS) matrix (Maki *et al.*, 1962) or the MNS-Pontecorvo matrix (Pontecorvo, 1968), which is usually parametrized in terms of three mixing angles (θ_{12}, θ_{13}, θ_{23}) and three CP-violating phases (δ, ρ, σ). A global analysis of current neutrino oscillation data yields $\theta_{12} \approx 34^\circ$, $\theta_{23} \approx 45^\circ$ and $\theta_{13} < 10^\circ$ (Fogli *et al.*, 2008; Schwetz *et al.*, 2008), but three CP-violating phases are entirely unrestricted due to the lack of relevant experimental information. The fact that θ_{12} and θ_{23} are remarkably larger than the largest quark mixing angle (i.e., the Cabibbo angle $\vartheta_{\mathrm{C}} \approx 13^\circ$) is an intriguing puzzle, implying an intrinsic difference between the origin of lepton flavor mixing and that of quark flavor mixing.

Neutrinos take part in both neutral- and charged-current weak interactions. The available experimental results for neutrino-electron scattering, neutrino-nucleus scattering and quasi-elastic or inelastic neutrino-nucleon scattering are all consistent with the SM. Hence the SM remains to be the standard theory of neutrino interactions even after neutrino oscillations have been discovered, and it is the guiding principle of various man-made experiments to produce and detect neutrinos. Up to now solar neutrinos, atmospheric neutrinos and Supernova 1987A neutrinos have been observed, thanks to the rapid development of detector techniques, so have geoneutrinos [5]. The technology of producing low- and high-energy neutrinos from reactors and accelerators has been very mature, too. We can therefore foresee a bright future in experimental neutrino physics and astronomy, which will finally help bring the true theory of massive neutrinos to light.

[5] Geoneutrinos are the low-energy neutrinos created in the decays of radioactive isotopes inside the Earth. They have been detected in the KamLAND and Borexino experiments (Araki *et al.*, 2005; Bellini *et al.*, 2010).

1.3.2 Open Questions on Neutrinos

Although we have known quite a lot about elusive neutrinos, as briefly summarized in Section 1.3.1, we have many open questions about their intrinsic properties and their unique roles in the Universe. The following is a partial list of some immediate and important questions in neutrino physics, neutrino astronomy and neutrino cosmology.

Question 1: are massive neutrinos the Dirac or Majorana particles? If massive neutrinos are the Dirac particles, just like the charged leptons and quarks, then they must be distinguishable from their antiparticles because of lepton number conservation. By definition, a Majorana neutrino is its own antiparticle (Majorana, 1937; Case, 1957). Hence the weak processes mediated by massive Majorana neutrinos can be lepton-number-violating. At present the only feasible way to identify the Majorana nature of three known neutrinos is to observe the $0\nu2\beta$ decays of some even-even nuclei (i.e., $N(A,Z) \to N(A,Z+2)+2e^-$ decays), which can naturally take place via the exchange of virtual Majorana neutrinos between two associated beta decays (Xing, 2004). No convincing evidence for an occurrence of the $0\nu2\beta$ decay has so far been established, although most theorists believe that massive neutrinos should be the Majorana particles and the origin of their masses must be different from that of charged-fermion masses.

Question 2: what is the absolute neutrino mass scale? There are three feasible ways to probe the absolute mass scale of three known neutrinos. The KATRIN experiment is the most promising next-generation direct-mass-search experiment. Its sensitivity to the effective mass of the tritium β-decay $\langle m \rangle_e \equiv \sqrt{m_1^2 |V_{e1}|^2 + m_2^2 |V_{e2}|^2 + m_3^2 |V_{e3}|^2}$ may hopefully reach ~ 0.2 eV (Bornschein *et al.*, 2003). If massive neutrinos are the Majorana particles, it is also possible to constrain their masses by observing the $0\nu2\beta$ decay and determining its effective mass $\langle m \rangle_{ee} \equiv |m_1 V_{e1}^2 + m_2 V_{e2}^2 + m_3 V_{e3}^2|$. The present $0\nu2\beta$ experiments are sensitive to $\langle m \rangle_{ee}$ of $\mathcal{O}(0.1)$ eV, while the future $0\nu2\beta$ experiments are likely to have sensitivities in the meV range (Avignone III *et al.*, 2008). In addition, one may obtain useful information on the absolute neutrino mass scale from cosmology or astrophysics. A global analysis of current cosmological data has provided us with a very stringent upper bound on the sum of light neutrino masses, whose magnitude is typically of $\mathcal{O}(0.1)$ eV to $\mathcal{O}(1)$ eV, but its explicit value depends on what assumptions are made and which data are used (Seljak *et al.*, 2006; Kayser, 2008). Note that the sign of Δm_{32}^2 has not been determined from the present neutrino oscillation experiments, implying that the neutrino mass spectrum can be either $m_3 > m_2 > m_1$ (normal hierarchy) or $m_2 > m_1 > m_3$ (inverted hierarchy). The upcoming long-baseline neutrino experiments and the future neutrino factory or superbeam facilities will be able to pin down the neutrino mass hierarchy (Bandyopadhyay *et al.*, 2009).

Question 3: how small is the neutrino mixing angle θ_{13}? Whether the smallest neutrino mixing angle θ_{13} is exactly vanishing or not is of great

importance in understanding the dynamics of lepton flavor mixing. While $\theta_{13} = 0$ might result from a certain flavor symmetry, it is in general unstable due to the flavor symmetry breaking or radiative corrections. The value of θ_{13}, after it is measured, may serve for a sensitive discriminator of various neutrino models. There will be no CP or T violation in neutrino oscillations if θ_{13} is vanishing, unless they get involved with non-standard neutrino interactions. If θ_{13} is too small, it will be extremely difficult or even impossible to discover CP violation in the lepton sector. A lesson learnt from the history of quark flavor physics is that a determination of the smallest quark mixing angle is a crucial turning-point in doing precision measurements, detecting CP violation and searching for new physics. It is therefore desirable to measure the smallest neutrino mixing angle θ_{13}. A number of long-baseline accelerator and reactor neutrino experiments are underway to determine or constrain this angle (Gonzalez-Garcia and Maltoni, 2008). In particular, the Daya Bay reactor antineutrino experiment in China will probe θ_{13} with a very impressive sensitivity: $\sin^2 2\theta_{13} \lesssim 0.01$ (Guo *et al.*, 2007).

Question 4: is there CP violation in the lepton sector? Within the SM the source of CP violation is the nontrivial Kobayashi-Maskawa (KM) phase which resides in the 3×3 quark mixing matrix (Kobayashi and Maskawa, 1973). The phenomena of CP violation have been observed in a number of K- and B-meson decays (e.g., Christenson *et al.*, 1964; Abe *et al.*, 2001; Aubert *et al.*, 2001), and all the experimental results are consistent with the KM mechanism (Nakamura *et al.*, 2010). Now that neutrinos are massive and lepton flavors are mixed, there should analogously exist CP violation in the lepton sector. The source of leptonic CP violation is expected to be a KM-like phase δ in the 3×3 MNS matrix V, but two additional CP-violating phases ought to be taken into account if massive neutrinos are the Majorana particles (Xing, 2004). The most promising way to discover leptonic CP violation is to measure an asymmetry between the probabilities of $\nu_e \to \nu_\mu$ and $\overline{\nu}_e \to \overline{\nu}_\mu$ transitions. Such a measurement can be done in a neutrino factory (Gonzalez-Garcia and Maltoni, 2008). Note that the strength of CP violation in neutrino oscillations depends both on the magnitude of δ itself and on the values of θ_{12}, θ_{13} and θ_{23}, and thus how small θ_{13} is turns out to be crucial in order to judge whether the effect of CP violation is practically observable or not.

Question 5: are there ultrahigh-energy cosmic neutrinos? The observation of solar and supernova neutrinos has initiated a new and rapidly-developing science — neutrino astronomy. Both solar and supernova neutrinos carry energies of $\mathcal{O}(1)$ MeV to $\mathcal{O}(10)$ MeV and reach the Earth without any attenuation, offering us some good opportunities to learn about the deep interior of a star (Bahcall, 1989). We believe that much more energetic neutrinos (from TeV to EeV) should be emitted from other astrophysical objects, such as supernova remnants, active galactic nuclei and gamma ray bursts, and from the annihilation of dark matter. For the time being the km^3-scale neutrino telescope IceCube is under construction at the South Pole, and it has already

constrained the flux of muon neutrinos emitted from the gamma ray bursts to be lower than 2.7×10^{-3} erg cm^{-2} in the energy range 3 TeV $< E_\nu <$ 2.8 PeV (Abbasi *et al.*, 2010). A km^3-scale underwater neutrino telescope, known as the KM3NeT (Carr *et al.*, 2007), is now under consideration. The discovery of ultrahigh-energy cosmic neutrinos will shed light on the origin of ultrahigh-energy cosmic rays and examine the intrinsic properties of neutrinos themselves. In particular, we hope that ultrahigh-energy cosmic neutrinos could finally become a useful messenger between human beings and the distant or even invisible Universe.

Question 6: how to detect cosmic background neutrinos? According to the standard Big Bang model of cosmology, today's abundance of relic neutrinos and that of relic photons are of the same order (Weinberg, 2008). The precision measurement of the CMB has remarkably improved our knowledge on the matter content and structure formation of the Universe. Unfortunately, it is a big challenge to directly detect the CνB because the energies of relic neutrinos are too low ($\sim 10^{-4}$ eV) and their interactions with matter are too weak. Current proposals for detecting relic neutrinos fall into three categories (Ringwald, 2009): (a) using the mechanical force — relic neutrinos scattering off the nuclei of a target will cause a mechanical force which can be measured by the Cavendish-type torsion balance; (b) using the capture on radioactive nuclei — relic neutrinos will be absorbed by radioactive nuclei via an inverse beta decay (e.g., $\nu_e + {}^3\mathrm{H} \to {}^3\mathrm{He} + e^-$); and (c) using the cutoff of an ultrahigh-energy neutrino spectrum — the ultrahigh-energy cosmic neutrinos with energies $E_\nu > 10^{21}$ eV will be absorbed or cut off by the CνB via the resonant reaction $\nu_\alpha + \overline{\nu}_\alpha \to Z^0 \to$ anything (Weiler, 1982, 1999; Fargion *et al.*, 1999). However, the sensitivities of such methods are limited by the present technology and still several orders of magnitude lower than that demanded by a successful detection of the CνB.

Question 7: what role is played by neutrinos in the evolution of the Universe? The existence of neutrinos in the early Universe has only indirectly been confirmed by the success of the standard Big Bang cosmology. Current observational data on the abundances of primordial light elements, the power spectra of CMB anisotropies and the large-scale structure formation all suggest that neutrinos be playing a crucial role in the evolution of the Universe (Hannestad, 2006). We expect that this intriguing picture can be further verified by the future observations. If the observed baryon number asymmetry of the Universe has something to do with the occurrence of heavy Majorana neutrinos in the early Universe (Fukugita and Yanagida, 1986), then they must have affected the evolution of the Universe. How to test such baryogenesis-via-leptogenesis mechanisms is another burning question in today's particle physics and cosmology (Xing, 2008).

So far we have only listed some experimental or observational questions about neutrinos. There are certainly many theoretical questions on the market. For example, we wonder what the origin of neutrino masses is, why the

pattern of lepton flavor mixing is so different from that of quark flavor mixing, what the origin of CP violation is, how the cosmological matter-antimatter asymmetry is related to CP violation at low energies, what the role of neutrinos is in dark matter, whether neutrinos have something to do with dark energy, whether there exist sterile neutrinos in the Universe, and so forth. Motivated by so many interesting and fundamental questions, we are trying to discover a new physics world with the help of neutrinos in the era of the Large Hadron Collider and in the era of precision astronomy and cosmology.

Last but not least, will neutrinos spring many more surprises on us? The history of neutrino physics is full of surprises. So it would be surprising if further surprises were not in store. In this sense one must be well prepared to encounter something that is completely unexpected, again and again, on the way of neutrino exploration. The road ahead must be bright and exciting!

References

Abbasi, R., *et al.* (HiRes Collaboration), 2008, Phys. Rev. Lett. **100**, 101101.
Abbasi, R., *et al.* (IceCube Collaboration), 2010, Astrophys. J. **710**, 346.
Abdurashitov, J. N., *et al.* (SAGE Collaboration), 2002, JETP **95**, 181.
Abe, K., *et al.* (Belle Collaboration), 2001, Phys. Rev. Lett. **87**, 091802.
Abraham, J., *et al.* (Pierre Auger Collaboration), 2008, Phys. Rev. Lett. **101**, 061101.
Ahmad, Q. R., *et al.* (SNO Collaboration), 2001, Phys. Rev. Lett. **87**, 071301.
Ahrens, J., *et al.* (IceCube Collaboration), 2003, Nucl. Phys. Proc. Suppl. **118**, 388.
Alekseev, E. N., *et al.*, 1987, JETP Lett. **45**, 589.
Allen, J. S., 1942, Phys. Rev. **61**, 692.
Alpher, R. A., Bethe, H., and Gamow, G., 1948, Phys. Rev. **73**, 803.
Altmann, M., *et al.* (GNO Collaboration), 2005, Phys. Lett. B **616**, 174.
Araki, T., *et al.* (KamLAND Collaboration), 2005, Nature **436**, 467.
Arnett, W. D., *et al.*, 1989, Annu. Rev. Astron. Astrophys. **27**, 629.
Aubert, B., *et al.* (BABAR Collaboration), 2001, Phys. Rev. Lett. **87**, 091801.
Avignone III, F. T., Elliot, S. R., and Engel, J., 2008, Rev. Mod. Phys. **80**, 481.
Bahcall, J. N., 1964, Phys. Rev. Lett. **12**, 300.
Bahcall, J. N., 1989, *Neutrino Astrophysics* (Cambridge University Press).
Bahcall, J. N., and Shaviv, G., 1968, Phys. Rev. Lett. **20**, 1209.
Bandyopadhyay, A., *et al.*, 2009, Rept. Prog. Phys. **72**, 106201.
Bardon, M., Franzini, P., and Lee, J., 1961, Phys. Rev. Lett. **7**, 23.
Bellini, G., *et al.* (Borexino Collaboration), 2010, Phys. Lett. B **687**, 299.
Bethe, H. A., 1939, Phys. Rev. **55**, 434.
Bethe, H. A., 1990, Rev. Mod. Phys. **62**, 801.
Bethe, H. A., and Bacher, R. F., 1936, Rev. Mod. Phys. **8**, 184.
Bethe, H. A., and Wilson, J. R., 1985, Astrophys. J. **295**, 14.
Bionta, R. M., *et al.* (IMB Collaboration), 1987, Phys. Rev. Lett. **58**, 1494.
Bornschein, L., *et al.* (KATRIN Collaboration), 2003, hep-ex/0309007.
Carr, J., *et al.* (KM3NeT Collaboration), 2007, arXiv:0711.2145.
Case, K. M., 1957, Phys. Rev. **107**, 307.

Chadwick, J., 1914, Verhandl. Deut. Phys. **16**, 383.
Chadwick, J., 1932, J. Proc. Roy. Soc. A **136**, 692.
Christenson, J. H., *et al.*, 1964, Phys. Rev. Lett. **13**, 138.
Cowan, C. L., Jr., *et al.*, 1956, Science **124**, 103.
Crane, H. R., 1948, Rev. Mod. Phys. **20**, 278.
Crane, H. R., and Halpern, J., 1939, Phys. Rev. **56**, 232.
Cyburt, R., *et al.*, 2005, Astropart. Phys. **23**, 313.
Danby, G., *et al.*, 1962, Phys. Rev. Lett. **9**, 36.
Davis, R. Jr., 1964, Phys. Rev. Lett. **13**, 303.
Davis, R. Jr., Harmer, D. S., and Hoffman, K. C., 1968, Phys. Rev. Lett. **20**, 1205.
Dondelson, S., 2003, *Modern Cosmology* (Academic Press).
Einstein, A., 1915, Sitzungsber. Preuss. Akad. Wiss. Berlin **48**, 844.
Ellis, C. D., and Wooster, W. A., 1927, Proc. Roy. Soc. London A **117**, 109.
Fargion, D., Mele, B., and Salis, A., 1999, Astrophys. J. **517**, 725.
Fermi, E., 1933, La Ricerca Scientifica **2**, 12.
Fermi, E., 1934, Z. Phys. **88**, 161.
Feynman, R. P., and Gell-Mann, M., 1958, Phys. Rev. **109**, 193.
Fogli, G. L., *et al.*, 2008, Phys. Rev. D **78**, 033010.
Franklin, A., 2000, *Are There Really Neutrinos?* (Perseus Books).
Friedman, J. I., and Telegdi, V. L., 1957, Phys. Rev. **105**, 1681.
Fukuda, S., *et al.* (Super-Kamiokande Collaboration), 2001, Phys. Rev. Lett. **86**, 5651.
Fukuda, Y., *et al.* (Kamiokande Collaboration), 1996, Phys. Rev. Lett. **77**, 1683.
Fukugita, M., and Yanagida, T., 1986, Phys. Lett.B **174**, 45.
Gaisser, T. K., 1991, *Cosmic Rays and Particle Physics* (Cambridge University Press).
Gamow, G., and Schönberg, M., 1940, Phys. Rev. **58**, 1117.
Gamow, G., and Schönberg, M., 1941, Phys. Rev. **59**, 539.
Gamow, G., and Teller, E., 1936, Phys. Rev. **49**, 895.
Garwin, R. L., Lederman, L. M., and Weinrich, M., 1957, Phys. Rev. **105**, 1415.
Goldhaber, M., Grodzins, L., and Sunyar, A. W., 1958, Phys. Rev. **109**, 1015.
Gonzalez-Garcia, M. C., and Maltoni, M., 2008, Phys. Rept. **460**, 1.
Greisen, K., 1966, Phys. Rev. Lett. **16**, 748.
Guo, X. H., *et al.* (Daya Bay Collaboration), 2007, arXiv:hep-ex/0701029.
Halzen, F., and Hooper, D., 2002, Rept. Prog. Phys. **65**, 1025.
Hampel, W., *et al.* (GALLEX Collaboration), 1999, Phys. Lett. B **447**, 127.
Hannestad, S., 2006, Ann. Rev. Nucl. Part. Sci. **56**, 137.
Heisenberg, W., 1932, Z. Phys. **77**, 1.
Heister, A., *et al.* (ALEPH Collaboration), 2001, Eur. Phys. J. C **22**, 217.
Heitler, W., and Herzberg, G., 1929, Naturwiss. **17**, 673.
Hirata, K., *et al.* (Kamiokande Collaboration), 1987, Phys. Rev. Lett. **58**, 1490.
Hubble, E. P., 1929, Proc. Nat. Acad. Sci. **15**, 168.
Ignatiev, A. Yu., and Joshi, G. C., 1995, Phys. Rev. D **51**, 2411.
Kayser, B., 2008, arXiv:0804.1497.
Kobayashi, M., and Maskawa, T., 1973, Prog. Theor. Phys. **49**, 652.
Kodama, K., *et al.* (DONUT Collaboration), 2001, Phys. Lett. B **504**, 218.
Komatsu, E., *et al.*, 2009, Astrophys. J. Suppl. **180**, 330.

Kronig, R. de L., 1928, Naturwiss. **16**, 335.
Landau, L., 1957, Nucl. Phys. **3**, 127.
Lee, T. D., and Yang, C. N., 1956, Phys. Rev. **104**, 254.
Lee, T. D., and Yang, C. N., 1957, Phys. Rev. **105**, 1671.
Lee, T. D., and Yang, C. N., 1960, in *Proceedings of the International Conference on High Energy Physics*, Rochester (New York: Interscience), p. 567.
Lemaitre, G., 1931, Nature **128**, 699.
Majorana, E., 1937, Nuovo Cim. **14**, 171.
Maki, Z., Nakagawa, M., and Sakata, S., 1962, Prog. Theor. Phys. **28**, 870.
Mikheyev, S. P., and Smirnov, A. Yu., 1986, Zh. Eksp. Teor. Fiz. **91**, 7.
Nakamura, K., *et al.* (Particle Data Group), 2010, J. Phys. G **37**, 075021.
Pauli, W., 1984, *Physik und Erkenntnistheorie* (Friedr, Vieweg, & Sohn, Braunschweig/Wiesbaden), p. 156.
Penzias, A. A., and Wilson, R. W., 1965, Astrophys. J. **142**, 419.
Perl, M. L., *et al.*, 1975, Phys. Rev. Lett. **35**, 1849.
Pontecorvo, B., 1946, Chalk River Lab. Report PD-205.
Pontecorvo, B., 1959, Zh. Eksp. Teor. Fiz. **36**, 1615.
Pontecorvo, B., 1968, JETP **26**, 984.
Raffelt, G. G., 1996, *Stars as Laboratories of Fundamental Physics* (The University of Chicago Press).
Raffelt, G. G., 1999, Phys. Rept. **320**, 319.
Rasetti, F., 1930, Z. Phys. **61**, 598.
Reines, F., 1979, Science **203**, 11.
Reines, F., *et al.*, 1960, Phys. Rev. **117**, 159.
Ringwald, A., 2009, Nucl. Phys. A **827**, 501c.
Salam, A., 1957, Nuovo Cim. **5**, 299.
Salam, A., 1968, in *Elementary Particle Physics (Nobel Symposium No. 8)*, edited by Svartholm N., (Almqvist and Wilsell), p. 367.
Schwetz, T., Tortola, M. A., and Valle, J. W. F., 2008, New J. Phys. **10**, 113011.
Seljak, U., Slosar, A., and McDonald, P., 2006, JCAP **0610**, 014.
Stanev, T., 2004, *High Energy Cosmic Rays* (Springer Praxis Books).
Sudarshan, E. C. G., and Marshak, R. E., 1958, Phys. Rev. **109**, 1860.
Wang, K. C., 1942, Phys. Rev. **61**, 97.
Weiler, T. J., 1982, Phys. Rev. Lett. **49**, 234.
Weiler, T. J., 1999, Astropart. Phys. **11**, 303.
Weinberg, S., 1967, Phys. Rev. Lett. **19**, 1264.
Weinberg, S., 2008, *Cosmology* (Oxford University Press).
Wolfenstein, L., 1978, Phys. Rev. D **17**, 2369.
Wu, C. S., *et al.*, 1957, Phys. Rev. **105**, 1413.
Xing, Z. Z., 2004, Int. J. Mod. Phys. A **19**, 1.
Xing, Z. Z., 2008, Int. J. Mod. Phys. A **23**, 4255.
Zatsepin, G. T., and Kuzmin, V. A., 1966, JETP Lett. **4**, 78.

2

Neutrinos within the Standard Model

Neutrinos are assumed to be massless in the standard model (SM) of particle physics. They can only have weak interactions with matter. In this chapter we shall first introduce the SM of electroweak interactions and then describe neutrino-electron scattering, neutrino-neutrino scattering and neutrino-nucleon interactions. The coherent forward scattering of neutrinos with matter, which is very important for neutrino oscillations in matter, will also be discussed in some detail.

2.1 Fundamentals of the Standard Model

There exist three generations of quarks and leptons which are the fundamental building blocks of matter. The interactions of these elementary particles can be described in the language of gauge field theories. For instance, the electromagnetic force between two charged particles is mediated by the photon, a gauge boson in quantum electrodynamics (QED) based on the Abelian group $U(1)$. The perfect agreement between the QED prediction and the experimental measurement of the muon anomalous magnetic moment $a_\mu \equiv (g-2)/2$ proves the usefulness and exactness of quantum field theories. We shall outline the structure of the SM, which unifies electromagnetic and weak interactions of elementary particles, in this section. Three indispensable ingredients of the SM — gauge principles, spontaneous symmetry breaking and renormalizability, will be explained in order.

2.1.1 Gauge Symmetries

Let us illustrate the gauge principle by examining QED, which exhibits the $U(1)$ gauge invariance. Consider the Lagrangian of a free electron described by the fermion field $\Psi(x)$,

$$\mathcal{L}_0 = \overline{\Psi}(x)\left(\mathrm{i}\partial\!\!\!/ - m\right)\Psi(x)\ , \tag{2.1}$$

where $\not{\partial} \equiv \gamma^\mu \partial_\mu$ is defined and m denotes the electron mass. It is easy to verify that $\mathcal{L}_0$ is invariant under the transformation $\Psi(x) \to \Psi'(x) = \mathrm{e}^{-\mathrm{i}\alpha}\Psi(x)$ with α being a spacetime-independent real constant. If one promotes the transformation into $\Psi(x) \to \Psi'(x) = \mathrm{e}^{-\mathrm{i}\alpha(x)}\Psi(x)$ with $\alpha(x)$ being an arbitrary real function of x, however, $\mathcal{L}_0$ will not be invariant under this new transformation. In order to preserve the local gauge invariance of $\mathcal{L}_0$, we introduce the covariant derivative $D_\mu \equiv \partial_\mu - \mathrm{i}eA_\mu(x)$, where e is the electric charge of the proton and $A_\mu(x)$ is a four-vector gauge field. The requirement that $D_\mu\Psi(x)$ transforms in the same way as $\Psi(x)$ allows us to determine how $A_\mu(x)$ transforms. More explicitly, we have

$$D_\mu\Psi(x) \to D'_\mu\Psi'(x) = \left[\partial_\mu - \mathrm{i}eA'_\mu(x)\right] \mathrm{e}^{-\mathrm{i}\alpha(x)}\Psi(x) = \mathrm{e}^{-\mathrm{i}\alpha(x)} D_\mu\Psi(x) \ , \quad (2.2)$$

which gives rise to

$$A_\mu(x) \to A'_\mu(x) = A_\mu(x) - \frac{1}{e}\partial_\mu\alpha(x) \ . \quad (2.3)$$

It is the local gauge invariance that necessitates the introduction of the gauge field $A_\mu(x)$ and uniquely fixes the interaction between the charged particles and $A_\mu(x)$. The kinetic term of $A_\mu(x)$ can be constructed from the strength tensor $F_{\mu\nu} \equiv \partial_\mu A_\nu(x) - \partial_\nu A_\mu(x)$, which is evidently gauge invariant as indicated by Eq. (2.3). Therefore, the total gauge-invariant Lagrangian of QED can be written as

$$\mathcal{L}_{\mathrm{QED}} = -\frac{1}{4}F^{\mu\nu}F_{\mu\nu} + \overline{\Psi}(x)\left(\mathrm{i}\not{D} - m\right)\Psi(x) \ , \quad (2.4)$$

where $\not{D} \equiv \gamma^\mu D_\mu$ is defined. From the above equation, one may easily derive the electron-photon vertex $e\overline{\Psi}(x)\gamma^\mu\Psi(x)A_\mu(x)$.

In 1954, Chen Ning Yang and Robert Mills proposed that the local isospin symmetry could be maintained in strong interactions (Yang and Mills, 1954). In this seminal paper the proton and neutron were combined to form a doublet under the non-Abelian group $SU(2)$. It is straightforward to generalize their idea to any non-Abelian group $SU(N)$. The generators of the group $SU(N)$ satisfy the commutation relation

$$\left[t^i, t^j\right] = \mathrm{i}c^{ijk}t^k \ , \quad (2.5)$$

where i, j, k run over $1, 2, \cdots, N^2 - 1$ and c^{ijk} is the structure constant which is fully antisymmetric with respect to the superscripts. The collective fields $\Psi(x) = [\psi_1(x), \psi_2(x), \cdots, \psi_N(x)]^T$ transform in the following way:

$$\Psi(x) \to \Psi'(x) = \mathrm{e}^{-\mathrm{i}\theta^k(x)T^k}\Psi(x) \ , \quad (2.6)$$

where T^k is the matrix representation of the generator t^k, and $\theta^k(x)$ (for $k = 1, 2, \cdots, N$) are the spacetime-dependent real functions. Similar to the Abelian gauge theory, the covariant derivative is now defined as

$$D_\mu = \partial_\mu - \mathrm{i}gT^k A_\mu^k(x) \ , \tag{2.7}$$

where $A_\mu^k(x)$ (for $k = 1, 2, \cdots, N$) stand for the gauge fields. If $D_\mu \Psi(x)$ is required to transform as $D_\mu \Psi(x) \to D'_\mu \Psi'(x) = \mathrm{e}^{-\mathrm{i}\theta^k(x)T^k} D_\mu \Psi(x)$, then $A_\mu^k(x)$ must transform as follows:

$$T^k A_\mu^k \to T^k A_\mu'^k = \mathrm{e}^{-\mathrm{i}\theta^k T^k} \left(T^k A_\mu^k\right) \mathrm{e}^{\mathrm{i}\theta^k T^k} - \frac{\mathrm{i}}{g} \left(\partial_\mu \mathrm{e}^{-\mathrm{i}\theta^k T^k}\right) \mathrm{e}^{\mathrm{i}\theta^k T^k} \ . \tag{2.8}$$

For the infinitesimal transformation, we have

$$A_\mu^k(x) \to A_\mu'^k(x) = A_\mu^k(x) - \frac{1}{g}\partial_\mu \theta^k(x) - c^{klm} A_\mu^l(x)\theta^m(x) \ . \tag{2.9}$$

The field strength tensor reads

$$F_{\mu\nu}^i = \partial_\mu A_\nu^i(x) - \partial_\nu A_\mu^i(x) + g c^{ijk} A_\mu^j(x) A_\nu^k(x) \ , \tag{2.10}$$

which constitutes the kinetic term of the gauge fields. It is obvious that the gauge-invariant Lagrangian takes the form

$$\mathcal{L}_{SU(N)} = -\frac{1}{4} F_{\mu\nu}^i F^{i\mu\nu} + \overline{\Psi}(x)\mathrm{i}\not{D}\Psi(x) \ . \tag{2.11}$$

One of the most successful examples of such a gauge theory is quantum chromodynamics (QCD), which describes the strong interactions of quarks with gluons (Fritzsch *et al.*, 1973). One of the experimentally-verified QCD predictions is the existence of three-gluon and four-gluon interaction vertices (Ellis *et al.*, 1976; Brandelik *et al.*, 1979), but glueballs (the bound states of gluons) have not been identified in any high-energy physics experiments.

2.1.2 Spontaneous Symmetry Breaking

Although the preliminary idea of gauge theories appeared as early as in the 1920's (Weyl, 1929) and the non-Abelian $SU(2)$ gauge symmetry was explored by Yang and Mills in the 1950's, their importance was not widely recognized until the mechanism of spontaneous symmetry breaking was invented in the 1960's. A simple reason is that the weak interactions must be mediated by massive gauge bosons, but a naive mass term like $mA_\mu^i A^{i\mu}$ explicitly violates the local gauge invariance. Inspired by the Bardeen-Cooper-Schrieffer theory of superconductivity, Yoichiro Nambu applied the concept of spontaneous symmetry breaking to particle physics (Nambu, 1960; Nambu and Jona-Lasinio, 1961a, 1961b; Goldstone, 1961) and paved the way for the Higgs mechanism and to a true gauge theory of weak interactions.

To explain the mechanism of spontaneous symmetry breaking, let us consider a scalar theory with the global $U(1)$ symmetry:

$$\mathcal{L}_{\phi} = \partial^{\mu}\phi^{\dagger}\partial_{\mu}\phi - \mu^{2}\phi^{\dagger}\phi - \lambda\left(\phi^{\dagger}\phi\right)^{2} \ , \tag{2.12}$$

where μ^2 and λ are real parameters. One can easily verify that $\mathcal{L}_{\phi}$ is invariant under the transformation $\phi \to \phi' = \mathrm{e}^{-\mathrm{i}\alpha}\phi$, or equivalently $\delta\phi \equiv \phi' - \phi = -\mathrm{i}\alpha\phi$ for the infinitely small constant α. We similarly have $\phi^{\dagger} \to \phi'^{\dagger} = \mathrm{e}^{\mathrm{i}\alpha}\phi^{\dagger}$ or $\delta\phi^{\dagger} = \mathrm{i}\alpha\phi^{\dagger}$ for the Hermitian-conjugate field $\phi^{\dagger}$. The variation of $\mathcal{L}_{\phi}$ with respect to $\delta\phi$ can be cast into

$$\begin{aligned}
\delta\mathcal{L}_{\phi} &= \frac{\partial\mathcal{L}_{\phi}}{\partial\phi}\delta\phi + \frac{\partial\mathcal{L}_{\phi}}{\partial(\partial^{\mu}\phi)}\partial^{\mu}\delta\phi \\
&= \frac{\partial\mathcal{L}_{\phi}}{\partial\phi}\delta\phi + \partial^{\mu}\left(\frac{\partial\mathcal{L}_{\phi}}{\partial(\partial^{\mu}\phi)}\delta\phi\right) - \partial^{\mu}\left(\frac{\partial\mathcal{L}_{\phi}}{\partial(\partial^{\mu}\phi)}\right)\delta\phi \\
&= \left[\frac{\partial\mathcal{L}_{\phi}}{\partial\phi} - \partial^{\mu}\left(\frac{\partial\mathcal{L}_{\phi}}{\partial(\partial^{\mu}\phi)}\right)\right]\delta\phi + \partial^{\mu}\left(\frac{\partial\mathcal{L}_{\phi}}{\partial(\partial^{\mu}\phi)}\delta\phi\right) \ .
\end{aligned} \tag{2.13}$$

As the equation of motion must be satisfied, the term inside the square brackets is vanishing. Requiring the theory to be invariant, one may define a symmetry current by identifying the remaining term in Eq. (2.13) as its divergence. This current turns out to be

$$J_{\mu} = \mathrm{i}\left(\phi^{\dagger}\partial_{\mu}\phi - \phi\partial_{\mu}\phi^{\dagger}\right) \ , \tag{2.14}$$

and the corresponding symmetry charge is

$$Q \equiv \int \mathrm{d}^{3}\mathbf{x} J_{0}(x) = \mathrm{i}\int \mathrm{d}^{3}\mathbf{x}\left(\phi^{\dagger}\dot{\phi} - \phi\dot{\phi}^{\dagger}\right) \ , \tag{2.15}$$

where the irrelevant constant α has been discarded. The conservation of the current $\partial_{\mu}J^{\mu} = 0$ implies that the charge is independent of time, namely $\dfrac{\mathrm{d}Q}{\mathrm{d}t} = 0$. The above discussion is actually a concise version of the famous Noether theorem, which states that there always exists a conserved current in the theory with a continuous symmetry (Noether, 1918). The commutators between the charge Q and the field operators (ϕ and $\phi^{\dagger}$) actually generate the transformations

$$[Q, \phi] = -\phi \ , \qquad \left[Q, \phi^{\dagger}\right] = +\phi^{\dagger} \ , \tag{2.16}$$

where the commutative relations between field operators and their conjugate momenta at the equal time have been used. Taking ϕ and $\phi^{\dagger}$ as independent variables, one can immediately verify

$$\left[\phi(t,\mathbf{x}), \dot{\phi}^{\dagger}(t,\mathbf{y})\right] = \left[\phi^{\dagger}(t,\mathbf{x}), \dot{\phi}(t,\mathbf{y})\right] = \mathrm{i}\delta^{3}(\mathbf{x}-\mathbf{y}) \ . \tag{2.17}$$

Note that the charge eigenvalues of ϕ and $\phi^{\dagger}$ are -1 and $+1$, respectively, as indicated by Eq. (2.16). Note also that one or more massless bosons, the

so-called Goldstone bosons or Nambu-Goldstone bosons, will appear in the theory if the original Lagrangian has a continuous symmetry but the vacuum state has a reduced symmetry (Goldstone, 1961; Goldstone *et al.*, 1962).

To see the occurrence of a Goldstone boson in this scalar theory, we define the complex field $\phi = (\eta + \mathrm{i}\chi)/\sqrt{2}$ and rewrite the Lagrangian $\mathcal{L}_\phi$ as

$$\mathcal{L}_\phi = \frac{1}{2}\partial^\mu\eta\partial_\mu\eta + \frac{1}{2}\partial^\mu\chi\partial_\mu\chi - \frac{1}{2}\mu^2(\eta^2+\chi^2) - \frac{1}{4}\lambda\left(\eta^2+\chi^2\right)^2 \ . \quad (2.18)$$

One can observe that $\mathcal{L}_\phi$ is invariant under the rotation

$$\begin{aligned} \eta &\to \eta' = +\eta\cos\alpha + \chi\sin\alpha \ , \\ \chi &\to \chi' = -\eta\sin\alpha + \chi\cos\alpha \ ; \end{aligned} \quad (2.19)$$

or equivalently,

$$\delta\eta = +\alpha\chi \ , \qquad \delta\chi = -\alpha\eta \ . \quad (2.20)$$

This transformation is just the rotation in the (x, y) plane, and the corresponding symmetry group is $SO(2)$ which is locally equivalent to the $U(1)$ group as it should be. If the vacuum expectation value (vev) of η is nonzero, $\langle\eta\rangle = u$ with u being real and positive, then the vacuum state is no longer invariant under the rotation as the preferred direction is along the x-axis. To find out the physical modes in the theory, one may disturb the field variables around their classical values and redefine $\eta = u + \tilde{\eta}$. Therefore, the minimization of the scalar potential in Eq. (2.18) determines the vev $u = \sqrt{-\mu^2/\lambda}$. Given $\lambda > 0$, μ^2 must be negative to produce a meaningful vev. Now we have

$$\mathcal{L}_\phi = \frac{1}{2}\partial^\mu\tilde{\eta}\partial_\mu\tilde{\eta} + \frac{1}{2}\partial^\mu\chi\partial_\mu\chi - \frac{1}{2}\left(-2\mu^2\right)(\tilde{\eta})^2 + \cdots \ , \quad (2.21)$$

where the ellipsis denotes those non-quadratic terms of $\tilde{\eta}$ and χ. It becomes evident that the masses of two scalar particles are given by $m_{\tilde{\eta}}^2 = -2\mu^2$ and $m_\chi^2 = 0$. The massless boson χ, known as the Goldstone boson, occurs after the spontaneous breaking of the global $U(1)$ symmetry.

In 1964, Peter Higgs and some other theorists applied the idea of spontaneous symmetry breaking to the local gauge theories and found that the massless gauge bosons could absorb those unwanted Goldstone bosons and then become massive (Higgs, 1964a, 1964b, 1966; Englert and Brout, 1964; Guralnik *et al.*, 1964). This is just the famous Higgs mechanism. Based on the $SU(2)_{\mathrm{L}} \times U(1)_{\mathrm{Y}}$ gauge symmetry (Glashow, 1961) and the Higgs mechanism, Steven Weinberg and Abdus Salam successfully proposed a coherent unified theory of electromagnetic and weak interactions — the SM of electroweak interactions (Weinberg, 1967; Salam, 1968).

2.1.3 Renormalizability

In quantum field theories one frequently encounters various infinities when going beyond the tree-level calculations. Richard Feynman, Julian Schwinger

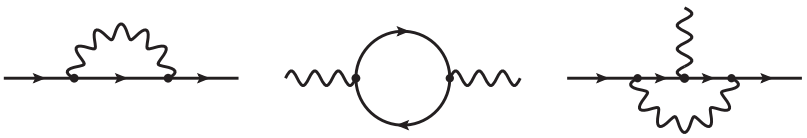

(a) (b) (c)

Fig. 2.1 The one-loop Feynman diagrams for (a) the electron self-energy, (b) the photon self-energy and (c) the electron-photon vertex in QED

and Sin-Itiro Tomonaga found a solution to this problem in QED in the late 1940's (Schwinger, 1958). In modern language, the mass and coupling parameters present in the classical Lagrangian are the so-called bare quantities which will receive radiative corrections at the quantum level. One must decompose the bare quantities into the renormalizable ones and the counterterms: the renormalizable quantities are physical and can be confronted with the experimental observables, while the counterterms are used to cancel the infinities arising from the quantum corrections. Hence we should rewrite the Lagrangian of QED in Eq. (2.4) in terms of bare quantities:

$$\mathcal{L}_{\rm QED} = -\frac{1}{4} F^0_{\mu\nu} F^{0\mu\nu} + \overline{\Psi^0} {\rm i}\gamma^\mu \left(\partial_\mu - {\rm i}e_0 A^0_\mu\right) \Psi^0 - m_0 \overline{\Psi^0} \Psi^0 \ , \quad (2.22)$$

where $F^0_{\mu\nu} = \partial_\mu A^0_\nu - \partial_\nu A^0_\mu$. It is well known that a quantum field theory is characterized by its Green functions. In order to see where the infinity comes from and how to deal with it, here we consider the simplest Green function of QED (i.e., the electron propagator) at the one-loop level. The tree-level propagator of a free electron is

$${\rm i}S_{\rm F}(\not{p}) = \frac{\rm i}{\not{p} - m_0 + {\rm i}\epsilon} \ . \quad (2.23)$$

The full propagator can be figured out by evaluating the one-loop electron self-energy $-{\rm i}\Sigma(\not{p})$, for which the Feynman diagram is given in Fig. 2.1(a). To be explicit, we have

$${\rm i}S'_{\rm F}(\not{p}) = {\rm i}S_{\rm F}(\not{p}) + {\rm i}S_{\rm F}(\not{p}) \left[-{\rm i}\Sigma(\not{p})\right] {\rm i}S_{\rm F}(\not{p}) + \cdots = \frac{\rm i}{\not{p} - m_0 - \Sigma(\not{p})} \ , \quad (2.24)$$

where the infinite insertions of the electron self-energy are implied, and $\Sigma(\not{p})$ can be treated as a perturbative quantity. Because of Lorentz invariance,

$$\Sigma(\not{p}) = A(p^2) + \not{p} B(p^2) \quad (2.25)$$

holds. Then the physical mass of the electron can be identified as the pole of the full propagator

$${\rm i}S'_{\rm F}(\not{p}) = \frac{{\rm i}Z_2}{\not{p} - m + {\rm i}\epsilon} \ . \quad (2.26)$$

where $m = Z_2(m_0 + A)$ is just the renormalized or physical mass of the electron with $Z_2^{-1} \equiv 1 - B$ being the wave function renormalization constant. One may similarly obtain the renormalized propagator of the photon: $\mathrm{i}D_{\mu\nu}(p^2) = -\mathrm{i}Z_3 g_{\mu\nu}/(p^2 + \mathrm{i}\epsilon)$, for which the one-loop Feynman diagram is shown in Fig. 2.1(b). We can absorb the constants Z_2 and Z_3 by rescaling the electron and photon fields $\Psi^0 \equiv Z_2^{1/2}\Psi$ and $A_\mu^0 = Z_3^{1/2} A_\mu$. As for radiative corrections to the electron-photon vertex in Fig. 2.1(c), one may introduce the physical electric charge e by using another renormalization constant $e_0 Z_2 Z_3^{1/2} = e Z_1$. The bare Lagrangian of QED can therefore be divided into the renormalized terms and their counterterms (Peskin and Schroeder, 1995)

$$\begin{aligned}\mathcal{L}_{\mathrm{QED}} = & -\frac{1}{4}F_{\mu\nu}F^{\mu\nu} + \overline{\Psi}\mathrm{i}\gamma^\mu\left(\partial_\mu - \mathrm{i}eA_\mu\right)\Psi - m\overline{\Psi}\Psi \\ & -\frac{1}{4}\delta Z_3 F_{\mu\nu}F^{\mu\nu} + \overline{\Psi}\mathrm{i}\gamma^\mu\left(\delta Z_2\partial_\mu - \mathrm{i}\delta Z_1 eA_\mu\right)\Psi - \delta m\overline{\Psi}\Psi \ , \quad (2.27)\end{aligned}$$

where $\delta Z_i \equiv Z_i - 1$ (for $i = 1, 2, 3$) and $\delta m \equiv Z_2 m_0 - m$ have been defined. Starting from this Lagrangian one can immediately read off the relevant Feynman rules and calculate the Green functions including the contributions from the counterterms. A detailed calculation shows that the infinities arise from the integration over the loop momentum. Such infinities can be removed by choosing suitable renormalization constants δZ_i and δm, for instance, by imposing the renormalization conditions

$$\Sigma(\not{p})\big|_{\not{p}=m} = 0 \ , \qquad \left.\frac{\mathrm{d}\Sigma(\not{p})}{\mathrm{d}\not{p}}\right|_{\not{p}=m} = 0 \ ; \quad (2.28)$$

and

$$\Pi(p^2)\big|_{p^2=0} = 0 \ , \qquad \mathrm{i}e\Gamma^\mu(p,p')\big|_{p-p'=0} = \mathrm{i}e\gamma^\mu \ , \quad (2.29)$$

where $\Pi(p^2)$ and $\Gamma^\mu(p,p')$ stand respectively for the photon self-energy and the proper electron-photon vertex. It is worth mentioning that the relation $Z_1 = Z_2$ exactly holds to all orders in QED as a consequence of the gauge invariance. This identity ensures that the physical electric charge e or the gauge coupling constant is universal for all the charged particles. The full renormalization of QED has been described in some standard textbooks of quantum field theories (Peskin and Schroeder, 1995; Weinberg, 1995).

A proof of the renormalizability of non-Abelian gauge theories is more complicated. First comes the quantization of non-Abelian gauge fields. To preserve the gauge invariance or to satisfy the Ward-Takahashi identity, Feynman found that scalar particles with the Fermi-Dirac statistics were necessary in the calculation of the one-loop self-energies of gauge bosons (Feynman, 1963). In the path-integral language Ludvig Faddeev and Victor Popov pointed out that these strange scalar particles arose from removing the freedom of gauge invariance (Faddeev and Popov, 1967; De Witt, 1967). It

was even unclear whether the spontaneous gauge symmetry breaking would spoil the renormalizability of the whole theory or not in the 1960's. In 1971, Gerardus 't Hooft gave the first complete proof of the renormalizability of non-Abelian gauge theories ('t Hooft, 1971a, 1971b; Lee and Zinn-Justin, 1972a, 1972b, 1972c). Since then, the Weinberg-Salam model has gradually been accepted to be the standard theory of electroweak interactions.

2.1.4 The Standard Electroweak Model

One of the greatest successes in particle physics is the establishment of the unified theory of electromagnetic and weak interactions, or the SM of electroweak interactions. This model is based on the $SU(2)_{\rm L} \times U(1)_{\rm Y}$ gauge group, and its gauge symmetry is spontaneously broken down to $U(1)_{\rm Q}$. The $U(1)_{\rm Q}$ gauge boson, which is just the photon, keeps massless due to the gauge invariance. In contrast, the $SU(2)_{\rm L}$ gauge bosons acquire their masses via the Higgs mechanism and mediate the short-range weak interactions. In the SM the left-handed components of quarks and leptons are assigned to be the $SU(2)_{\rm L}$ doublets

$$Q_{\rm L} \equiv \begin{pmatrix} u_{\rm L} \\ d_{\rm L} \end{pmatrix} , \begin{pmatrix} c_{\rm L} \\ s_{\rm L} \end{pmatrix} , \begin{pmatrix} t_{\rm L} \\ b_{\rm L} \end{pmatrix} ; \quad \ell_{\rm L} \equiv \begin{pmatrix} \nu_{e{\rm L}} \\ e_{\rm L} \end{pmatrix} , \begin{pmatrix} \nu_{\mu{\rm L}} \\ \mu_{\rm L} \end{pmatrix} , \begin{pmatrix} \nu_{\tau{\rm L}} \\ \tau_{\rm L} \end{pmatrix} . \quad (2.30)$$

The right-handed components of quarks and leptons are all the $SU(2)_{\rm L}$ singlets defined as

$$U_{\rm R} \equiv u_{\rm R},\ c_{\rm R},\ t_{\rm R} ; \quad D_{\rm R} \equiv d_{\rm R},\ s_{\rm R},\ b_{\rm R} ; \quad E_{\rm R} \equiv e_{\rm R},\ \mu_{\rm R},\ \tau_{\rm R} . \quad (2.31)$$

Note that only the left-handed components of three neutrinos take part in weak interactions, because they have been assumed to be the massless Weyl particles in the SM [1]. Quarks and leptons also carry the hypercharges Y, which are related to the weak isospin I^3 components and the electric charges Q through the relation $Q = I^3 + Y$. Table 2.1 is a list of all the quantum numbers of quarks and leptons in the SM.

As discussed in Section 2.1.1, the gauge fields should be introduced to maintain the local gauge invariance via the definition of covariant derivatives. Hence the kinetic terms of fermion fields are

$$\mathcal{L}_{\rm F} = \overline{Q_{\rm L}} {\rm i} \not{D} Q_{\rm L} + \overline{\ell_{\rm L}} {\rm i} \not{D} \ell_{\rm L} + \overline{U_{\rm R}} {\rm i} \not{\partial}' U_{\rm R} + \overline{D_{\rm R}} {\rm i} \not{\partial}' D_{\rm R} + \overline{E_{\rm R}} {\rm i} \not{\partial}' E_{\rm R} , \quad (2.32)$$

where the covariant derivatives are defined as

$$D_\mu \equiv \partial_\mu - {\rm i} g \tau^k W_\mu^k - {\rm i} g' Y B_\mu ,$$

[1] The discovery of neutrino oscillations implies that neutrinos must be massive. Hence the SM is actually incomplete. The possibilities of incorporating massive neutrinos into the SM will be discussed in Chapters 3 and 4.

Table 2.1 Quantum numbers of quarks and leptons in the SM

Particle content	Weak isospin I^3	Hypercharge Y	Electric charge Q
$Q_{\rm L} \equiv \begin{pmatrix} u_{\rm L} \\ d_{\rm L} \end{pmatrix}, \begin{pmatrix} c_{\rm L} \\ s_{\rm L} \end{pmatrix}, \begin{pmatrix} t_{\rm L} \\ b_{\rm L} \end{pmatrix}$	$\begin{pmatrix} +1/2 \\ -1/2 \end{pmatrix}$	$+1/6$	$\begin{pmatrix} +2/3 \\ -1/3 \end{pmatrix}$
$\ell_{\rm L} \equiv \begin{pmatrix} \nu_{e{\rm L}} \\ e_{\rm L} \end{pmatrix}, \begin{pmatrix} \nu_{\mu{\rm L}} \\ \mu_{\rm L} \end{pmatrix}, \begin{pmatrix} \nu_{\tau{\rm L}} \\ \tau_{\rm L} \end{pmatrix}$	$\begin{pmatrix} +1/2 \\ -1/2 \end{pmatrix}$	$-1/2$	$\begin{pmatrix} 0 \\ -1 \end{pmatrix}$
$U_{\rm R} \equiv u_{\rm R},\ c_{\rm R},\ t_{\rm R}$	0	$+2/3$	$+2/3$
$D_{\rm R} \equiv d_{\rm R},\ s_{\rm R},\ b_{\rm R}$	0	$-1/3$	$-1/3$
$E_{\rm R} \equiv e_{\rm R},\ \mu_{\rm R},\ \tau_{\rm R}$	0	-1	-1

$$\partial'_\mu \equiv \partial_\mu - {\rm i}g' Y B_\mu \ . \tag{2.33}$$

Note that $\tau_k \equiv \sigma_k/2$ (for $k = 1, 2, 3$) and Y denote the generators of the gauge groups $SU(2)_{\rm L}$ and $U(1)_{\rm Y}$, respectively. In Eq. (2.33), g and g' are the corresponding gauge coupling constants. Since the gauge fields are also dynamic, their kinetic terms are given by

$$\mathcal{L}_{\rm G} = -\frac{1}{4} W^{i\mu\nu} W^i_{\mu\nu} - \frac{1}{4} B^{\mu\nu} B_{\mu\nu} \tag{2.34}$$

with

$$\begin{aligned} W^i_{\mu\nu} &\equiv \partial_\mu W^i_\nu - \partial_\nu W^i_\mu + g\varepsilon^{ijk} W^j_\mu W^k_\nu \ , \\ B_{\mu\nu} &\equiv \partial_\mu B_\nu - \partial_\nu B_\mu \ , \end{aligned} \tag{2.35}$$

where W^i_μ (for $i = 1, 2, 3$) and B_μ are the $SU(2)_{\rm L}$ and $U(1)_{\rm Y}$ gauge bosons, respectively. It is straightforward to verify that Eqs. (2.32) and (2.34) are gauge-invariant. However, the local gauge symmetry must be broken; i.e., $SU(2)_{\rm L} \times U(1)_{\rm Y} \to U(1)_{\rm Q}$, where $U(1)_{\rm Q}$ is just the gauge group of QED. The symmetry breaking can be realized by adding a doublet scalar $H \equiv (\phi^+, \phi^0)^T$, which has the hypercharge $Y(H) = +1$. The gauge-invariant Lagrangian for the scalar fields reads

$$\mathcal{L}_{\rm H} = (D^\mu H)^\dagger \left(D_\mu H\right) - \mu^2 H^\dagger H - \lambda \left(H^\dagger H\right)^2 \ , \tag{2.36}$$

where μ^2 is real and λ is real and positive. To figure out the particle spectrum, one has to determine the vacuum of the theory by minimizing the scalar potential. If $\mu^2 > 0$, the minimum is located at the original point (i.e., $\langle H \rangle \equiv \langle 0|H|0\rangle = 0$). In this case the vacuum state is also invariant under the gauge

transformation, such that the gauge symmetry of the theory is preserved. If $\mu^2 < 0$, the minima are fixed by [2]

$$|\langle H \rangle|^2 = \frac{1}{2} v^2 \ , \tag{2.37}$$

where $v = \sqrt{-\mu^2/\lambda}$ is the vev of H. Eq. (2.37) shows that there exist infinite and degenerate vacua. Once one chooses a special direction,

$$\langle H \rangle = \frac{1}{\sqrt{2}} \begin{pmatrix} 0 \\ v \end{pmatrix} \ , \tag{2.38}$$

the gauge symmetry is broken down and the corresponding gauge bosons get masses. To make this point clear, we parametrize the Higgs doublet as

$$H = \mathrm{e}^{\mathrm{i}\tau^k \xi^k(x)/v} \frac{1}{\sqrt{2}} \begin{pmatrix} 0 \\ v + h(x) \end{pmatrix} \ , \tag{2.39}$$

where $\xi^k(x)$ (for $k = 1, 2, 3$) and $h(x)$ stand for the four degrees of freedom in the doublet H. After performing the gauge transformation with $U(\xi) = \mathrm{e}^{-\mathrm{i}\tau^k \xi^k(x)/v}$, we turn to the unitary gauge. In this case the transformed Higgs and gauge fields are

$$\begin{aligned} H &= \frac{1}{\sqrt{2}} \begin{pmatrix} 0 \\ v + h(x) \end{pmatrix} \ , \\ \tau^k \widetilde{W}^k_\mu &= U(\xi) \tau^k W^k_\mu U^{-1}(\xi) - \frac{\mathrm{i}}{g} \left[\partial_\mu U(\xi) \right] U^{-1}(\xi) \ . \end{aligned} \tag{2.40}$$

In the unitary gauge only one physical scalar boson h survives, and the gauge bosons are no longer massless. The latter can be understood from the second equation in Eq. (2.40): there is a longitudinal polarization of $\widetilde{W}^k_\mu$ in contrast with the massless or transverse W^k_μ gauge bosons.

After spontaneous gauge symmetry breaking, let us proceed to discuss the particle spectrum of the SM.

(1) The masses of gauge bosons come from the first term in Eq. (2.36):

$$\begin{aligned} & \frac{v^2}{8} \left(0 \ 1 \right) \left(g \sigma^k W^k_\mu + g' B_\mu \right) \left(g \sigma^k W^{k\mu} + g' B^\mu \right) \begin{pmatrix} 0 \\ 1 \end{pmatrix} \\ = & \frac{v^2}{8} \left(W^1_\mu \ W^2_\mu \ W^3_\mu \ B_\mu \right) \begin{pmatrix} g^2 & 0 & 0 & 0 \\ 0 & g^2 & 0 & 0 \\ 0 & 0 & g^2 & -gg' \\ 0 & 0 & -gg' & g^2 \end{pmatrix} \begin{pmatrix} W^{1\mu} \\ W^{2\mu} \\ W^{3\mu} \\ B^\mu \end{pmatrix} \ . \end{aligned} \tag{2.41}$$

As usual, we define the physical gauge bosons

[2] One might wonder what will happen if $\mu^2 = 0$. In fact, it has been proved that the spontaneous gauge symmetry breaking can be triggered by radiative corrections even if μ^2 is vanishing at the tree-level (Coleman and Weinberg, 1973).

$$W_\mu^\pm \equiv \frac{1}{\sqrt{2}} \left(W_\mu^1 \mp \mathrm{i} W_\mu^2 \right) \tag{2.42}$$

and

$$\begin{pmatrix} Z_\mu \\ A_\mu \end{pmatrix} = \begin{pmatrix} \cos\theta_\mathrm{w} & -\sin\theta_\mathrm{w} \\ \sin\theta_\mathrm{w} & \cos\theta_\mathrm{w} \end{pmatrix} \begin{pmatrix} W_\mu^3 \\ B_\mu \end{pmatrix} \ . \tag{2.43}$$

The weak mixing angle θ_w and masses of gauge bosons can be determined from the diagonalization of the mass matrix in Eq. (2.41):

$$\tan\theta_\mathrm{w} = \frac{g'}{g} \ , \quad M_{W^\pm}^2 = \frac{1}{2} g v \ , \quad M_{Z^0}^2 = \frac{1}{2} \sqrt{g^2 + g'^2}\ v \ . \tag{2.44}$$

Note that A_μ describes the photon, whose mass keeps vanishing because the $U(1)_\mathrm{Q}$ gauge symmetry is unbroken. Both the charged gauge bosons $W^\pm$ and the neutral gauge boson Z^0 are massive, and their masses are proportional to the vev of the Higgs field. The $W^\pm$ and Z^0 particles were experimentally discovered by Carlo Rubbia, Simon van der Meer and the UA1 Collaboration in 1983 at CERN (Arnison *et al.*, 1983a, 1983b). Their masses, together with the weak mixing angle θ_w, have now been measured to a high degree of accuracy: $M_W = (80.398 \pm 0.025)$ GeV, $M_Z = (91.1876 \pm 0.0021)$ GeV and $\sin^2\theta_\mathrm{w} = 0.23119 \pm 0.00014$ (Nakamura *et al.*, 2010).

(2) The mass of the Higgs boson arises from the last two terms (i.e., the Higgs potential) in Eq. (2.36). More explicitly,

$$V(H) \equiv \mu^2 H^\dagger H + \lambda \left(H^\dagger H \right)^2 = -\mu^2 h^2 + \lambda v h^3 + \frac{\lambda}{4} h^4 + \frac{1}{4} \mu^2 v^2 \ . \tag{2.45}$$

Hence the mass of the Higgs boson h is $M_h = \sqrt{-2\mu^2}$. It is worth stressing that the Higgs boson is the only SM particle that has not been observed. Current experimental lower bound on M_h is $M_h > 114.4$ GeV at the 95% confidence level (Nakamura *et al.*, 2010). Recently, a combined analysis of the data from the CDF and D0 Collaborations at the Fermilab Tevatron has excluded a SM Higgs boson in the mass range 162 GeV $< M_h <$ 166 GeV at the 95% confidence level (Aaltonen *et al.*, 2010). The search for the Higgs boson is the main mission of the Large Hadron Collider (LHC), which is running with the center-of-mass energy $\sqrt{s}$ from 7 TeV to 14 TeV at CERN.

(3) The masses of six quarks and three charged leptons stem from the Yukawa interactions

$$\mathcal{L}_\mathrm{Y} = -\overline{Q_\mathrm{L}} Y_\mathrm{u} \tilde{H} U_\mathrm{R} - \overline{Q_\mathrm{L}} Y_\mathrm{d} H D_\mathrm{R} - \overline{\ell_\mathrm{L}} Y_l H E_\mathrm{R} + \mathrm{h.c.} \ , \tag{2.46}$$

where $\tilde{H} \equiv \mathrm{i}\sigma_2 H^*$ is defined, Y_u, Y_d and Y_l are the 3×3 Yukawa coupling matrices. After the Higgs field acquires its vev, the mass matrices of up-type quarks, down-type quarks and charged leptons are respectively given by

$$M_\mathrm{u} = \frac{1}{\sqrt{2}} v Y_\mathrm{u} \ , \quad M_\mathrm{d} = \frac{1}{\sqrt{2}} v Y_\mathrm{d} \ , \quad M_l = \frac{1}{\sqrt{2}} v Y_l \ , \tag{2.47}$$

where $v \simeq 246$ GeV. They can simply be diagonalized by means of the bi-unitary transformations

$$U_{\rm u}^\dagger M_{\rm u} U_{\rm u}' = {\rm Diag}\{m_u,\ m_c,\ m_t\}\ , \quad U_{\rm d}^\dagger M_{\rm d} U_{\rm d}' = {\rm Diag}\{m_d,\ m_s,\ m_b\}\ ,$$
$$U_l^\dagger M_l U_l' = {\rm Diag}\left\{m_e,\ m_\mu,\ m_\tau\right\}\ , \tag{2.48}$$

where m_q (for $q = u, c, t$ or d, s, b) and m_α (for $\alpha = e, \mu, \tau$) stand respectively for the physical masses of quarks and charged leptons. These nine fundamental parameters of the SM have all been determined with the help of QED, QCD and relevant experimental data (Nakamura *et al.*, 2010), and their values at a given energy scale exhibit the puzzling hierarchies $m_u \ll m_c \ll m_t$, $m_d \ll m_s \ll m_b$ and $m_e \ll m_\mu \ll m_\tau$.

A combination of Eqs. (2.32), (2.34), (2.36) and (2.46) leads us to the full Lagrangian of the SM at the classical level. The quantization of the non-Abelian gauge fields will involve the gauge-fixing terms and the Faddeev-Popov ghost fields, as excellently described in some standard textbooks (Cheng and Li, 1988; Peskin and Schroeder, 1995; Weinberg, 1995). In the subsequent sections we shall focus our attention on the interactions of neutrinos with quarks and leptons within the SM.

2.2 Standard Interactions of Neutrinos

In view of the fact that neutrinos can weakly interact with other elementary particles via $W^\pm$ and Z^0, let us first of all give a brief summary of the charged-current and neutral-current interactions of quarks, charged leptons and neutrinos in the SM.

(1) Eq. (2.32) allows us to fix the charged-current interactions of quarks:

$$\begin{aligned}\mathcal{L}_{\rm cc}^q &= g\overline{Q_{\rm L}}\gamma^\mu \left(\tau_1 W_\mu^1 + \tau_2 W_\mu^2\right) Q_{\rm L} = \frac{g}{\sqrt{2}}\overline{Q_{\rm L}}\gamma^\mu \tau^+ W_\mu^+ Q_{\rm L} + {\rm h.c.} \\ &= \frac{g}{\sqrt{2}}\overline{\left(u\ c\ t\right)_{\rm L}}\gamma^\mu \begin{pmatrix} d \\ s \\ b \end{pmatrix}_{\rm L} W_\mu^+ + {\rm h.c.}\ ,\end{aligned} \tag{2.49}$$

where W_μ^+ and W_μ^- have been defined in Eq. (2.42), and

$$\tau^+ \equiv \tau_1 + {\rm i}\tau_2 = \begin{pmatrix} 0 & 1 \\ 0 & 0 \end{pmatrix}\ , \quad \tau^- \equiv \tau_1 - {\rm i}\tau_2 = \begin{pmatrix} 0 & 0 \\ 1 & 0 \end{pmatrix}\ . \tag{2.50}$$

As shown in Eq. (2.48), one may always diagonalize the quark mass matrices $M_{\rm u}$ and $M_{\rm d}$ by using the bi-unitary transformations. This treatment is equivalent to transforming the flavor eigenstates of up- and down-type quarks into their mass eigenstates (u', c', t' and d', s', b'). Then $\mathcal{L}_{\rm cc}^q$ can be rewritten as

$$\mathcal{L}^q_{\rm cc} = \frac{g}{\sqrt{2}} \overline{\left(u'\ c'\ t'\right)_{\rm L}} \gamma^\mu V \begin{pmatrix} d' \\ s' \\ b' \end{pmatrix}_{\rm L} W^+_\mu + {\rm h.c.}\ , \tag{2.51}$$

where $V \equiv U^\dagger_{\rm u} U_{\rm d}$ is the Cabibbo-Kobayashi-Maskawa (CKM) quark flavor mixing matrix (Cabibbo, 1963; Kobayashi and Maskawa, 1973). A full parametrization of V needs three mixing angles and one CP-violating phase, whose values have all been measured to a very good degree of accuracy (Nakamura *et al.*, 2010). Similarly, the charged-current interactions of leptons are described by

$$\mathcal{L}^l_{\rm cc} = \frac{g}{\sqrt{2}} \overline{\left(e\ \mu\ \tau\right)_{\rm L}} \gamma^\mu \begin{pmatrix} \nu_e \\ \nu_\mu \\ \nu_\tau \end{pmatrix}_{\rm L} W^-_\mu + {\rm h.c.}\ . \tag{2.52}$$

Since neutrinos are massless in the SM, it is always possible to make the mass eigenstates of charged leptons and neutrinos simultaneously coincide with their corresponding flavor eigenstates. In other words, there is no lepton flavor mixing. If three neutrinos have non-degenerate masses, however, a CKM-like lepton flavor mixing matrix will appear in $\mathcal{L}^l_{\rm cc}$. The phenomenology of neutrino masses and lepton flavor mixing will be discussed in Chapter 3.

(2) Eq. (2.32) can also allow us to determine the neutral-current interactions of quarks:

$$\begin{aligned} \mathcal{L}^q_{\rm nc} &= g \overline{Q_{\rm L}} \gamma^\mu \tau_3 Q_{\rm L} W^3_\mu + g' \left(\overline{Q_{\rm L}} \gamma^\mu Y Q_{\rm L} + \overline{U_{\rm R}} \gamma^\mu Y U_{\rm R} + \overline{D_{\rm R}} \gamma^\mu Y D_{\rm R} \right) B_\mu \\ &= \sum_{i=1}^{3} \left[g \overline{\left(q_i\ q'_i\right)_{\rm L}} \gamma^\mu \begin{pmatrix} I^3_{q_{i\rm L}} & 0 \\ 0 & I^3_{q'_{i\rm L}} \end{pmatrix} \begin{pmatrix} q_i \\ q'_i \end{pmatrix}_{\rm L} W^3_\mu \right. \\ &\quad + g' \overline{\left(q_i\ q'_i\right)_{\rm L}} \gamma^\mu \begin{pmatrix} Y_{q_{i\rm L}} & 0 \\ 0 & Y_{q'_{i\rm L}} \end{pmatrix} \begin{pmatrix} q_i \\ q'_i \end{pmatrix}_{\rm L} B_\mu \\ &\quad \left. + g' \overline{\left(q_i\ q'_i\right)_{\rm R}} \gamma^\mu \begin{pmatrix} Y_{q_{i\rm R}} & 0 \\ 0 & Y_{q'_{i\rm R}} \end{pmatrix} \begin{pmatrix} q_i \\ q'_i \end{pmatrix}_{\rm R} B_\mu \right] , \end{aligned} \tag{2.53}$$

where q_i and q'_i (for $i = 1, 2, 3$) run over (u, c, t) and (d, s, b), respectively. The neutral-current interactions of leptons can analogously be written out. With the help of Eq. (2.43), we express the weak neutral-current interactions of quarks and leptons in terms of the physical gauge field Z_μ:

$$\mathcal{L}_{\rm nc} = \frac{g}{\cos\theta_{\rm w}} \sum_f \left(C^f_{\rm L} \overline{f_{\rm L}} \gamma^\mu f_{\rm L} Z_\mu + C^f_{\rm R} \overline{f_{\rm R}} \gamma^\mu f_{\rm R} Z_\mu \right) , \tag{2.54}$$

where $C^f_{\rm L} \equiv I^3_{f_{\rm L}} - Q_f \sin^2\theta_{\rm w}$, $C^f_{\rm R} \equiv I^3_{f_{\rm R}} - Q_f \sin^2\theta_{\rm w}$, and f runs over all quarks and leptons. The explicit results of $C^f_{\rm L}$ and $C^f_{\rm R}$ are listed in Table 2.2. In addition, the electromagnetic interactions of leptons and quarks take the same form as in QED:

$$\mathcal{L}_{\rm EM} = e \sum_f Q_f \overline{f} \gamma^\mu f A_\mu \ , \tag{2.55}$$

with $Q_f = I_f^3 + Y_f$. Sometimes it is more convenient to express $\mathcal{L}_{\rm nc}$ as a sum of the vector- and pseudovector-current contributions. In this case,

$$\mathcal{L}_{\rm nc} = \frac{g}{\cos\theta_{\rm w}} \sum_f \overline{f} \gamma^\mu \left(C_{\rm V}^f - C_{\rm A}^f \gamma_5 \right) f Z_\mu \ , \tag{2.56}$$

where

$$C_{\rm V}^f \equiv C_{\rm L}^f + C_{\rm R}^f \ , \quad C_{\rm A}^f \equiv C_{\rm L}^f - C_{\rm R}^f \ . \tag{2.57}$$

The explicit results of $C_{\rm V}^f$ and $C_{\rm A}^f$ are also given in Table 2.2.

Table 2.2 The coefficients $C_{\rm L}^f$ and $C_{\rm R}^f$ versus $C_{\rm V}^f$ and $C_{\rm A}^f$ for weak neutral-current interactions of leptons and quarks in the SM, where f = u, d, l or ν denotes the up-type quarks, down-type quarks, charged leptons or neutrinos, respectively

	$f = {\rm u}$	$f = {\rm d}$	$f = l$	$f = \nu$
$C_{\rm L}^f$	$+\frac{1}{2} - \frac{2}{3}\sin^2\theta_{\rm w}$	$-\frac{1}{2} + \frac{1}{3}\sin^2\theta_{\rm w}$	$-\frac{1}{2} + \sin^2\theta_{\rm w}$	$+\frac{1}{2}$
$C_{\rm R}^f$	$-\frac{2}{3}\sin^2\theta_{\rm w}$	$+\frac{1}{3}\sin^2\theta_{\rm w}$	$\sin^2\theta_{\rm w}$	0
$C_{\rm V}^f$	$+\frac{1}{2} - \frac{4}{3}\sin^2\theta_{\rm w}$	$-\frac{1}{2} + \frac{2}{3}\sin^2\theta_{\rm w}$	$-\frac{1}{2} + 2\sin^2\theta_{\rm w}$	$+\frac{1}{2}$
$C_{\rm A}^f$	$+\frac{1}{2}$	$-\frac{1}{2}$	$-\frac{1}{2}$	$+\frac{1}{2}$

In the following we shall elaborate on the neutrino interactions by taking a few typical examples — neutrino-electron, neutrino-neutrino and neutrino-nucleon scattering processes.

2.2.1 Neutrino-electron Scattering

Let us first calculate the cross section of the elastic neutrino-electron scattering process $\nu_e + e^- \to \nu_e + e^-$, which has played an important role in detecting solar neutrinos. The invariant amplitude for $\nu_e(p, s_\nu) + e^-(q, s_e) \to \nu_e(p', s'_\nu) + e^-(q', s'_e)$ receives contributions from both neutral- and charged-current interactions, as shown in Fig. 2.2. We ignore the transferred energy in the low-energy region since it is much smaller than M_W and M_Z. In this good approximation the amplitude for neutral-current interactions is

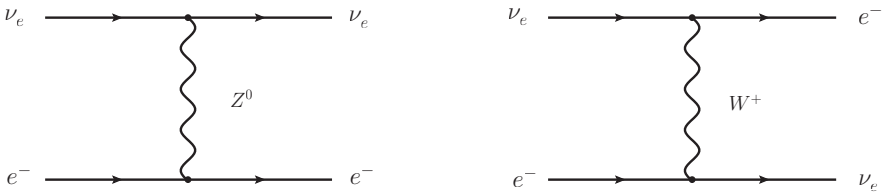

Fig. 2.2 Feynman diagrams for the elastic neutrino-electron scattering process $\nu_e + e^- \to \nu_e + e^-$ in the SM

$$\mathcal{M}^{\rm nc}(s_\nu, s_e; s'_\nu, s'_e) = \frac{-g^2}{4M_Z^2 \cos^2\theta_{\rm w}} C_{\rm L}^{\nu} \overline{u}(p', s'_\nu)\gamma^\mu(1-\gamma_5)u(p, s_\nu) \times \overline{u}(q', s'_e)\gamma_\mu \left[C_{\rm L}^{l}(1-\gamma_5) + C_{\rm R}^{l}(1+\gamma_5)\right] u(q, s_e) \; , \tag{2.58}$$

and the amplitude for charged-current interactions reads

$$\mathcal{M}^{\rm cc}(s_\nu, s_e; s'_\nu, s'_e) = \frac{-g^2}{8M_W^2} \overline{u}(q', s'_e)\gamma^\mu(1-\gamma_5)u(p, s_\nu) \times \overline{u}(p', s'_\nu)\gamma_\mu(1-\gamma_5)u(q, s_e) \; . \tag{2.59}$$

The overall amplitude is the sum of Eqs. (2.58) and (2.59). Before going into the details of our calculations, we briefly review the Fierz transformations. It is well known that an arbitrary 4×4 matrix can be expanded in the basis of sixteen independent matrices Γ^r (for $r = 1, 2, \cdots, 16$) defined as

$$\begin{aligned} \Gamma^1 &\equiv \mathbf{1}_4 \; , \\ \Gamma^{2,3,4,5} &\equiv \gamma^\mu \; , \qquad (\text{for } \mu = 0, 1, 2, 3) \; , \\ \Gamma^{6,7,8,9,10,11} &\equiv \sigma^{\mu\nu} \; , \qquad (\text{for } \mu, \nu = 0, 1, 2, 3 \;\; \text{and} \;\; \mu < \nu) \; , \\ \Gamma^{12,13,14,15} &\equiv {\rm i}\gamma^\mu\gamma_5 \; , \qquad (\text{for } \mu = 0, 1, 2, 3) \; , \\ \Gamma^{16} &\equiv \gamma_5 \; . \end{aligned} \tag{2.60}$$

It is easy to verify that the normalization relation

$$\mathrm{Tr}\left[\Gamma^r \Gamma_s\right] = 4\delta^r_s \tag{2.61}$$

holds (for $r, s = 1, 2, \cdots, 16$), where the subscripts imply that the corresponding Lorentz indices should be lowered down by the metric tensor. Consider the product

$$\begin{aligned} \mathcal{P} &= \sum_{r=1}^{16} g_r \overline{\Psi_1} \Gamma^r \Psi_2 \overline{\Psi_3} \Gamma_r \Psi_4 \\ &= \sum_{r=1}^{16} g_r \left(\Gamma^r\right)_{\alpha\beta} \left(\Gamma_r\right)_{\eta\lambda} \left(\overline{\Psi_1}\right)_\alpha \left(\Psi_2\right)_\beta \left(\overline{\Psi_3}\right)_\eta \left(\Psi_4\right)_\lambda \; , \end{aligned} \tag{2.62}$$

where Ψ_i (for $i = 1, 2, 3, 4$) are Dirac spinors with the Greek subscripts being the spinor indices. This product should obviously be equivalent to

$$\mathcal{P} = -\sum_{s=1}^{16} \hat{g}_s \left(\Gamma^s\right)_{\alpha\lambda} \left(\Gamma_s\right)_{\eta\beta} \left(\overline{\Psi_1}\right)_\alpha \left(\Psi_4\right)_\lambda \left(\overline{\Psi_3}\right)_\eta \left(\Psi_2\right)_\beta \ , \tag{2.63}$$

where the minus sign comes from the exchange of fermion field operators. Identifying the coefficients in front of the fermion fields in these two equations,

$$\sum_{s=1}^{16} \hat{g}_s \left(\Gamma^s\right)_{\alpha\lambda} \left(\Gamma_s\right)_{\eta\beta} = -\sum_{r=1}^{16} g_r \left(\Gamma^r\right)_{\alpha\beta} \left(\Gamma_r\right)_{\eta\lambda} \ , \tag{2.64}$$

and multiplying both sides of Eq. (2.64) by $\left(\Gamma_p\right)_{\lambda\alpha} \left(\Gamma^q\right)_{\beta\eta}$, we obtain

$$\hat{g}_p = -\frac{1}{16} \sum_{r=1}^{16} \mathrm{Tr}\left[\Gamma_r \Gamma_p \Gamma^r \Gamma^p\right] g_r \ , \tag{2.65}$$

where the normalization relation in Eq. (2.61) has been used. In view of Lorentz invariance, one usually needs to treat the interactions with Γ^I (for $I = S, V, T, A, P$) defined in Eq. (2.60). In this case one may find the relations between $\hat{g}_I$ and g_I by using Eq. (2.65):

$$\begin{pmatrix} \hat{g}_S \\ \hat{g}_V \\ \hat{g}_T \\ \hat{g}_A \\ \hat{g}_P \end{pmatrix} = -\frac{1}{4} \begin{pmatrix} 1 & 4 & 6 & 4 & 1 \\ 1 & -2 & 0 & 2 & -1 \\ 1 & 0 & -2 & 0 & 1 \\ 1 & 2 & 0 & -2 & -1 \\ 1 & -4 & 6 & -4 & 1 \end{pmatrix} \begin{pmatrix} g_S \\ g_V \\ g_T \\ g_A \\ g_P \end{pmatrix} \ . \tag{2.66}$$

For the $(V-A)$-type interaction, it is straightforward to get

$$\overline{\Psi_1}\gamma^\mu(1-\gamma_5)\Psi_2\overline{\Psi_3}\gamma_\mu(1-\gamma_5)\Psi_4 = \overline{\Psi_1}\gamma^\mu(1-\gamma_5)\Psi_4\overline{\Psi_3}\gamma_\mu(1-\gamma_5)\Psi_2 \ . \tag{2.67}$$

Applying this Fierz identity to Eq. (2.59), we can simplify the overall amplitude $\mathcal{M} = \mathcal{M}^{\rm nc} + \mathcal{M}^{\rm cc}$ for the elastic neutrino-electron scattering:

$$\begin{aligned} \mathcal{M}(s_\nu, s_e; s'_\nu, s'_e) = \frac{G_{\rm F}}{\sqrt{2}} &\overline{u}(p', s'_\nu)\gamma^\mu(1-\gamma_5)u(p, s_\nu)\overline{u}(q', s'_e)\gamma_\mu \\ &\times \left[(1+C_{\rm L}^l)(1-\gamma_5) + C_{\rm R}^l(1+\gamma_5)\right] u(q, s_e) \ , \end{aligned} \tag{2.68}$$

where $M_Z^2 \cos^2\theta_{\rm w} = M_W^2$ has been used, and $G_{\rm F} = g^2/(4\sqrt{2}M_W^2)$ is the Fermi constant. Note that $|\mathcal{M}|^2$ should be summed over the spins of the final state and averaged over the spins of the initial state:

$$\frac{1}{2}\sum_{\rm spin} |\mathcal{M}|^2 = \frac{G_{\rm F}^2}{4} L^-_{\mu\nu}(p, p') \left[\left(1 + C_{\rm L}^l\right)^2 L^{-\mu\nu}(q, q')\right.$$

$$+16m_e^2 g^{\mu\nu}(1+C_{\rm L}^l)C_{\rm R}^l + \left(C_{\rm R}^l\right)^2 L^{+\mu\nu}(q,q')\Big] \ , \quad (2.69)$$

where

$$\begin{aligned} L_{\mu\nu}^{\pm}(p,p') &\equiv {\rm Tr}\left[\not{p}\gamma_\mu(1\pm\gamma_5)\not{p}'\gamma_\nu(1\pm\gamma_5)\right] \\ &= 8\left(p_\mu p'_\nu + p_\nu p'_\mu - p\cdot p' g_{\mu\nu} \pm {\rm i}\varepsilon_{\mu\nu\rho\sigma}p^\rho p'^\sigma\right) \end{aligned} \quad (2.70)$$

have been defined. Note also that neutrinos are always left-handed in the SM, so an average over the spins of the initial state is only acting on the electron. Given $p+q=p'+q'$, Eq. (2.69) is simplified to

$$\begin{aligned} \frac{1}{2}\sum_{\rm spin}|\mathcal{M}|^2 = 64G_{\rm F}^2\Big[&\left(1+C_{\rm L}^l\right)^2(p\cdot q)^2 + \left(C_{\rm R}^l\right)^2(p'\cdot q)^2 \\ &- \left(1+C_{\rm L}^l\right)C_{\rm R}^l m_e^2(p\cdot p')\Big] \ . \end{aligned} \quad (2.71)$$

In the laboratory frame where the electron is at rest, we have

$$q = \left(m_e, 0, 0, 0\right) \ , \qquad p = \left(E_\nu, \mathbf{p}\right) \ , \quad (2.72)$$

and $E_\nu = |\mathbf{p}|$. Denoting the energy of the outgoing electron as E_e and that of the scattered neutrino as E'_ν, we express the total cross section of the elastic neutrino-electron scattering as follows:

$$\begin{aligned} \sigma^{\rm ES}(\nu_e e^-) = \frac{1}{4E_\nu m_e}\int &\frac{{\rm d}^3\mathbf{p}'}{(2\pi)^3 2E'_\nu}\frac{{\rm d}^3\mathbf{q}'}{(2\pi)^3 2E_e}(2\pi)^4\delta^4(p+q-p'-q') \\ &\times 64G_{\rm F}^2 m_e^2 E_\nu^2\Bigg[\left(1+C_{\rm L}^l\right)^2 + \left(C_{\rm R}^l\right)^2\left(1-\frac{T}{E_\nu}\right)^2 \\ &- \left(1+C_{\rm L}^l\right)C_{\rm R}^l\left(1-\cos\theta\right)\frac{E'_\nu}{E_\nu}\Bigg] \ , \end{aligned} \quad (2.73)$$

where the kinetic energy of the recoil electron is defined as $T = E_e - m_e$, and $\cos\theta$ is the cosine of the angle between the momenta of the scattered and incident neutrinos. With the help of Eq. (2.73), it is easy to obtain the differential cross section ('t Hooft, 1971c; Marciano and Parsa, 2003)

$$\frac{{\rm d}\sigma^{\rm ES}}{{\rm d}T}(E_\nu, T) = \frac{G_{\rm F}^2 m_e}{2\pi}\left[\epsilon_+^2 + \epsilon_-^2\left(1-\frac{T}{E_\nu}\right)^2 - \epsilon_+\epsilon_-\frac{m_e T}{E_\nu^2}\right] \ , \quad (2.74)$$

where $\epsilon_\pm \equiv g_{\rm V}^e \pm g_{\rm A}^e$ and

$$g_{\rm V}^e \equiv 1 + C_{\rm V}^l \ , \quad g_{\rm A}^e \equiv 1 + C_{\rm A}^l \ . \quad (2.75)$$

A measurement of this differential cross section allows one to pin down the coefficients $g_{\rm V}^e$ and $g_{\rm A}^e$, so as to test the SM.

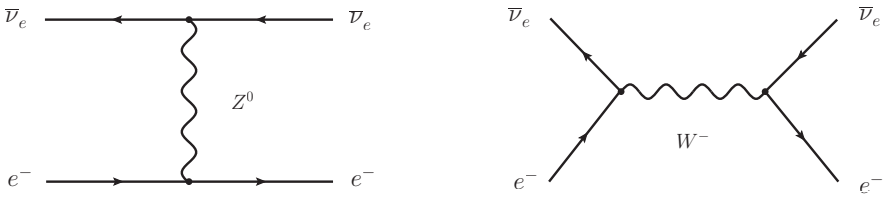

Fig. 2.3 Feynman diagrams for the elastic antineutrino-electron scattering process $\overline{\nu}_e + e^- \to \overline{\nu}_e + e^-$ in the SM

If the energy of the incident neutrino is much larger than the electron mass (i.e., $E_\nu \gg m_e$), then the total cross section given in Eq. (2.73) can safely approximate to

$$\sigma^{\rm ES}(\nu_e e^-) = \frac{2G_{\rm F}^2}{\pi} m_e E_\nu \left[\left(1 + C_{\rm L}^l\right)^2 + \frac{1}{3} \left(C_{\rm R}^l\right)^2 \right] . \tag{2.76}$$

One may similarly figure out the total cross section of the elastic antineutrino-electron scattering, which takes place via the Feynman diagrams shown in Fig. 2.3. The result is

$$\sigma^{\rm ES}(\overline{\nu}_e e^-) = \frac{2G_{\rm F}^2}{\pi} m_e E_\nu \left[\frac{1}{3} \left(1 + C_{\rm L}^l\right)^2 + \left(C_{\rm R}^l\right)^2 \right] . \tag{2.77}$$

For the sake of completeness, we also consider the neutral-current scattering processes $\nu_x + e^- \to \nu_x + e^-$ and $\overline{\nu}_x + e^- \to \overline{\nu}_x + e^-$ (for $x = \mu$ or τ). Their Feynman diagrams are given in Fig. 2.4, and their total cross sections read

$$\begin{aligned} \sigma^{\rm ES}(\nu_x e^-) &= \frac{2G_{\rm F}^2}{\pi} m_e E_\nu \left[\left(C_{\rm L}^l\right)^2 + \frac{1}{3} \left(C_{\rm R}^l\right)^2 \right] , \\ \sigma^{\rm ES}(\overline{\nu}_x e^-) &= \frac{2G_{\rm F}^2}{\pi} m_e E_\nu \left[\frac{1}{3} \left(C_{\rm L}^l\right)^2 + \left(C_{\rm R}^l\right)^2 \right] , \end{aligned} \tag{2.78}$$

where $x = \mu$ or τ. The ratio of $\sigma^{\rm ES}(\nu_x e^-)$ to $\sigma^{\rm ES}(\nu_e e^-)$ turns out to be

$$\frac{\sigma^{\rm ES}(\nu_x e^-)}{\sigma^{\rm ES}(\nu_e e^-)} = \frac{3\left(C_{\rm L}^l\right)^2 + \left(C_{\rm R}^l\right)^2}{3\left(1 + C_{\rm L}^l\right)^2 + \left(C_{\rm R}^l\right)^2} \approx 0.155 , \tag{2.79}$$

where $C_{\rm L}^l$ and $C_{\rm R}^l$ can be found in Table 2.2, and $\sin^2\theta_{\rm w} \approx 0.2381$ (Porsev *et al.*, 2009) has been input. It is worth stressing that gauge coupling constants depend on the energy scale where the interactions take place. At the electroweak scale we have $\sin^2\theta_{\rm w} = 0.23119 \pm 0.00014$ (Nakamura *et al.*, 2010), which is slightly smaller than the values measured at extremely low energies.

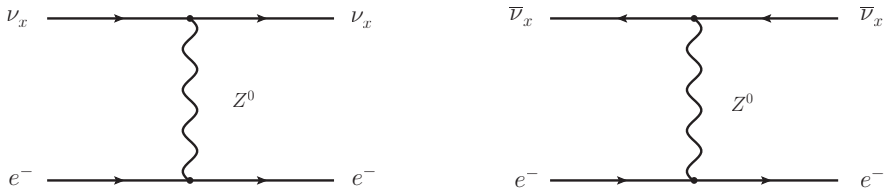

Fig. 2.4 Feynman diagrams for the elastic neutrino-electron scattering processes $\nu_x + e^- \to \nu_x + e^-$ and $\overline{\nu}_x + e^- \to \overline{\nu}_x + e^-$ (for $x = \mu$ or τ) in the SM

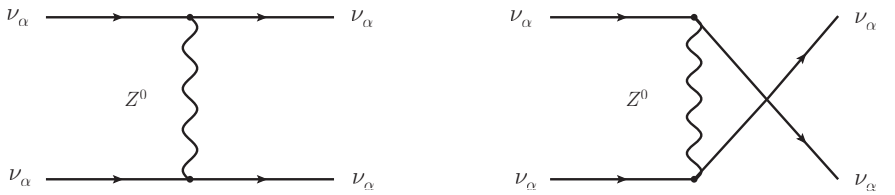

Fig. 2.5 Feynman diagrams for the elastic neutrino-neutrino scattering processes $\nu_\alpha + \nu_\alpha \to \nu_\alpha + \nu_\alpha$ (for $\alpha = e, \mu, \tau$) in the SM

2.2.2 Neutrino-neutrino Scattering

Contrary to the elastic neutrino-electron scattering, the elastic neutrino-neutrino scattering seems less important in the development of particle physics. However, it has recently been noticed that the coherent neutrino-neutrino scattering processes in supernovae are essential to the flavor conversions of supernova neutrinos (Dighe, 2008; Duan and Kneller, 2009). Neutrino-neutrino interactions are also expected to be significant in the neutrino-decoupling era of the early Universe. In this subsection we shall briefly discuss the total cross sections of elastic neutrino-neutrino scattering and neutrino-antineutrino annihilation.

Fig. 2.5 shows the Feynman diagrams for the elastic neutrino-neutrino scattering process $\nu_\alpha(p) + \nu_\alpha(q) \to \nu_\alpha(p') + \nu_\alpha(q')$ (for $\alpha = e, \mu, \tau$). Although only the neutral-current interactions contribute to this process, there are two different channels due to the exchange of the final-state neutrinos. The overall amplitude can be written as

$$\mathcal{M} = -\frac{G_{\rm F}}{\sqrt{2}} \overline{u}(p')\gamma^\mu(1-\gamma_5)u(p)\overline{u}(q')\gamma_\mu(1-\gamma_5)u(q) \;, \tag{2.80}$$

where the Fierz identity has been used to combine the t- and u-channels. The total cross section is found to be

$$\sigma^{\rm ES}(\nu_\alpha\nu_\alpha) = \frac{G_{\rm F}^2 s}{\pi} \;, \tag{2.81}$$

where $s \equiv (p+q)^2$. It is worth mentioning that the above result multiplied by a factor 1/2 will be applicable to the elastic $\nu_\alpha + \nu_\beta \to \nu_\alpha + \nu_\beta$ reactions (for $\beta \neq \alpha$). The reason is simply that these processes only have the t-channel contributions and their final-state neutrinos are not identical. Furthermore, one can immediately figure out the total cross sections of the elastic antineutrino-antineutrino scattering processes. The final results are

$$\sigma^{\rm ES}(\overline{\nu}_\alpha \overline{\nu}_\alpha) = \sigma^{\rm ES}(\nu_\alpha \nu_\alpha) = \frac{G_{\rm F}^2 s}{\pi} \; ,$$
$$\sigma^{\rm ES}(\overline{\nu}_\alpha \overline{\nu}_\beta) = \sigma^{\rm ES}(\nu_\alpha \nu_\beta) = \frac{G_{\rm F}^2 s}{2\pi} \; , \tag{2.82}$$

where $\alpha \neq \beta$. The two equalities obtained above are guaranteed by the CPT theorem, which is always valid in the local and Lorentz-invariant field theories (Schwinger, 1951; Pauli, 1955; Bell, 1955; Lüders, 1957). Following the elastic neutrino-neutrino scattering, one may write out the amplitude for the elastic neutrino-antineutrino scattering process $\nu_\alpha(p) + \overline{\nu}_\alpha(q) \to \nu_\alpha(p') + \overline{\nu}_\alpha(q')$, whose Feynman diagrams are given in Fig. 2.6:

$$\mathcal{M} = -\frac{G_{\rm F}}{\sqrt{2}} \overline{u}(p') \gamma^\mu (1-\gamma_5) u(p) \overline{v}(q') \gamma_\mu (1-\gamma_5) v(q) \; . \tag{2.83}$$

Different from the elastic $\nu_\alpha \nu_\alpha$ scattering, the elastic $\nu_\alpha \overline{\nu}_\alpha$ scattering does not involve the symmetry factor 1/2 originating from the identical final-state particles. Therefore,

$$\sigma^{\rm ES}(\nu_\alpha \overline{\nu}_\alpha) = 2\sigma^{\rm ES}(\nu_\alpha \nu_\alpha) = \frac{2G_{\rm F}^2 s}{\pi} \; . \tag{2.84}$$

Note that the elastic $\nu_\alpha + \overline{\nu}_\beta \to \nu_\alpha + \overline{\nu}_\beta$ scattering processes (for $\beta \neq \alpha$) can only take place via the t-channel. Hence it is straightforward to obtain $\sigma^{\rm ES}(\nu_\alpha \overline{\nu}_\beta) = \sigma^{\rm ES}(\nu_\alpha \nu_\beta) = \sigma^{\rm ES}(\nu_\alpha \overline{\nu}_\alpha)/4$. Note also that one should perform the thermal average over the initial particles if the frequent scattering occurs in a thermal bath, such as in the early Universe or in the interior of a massive star. In this case it is evident that the neutrino-antineutrino scattering process should be most important. Nevertheless, the total cross sections for neutrino interactions are extremely small and can be neglected in most cases. As we shall show later, the coherent forward scattering of neutrinos off matter or other neutrinos plays a crucial role in astrophysics and cosmology (e.g., it has to be taken into account in understanding solar neutrino oscillations and supernova neutrino oscillations).

2.2.3 Neutrino-nucleon Interactions

The first detection of electron antineutrinos in 1956 made use of a kind of neutrino-nucleon interactions — the inverse beta decay $\overline{\nu}_e + p \to e^+ + n$

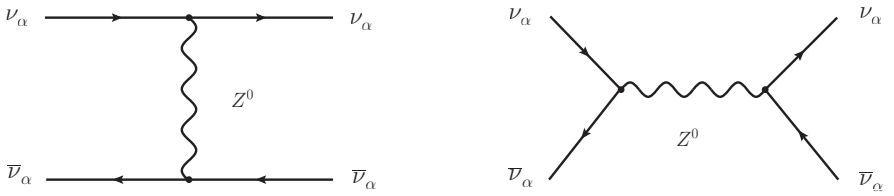

Fig. 2.6 Feynman diagrams for the elastic neutrino-antineutrino scattering processes $\nu_\alpha + \overline{\nu}_\alpha \to \nu_\alpha + \overline{\nu}_\alpha$ $(\alpha = e, \mu, \tau)$ in the SM

(Cowan *et al.*, 1956; Reines and Cowan, 1956). In the SM both the beta decay and the inverse beta decay take place via the charged-current interactions of quarks and leptons. It remains difficult to quantitatively describe how quarks interact and form hadrons at low energies, so one has to find out a consistent way to convert the neutrino interactions with quarks into those with nucleons. The effective Lagrangian responsible for the inverse beta decay is given by

$$\mathcal{L}_{\rm eff} = \frac{G_{\rm F}}{\sqrt{2}} J^l_\mu J^{q\mu} + \text{h.c.} = \frac{G_{\rm F}}{\sqrt{2}} V_{ud} \overline{l_\alpha} \gamma_\mu (1 - \gamma_5) \nu_\alpha \overline{u} \gamma^\mu (1 - \gamma_5) d + \text{h.c.} \,, \quad (2.85)$$

where J^l_μ and J^q_μ stand respectively for the charged currents of leptons and quarks, and V_{ud} is an element of the CKM matrix V. The amplitude for the quasi-elastic scattering $\overline{\nu}_e(k) + p(q) \to e^+(k') + n(q')$ can therefore be read off from $\mathcal{L}_{\rm eff}$:

$$\mathcal{M} = \frac{G_{\rm F}}{\sqrt{2}} \overline{v_\nu}(k) \gamma^\mu (1 - \gamma_5) v_e(k') \langle n(q') | J^{q\dagger}_\mu | p(q) \rangle \,, \quad (2.86)$$

where we have replaced the charged current of quarks with the corresponding nucleon matrix element. Although protons and neutrons are not elementary particles, they must obey the Fermi-Dirac statistics and satisfy the Dirac equation. It is instructive to divide the charged current J^q_μ into the vector component $v^q_\mu = \overline{u} \gamma_\mu d$ and the pseudovector component $a^q_\mu = \overline{u} \gamma_\mu \gamma^5 d$, such that $J^q_\mu = V_{ud}(v^q_\mu - a^q_\mu)$. With the help of Lorentz invariance and Dirac equations, the nucleon matrix element can be written as (Llewellyn Smith, 1971; Alberico *et al.*, 2002)

$$\langle n(q') | v^q_\mu(0) | p(q) \rangle = \overline{u_n}(q') \left[\gamma_\mu F_1(Q^2) + \frac{\mathrm{i} \sigma_{\mu\nu} q^\nu_-}{2 m_N} F_2(Q^2) \right] u_p(q) \,, \quad (2.87)$$

and

$$\langle n(q') | a^q_\mu(0) | p(q) \rangle = \overline{u_n}(q') \left[\gamma_\mu \gamma^5 G_{\rm A}(Q^2) + \frac{q_{-\mu}}{m_N} \gamma^5 G_{\rm P}(Q^2) \right] u_p(q) \,, \quad (2.88)$$

where $q_- \equiv q' - q$ and $Q^2 \equiv -q^2_-$ are defined, and $m_p \approx m_n \equiv m_N$ is taken. Let us give some comments on the form factors in Eqs. (2.87) and (2.88).

First, the time reversal invariance makes all the form factors real [3]. Second, the isospin symmetry in strong interactions makes the second-class currents vanishing (Weinberg, 1958). Among the four form factors, F_1 and F_2 are associated with the electromagnetic properties of nucleons, while $G_{\rm A}$ and $G_{\rm P}$ are related with the weak interactions. All of them can be extracted from the relevant experimental results (Cheng and Li, 1988). Combining Eqs. (2.86), (2.87) and (2.88), one obtains the differential cross section in the laboratory frame (Llewellyn Smith, 1971):

$$\frac{{\rm d}\sigma(\overline{\nu}_e p)}{{\rm d}Q^2} = \frac{G_{\rm F}^2 \left|V_{ud}\right|^2 m_N^4}{8\pi (k\cdot q)^2} \left[C_1 - C_2 \frac{s-u}{m_N^2} + C_3 \frac{(s-u)^2}{m_N^4}\right] , \qquad (2.89)$$

where C_i (for $i = 1, 2, 3$) are the analytical functions of Q^2 depending on the form factors defined above, and $s = (k+q)^2$, $t = (q'-q)^2$ and $u = (k'-q)^2$ are the Mandelstam invariants. The results of C_i are summarized as follows (Llewellyn Smith, 1971):

$$\begin{aligned} C_1 &= 4\kappa \left[(1+\kappa) G_{\rm A}^2 - (1-\kappa)\left(F_1^2 - \kappa F_2^2\right) + 4\kappa F_1 F_2\right] , \\ C_2 &= 4\kappa G_{\rm A}^2 , \\ C_3 &= \frac{1}{4}\left(G_{\rm A}^2 + F_1^2 + \kappa F_2^2\right) , \end{aligned} \qquad (2.90)$$

where $\kappa \equiv Q^2/(4m_N^2)$, and the terms involving m_e^2/m_N^2 have been neglected. For low-energy neutrinos ($E_\nu \ll m_N$) in the laboratory frame, where the nucleon is at rest, the total cross section of the inverse beta decay reads

$$\sigma(\overline{\nu}_e p) \approx \frac{G_{\rm F}^2 \left|V_{ud}\right|^2}{\pi} \left(1 + 3g_{\rm A}^2\right) E_\nu^2 , \qquad (2.91)$$

where the vector and pseudovector couplings of nucleons are $g_{\rm V} \equiv F_1(0) \approx 1$ and $g_{\rm A} \equiv G_{\rm A}(0) \approx 1.25$. The total cross section of the quasi-elastic scattering $\nu_e + n \to e^- + p$, defined as $\sigma(\nu_e n)$, is found to be equal to $\sigma(\overline{\nu}_e p)$ in the same approximation. Taking $G_{\rm F} = 1.166 \times 10^{-5}$ GeV^{-2} and $|V_{ud}| = 0.973$ (Nakamura *et al.*, 2010), we obtain

$$\sigma(\overline{\nu}_e p) = \sigma(\nu_e n) \approx 9.1 \times 10^{-44} \left(\frac{E_\nu}{\rm MeV}\right)^2 {\rm cm}^2 . \qquad (2.92)$$

It is worth mentioning that the first theoretical estimation of the total cross section of the neutrino-nucleon scattering was done by Hans Bethe and Rudolf Peierls in 1934 (Bethe and Peierls, 1934), soon after Enrico Fermi formulated his effective theory for the beta decay (Fermi, 1933). Their result is amazingly consistent with the one given in Eq. (2.92).

[3] The C, P and T transformations and their implications in quantum field theories will be discussed in Section 3.3.

We have discussed the neutrino-nucleon scattering processes mediated by weak charged-current interactions. Note that the elastic scattering processes $\nu_\alpha + N \to \nu_\alpha + N$ (for $\alpha = e, \mu, \tau$) can take place via weak neutral-current interactions, and they have been used to extract the weak mixing angle in the SM. To study the high-energy neutrino interactions with nucleons, however, one has to consider the fine structure of a proton or a neutron (e.g., its parton distributions) (Llewellyn Smith, 1971).

2.3 Neutrino Propagation in a Medium

In 1978, Lincoln Wolfenstein pointed out that the coherent forward scattering of neutrinos off matter could be very important in studying the behavior of neutrino flavor conversions in a dense medium (Wolfenstein, 1978). This observation has been verified in understanding solar neutrino oscillations, since the Sun itself is just a dense medium in which the propagation of solar ν_e neutrinos may be modified by their interactions with the ambient electrons and nucleons. The main effects induced by a medium can be described by an effective potential, or equivalently a neutrino refractive index. In this section we present three different approaches for calculating the effective potential of neutrinos propagating in a medium: (1) to compute the coherent forward scattering amplitudes and then derive neutrino refractive indices; (2) to evaluate the effective potential directly from the effective Hamiltonian; (3) to calculate the neutrino self-energy in a medium and then extract the effective potential via the dispersion relation. We show that these three methods are equivalent and lead to the same result. We also apply the result to two interesting cases — neutrinos propagating in a normal matter environment and in a dense neutrino environment. The detailed discussions of matter effects on neutrino flavor conversions will be given in Chapter 5, while the applications to solar and supernova neutrinos can be found in Chapters 6 and 7.

2.3.1 Coherent Forward Scattering

In quantum field theories, the probability amplitude of the scattering process $\alpha \to \beta$ is given by the S-matrix element

$$S_{\beta\alpha} \equiv \langle \Phi_\beta^{\rm out} | \Phi_\alpha^{\rm in} \rangle \; , \tag{2.93}$$

where $\Phi_\alpha^{\rm in}$ and $\Phi_\beta^{\rm out}$ are the *in* and *out* states, respectively. Here the subscripts α and β stand for the momentum, spin and other quantum numbers characterizing the corresponding particles. If there is no any interaction, the in-state must be identical to the out-state such that the probability for $\alpha \to \alpha$ is unity. Hence the transition amplitude of the scattering process $\alpha \to \beta$ (for $\alpha \neq \beta$) can be defined through $S \equiv \mathbf{1} + {\rm i}T$ and written as

$$\mathrm{i}T_{\beta\alpha} = (2\pi)^4\,\mathrm{i}\delta^4(p_\alpha - p_\beta)\mathcal{M}_{\beta\alpha}\ , \tag{2.94}$$

where the Feynman amplitude $\mathcal{M}_{\beta\alpha}$ is free of the delta functions. It is straightforward to compute the differential cross section for the reaction $1+2 \to 3+4+\cdots+n$ with $n-2$ particles in the final state (Cheng and Li, 1988; Peskin and Schroeder, 1995):

$$\mathrm{d}\sigma = \frac{(2\pi)^4\,\delta^4\left(p_1+p_2-p_3-\cdots-p_n\right)}{4\sqrt{\left(p_1\cdot p_2\right)^2 - m_1^2 m_2^2}}\,|\mathcal{M}|^2 \prod_{j=3}^{n}\frac{\mathrm{d}^3\mathbf{p}_j}{(2\pi)^3 2E_j}\ , \tag{2.95}$$

where p_i, $\mathbf{p}_i$ and $E_i = \sqrt{|\mathbf{p}_i|^2 + m_i^2}$ (for $i = 1, 2, \cdots, n$) stand respectively for the four-momenta, three-momenta and energies of relevant particles with m_i being their masses. Let us consider a two-body scattering process $a+b \to c+d$ for example. Its differential cross section involves the integration over the final-state phase space

$$(2\pi)^4\delta^4(p_a+p_b-p_c-p_d)\frac{\mathrm{d}^3\mathbf{p}_c}{(2\pi)^3 2E_c}\cdot\frac{\mathrm{d}^3\mathbf{p}_d}{(2\pi)^3 2E_d}\ . \tag{2.96}$$

In the center-of-mass frame we have $\mathbf{p}_a + \mathbf{p}_b = 0$. The total energy of the initial particles is $E = E_a + E_b$. The integration over $\mathbf{p}_d$ is equivalent to dropping the three-dimensional delta function $\delta^3(\mathbf{p}_c + \mathbf{p}_d)$ and replacing the three-momentum $\mathbf{p}_d$ with $-\mathbf{p}_c$ in the integrand. The phase-space factor in Eq. (2.96) is therefore simplified to

$$\frac{1}{16\pi^2 E_c E_d}\delta(E_c + E_d - E)\,|\mathbf{p}_c|^2\,\mathrm{d}|\mathbf{p}_c|\mathrm{d}\Omega\ , \tag{2.97}$$

where $E_c = \sqrt{|\mathbf{p}_c|^2 + m_c^2}$ and $E_d = \sqrt{|\mathbf{p}_c|^2 + m_d^2}$, and $\mathrm{d}\Omega \equiv \sin\theta\mathrm{d}\theta\mathrm{d}\phi$ is the differential element of the solid angle. The integration of the delta function over $\mathrm{d}|\mathbf{p}_c|$ requires us to find out the zero point of the argument of the delta function. Namely,

$$\sqrt{|\mathbf{p}_c'|^2 + m_c^2}\ + \sqrt{|\mathbf{p}_c'|^2 + m_d^2}\ = E \tag{2.98}$$

leads us to the solution

$$|\mathbf{p}_c'| = \frac{1}{2E}\sqrt{\left(E^2 - m_c^2 - m_d^2\right)^2 - 4m_c^2 m_d^2}\ . \tag{2.99}$$

It is then straightforward to see that the integration with the delta function $\delta(E_c + E_d - E)$ contributes the factor

$$\left[\frac{\mathrm{d}}{\mathrm{d}|\mathbf{p}_c|}\left(\sqrt{|\mathbf{p}_c|^2 + m_c^2} + \sqrt{|\mathbf{p}_c|^2 + m_d^2} - E\right)\right]^{-1}_{|\mathbf{p}_c| = |\mathbf{p}_c'|} = \frac{E_c' E_d'}{|\mathbf{p}_c'|E}\ , \tag{2.100}$$

where $E'_c = \sqrt{|\mathbf{p}'_c|^2 + m_c^2}$ and $E'_d = \sqrt{|\mathbf{p}'_c|^2 + m_d^2}$. Combining Eqs. (2.96), (2.97), (2.99) and (2.100) with Eq. (2.95), we arrive at the differential cross section of the two-body scattering process $a + b \to c + d$ as follows:

$$\mathrm{d}\sigma(a + b \to c + d) = \frac{1}{64\pi^2} \cdot \frac{|\mathbf{p}'_c|}{|\mathbf{p}_a| E^2} \left|\mathcal{M}(a + b \to c + d)\right|^2 \mathrm{d}\Omega \qquad (2.101)$$

in the center-of-mass frame. This result will be used later on to discuss the propagation of neutrinos in matter. When a neutrino beam propagates in matter, the scattered neutrino waves may coherently interfere in the forward direction. We shall show that this coherent forward scattering of neutrinos off matter is very important in some astrophysical environments where neutrinos are copiously produced (Wolfenstein, 1978, 1979; Mikheyev and Smirnov, 1985; Raffelt, 1996).

Now let us consider that a neutrino beam propagating with momentum $\mathbf{k}$ in the direction of the z-axis interacts with a scatterer at the location $\mathbf{r} = 0$. Such a neutrino beam is usually described by the plane wave $\Psi = \mathrm{e}^{\mathrm{i}kz}$, and the wave function of the system at extremely far distances after scattering can be regarded as a superposition of the original and the scattered waves (Landau and Lifshitz, 1977):

$$\Psi_{\mathrm{f}}(\mathbf{r}) \approx \mathrm{e}^{\mathrm{i}kz} + f(\theta) \frac{\mathrm{e}^{\mathrm{i}kr}}{r} \; , \qquad (2.102)$$

where $f(\theta)$ is the scattering amplitude. The differential cross section of this scattering process is then given by $\mathrm{d}\sigma = \left|f(\theta)\right|^2 \mathrm{d}\Omega$. Linking it to the differential cross section of a two-body scattering process $a + b \to c + d$, we can establish the relation between the Feynman amplitude $\mathcal{M}(a + b \to c + d)$ in the center-of-mass frame and the scattering amplitude $f(\theta)$ [4]:

$$f(\theta) = \frac{1}{8\pi E} \sqrt{\frac{|\mathbf{p}'_c|}{|\mathbf{p}_a|}} \mathcal{M}(a + b \to c + d) \; . \qquad (2.103)$$

In a perturbation theory one may first calculate the Feynman amplitude order by order and then compute the forward scattering amplitude $f(0)$, which can be used to derive the refractive index of neutrinos propagating in matter.

For this purpose, we consider the neutrino beam to be a plane wave $\mathrm{e}^{\mathrm{i}kz}$ incident on a slab which is located at $z = 0$ and perpendicular to the z-axis. We assume that the slab has an infinitesimal thickness δ and is infinitely large in both the x-axis and the y-axis. After traversing the slab, the neutrino wave is still a plane wave at the distance $z \gg 2\pi/k$ but it has attained a phase $\mathrm{e}^{\mathrm{i}k[z+(n-1)\delta]}$ with n being the neutrino refractive index. On the other hand,

[4] The sign of the scattering amplitude has been chosen in such a way that $f(\theta)$ is just the coefficient of the outgoing wave in the solution of the time-dependent Schrödinger equation (Weinberg, 1995).

the asymptotic form of the original and scattered waves reads (Fermi, 1949; Sakurai, 1967; Raffelt, 1996)

$$\Psi_{\rm f}(z) = {\rm e}^{{\rm i}kz} + 2\pi \int_0^\infty N\delta f(\theta) \frac{{\rm e}^{{\rm i}kr}}{r} \rho {\rm d}\rho \; , \tag{2.104}$$

where $\rho = \sqrt{x^2 + y^2}$ and $\theta = \arctan(\rho/z)$, and N is the number of the scatterers per unit volume. Note that $\rho {\rm d}\rho = r{\rm d}r$ holds. Replacing k by $k + {\rm i}\epsilon$ with $\epsilon \to 0^+$ in the integrand in Eq. (2.104), one obtains

$$\Psi_{\rm f}(z) = {\rm e}^{{\rm i}kz} \left[1 + {\rm i} \frac{2\pi f(0) N\delta}{k} \right] \; . \tag{2.105}$$

For the slab with a finite thickness $d \equiv m\delta$, where m can be taken as the number of the layers and $m \to \infty$ holds, it is straightforward to obtain

$$\Psi_{\rm f}(z) = \lim_{m\to\infty} {\rm e}^{{\rm i}kz} \left[1 + {\rm i} \frac{2\pi f(0) N d}{mk} \right]^m = {\rm e}^{{\rm i}kz} {\rm e}^{{\rm i}2\pi f(0) N d/k} \; , \tag{2.106}$$

which should be identified with the plane wave ${\rm e}^{{\rm i}k[z+(n-1)d]}$. The refractive index of neutrinos in matter turns out to be (Wolfenstein, 1978)

$$n = 1 + \frac{2\pi}{k^2} N f(0) \; . \tag{2.107}$$

Note that the energy dependence of the forward scattering amplitude $f(0)$ is implied. A nonzero refractive index means that the dispersion relation of neutrinos is modified in matter, so is their flavor oscillation in matter. This mechanism has offered a natural solution to the longstanding solar neutrino problem (Wolfenstein, 1978; Mikheyev and Smirnov, 1985). The details of neutrino oscillations in matter will be discussed in Chapter 5.

Now that a relationship between the scattering amplitude $f(\theta)$ and the Feynman amplitude $\mathcal{M}(a + b \to c + d)$ has been established, it is ready to calculate the forward scattering amplitude $f(0)$ by using the same techniques in perturbative quantum field theories. For instance, we shall compute $f(0)$ for ν_e-e^- scattering in matter in Section 2.3.2. Here let us figure out the charged-current contribution to $f(0)$ in the elastic ν_e-e^- scattering process. The relevant Feynman amplitude has been given in Eq. (2.59). One may set $|\mathbf{p}_a| = |\mathbf{p}'_c|$ in Eq. (2.103) for the elastic forward scattering under consideration. Using the normalization conditions $u^\dagger(\mathbf{p}, r)u(\mathbf{p}, s) = 2E\delta_{rs}$ for Dirac spinors, one can then arrive at

$$f(0) = -\frac{G_{\rm F}}{\sqrt{2}\pi} E \; . \tag{2.108}$$

This result, together with Eq. (2.107), leads to the neutrino refractive index $n - 1 = -\sqrt{2} G_{\rm F} n_e / E$, where n_e is the number density of electrons in matter.

The distribution of electrons in matter is assumed to be isotropic, and thus the average of their three-momenta is vanishing. One should take account of both neutral- and charged-current contributions to $f(0)$ in a complete analysis of the elastic forward scattering of neutrinos in matter, but only the differences between the refractive indices of different neutrinos are relevant to neutrino flavor conversions.

2.3.2 The Effective Potential

The neutrino waves scattered by the background particles may coherently interfere in the forward direction. This matter-induced effect on the propagation of neutrinos can be described by an effective potential. Since neutrinos are massless in the SM, their dispersion relation in matter is modified to $|\mathbf{p}| = nE$, where n is just the refractive index. Since neutrinos only have weak interactions with matter, $(n-1) \ll 1$ must hold. In this case one may define the effective potential of the neutrino beam in matter as

$$\mathcal{V} \equiv E - |\mathbf{p}| = -(n-1)E = -\frac{2\pi N}{E} f(0) \; , \tag{2.109}$$

where Eq. (2.107) has been used. This relationship links the effective potential $\mathcal{V}$ to the refractive index n, or equivalently, to the forward scattering amplitude $f(0)$. If only the charged-current interactions are taken into account, then the effective potential of electron neutrinos in an electron background can be given by

$$\mathcal{V} = -\frac{2\pi N}{E} f(0) = \sqrt{2}\, G_{\rm F} n_e \; , \tag{2.110}$$

where Eq. (2.108) has been used. Hence a dense medium is possible to affect the behavior of neutrino propagation, in particular the oscillation of neutrino flavors. Because neutrinos are massless and lepton flavors are conserved in the SM, the phenomenon of neutrino oscillations is impossible to take place either in vacuum or in matter unless non-standard neutrino interactions are introduced (Wolfenstein, 1978). Although three neutrinos may have finite masses beyond the SM, the precision measurements of electroweak interactions have indicated that their interactions with other SM particles can still be described by the SM to an excellent degree of accuracy (Nakamura *et al.*, 2010). Hence the neutrino refractive indices calculated in the SM are applicable, at least in the leading-order approximation, to those reasonable extensions of the SM which can naturally accommodate massive neutrinos.

Now we consider the ordinary matter which is made of electrons and nucleons but electrically neutral as a whole. In this case the number densities of electrons and protons are equal (i.e., $n_e = n_p$). The forward scattering of ν_e neutrinos off electrons is caused by both charged- and neutral-current interactions, while that of ν_μ or ν_τ neutrinos off electrons can only be caused

by neutral-current interactions. The Feynman amplitude of $\nu_e + e^- \to \nu_e + e^-$ scattering has been given in Eq. (2.68) and can be rewritten as

$$\mathcal{M}(\nu_e e^-) = -\frac{G_{\rm F}}{\sqrt{2}} \overline{u_\nu}(p') \gamma^\mu (1-\gamma_5) u_\nu(p) \overline{u_e}(q') \gamma_\mu \left(g_{\rm V}^e - g_{\rm A}^e \gamma_5\right) u_e(q) \; , \tag{2.111}$$

where $g_{\rm V}^e \equiv 1 + C_{\rm V}^l$ and $g_{\rm A}^e \equiv 1 + C_{\rm A}^l$ have been defined in Eq. (2.75). The Feynman amplitude of $\nu_\mu + e^- \to \nu_\mu + e^-$ scattering or $\nu_\tau + e^- \to \nu_\tau + e^-$ scattering can directly be read off from Eq. (2.111) by replacing the coefficients $g_{\rm V}^e$ and $g_{\rm A}^e$ with $C_{\rm V}^l$ and $C_{\rm A}^l$ given in Table 2.2. One may construct a low-energy effective Hamiltonian for elastic ν_e-e^- scattering, which should be able to reproduce the exact Feynman amplitude in Eq. (2.111). Such a requirement is a common criterion for constructing the effective Hamiltonians in quantum field theories.

The fact that neutrinos propagating in matter may interact with the background particles can be described by means of the picture of free neutrinos traveling in an effective potential. The first step to derive the effective potential is to write down the effective Hamiltonian at an energy scale much lower than the masses of $W^\pm$ and Z^0 bosons. The effective Hamiltonian density responsible for the interactions of ν_e neutrinos with electrons is

$$\mathcal{H}_{\rm eff}(x) = \frac{G_{\rm F}}{\sqrt{2}} \overline{\nu}_e(x) \gamma^\mu (1-\gamma_5) \nu_e(x) \bar{e}(x) \gamma_\mu \left(g_{\rm V}^e - g_{\rm A}^e \gamma_5\right) e(x) \; . \tag{2.112}$$

Assuming the background electrons to be thermally distributed and unpolarized, we should average the effective Hamiltonian over the electron states. This can be done in the following way:

$$\overline{\mathcal{H}}_{\rm eff}(x) = \frac{1}{2} \sum_{s_e} \int \frac{{\rm d}^3 \mathbf{p}}{(2\pi)^3} g_e f(p,T) \langle e(\mathbf{p}, s_e) | \mathcal{H}_{\rm eff}(x) | e(\mathbf{p}, s_e) \rangle \; , \tag{2.113}$$

where $g_e = 2$ denotes an internal degree of freedom, $f(p,T)$ is the distribution function of electrons in the phase space, and $|e(\mathbf{p}, s_e)\rangle = \sqrt{2E_{\mathbf{p}}}\; b_e^\dagger(\mathbf{p}, s_e)|0\rangle$ stands for the one-particle electron state with the momentum $\mathbf{p}$ and the spin eigenvalue s_e. Recalling the quantization of the electron field,

$$e(x) = \int {\rm d}\Pi_{\mathbf{q}} \sum_s \left[b_e(\mathbf{q}, s) u_e(\mathbf{q}, s) {\rm e}^{-{\rm i}qx} + d_e^\dagger(\mathbf{q}, s) v_e(\mathbf{q}, s) {\rm e}^{{\rm i}qx} \right] \tag{2.114}$$

with the phase element ${\rm d}\Pi_{\mathbf{q}} \equiv {\rm d}^3\mathbf{q}/[(2\pi)^3 \sqrt{2E_{\mathbf{q}}}]$, one may figure out the averaged effective Hamiltonian in Eq. (2.113):

$$\overline{\mathcal{H}}_{\rm eff}(x) = \frac{G_{\rm F}}{\sqrt{2}} n_e g_{\rm V}^e \overline{\nu}_e(x) \gamma^0 (1-\gamma_5) \nu_e(x) \; , \tag{2.115}$$

where the integration over the distribution function gives rise to the number density of electrons n_e, and the three-momentum $\mathbf{p}$ is taken to be isotropic.

Therefore, the electrons in matter contribute an effective potential for the left-handed electron neutrinos:

$$\mathcal{V}_e = \int \frac{\mathrm{d}^3\mathbf{p}\ \mathrm{d}^3\mathbf{x}}{(2\pi)^3 2E_{\mathbf{p}}} \langle \nu_{e\mathrm{L}}(\mathbf{p},s)|\overline{\mathcal{H}}_{\mathrm{eff}}(x)|\nu_{e\mathrm{L}}(\mathbf{p},s)\rangle = \sqrt{2}\ G_{\mathrm{F}} n_e g_{\mathrm{V}}^e\ , \quad (2.116)$$

where we have introduced the one-particle state $|\nu_{e\mathrm{L}}(\mathbf{p},s)\rangle$ corresponding to the left-handed neutrino field $\nu_{e\mathrm{L}}(x)$. Note that $(1-\gamma_5)\nu_{e\mathrm{L}}(x) = 2\nu_{e\mathrm{L}}(x)$ and the normalization relation of the one-particle states $\langle \nu_{e\mathrm{L}}(\mathbf{p},s)|\nu_{e\mathrm{L}}(\mathbf{q},s')\rangle = 2E_{\mathbf{p}}(2\pi)^3\delta^3(\mathbf{p}-\mathbf{q})\delta_{ss'}$ should be carefully taken into account in the above calculation. For this reason, a similar calculation done in the finite-volume quantization scheme is somewhat more transparent and simpler (Linder, 2005; Giunti and Kim, 2007).

In comparison, the effective Hamiltonian responsible for ν_μ or ν_τ neutrinos propagating in matter only arises from neutral-current interactions and can therefore be written as

$$\mathcal{H}_{\mathrm{eff}}(x) = \frac{G_{\mathrm{F}}}{\sqrt{2}} \overline{\nu}_\alpha(x)\gamma^\mu(1-\gamma_5)\nu_\alpha(x)\overline{e}(x)\gamma_\mu(C_{\mathrm{V}}^l - C_{\mathrm{A}}^l\gamma_5)e(x)\ , \quad (2.117)$$

where $\alpha = \mu$ or τ. Following a way similar to the treatment of electron neutrinos, one may easily figure out the effective potentials of muon and tau neutrinos in normal matter:

$$\mathcal{V}_\mu = \mathcal{V}_\tau = \sqrt{2}\ G_{\mathrm{F}} n_e C_{\mathrm{V}}^l\ . \quad (2.118)$$

Note that the equality $\mathcal{V}_\mu = \mathcal{V}_\tau$ will no more hold if the radiative corrections are taken into account (Botella *et al.*, 1987). The difference between $\mathcal{V}_\mu$ and $\mathcal{V}_\tau$ is likely to impact the flavor conversions of supernova neutrinos (Esteban-Pretel *et al.*, 2008).

We proceed to consider the effective Hamiltonian responsible for neutrino-nucleon interactions. The above results indicate that an effective potential of neutrinos propagating in isotropic matter is independent of the pseudovector couplings. In addition, the conservation of vector currents implies that the vector couplings of nucleons can simply be taken as a sum over the vector couplings of valence quarks. Both neutrino-proton and neutrino-neutron scattering processes are mediated by the neutral gauge boson Z^0, so their effective Hamiltonian takes the form

$$\mathcal{H}_{\mathrm{eff}}(x) = \frac{G_{\mathrm{F}}}{\sqrt{2}} \overline{\nu}_\alpha(x)\gamma_\mu(1-\gamma_5)\nu_\alpha(x)\overline{N}(x)\gamma^\mu \left(C_{\mathrm{V}}^N - \gamma_5 C_{\mathrm{A}}^N\right) N(x)\ , \quad (2.119)$$

where $C_{\mathrm{V,A}}^N \equiv 2C_{\mathrm{V,A}}^{\mathrm{u}} + C_{\mathrm{V,A}}^{\mathrm{d}}$ for protons $N(x) = p(x)$, or $C_{\mathrm{V,A}}^N \equiv 2C_{\mathrm{V,A}}^{\mathrm{d}} + C_{\mathrm{V,A}}^{\mathrm{u}}$ for neutrons $N(x) = n(x)$. One can then work out the effective potentials of neutrinos induced by the background protons and neutrons in matter:

$$\mathcal{V}_\alpha^p = \sqrt{2}\ G_{\mathrm{F}} n_p \left(2C_{\mathrm{V}}^{\mathrm{u}} + C_{\mathrm{V}}^{\mathrm{d}}\right) = \frac{1}{\sqrt{2}} G_{\mathrm{F}} n_p \left(1 - 4\sin^2\theta_{\mathrm{w}}\right)\ ,$$

$$\mathcal{V}_\alpha^n = \sqrt{2}\, G_{\rm F} n_n \left(2C_{\rm V}^{\rm d} + C_{\rm V}^{\rm u}\right) = -\frac{1}{\sqrt{2}} G_{\rm F} n_n \; , \tag{2.120}$$

where $\alpha = e, \mu$ or τ, n_p and n_n stand respectively for the number densities of protons and neutrons, and the values of $C_{\rm V}^{\rm u}$ and $C_{\rm V}^{\rm d}$ given in Table 2.3 have been used. Note that the neutral-current contributions are universal for all three types of neutrinos. Note also that the total effective potential for electron neutrinos is $\mathcal{V}_e + \mathcal{V}_e^p + \mathcal{V}_e^n = \sqrt{2}\, G_{\rm F} n_e + \mathcal{V}_\alpha^n$, but the total effective potential for muon (or tau) neutrinos is $\mathcal{V}_\mu + \mathcal{V}_\mu^p + \mathcal{V}_\mu^n = \mathcal{V}_\alpha^n$, where $n_e = n_p$ is taken as a consequence of the electric neutrality of matter. The difference between the potentials of electron and muon (or tau) neutrinos turns out to be $\Delta\mathcal{V} = \mathcal{V}_e - \mathcal{V}_\mu = \sqrt{2}\, G_{\rm F} n_e$. An important comment should be made on the effective potentials of antineutrinos in matter. The effective Hamiltonian of neutrinos is also applicable to the corresponding antineutrinos. But a difference appears when evaluating the effective potential in Eq. (2.116). For neutrinos, we are left with a unique non-vanishing matrix element of $\overline{\mathcal{H}}_{\rm eff}$ (Linder, 2005):

$$\langle \nu_\alpha(\mathbf{p}) | \overline{\mathcal{H}}_{\rm eff}(x) | \nu_\alpha(\mathbf{p}) \rangle \propto \langle 0 | b_\nu(\mathbf{p}) \left[\int {\rm d}^3\mathbf{q}\; b_\nu^\dagger(\mathbf{q}) b_\nu(\mathbf{q}) \right] b_\nu^\dagger(\mathbf{p}) | 0 \rangle \; ; \tag{2.121}$$

while for antineutrinos, the corresponding matrix element of $\overline{\mathcal{H}}_{\rm eff}$ reads

$$\begin{aligned} \langle \overline{\nu}_\alpha(\mathbf{p}) | \overline{\mathcal{H}}_{\rm eff}(x) | \overline{\nu}_\alpha(\mathbf{p}) \rangle &\propto \langle 0 | d_\nu(\mathbf{p}) \left[\int {\rm d}^3\mathbf{q}\; d_\nu(\mathbf{q}) d_\nu^\dagger(\mathbf{q}) \right] d_\nu^\dagger(\mathbf{p}) | 0 \rangle \\ &= -\langle 0 | d_\nu(\mathbf{p}) \left[\int {\rm d}^3\mathbf{q}\; d_\nu^\dagger(\mathbf{q}) d_\nu(\mathbf{q}) \right] d_\nu^\dagger(\mathbf{p}) | 0 \rangle \; , \end{aligned} \tag{2.122}$$

where the quantization of neutrino fields is the same as that in Eq. (2.114). Hence we conclude that the effective potentials responsible for neutrinos and antineutrinos propagating in matter have the opposite signs. For the same reason, we can see from Eq. (2.113) that the effective potentials of neutrinos will change their signs if the background particles are replaced by the corresponding antiparticles.

Finally, let us turn to the coherent forward scattering of neutrinos off their ambient neutrinos — a phenomenon which can be extremely important for the flavor conversions of supernova neutrinos. It is obvious that only the neutral-current interactions contribute to this process. The Feynman amplitude of $\nu_\alpha + \nu_\alpha \to \nu_\alpha + \nu_\alpha$ scattering has been given in Eq. (2.80), which corresponds to the following effective Hamiltonian:

$$\mathcal{H}_{\rm eff}(x) = \frac{G_{\rm F}}{2\sqrt{2}} \overline{\nu}_\alpha(x) \gamma^\mu (1 - \gamma_5) \nu_\alpha(x) \overline{\nu}_\alpha(x) \gamma_\mu (1 - \gamma_5) \nu_\alpha(x) \; . \tag{2.123}$$

It is straightforward to reproduce Eq. (2.80) from Eq. (2.123). An average over the background neutrinos receives contributions from both spinor bilinears

in Eq. (2.123) and thus gives rise to a factor 2. Taking account of this factor, one can work out the effective potential for ν_α neutrinos propagating in the background of ν_α neutrinos:

$$\mathcal{V}_{\nu_\alpha} = 2\sqrt{2}\, G_{\rm F} n_{\nu_\alpha} \,, \tag{2.124}$$

where n_{ν_α} is the number density of the background neutrinos. One should keep in mind that neutrinos are always left-handed in the SM when doing the above calculation. One may analogously find that the effective potential for ν_α neutrinos traveling in the background of ν_β neutrinos (for $\beta \neq \alpha$) is simply $\mathcal{V}_{\nu_\alpha} = \sqrt{2}\, G_{\rm F} n_{\nu_\beta}$. Hence the effective potential of neutrino-neutrino scattering can be recast into a much more compact form: $\mathcal{V}_{\nu_\alpha} = \sqrt{2}\, G_{\rm F}(1+\delta_{\alpha\beta}) n_{\nu_\beta}$. The angular correlation between the incident and background neutrinos is very important in the case of supernova neutrinos. This effect is neglected here but it will be discussed in detail in Chapter 7.

2.3.3 Neutrino Self-energy Approach

In the astrophysical and cosmological environments, such as in the core of a supernova or in the early Universe, there may exist neutrinos in thermal equilibrium with other particles. In this case it is more reasonable to deal with the system by means of quantum field theories at finite temperatures (Landsman and van Weert, 1987; Kapusta, 1989; Quiros, 1999). On the other hand, it is certainly inappropriate to treat neutrinos in the early Universe as a beam of free particles. A proper strategy is to calculate the self-energies of neutrinos in the presence of background particles and then extract the effective potential by using the dispersion relation. The dispersion relation can be derived from (Nötzold and Raffelt, 1988)

$$\text{Det}\left[\not{p} - \Sigma(\not{p})\right] = 0 \,, \tag{2.125}$$

where $\Sigma(\not{p})$ denotes the self-energy of a fermion. For a free fermion with mass m, we have $\Sigma(\not{p}) = m$. Then an explicit calculation of the determinant in Eq. (2.125) yields the dispersion relation $E^2 = |\mathbf{p}|^2 + m^2$. In the presence of interactions, the general form of the neutrino self-energy in the SM can be written as $\Sigma(\not{p}) = \{c_1 \not{p} + c_2 \not{u} + c_3 [\not{p}, \not{u}]\} P_{\rm L}$ with u^μ being the four-velocity of the medium (Weldon, 1982). A calculation of the coefficients c_i (for $i = 1, 2, 3$) involves the Feynman rules in quantum field theories at finite temperatures, which will be briefly discussed in the following.

Consider a thermal system at rest with the Hamiltonian H and the conserved charge Q. The equilibrium states are then described by the grand-canonical density operator [5]

[5] The grand canonical ensemble can exchange the energy and particles with the thermal reservoir, but its temperature, volume and chemical potential are fixed.

$$\rho = \frac{1}{\mathcal{N}} \mathrm{e}^{-\beta(H-\mu Q)} \ , \tag{2.126}$$

where $\mathcal{N} \equiv \mathrm{Tr}\left[\mathrm{e}^{-\beta(H-\mu Q)}\right]$ is the normalization factor, μ denotes the chemical potential, and $\beta = 1/T$ with T being the temperature is introduced. Here the normalization $\mathrm{Tr}[\rho] = 1$ is implied. The thermal average of an operator $\mathcal{O}$ is then defined as

$$\langle \mathcal{O} \rangle = \mathrm{Tr}\left[\rho \mathcal{O}\right] \ . \tag{2.127}$$

For simplicity, we temporarily ignore the chemical potential μ and discuss the case of real scalar particles. In the Heisenberg picture one may write the scalar field operator as $\phi(x) = \mathrm{e}^{\mathrm{i}Ht}\phi(0,\mathbf{x})\mathrm{e}^{-\mathrm{i}Ht}$, where the time $x^0 = t$ is to be analytically continued to the complex plane. As usual, the two-point Green function is defined as the thermal average of the time-ordered field operators:

$$\begin{aligned} G^C(x-y) &\equiv \langle T_C\left[\phi(x)\phi(y)\right]\rangle \\ &\equiv \Theta_C\left(x^0-y^0\right)\langle\phi(x)\phi(y)\rangle + \Theta_C\left(y^0-x^0\right)\langle\phi(y)\phi(x)\rangle \ , \end{aligned} \tag{2.128}$$

where the T_C-ordering indicates that the fields should be ordered along the path C in the complex-time plane. We explicitly parametrize the path as $t = z(\tau)$ with τ being a real parameter, then the ordering in t is defined as that in τ. In addition, we have the step function $\Theta_C(t) = \Theta(\tau)$ and the Dirac delta function $\delta_C(t) = \left(\frac{\mathrm{d}z}{\mathrm{d}\tau}\right)^{-1}\delta(\tau)$. The functional formalism in quantum field theories is also applicable, so one may similarly define the generating functional of Green functions and that of the one-particle irreducible Green functions (Landsman and van Weert, 1987). The two-point Green function defined in Eq. (2.128) can be rewritten as

$$G^C(x-y) \equiv \Theta_C(x^0-y^0)G_+(x-y) + \Theta_C(y^0-x^0)G_-(x-y) \ , \tag{2.129}$$

where $G_+(x-y) \equiv \langle\phi(x)\phi(y)\rangle$ and $G_-(x-y) = G_+(y-x)$. Now we evaluate $G_+(x-y)$ at the point $\mathbf{x} = \mathbf{y} = 0$ by implementing the complete set of eigenstates $|n\rangle$ of the Hamiltonian (i.e., $H|n\rangle = E_n|n\rangle$). More explicitly,

$$\begin{aligned} G_+(x^0-y^0) &= \frac{1}{\mathcal{N}}\sum_n \langle n|\mathrm{e}^{-\beta H}\mathrm{e}^{\mathrm{i}Hx^0}\phi(0)\mathrm{e}^{-\mathrm{i}H(x^0-y^0)}\phi(0)\mathrm{e}^{-\mathrm{i}Hy^0}|n\rangle \\ &= \frac{1}{\mathcal{N}}\sum_{m,n} \left|\langle m|\phi(0)|n\rangle\right|^2 \mathrm{e}^{-\mathrm{i}E_m(x^0-y^0)}\mathrm{e}^{\mathrm{i}E_n(x^0-y^0+\mathrm{i}\beta)} \ . \end{aligned} \tag{2.130}$$

To assure the summation to be convergent, we require $-\beta \leqslant \mathrm{Im}(x^0-y^0) \leqslant 0$ together with $\Theta_C(x^0-y^0) = 0$ for $\mathrm{Im}(x^0-y^0) > 0$. A similar analysis of $G_-(x^0-y^0)$ yields the condition $0 \leqslant \mathrm{Im}(x^0-y^0) \leqslant \beta$ together with $\Theta_C(y^0-x^0) = 0$ for $\mathrm{Im}(x^0-y^0) < 0$. Consequently, the convergence of the

Green function in the range $-\beta \leqslant \mathrm{Im}(x^0 - y^0) \leqslant \beta$ restricts us to define $\Theta_C(t) = 0$ for $\mathrm{Im}(t) > 0$. The latter implies that the point along the chosen path C should have a constant or monotonically decreasing imaginary part (Quiros, 1999). Starting with the definition of the two-point Green function, we can further derive

$$\begin{aligned} G_+(t - \mathrm{i}\beta, \mathbf{x}) &\equiv \langle \phi(t - \mathrm{i}\beta, \mathbf{x})\phi(0)\rangle \\ &= \frac{1}{\mathcal{N}}\mathrm{Tr}\left[\mathrm{e}^{-\beta H}\mathrm{e}^{\mathrm{i}H(-\mathrm{i}\beta)}\phi(t, \mathbf{x})\mathrm{e}^{-\mathrm{i}H(-\mathrm{i}\beta)}\phi(0)\right] \\ &= \frac{1}{\mathcal{N}}\mathrm{Tr}\left[\mathrm{e}^{-\beta H}\phi(0)\phi(t, \mathbf{x})\right] = G_+(-t, -\mathbf{x}) = G_-(t, \mathbf{x}) \ , \end{aligned} \tag{2.131}$$

where the cyclic invariance of the trace and the identity $G_-(x-y) = G_+(y-x)$ have been used. This is just the famous Kubo-Martin-Schwinger relation (Kubo, 1957; Martin and Schwinger, 1959).

Now we calculate the thermal two-point Green function for a free real scalar field, whose Hamiltonian can be written as

$$H = \int \frac{\mathrm{d}^3\mathbf{p}}{(2\pi)^3} E_{\mathbf{p}} a^\dagger_{\mathbf{p}} a_{\mathbf{p}} \ , \tag{2.132}$$

where $E_{\mathbf{p}} = \sqrt{|\mathbf{p}|^2 + m^2}$. Note that $a^\dagger$ and a stand respectively for the creation and annihilation operators, which satisfy the commutation relation $\left[a_{\mathbf{p}}, a^\dagger_{\mathbf{q}}\right] = (2\pi)^3\delta^3(\mathbf{p}-\mathbf{q})$. We first consider a system with a single momentum mode and the energy ω. Its Hamiltonian is $H = \omega a^\dagger a$, and its complete set of eigenstates are denoted by $|n\rangle$. We get

$$\mathrm{Tr}\left[\mathrm{e}^{-\beta H}\right] = \sum_{n=0}^{\infty}\langle n|\mathrm{e}^{-\beta H}|n\rangle = \sum_{n=0}^{\infty}\mathrm{e}^{-n\beta\omega} = \frac{1}{1 - \mathrm{e}^{-\beta\omega}} \ , \tag{2.133}$$

and

$$\mathrm{Tr}\left[\mathrm{e}^{-\beta H}a^\dagger a\right] = \sum_{n=0}^{\infty} n\mathrm{e}^{-n\beta\omega} = \frac{\mathrm{e}^{-\beta\omega}}{\left(1 - \mathrm{e}^{-\beta\omega}\right)^2} \ . \tag{2.134}$$

Therefore, the thermal average of the number operator reads $\langle a^\dagger a\rangle = n_{\mathrm{B}}(\omega)$ and $\langle aa^\dagger\rangle = 1 + n_{\mathrm{B}}(\omega)$, where $n_{\mathrm{B}}(\omega) \equiv 1/(\mathrm{e}^{\beta\omega} - 1)$ is the Bose-Einstein distribution function. Then it is straightforward to obtain the results for any momentum mode:

$$\begin{aligned} \langle a^\dagger_{\mathbf{p}} a_{\mathbf{q}}\rangle &= n_{\mathrm{B}}(E_{\mathbf{p}})(2\pi)^3\delta^3(\mathbf{p} - \mathbf{q}) \ , \\ \langle a_{\mathbf{p}} a^\dagger_{\mathbf{q}}\rangle &= \left[1 + n_{\mathrm{B}}(E_{\mathbf{p}})\right](2\pi)^3\delta^3(\mathbf{p} - \mathbf{q}) \ . \end{aligned} \tag{2.135}$$

Recalling the quantization of a real scalar field and using Eq. (2.135), we compute the two-point Green function (Altherr, 1993)

$$G^C(x-y) = \int \Big\{ \Theta_C(x^0-y^0) \left[\langle a^\dagger_{\mathbf{p}} a_{\mathbf{q}} \rangle \mathrm{e}^{\mathrm{i}(px-qy)} + \langle a_{\mathbf{p}} a^\dagger_{\mathbf{q}} \rangle \mathrm{e}^{-\mathrm{i}(px-qy)} \right] + \Theta_C(y^0-x^0) \left[\langle a_{\mathbf{q}} a^\dagger_{\mathbf{p}} \rangle \mathrm{e}^{\mathrm{i}(px-qy)} + \langle a^\dagger_{\mathbf{q}} a_{\mathbf{p}} \rangle \mathrm{e}^{-\mathrm{i}(px-qy)} \right] \Big\}$$
$$= \int \frac{\mathrm{d}^4 p}{(2\pi)^4} \kappa(p) \mathrm{e}^{-\mathrm{i}p(x-y)} \left[\Theta_C(x^0-y^0) + n_{\mathrm{B}}(p^0) \right] , \qquad (2.136)$$

where the integration over the phase space in the first equality is implied, and the spectrum function $\kappa(p) \equiv 2\pi\delta(p^2-m^2)\left[\Theta(p^0)-\Theta(-p^0)\right]$ has been introduced. It is worth pointing out that the specific expression of $G^C(x-y)$ definitely depends on the choice of the path C. There exist two conventional options — the imaginary- and real-time formalisms (Landsman and van Weert, 1987). We shall concentrate on the real-time formalism, in which the path C is chosen in the complex-time plane as follows: (1) from the initial real time t_i along the real axis to the final real time t_f; (2) from t_f to $t_f - \mathrm{i}\sigma$ along the imaginary axis with $0 < \sigma < \beta$; (3) from $t_f - \mathrm{i}\sigma$ to $t_i - \mathrm{i}\sigma$ in the opposite direction of the real axis; and (4) from $t_i - \mathrm{i}\sigma$ to $t_i - \mathrm{i}\beta$. In this formalism four distinct propagators arise from Eq. (2.136) and they can be expressed in the momentum space as

$$G^C(p) = \begin{pmatrix} G^{11}(p) & G^{12}(p) \\ G^{21}(p) & G^{22}(p) \end{pmatrix} = U(\beta,p) \begin{pmatrix} \Delta(p) & 0 \\ 0 & \Delta^*(p) \end{pmatrix} U(\beta,p) , \quad (2.137)$$

where

$$U(\beta,p) = \begin{pmatrix} \cosh\theta_p & \sinh\theta_p \\ \sinh\theta_p & \cosh\theta_p \end{pmatrix} \qquad (2.138)$$

with $\cosh\theta_p \equiv 1/\sqrt{1-\mathrm{e}^{-\beta E_{\mathbf{p}}}}$, and $\Delta(p)$ is just the usual Feynman propagator at zero temperature. Although there are propagators associated with the superscript "2", the physical fields are only related to $G^{11}(p)$. Explicitly, we have (Bernard, 1974; Dolan and Jackiw, 1974; Weinberg, 1974; Landsman and van Weert, 1987)

$$G^{11}(p) = \frac{\mathrm{i}}{p^2-m^2+\mathrm{i}\epsilon} + 2\pi n_{\mathrm{B}}(E_{\mathbf{p}})\delta(p^2-m^2) . \qquad (2.139)$$

One may discuss the case of fermions in a similar way. The fermionic Green function can be written as

$$S^C(p) = \begin{pmatrix} S^{11}(p) & S^{12}(p) \\ S^{21}(p) & S^{22}(p) \end{pmatrix} = V(\beta,p) \begin{pmatrix} S_{\mathrm{F}}(p) & 0 \\ 0 & S^*_{\mathrm{F}}(p) \end{pmatrix} V(\beta,p) , \quad (2.140)$$

where

$$V(\beta,p) = \begin{pmatrix} \cos\theta_p & \sin\theta_p \\ \sin\theta_p & \cos\theta_p \end{pmatrix} \qquad (2.141)$$

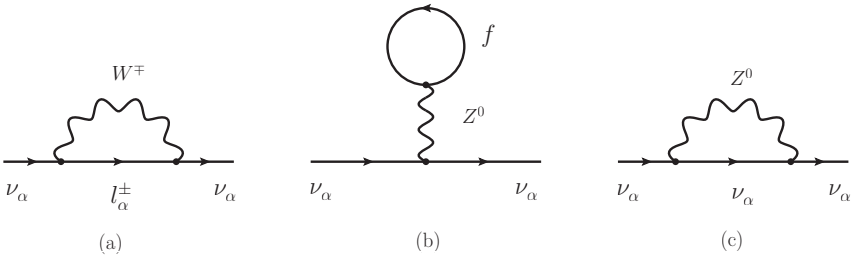

Fig. 2.7 The Feynman diagrams for the self-energy of neutrinos in the presence of background particles: (a) charged-current contributions; (b) neutral-current contributions with f being all the relevant particles in a medium; and (c) contributions from the background neutrinos

with $\cos\theta_p \equiv [\Theta(p^0) - \Theta(-p^0)]/\sqrt{1 + \mathrm{e}^{-\beta E_{\mathbf{P}}}}$, and $S_{\mathrm{F}}(p)$ is just the fermionic propagator at zero temperature. Eq. (2.140) allows us to obtain the physical component of the Green function:

$$S^{11}(p) = \left(\not{p} + m\right)\left[\frac{\mathrm{i}}{p^2 - m^2 + \mathrm{i}\epsilon} - 2\pi n_{\mathrm{F}}(E_{\mathbf{p}})\delta(p^2 - m^2)\right] , \quad (2.142)$$

where $n_{\mathrm{F}}(E_{\mathbf{p}}) \equiv 1/(\mathrm{e}^{\beta E_{\mathbf{P}}} + 1)$ is the Fermi-Dirac distribution function. In fact, the Feynman diagrams of a specific process in the real-time formalism is the same as those in the zero-temperature field theory. But all the vertices should be labeled by "1" or "2", and the physical legs must be assigned as "1". The Feynman rules for the vertex "1" are the same as those in the zero-temperature field theory, and those for the vertex "2" are just the Hermitian conjugate (Landsman and van Weert, 1987).

Now we are ready to calculate the self-energy of neutrinos in the presence of background particles. To be more specific, we consider the ordinary matter in which there are electrons and nucleons or neutrinos themselves. The Feynman diagrams for possible contributions to the neutrino self-energy are shown in Fig. 2.7, where the unitary gauge is implied. So far we have only discussed the propagators of bosons and fermions in a thermal system at rest. It has been proposed that all the calculations at finite temperatures can be performed in a Lorentz-invariant way by introducing the four-velocity u^μ of the thermal bath (Weldon, 1982). In this case the propagator of electron fields is (Landsman and van Weert, 1987)

$$S_{\mathrm{F}}^{11}(p) = \left(\not{p} + m_e\right)\left[\frac{\mathrm{i}}{p^2 - m_e^2 + \mathrm{i}\epsilon} - 2\pi\delta(p^2 - m_e^2)\eta(p\cdot u)\right] , \quad (2.143)$$

where we have defined

$$\eta(p\cdot u) \equiv \frac{\Theta(p\cdot u)}{\mathrm{e}^{\beta(p\cdot u - \mu)} + 1} + \frac{\Theta(-p\cdot u)}{\mathrm{e}^{-\beta(p\cdot u - \mu)} + 1} \quad (2.144)$$

with μ being the chemical potential. In the absence of the chemical potential and in the rest frame, one can easily reproduce the propagator in Eq. (2.142). For instance, we look at the background-dependent term in the neutrino self-energy from Fig. 2.7(a) (Nötzold and Raffelt, 1988; Nieves, 1992):

$$-\mathrm{i}\Sigma^a(k) = \left(\frac{\mathrm{i}g}{\sqrt{2}}\right)^2 \int \frac{\mathrm{d}^4p}{(2\pi)^4}\gamma^\mu P_\mathrm{L} \frac{-\mathrm{i}}{(p-k)^2 - M_W^2} \tilde{S}_\mathrm{F}^{11}(p)\gamma_\mu P_\mathrm{L} \ , \quad (2.145)$$

where $\tilde{S}_\mathrm{F}^{11}$ singles out the temperature-dependent part of the full electron propagator, $P_\mathrm{L} \equiv (1-\gamma_5)/2$ is the left-handed projection operator, and the terms suppressed by m_e^2/M_W^2 have been neglected. Assuming $(p-k)^2 \ll M_W^2$ and using the identity $\gamma^\mu \not{p} \gamma_\mu = -2\not{p}$, we simplify Eq. (2.145) to

$$\Sigma^a(k) = \frac{g^2}{M_W^2} \int \frac{\mathrm{d}^4p}{(2\pi)^3} \delta(p^2 - m_e^2) \not{p} P_\mathrm{L} \eta(p\cdot u) \ . \quad (2.146)$$

Given its Lorentz structure, the above integration should uniquely depend on $\not{u}$. In order to further identify the coefficient, we work in the rest frame of the medium with $u^\mu = (1, \mathbf{0})$. Then Eq. (2.146) becomes

$$\begin{aligned} \Sigma^a(k)|_{u^\mu=(1,\mathbf{0})} &= \frac{g^2}{M_W^2}\gamma^0 P_\mathrm{L} \int \frac{\mathrm{d}^4p}{(2\pi)^3} p^0 \delta(p^2 - m_e^2)\eta(p^0) \\ &= \frac{g^2}{M_W^2}\gamma^0 P_\mathrm{L} \int \frac{\mathrm{d}^3\mathbf{p}}{(2\pi)^3} \int_{-\infty}^{+\infty} p^0 \delta(p^2 - m_e^2)\eta(p^0)\mathrm{d}p^0 \ , \end{aligned} \quad (2.147)$$

and the integration over $\mathrm{d}p^0$ can be evaluated as follows:

$$\begin{aligned} &\int_{-\infty}^{+\infty} p^0 \frac{1}{2|p^0|}\left[\delta(p^0 - E_\mathbf{p}) + \delta(p^0 + E_\mathbf{p})\right]\eta(p^0)\mathrm{d}p^0 \\ &= \frac{1}{2}\int_0^{+\infty} \frac{\delta(p^0 - E_\mathbf{p})\Theta(p^0)\mathrm{d}p^0}{\mathrm{e}^{\beta(p^0-\mu)}+1} - \frac{1}{2}\int_{-\infty}^0 \frac{\Theta(-p^0)\delta(p^0 + E_\mathbf{p})\mathrm{d}p^0}{\mathrm{e}^{-\beta(p^0-\mu)}+1} \\ &= \frac{1}{2}\left(\frac{1}{\mathrm{e}^{\beta(E_\mathbf{p}-\mu)}+1} - \frac{1}{\mathrm{e}^{\beta(E_\mathbf{p}+\mu)}+1}\right) \end{aligned} \quad (2.148)$$

with $E_\mathbf{p} \equiv \sqrt{|\mathbf{p}|^2 + m_e^2}$. Substituting Eq. (2.148) into Eq. (2.147), we find

$$\Sigma^a(k)|_{u^\mu=(1,\mathbf{0})} = \frac{g^2}{4M_W^2}\gamma^0 P_\mathrm{L}(n_{e^-} - n_{e^+}) \ , \quad (2.149)$$

where n_{e^-} (or n_{e^+}) denotes the number density of electrons (or positrons):

$$n_{e^+} \equiv g_{e^+} \int \frac{\mathrm{d}^3\mathbf{p}}{(2\pi)^3} \cdot \frac{1}{\mathrm{e}^{\beta(E_\mathbf{p} \mp \mu)}+1} \quad (2.150)$$

with $g_{e^\mp} = 2$ being an internal degree of freedom. The general covariant form of the neutrino self-energy in Eq. (2.146) turns out to be

$$\Sigma^a(k) = \sqrt{2}\, G_{\rm F}(n_{e^-} - n_{e^+}) \not{n} P_{\rm L} \ . \tag{2.151}$$

Now let us examine how the above self-energy in the rest frame of the medium affects the dispersion relation of neutrinos. The latter is just the solution to the equation

$$\begin{aligned} 0 &= {\rm Det}\left[\not{k} - \Sigma^a(k)\right] \\ &= {\rm Det}\left[\begin{pmatrix} E - c_2 & \mathbf{k}\cdot\boldsymbol{\sigma} \\ -\mathbf{k}\cdot\boldsymbol{\sigma} & c_2 - E \end{pmatrix}\right] \\ &= \left[(E - c_2)^2 - |\mathbf{k}|^2\right]^2 \ , \end{aligned} \tag{2.152}$$

where $c_2 = \sqrt{2}\, G_{\rm F}(n_{e^-} - n_{e^+})$. It becomes evident that the dispersion relation for massless neutrinos is $c_2 = E - |\mathbf{k}|$, so c_2 is just the effective potential $\mathcal{V}$ defined in Eq. (2.109). This result is consistent with our previous calculations by means of the coherent scattering amplitude and the effective Hamiltonian in the absence of positrons in matter. One may follow a similar procedure to compute the effective potentials or the refractive indices of neutrinos induced by the processes in Fig. 2.7(b) and Fig. 2.7(c). The final results for the effective potentials are summarized below (Nötzold and Raffelt, 1988).

(1) In the $e^{\pm}$ background:

$$\begin{aligned} \mathcal{V}_e &= \mathcal{V}_e^{\rm cc} + \mathcal{V}_e^{\rm nc} = \frac{1}{\sqrt{2}} G_{\rm F}\left(1 + 4\sin^2\theta_{\rm w}\right)\left(n_{e^-} - n_{e^+}\right) \ , \\ \mathcal{V}_\mu &= \mathcal{V}_\tau = \mathcal{V}_\mu^{\rm nc} = \mathcal{V}_\tau^{\rm nc} = -\frac{1}{\sqrt{2}} G_{\rm F}\left(1 - 4\sin^2\theta_{\rm w}\right)\left(n_{e^-} - n_{e^+}\right) \ . \end{aligned} \tag{2.153}$$

(2) In the nucleon background:

$$\begin{aligned} \mathcal{V}_\alpha^p &= \frac{1}{\sqrt{2}} G_{\rm F}\left(1 - 4\sin^2\theta_{\rm w}\right)\left(n_p - n_{\overline{p}}\right) \ , \\ \mathcal{V}_\alpha^n &= -\frac{1}{\sqrt{2}} G_{\rm F}\left(n_n - n_{\overline{n}}\right) \ , \end{aligned} \tag{2.154}$$

where $\alpha = e$, μ or τ.

(3) In the neutrino background:

$$\mathcal{V}_{\nu_\alpha} = \sqrt{2}\, G_{\rm F}\left(1 + \delta_{\alpha\beta}\right)\left(n_{\nu_\beta} - n_{\overline{\nu}_\beta}\right) \ , \tag{2.155}$$

where ν_β (or $\overline{\nu}_\beta$) denote the background neutrinos (or antineutrinos).

For the antineutrino beam in a given medium, the corresponding effective potential takes the opposite sign. Note that only the leading-order results have been presented here. More general results including the next-to-leading-order corrections can be found in some literature (Botella *et al.*, 1987; Nötzold and Raffelt, 1988; Nieves, 1992; Mirizzi *et al.*, 2009).

References

Aaltonen, T., *et al.* (CDF and D0 Collaborations), 2010, Phys. Rev. Lett. **104**, 061802.

Alberico, W. M., Bilenky, S. M., and Maieron, C., 2002, Phys. Rept. **358**, 227.

Altherr, T., 1993, arXiv:hep-ph/9307277.

Arnison, G., *et al.* (UA1 Collaboration), 1983a, Phys. Lett. B **122**, 103.

Arnison, G., *et al.* (UA1 Collaboration), 1983b, Phys. Lett. B **126**, 398.

Bell, J. S., 1955, Proc. Roy. Soc. A **231**, 79.

Bernard, C., 1974, Phys. Rev. D **9**, 3312.

Bethe, H., and Peierls, R., 1934, Nature **133**, 532.

Botella, F. J., Lim, C. S., and Marciano, W. J., 1987, Phys. Rev. D **35**, 896.

Brandelik, R., *et al.*, 1979, Phys. Lett. B **86**, 243.

Cabibbo, N., 1963, Phys. Rev. Lett. **10**, 531.

Cheng, T. P., and Li, L. F., 1988, *Gauge Theory of Elementary Particle Physics* (Oxford University Press).

Coleman, S. R., and Weinberg, E. J., 1973, Phys. Rev. D **7**, 1888.

Cowan, J. L. Jr., *et al.*, 1956, Science **124**, 103.

De Witt, B. S., 1967, Phys. Rev. **162**, 1195.

Dighe, A., 2008, J. Phys. Conf. Ser. **136**, 022041.

Dolan, L., and Jackiw, R., 1974, Phys. Rev. D **9**, 3320.

Duan, H., and Kneller, J. P., 2009, J. Phys. G **36**, 113201.

Ellis, J. R., Gaillard, M. K., and Ross, G. G., 1976, Nucl. Phys. B **111**, 253.

Englert, F., and Brout, R., 1964, Phys. Rev. Lett. **13**, 321.

Esteban-Pretel, A., *et al.*, 2008, Phys. Rev. D **77**, 065024.

Fadeev, L. D., and Popov, V. N., 1967, Phys. Lett. B **25**, 29.

Fermi, E., 1933, La Ricerca Scientifica **2**, 12.

Fermi, E., 1949, *Nuclear Physics* (The University of Chicago Press).

Feynman, R. P., 1963, Acta Phys. Pol. **24**, 697.

Fritzsch, H., Gell-Mann, M., and Leutwyler, H., 1973, Phys. Lett. B **47**, 365.

Giunti, C., and Kim, C. W., 2007, *Fundamentals of Neutrino Physics and Astrophysics* (Oxford University Press).

Glashow, S. L., 1961, Nucl. Phys. **22**, 579.

Goldstone, J., 1961, Nuovo Cim. **19**, 154.

Goldstone, J., Salam, A., and Weinberg, S., 1962, Phys. Rev. **127**, 965.

Guralnik, G. S., Hagen, C. R., and Kibble, T. W. B., 1964, Phys. Rev. Lett. **13**, 585.

Higgs, P. W., 1964a, Phys. Lett. **12**, 132.

Higgs, P. W., 1964b, Phys. Rev. Lett. **13**, 508.

Higgs, P. W., 1966, Phys. Rev. **145**, 1156.

Kapusta, J. I., 1989, *Finite-temperature Field Theory* (Cambridge University Press).

Kobayashi, M., and Maskawa, T., 1973, Prog. Theor. Phys. **49**, 652.

Kubo, R., 1957, J. Phys. Soc. Japan **12**, 570.

Landau, L. D., and Lifshitz, E. M., 1977, *Quantum Mechanics: Non-relativistic Theory* (Pergamon Press).

Landsman, N. P., and van Weert, C. G., 1987, Phys. Rept. **145**, 141.

Lee, B. W., and Zinn-Justin, J., 1972a, Phys. Rev. D **5**, 3121.

Lee, B. W., and Zinn-Justin, J., 1972b, Phys. Rev. D **5**, 3137.
Lee, B. W., and Zinn-Justin, J., 1972c, Phys. Rev. D **5**, 3155.
Linder, J., 2005, arXiv:hep-ph/0504264.
Llewellyn Smith, C. H., 1971, Phys. Rept. **3**, 261.
Lüders, G., 1957, Ann. Phys. **2**, 1.
Marciano, W. J., and Parsa, Z., 2003, J. Phys. G **29**, 2629.
Martin, P. C., and Schwinger, J., 1959, Phys. Rev. **115**, 1342.
Mikheyev, S. P., and Smirnov, A. Yu., 1985, Sov. J. Nucl. Phys. **42**, 913.
Mirizzi, A., *et al.*, 2009, JHEP **0910**, 020.
Nakamura, K., *et al.* (Particle Data Group), 2010, J. Phys. G **37**, 075021.
Nambu, Y., 1960, Phys. Rev. Lett. **4**, 380.
Nambu, Y., and Jona-Lasinio, G., 1961a, Phys. Rev. **122**, 345.
Nambu, Y., and Jona-Lasinio, G., 1961b, Phys. Rev. **124**, 246.
Nieves, J. F., 1992, in *Proceedings of 4th Mexican School of Particles and Fields*, edited by Lucio, J. L., and Zepeda, A. (World Scientific), p. 510.
Noether, E., 1918, Nachr. D. König. Gesellsch. D. Wiss. Zu Göttingen, Math-phys. Klasse 1918, 235.
Nötzold, D., and Raffelt, G. G., 1988, Nucl. Phys. B **307**, 924.
Pauli, W., 1955, in *Niels Bohr and the Development of Physics*, edited by W. Pauli (Pergamon Press), p. 30.
Peskin, M. E., and Schroeder, D. V., 1995, *An Introduction to Quantum Field Theory* (Perseus Books Publishing, L.L.C).
Porsev, S. G., Beloy, K., and Derevianko, A., 2009, Phys. Rev. Lett. **102**, 181601.
Quiros, M., 1999, arXiv:hep-ph/9901312.
Raffelt, G. G., 1996, *Stars as Laboratories for Fundamental Physics* (The University of Chicago Press).
Reines, F., and Cowan, C. L., 1956, Nature **178**, 446.
Sakurai, J. J., 1967, *Advanced Quantum Mechanics* (Addison-Wesley Publishing Company).
Salam, A., 1968, in *Elementary Particle Physics (Nobel Symposium No. 8)*, edited by N. Svartholm (Almqvist and Wilsell), p. 367.
Schwinger, J., 1951, Phys. Rev. **82**, 914.
Schwinger, J., 1958, *Quantum Electrodynamics* (Dover Publications).
't Hooft, G., 1971a, Nucl. Phys. B **33**, 173.
't Hooft, G., 1971b, Nucl. Phys. B **35**, 167.
't Hooft, G., 1971c, Phys. Lett. B **37**, 195.
Weinberg, S., 1958, Phys. Rev. **112**, 1375.
Weinberg, S., 1967, Phys. Rev. Lett. **19**, 1264.
Weinberg, S., 1974, Phys. Rev. D **9**, 3357.
Weinberg, S., 1995, *The Quantum Theory of Fields* (Cambridge University Press).
Weldon, H. A., 1982, Phys. Rev. D **26**, 2789.
Weyl, H., 1929, Z. Phys. **56**, 330.
Wolfenstein, L., 1978, Phys. Rev. D **17**, 2369.
Wolfenstein, L., 1979, Phys. Rev. D **20**, 2634.
Yang, C. N., and Mills, R., 1954, Phys. Rev. **96**, 191.

3

Neutrinos beyond the Standard Model

Some salient and model-independent properties of massive neutrinos will be introduced in this chapter. First of all, we shall summarize current experimental evidence for neutrino oscillations, which point to finite neutrino masses and lepton flavor mixing angles. Then we shall describe how to write out the mass terms of Dirac and Majorana neutrinos, analyze their C, P and T properties, and discuss their electromagnetic properties. The phenomenology of lepton flavor mixing and CP violation, together with the running behaviors of neutrino mass parameters from one energy scale to another, will also be discussed in some detail.

3.1 Experimental Evidence for Neutrino Masses

The mass of an elementary particle represents its inertial energy when it exists at rest. Hence a massless particle has no way to exist at rest — instead, it must always move at the speed of light. A massive fermion must exist in both left-handed and right-handed states, because the field operators responsible for the non-vanishing mass of a fermion have to be bilinear products of the spinor fields which flip the fermion's handedness or chirality (Xing, 2004).

The standard model (SM) of electroweak interactions contains three neutrinos $(\nu_e, \nu_\mu, \nu_\tau)$ which are purely left-handed and massless. Note that the masslessness of the photon in the SM is guaranteed by the electromagnetic $U(1)_{\rm Q}$ gauge symmetry. Although the masslessness of three neutrinos corresponds to the lepton number conservation [1], the latter is an accidental symmetry rather than a fundamental symmetry of the SM. Therefore, many

[1] It is actually the $B-L$ symmetry that makes neutrinos exactly massless in the SM, where B = baryon number and L = lepton number. The reason is simply that a neutrino and an antineutrino have different values of $B-L$ (Witten, 2001). Thus the naive argument for massless neutrinos is valid to all orders in perturbation and non-perturbation theories, if $B-L$ is an exact symmetry.

physicists strongly believed that neutrinos should be massive even long before some incontrovertible experimental evidence for massive neutrinos were accumulated. A good reason for this belief is that neutrinos are more natural to be massive than to be massless in some grand unified theories (GUTs), such as the $SO(10)$ theory (Fritzsch and Minkowski, 1975; Georgi, 1975), which try to unify the electromagnetic, weak and strong interactions on the one hand and the leptons and quarks on the other hand.

If neutrinos are massive and their masses are non-degenerate, it will in general be impossible to find a flavor basis in which the coincidence between flavor and mass eigenstates holds both for charged leptons (e, μ, τ) and for neutrinos $(\nu_e, \nu_\mu, \nu_\tau)$. In other words, the phenomenon of flavor mixing is naturally expected to appear between three charged leptons and three massive neutrinos, just like the phenomenon of flavor mixing between three up-type quarks (u, c, t) and three down-type quarks (d, s, b) (Cabibbo, 1963; Kobayashi and Maskawa, 1973).

The neutrino oscillation, or the spontaneous periodic change from one neutrino flavor eigenstate to another, is a wonderful quantum phenomenon which can naturally take place if neutrinos are massive and lepton flavors are mixed. In a simple two-neutrino mixing scheme, the neutrino flavor eigenstates ν_α and ν_β are linear combinations of the neutrino mass eigenstates ν_a and ν_b (Maki *et al.*, 1962): $\nu_\alpha = \nu_a \cos\theta + \nu_b \sin\theta$ and $\nu_\beta = \nu_b \cos\theta - \nu_a \sin\theta$, where θ denotes the flavor mixing angle. Then the probabilities of neutrino oscillations are governed by two characteristic parameters: one is the neutrino mass-squared difference $\Delta m^2 \equiv m_b^2 - m_a^2$ (in units of eV^2) and the other is the flavor mixing factor $\sin^2 2\theta$. Corresponding to the "disappearance" and "appearance" neutrino experiments, the survival and conversion probabilities of a neutrino flavor eigenstate ν_α can explicitly be expressed as

$$P(\nu_\alpha \to \nu_\alpha) = 1 - \sin^2 2\theta \sin^2 \left(1.27 \frac{\Delta m^2 L}{E} \right) \tag{3.1}$$

and $P(\nu_\alpha \to \nu_\beta) = 1 - P(\nu_\alpha \to \nu_\alpha)$ with $\beta \neq \alpha$, where E is the neutrino beam energy (in units of GeV), and L denotes the distance between the neutrino source and the neutrino detector (in units of km). A lot of data, including those from solar, atmospheric, reactor and accelerator neutrino oscillation experiments, have been analyzed by using Eq. (3.1) as a good approximation.

3.1.1 Atmospheric Neutrino Oscillations

The first compelling and model-independent evidence for neutrino oscillations was achieved from the Super-Kamiokande (SK) experiment (Fukuda *et al.*, 1998b) on atmospheric neutrinos, which are produced in the Earth's atmosphere by cosmic rays and are detected in an underground detector. If there were no neutrino oscillation, the atmospheric ν_e (or $\overline{\nu}_e$) and ν_μ (or $\overline{\nu}_\mu$) neutrinos entering and exiting the detector should have an almost perfect

spherical symmetry. In other words, the downward-going and upward-going neutrino fluxes should be equal to each other: $\Phi_\alpha(\theta_z) = \Phi_\alpha(\pi - \theta_z)$ versus the zenith angle θ_z (for $\alpha = e$ or μ). The SK Collaboration has observed an approximate up-down flux symmetry for atmospheric ν_e neutrinos (or $\overline{\nu}_e$ antineutrinos) and a significant up-down flux asymmetry for atmospheric ν_μ neutrinos (or $\overline{\nu}_\mu$ antineutrinos). For example (Ashie *et al.*, 2005),

$$\begin{aligned} \frac{\Phi_e(-1 \leqslant \cos\theta_z \leqslant -0.2)}{\Phi_e(+0.2 \leqslant \cos\theta_z \leqslant +1)} &= 0.961^{+0.086}_{-0.079} \pm 0.016 \; , \\ \frac{\Phi_\mu(-1 \leqslant \cos\theta_z \leqslant -0.2)}{\Phi_\mu(+0.2 \leqslant \cos\theta_z \leqslant +1)} &= 0.551^{+0.035}_{-0.033} \pm 0.004 \; , \end{aligned} \tag{3.2}$$

for the multi-GeV e-like events and for the single-ring multi-GeV μ-like events plus partially-contained events, respectively. This result can well be interpreted in the assumption of $\nu_\mu \to \nu_\tau$ neutrino oscillations. Current neutrino oscillation experiments have convincingly ruled out the possibility that the atmospheric neutrino anomaly is dominantly attributed to $\nu_\mu \to \nu_e$ or $\nu_\mu \to \nu_s$ oscillations, where ν_s stands for a "sterile" neutrino which does not take part in the normal electroweak interactions.

The SK Collaboration studied the ν_μ disappearance probability as a function of the neutrino flight length L over the neutrino energy E and claimed the first *direct* evidence for atmospheric neutrino oscillations (Ashie *et al.*, 2004). A dip in the L/E distribution was observed in the experimental data (see Fig. 3.1 for illustration), as predicted from the sinusoidal flavor transition probability of neutrino oscillations. We observe that the exotic neutrino decay and neutrino decoherence scenarios are disfavored by the data, because they are unable to reproduce the dip. In addition, the no-oscillation case is strongly disfavored by the data at large L/E.

3.1.2 Accelerator Neutrino Oscillations

If the atmospheric ν_μ disappearance is attributed to $\nu_\mu \to \nu_\tau$ oscillations, then a significant fraction of the accelerator-produced ν_μ events should also disappear on their way to a sufficiently distant detector. This expectation has been confirmed by the long-baseline K2K (Ahn *et al.*, 2003) and MINOS (Michael *et al.*, 2006) experiments. As for the K2K experiment, the ν_μ beam was produced at the KEK accelerator, first measured by a near detector before any oscillation was developed, and then measured 250 km away by the SK detector at the Kamiokande. In comparison, the baseline length of the MINOS experiment is 735 km, from Fermilab (the source of ν_μ neutrinos) to northern Minnesota (the location of the far detector). Both experiments have observed a reduction of the ν_μ flux and a distortion of the ν_μ energy spectrum, which must take place in the presence of $\nu_\mu \to \nu_\tau$ oscillations.

The atmospheric neutrino data from the SK experiment and the accelerator neutrino data from the K2K and MINOS experiments can simultaneously

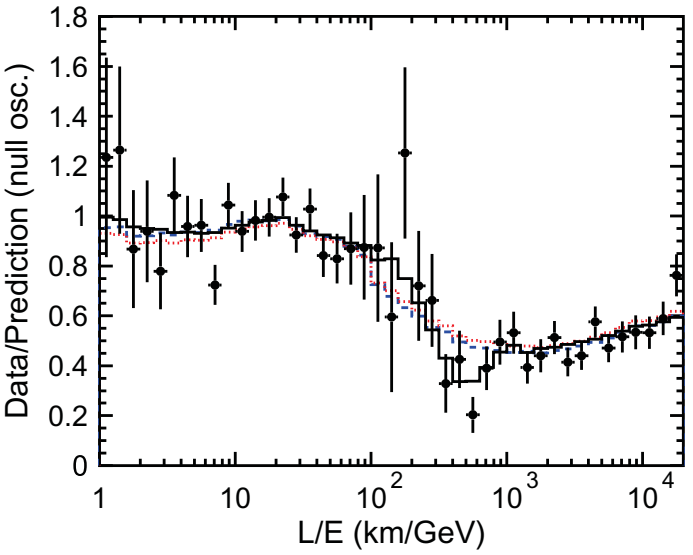

Fig. 3.1 A ratio of the experimental data to the Monte Carlo events without neutrino oscillations (points) as a function of the reconstructed L/E together with the best-fit expectation for $\nu_\mu \to \nu_\tau$ oscillations (solid line). As a comparison, the best-fit expectations for the neutrino decay (dashed line) and the neutrino decoherence (dotted line) are also shown in this plot (Ashie *et al.*, 2004. With permission from the American Physical Society)

be interpreted as the standard $\nu_\mu \to \nu_\tau$ oscillations. Fig. 3.2 shows the allowed region of Δm^2 and $\sin^2 2\theta$ constrained by these data (Adamson *et al.*, 2008). One can see that the best-fit point of the MINOS measurement corresponds to $|\Delta m^2| = 2.43 \times 10^{-3}$ eV^2 and $\sin^2 2\theta = 1.0$.

In spite of a careful search for the ν_τ appearance from atmospheric neutrino oscillations, no significant evidence has been established by the SK Collaboration (Abe *et al.*, 2006). It is expected that the ν_τ appearance can be observed from $\nu_\mu \to \nu_\tau$ oscillations in the OPERA experiment (Acquafredda *et al.*, 2006), which possesses a much higher neutrino beam energy ($E \sim 5$ GeV to 30 GeV, above the $\nu_\tau \to \tau$ production threshold) and a suitable baseline length ($L = 730$ km, from CERN to Gran Sasso).

3.1.3 Solar Neutrino Oscillations

The long-standing problem associated with solar neutrinos is that the flux of solar ν_e neutrinos measured in almost all experiments, such as the SK (Fukuda *et al.*, 1998a) and SNO (Ahmad *et al.*, 2002) experiments as well as the earlier Homestake (Cleveland *et al.*, 1998), GALLEX/GNO (Hampel *et al.*, 1999; Altmann *et al.*, 2000) and SAGE (Abdurashitov *et al.*, 2002)

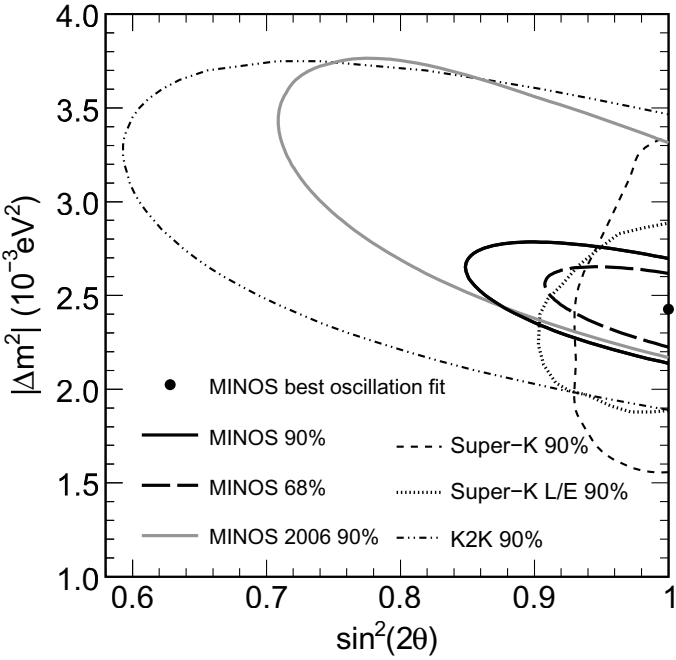

Fig. 3.2 Contours for the oscillation fit to the MINOS data taken in 2008. Also shown are the results from the SK and K2K measurements (Adamson *et al.*, 2008. With permission from the American Physical Society)

experiments, is significantly smaller than that predicted by the standard solar model (SSM) (Bahcall *et al.*, 2001). The deficits of solar neutrinos are not the same in different experiments, implying that the relevant physical effects are energy-dependent. Before the SNO experiment, it had been hypothesized that the solar neutrino anomaly was due to the conversion of solar ν_e neutrinos into other active or sterile neutrinos on their way from the core of the Sun to the detectors on the Earth. The SNO measurement has model-independently demonstrated that $\nu_e \to \nu_\mu$ and $\nu_e \to \nu_\tau$ transitions are dominantly responsible for the solar neutrino deficit. It is actually the $\nu_e \to \nu_\mu$ oscillation with a large mixing angle that dominates the solar neutrino flavor change.

What the SNO Collaboration has measured is the flux of solar ^{8}B neutrinos via the charged-current (CC), neutral-current (NC) and elastic-scattering (ES) reactions (Ahmad *et al.*, 2002): $\nu_e + \mathrm{D} \to e^- + p + p$, $\nu_\alpha + \mathrm{D} \to \nu_\alpha + p + n$ and $\nu_\alpha + e^- \to \nu_\alpha + e^-$ (for $\alpha = e$, μ or τ). In the presence of flavor conversion, the observed neutrino fluxes in different reactions satisfy

$$\phi_{\mathrm{CC}} = \phi_e \ , \quad \phi_{\mathrm{NC}} = \phi_e + \phi_{\mu\tau} \ , \quad \phi_{\mathrm{ES}} = \phi_e + \frac{\sigma_\mu}{\sigma_e}\phi_{\mu\tau} \approx \phi_e + 0.155\phi_{\mu\tau} \ , \quad (3.3)$$

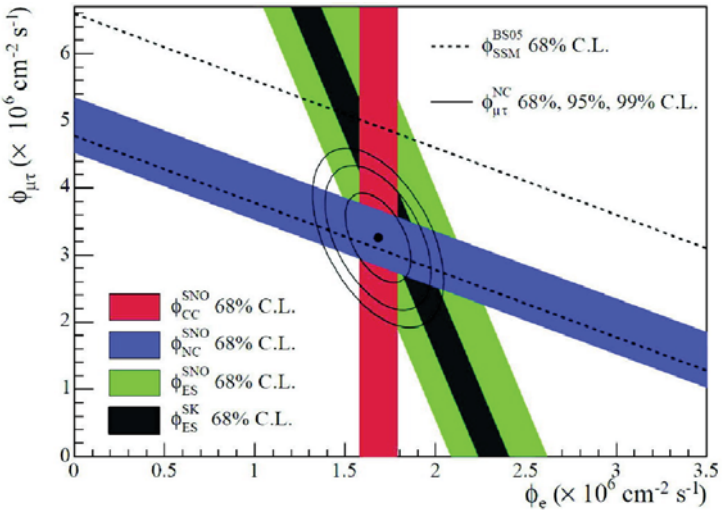

Fig. 3.3 The ν_μ+ν_τ flux versus the ν_e flux determined from the SNO data. The total ^{8}B solar neutrino flux predicted by the SSM is shown as dashed lines, parallel to the NC measurement. The narrow band parallel to the SNO's ES measurement corresponds to the SK's ES result. The best-fit point is obtained using only the SNO data (Aharmim *et al.*, 2005. With permission from the American Physical Society)

where $\sigma_\mu/\sigma_e \approx 0.155$ is the ratio of elastic ν_μ-e and ν_e-e scattering cross-sections, and $\phi_{\mu\tau}$ denotes the flux of active non-electron neutrinos. Of course, $\phi_{\mu\tau} = 0$ or equivalently $\phi_{\rm CC} = \phi_{\rm NC} = \phi_{\rm ES}$ would hold, if there were no flavor conversion. The SNO data yield (Aharmim *et al.*, 2005)

$$\begin{aligned}
\phi_{\rm CC} &= 1.68^{+0.06}_{-0.06}({\rm stat.})^{+0.08}_{-0.09}({\rm syst.}) \,, \\
\phi_{\rm ES} &= 2.35^{+0.22}_{-0.22}({\rm stat.})^{+0.15}_{-0.15}({\rm syst.}) \,, \\
\phi_{\rm NC} &= 4.94^{+0.21}_{-0.21}({\rm stat.})^{+0.38}_{-0.34}({\rm syst.}) \,,
\end{aligned} \tag{3.4}$$

from which the flavor composition of ^{8}B solar neutrinos is determined and summarized in Fig. 3.3. This impressive result is consistent with the SSM prediction (Bahcall *et al.*, 2005) and indicates the existence of ν_μ and ν_τ neutrinos in the flux of solar neutrinos onto the Earth.

The flavor conversion of solar ^{8}B neutrinos, whose typical energies are about 6 MeV to 7 MeV, is most likely due to $\nu_e \to \nu_\mu$ oscillations associated with the Mikheyev-Smirnov-Wolfenstein (MSW) matter effects (Wolfenstein, 1978; Mikheyev and Smirnov, 1985). Before the KamLAND reactor neutrino experiment (Eguchi *et al.*, 2003), a global analysis of all available experimental data on solar neutrinos (in particular, those from the SK and SNO measurements) in the two-flavor oscillation scheme led to several allowed re-

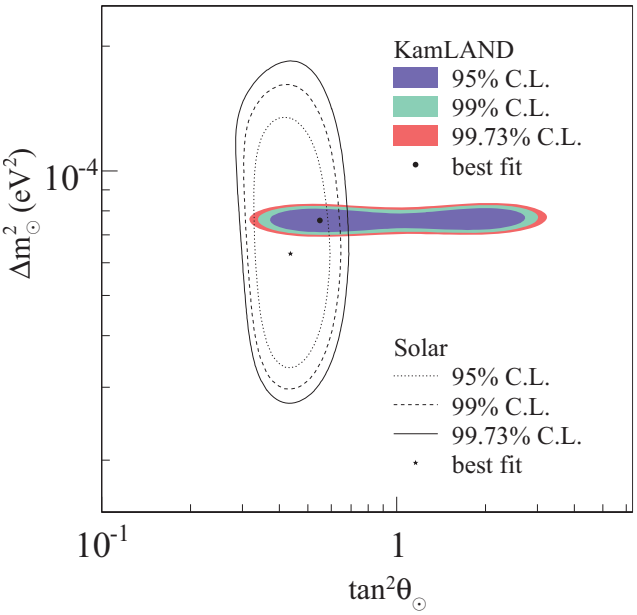

Fig. 3.4 Allowed region for two-flavor neutrino oscillation parameters from the solar neutrino and KamLAND experiments (Abe *et al.*, 2008. With permission from the American Physical Society)

gions of $\Delta m^2_\odot$ and $\tan^2\theta_\odot$: the SMA (small mixing angle), LMA (large mixing angle) and LOW (low mass-squared difference) regions based on the MSW mechanism as well as the VO (vacuum oscillation) and other possible regions. It was the KamLAND measurement that singled out the LMA MSW solution as the only acceptable solution to the solar neutrino problem.

Note also that the Borexino experiment (Arpesella *et al.*, 2008a; 2008b) has provided the first real-time detection of the mono-energetic solar ^{7}Be neutrinos with $E = 0.862$ MeV and observed a remarkable deficit corresponding to $P(\nu_e \to \nu_e) = 0.56 \pm 0.1$. This result can be interpreted as $\nu_e \to \nu_\mu$ oscillations in vacuum, as the matter effects on low-energy ^{7}Be neutrino oscillations are fairly insignificant (Kayser, 2008). More accurate measurements of ^{7}Be-associated ν_e events will be very important for much better understanding of the interplay between solar neutrino oscillations and MSW matter effects.

3.1.4 Reactor Neutrino Oscillations

The KamLAND Collaboration has measured the partial disappearance of $\overline{\nu}_e$ events, which were originally produced from distant nuclear reactors, by means of the inverse β-decay reaction $\overline{\nu}_e + p \to e^+ + n$ (Eguchi *et al.*, 2003; Abe *et al.*, 2008). The typical baseline of this experiment is 180 km, allowing

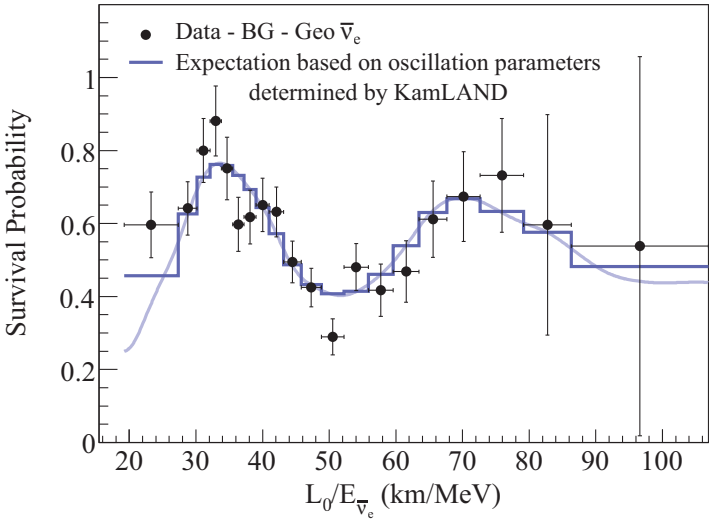

Fig. 3.5 Ratio of the background and geoneutrino-subtracted $\overline{\nu}_e$ spectrum to the no-oscillation expectation as a function of L_0/E, where $L_0 = 180$ km is the effective KamLAND baseline taken as a flux-weighted average (Abe *et al.*, 2008. With permission from the American Physical Society)

a terrestrial test of the LMA solution to the solar neutrino problem. The ratio of the observed inverse β-decay events to the expected number without $\overline{\nu}_e$ disappearance turns out to be convincingly smaller than one. Such a deficit can naturally be interpreted in the hypothesis of $\overline{\nu}_e \to \overline{\nu}_\mu$ oscillations, and the corresponding parameter space shown in Fig. 3.4 is compatible very well with the LMA region of solar $\nu_e \to \nu_\mu$ oscillations under CPT invariance (Abe *et al.*, 2008): $\Delta m^2_\odot = (7.59 \pm 0.21) \times 10^{-5}$ eV^2 and $\tan^2\theta_\odot = 0.47^{+0.06}_{-0.05}$.

In particular, $P(\overline{\nu}_e \to \overline{\nu}_e)$ measured in the KamLAND experiment displays a striking sinusoidal behavior of two-flavor oscillations (see Fig. 3.5). Note that the KamLAND detector detects $\overline{\nu}_e$ events coming from a number of reactors at different distances, so the distance L travelled by any given $\overline{\nu}_e$ is unknown (Kayser, 2008). For this reason, Fig. 3.5 plots the experimental data versus L_0/E with $L_0 = 180$ km being a flux-weighted average distance. The oscillatory curve and histogram in this figure have taken account of the actual distances to the individual reactors. One can see almost two cycles of the sinusoidal structure of neutrino oscillations.

The CHOOZ (Apollonio *et al.*, 1998) and Palo Verde (Boehm *et al.*, 2000) reactor antineutrino experiments were done to search for $\overline{\nu}_e \to \overline{\nu}_e$ oscillations in the atmospheric range of Δm^2. No indication in favor of neutrino oscillations was found from both experiments, leading to a strong constraint on the smallest neutrino mixing angle: $\sin^2 2\theta_{\rm chz} < 0.10$ for $\Delta m^2_{\rm chz} > 3.5 \times 10^{-3}$ eV^2; or $\sin^2 2\theta_{\rm chz} < 0.18$ for $\Delta m^2_{\rm chz} > 2.0 \times 10^{-3}$ eV^2.

3.1.5 Implications of Experimental Data

The neutrino experiments that we have briefly summarized involve different neutrino sources, different neutrino flavors, different neutrino beam energies and (or) different neutrino travel distances. But the observed neutrino deficits can all be explained in the framework of three-flavor oscillations, only if three known neutrinos have non-degenerate masses and nontrivial mixing angles. Such a solution is natural and economical in the sense that it does not invoke any (exotic) new particles or new forces, or change the SSM, or fine-tune the parameter space (Xing, 2008a). We conclude that neutrino oscillations have definitely been observed, implying that at least two neutrinos must be massive. This is the only new physics beyond the SM which has been established on solid experimental ground in the past four decades.

A global three-flavor analysis of all the available experimental data on solar (SNO, SK, Borexino), atmospheric (SK), reactor (KamLAND and CHOOZ) and accelerator (K2K and MINOS) neutrino oscillations has been done by two different groups (Schwetz *et al.*, 2008; Fogli *et al.*, 2008a). Tables 3.1 and 3.2 list their main results for two neutrino mass-squared differences and three neutrino mixing angles, respectively. One can see that the numerical results of these two analyses are essentially compatible with each other. Although $\sin^2\theta_{13} = 0.016 \pm 0.010$ (1σ) is claimed to be an interesting hint at $\theta_{13} > 0$ (Fogli *et al.*, 2008b), its significance remains quite poor.

Only some upper bounds on the absolute neutrino mass scale have been obtained from current data on the beta decay, the neutrinoless double-beta $(0\nu 2\beta)$ decay and cosmology (Strumia and Vissani, 2006; Seljak *et al.*, 2006). The following statements should be true: (a) every neutrino mass must be below $\mathcal{O}(1)$ eV; (b) one neutrino mass must be larger than $\sqrt{|\Delta m^2_{31}|} \sim 0.05$ eV; and (c) the smallest neutrino mass can be zero. The origin of finite neutrino masses demands a kind of new physics beyond the SM.

3.2 Dirac and Majorana Neutrino Mass Terms

To write out the mass term for three known neutrinos, let us make a minimal extension of the SM by introducing three right-handed neutrinos. Then we totally have six neutrino fields [2]:

$$\nu_{\rm L} = \begin{pmatrix} \nu_{e{\rm L}} \\ \nu_{\mu{\rm L}} \\ \nu_{\tau{\rm L}} \end{pmatrix} \; , \qquad N_{\rm R} = \begin{pmatrix} N_{1{\rm R}} \\ N_{2{\rm R}} \\ N_{3{\rm R}} \end{pmatrix} \; , \tag{3.5}$$

[2] The left- and right-handed components of a fermion field $\psi(x)$ are denoted as $\psi_{\rm L}(x) = P_{\rm L}\psi(x)$ and $\psi_{\rm R}(x) = P_{\rm R}\psi(x)$, respectively, where $P_{\rm L} \equiv (1-\gamma_5)/2$ and $P_{\rm R} \equiv (1+\gamma_5)/2$ are the chiral projection operators. Note, however, that $\nu_{\rm L} = P_{\rm L}\nu_{\rm L}$ and $N_{\rm R} = P_{\rm R}N_{\rm R}$ are in general independent of each other.

Table 3.1 Best-fit values with 1σ errors together with 2σ and 3σ intervals for three-flavor neutrino oscillation parameters from a global analysis of current data (Schwetz *et al.*, 2008. With permission from the Institute of Physics). Here $\Delta m^2_{21} \equiv m^2_2 - m^2_1$ and $\Delta m^2_{31} \equiv m^2_3 - m^2_1$ are defined

Parameter	Best fit + 1σ	2σ	3σ
$\Delta m^2_{21}\left(10^{-5}\ \mathrm{eV}^2\right)$	$7.65^{+0.23}_{-0.20}$	7.25 to 8.11	7.05 to 8.34
$\lvert\Delta m^2_{31}\rvert\left(10^{-3}\ \mathrm{eV}^2\right)$	$2.40^{+0.12}_{-0.11}$	2.18 to 2.64	2.07 to 2.75
$\sin^2\theta_{12}$	$0.304^{+0.022}_{-0.016}$	0.27 to 0.35	0.25 to 0.37
$\sin^2\theta_{23}$	$0.50^{+0.07}_{-0.06}$	0.39 to 0.63	0.36 to 0.67
$\sin^2\theta_{13}$	$0.01^{+0.016}_{-0.011}$	$\leqslant 0.040$	$\leqslant 0.056$

Table 3.2 Best-fit values and allowed 1σ, 2σ and 3σ ranges for three-flavor neutrino oscillation parameters from a global analysis of current data (Fogli *et al.*, 2008a. With permission from the American Physical Society). Here $\delta m^2 \equiv m^2_2 - m^2_1$ and $\Delta m^2 \equiv |m^2_3 - (m^2_1 + m^2_2)/2|$ are defined

Parameter	Best fit	1σ	2σ	3σ
$\delta m^2\left(10^{-5}\ \mathrm{eV}^2\right)$	7.67	7.48 to 7.83	7.31 to 8.01	7.14 to 8.19
$\Delta m^2\left(10^{-3}\ \mathrm{eV}^2\right)$	2.39	2.31 to 2.50	2.19 to 2.66	2.06 to 2.81
$\sin^2\theta_{12}$	0.312	0.294 to 0.331	0.278 to 0.352	0.263 to 0.375
$\sin^2\theta_{23}$	0.466	0.408 to 0.539	0.366 to 0.602	0.331 to 0.644
$\sin^2\theta_{13}$	0.016	0.006 to 0.026	< 0.036	< 0.046

where only the left-handed fields take part in the electroweak interactions. The charge-conjugate counterparts of ν_{L} and N_{R} are defined as

$$(\nu_{\mathrm{L}})^c \equiv \mathcal{C}\overline{\nu_{\mathrm{L}}}^T\ , \qquad (N_{\mathrm{R}})^c \equiv \mathcal{C}\overline{N_{\mathrm{R}}}^T\ ; \tag{3.6}$$

and accordingly,

$$\overline{(\nu_{\mathrm{L}})^c} = (\nu_{\mathrm{L}})^T\mathcal{C}\ , \qquad \overline{(N_{\mathrm{R}})^c} = (N_{\mathrm{R}})^T\mathcal{C}\ , \tag{3.7}$$

where $\mathcal{C}$ denotes the charge-conjugation matrix and satisfies the conditions

$$\mathcal{C}\gamma^T_\mu\mathcal{C}^{-1} = -\gamma_\mu\ , \qquad \mathcal{C}\gamma^T_5\mathcal{C}^{-1} = \gamma_5\ , \qquad \mathcal{C}^{-1} = \mathcal{C}^\dagger = \mathcal{C}^T = -\mathcal{C}\ . \tag{3.8}$$

It is easy to check that $P_{\mathrm{L}}(N_{\mathrm{R}})^c = (N_{\mathrm{R}})^c$ and $P_{\mathrm{R}}(\nu_{\mathrm{L}})^c = (\nu_{\mathrm{L}})^c$ hold; namely, $(\nu_{\mathrm{L}})^c = (\nu^c)_{\mathrm{R}}$ and $(N_{\mathrm{R}})^c = (N^c)_{\mathrm{L}}$ hold. Hence $(\nu_{\mathrm{L}})^c$ and $(N_{\mathrm{R}})^c$ are right- and left-handed fields, respectively. One may then use the neutrino fields ν_{L},

$N_{\rm R}$ and their charge-conjugate partners to write out the gauge-invariant and Lorentz-invariant neutrino mass terms.

In the SM the weak charged-current interactions of three active neutrinos are given by

$$\mathcal{L}_{\rm cc} = \frac{g}{\sqrt{2}} \overline{(e\ \mu\ \tau)_{\rm L}}\ \gamma^\mu \begin{pmatrix} \nu_e \\ \nu_\mu \\ \nu_\tau \end{pmatrix}_{\rm L} W^-_\mu + {\rm h.c.} \; . \tag{3.9}$$

Without loss of generality, we choose the basis in which the mass eigenstates of three charged leptons are identified with their flavor eigenstates. If neutrinos have nonzero and non-degenerate masses, their flavor and mass eigenstates are in general not identical in the chosen basis. This mismatch signifies the phenomenon of lepton flavor mixing (Maki *et al.*, 1962).

3.2.1 Dirac Masses and Lepton Number Conservation

A Dirac neutrino is described by a four-component Dirac spinor $\nu = \nu_{\rm L} + N_{\rm R}$, whose left-handed and right-handed components are just $\nu_{\rm L}$ and $N_{\rm R}$. The Dirac neutrino mass term comes from the Yukawa interactions

$$-\mathcal{L}_{\rm Dirac} = \overline{\ell_{\rm L}} Y_\nu \tilde{H} N_{\rm R} + {\rm h.c.} \; , \tag{3.10}$$

where $\tilde{H} \equiv {\rm i}\sigma_2 H^*$ with H being the SM Higgs doublet, and $\ell_{\rm L}$ denotes the left-handed lepton doublet. After spontaneous gauge symmetry breaking (i.e., $SU(2)_{\rm L} \times U(1)_{\rm Y} \to U(1)_{\rm Q}$), we obtain

$$-\mathcal{L}'_{\rm Dirac} = \overline{\nu_{\rm L}} M_{\rm D} N_{\rm R} + {\rm h.c.} \; , \tag{3.11}$$

where $M_{\rm D} = Y_\nu \langle H \rangle$ with $\langle H \rangle \simeq 174$ GeV being the vacuum expectation value of H. This mass matrix can be diagonalized by a bi-unitary transformation: $V^\dagger M_{\rm D} U = \widehat{M}_\nu \equiv {\rm Diag}\{m_1, m_2, m_3\}$ with m_i being the neutrino masses (for $i = 1, 2, 3$). After this diagonalization, Eq. (3.11) becomes

$$-\mathcal{L}'_{\rm Dirac} = \overline{\nu'_{\rm L}} \widehat{M}_\nu N'_{\rm R} + {\rm h.c.} \; , \tag{3.12}$$

where $\nu'_{\rm L} = V^\dagger \nu_{\rm L}$ and $N'_{\rm R} = U^\dagger N_{\rm R}$. Then the four-component Dirac spinor

$$\nu' = \nu'_{\rm L} + N'_{\rm R} = \begin{pmatrix} \nu_1 \\ \nu_2 \\ \nu_3 \end{pmatrix} \; , \tag{3.13}$$

which automatically satisfies $P_{\rm L} \nu' = \nu'_{\rm L}$ and $P_{\rm R} \nu' = N'_{\rm R}$, describes the mass eigenstates of three Dirac neutrinos. In other words,

$$-\mathcal{L}'_{\rm Dirac} = \overline{\nu'} \widehat{M}_\nu \nu' = \sum_{i=1}^{3} m_i \overline{\nu_i} \nu_i \; . \tag{3.14}$$

The kinetic term of Dirac neutrinos turns out to be

$$\mathcal{L}_{\rm kinetic} = {\rm i}\overline{\nu_{\rm L}}\gamma_\mu\partial^\mu\nu_{\rm L} + {\rm i}\overline{N_{\rm R}}\gamma_\mu\partial^\mu N_{\rm R} = {\rm i}\overline{\nu'}\gamma_\mu\partial^\mu\nu' = {\rm i}\sum_{k=1}^{3}\overline{\nu_k}\gamma_\mu\partial^\mu\nu_k \; , \quad (3.15)$$

where $V^\dagger V = V V^\dagger = \mathbf{1}$ and $U^\dagger U = U U^\dagger = \mathbf{1}$ have been used.

Now we rewrite the weak charged-current interactions of three neutrinos in Eq. (3.9) in terms of their mass eigenstates $\nu'_{\rm L} = V^\dagger \nu_{\rm L}$ in the chosen basis where the flavor and mass eigenstates of three charged leptons are identical:

$$\mathcal{L}_{\rm cc} = \frac{g}{\sqrt{2}}\overline{(e\ \mu\ \tau)_{\rm L}}\ \gamma^\mu V \begin{pmatrix}\nu_1\\ \nu_2\\ \nu_3\end{pmatrix}_{\rm L} W^-_\mu + {\rm h.c.} \; . \quad (3.16)$$

The 3×3 unitary matrix V, which actually links the neutrino mass eigenstates (ν_1, ν_2, ν_3) to the neutrino flavor eigenstates $(\nu_e, \nu_\mu, \nu_\tau)$, just measures the phenomenon of neutrino mixing.

A salient feature of massive Dirac neutrinos is lepton number conservation. Table 3.3 lists the lepton number L and the lepton flavor (family) number L_α of every lepton in the SM. To see why massive Dirac neutrinos are lepton-number-conserving, we make the global phase transformations

$$l(x) \to {\rm e}^{{\rm i}\Phi} l(x) \; , \quad \nu'_{\rm L}(x) \to {\rm e}^{{\rm i}\Phi}\nu'_{\rm L}(x) \; , \quad N'_{\rm R}(x) \to {\rm e}^{{\rm i}\Phi} N'_{\rm R}(x) \; , \quad (3.17)$$

where l denotes the column vector of e, μ and τ fields, and Φ is an arbitrary spacetime-independent phase. Because the mass term $\mathcal{L}'_{\rm Dirac}$, the kinetic term $\mathcal{L}_{\rm kinetic}$ and the charged-current interaction term $\mathcal{L}_{\rm cc}$ are all invariant under these transformations, the lepton number must be conserved for massive Dirac neutrinos. It is evident that lepton flavors are violated, unless $M_{\rm D}$ is diagonal or equivalently V is the identity matrix. In other words, lepton flavor mixing leads to lepton flavor violation, or vice versa.

Table 3.3 Lepton number L and lepton flavor (family) number L_α of charged leptons and neutrinos (for $\alpha = e, \mu, \tau$) in the SM

	e^-	ν_e	e^+	$\overline{\nu}_e$	μ^-	ν_μ	μ^+	$\overline{\nu}_\mu$	τ^-	ν_τ	τ^+	$\overline{\nu}_\tau$
L	+1	+1	−1	−1	+1	+1	−1	−1	+1	+1	−1	−1
L_e	+1	+1	−1	−1	0	0	0	0	0	0	0	0
L_μ	0	0	0	0	+1	+1	−1	−1	0	0	0	0
L_τ	0	0	0	0	0	0	0	0	+1	+1	−1	−1

For example, the decay mode $\pi^- \to \mu^- + \overline{\nu}_\mu$ preserves both the lepton number and lepton flavors. In contrast, $\mu^+ \to e^+ + \gamma$ preserves the lepton

number but violates the lepton flavors. The observed phenomena of neutrino oscillations verify the existence of neutrino flavor violation. Note that the $0\nu2\beta$ decay $(A, Z) \to (A, Z+2) + 2e^-$ violates the lepton number. This process cannot take place if neutrinos are massive Dirac particles, but it may naturally happen if neutrinos are massive Majorana particles.

3.2.2 Majorana Masses and Lepton Number Violation

The left-handed neutrino field $\nu_{\rm L}$ and its charge-conjugate counterpart $(\nu_{\rm L})^c$ can in principle form a neutrino mass term, as $(\nu_{\rm L})^c$ is actually right-handed. But this Majorana mass term is forbidden by the $SU(2)_{\rm L} \times U(1)_{\rm Y}$ gauge symmetry in the SM, which contains only one $SU(2)_{\rm L}$ Higgs doublet and preserves lepton number conservation. We shall show in Section 4.1.2 that the introduction of an $SU(2)_{\rm L}$ Higgs triplet into the SM can accommodate such a neutrino mass term with gauge invariance. Here we ignore the details of the Higgs triplet models and focus on the Majorana neutrino mass term itself (Gribov and Pontecorvo, 1969):

$$-\mathcal{L}'_{\rm Majorana} = \frac{1}{2}\overline{\nu_{\rm L}} M_{\rm L} (\nu_{\rm L})^c + {\rm h.c.} \; . \tag{3.18}$$

Note that the mass matrix $M_{\rm L}$ must be symmetric. Because the mass term is a Lorentz scalar whose transpose keeps unchanged, we have

$$\overline{\nu_{\rm L}} M_{\rm L} (\nu_{\rm L})^c = [\overline{\nu_{\rm L}} M_{\rm L} (\nu_{\rm L})^c]^T = -\overline{\nu_{\rm L}} \mathcal{C}^T M_{\rm L}^T \overline{\nu_{\rm L}}^T = \overline{\nu_{\rm L}} M_{\rm L}^T (\nu_{\rm L})^c \; , \tag{3.19}$$

where a minus sign appears when interchanging two fermion field operators, and $\mathcal{C}^T = -\mathcal{C}$ has been used. Hence $M_{\rm L}^T = M_{\rm L}$ holds. This symmetric mass matrix can be diagonalized by the transformation $V^\dagger M_{\rm L} V^* = \widehat{M}_\nu \equiv {\rm Diag}\{m_1, m_2, m_3\}$, where V is a unitary matrix [3]. After this diagonalization, Eq. (3.18) becomes

$$-\mathcal{L}'_{\rm Majorana} = \frac{1}{2}\overline{\nu'_{\rm L}} \widehat{M}_\nu (\nu'_{\rm L})^c + {\rm h.c.} \; , \tag{3.20}$$

where $\nu'_{\rm L} = V^\dagger \nu_{\rm L}$ and $(\nu'_{\rm L})^c = \mathcal{C}\overline{\nu'_{\rm L}}^T$. Then the field

$$\nu' = \nu'_{\rm L} + (\nu'_{\rm L})^c = \begin{pmatrix} \nu_1 \\ \nu_2 \\ \nu_3 \end{pmatrix} \; , \tag{3.21}$$

which satisfies the Majorana condition $(\nu')^c = \nu'$ (Majorana, 1937), describes the mass eigenstates of three Majorana neutrinos. In other words,

[3] A proof of this theorem is very easy (see, e.g., Bilenky and Petcov, 1987; Dreiner *et al.*, 2008; and references therein).

$$-\mathcal{L}'_{\rm Majorana} = \frac{1}{2}\overline{\nu'}\widehat{M}_\nu\nu' = \frac{1}{2}\sum_{i=1}^{3} m_i\overline{\nu_i}\nu_i \; . \tag{3.22}$$

The kinetic term of Majorana neutrinos turns out to be

$$\mathcal{L}_{\rm kinetic} = {\rm i}\overline{\nu_{\rm L}}\gamma_\mu\partial^\mu\nu_{\rm L} = {\rm i}\overline{\nu'_{\rm L}}\gamma_\mu\partial^\mu\nu'_{\rm L} = \frac{\rm i}{2}\overline{\nu'}\gamma_\mu\partial^\mu\nu' = \frac{\rm i}{2}\sum_{k=1}^{3}\overline{\nu_k}\gamma_\mu\partial^\mu\nu_k \; , \tag{3.23}$$

where we have used a generic relationship $\overline{(\psi_{\rm L})^c}\gamma_\mu\partial^\mu(\psi_{\rm L})^c = \overline{\psi_{\rm L}}\gamma_\mu\partial^\mu\psi_{\rm L}$. This relationship can easily be proved by taking account of $\partial^\mu\left[\overline{(\psi_{\rm L})^c}\gamma_\mu(\psi_{\rm L})^c\right] = 0$; i.e., we have

$$\begin{aligned}\overline{(\psi_{\rm L})^c}\gamma_\mu\partial^\mu(\psi_{\rm L})^c &= -\partial^\mu\overline{(\psi_{\rm L})^c}\gamma_\mu(\psi_{\rm L})^c = -\left[\partial^\mu\overline{(\psi_{\rm L})^c}\gamma_\mu(\psi_{\rm L})^c\right]^T \\ &= \left(\mathcal{C}\overline{\psi_{\rm L}}^T\right)^T\gamma_\mu^T\partial^\mu\left[(\psi_{\rm L})^T\mathcal{C}\right]^T = \overline{\psi_{\rm L}}\gamma_\mu\partial^\mu\psi_{\rm L} \; ,\end{aligned} \tag{3.24}$$

where $\mathcal{C}^T\gamma_\mu^T\mathcal{C}^T = \gamma_\mu$, which can be read off from Eq. (3.8), has been used.

It is worth pointing out that the factor 1/2 in $\mathcal{L}'_{\rm Majorana}$ allows us to get the Dirac equation of massive Majorana neutrinos analogous to that of massive Dirac neutrinos. To see this point more clearly, let us consider the Lagrangian of free Majorana neutrinos (i.e., their kinetic and mass terms):

$$\begin{aligned}\mathcal{L}_\nu &= {\rm i}\overline{\nu_{\rm L}}\gamma_\mu\partial^\mu\nu_{\rm L} - \left[\frac{1}{2}\overline{\nu_{\rm L}}M_{\rm L}(\nu_{\rm L})^c + {\rm h.c.}\right] \\ &= {\rm i}\overline{\nu'_{\rm L}}\gamma_\mu\partial^\mu\nu'_{\rm L} - \left[\frac{1}{2}\overline{\nu'_{\rm L}}\widehat{M}_\nu(\nu'_{\rm L})^c + {\rm h.c.}\right] \\ &= \frac{1}{2}\left({\rm i}\overline{\nu'}\gamma_\mu\partial^\mu\nu' - \overline{\nu'}\widehat{M}_\nu\nu'\right) = -\frac{1}{2}\left({\rm i}\partial^\mu\overline{\nu'}\gamma_\mu\nu' + \overline{\nu'}\widehat{M}_\nu\nu'\right) \; ,\end{aligned} \tag{3.25}$$

where $\partial^\mu(\overline{\nu'}\gamma_\mu\nu') = 0$ has been used. Then we substitute $\mathcal{L}_\nu$ into the Euler-Lagrange equation

$$\partial^\mu\frac{\partial\mathcal{L}_\nu}{\partial\left(\partial^\mu\overline{\nu'}\right)} - \frac{\partial\mathcal{L}_\nu}{\partial\overline{\nu'}} = 0 \tag{3.26}$$

and obtain the Dirac equation

$${\rm i}\gamma_\mu\partial^\mu\nu' - \widehat{M}_\nu\nu' = 0 \; . \tag{3.27}$$

More explicitly, ${\rm i}\gamma_\mu\partial^\mu\nu_k - m_k\nu_k = 0$ holds (for $k = 1, 2, 3$). That is why the factor 1/2 in $\mathcal{L}'_{\rm Majorana}$ makes sense.

The weak charged-current interactions of three neutrinos in Eq. (3.9) can now be rewritten in terms of their mass eigenstates $\nu'_{\rm L} = V^\dagger\nu_{\rm L}$. In the chosen basis where the flavor and mass eigenstates of three charged leptons are identical, the expression of $\mathcal{L}_{\rm cc}$ for Majorana neutrinos is the same as

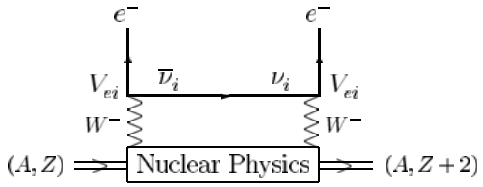

Fig. 3.6 The $0\nu2\beta$ decay of some even-even nuclei via the exchange of virtual Majorana neutrinos between two beta decays

that given in Eq. (3.16) for Dirac neutrinos. The unitary matrix V is just the 3×3 Majorana neutrino mixing matrix, which contains two more irremovable CP-violating phases than the 3×3 Dirac neutrino mixing matrix (see Section 3.5 for detailed discussions).

The most salient feature of massive Majorana neutrinos is lepton number violation. Let us make the global phase transformations

$$l(x) \to \mathrm{e}^{\mathrm{i}\Phi} l(x) \; , \quad \nu'_{\mathrm{L}}(x) \to \mathrm{e}^{\mathrm{i}\Phi} \nu'_{\mathrm{L}}(x) \; , \tag{3.28}$$

where l stands for the column vector of e, μ and τ fields, and Φ is an arbitrary spacetime-independent phase. One can immediately see that the kinetic term $\mathcal{L}_{\rm kinetic}$ and the charged-current interaction term $\mathcal{L}_{\rm cc}$ are invariant under these transformations, but the mass term $\mathcal{L}'_{\rm Majorana}$ is not invariant because of both $\overline{\nu'_{\mathrm{L}}} \to \mathrm{e}^{-\mathrm{i}\Phi} \overline{\nu'_{\mathrm{L}}}$ and $(\nu'_{\mathrm{L}})^c \to \mathrm{e}^{-\mathrm{i}\Phi} (\nu'_{\mathrm{L}})^c$. The lepton number is therefore violated for massive Majorana neutrinos. Similar to the case of Dirac neutrinos, the lepton flavor violation of Majorana neutrinos is described by V.

The $0\nu2\beta$ decay $(A, Z) \to (A, Z+2) + 2e^-$ is a clean signature of the Majorana nature of massive neutrinos. Fig. 3.6 shows that this lepton-number-violating process can occur when there exists neutrino-antineutrino mixing induced by the Majorana mass term (i.e., the neutrino mass eigenstates are self-conjugate, $\overline{\nu}_i = \nu_i$). The effective mass of the $0\nu2\beta$ decay is defined as

$$\langle m \rangle_{ee} \equiv \left| \sum_i m_i V_{ei}^2 \right| \; , \tag{3.29}$$

where m_i comes from the helicity suppression factor m_i/E for the $\nu_i = \overline{\nu}_i$ exchange between two ordinary beta decays with E being the energy of the virtual ν_i or $\overline{\nu}_i$. Current experimental data only yield an upper bound $\langle m \rangle_{ee} < 0.23$ eV (or < 0.85 eV as a more conservative bound) at the 2σ level (Fogli *et al.*, 2008a).

3.2.3 Hybrid Mass Terms and Seesaw Mechanisms

Similar to Eq. (3.18), N_{R} and its charge-conjugate counterpart $(N_{\mathrm{R}})^c$ can also form a Majorana mass term. Hence it is possible to write out the following hybrid neutrino mass terms in terms of ν_{L}, N_{R}, $(\nu_{\mathrm{L}})^c$ and $(N_{\mathrm{R}})^c$ fields:

$$
\begin{aligned}
-\mathcal{L}'_{\rm hybrid} &= \overline{\nu_{\rm L}} M_{\rm D} N_{\rm R} + \frac{1}{2}\overline{\nu_{\rm L}} M_{\rm L} (\nu_{\rm L})^c + \frac{1}{2}\overline{(N_{\rm R})^c} M_{\rm R} N_{\rm R} + {\rm h.c.} \\
&= \frac{1}{2} \left[\overline{\nu_{\rm L}} \;\; \overline{(N_{\rm R})^c} \right] \begin{pmatrix} M_{\rm L} & M_{\rm D} \\ M_{\rm D}^T & M_{\rm R} \end{pmatrix} \begin{bmatrix} (\nu_{\rm L})^c \\ N_{\rm R} \end{bmatrix} + {\rm h.c.} \; , \qquad (3.30)
\end{aligned}
$$

where $M_{\rm L}$ and $M_{\rm R}$ are symmetric mass matrices because the corresponding mass terms are of the Majorana type, and the relationship

$$
\overline{(N_{\rm R})^c} M_{\rm D}^T (\nu_{\rm L})^c = \left[(N_{\rm R})^T \mathcal{C} M_{\rm D}^T \mathcal{C} \overline{\nu_{\rm L}}^T \right]^T = \overline{\nu_{\rm L}} M_{\rm D} N_{\rm R} \qquad (3.31)
$$

has been used. The overall 6×6 mass matrix in Eq. (3.30) is also symmetric and can be diagonalized by a 6×6 unitary matrix through the transformation

$$
\begin{pmatrix} V & R \\ S & U \end{pmatrix}^\dagger \begin{pmatrix} M_{\rm L} & M_{\rm D} \\ M_{\rm D}^T & M_{\rm R} \end{pmatrix} \begin{pmatrix} V & R \\ S & U \end{pmatrix}^* = \begin{pmatrix} \widehat{M}_\nu & \mathbf{0} \\ \mathbf{0} & \widehat{M}_N \end{pmatrix} \; , \qquad (3.32)
$$

where $\widehat{M}_\nu \equiv {\rm Diag}\{m_1, m_2, m_3\}$, $\widehat{M}_N \equiv {\rm Diag}\{M_1, M_2, M_3\}$, and the 3×3 sub-matrices V, R, S and U satisfy the unitarity conditions

$$
\begin{aligned}
& V V^\dagger + R R^\dagger = S S^\dagger + U U^\dagger = \mathbf{1} \; , \\
& V^\dagger V + S^\dagger S = R^\dagger R + U^\dagger U = \mathbf{1} \; , \\
& V S^\dagger + R U^\dagger = V^\dagger R + S^\dagger U = \mathbf{0} \; . \qquad (3.33)
\end{aligned}
$$

After this diagonalization, Eq. (3.30) becomes

$$
-\mathcal{L}'_{\rm hybrid} = \frac{1}{2} \left[\overline{\nu'_{\rm L}} \;\; \overline{(N'_{\rm R})^c} \right] \begin{pmatrix} \widehat{M}_\nu & \mathbf{0} \\ \mathbf{0} & \widehat{M}_N \end{pmatrix} \begin{bmatrix} (\nu'_{\rm L})^c \\ N'_{\rm R} \end{bmatrix} + {\rm h.c.} \; , \qquad (3.34)
$$

where $\nu'_{\rm L} = V^\dagger \nu_{\rm L} + S^\dagger (N_{\rm R})^c$ and $N'_{\rm R} = R^T (\nu_{\rm L})^c + U^T N_{\rm R}$ together with $(\nu'_{\rm L})^c = \mathcal{C} \overline{\nu'_{\rm L}}^T$ and $(N'_{\rm R})^c = \mathcal{C} \overline{N'_{\rm R}}^T$. Then the field

$$
\nu' = \begin{bmatrix} \nu'_{\rm L} \\ (N'_{\rm R})^c \end{bmatrix} + \begin{bmatrix} (\nu'_{\rm L})^c \\ N'_{\rm R} \end{bmatrix} = \begin{pmatrix} \nu_1 \\ \nu_2 \\ \nu_3 \\ N_1 \\ N_2 \\ N_3 \end{pmatrix} \qquad (3.35)
$$

satisfies the Majorana condition $(\nu')^c = \nu'$ and describes the mass eigenstates of six Majorana neutrinos. In other words,

$$
-\mathcal{L}'_{\rm hybrid} = \frac{1}{2} \overline{\nu'} \begin{pmatrix} \widehat{M}_\nu & \mathbf{0} \\ \mathbf{0} & \widehat{M}_N \end{pmatrix} \nu' = \frac{1}{2} \sum_{i=1}^{3} \left(m_i \overline{\nu_i} \nu_i + M_i \overline{N_i} N_i \right) \; . \qquad (3.36)
$$

Because of $\nu_{\rm L} = V \nu'_{\rm L} + R (N'_{\rm R})^c$ and $N_{\rm R} = S^* (\nu'_{\rm L})^c + U^* N'_{\rm R}$, we immediately have $(\nu_{\rm L})^c = V^* (\nu'_{\rm L})^c + R^* N'_{\rm R}$ and $(N_{\rm R})^c = S \nu'_{\rm L} + U (N'_{\rm R})^c$. Given the relations $\overline{(\psi_{\rm L})^c} \gamma_\mu \partial^\mu (\psi_{\rm L})^c = \overline{\psi_{\rm L}} \gamma_\mu \partial^\mu \psi_{\rm L}$ and $\overline{(\psi_{\rm R})^c} \gamma_\mu \partial^\mu (\psi_{\rm R})^c = \overline{\psi_{\rm R}} \gamma_\mu \partial^\mu \psi_{\rm R}$ for an arbitrary fermion field ψ, the kinetic term of Majorana neutrinos reads

$$
\begin{aligned}
\mathcal{L}_{\rm kinetic} &= {\rm i}\overline{\nu_{\rm L}}\gamma_\mu\partial^\mu\nu_{\rm L} + {\rm i}\overline{N_{\rm R}}\gamma_\mu\partial^\mu N_{\rm R} \\
&= \frac{\rm i}{2}\left[\overline{\nu_{\rm L}} \;\; \overline{(N_{\rm R})^c}\right]\gamma_\mu\partial^\mu\begin{bmatrix}\nu_{\rm L} \\ (N_{\rm R})^c\end{bmatrix} + \frac{\rm i}{2}\left[\overline{(\nu_{\rm L})^c} \;\; \overline{N_{\rm R}}\right]\gamma_\mu\partial^\mu\begin{bmatrix}(\nu_{\rm L})^c \\ N_{\rm R}\end{bmatrix} \\
&= \frac{\rm i}{2}\left[\overline{\nu'_{\rm L}} \;\; \overline{(N'_{\rm R})^c}\right]\gamma_\mu\partial^\mu\begin{pmatrix}V & R \\ S & U\end{pmatrix}^\dagger\begin{pmatrix}V & R \\ S & U\end{pmatrix}\begin{bmatrix}\nu'_{\rm L} \\ (N'_{\rm R})^c\end{bmatrix} \\
&\quad + \frac{\rm i}{2}\left[\overline{(\nu'_{\rm L})^c} \;\; \overline{N'_{\rm R}}\right]\gamma_\mu\partial^\mu\begin{pmatrix}V & R \\ S & U\end{pmatrix}^T\begin{pmatrix}V & R \\ S & U\end{pmatrix}^*\begin{bmatrix}(\nu'_{\rm L})^c \\ N'_{\rm R}\end{bmatrix} \\
&= \frac{\rm i}{2}\left[\overline{\nu'_{\rm L}} \;\; \overline{(N'_{\rm R})^c}\right]\gamma_\mu\partial^\mu\begin{bmatrix}\nu'_{\rm L} \\ (N'_{\rm R})^c\end{bmatrix} + \frac{\rm i}{2}\left[\overline{(\nu'_{\rm L})^c} \;\; \overline{N'_{\rm R}}\right]\gamma_\mu\partial^\mu\begin{bmatrix}(\nu'_{\rm L})^c \\ N'_{\rm R}\end{bmatrix} \\
&= {\rm i}\overline{\nu'_{\rm L}}\gamma_\mu\partial^\mu\nu'_{\rm L} + {\rm i}\overline{N'_{\rm R}}\gamma_\mu\partial^\mu N'_{\rm R} \\
&= \frac{\rm i}{2}\overline{\nu'}\gamma_\mu\partial^\mu\nu' = \frac{\rm i}{2}\sum_{k=1}^{3}\left(\overline{\nu_k}\gamma_\mu\partial^\mu\nu_k + \overline{N_k}\gamma_\mu\partial^\mu N_k\right) \; , \qquad (3.37)
\end{aligned}
$$

where the unitarity conditions given in Eq. (3.33) have been used.

The weak charged-current interactions of active neutrinos in Eq. (3.9) can now be rewritten in terms of the mass eigenstates of six Majorana neutrinos via $\nu_{\rm L} = V\nu'_{\rm L} + R(N'_{\rm R})^c$. In the chosen basis where the flavor and mass eigenstates of three charged leptons are identical, we have

$$
\mathcal{L}_{\rm cc} = \frac{g}{\sqrt{2}}\overline{(e \;\; \mu \;\; \tau)_{\rm L}}\;\gamma^\mu\left[V\begin{pmatrix}\nu_1 \\ \nu_2 \\ \nu_3\end{pmatrix}_{\rm L} + R\begin{pmatrix}N_1 \\ N_2 \\ N_3\end{pmatrix}_{\rm L}\right]W^-_\mu + {\rm h.c.} \; . \qquad (3.38)
$$

Note that V and R are responsible for the charged-current interactions of three known neutrinos ν_i and three new neutrinos N_i (for $i = 1, 2, 3$), respectively. Their correlation is described by $VV^\dagger + RR^\dagger = \mathbf{1}$, and thus V is not unitary unless ν_i and N_i are completely decoupled (i.e., $R = \mathbf{0}$). A parametrization of V and R in terms of some mixing angles and CP-violating phases will be presented in section 4.5.2 (Xing, 2008b).

As a consequence of lepton number violation, the $0\nu2\beta$ decay $(A, Z) \to (A, Z + 2) + 2e^-$ can now take place via the exchanges of both ν_i and N_i between two beta decays, whose coupling matrix elements are V_{ei} and R_{ei} respectively. The relative contributions of ν_i and N_i to this lepton-number-violating process depend not only on m_i, M_i, V_{ei} and R_{ei} but also on the relevant nuclear matrix elements which cannot be reliably evaluated (Haxton and Stephenson, 1984). For a realistic seesaw mechanism working at the TeV scale (i.e., $M_i \sim \mathcal{O}(1)$ TeV) or at a superhigh-energy scale, however, the contribution of ν_i to the $0\nu2\beta$ decay is in most cases dominant (Xing, 2009b).

The hybrid neutrino mass terms in Eq. (3.30) provide us with the necessary ingredients of a dynamic mechanism to interpret why three known neutrinos have nonzero but tiny masses. The key point is that the mass scales of $M_{\rm L}$, $M_{\rm D}$ and $M_{\rm R}$ may have a strong hierarchy. First, $M_{\rm D} \sim \langle H\rangle \approx 174$ GeV is naturally characterized by the electroweak symmetry breaking scale.

Second, $M_{\rm L} \ll \langle H \rangle$ satisfies 't Hooft's naturalness criterion ('t Hooft, 1980) because this Majorana mass term violates lepton number conservation. Third, $M_{\rm R} \gg \langle H \rangle$ is naturally expected since right-handed neutrinos are $SU(2)_{\rm L}$ gauge singlets and thus their mass term is not subject to the electroweak symmetry breaking scale. The hierarchy $M_{\rm R} \gg M_{\rm D} \gg M_{\rm L}$ can therefore allow us to make reliable approximations in deriving the effective mass matrix of three active neutrinos $(\nu_e, \nu_\mu, \nu_\tau)$ from Eq. (3.32). The latter yields

$$\begin{aligned} R\widehat{M}_N &= M_{\rm L} R^* + M_{\rm D} U^* \; , \\ S\widehat{M}_\nu &= M_{\rm D}^T V^* + M_{\rm R} S^* \; ; \end{aligned} \tag{3.39}$$

and

$$\begin{aligned} U\widehat{M}_N &= M_{\rm R} U^* + M_{\rm D}^T R^* \; , \\ V\widehat{M}_\nu &= M_{\rm L} V^* + M_{\rm D} S^* \; . \end{aligned} \tag{3.40}$$

Given $M_{\rm R} \gg M_{\rm D} \gg M_{\rm L}$, $R \sim S \sim \mathcal{O}(M_{\rm D}/M_{\rm R})$ naturally holds, implying that U and V are almost unitary up to the accuracy of $\mathcal{O}(M_{\rm D}^2/M_{\rm R}^2)$ (Xing and Zhou, 2006). Hence Eq. (3.40) leads to

$$\begin{aligned} U\widehat{M}_N U^T &= M_{\rm R} (UU^\dagger)^T + M_{\rm D}^T (R^* U^T) \approx M_{\rm R} \; , \\ V\widehat{M}_\nu V^T &= M_{\rm L} (VV^\dagger)^T + M_{\rm D} (S^* V^T) \; \approx M_{\rm L} + M_{\rm D} (S^* V^T) \; . \end{aligned} \tag{3.41}$$

Note that $S^* V^T = M_{\rm R}^{-1} S \widehat{M}_\nu V^T - M_{\rm R}^{-1} M_{\rm D}^T (VV^\dagger)^T \approx -M_{\rm R}^{-1} M_{\rm D}^T$ can be derived from Eq. (3.39). We substitute this expression into Eq. (3.41) and then obtain

$$M_\nu \equiv V \widehat{M}_\nu V^T \approx M_{\rm L} - M_{\rm D} M_{\rm R}^{-1} M_{\rm D}^T \; . \tag{3.42}$$

This result, known as the type-(I+II) seesaw relation, is just the effective mass matrix of three light neutrinos. The small mass scale of M_ν is attributed to the small mass scale of $M_{\rm L}$ and the large mass scale of $M_{\rm R}$. There are two particularly interesting limits.

- If the mass term $M_{\rm L}$ is absent from Eq. (3.30), one will be left with the canonical or type-I seesaw relation $M_\nu \approx -M_{\rm D} M_{\rm R}^{-1} M_{\rm D}^T$ (Fritzsch *et al.*, 1975; Minkowski, 1977; Yanagida, 1979; Gell-Mann *et al.*, 1979; Glashow, 1980; Mohapatra and Senjanovic, 1980).
- If only the mass term $M_{\rm L}$ is present in Eq. (3.30), one will be left with the type-II seesaw relation $M_\nu = M_{\rm L}$ (Konetschny and Kummer, 1977; Magg and Wetterich, 1980; Schechter and Valle, 1980; Cheng and Li, 1980; Lazarides *et al.*, 1981; Mohapatra and Senjanovic, 1981).

More detailed discussions about various seesaw mechanisms and their phenomenological consequences will be presented in Chapter 4.

3.3 C, P and T Properties of Fermion Fields

CP violation is one of a few central concepts in flavor physics. The phenomenon of CP violation was first observed by James Cronin and Val Fitch in the decay mode $K_{\rm L} \to \pi^+\pi^-$ (Christenson *et al.*, 1964). Large CP-violating effects were predicted to appear in a variety of B-meson decays based on the Kobayashi-Maskawa mechanism of CP violation within the SM (Kobayashi and Maskawa, 1973), and they were observed to a good degree of accuracy at B-meson factories (Aubert *et al.*, 2001; Abe *et al.*, 2001). Nevertheless, the magnitude of CP violation in the quark sector is insufficient to account for the cosmological matter-antimatter asymmetry. Hence one wonders whether there is CP violation in the lepton sector and whether it can account for the observed baryon-antibaryon asymmetry of the Universe. We shall see in Chapter 11 that it is possible to realize baryogenesis via leptogenesis thanks to CP violation in the neutrino sector,

In this section we shall first discuss the C, P, T, CP and CPT properties of quark and lepton fields, and then diagnose both the origin of CP violation in the quark sector of the SM and that in the lepton sector for a minimal extension of the SM to accommodate finite neutrino masses. It will be demonstrated that CP violation arises from the coexistence of the charged-current interactions of fermions with the $W^\pm$ bosons and the Yukawa interactions of fermions with the Higgs boson.

3.3.1 C, P and T Transformations of Spinor Bilinears

We begin with a brief summary of the transformation properties of quantum fields under the discrete space-time symmetries of parity (P), charge conjugation (C) and time reversal (T). The parity transformation changes the space coordinates $\mathbf{x}$ into $-\mathbf{x}$. The charge conjugation flips the signs of internal charges of a particle, such as the electric charge and the lepton (baryon) number. The time reversal reflects the time coordinate t into $-t$. The transformation properties of scalar (S), pseudoscalar (P), vector (V_μ) and pseudovector (A_μ) fields under C, P and T, which are summarized in Table 3.4, have been discussed in detail in some literature (Jarlskog, 1989; Peskin and Schroeder, 1995; Branco *et al.*, 1999; Bigi and Sanda, 2000). Note that V_μ annihilates a vector particle and creates its antiparticle, while $V_\mu^\dagger$ does the opposite operation. So do S, P, A_μ and $S^\dagger$, $P^\dagger$, $A_\mu^\dagger$. Hence the roles of particles and antiparticles are interchanged under C.

A free Dirac spinor $\psi(t,\mathbf{x})$ or $\overline{\psi}(t,\mathbf{x})$ transforms under C, P and T as [4]

$$\psi(t,\mathbf{x}) \stackrel{\rm C}{\longrightarrow} \mathcal{C}\overline{\psi}^T(t,\mathbf{x}) \; , \qquad \overline{\psi}(t,\mathbf{x}) \stackrel{\rm C}{\longrightarrow} -\psi^T(t,\mathbf{x})\mathcal{C}^{-1} \; ,$$

[4] For simplicity, here we have omitted a phase factor associated with each transformation. Because one is always interested in the spinor bilinears, the relevant phase factor usually plays no physical role.

Table 3.4 Transformation properties of scalar (S), pseudoscalar (P), vector (V_μ) and pseudovector (A_μ) fields under C, P and T

	$S(t,\mathbf{x})$	$P(t,\mathbf{x})$	$V_\mu(t,\mathbf{x})$	$A_\mu(t,\mathbf{x})$
C	$S^\dagger(t,\mathbf{x})$	$P^\dagger(t,\mathbf{x})$	$-V_\mu^\dagger(t,\mathbf{x})$	$A_\mu^\dagger(t,\mathbf{x})$
P	$S(t,-\mathbf{x})$	$-P(t,-\mathbf{x})$	$V^\mu(t,-\mathbf{x})$	$-A^\mu(t,-\mathbf{x})$
T	$S(-t,\mathbf{x})$	$P(-t,\mathbf{x})$	$V^\mu(-t,\mathbf{x})$	$A^\mu(-t,\mathbf{x})$
CP	$S^\dagger(t,-\mathbf{x})$	$-P^\dagger(t,-\mathbf{x})$	$-V^{\mu\,\dagger}(t,-\mathbf{x})$	$-A^{\mu\,\dagger}(t,-\mathbf{x})$
CPT	$S^\dagger(-t,-\mathbf{x})$	$-P^\dagger(-t,-\mathbf{x})$	$-V_\mu^\dagger(-t,-\mathbf{x})$	$-A_\mu^\dagger(-t,-\mathbf{x})$

$$\begin{aligned}
&\psi(t,\mathbf{x}) \xrightarrow{\rm P} \mathcal{P}\psi(t,-\mathbf{x})\;, \quad && \overline{\psi}(t,\mathbf{x}) \xrightarrow{\rm P} \overline{\psi}(t,-\mathbf{x})\mathcal{P}^\dagger\;,\\
&\psi(t,\mathbf{x}) \xrightarrow{\rm T} \mathcal{T}\psi(-t,\mathbf{x})\;, \quad && \overline{\psi}(t,\mathbf{x}) \xrightarrow{\rm T} \overline{\psi}(-t,\mathbf{x})\mathcal{T}^\dagger\;,
\end{aligned} \tag{3.43}$$

where $\mathcal{C} = {\rm i}\gamma_2\gamma_0$, $\mathcal{P} = \gamma_0$ and $\mathcal{T} = \gamma_1\gamma_3$ in the Dirac-Pauli representation. These transformation properties can simply be deduced from the requirement that the Dirac equation ${\rm i}\gamma_\mu\partial^\mu\psi(t,\mathbf{x}) = m\psi(t,\mathbf{x})$ be invariant under C, P or T operation. Note that all the classical numbers (or c-numbers), such as the coupling constants and γ-matrix elements, must be complex-conjugated under T. Note also that the charge-conjugation matrix $\mathcal{C}$ satisfies the conditions given in Eq. (3.8). It is very important to figure out how the Dirac spinor bilinears transform under C, P and T, because both leptons and quarks are described by spinor fields and they always appear in the bilinear forms in a Lorentz-invariant Lagrangian. Let us consider the following scalar-, pseudoscalar-, vector-, pseudovector- and tensor-like spinor bilinears:

$$\overline{\psi_1}\psi_2\;, \quad {\rm i}\overline{\psi_1}\gamma_5\psi_2\;, \quad \overline{\psi_1}\gamma_\mu\psi_2\;, \quad \overline{\psi_1}\gamma_\mu\gamma_5\psi_2\;, \quad \overline{\psi_1}\sigma_{\mu\nu}\psi_2\;, \tag{3.44}$$

where $\sigma_{\mu\nu} \equiv {\rm i}[\gamma_\mu,\gamma_\nu]/2$ is defined. One may easily verify that all these bilinears are Hermitian, if $\psi_1 = \psi_2$ is taken. Under C, P and T, for example,

$$\begin{aligned}
&\overline{\psi_1}\gamma_\mu\psi_2 \xrightarrow{\rm C} -\psi_1^T\mathcal{C}^{-1}\gamma_\mu\mathcal{C}\overline{\psi_2}^T = \psi_1^T\gamma_\mu^T\overline{\psi_2}^T = -\left[\overline{\psi_2}\gamma_\mu\psi_1\right]^T = -\overline{\psi_2}\gamma_\mu\psi_1\;,\\
&\overline{\psi_1}\gamma_\mu\psi_2 \xrightarrow{\rm P} \overline{\psi_1}\gamma_0\gamma_\mu\gamma_0\psi_2 = \overline{\psi_1}\gamma^\mu\psi_2\;,\\
&\overline{\psi_1}\gamma_\mu\psi_2 \xrightarrow{\rm T} \overline{\psi_1}\left(\gamma_1\gamma_3\right)^\dagger\gamma_\mu^*\left(\gamma_1\gamma_3\right)\psi_2 = \overline{\psi_1}\gamma^\mu\psi_2\;;
\end{aligned} \tag{3.45}$$

and thus

$$\overline{\psi_1}\gamma_\mu\psi_2 \xrightarrow{\rm CP} -\overline{\psi_2}\gamma^\mu\psi_1\;, \quad \overline{\psi_1}\gamma_\mu\psi_2 \xrightarrow{\rm CPT} -\overline{\psi_2}\gamma_\mu\psi_1\;, \tag{3.46}$$

with $\mathbf{x} \to -\mathbf{x}$ under P and $t \to -t$ under T for ψ_1 and ψ_2. The transformation properties of five spinor bilinears under C, P, T, CP and CPT are summarized in Table 3.5, where one should keep in mind that all the c-numbers are complex-conjugated under T and CPT. Comparing between Table 3.4 and

Table 3.5, we arrive at $S(t,\mathbf{x}) = \overline{\psi_1}(t,\mathbf{x})\psi_2(t,\mathbf{x})$, $P(t,\mathbf{x}) = \overline{\psi_1}(t,\mathbf{x})\gamma_5\psi_2(t,\mathbf{x})$, $V_\mu(t,\mathbf{x}) = \overline{\psi_1}(t,\mathbf{x})\gamma_\mu\psi_2(t,\mathbf{x})$ and $A_\mu(t,\mathbf{x}) = \overline{\psi_1}(t,\mathbf{x})\gamma_\mu\gamma_5\psi_2(t,\mathbf{x})$, corresponding to scalar, pseudoscalar, vector and pseudovector fields. Note that $\overline{\psi}(t,\mathbf{x})\gamma_5\psi(t,\mathbf{x})$ itself is not Hermitian, but $\mathrm{i}\overline{\psi}(t,\mathbf{x})\gamma_5\psi(t,\mathbf{x})$ is Hermitian just because it contains i.

Table 3.5 Transformation properties of the scalar-, pseudoscalar-, vector-, pseudovector- and tensor-like spinor bilinears under C, P and T. Here $\mathbf{x} \to -\mathbf{x}$ under P, CP and CPT, together with $t \to -t$ under T and CPT, is hidden and self-explaining for ψ_1 and ψ_2

	$\overline{\psi_1}\psi_2$	$\mathrm{i}\overline{\psi_1}\gamma_5\psi_2$	$\overline{\psi_1}\gamma_\mu\psi_2$	$\overline{\psi_1}\gamma_\mu\gamma_5\psi_2$	$\overline{\psi_1}\sigma_{\mu\nu}\psi_2$
C	$\overline{\psi_2}\psi_1$	$\mathrm{i}\overline{\psi_2}\gamma_5\psi_1$	$-\overline{\psi_2}\gamma_\mu\psi_1$	$\overline{\psi_2}\gamma_\mu\gamma_5\psi_1$	$-\overline{\psi_2}\sigma_{\mu\nu}\psi_1$
P	$\overline{\psi_1}\psi_2$	$-\mathrm{i}\overline{\psi_1}\gamma_5\psi_2$	$\overline{\psi_1}\gamma^\mu\psi_2$	$-\overline{\psi_1}\gamma^\mu\gamma_5\psi_2$	$\overline{\psi_1}\sigma^{\mu\nu}\psi_2$
T	$\overline{\psi_1}\psi_2$	$-\mathrm{i}\overline{\psi_1}\gamma_5\psi_2$	$\overline{\psi_1}\gamma^\mu\psi_2$	$\overline{\psi_1}\gamma^\mu\gamma_5\psi_2$	$-\overline{\psi_1}\sigma^{\mu\nu}\psi_2$
CP	$\overline{\psi_2}\psi_1$	$-\mathrm{i}\overline{\psi_2}\gamma_5\psi_1$	$-\overline{\psi_2}\gamma^\mu\psi_1$	$-\overline{\psi_2}\gamma^\mu\gamma_5\psi_1$	$-\overline{\psi_2}\sigma^{\mu\nu}\psi_1$
CPT	$\overline{\psi_2}\psi_1$	$\mathrm{i}\overline{\psi_2}\gamma_5\psi_1$	$-\overline{\psi_2}\gamma_\mu\psi_1$	$-\overline{\psi_2}\gamma_\mu\gamma_5\psi_1$	$\overline{\psi_2}\sigma_{\mu\nu}\psi_1$

It is well known that CPT is a good symmetry in a local quantum field theory which is Lorentz-invariant and possesses a Hermitian Lagrangian (Schwinger, 1951; Lüders, 1954; Pauli, 1955). The latter is necessary in order to have a unitary transition operator (i.e., the S-matrix). The CPT invariance of a theory implies that CP and T must be simultaneously conserving or broken, as already examined in the quark sector of the SM via the K^0-$\bar{K}^0$ mixing system (Nakamura *et al.*, 2010). After a slight modification of the SM by introducing the Dirac or Majorana mass term for three neutrinos, one may also look at possible sources of CP or T violation in the lepton sector.

3.3.2 CP Violation in Quark and Lepton Sectors

As discussed in Chapter 2, the SM of electroweak interactions is based on the $SU(2)_{\mathrm{L}} \times U(1)_{\mathrm{Y}}$ gauge symmetry and the Higgs mechanism. The latter triggers the spontaneous symmetry breaking $SU(2)_{\mathrm{L}} \times U(1)_{\mathrm{Y}} \to U(1)_{\mathrm{Q}}$, such that three gauge bosons, three charged leptons and six quarks can all acquire masses. But this mechanism itself does not spontaneously break CP, and thus one may examine the source of CP violation in the SM either before or after spontaneous symmetry breaking.

The Lagrangian of the SM $\mathcal{L} = \mathcal{L}_{\mathrm{G}} + \mathcal{L}_{\mathrm{H}} + \mathcal{L}_{\mathrm{F}} + \mathcal{L}_{\mathrm{Y}}$ is composed of four parts: the kinetic term of the gauge fields and their self-interactions ($\mathcal{L}_{\mathrm{G}}$), the kinetic term of the Higgs doublet and its potential and interactions with the

gauge fields ($\mathcal{L}_{\rm H}$), the kinetic term of the fermion fields and their interactions with the gauge fields ($\mathcal{L}_{\rm F}$), and the Yukawa interactions of the fermion fields with the Higgs doublet ($\mathcal{L}_{\rm Y}$):

$$\begin{aligned}
\mathcal{L}_{\rm G} &= -\frac{1}{4}\left(W^{i\mu\nu}W^{i}_{\mu\nu} + B^{\mu\nu}B_{\mu\nu}\right) \ , \\
\mathcal{L}_{\rm H} &= \left(D^{\mu}H\right)^{\dagger}\left(D_{\mu}H\right) - \mu^2 H^{\dagger}H - \lambda\left(H^{\dagger}H\right)^2 \ , \\
\mathcal{L}_{\rm F} &= \overline{Q_{\rm L}}{\rm i}\not{D}Q_{\rm L} + \overline{\ell_{\rm L}}{\rm i}\not{D}\ell_{\rm L} + \overline{U_{\rm R}}{\rm i}\not{\partial}' U_{\rm R} + \overline{D_{\rm R}}{\rm i}\not{\partial}' D_{\rm R} + \overline{E_{\rm R}}{\rm i}\not{\partial}' E_{\rm R} \ , \\
\mathcal{L}_{\rm Y} &= -\overline{Q_{\rm L}}Y_{\rm u}\tilde{H}U_{\rm R} - \overline{Q_{\rm L}}Y_{\rm d}HD_{\rm R} - \overline{\ell_{\rm L}}Y_{l}HE_{\rm R} + {\rm h.c.} \ ,
\end{aligned} \tag{3.47}$$

whose notations have been explained in Section 2.1.4. To accommodate finite neutrino masses, the simplest way is to slightly modify the $\mathcal{L}_{\rm F}$ and $\mathcal{L}_{\rm Y}$ parts of the SM (e.g., by introducing three right-handed neutrinos into the SM and allowing for the Yukawa interactions between neutrinos and the Higgs doublet). CP violation is due to the coexistence of $\mathcal{L}_{\rm F}$ and $\mathcal{L}_{\rm Y}$.

We first show that $\mathcal{L}_{\rm G}$ is always invariant under CP. The transformation properties of gauge fields B_{μ} and W^{i}_{μ} under C and P are

$$\begin{aligned}
\left[B_{\mu},\, W^{1}_{\mu},\, W^{2}_{\mu},\, W^{3}_{\mu}\right] &\xrightarrow{\rm C} \left[-B_{\mu},\, -W^{1}_{\mu},\, +W^{2}_{\mu},\, -W^{3}_{\mu}\right] \ , \\
\left[B_{\mu},\, W^{1}_{\mu},\, W^{2}_{\mu},\, W^{3}_{\mu}\right] &\xrightarrow{\rm P} \left[B^{\mu},\, W^{1\mu},\, W^{2\mu},\, W^{3\mu}\right] \ , \\
\left[B_{\mu},\, W^{1}_{\mu},\, W^{2}_{\mu},\, W^{3}_{\mu}\right] &\xrightarrow{\rm CP} \left[-B^{\mu},\, -W^{1\mu},\, +W^{2\mu},\, -W^{3\mu}\right]
\end{aligned} \tag{3.48}$$

with $\mathbf{x} \to -\mathbf{x}$ under P and CP for relevant fields. Then the gauge field tensors $B_{\mu\nu}$ and $W^{i}_{\mu\nu}$ transform under CP as follows:

$$\left[B_{\mu\nu},\, W^{1}_{\mu\nu},\, W^{2}_{\mu\nu},\, W^{3}_{\mu\nu}\right] \xrightarrow{\rm CP} \left[-B^{\mu\nu},\, -W^{1\mu\nu},\, +W^{2\mu\nu},\, -W^{3\mu\nu}\right] \ . \tag{3.49}$$

Hence $\mathcal{L}_{\rm G}$ is formally invariant under CP.

We proceed to show that $\mathcal{L}_{\rm H}$ is also invariant under CP. The Higgs doublet H contains two scalar components ϕ^{+} and ϕ^{0}; i.e.,

$$H = \begin{pmatrix} \phi^{+} \\ \phi^{0} \end{pmatrix} \ , \quad H^{\dagger} = \begin{pmatrix} \phi^{-} & \phi^{0*} \end{pmatrix} \ . \tag{3.50}$$

One can directly read off the transformation properties of $\phi^{\pm}$ and ϕ^{0} under CP from Table 3.4. Therefore,

$$H(t,\mathbf{x}) \xrightarrow{\rm CP} H^{*}(t,-\mathbf{x}) = \begin{pmatrix} \phi^{-} \\ \phi^{0*} \end{pmatrix} \ . \tag{3.51}$$

It is very trivial to prove that the $H^{\dagger}H$ and $(H^{\dagger}H)^2$ terms of $\mathcal{L}_{\rm H}$ are CP-invariant. To examine how the $(D^{\mu}H)^{\dagger}(D_{\mu}H)$ term of $\mathcal{L}_{\rm H}$ transforms under CP, we explicitly write out

$$D_\mu H = \left(\partial_\mu - \mathrm{i}g\tau^k W_\mu^k - \mathrm{i}g' Y B_\mu\right) H = \begin{pmatrix} \partial_\mu \phi^+ - \mathrm{i}X_\mu^+ \phi^0 - \mathrm{i}Y_\mu^+ \phi^+ \\ \partial_\mu \phi^0 - \mathrm{i}X_\mu^- \phi^+ + \mathrm{i}Y_\mu^- \phi^0 \end{pmatrix} \quad (3.52)$$

with $X_\mu^\pm \equiv gW_\mu^\pm/\sqrt{2} = g(W_\mu^1 \mp \mathrm{i}W_\mu^2)/2$ and $Y_\mu^\pm \equiv \pm g' Y B_\mu + gW_\mu^3/2$. Then

$$\begin{aligned} \left(D^\mu H\right)^\dagger \left(D_\mu H\right) = {} & \partial^\mu \phi^- \partial_\mu \phi^+ - \mathrm{i}\partial^\mu \phi^- X_\mu^+ \phi^0 - \mathrm{i}\partial^\mu \phi^- Y_\mu^+ \phi^+ \\ & + \mathrm{i}X^{-\mu} \phi^{0^*} \partial_\mu \phi^+ + X^{-\mu} X_\mu^+ |\phi^0|^2 + X^{-\mu} \phi^{0^*} Y_\mu^+ \phi^+ \\ & + \mathrm{i}Y^{+\mu} \phi^- \partial_\mu \phi^+ + Y^{+\mu} X_\mu^+ \phi^- \phi^0 + Y^{+\mu} Y_\mu^+ |\phi^+|^2 \\ & + \partial^\mu \phi^{0^*} \partial_\mu \phi^0 - \mathrm{i}\partial^\mu \phi^{0^*} X_\mu^- \phi^+ + \mathrm{i}\partial^\mu \phi^{0^*} Y_\mu^- \phi^0 \\ & + \mathrm{i}X^{+\mu} \phi^- \partial_\mu \phi^0 + X^{+\mu} X_\mu^- |\phi^+|^2 - X^{+\mu} \phi^- Y_\mu^- \phi^0 \\ & - \mathrm{i}Y^{-\mu} \phi^{0^*} \partial_\mu \phi^0 - Y^{-\mu} X_\mu^- \phi^{0^*} \phi^+ + Y^{-\mu} Y_\mu^- |\phi^0|^2 \ . \end{aligned} \quad (3.53)$$

Note that

$$X_\mu^\pm \xrightarrow{\text{CP}} -X^{\mp\mu} \ , \qquad Y_\mu^\pm \xrightarrow{\text{CP}} -Y^{\pm\mu} \ , \quad (3.54)$$

together with $\partial_\mu \to \partial^\mu$, $\phi^\pm \to \phi^\mp$ and $\phi^0 \to \phi^{0^*}$ under CP. So $(D^\mu H)^\dagger (D_\mu H)$ is also CP-invariant. Therefore, $\mathcal{L}_\mathrm{H}$ is formally invariant under CP.

The next step is to examine the CP invariance of $\mathcal{L}_\mathrm{F}$. To be more specific, we divide $\mathcal{L}_\mathrm{F}$ into the quark sector and the lepton sector; i.e., $\mathcal{L}_\mathrm{F} = \mathcal{L}_q + \mathcal{L}_l$. We only analyze the CP property of $\mathcal{L}_q$ in the following, because that of $\mathcal{L}_l$ can be analyzed in the same way. The explicit form of $\mathcal{L}_q$ reads

$$\begin{aligned} \mathcal{L}_q &= \overline{Q_\mathrm{L}} \mathrm{i}\not{\partial} Q_\mathrm{L} + \overline{U_\mathrm{R}} \mathrm{i}\not{\partial}' U_\mathrm{R} + \overline{D_\mathrm{R}} \mathrm{i}\not{\partial}' D_\mathrm{R} \\ &= \sum_{j=1}^{3} \left[\overline{\left(q_j \ q_j'\right)_\mathrm{L}} \mathrm{i}\gamma^\mu \left(\partial_\mu - \mathrm{i}g\tau^k W_\mu^k - \mathrm{i}\frac{g'}{6} B_\mu\right) \begin{pmatrix} q_j \\ q_j' \end{pmatrix}_\mathrm{L} \right. \\ &\quad \left. + \overline{q_{j\mathrm{R}}} \mathrm{i}\gamma^\mu \left(\partial_\mu - \mathrm{i}\frac{2g'}{3} B_\mu\right) q_{j\mathrm{R}} + \overline{q_{j\mathrm{R}}'} \mathrm{i}\gamma^\mu \left(\partial_\mu + \mathrm{i}\frac{g'}{3} B_\mu\right) q_{j\mathrm{R}}' \right] \\ &= \sum_{j=1}^{3} \left\{ \frac{g}{4} \left[\overline{q_j'} \gamma^\mu \left(1 - \gamma_5\right) W_\mu^1 q_j + \overline{q_j} \gamma^\mu \left(1 - \gamma_5\right) W_\mu^1 q_j' \right] \right. \\ &\quad + \frac{g}{4} \left[\mathrm{i}\overline{q_j'} \gamma^\mu \left(1 - \gamma_5\right) W_\mu^2 q_j - \mathrm{i}\overline{q_j} \gamma^\mu \left(1 - \gamma_5\right) W_\mu^2 q_j' \right] \\ &\quad + \frac{g}{4} \left[\overline{q_j} \gamma^\mu \left(1 - \gamma_5\right) W_\mu^3 q_j - \overline{q_j'} \gamma^\mu \left(1 - \gamma_5\right) W_\mu^3 q_j' \right] \\ &\quad + \frac{\mathrm{i}}{2} \left[\overline{q_j} \gamma^\mu \left(1 - \gamma_5\right) \left(\partial_\mu - \mathrm{i}\frac{g'}{6} B_\mu\right) q_j \right] \\ &\quad + \frac{\mathrm{i}}{2} \left[\overline{q_j'} \gamma^\mu \left(1 - \gamma_5\right) \left(\partial_\mu - \mathrm{i}\frac{g'}{6} B_\mu\right) q_j' \right] \\ &\quad + \frac{\mathrm{i}}{2} \left[\overline{q_j} \gamma^\mu \left(1 + \gamma_5\right) \left(\partial_\mu - \mathrm{i}\frac{2g'}{3} B_\mu\right) q_j \right] \\ &\quad \left. + \frac{\mathrm{i}}{2} \left[\overline{q_j'} \gamma^\mu \left(1 + \gamma_5\right) \left(\partial_\mu + \mathrm{i}\frac{g'}{3} B_\mu\right) q_j' \right] \right\} \ , \end{aligned} \quad (3.55)$$

where q_j and q'_j (for $j = 1, 2, 3$) run over (u, c, t) and (d, s, b), respectively. The transformation properties of gauge fields B_μ and W^i_μ under C and P have been given in Eq. (3.48). With the help of Table 3.5, one can see that the relevant spinor bilinears transform under C and P as follows:

$$\begin{aligned}
\overline{\psi_1}\gamma_\mu\left(1 \pm \gamma_5\right)\psi_2 &\xrightarrow{\text{C}} -\overline{\psi_2}\gamma_\mu\left(1 \mp \gamma_5\right)\psi_1 \,, \\
\overline{\psi_1}\gamma_\mu\left(1 \pm \gamma_5\right)\psi_2 &\xrightarrow{\text{P}} +\overline{\psi_1}\gamma^\mu\left(1 \mp \gamma_5\right)\psi_2 \,, \\
\overline{\psi_1}\gamma_\mu\left(1 \pm \gamma_5\right)\psi_2 &\xrightarrow{\text{CP}} -\overline{\psi_2}\gamma^\mu\left(1 \pm \gamma_5\right)\psi_1 \,,
\end{aligned} \tag{3.56}$$

with $\mathbf{x} \to -\mathbf{x}$ under P and CP for ψ_1 and ψ_2. Furthermore,

$$\begin{aligned}
\overline{\psi_1}\gamma_\mu\left(1 \pm \gamma_5\right)\partial^\mu\psi_2 &\xrightarrow{\text{C}} \overline{\psi_2}\gamma_\mu\left(1 \mp \gamma_5\right)\partial^\mu\psi_1 \,, \\
\overline{\psi_1}\gamma_\mu\left(1 \pm \gamma_5\right)\partial^\mu\psi_2 &\xrightarrow{\text{P}} \overline{\psi_1}\gamma^\mu\left(1 \mp \gamma_5\right)\partial_\mu\psi_2 \,, \\
\overline{\psi_1}\gamma_\mu\left(1 \pm \gamma_5\right)\partial^\mu\psi_2 &\xrightarrow{\text{CP}} \overline{\psi_2}\gamma^\mu\left(1 \pm \gamma_5\right)\partial_\mu\psi_1 \,,
\end{aligned} \tag{3.57}$$

with $\mathbf{x} \to -\mathbf{x}$ under P and CP for ψ_1 and ψ_2. Then it is straightforward to check that $\mathcal{L}_q$ in Eq. (3.55) is formally invariant under CP. Following the same procedure and using Eqs. (3.48), (3.56) and (3.57), one can easily show that $\mathcal{L}_l = \overline{\ell_{\text{L}}}\text{i}\not{D}\ell_{\text{L}} + \overline{E_{\text{R}}}\text{i}\not{\partial}' E_{\text{R}}$ is also CP-invariant. Thus we conclude that $\mathcal{L}_{\text{F}}$ is invariant under CP.

The last step is to examine whether $\mathcal{L}_{\text{Y}}$ is CP-conserving or not. Explicitly,

$$\begin{aligned}
-\mathcal{L}_{\text{Y}} &= \overline{Q_{\text{L}}}Y_{\text{u}}\tilde{H}U_{\text{R}} + \overline{Q_{\text{L}}}Y_{\text{d}}HD_{\text{R}} + \overline{\ell_{\text{L}}}Y_l HE_{\text{R}} + \text{h.c.} \\
&= \sum_{j,k=1}^{3}\left[(Y_{\text{u}})_{jk}\overline{\left(q_j\ q'_j\right)_{\text{L}}}\begin{pmatrix}\phi^{0*}\\ -\phi^-\end{pmatrix}q_{k\text{R}} + (Y_{\text{d}})_{jk}\overline{\left(q_j\ q'_j\right)_{\text{L}}}\begin{pmatrix}\phi^+\\ \phi^0\end{pmatrix}q'_{k\text{R}}\right. \\
&\quad \left. + (Y_l)_{jk}\overline{\left(\nu_j\ l_j\right)_{\text{L}}}\begin{pmatrix}\phi^+\\ \phi^0\end{pmatrix}l_{k\text{R}} + \text{h.c.}\right] \\
&= \sum_{j,k=1}^{3}\left\{\frac{(Y_{\text{u}})_{jk}}{2}\left[\overline{q_j}\left(1+\gamma_5\right)q_k\phi^{0*} - \overline{q'_j}\left(1+\gamma_5\right)q_k\phi^-\right]\right. \\
&\quad + \frac{(Y_{\text{u}})^*_{jk}}{2}\left[\overline{q_k}\left(1-\gamma_5\right)q_j\phi^0 - \overline{q_k}\left(1-\gamma_5\right)q'_j\phi^+\right] \\
&\quad + \frac{(Y_{\text{d}})_{jk}}{2}\left[\overline{q_j}\left(1+\gamma_5\right)q'_k\phi^+ + \overline{q'_j}\left(1+\gamma_5\right)q'_k\phi^0\right] \\
&\quad + \frac{(Y_{\text{d}})^*_{jk}}{2}\left[\overline{q'_k}\left(1-\gamma_5\right)q_j\phi^- + \overline{q'_k}\left(1-\gamma_5\right)q'_j\phi^{0*}\right] \\
&\quad + \frac{(Y_l)_{jk}}{2}\left[\overline{\nu_j}\left(1+\gamma_5\right)l_k\phi^+ + \overline{l_j}\left(1+\gamma_5\right)l_k\phi^0\right] \\
&\quad \left. + \frac{(Y_l)^*_{jk}}{2}\left[\overline{l_k}\left(1-\gamma_5\right)\nu_j\phi^- + \overline{l_k}\left(1-\gamma_5\right)l_j\phi^{0*}\right]\right\} \,,
\end{aligned} \tag{3.58}$$

where q_j and q'_j (for $j = 1, 2, 3$) run over (u, c, t) and (d, s, b), respectively; while ν_j and l_j (for $j = 1, 2, 3$) run over $(\nu_e, \nu_\mu, \nu_\tau)$ and (e, μ, τ), respectively. Because of $\phi^\pm \to \phi^\mp$, $\phi^0 \to \phi^{0*}$ and $\overline{\psi_1}(1 \pm \gamma_5)\psi_2 \to \overline{\psi_2}(1 \mp \gamma_5)\psi_1$ under CP as shown in Tables 3.4 and 3.5, we immediately arrive at

$$\begin{aligned} -\mathcal{L}_{\rm Y} \xrightarrow{\rm CP} \sum_{j,k=1}^{3} \Bigg\{ & \frac{(Y_{\rm u})_{jk}}{2} \left[\overline{q_k} \, (1 - \gamma_5) \, q_j \phi^0 - \overline{q_k} \, (1 - \gamma_5) \, q'_j \phi^+ \right] \\ & + \frac{(Y_{\rm u})^*_{jk}}{2} \left[\overline{q_j} \, (1 + \gamma_5) \, q_k \phi^{0*} - \overline{q'_j} \, (1 + \gamma_5) \, q_k \phi^- \right] \\ & + \frac{(Y_{\rm d})_{jk}}{2} \left[\overline{q'_k} \, (1 - \gamma_5) \, q_j \phi^- + \overline{q'_k} \, (1 - \gamma_5) \, q'_j \phi^{0*} \right] \\ & + \frac{(Y_{\rm d})^*_{jk}}{2} \left[\overline{q_j} \, (1 + \gamma_5) \, q'_k \phi^+ + \overline{q'_j} \, (1 + \gamma_5) \, q'_k \phi^0 \right] \\ & + \frac{(Y_l)_{jk}}{2} \left[\overline{l_k} \, (1 - \gamma_5) \, \nu_j \phi^- + \overline{l_k} \, (1 - \gamma_5) \, l_j \phi^{0*} \right] \\ & + \frac{(Y_l)^*_{jk}}{2} \left[\overline{\nu_j} \, (1 + \gamma_5) \, l_k \phi^+ + \overline{l_j} \, (1 + \gamma_5) \, l_k \phi^0 \right] \Bigg\} \; , \end{aligned} \tag{3.59}$$

with $\mathbf{x} \to -\mathbf{x}$ for both scalar and spinor fields under consideration. Comparing between Eqs. (3.58) and (3.59), we see that $\mathcal{L}_{\rm Y}$ will be formally invariant under CP if the conditions

$$(Y_{\rm u})_{jk} = (Y_{\rm u})^*_{jk} \; , \quad (Y_{\rm d})_{jk} = (Y_{\rm d})^*_{jk} \; , \quad (Y_l)_{jk} = (Y_l)^*_{jk} \tag{3.60}$$

are satisfied. In other words, the Yukawa coupling matrices $Y_{\rm u}$, $Y_{\rm d}$ and Y_l must be real to guarantee the CP invariance of $\mathcal{L}_{\rm Y}$. Given three massless neutrinos in the SM, it is always possible to make Y_l real by redefining the phases of charged-lepton fields. But it is in general impossible to make both $Y_{\rm u}$ and $Y_{\rm d}$ real for three families of quarks (Kobayashi and Maskawa, 1973), and thus CP violation can only appear in the quark sector.

Given massive neutrinos beyond the SM, $\mathcal{L}_{\rm Y}$ must be modified. The simplest way is to introduce three right-handed neutrinos and incorporate the Dirac neutrino mass term in Eq. (3.10) into $\mathcal{L}_{\rm Y}$. In this case one should also add the kinetic term of three right-handed neutrinos into $\mathcal{L}_{\rm F}$. It is straightforward to show that the conditions of CP invariance in the lepton sector turn out to be

$$Y_\nu = Y^*_\nu \; , \qquad Y_l = Y^*_l \; , \tag{3.61}$$

exactly in parallel with the quark sector. If an effective Majorana mass term is introduced into $\mathcal{L}_{\rm Y}$, as shown in Eq. (3.18), then the conditions of CP invariance in the lepton sector become

$$M_{\rm L} = M^*_{\rm L} \; , \quad Y_l = Y^*_l \; , \tag{3.62}$$

where $M_{\rm L}$ is the effective Majorana neutrino mass matrix. One may diagonalize both Y_ν (or $M_{\rm L}$) and Y_l to make them real and positive, but such

a treatment will transfer CP violation from the Yukawa interactions to the weak charged-current interactions. Then lepton flavor mixing and CP violation are described by the 3×3 unitary matrix V given in Eq. (3.16), analogous to the 3×3 unitary matrix of quark flavor mixing and CP violation given in Eq. (2.50). In other words, the source of CP violation is the irremovable complex phase(s) in the flavor mixing matrix of quarks or leptons. That is why we claim that CP violation stems from the coexistence of $\mathcal{L}_{\rm F}$ and $\mathcal{L}_{\rm Y}$ within the SM and, in most cases, beyond the SM.

It is worth reiterating that the process of spontaneous gauge symmetry breaking in the SM does not spontaneously violate CP. After the Higgs doublet H acquires its vacuum expectation value (i.e., $\phi^+ \to 0$ and $\phi^0 \to v/\sqrt{2}$ with v being real), as described in Section 2.1.4, we obtain three massive gauge bosons $W^{\pm}_{\mu}$ and Z_{μ} as well as one massless gauge boson A_{μ}. According to their relations with W^i_{μ} and B_{μ} shown in Eqs. (2.42) and (2.43), it is easy to find out the transformation properties of these physical fields under CP:

$$W^{\pm}_{\mu} \xrightarrow{\rm CP} -W^{\mp\mu} \; , \quad Z_{\mu} \xrightarrow{\rm CP} -Z^{\mu} \; , \quad A_{\mu} \xrightarrow{\rm CP} -A^{\mu} \; , \tag{3.63}$$

with $\mathbf{x} \to -\mathbf{x}$ under P and CP for each field. In contrast, the neutral Higgs boson h is a CP-even particle. After spontaneous electroweak symmetry breaking, we are left with the quark mass matrices $M_{\rm u} = vY_{\rm u}/\sqrt{2}$ and $M_{\rm d} = vY_{\rm d}/\sqrt{2}$ or the lepton mass matrices $M_{\rm D} = vY_{\nu}/\sqrt{2}$ and $M_l = vY_l/\sqrt{2}$. The conditions of CP invariance given in Eq. (3.60), (3.61) or (3.62) can therefore be replaced with the corresponding mass matrices.

3.4 Electromagnetic Properties of Massive Neutrinos

The effective electromagnetic vertex of a fermion interacting with the photon is illustrated in Fig. 3.7. Although a neutrino does not possess any electric charge, it can have electromagnetic interactions via quantum loops. One may summarize such interactions by means of the following effective interaction term (Mohapatra and Pal, 2004):

$$\mathcal{L}_{\rm EM} = \overline{\psi} \Gamma_{\mu} \psi A^{\mu} \equiv J_{\mu}(x) A^{\mu}(x) \; , \tag{3.64}$$

where the form of the electromagnetic current $J_{\mu}(x)$ is our present concern. Dirac and Majorana neutrinos couple to the photon in different ways, which are described by their respective electromagnetic form factors.

3.4.1 Electromagnetic Form Factors

For an arbitrary Dirac particle (e.g., a Dirac neutrino), let us write down the matrix element of $J_{\mu}(x)$ between two one-particle states:

$$\langle \psi(p') | J_{\mu}(x) | \psi(p) \rangle = {\rm e}^{-{\rm i}qx} \langle \psi(p') | J_{\mu}(0) | \psi(p) \rangle$$

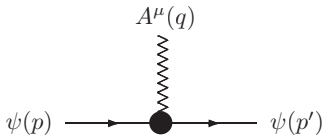

Fig. 3.7 The effective electromagnetic vertex of a fermion, where A^μ is the photon field with $q = p - p'$

$$= \mathrm{e}^{-\mathrm{i}qx}\overline{u}(\mathbf{p}')\Gamma_\mu(p,p')u(\mathbf{p}) \tag{3.65}$$

with $q = p - p'$. Because $J_\mu(x)$ is a Lorentz vector, the electromagnetic vertex function $\Gamma_\mu(p,p')$ must be a Lorentz vector too. The electromagnetic current conservation (or $U(1)_{\mathrm{Q}}$ gauge symmetry) requires $\partial^\mu J_\mu(x) = 0$, leading to

$$\langle\psi(p')|\partial^\mu J_\mu(x)|\psi(p)\rangle = (-\mathrm{i}q^\mu)\,\mathrm{e}^{-\mathrm{i}qx}\overline{u}(\mathbf{p}')\Gamma_\mu(p,p')u(\mathbf{p}) = 0\ . \tag{3.66}$$

Thus

$$q^\mu\overline{u}(\mathbf{p}')\Gamma_\mu(p,p')u(\mathbf{p}) = 0 \tag{3.67}$$

holds as one of the model-independent constraints on the form of $\Gamma_\mu(p,p')$. In addition, the Hermiticity of $J_\mu(x)$ or its matrix element implies

$$\begin{aligned}\mathrm{e}^{-\mathrm{i}qx}\overline{u}(\mathbf{p}')\Gamma_\mu(p,p')u(\mathbf{p}) &= \mathrm{e}^{+\mathrm{i}qx}\left[\overline{u}(\mathbf{p}')\Gamma_\mu(p,p')u(\mathbf{p})\right]^\dagger \\ &= \mathrm{e}^{+\mathrm{i}qx}\overline{u}(\mathbf{p})\left[\gamma_0\Gamma_\mu^\dagger(p,p')\gamma_0\right]u(\mathbf{p}') \\ &= \mathrm{e}^{-\mathrm{i}qx}\overline{u}(\mathbf{p}')\left[\gamma_0\Gamma_\mu^\dagger(p',p)\gamma_0\right]u(\mathbf{p})\ ,\end{aligned} \tag{3.68}$$

from which we immediately arrive at the second constraint on $\Gamma_\mu(p,p')$:

$$\Gamma_\mu(p,p') = \gamma_0\Gamma_\mu^\dagger(p',p)\gamma_0\ . \tag{3.69}$$

Because of $p^2 = p'^2 = m^2$ with m being the fermion mass, we have $(p+p')^2 = 4m^2 - q^2$. Hence $\Gamma_\mu(p,p')$ depends only on the Lorentz-invariant quantity q^2.

A careful analysis of the Lorentz structure of $\overline{u}(\mathbf{p}')\Gamma_\mu(p,p')u(\mathbf{p})$, with the help of the Gordon-like identities and the constraints given in Eqs. (3.67) and (3.69), shows that $\Gamma_\mu(p,p')$ may in general consist of four independent terms (Kayser, 1982; 1984; Nieves, 1982; Mohapatra and Pal, 2004; Nowakowski *et al.*, 2005; Giunti and Studenikin, 2009):

$$\begin{aligned}\Gamma_\mu(p,p') = {} & f_{\mathrm{Q}}(q^2)\gamma_\mu + f_{\mathrm{M}}(q^2)\mathrm{i}\sigma_{\mu\nu}q^\nu + f_{\mathrm{E}}(q^2)\sigma_{\mu\nu}q^\nu\gamma_5 \\ & + f_{\mathrm{A}}(q^2)\left(q^2\gamma_\mu - q_\mu\not{q}\right)\gamma_5\ ,\end{aligned} \tag{3.70}$$

where $f_{\mathrm{Q}}(q^2)$, $f_{\mathrm{M}}(q^2)$, $f_{\mathrm{E}}(q^2)$ and $f_{\mathrm{A}}(q^2)$ are usually referred to as the charge, magnetic dipole, electric dipole and anapole form factors, respectively. In the non-relativistic limit of $\mathcal{L}_{\mathrm{EM}}$, it is easy to find that $f_{\mathrm{Q}}(0) = Q$ represents

the electric charge of the particle, $f_{\rm M}(0) \equiv \mu$ denotes the magnetic dipole moment of the particle (i.e., $\mathcal{L}_{\rm EM}(f_{\rm M}) = -\mu\boldsymbol{\sigma}\cdot\mathbf{B}$ with $\mathbf{B}$ being the static magnetic field), $f_{\rm E}(0) \equiv \epsilon$ stands for the electric dipole moment of the particle (i.e., $\mathcal{L}_{\rm EM}(f_{\rm E}) = -\epsilon\boldsymbol{\sigma}\cdot\mathbf{E}$ with $\mathbf{E}$ being the static electric field), and $f_{\rm A}(0)$ corresponds to the Zeldovich anapole moment of the particle (i.e., $\mathcal{L}_{\rm EM}(f_{\rm A}) \propto f_{\rm A}(0)\boldsymbol{\sigma}\cdot[\nabla\times\mathbf{B}-\dot{\mathbf{E}}]$) (see, e.g., Nowakowski *et al.*, 2005). One can observe that these form factors are not only Lorentz-invariant but also real (i.e., ${\rm Im}f_{\rm Q} = {\rm Im}f_{\rm M} = {\rm Im}f_{\rm E} = {\rm Im}f_{\rm A} = 0$). The latter is actually guaranteed by the Hermiticity condition in Eq. (3.69).

Given the form of Γ_μ in Eq. (3.70), it is straightforward to check the CP properties of $\mathcal{L}_{\rm EM}$ in Eq. (3.64). Note that the photon field transforms as $A^\mu \to -A_\mu$ under CP, and [5]

$$\begin{aligned}
&\overline{\psi}\gamma_\mu\psi \xrightarrow{\rm CP} -\overline{\psi}\gamma^\mu\psi\ , \qquad \overline{\psi}\gamma_\mu\gamma_5\psi \xrightarrow{\rm CP} -\overline{\psi}\gamma^\mu\gamma_5\psi\ , \\
&\overline{\psi}\sigma_{\mu\nu}\psi \xrightarrow{\rm CP} -\overline{\psi}\sigma^{\mu\nu}\psi\ , \qquad \overline{\psi}\sigma_{\mu\nu}\gamma_5\psi \xrightarrow{\rm CP} +\overline{\psi}\sigma^{\mu\nu}\gamma_5\psi\ .
\end{aligned} \tag{3.71}$$

Therefore, only the term proportional to $f_{\rm E}$ in $\mathcal{L}_{\rm EM}$ is CP-violating. If CP were conserved, then this term would vanish (i.e., $f_{\rm E} = 0$ would hold). Although there is no experimental hint at CP violation in the lepton sector, we expect that it should exist as in the quark sector. In any case, all four form factors are finite for a Dirac neutrino.

If neutrinos are massive Majorana particles, their electromagnetic properties will be rather different. The reason is simply that Majorana particles are their own antiparticles and thus can be described by using a smaller number of degrees of freedom. A free Majorana neutrino field ψ is by definition equal to its charge-conjugate field $\psi^c = \mathcal{C}\overline{\psi}^T$ up to a global phase. Then

$$\overline{\psi}\Gamma_\mu\psi = \overline{\psi^c}\Gamma_\mu\psi^c = \psi^T\mathcal{C}\Gamma_\mu\mathcal{C}\overline{\psi}^T = \left(\psi^T\mathcal{C}\Gamma_\mu\mathcal{C}\overline{\psi}^T\right)^T = -\overline{\psi}\mathcal{C}^T\Gamma_\mu^T\mathcal{C}^T\psi\ , \tag{3.72}$$

from which one arrives at

$$\Gamma_\mu = -\mathcal{C}^T\Gamma_\mu^T\mathcal{C}^T = \mathcal{C}\Gamma_\mu^T\mathcal{C}^{-1}\ . \tag{3.73}$$

Substituting Eq. (3.70) into the right-hand side of Eq. (3.73) and taking account of $\mathcal{C}\gamma_\mu^T\mathcal{C}^{-1} = -\gamma_\mu$, $\mathcal{C}(\gamma_\mu\gamma_5)^T\mathcal{C}^{-1} = +\gamma_\mu\gamma_5$, $\mathcal{C}\sigma_{\mu\nu}^T\mathcal{C}^{-1} = -\sigma_{\mu\nu}$ and $\mathcal{C}(\sigma_{\mu\nu}\gamma_5)^T\mathcal{C}^{-1} = -\sigma_{\mu\nu}\gamma_5$, we obtain

$$\begin{aligned}
\Gamma_\mu(p,p') = &-f_{\rm Q}(q^2)\gamma_\mu - f_{\rm M}(q^2){\rm i}\sigma_{\mu\nu}q^\nu - f_{\rm E}(q^2)\sigma_{\mu\nu}q^\nu\gamma_5 \\
&+f_{\rm A}(q^2)\left(q^2\gamma_\mu - q_\mu\not{q}\right)\gamma_5\ .
\end{aligned} \tag{3.74}$$

A comparison between Eqs. (3.70) and (3.74) leads to

[5] Taking account of $\mathcal{C}^{-1}\sigma_{\mu\nu}\mathcal{C} = -\sigma_{\mu\nu}^T$ and $\mathcal{C}^{-1}\gamma_5\mathcal{C} = \gamma_5^T$, one may easily prove that $\overline{\psi}\sigma_{\mu\nu}\gamma_5\psi$ is odd under both C and P. Thus $\overline{\psi}\sigma_{\mu\nu}\gamma_5\psi$ is CP-even.

$$f_{\rm Q}(q^2) = f_{\rm M}(q^2) = f_{\rm E}(q^2) = 0 \ . \tag{3.75}$$

This result means that a Majorana neutrino only has the anapole form factor $f_{\rm A}(q^2)$ (Schechter and Valle, 1981; Nieves, 1982).

More generally, one may write out the matrix elements of the electromagnetic current $J_\mu(x)$ between two different states (i.e., the incoming and outgoing particles are different):

$$\langle \psi_j(p')|J_\mu(x)|\psi_i(p)\rangle = {\rm e}^{-{\rm i}qx}\overline{u_j}(\mathbf{p}')\Gamma_\mu^{ij}(p,p')u_i(\mathbf{p}) \ , \tag{3.76}$$

where $q = p - p'$ together with $p^2 = m_i^2$ and $p'^2 = m_j^2$ (for $i \neq j$). Here the electromagnetic vertex matrix $\Gamma_\mu(p,p')$ can be decomposed into the following Lorentz-invariant form in terms of four form factors:

$$\begin{aligned}\Gamma_\mu(p,p') = {} & F_{\rm Q}(q^2)\left(q^2\gamma_\mu - q_\mu \not{q}\right) + F_{\rm M}(q^2){\rm i}\sigma_{\mu\nu}q^\nu \\ & + F_{\rm E}(q^2)\sigma_{\mu\nu}q^\nu\gamma_5 + F_{\rm A}(q^2)\left(q^2\gamma_\mu - q_\mu \not{q}\right)\gamma_5 \ ,\end{aligned} \tag{3.77}$$

where $F_{\rm Q}$, $F_{\rm M}$, $F_{\rm E}$ and $F_{\rm A}$ are all the 2×2 matrices in the space of neutrino mass eigenstates (Shrock, 1982). The diagonal case (i.e., $i = j$) has been discussed above, from Eq. (3.65) to Eq. (3.75). In the off-diagonal case (i.e., $i \neq j$), the Hermiticity of $J_\mu(x)$ is no more a constraint on $\Gamma_\mu(p,p')$ for Dirac neutrinos because Eq. (3.68) only holds for $i = j$. It is now possible for Majorana neutrinos to have finite *transition* dipole moments, simply because Eqs. (3.72)—(3.75) do not hold when ψ_i and ψ_j represent different flavors.

We conclude that Dirac neutrinos may have both electric and magnetic dipole moments, while Majorana neutrinos have neither electric nor magnetic dipole moments. But massive Majorana neutrinos can have *transition* dipole moments which involve two different neutrino flavors in the initial and final states, so can massive Dirac neutrinos.

3.4.2 Magnetic and Electric Dipole Moments

The magnetic and electric dipole moments of massive neutrinos, denoted as $\mu \equiv F_{\rm M}(0)$ and $\epsilon \equiv F_{\rm E}(0)$, are interesting in both theories and experiments because they are closely related to the dynamics of neutrino mass generation and to the characteristic of new physics.

Let us consider a minimal extension of the SM in which three right-handed neutrinos are introduced and lepton number conservation is required, just as described in Section 3.2.1. In this case massive neutrinos are Dirac particles and their magnetic and electric dipole moments can be evaluated by calculating the Feynman diagrams in Fig. 3.8 (Marciano and Sanda, 1977; Lee and Shrock, 1977; Fujikawa and Shrock, 1980; Shrock, 1982; Pal and Wolfenstein, 1982). Taking account of the smallness of both m_α^2/M_W^2 and m_i^2/M_W^2, where m_α (for $\alpha = e, \mu, \tau$) and m_i (for $i = 1, 2, 3$) stand respectively for the charged-lepton and neutrino masses, one obtains (Cabral-Rosetti *et al.*, 2000; Dvornikov and Studenikin, 2004; Giunti and Studenikin, 2009)

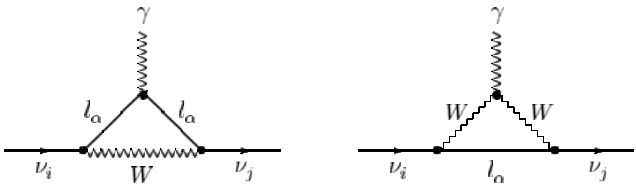

Fig. 3.8 One-loop Feynman diagrams contributing to the magnetic and electric dipole moments of massive Dirac neutrinos, where $\alpha = e, \mu, \tau$ and $i, j = 1, 2, 3$

$$\mu_{ij}^{\rm D} = \frac{3eG_{\rm F}m_i}{32\sqrt{2}\pi^2}\left(1+\frac{m_j}{m_i}\right)\sum_\alpha\left(2-\frac{m_\alpha^2}{M_W^2}\right)V_{\alpha i}V_{\alpha j}^* \ ,$$
$$\epsilon_{ij}^{\rm D} = \frac{3eG_{\rm F}m_i}{32\sqrt{2}\pi^2}\left(1-\frac{m_j}{m_i}\right)\sum_\alpha\left(2-\frac{m_\alpha^2}{M_W^2}\right)V_{\alpha i}V_{\alpha j}^* \ , \tag{3.78}$$

to an excellent degree of accuracy. Here $V_{\alpha i}$ and $V_{\alpha j}$ are the elements of the unitary lepton flavor mixing matrix V. Some discussions are in order.

(1) In the diagonal case (i.e., $i = j$), we are left with vanishing electric dipole moments (i.e., $\epsilon_{ii}^{\rm D} = 0$). The magnetic dipole moments $\mu_{ii}^{\rm D}$ are finite and proportional to the neutrino masses m_i (for $i = 1, 2, 3$):

$$\mu_{ii}^{\rm D} = \frac{3eG_{\rm F}m_i}{8\sqrt{2}\pi^2}\left(1-\frac{1}{2}\sum_\alpha\frac{m_\alpha^2}{M_W^2}|V_{\alpha i}|^2\right) \ . \tag{3.79}$$

Hence a massless Dirac neutrino in the SM has no magnetic dipole moment. In the leading-order approximation, $\mu_{ii}^{\rm D}$ are independent of the strength of lepton flavor mixing and have tiny values

$$\mu_{ii}^{\rm D} \approx \frac{3eG_{\rm F}m_i}{8\sqrt{2}\pi^2} \approx 3\times 10^{-19}\left(\frac{m_i}{1\ {\rm eV}}\right)\mu_{\rm B} \ , \tag{3.80}$$

where $\mu_{\rm B} = e\hbar/(2m_e)$ is the Bohr magneton. Given $m_i \lesssim 1$ eV, the magnitude of $\mu_{ii}^{\rm D}$ is far below its present experimental upper bound ($<$ a few $\times 10^{-11}\mu_{\rm B}$).

(2) In the off-diagonal case (i.e., $i \neq j$), the unitarity of V allows us to simplify Eq. (3.78) to

$$\mu_{ij}^{\rm D} = -\frac{3eG_{\rm F}m_i}{32\sqrt{2}\pi^2}\left(1+\frac{m_j}{m_i}\right)\sum_\alpha\frac{m_\alpha^2}{M_W^2}V_{\alpha i}V_{\alpha j}^* \ ,$$
$$\epsilon_{ij}^{\rm D} = -\frac{3eG_{\rm F}m_i}{32\sqrt{2}\pi^2}\left(1-\frac{m_j}{m_i}\right)\sum_\alpha\frac{m_\alpha^2}{M_W^2}V_{\alpha i}V_{\alpha j}^* \ . \tag{3.81}$$

We see that the magnitudes of $\mu_{ij}^{\rm D}$ and $\epsilon_{ij}^{\rm D}$ (for $i \neq j$), compared with that of $\mu_{ii}^{\rm D}$, are further suppressed due to the smallness of m_α^2/M_W^2. Similar to the expression given in Eq. (3.80),

$$\mu^{\rm D}_{ij} \approx -4\times 10^{-23}\left(\frac{m_i+m_j}{1\ {\rm eV}}\right)\left(\sum_\alpha \frac{m^2_\alpha}{m^2_\tau}V_{\alpha i}V^*_{\alpha j}\right)\mu_{\rm B}\ ,$$
$$\epsilon^{\rm D}_{ij} \approx -4\times 10^{-23}\left(\frac{m_i-m_j}{1\ {\rm eV}}\right)\left(\sum_\alpha \frac{m^2_\alpha}{m^2_\tau}V_{\alpha i}V^*_{\alpha j}\right)\mu_{\rm B}\ , \qquad (3.82)$$

which can illustrate how small $\mu^{\rm D}_{ij}$ and $\epsilon^{\rm D}_{ij}$ are (see, e.g., Raffelt, 1996, 1999; Giunti and Studenikin, 2009).

(3) Although Majorana neutrinos do not have intrinsic ($i = j$) magnetic and electric dipole moments, they may have finite transition ($i \neq j$) dipole moments as we have pointed out in Section 3.4.1. Because of the fact that Majorana neutrinos are their own antiparticles, their magnetic and electric dipole moments can also get contributions from two additional one-loop Feynman diagrams involving the charge-conjugate fields of ν_i, ν_j, l_α, $W^\pm$ and γ shown in Fig. 3.8 [6]. In this case one obtains (Shrock, 1982)

$$\mu^{\rm M}_{ij} = -\frac{3eG_{\rm F}{\rm i}}{16\sqrt{2}\pi^2}\left(m_i+m_j\right)\sum_\alpha \frac{m^2_\alpha}{M^2_W}{\rm Im}\left(V_{\alpha i}V^*_{\alpha j}\right)\ ,$$
$$\epsilon^{\rm M}_{ij} = -\frac{3eG_{\rm F}}{16\sqrt{2}\pi^2}\left(m_i-m_j\right)\sum_\alpha \frac{m^2_\alpha}{M^2_W}{\rm Re}\left(V_{\alpha i}V^*_{\alpha j}\right)\ , \qquad (3.83)$$

where $m_i \neq m_j$ must hold. Comparing between Eqs. (3.81) and (3.83), we observe that the magnitudes of $\mu^{\rm M}_{ij}$ and $\epsilon^{\rm M}_{ij}$ are the same order as those of $\mu^{\rm D}_{ij}$ and $\epsilon^{\rm D}_{ij}$ in most cases, although the CP-violating phases hidden in $V_{\alpha i}V^*_{\alpha j}$ are possible to give rise to significant cancellations in some cases.

(4) The fact that μ_{ij} and ϵ_{ij} are proportional to m_i or m_j can be understood in the following way. Note that both tensor- and pseudotensor-like spinor bilinears are chirality-changing operators, which link the left-handed state to the right-handed one (Mohapatra and Pal, 2004) [7]:

$$\overline{\psi}\sigma_{\mu\nu}\psi = \overline{\psi_{\rm L}}\sigma_{\mu\nu}\psi_{\rm R} + {\rm h.c.}\ , \quad \overline{\psi}\sigma_{\mu\nu}\gamma_5\psi = \overline{\psi_{\rm L}}\sigma_{\mu\nu}\gamma_5\psi_{\rm R} - {\rm h.c.}\ . \qquad (3.84)$$

Note also that the same relations hold when ψ is replaced by its charge-conjugate field ψ^c for Majorana neutrinos. Because $(\nu_i)_{\rm R}$ and $(\nu_j)_{\rm R}$ do not have any interactions with $W^\pm$ in Fig. 3.8, it seems that only $(\nu_i)_{\rm L}$ and $(\nu_j)_{\rm L}$ are flowing along the external fermion lines. To obtain a chirality-changing contribution from the effective (one-loop) electromagnetic vertex, one has to put a mass insertion on one of the external legs in the Feynman diagrams. As a result, the magnetic and electric dipole moments must involve m_i and m_j, the masses of ν_i and ν_j neutrinos.

[6] Here we confine ourselves to a simple extension of the SM with three known neutrinos to be massive Majorana particles, as discussed in Section 3.2.2.

[7] That is why both magnetic and electric dipole moments must vanish for a Weyl neutrino, because it is massless and does not possess the right-handed component.

(5) Is the magnetic or electric dipole moment of a neutrino always proportional to its mass? The answer may be negative if new physics beyond the $SU(2)_{\rm L} \times U(1)_{\rm Y}$ gauge theory is involved (Giunti and Studenikin, 2009). For instance, a new term proportional to the charged-lepton mass can contribute to the magnetic dipole moment of a massive Dirac neutrino in the $SU(2)_{\rm L} \times SU(2)_{\rm R} \times U(1)_{\rm Y}$ model with broken left-right symmetry (Kim, 1976; Marciano and Sanda, 1977; Czakon *et al.*, 1999). Depending on the details of this model, such a term might cancel or exceed the term proportional to the neutrino mass in the expression of the magnetic dipole moment.

Finite magnetic and electric dipole moments of massive neutrinos may produce a variety of new processes beyond the SM (Strumia and Vissani, 2006; Giunti and Studenikin, 2009). For example, (a) radiative neutrino decays $\nu_i \to \nu_j + \gamma$ can happen, so can the Cherenkov radiation of neutrinos in an external electromagnetic field; (b) the elastic neutrino-electron or neutrino-nucleon scattering can be mediated by the magnetic and electric dipole moments; (c) the phenomenon of precession of the neutrino spin can occur in an external magnetic field; (d) the photon (or plasmon) can decay into a neutrino-antineutrino pair in a plasma (i.e., $\gamma^* \to \nu\overline{\nu}$). Of course, non-vanishing electromagnetic dipole moments contribute to neutrino masses too. The following two subsections will briefly cover the topics of radiative neutrino decays and electromagnetic neutrino-electron scattering effects.

3.4.3 Radiative Decays of Massive Neutrinos

If the electromagnetic moments of a massive neutrino ν_i are finite, it can decay into a lighter neutrino ν_j and a photon γ via Fig. 3.7, where the incoming and outgoing fermions are replaced respectively by ν_i and ν_j. The Lorentz-invariant vertex matrix of this $\nu_i \to \nu_j + \gamma$ process is in general described by $\Gamma_\mu(p, p')$ in Eq. (3.77). Because $q^2 = 0$ and $q_\mu \varepsilon^\mu = 0$ hold for a real photon γ (Mohapatra and Pal, 2004), where ε^μ represents the photon polarization vector, the form of $\Gamma_\mu(p, p')$ can be simplified to

$$\Gamma_\mu(p, p') = [{\rm i}F_{\rm M}(0) + F_{\rm E}(0)\gamma_5]\, \sigma_{\mu\nu} q^\nu \; . \tag{3.85}$$

By definition, $F^{ij}_{\rm M}(0) \equiv \mu_{ij}$ and $F^{ij}_{\rm E}(0) \equiv \epsilon_{ij}$ are just the magnetic and electric transition dipole moments between ν_i and ν_j neutrinos. Given the transition matrix element $\overline{u_j}(\mathbf{p}')\Gamma^{ij}_\mu(p, p')u_i(\mathbf{p})$, it is straightforward to calculate the decay rate. In the rest frame of the decaying neutrino ν_i, one obtains

$$\Gamma_{\nu_i \to \nu_j + \gamma} = \frac{\left(m_i^2 - m_j^2\right)^3}{8\pi m_i^3} \left(\left|\mu_{ij}\right|^2 + \left|\epsilon_{ij}\right|^2 \right) \; . \tag{3.86}$$

This result is valid for both Dirac and Majorana neutrinos.

In the framework of the $SU(2)_{\rm L} \times U(1)_{\rm Y}$ gauge theory with three massive Dirac (or Majorana) neutrinos, the radiative decay $\nu_i \to \nu_j + \gamma$ is mediated

by the one-loop Feynman diagrams (and their charge-conjugate diagrams) shown in Fig. 3.8. The explicit expressions of μ_{ij} and ϵ_{ij} have been given in Eq. (3.81) for Dirac neutrinos and in Eq. (3.83) for Majorana neutrinos. As a result,

$$\begin{aligned}\Gamma^{(\rm D)}_{\nu_i\to\nu_j+\gamma} &= \frac{\left(m_i^2-m_j^2\right)^3}{8\pi m_i^3}\left(\left|\mu^{\rm D}_{ij}\right|^2+\left|\epsilon^{\rm D}_{ij}\right|^2\right) \\ &= \frac{9\alpha_{\rm em}G_{\rm F}^2 m_i^5}{2^{11}\pi^4}\left(1-\frac{m_j^2}{m_i^2}\right)^3\left(1+\frac{m_j^2}{m_i^2}\right)\left|\sum_\alpha \frac{m_\alpha^2}{M_W^2}V_{\alpha i}V^*_{\alpha j}\right|^2 \end{aligned} \tag{3.87}$$

for Dirac neutrinos (Lee and Shrock, 1977; Marciano and Sanda, 1977; Shrock, 1982; Pal and Wolfenstein, 1982); or

$$\begin{aligned}\Gamma^{(\rm M)}_{\nu_i\to\nu_j+\gamma} &= \frac{\left(m_i^2-m_j^2\right)^3}{8\pi m_i^3}\left(\left|\mu^{\rm M}_{ij}\right|^2+\left|\epsilon^{\rm M}_{ij}\right|^2\right) \\ &= \frac{9\alpha_{\rm em}G_{\rm F}^2 m_i^5}{2^{10}\pi^4}\left(1-\frac{m_j^2}{m_i^2}\right)^3\left\{\left(1+\frac{m_j}{m_i}\right)^2\left[\sum_\alpha \frac{m_\alpha^2}{M_W^2}{\rm Im}\left(V_{\alpha i}V^*_{\alpha j}\right)\right]^2\right. \\ &\quad \left.+\left(1-\frac{m_j}{m_i}\right)^2\left[\sum_\alpha \frac{m_\alpha^2}{M_W^2}{\rm Re}\left(V_{\alpha i}V^*_{\alpha j}\right)\right]^2\right\} \end{aligned} \tag{3.88}$$

for Majorana neutrinos (Shrock, 1982), where $\alpha_{\rm em} = e^2/(4\pi)$ denotes the electromagnetic fine-structure constant.

To compare $\Gamma_{\nu_i\to\nu_j+\gamma}$ with the experimental data in a simpler way, one may define an effective magnetic dipole moment

$$\mu_{\rm eff} \equiv \sqrt{\left|\mu_{ij}\right|^2+\left|\epsilon_{ij}\right|^2} \ . \tag{3.89}$$

Eq. (3.86) can then be expressed as

$$\Gamma_{\nu_i\to\nu_j+\gamma} = 5.3\times\left(1-\frac{m_j^2}{m_i^2}\right)^3\left(\frac{m_i}{1\ {\rm eV}}\right)^3\left(\frac{\mu_{\rm eff}}{\mu_{\rm B}}\right)^2 {\rm s}^{-1} \ . \tag{3.90}$$

Although $\mu_{\rm eff}$ is extremely small in some simple extensions of the SM like the one discussed in Section 3.4.2, it could be sufficiently large in some more complicated or exotic scenarios beyond the SM, such as a class of extra-dimension models (Mohapatra *et al.*, 2004). Experimentally, radiative decays of massive neutrinos can be constrained by seeing no emission of the photons from solar ν_e and reactor $\overline{\nu}_e$ fluxes. Much stronger constraints on $\mu_{\rm eff}$ can be obtained from the Supernova 1987A limit on the neutrino decay and from the astrophysical limit on distortions of the cosmic microwave background (CMB) radiation (Raffelt, 1996, 1999), as shown in Fig. 3.9. A brief summary of these limits is (Raffelt, 1999; Giunti and Studenikin, 2009)

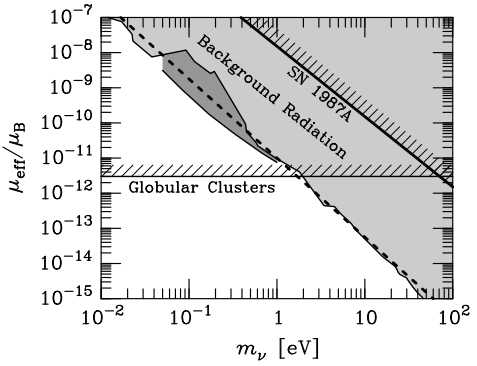

Fig. 3.9 Astrophysical bounds on the effective magnetic dipole moment $\mu_{\rm eff}$ in radiative neutrino decays (Raffelt, 1996, 1999. With permission from the University of Chicago Press and Elsevier)

$$\frac{\mu_{\rm eff}}{\mu_{\rm B}} < \begin{cases} 0.9 \times 10^{-1} \left(\dfrac{\rm eV}{m_\nu}\right)^2 & \text{Reactor } (\overline{\nu}_e)\ , \\ 0.5 \times 10^{-5} \left(\dfrac{\rm eV}{m_\nu}\right)^2 & \text{Sun } (\nu_e)\ , \\ 1.5 \times 10^{-8} \left(\dfrac{\rm eV}{m_\nu}\right)^2 & \text{SN 1987A (all flavors)}\ , \\ 1.0 \times 10^{-11} \left(\dfrac{\rm eV}{m_\nu}\right)^{9/4} & \text{CMB (all flavors)}\ , \end{cases} \tag{3.91}$$

in which m_ν is used to denote the effective mass of the decaying neutrino (i.e., $m_\nu = m_i$).

3.4.4 Electromagnetic Neutrino-electron Scattering

In practice, the most sensitive way of probing the electromagnetic dipole moments of a massive neutrino is to measure the cross section of elastic neutrino-electron (or antineutrino-electron) scattering, which can be expressed as a sum of the contribution from the SM (σ_0) and that from the electromagnetic dipole moments of massive neutrinos (σ_μ):

$$\frac{{\rm d}\sigma}{{\rm d}T} = \frac{{\rm d}\sigma_0}{{\rm d}T} + \frac{{\rm d}\sigma_\mu}{{\rm d}T}\ , \tag{3.92}$$

where $T = E_e - m_e$ denotes the kinetic energy of the recoil electron in this process. Following the calculations done in section 2.2.1, we have

$$\frac{{\rm d}\sigma_0}{{\rm d}T} = \frac{G_{\rm F}^2 m_e}{2\pi} \left[g_+^2 + g_-^2 \left(1 - \frac{T}{E_\nu}\right)^2 - g_+ g_- \frac{m_e T}{E_\nu^2} \right] \tag{3.93}$$

for neutrino-electron scattering ('t Hooft, 1971; Marciano and Parsa, 2003), where $g_+ = 2\sin^2\theta_{\rm w} + 1$ for ν_e, $g_+ = 2\sin^2\theta_{\rm w} - 1$ for ν_μ and ν_τ, and $g_- = 2\sin^2\theta_{\rm w}$ for all flavors. Note that Eq. (3.93) is also valid for antineutrino-electron scattering if one simply exchanges the positions of g_+ and g_-. On the other hand (Bardin *et al.*, 1970; Kyuldjiev, 1984; Vogel and Engel, 1989),

$$\frac{{\rm d}\sigma_\mu}{{\rm d}T} = \frac{\alpha_{\rm em}^2\pi}{m_e^2}\left(\frac{1}{T} - \frac{1}{E_\nu}\right)\left(\frac{\mu_\nu}{\mu_{\rm B}}\right)^2 \tag{3.94}$$

with $\mu_\nu^2 \equiv |\mu_{ii}^{\rm D}|^2 + |\epsilon_{ii}^{\rm D}|^2$ (for $i = 1$, 2 or 3), which holds for both neutrinos and antineutrinos. In obtaining Eqs. (3.93) and (3.94) one has assumed the scattered neutrino to be a Dirac particle and omitted the effects of finite neutrino masses and flavor mixing (i.e., $\nu_e = \nu_1$, $\nu_\mu = \nu_2$ and $\nu_\tau = \nu_3$ have been taken). Hence there is no interference between the contributions coming from the SM and electromagnetic dipole moments — the latter leads to a helicity flip of the neutrino but the former is always helicity-conserving. While an interference term will appear if one takes account of neutrino masses and flavor mixing, its magnitude linearly depends on the neutrino masses and thus is strongly suppressed in comparison with the pure weak and electromagnetic terms (Grimus and Stockinger, 1998). So the incoherent sum of $\dfrac{{\rm d}\sigma_0}{{\rm d}T}$ and $\dfrac{{\rm d}\sigma_\mu}{{\rm d}T}$ in Eq. (3.92) is actually an excellent approximation of $\dfrac{{\rm d}\sigma}{{\rm d}T}$.

It is obvious that the two terms of $\dfrac{{\rm d}\sigma}{{\rm d}T}$ depend on the kinetic energy of the recoil electron in quite different ways. In particular, $\dfrac{{\rm d}\sigma_\mu}{{\rm d}T}$ grows rapidly with decreasing values of T. Hence a measurement of smaller T can probe smaller μ_ν in this kind of experiments. The magnitude of $\dfrac{{\rm d}\sigma_\mu}{{\rm d}T}$ becomes larger than that of $\dfrac{{\rm d}\sigma_0}{{\rm d}T}$ if the condition

$$T \lesssim \frac{\alpha_{\rm em}^2\pi^2}{G_{\rm F}^2 m_e^3}\left(\frac{\mu_\nu}{\mu_{\rm B}}\right)^2 \approx 3\times 10^{22}\left(\frac{\mu_\nu}{\mu_{\rm B}}\right)^2 {\rm keV} \tag{3.95}$$

is roughly satisfied, as one can easily see from Eqs. (3.93) and (3.94). No distortion of the recoil electron energy spectrum of $\nu_\alpha e^-$ or $\overline{\nu}_\alpha e^-$ scattering (for $\alpha = e, \mu, \tau$) has so far been observed in any direct laboratory experiments, and thus only the upper bounds on μ_ν can be derived (Wong and Li, 2005; Beda *et al.*, 2007). For instance, an analysis of the T-spectrum in the SK experiment yields $\mu_\nu < 1.1\times 10^{-10}\mu_{\rm B}$ (Liu *et al.*, 2004); several recent reactor experiments on $\overline{\nu}_e e^-$ scattering yield

$$\mu_\nu < \begin{cases} 9.0\times 10^{-11}\mu_{\rm B} & \text{MUNU (Darakchieva } et\ al.,\ 2005)\ , \\ 7.4\times 10^{-11}\mu_{\rm B} & \text{TEXONO (Wong } et\ al.,\ 2007)\ , \\ 5.8\times 10^{-11}\mu_{\rm B} & \text{GEMMA (Beda } et\ al.,\ 2007)\ ; \end{cases} \tag{3.96}$$

and the present Borexino experiment yields $\mu_\nu < 5.4 \times 10^{-11} \mu_{\rm B}$ (Arpesella *et al.*, 2008b). More stringent bounds on μ_ν can hopefully be achieved from the future experiments of these types (Giunti and Studenikin, 2009).

In view of current experimental data on neutrino oscillations, we know that neutrinos are actually massive. Hence the effects of finite neutrino masses and flavor mixing should be taken into account in calculating the cross section of elastic neutrino-electron or antineutrino-electron scattering (Grimus and Stockinger, 1998; Beacom and Vogel, 1999). Here let us illustrate how the neutrino oscillation may affect the weak and electromagnetic terms of elastic $\overline{\nu}_e e^-$ scattering in a reactor experiment, where the electron antineutrinos are produced from the beta decay of fission products and detected by their elastic scattering with electrons in a detector. The antineutrino state created in this beta decay (via $W^- \to e^- + \overline{\nu}_e$) at the reactor is a superposition of three antineutrino mass eigenstates:

$$|\overline{\nu}_e(0)\rangle = \sum_{j=1}^{3} V_{ej} |\overline{\nu}_j\rangle \; , \tag{3.97}$$

where V is the 3×3 neutrino mixing matrix. Such a $\overline{\nu}_e$ beam propagates over the distance L to the detector,

$$|\overline{\nu}_e(L)\rangle = \sum_{j=1}^{3} {\rm e}^{{\rm i}q_j L} V_{ej} |\overline{\nu}_j\rangle \; , \tag{3.98}$$

in which $q_j = \sqrt{E_\nu^2 - m_j^2}$ is the momentum of ν_j with E_ν being the beam energy and m_j being the mass of ν_j. After taking account of the effect of neutrino oscillations, one obtains the differential cross section of elastic antineutrino-electron scattering as follows (Grimus and Stockinger, 1998):

$$\frac{{\rm d}\sigma'}{{\rm d}T} = \frac{{\rm d}\sigma'_0}{{\rm d}T} + \frac{{\rm d}\sigma'_\mu}{{\rm d}T} \; , \tag{3.99}$$

where

$$\begin{aligned} \frac{{\rm d}\sigma'_0}{{\rm d}T} = \frac{G_{\rm F}^2 m_e}{2\pi} \Bigg\{ & g_-^2 + \left(g_- - 1\right)^2 \left(1 - \frac{T}{E_\nu}\right)^2 - g_- \left(g_- - 1\right) \frac{m_e T}{E_\nu^2} \\ & + 2 g_- \left| \sum_{j=1}^{3} {\rm e}^{{\rm i}q_j L} |V_{ej}|^2 \right|^2 \left[2 \left(1 - \frac{T}{E_\nu}\right)^2 - \frac{m_e T}{E_\nu^2} \right] \Bigg\} \end{aligned} \tag{3.100}$$

with $g_- = 2 \sin^2 \theta_{\rm w}$ for $\overline{\nu}_e$, and

$$\frac{{\rm d}\sigma'_\mu}{{\rm d}T} = \frac{\alpha_{\rm em}^2 \pi}{m_e^2} \sum_{k=1}^{3} \left| \sum_{j=1}^{3} {\rm e}^{{\rm i}q_j L} V_{ej} \left({\rm i} \frac{\mu_{jk}}{\mu_{\rm B}} + \frac{\epsilon_{jk}}{\mu_{\rm B}} \right) \right|^2 \left(\frac{1}{T} - \frac{1}{E_\nu} \right) \tag{3.101}$$

with μ_{jk} and ϵ_{jk} being the magnetic and electric transition dipole moments between ν_j and ν_k neutrinos as defined in Eq. (3.85). Because different neutrino mass eigenstates are in principle distinguishable in the electromagnetic $\overline{\nu}_e e^-$ scattering, their contributions to the total cross section are incoherent. Eq. (3.101) shows that it is in general difficult to determine or constrain the magnitudes of μ_{jk} and ϵ_{jk} (for $j,k=1,2,3$) from a single measurement. But it is possible to simplify the above expression for $\dfrac{\mathrm{d}\sigma'_\mu}{\mathrm{d}T}$ in a few special cases (Beacom and Vogel, 1999).

3.5 Lepton Flavor Mixing and CP Violation

Regardless of the origin of tiny neutrino masses [8], we may discuss lepton flavor mixing by taking account of the effective mass terms of charged leptons and Majorana neutrinos at low energies [9],

$$-\mathcal{L}'_{\rm lepton} = \overline{(e\ \mu\ \tau)_{\rm L}}\ M_l \begin{pmatrix} e \\ \mu \\ \tau \end{pmatrix}_{\rm R} + \frac{1}{2}\overline{\left(\nu_e\ \nu_\mu\ \nu_\tau\right)_{\rm L}}\ M_\nu \begin{pmatrix} \nu_e^c \\ \nu_\mu^c \\ \nu_\tau^c \end{pmatrix}_{\rm R} + \text{h.c.}\ . \quad (3.102)$$

The phenomenon of lepton flavor mixing arises from a mismatch between the diagonalizations of M_l and M_ν in an arbitrary flavor basis: $V_l^\dagger M_l U_l = {\rm Diag}\{m_e, \mu_\mu, m_\tau\}$ and $V_\nu^\dagger M_\nu V_\nu^* = {\rm Diag}\{m_1, m_2, m_3\}$, where V_l, U_l and V_ν are the 3×3 unitary matrices. In the basis of mass eigenstates, it is the unitary matrix $V = V_l^\dagger V_\nu$ that will appear in the weak charged-current interactions in Eq. (3.9). Although the basis of $M_l = {\rm Diag}\{m_e, m_\mu, m_\tau\}$ with $V_l = \mathbf{1}$ and $V = V_\nu$ is often chosen in neutrino phenomenology, one should keep in mind that both the charged-lepton and neutrino sectors may in general contribute to lepton flavor mixing. In other words, both V_l and V_ν are not fully physical, and only their product $V = V_l^\dagger V_\nu$ is a physical description of lepton flavor mixing and CP violation at low energies.

3.5.1 Classification of Different Parametrizations

Flavor mixing among n different lepton families can be described by an $n\times n$ unitary matrix V, whose number of independent parameters relies on the nature of neutrinos. If neutrinos are Dirac particles, one may make use of $n(n-1)/2$ rotation angles and $(n-1)(n-2)/2$ phase angles to parametrize

[8] For simplicity, here we do not consider possible non-unitarity of the 3×3 neutrino mixing matrix because its effects are either absent or very small.

[9] As for Dirac neutrinos, the corresponding mass term is the same as that given in Eq. (3.11). In this case the neutrino mass matrix M_ν is in general not symmetric and can be diagonalized by means of the transformation $V_\nu^\dagger M_\nu U_\nu = {\rm Diag}\{m_1, m_2, m_3\}$, where both V_ν and U_ν are unitary.

V. If neutrinos are Majorana particles, however, a full parametrization of V needs $n(n-1)/2$ rotation angles and the same number of phase angles [10]. The flavor mixing between charged leptons and Dirac neutrinos is completely analogous to that of quarks, for which a number of different parametrizations have been proposed and classified in the literature (Fritzsch and Xing, 1998a). Here we classify all possible parametrizations for the flavor mixing between charged leptons and Majorana neutrinos with $n = 3$. Regardless of the freedom of phase reassignments, we find that there are nine structurally different parametrizations for the 3×3 lepton flavor mixing matrix V.

The 3×3 lepton flavor mixing matrix V, which is often called the Maki-Nakagawa-Sakata (MNS) matrix (Maki *et al.*, 1962), can be expressed as a product of three unitary matrices O_1, O_2 and O_3. They correspond to simple rotations in the complex (1,2), (2,3) and (3,1) planes:

$$O_1(\theta_1,\alpha_1,\beta_1,\gamma_1) = \begin{pmatrix} c_1 e^{i\alpha_1} & s_1 e^{-i\beta_1} & 0 \\ -s_1 e^{i\beta_1} & c_1 e^{-i\alpha_1} & 0 \\ 0 & 0 & e^{i\gamma_1} \end{pmatrix} ,$$

$$O_2(\theta_2,\alpha_2,\beta_2,\gamma_2) = \begin{pmatrix} e^{i\gamma_2} & 0 & 0 \\ 0 & c_2 e^{i\alpha_2} & s_2 e^{-i\beta_2} \\ 0 & -s_2 e^{i\beta_2} & c_2 e^{-i\alpha_2} \end{pmatrix} ,$$

$$O_3(\theta_3,\alpha_3,\beta_3,\gamma_3) = \begin{pmatrix} c_3 e^{i\alpha_3} & 0 & s_3 e^{-i\beta_3} \\ 0 & e^{i\gamma_3} & 0 \\ -s_3 e^{i\beta_3} & 0 & c_3 e^{-i\alpha_3} \end{pmatrix} , \tag{3.103}$$

where $s_i \equiv \sin\theta_i$ and $c_i \equiv \cos\theta_i$ (for $i = 1, 2, 3$). Obviously $O_i O_i^\dagger = O_i^\dagger O_i = \mathbf{1}$ holds, and any two rotation matrices do not commute with each other. We find twelve different ways to arrange the product of O_1, O_2 and O_3, which can cover the whole 3×3 space and provide a full description of V (Fritzsch and Xing, 2001). Explicitly, six of the twelve different combinations of O_i belong to the type

$$V = O_i(\theta_i,\alpha_i,\beta_i,\gamma_i) \otimes O_j(\theta_j,\alpha_j,\beta_j,\gamma_j) \otimes O_i(\theta_i',\alpha_i',\beta_i',\gamma_i') \tag{3.104}$$

with $i \neq j$, where the complex rotation matrix O_i occurs twice; and the other six belong to the type

$$V = O_i(\theta_i,\alpha_i,\beta_i,\gamma_i) \otimes O_j(\theta_j,\alpha_j,\beta_j,\gamma_j) \otimes O_k(\theta_k,\alpha_k,\beta_k,\gamma_k) \tag{3.105}$$

with $i \neq j \neq k$, in which the rotations take place in three different complex planes. Note that the products $O_i O_j O_i$ and $O_i O_k O_i$ (for $j \neq k$) in Eq. (3.104) are correlated with each other, if the relevant phase parameters are switched

[10] No matter whether neutrinos are Dirac or Majorana particles, the $n \times n$ unitary flavor mixing matrix has $(n-1)^2(n-2)^2/4$ Jarlskog invariants of CP violation defined as $\mathcal{J}^{ij}_{\alpha\beta} \equiv \mathrm{Im}\left(V_{\alpha i} V_{\beta j} V^*_{\alpha j} V^*_{\beta i}\right)$ (Botella and Chau, 1986).

off. Hence only nine of the twelve parametrizations, three from Eq. (3.104) and six from Eq. (3.105), are structurally different (Xing, 2004).

In each parametrization of V, there apparently exist nine phase parameters. Some of them or their combinations can be absorbed by redefining the relevant phases of charged-lepton and neutrino fields. For example,

$$\begin{pmatrix} e^{i\gamma_2} & 0 & 0 \\ 0 & c_2 e^{i\alpha_2} & s_2 e^{-i\beta_2} \\ 0 & -s_2 e^{i\beta_2} & c_2 e^{-i\alpha_2} \end{pmatrix} \begin{pmatrix} c_3 e^{i\alpha_3} & 0 & s_3 e^{-i\beta_3} \\ 0 & e^{i\gamma_3} & 0 \\ -s_3 e^{i\beta_3} & 0 & c_3 e^{-i\alpha_3} \end{pmatrix} \begin{pmatrix} c_1 e^{i\alpha_1} & s_1 e^{-i\beta_1} & 0 \\ -s_1 e^{i\beta_1} & c_1 e^{-i\alpha_1} & 0 \\ 0 & 0 & e^{i\gamma_1} \end{pmatrix}$$
$$= P \begin{pmatrix} c_1 c_3 & s_1 c_3 & s_3 e^{-i\delta} \\ -s_1 c_2 - c_1 s_2 s_3 e^{i\delta} & c_1 c_2 - s_1 s_2 s_3 e^{i\delta} & s_2 c_3 \\ s_1 s_2 - c_1 c_2 s_3 e^{i\delta} & -c_1 s_2 - s_1 c_2 s_3 e^{i\delta} & c_2 c_3 \end{pmatrix} P' \,, \tag{3.106}$$

where $\delta = (\alpha_1 - \beta_1) - (\alpha_2 + \beta_2) + (\beta_3 - \gamma_3)$, $P = \mathrm{Diag}\{e^{ia}, e^{ib}, e^{ic}\}$ with $a = (\alpha_1 - \beta_1) - (\alpha_2 + \beta_2 - \gamma_2) - \gamma_3$, $b = -(\beta_2 + \alpha_3)$ and $c = -(\alpha_2 + \alpha_3)$, and $P' = \mathrm{Diag}\{e^{ix}, e^{iy}, e^{iz}\}$ with $x = \beta_1 + (\alpha_2 + \beta_2) + (\alpha_3 + \gamma_3)$, $y = -\alpha_1 + (\alpha_2 + \beta_2) + (\alpha_3 + \gamma_3)$ and $z = \gamma_1$. If neutrinos are Dirac particles, one can always remove both P and P' such that only δ is left as the single nontrivial CP-violating phase. If neutrinos are Majorana particles, however, there is no freedom to rearrange the relative phases of three Majorana neutrino fields. Hence only P itself and one common phase of P' are removable; namely, we are left with three nontrivial CP-violating phases in the Majorana case (δ and two Majorana phases in P'). Both CP- and T-violating effects in neutrino oscillations depend only upon the Dirac-like phase δ.

Different parametrizations of V are mathematically equivalent, so adopting any of them does not directly point to physical significance. But it is very likely that one particular parametrization is more useful and transparent than the others in studying the neutrino phenomenology and (or) exploring the underlying dynamics responsible for lepton mass generation and CP violation. Here we highlight two particular parametrizations of the MNS matrix V. The first one is the so-called "standard" parametrization advocated by the Particle Data Group (Nakamura *et al.*, 2010):

$$V = \begin{pmatrix} 1 & 0 & 0 \\ 0 & c_{23} & s_{23} \\ 0 & -s_{23} & c_{23} \end{pmatrix} \begin{pmatrix} c_{13} & 0 & s_{13} e^{-i\delta} \\ 0 & 1 & 0 \\ -s_{13} e^{i\delta} & 0 & c_{13} \end{pmatrix} \begin{pmatrix} c_{12} & s_{12} & 0 \\ -s_{12} & c_{12} & 0 \\ 0 & 0 & 1 \end{pmatrix} P'$$
$$= \begin{pmatrix} c_{12} c_{13} & s_{12} c_{13} & s_{13} e^{-i\delta} \\ -s_{12} c_{23} - c_{12} s_{23} s_{13} e^{i\delta} & c_{12} c_{23} - s_{12} s_{23} s_{13} e^{i\delta} & s_{23} c_{13} \\ s_{12} s_{23} - c_{12} c_{23} s_{13} e^{i\delta} & -c_{12} s_{23} - s_{12} c_{23} s_{13} e^{i\delta} & c_{23} c_{13} \end{pmatrix} P' \,, \tag{3.107}$$

where $c_{ij} \equiv \cos\theta_{ij}$ and $s_{ij} \equiv \sin\theta_{ij}$ (for $ij = 12, 13, 23$) together with the Majorana phase matrix $P' = \mathrm{Diag}\{e^{i\rho}, e^{i\sigma}, 1\}$. Without loss of generality, the three mixing angles $(\theta_{12}, \theta_{13}, \theta_{23})$ can all be arranged to lie in the first quadrant. Arbitrary values between 0 and 2π are allowed for three CP-violating phases (δ, ρ, σ). A remarkable merit of this parametrization is that its three

mixing angles are approximately equivalent to the mixing angles of solar (θ_{12}), atmospheric (θ_{23}) and CHOOZ reactor (θ_{13}) neutrino oscillation experiments. Another useful parametrization is the Fritzsch-Xing (FX) parametrization proposed originally for quark mixing (Fritzsch and Xing, 1997) and later for lepton mixing (Fritzsch and Xing, 1998b):

$$\begin{aligned} V &= \begin{pmatrix} c_l & s_l & 0 \\ -s_l & c_l & 0 \\ 0 & 0 & 1 \end{pmatrix} \begin{pmatrix} \mathrm{e}^{-\mathrm{i}\phi} & 0 & 0 \\ 0 & c & s \\ 0 & -s & c \end{pmatrix} \begin{pmatrix} c_\nu & -s_\nu & 0 \\ s_\nu & c_\nu & 0 \\ 0 & 0 & 1 \end{pmatrix} P' \\ &= \begin{pmatrix} s_l s_\nu c + c_l c_\nu \mathrm{e}^{-\mathrm{i}\phi} & s_l c_\nu c - c_l s_\nu \mathrm{e}^{-\mathrm{i}\phi} & s_l s \\ c_l s_\nu c - s_l c_\nu \mathrm{e}^{-\mathrm{i}\phi} & c_l c_\nu c + s_l s_\nu \mathrm{e}^{-\mathrm{i}\phi} & c_l s \\ -s_\nu s & -c_\nu s & c \end{pmatrix} P' \,, \end{aligned} \tag{3.108}$$

where $c_{l,\nu} \equiv \cos\theta_{l,\nu}$, $s_{l,\nu} \equiv \sin\theta_{l,\nu}$, $c \equiv \cos\theta$, $s \equiv \sin\theta$, and P' is a diagonal phase matrix containing two nontrivial CP-violating phases. Although the form of V in Eq. (3.108) is apparently different from that in Eq. (3.107), their corresponding flavor mixing angles $(\theta_l, \theta_\nu, \theta)$ and $(\theta_{12}, \theta_{13}, \theta_{23})$ have quite similar meanings in interpreting the experimental data on neutrino oscillations. In the limit $\theta_l = \theta_{13} = 0$, one easily arrives at $\theta_\nu = \theta_{12}$ and $\theta = \theta_{23}$. As a natural consequence of very small θ_l, three mixing angles of the FX parametrization can also be related to those of solar (θ_ν), atmospheric (θ) and CHOOZ reactor ($\theta_l \sin\theta$) neutrino oscillation experiments in the leading-order approximation (Xing, 2009a). A striking merit of this parametrization is that its six parameters have very simple renormalization-group equations when they run from a superhigh-energy scale to the electroweak scale or vice versa (Xing, 2006), as one will see in Section 3.6.

3.5.2 Democratic and Tri-bimaximal Mixing Patterns

Tables 3.1 and 3.2 indicate the essential feature of lepton flavor mixing: two mixing angles are quite large ($\theta_{12} \sim 34^\circ$ and $\theta_{23} \sim 45^\circ$) while the third one is very small ($\theta_{13} < 10^\circ$). Such a flavor mixing pattern is far beyond the original imagination of most people because it is rather different from the well-known quark mixing pattern ($\vartheta_{12} \approx 13^\circ$, $\vartheta_{23} \approx 2.3^\circ$, $\vartheta_{13} \approx 0.22^\circ$ and $\delta \approx 69^\circ$) described by the same parametrization of the Cabibbo-Kobayashi-Maskawa (CKM) matrix (Cabibbo, 1963; Kobayashi and Maskawa, 1973). To understand this difference, a number of constant lepton mixing patterns have been proposed as the starting point of model building (Xing, 2004). Possible flavor symmetries and their spontaneous or explicit breaking mechanisms hidden in those constant patterns might finally help us pin down the dynamics responsible for lepton mass generation and flavor mixing. To illustrate, let us first comment on the "democratic" neutrino mixing pattern and then pay more attention to the "tri-bimaximal" neutrino mixing pattern.

The "democratic" lepton flavor mixing pattern

$$U_0 = \begin{pmatrix} \frac{1}{\sqrt{2}} & \frac{1}{\sqrt{2}} & 0 \\ \frac{-1}{\sqrt{6}} & \frac{1}{\sqrt{6}} & \frac{\sqrt{2}}{\sqrt{3}} \\ \frac{1}{\sqrt{3}} & \frac{-1}{\sqrt{3}} & \frac{1}{\sqrt{3}} \end{pmatrix} \tag{3.109}$$

was originally obtained by Fritzsch and Xing as the leading term of the 3×3 lepton mixing matrix from the breaking of flavor democracy or $S(3)_{\rm L} \times S(3)_{\rm R}$ symmetry of the charged-lepton mass matrix in the basis where the Majorana neutrino mass matrix is diagonal and possesses the $S(3)$ symmetry (Fritzsch and Xing, 1996). Its naive predictions $\theta_{12} = 45^\circ$ and $\theta_{23} \approx 54.7^\circ$ are no more favored today, but they may receive proper corrections from the symmetry-breaking perturbations so as to fit current neutrino oscillation data (See, e.g., Fritzsch and Xing, 1998b, 2000a, 2004; Xing *et al.*, 2010).

Today's most popular constant pattern of neutrino mixing is the "tri-bimaximal" mixing matrix (Harrison *et al.*, 2002; Xing, 2002a; He and Zee, 2003):

$$V_0 = \begin{pmatrix} \frac{\sqrt{2}}{\sqrt{3}} & \frac{1}{\sqrt{3}} & 0 \\ \frac{-1}{\sqrt{6}} & \frac{1}{\sqrt{3}} & \frac{1}{\sqrt{2}} \\ \frac{1}{\sqrt{6}} & \frac{-1}{\sqrt{3}} & \frac{1}{\sqrt{2}} \end{pmatrix} \tag{3.110}$$

which looks like a twisted form of the democratic mixing pattern with the same entries. Its strange name comes from the fact that this flavor mixing pattern is actually a product of the "tri-maximal" mixing matrix (Cabibbo, 1978) and a "bi-maximal" mixing matrix:

$$V_0' = \begin{pmatrix} \frac{1}{\sqrt{3}} & \frac{1}{\sqrt{3}} & \frac{1}{\sqrt{3}} \\ \frac{1}{\sqrt{3}} & \frac{\omega}{\sqrt{3}} & \frac{\omega^2}{\sqrt{3}} \\ \frac{1}{\sqrt{3}} & \frac{\omega^2}{\sqrt{3}} & \frac{\omega}{\sqrt{3}} \end{pmatrix} \begin{pmatrix} \frac{1}{\sqrt{2}} & 0 & \frac{-1}{\sqrt{2}} \\ 0 & 1 & 0 \\ \frac{1}{\sqrt{2}} & 0 & \frac{1}{\sqrt{2}} \end{pmatrix} = P V_0 P' \; , \tag{3.111}$$

where $\omega = {\rm e}^{{\rm i}2\pi/3}$ denotes the complex cube-root of unity (i.e., $\omega^3 = 1$), and $P = {\rm Diag}\{1, \omega, \omega^2\}$ and $P' = {\rm Diag}\{1, 1, i\}$ are two diagonal phase matrices. V_0 or V_0' predicts $\theta_{12} = \arctan(1/\sqrt{2}) \approx 35.3^\circ$, $\theta_{13} = 0^\circ$ and $\theta_{23} = 45^\circ$, consistent quite well with current neutrino oscillation data. Because the entries of U_0 or V_0 are all formed from small integers (0, 1, 2 and 3) and their square roots, it is often suggestive of certain discrete flavor symmetries in the language of group theories. That is why the democratic or tri-bimaximal neutrino mixing pattern can serve as a good starting point of model building based on a variety of flavor symmetries, such as Z_2, Z_3, S_3, S_4, A_4, D_4, D_5, Q_4, Q_6, $\Delta(27)$ and $\Sigma(81)$ (Ma, 2007; King and Luhn, 2009). In particular, a lot of interest has been paid to the derivation of V_0 with the help of the non-Abelian discrete A_4 symmetry (see, e.g., Ma, 2004; Altarelli and Feruglio, 2005; Zee, 2006; He *et al.*, 2006) or the Friedberg-Lee symmetry (Friedberg and Lee, 2006, 2008, 2010; Xing *et al.*, 2006; Xing, 2007; Chan *et al.*, 2009).

Note that the democratic mixing matrix U_0 and the tri-bimaximal mixing matrix V_0 are related with each other via the following transformation:

$$V_0 = \begin{pmatrix} 1 & 0 & 0 \\ 0 & \cos\theta_0 & -\sin\theta_0 \\ 0 & \sin\theta_0 & \cos\theta_0 \end{pmatrix} U_0 \begin{pmatrix} \cos\theta_0 & -\sin\theta_0 & 0 \\ \sin\theta_0 & \cos\theta_0 & 0 \\ 0 & 0 & 1 \end{pmatrix} , \tag{3.112}$$

where $\theta_0 = \arctan(\sqrt{2}-1)^2 \approx 9.7^\circ$. This angle is actually a measure of the difference between the mixing angles of U_0 and V_0 (namely, $45^\circ - 35.3^\circ = 54.7^\circ - 45^\circ = 9.7^\circ$). In this sense, we argue that it is worthwhile to explore possible flavor symmetries behind both V_0 and U_0 so as to build realistic models for neutrino mass generation and lepton flavor mixing.

Note also that it is possible to construct different but viable neutrino mixing patterns with a few small integers and their square roots. Here we give an interesting example in terms of only two small integers 1 and 2 together with their square roots and the imaginary unit i (Xing, 2008c):

$$V = \frac{1}{2} \begin{pmatrix} 1+\frac{1}{\sqrt{2}} & 1 & 1-\frac{1}{\sqrt{2}} \\ \frac{-1}{\sqrt{2}}\left[1-\mathrm{i}\left(1-\frac{1}{\sqrt{2}}\right)\right] & 1-\mathrm{i}\frac{1}{\sqrt{2}} & \frac{1}{\sqrt{2}}\left[1+\mathrm{i}\left(1+\frac{1}{\sqrt{2}}\right)\right] \\ \frac{-1}{\sqrt{2}}\left[1+\mathrm{i}\left(1-\frac{1}{\sqrt{2}}\right)\right] & 1+\mathrm{i}\frac{1}{\sqrt{2}} & \frac{1}{\sqrt{2}}\left[1-\mathrm{i}\left(1+\frac{1}{\sqrt{2}}\right)\right] \end{pmatrix} . \tag{3.113}$$

We refer to this ansatz as the "tetra-maximal" mixing pattern because it can be expressed as a product of four rotation matrices whose mixing angles are all $\pi/4$ in the complex plane. It predicts $\theta_{12} = \arctan(2-\sqrt{2}) \approx 30.4^\circ$, $\theta_{13} = \arcsin[(\sqrt{2}-1)/(2\sqrt{2})] \approx 8.4^\circ$, $\theta_{23} = 45^\circ$ and $\delta = 90^\circ$ in the standard parametrization. These results are certainly compatible with current neutrino oscillation data and will soon be tested in the upcoming and more accurate neutrino oscillation experiments.

Let us remark that a specific constant mixing pattern should be regarded as the leading-order approximation of the "true" lepton flavor mixing matrix, whose mixing angles should in general depend on both the ratios of charged-lepton masses and those of neutrino masses. We may at least make the following naive speculation about how to phenomenologically understand the observed pattern of lepton flavor mixing (Xing, 2004):

- Large values of θ_{12} and θ_{23} could arise from a weak hierarchy or a near degeneracy of the neutrino mass spectrum, because the strong hierarchy of charged-lepton masses implies that $m_e/m_\mu \approx 4.7 \times 10^{-3}$ and $m_\mu/m_\tau \approx 5.9 \times 10^{-2}$ at the electroweak scale are unlikely to contribute to θ_{12} and θ_{23} in a dominant way.
- Special values of θ_{12} and θ_{23} might stem from an underlying flavor symmetry of the charged-lepton mass matrix or the neutrino mass matrix. Then the contributions of lepton mass ratios to flavor mixing angles, due to flavor symmetry breaking, are expected to serve as the perturbative corrections to U_0 or V_0, or another constant flavor mixing pattern.
- Vanishing or small θ_{13} could be a natural consequence of the explicit textures of lepton mass matrices. It might also be related to the flavor symmetry which gives rise to sizable θ_{12} and θ_{23} (e.g., in U_0 or V_0).

- Small corrections to a constant flavor mixing pattern may also result from the renormalization-group running effects of leptons and quarks, e.g., from a superhigh-energy scale to low energies or vice versa.

We admit that there are too many possibilities of linking the observed pattern of lepton flavor mixing to a certain flavor symmetry, and none of them is unique from the theoretical point of view. In this sense flavor symmetries might not be a perfect guiding principle of model building.

3.5.3 Rephasing Invariants and Unitarity Triangles

In the basis where the flavor eigenstates of charged leptons are identified with their mass eigenstates, the MNS matrix V relates the neutrino mass eigenstates (ν_1, ν_2, ν_3) to the neutrino flavor eigenstates $(\nu_e, \nu_\mu, \nu_\tau)$:

$$\begin{pmatrix} \nu_e \\ \nu_\mu \\ \nu_\tau \end{pmatrix} = \begin{pmatrix} V_{e1} & V_{e2} & V_{e3} \\ V_{\mu 1} & V_{\mu 2} & V_{\mu 3} \\ V_{\tau 1} & V_{\tau 2} & V_{\tau 3} \end{pmatrix} \begin{pmatrix} \nu_1 \\ \nu_2 \\ \nu_3 \end{pmatrix} \; . \tag{3.114}$$

The unitarity of V represents two sets of normalization and orthogonality conditions:

$$\sum_i \left(V_{\alpha i} V^*_{\beta i} \right) = \; \delta_{\alpha\beta} \; , \qquad \sum_\alpha \left(V_{\alpha i} V^*_{\alpha j} \right) = \delta_{ij} \; , \tag{3.115}$$

where Greek and Latin subscripts run over (e, μ, τ) and $(1, 2, 3)$, respectively. In the complex plane the six orthogonality relations in Eq. (3.115) define six triangles $(\triangle_e, \triangle_\mu, \triangle_\tau)$ and $(\triangle_1, \triangle_2, \triangle_3)$ shown in Fig. 3.10, the so-called unitarity triangles. These six triangles have eighteen different sides and nine different inner (or outer) angles. But the unitarity of V requires that all six triangles have the same area amounting to $\mathcal{J}/2$, where $\mathcal{J}$ is the Jarlskog invariant of CP violation (Jarlskog, 1985; Wu, 1986) defined through

$$\mathrm{Im} \left(V_{\alpha i} V_{\beta j} V^*_{\alpha j} V^*_{\beta i} \right) = \mathcal{J} \sum_\gamma \epsilon_{\alpha\beta\gamma} \sum_k \epsilon_{ijk} \; . \tag{3.116}$$

One has $\mathcal{J} = c_{12} s_{12} c^2_{13} s_{13} c_{23} s_{23} \sin\delta$ in the standard parametrization of V and $\mathcal{J} = c_l s_l c_\nu s_\nu c s^2 \sin\phi$ in the FX parametrization of V. No matter whether neutrinos are Dirac or Majorana particles, the strength of CP or T violation in neutrino oscillations depends only upon $\mathcal{J}$.

To show why the areas of six unitarity triangles are identical with one another, let us take triangles $\triangle_\tau$ and $\triangle_3$ for example. They correspond to the orthogonality relations

$$\begin{aligned} V_{e1} V^*_{\mu 1} + V_{e2} V^*_{\mu 2} + V_{e3} V^*_{\mu 3} \; &= \; 0 \; , \\ V_{e1} V^*_{e 2} + V_{\mu 1} V^*_{\mu 2} + V_{\tau 1} V^*_{\tau 2} \; &= \; 0 \; . \end{aligned} \tag{3.117}$$

Multiplying these two equations by $V_{\mu 2} V^*_{e 2}$ and $V_{\mu 2} V^*_{\mu 1}$ respectively, we arrive at two rescaled triangles which share the side

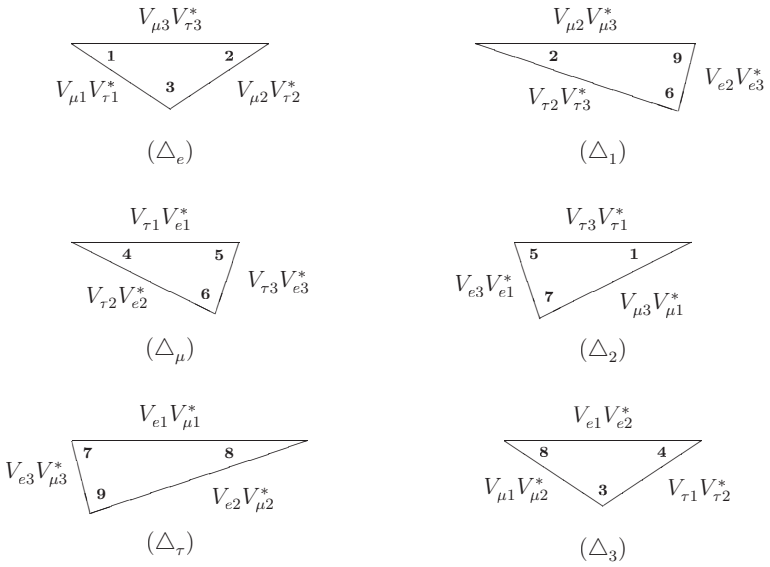

Fig. 3.10 Unitarity triangles of the 3×3 MNS matrix in the complex plane. Each triangle is named by the index that does not manifest in its three sides

$$\begin{aligned} V_{e1}V_{\mu2}V_{e2}^*V_{\mu1}^* &= -|V_{e2}V_{\mu2}|^2 - V_{e3}V_{\mu2}V_{e2}^*V_{\mu3}^* \\ &= -|V_{\mu1}V_{\mu2}|^2 - V_{\mu2}V_{\tau1}V_{\mu1}^*V_{\tau2}^* \,. \end{aligned} \tag{3.118}$$

This result is apparently consistent with the definition of $\mathcal{J}$ in Eq. (3.116); i.e., $\mathrm{Im}(V_{e1}V_{\mu2}V_{e2}^*V_{\mu1}^*) = \mathcal{J}$ and $\mathrm{Im}(V_{e3}V_{\mu2}V_{e2}^*V_{\mu3}^*) = \mathrm{Im}(V_{\mu2}V_{\tau1}V_{\mu1}^*V_{\tau2}^*) = -\mathcal{J}$. The latter simultaneously implies that the areas of $\triangle_\tau$ and $\triangle_3$ are equal to $\mathcal{J}/2$. One may analogously prove that all the six unitarity triangles have the same area $\mathcal{J}/2$. If CP or T were an exact symmetry, $\mathcal{J} = 0$ would hold and those unitarity triangles would collapse into lines in the complex plane. Note that the shape and area of each unitarity triangle are irrelevant to the nature of neutrinos; i.e., they are the same for Dirac and Majorana neutrinos.

Because of $V_{e1}^*V_{\mu1} + V_{e2}^*V_{\mu2} = -V_{e3}^*V_{\mu3}$ or equivalently $|V_{e1}V_{\mu1}^* + V_{e2}V_{\mu2}^*|^2 = |V_{e3}V_{\mu3}^*|^2$, it is easy to obtain

$$2\mathrm{Re}\left(V_{e1}V_{\mu2}V_{e2}^*V_{\mu1}^*\right) = |V_{e3}|^2|V_{\mu3}|^2 - |V_{e1}|^2|V_{\mu1}|^2 - |V_{e2}|^2|V_{\mu2}|^2 \,. \tag{3.119}$$

Combining $V_{e1}V_{\mu2}V_{e2}^*V_{\mu1}^* = \mathrm{Re}(V_{e1}V_{\mu2}V_{e2}^*V_{\mu1}^*) + \mathrm{i}\mathcal{J}$ with Eq. (3.119) leads us to the result

$$\begin{aligned} \mathcal{J}^2 &= |V_{e1}|^2|V_{\mu2}|^2|V_{e2}|^2|V_{\mu1}|^2 - \frac{1}{4}\left(|V_{e3}|^2|V_{\mu3}|^2 - |V_{e1}|^2|V_{\mu1}|^2 - |V_{e2}|^2|V_{\mu2}|^2\right)^2 \\ &= |V_{e1}|^2|V_{\mu2}|^2|V_{e2}|^2|V_{\mu1}|^2 - \frac{1}{4}\left(1 + |V_{e1}|^2|V_{\mu2}|^2 + |V_{e2}|^2|V_{\mu1}|^2\right. \\ &\quad \left. -|V_{e1}|^2 - |V_{\mu2}|^2 - |V_{e2}|^2 - |V_{\mu1}|^2\right)^2 \,. \end{aligned} \tag{3.120}$$

As a straightforward generalization of Eq. (3.120), $\mathcal{J}^2$ can be expressed in terms of the moduli of any four independent matrix elements of V (Sasaki, 1986; Hamzaoui, 1988; Fritzsch and Xing, 2000b):

$$\mathcal{J}^2 = |V_{\alpha i}|^2 |V_{\beta j}|^2 |V_{\alpha j}|^2 |V_{\beta i}|^2 - \frac{1}{4} \left(1 + |V_{\alpha i}|^2 |V_{\beta j}|^2 + |V_{\alpha j}|^2 |V_{\beta i}|^2 - |V_{\alpha i}|^2 - |V_{\beta j}|^2 - |V_{\alpha j}|^2 - |V_{\beta i}|^2\right)^2 , \tag{3.121}$$

in which $\alpha \neq \beta$ running over (e, μ, τ) and $i \neq j$ running over $(1, 2, 3)$. The implication of this result is very obvious: the information about leptonic CP violation can in principle be extracted from the measured moduli of the neutrino mixing matrix elements.

As a consequence of the unitarity of V, two interesting relations can be derived from the normalization conditions in Eq. (3.115):

$$\begin{aligned} |V_{e2}|^2 - |V_{\mu 1}|^2 &= |V_{\mu 3}|^2 - |V_{\tau 2}|^2 = |V_{\tau 1}|^2 - |V_{e3}|^2 \equiv \Delta_{\rm L} , \\ |V_{e2}|^2 - |V_{\mu 3}|^2 &= |V_{\mu 1}|^2 - |V_{\tau 2}|^2 = |V_{\tau 3}|^2 - |V_{e1}|^2 \equiv \Delta_{\rm R} . \end{aligned} \tag{3.122}$$

The off-diagonal asymmetries $\Delta_{\rm L}$ and $\Delta_{\rm R}$ characterize the geometrical structure of V about its V_{e1}-$V_{\mu 2}$-$V_{\tau 3}$ and V_{e3}-$V_{\mu 2}$-$V_{\tau 1}$ axes, respectively (Xing, 2002b). For instance, $\Delta_{\rm L} = 1/6$ and $\Delta_{\rm R} = -1/6$ hold for the tri-bimaximal neutrino mixing pattern V_0. If $\Delta_{\rm L} = 0$ (or $\Delta_{\rm R} = 0$) held, V would be symmetric about the V_{e1}-$V_{\mu 2}$-$V_{\tau 3}$ (or V_{e3}-$V_{\mu 2}$-$V_{\tau 1}$) axis. Geometrically this would correspond to the congruence between two unitarity triangles; i.e.,

$$\begin{aligned} \Delta_{\rm L} = 0 \quad &\Longrightarrow \quad \triangle_e \cong \triangle_1 , \quad \triangle_\mu \cong \triangle_2 , \quad \triangle_\tau \cong \triangle_3 ; \\ \Delta_{\rm R} = 0 \quad &\Longrightarrow \quad \triangle_e \cong \triangle_3 , \quad \triangle_\mu \cong \triangle_2 , \quad \triangle_\tau \cong \triangle_1 . \end{aligned} \tag{3.123}$$

Indeed the counterpart of $\Delta_{\rm L}$ in the quark sector is only of $\mathcal{O}(10^{-5})$ (Xing, 1996a, 1996b); i.e., the CKM matrix is almost symmetric about its V_{ud}-V_{cs}-V_{tb} axis. An exactly symmetric flavor mixing matrix might hint at an underlying flavor symmetry, from which some deeper understanding of the fermion mass texture could be achieved.

3.5.4 Flavor Problems in Particle Physics

In the subatomic world the fundamental building blocks of matter have twelve flavors: six quarks and six leptons (and their antiparticles). Table 3.6 is a brief list of some important discoveries in flavor physics, which can partly give people a ball-park feeling of a century of developments in particle physics. The SM of electromagnetic and weak interactions contain thirteen free parameters in its lepton and quark sectors: three charged-lepton masses, six quark masses, three quark flavor mixing angles and one CP-violating phase. If three known neutrinos are massive Majorana particles, one has to introduce nine free parameters to describe their flavor properties: three neutrino masses, three

lepton flavor mixing angles and three CP-violating phases. Thus an effective theory of electroweak interactions at low energies totally consists of twenty-two flavor parameters which can only be determined from experiments. Why is the number of degrees of freedom so big in the flavor sector? What is the fundamental physics behind these parameters? Such puzzles constitute the flavor problems in modern particle physics.

Table 3.6 Some important discoveries in the developments of flavor physics

	Discoveries of lepton flavors, quark flavors and CP violation
1897	electron (Thomson, 1897)
1919	proton (up and down quarks) (Rutherford, 1919)
1932	neutron (up and down quarks) (Chadwick, 1932)
1933	positron (Anderson, 1933)
1937	muon (Neddermeyer and Anderson, 1937)
1947	Kaon (strange quark) (Rochester and Butler, 1947)
1956	electron antineutrino (Cowan *et al.*, 1956)
1962	muon neutrino (Danby *et al.*, 1962)
1964	CP violation in s-quark decays (Christenson *et al.*, 1964)
1974	charm quark (Aubert *et al.*, 1974; Abrams *et al.*, 1974)
1975	tau (Perl *et al.*, 1975)
1977	bottom quark (Herb *et al.*, 1977)
1995	top quark (Abe *et al.*, 1995; Abachi *et al.*, 1995)
2000	tau neutrino (Kodama *et al.*, 2000)
2001	CP violation in b-quark decays (Aubert *et al.*, 2001; Abe *et al.*, 2001)

Fig. 3.11 is a schematic plot for the mass spectra of six quarks and six leptons at the electroweak scale (Li and Xing, 2010), where we have used the allowed ranges of neutrino masses with a normal hierarchy (Gonzalez-Garcia *et al.*, 2010) and the central values of charged-lepton and quark masses (Xing *et al.*, 2008). One can see that the span between m_1 and m_t is at least twelve orders of magnitude. Furthermore, the "desert" between the heaviest neutrino ν_3 and the lightest charged fermion e^- spans at least six orders of magnitude. Why do twelve fermions have such a strange mass pattern or such hierarchy and desert puzzles? The answer to this fundamental question remains open. As shown in Table 3.1, current neutrino oscillation data only tell us $m_1 < m_2$. It remains unknown whether m_3 is larger than m_2 (normal hierarchy) or smaller than m_1 (inverted hierarchy). The possibility $m_1 \approx m_2 \approx m_3$ (near degeneracy) cannot be excluded at present. In contrast, three families of charged fermions have strong mass hierarchies (Xing *et al.*, 2008):

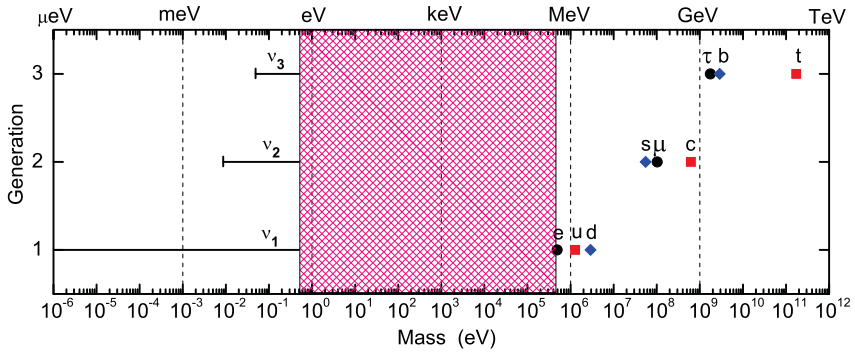

Fig. 3.11 A schematic illustration of the flavor "hierarchy" and "desert" problems in the SM fermion mass spectrum at the electroweak scale (Li and Xing, 2010)

$$\frac{m_e}{m_\mu} \sim \frac{m_u}{m_c} \sim \frac{m_c}{m_t} \sim \lambda^4 \; , \\ \frac{m_\mu}{m_\tau} \sim \frac{m_d}{m_s} \sim \frac{m_s}{m_b} \sim \lambda^2 \; , \tag{3.124}$$

where $\lambda \equiv \sin\theta_{\rm C} \approx 0.22$ with $\theta_{\rm C}$ being the Cabibbo angle of quark flavor mixing (Cabibbo, 1963). In the standard parametrization of the CKM matrix, three quark mixing angles exhibit an impressive hierarchy:

$$\vartheta_{12} \sim \lambda \; , \quad \vartheta_{23} \sim \lambda^2 \; , \quad \vartheta_{13} \sim \lambda^4 \; . \tag{3.125}$$

These two kinds of hierarchies might intrinsically be related to each other, because the flavor mixing angles actually measure a mismatch between the mass and flavor eigenstates of up- and down-type quarks. For example, the relations $\vartheta_{12} \approx \sqrt{m_d/m_s}$, $\vartheta_{23} \approx \sqrt{m_d/m_b}$ and $\vartheta_{13} \approx \sqrt{m_u/m_t}$ are compatible with Eqs. (3.124) and (3.125). They can be derived from a specific pattern of up- and down-type quark mass matrices with five texture zeros (Chkareuli and Froggatt, 1999). On the other hand, it seems quite difficult to find a simple way of linking two large lepton flavor mixing angles $\theta_{12} \sim \pi/6$ and $\theta_{23} \sim \pi/4$ to small m_e/m_μ and m_μ/m_τ. One might ascribe the largeness of θ_{12} and θ_{23} to a very weak hierarchy of three neutrino masses and the smallness of θ_{13} to the strong mass hierarchy in the charged-lepton sector (Fritzsch and Xing, 2006, 2009). There are of course many possibilities of model building to understand the observed lepton flavor mixing pattern, but none of them has experimentally and theoretically been justified.

Among a number of concrete flavor puzzles that are currently facing us, the following three are particularly intriguing.

- The pole masses of three charged leptons satisfy the equality (Koide, 1983)

$$\frac{m_e + m_\mu + m_\tau}{\left(\sqrt{m_e} + \sqrt{m_\mu} + \sqrt{m_\tau}\right)^2} = \frac{2}{3} \tag{3.126}$$

to an amazingly good degree of accuracy — its error bar is only of $\mathcal{O}(10^{-5})$ (Xing and Zhang, 2006).

- There are two quark-lepton "complementarity" relations in flavor mixing:

$$\theta_{12} + \vartheta_{12} \approx \theta_{23} + \vartheta_{23} \approx \frac{\pi}{4} \; , \tag{3.127}$$

which are compatible with the present experimental data (Xing, 2005).

- Two unitarity triangles of the CKM matrix, defined by the orthogonality conditions $V_{ud} V^*_{ub} + V_{cd} V^*_{cb} + V_{td} V^*_{tb} = 0$ and $V_{tb} V^*_{ub} + V_{ts} V^*_{us} + V_{td} V^*_{ud} = 0$, are almost the right triangles. Namely, the common inner angle of these two triangles satisfies (Xing, 2009a)

$$\alpha \equiv \arg\left(-\frac{V_{ud} V^*_{ub}}{V_{td} V^*_{tb}}\right) \approx \frac{\pi}{2} \; , \tag{3.128}$$

indicated by current experimental data on quark mixing and CP violation.

Such special numerical relations might just be accidental. One or two of them might also be possible to result from a certain (underlying) flavor symmetry.

3.6 Running Behaviors of Neutrino Mass Parameters

The spirit of seesaw mechanisms (to be described in Chapter 4) is to attribute the small masses of three known neutrinos to the existence of some heavy degrees of freedom, such as the $SU(2)_{\rm L}$ gauge-singlet fermions, the $SU(2)_{\rm L}$ gauge-triplet scalars or the $SU(2)_{\rm L}$ gauge-triplet fermions. All of them point to the unique dimension-5 Weinberg operator in an effective theory after the corresponding heavy particles are integrated out (Weinberg, 1979):

$$\frac{\mathcal{L}_{\rm d=5}}{\Lambda} = \frac{1}{2} \kappa_{\alpha\beta} \overline{\ell_{\alpha \rm L}} \tilde{H} \tilde{H}^T \ell^c_{\beta \rm L} + {\rm h.c.} \; , \tag{3.129}$$

where Λ is the cutoff scale, $\ell_{\rm L}$ denotes the left-handed lepton doublet, $\tilde{H} \equiv {\rm i}\sigma_2 H^*$ with H being the SM Higgs doublet, and κ stands for the effective neutrino coupling matrix. After spontaneous gauge symmetry breaking, $\tilde{H}$ gains its vacuum expectation value $\langle \tilde{H} \rangle = v/\sqrt{2}$ with $v \approx 246$ GeV. We are then left with the effective Majorana mass matrix $M_\nu = \kappa v^2/2$ for three light neutrinos from Eq. (3.129). If the dimension-5 Weinberg operator is obtained in the framework of the minimal supersymmetric standard model (MSSM), one will be left with $M_\nu = \kappa (v \sin\beta)^2/2$, where $\tan\beta$ denotes the ratio of the vacuum expectation values of two MSSM Higgs doublets.

Eq. (3.129) or its supersymmetric counterpart can provide a simple but generic way of generating tiny neutrino masses. There are a number of interesting possibilities of building renormalizable gauge models to realize the effective Weinberg mass operator, either radiatively or at the tree level. The

latter case is just associated with the well-known seesaw mechanisms to be discussed in Section 4.1. Here we assume that $\mathcal{L}_{\rm d=5}/\Lambda$ arises from an underlying seesaw model, whose lightest heavy particle has a mass of $\mathcal{O}(\Lambda)$. In other words, Λ characterizes the seesaw scale. Above Λ there may exist one or more energy thresholds corresponding to the masses of heavier seesaw particles (King and Singh, 2000; Antusch *et al.*, 2002a; Mei, 2005; Antusch *et al.*, 2005; Chao and Zhang, 2007; Schmidt, 2007; Chakrabortty *et al.*, 2009). Below Λ the energy dependence of the effective neutrino coupling matrix κ is described by its renormalization-group equation (RGE). The evolution of κ from Λ down to the electroweak scale is formally independent of any details of the relevant seesaw model from which κ is derived.

3.6.1 One-loop Renormalization-group Equations

At the one-loop level κ obeys the RGE (Chankowski and Pluciennik, 1993; Babu *et al.*, 1993; Antusch *et al.*, 2001; 2002b)

$$16\pi^2 \frac{{\rm d}\kappa}{{\rm d}t} = \alpha_\kappa \kappa + C_\kappa \left[(Y_l Y_l^\dagger)\kappa + \kappa (Y_l Y_l^\dagger)^T \right] \; , \tag{3.130}$$

where $t \equiv \ln(\mu/\Lambda)$ with μ being an arbitrary renormalization scale between the electroweak scale and the seesaw scale, and Y_l is the charged-lepton Yukawa coupling matrix. The RGE of Y_l and those of $Y_{\rm u}$ (up-type quarks) and $Y_{\rm d}$ (down-type quarks) are given by

$$\begin{aligned} 16\pi^2 \frac{{\rm d}Y_l}{{\rm d}t} &= \left[\alpha_l + C_l^l (Y_l Y_l^\dagger) \right] Y_l \; , \\ 16\pi^2 \frac{{\rm d}Y_{\rm u}}{{\rm d}t} &= \left[\alpha_{\rm u} + C_{\rm u}^{\rm u} (Y_{\rm u} Y_{\rm u}^\dagger) + C_{\rm u}^{\rm d} (Y_{\rm d} Y_{\rm d}^\dagger) \right] Y_{\rm u} \; , \\ 16\pi^2 \frac{{\rm d}Y_{\rm d}}{{\rm d}t} &= \left[\alpha_{\rm d} + C_{\rm d}^{\rm u} (Y_{\rm u} Y_{\rm u}^\dagger) + C_{\rm d}^{\rm d} (Y_{\rm d} Y_{\rm d}^\dagger) \right] Y_{\rm d} \; . \end{aligned} \tag{3.131}$$

In the framework of the SM we have

$$C_\kappa = C_{\rm u}^{\rm d} = C_{\rm d}^{\rm u} = -C_l^l = -C_{\rm u}^{\rm u} = -C_{\rm d}^{\rm d} = -\frac{3}{2} \; , \tag{3.132}$$

and

$$\begin{aligned} \alpha_\kappa &= -3g_2^2 + \lambda + 2{\rm Tr}\left[3(Y_{\rm u} Y_{\rm u}^\dagger) + 3(Y_{\rm d} Y_{\rm d}^\dagger) + (Y_l Y_l^\dagger) \right] \; , \\ \alpha_l &= -\frac{9}{4} g_1^2 - \frac{9}{4} g_2^2 + {\rm Tr}\left[3(Y_{\rm u} Y_{\rm u}^\dagger) + 3(Y_{\rm d} Y_{\rm d}^\dagger) + (Y_l Y_l^\dagger) \right] \; , \\ \alpha_{\rm u} &= -\frac{17}{20} g_1^2 - \frac{9}{4} g_2^2 - 8 g_3^2 + {\rm Tr}\left[3(Y_{\rm u} Y_{\rm u}^\dagger) + 3(Y_{\rm d} Y_{\rm d}^\dagger) + (Y_l Y_l^\dagger) \right] \; , \\ \alpha_{\rm d} &= -\frac{1}{4} g_1^2 - \frac{9}{4} g_2^2 - 8 g_3^2 + {\rm Tr}\left[3(Y_{\rm u} Y_{\rm u}^\dagger) + 3(Y_{\rm d} Y_{\rm d}^\dagger) + (Y_l Y_l^\dagger) \right] \; ; \end{aligned} \tag{3.133}$$

and in the framework of the MSSM we have

$$C_\kappa = C_{\rm u}^{\rm d} = C_{\rm d}^{\rm u} = \frac{C_l^l}{3} = \frac{C_{\rm u}^{\rm u}}{3} = \frac{C_{\rm d}^{\rm d}}{3} = 1 \ , \tag{3.134}$$

and

$$\begin{aligned}
\alpha_\kappa &= -\frac{6}{5} g_1^2 - 6 g_2^2 + 6{\rm Tr}(Y_{\rm u} Y_{\rm u}^\dagger) \ , \\
\alpha_l &= -\frac{9}{5} g_1^2 - 3 g_2^2 + {\rm Tr}\left[3(Y_{\rm d} Y_{\rm d}^\dagger) + (Y_l Y_l^\dagger)\right] \ , \\
\alpha_{\rm u} &= -\frac{13}{15} g_1^2 - 3 g_2^2 - \frac{16}{3} g_3^2 + 3{\rm Tr}(Y_{\rm u} Y_{\rm u}^\dagger) \ , \\
\alpha_{\rm d} &= -\frac{7}{15} g_1^2 - 3 g_2^2 - \frac{16}{3} g_3^2 + {\rm Tr}\left[3(Y_{\rm d} Y_{\rm d}^\dagger) + (Y_l Y_l^\dagger)\right] \ .
\end{aligned} \tag{3.135}$$

Here g_1, g_2 and g_3 are the gauge couplings and satisfy their RGEs

$$16\pi^2 \frac{{\rm d}g_i}{{\rm d}t} = b_i g_i^3 \ , \tag{3.136}$$

where $(b_1, b_2, b_3) = (41/10, -19/6, -7)$ in the SM or $(33/5, 1, -3)$ in the MSSM. In addition, λ is the Higgs self-coupling parameter of the SM and obeys the RGE (Antusch *et al.*, 2003)

$$\begin{aligned}
16\pi^2 \frac{{\rm d}\lambda}{{\rm d}t} = {} & 6\lambda^2 - 3\lambda\left(\frac{3}{5} g_1^2 + 3 g_2^2\right) + \frac{3}{2}\left(\frac{3}{5} g_1^2 + g_2^2\right)^2 + 3 g_2^4 \\
& + 4\lambda {\rm Tr}\left[3(Y_{\rm u} Y_{\rm u}^\dagger) + 3(Y_{\rm d} Y_{\rm d}^\dagger) + (Y_l Y_l^\dagger)\right] \\
& - 8{\rm Tr}\left[3(Y_{\rm u} Y_{\rm u}^\dagger)^2 + 3(Y_{\rm d} Y_{\rm d}^\dagger)^2 + (Y_l Y_l^\dagger)^2\right] \ .
\end{aligned} \tag{3.137}$$

The relation between λ and the Higgs mass M_h is given by $\lambda = M_h^2/(2v^2)$, where $v \approx 246$ GeV is the vacuum expectation value of the Higgs field.

Although massive neutrinos are most likely to be Majorana particles, the possibility that they could be Dirac particles cannot be ruled out at present. A combination of the Yukawa interactions of Dirac neutrinos in Eq. (3.10) and those of charged fermions in Eq. (3.47) allows one to derive their RGEs (Cheng *et al.*, 1974; Machacek and Vaughn, 1984). At the one-loop level we have the RGEs of Dirac fermions:

$$\begin{aligned}
16\pi^2 \frac{{\rm d}Y_\nu}{{\rm d}t} &= \left[\alpha_\nu + C_\nu^\nu (Y_\nu Y_\nu^\dagger) + C_\nu^l (Y_l Y_l^\dagger)\right] Y_\nu \ , \\
16\pi^2 \frac{{\rm d}Y_l}{{\rm d}t} &= \left[\alpha_l + C_l^\nu (Y_\nu Y_\nu^\dagger) + C_l^l (Y_l Y_l^\dagger)\right] Y_l \ , \\
16\pi^2 \frac{{\rm d}Y_{\rm u}}{{\rm d}t} &= \left[\alpha_{\rm u} + C_{\rm u}^{\rm u} (Y_{\rm u} Y_{\rm u}^\dagger) + C_{\rm u}^{\rm d} (Y_{\rm d} Y_{\rm d}^\dagger)\right] Y_{\rm u} \ , \\
16\pi^2 \frac{{\rm d}Y_{\rm d}}{{\rm d}t} &= \left[\alpha_{\rm d} + C_{\rm d}^{\rm u} (Y_{\rm u} Y_{\rm u}^\dagger) + C_{\rm d}^{\rm d} (Y_{\rm d} Y_{\rm d}^\dagger)\right] Y_{\rm d} \ .
\end{aligned} \tag{3.138}$$

In the framework of the SM

$$C_\nu^\nu = C_l^l = C_{\rm u}^{\rm u} = C_{\rm d}^{\rm d} = +\frac{3}{2} \; ,$$
$$C_\nu^l = C_l^\nu = C_{\rm u}^{\rm d} = C_{\rm d}^{\rm u} = -\frac{3}{2} \; , \tag{3.139}$$

and

$$\alpha_\nu = -\frac{9}{20} g_1^2 - \frac{9}{4} g_2^2 + T_{\rm SM} \; ,$$
$$\alpha_l = -\frac{9}{4} g_1^2 - \frac{9}{4} g_2^2 + T_{\rm SM} \; ,$$
$$\alpha_{\rm u} = -\frac{17}{20} g_1^2 - \frac{9}{4} g_2^2 - 8 g_3^2 + T_{\rm SM} \; ,$$
$$\alpha_{\rm d} = -\frac{1}{4} g_1^2 - \frac{9}{4} g_2^2 - 8 g_3^2 + T_{\rm SM} \; , \tag{3.140}$$

in which $T_{\rm SM} = {\rm Tr}\left[3(Y_{\rm u} Y_{\rm u}^\dagger) + 3(Y_{\rm d} Y_{\rm d}^\dagger) + (Y_\nu Y_\nu^\dagger) + (Y_l Y_l^\dagger)\right]$ (Lindner *et al.*, 2005); and in the framework of the MSSM

$$C_\nu^\nu = C_l^l = C_{\rm u}^{\rm u} = C_{\rm d}^{\rm d} = +3 \; ,$$
$$C_\nu^l = C_l^\nu = C_{\rm u}^{\rm d} = C_{\rm d}^{\rm u} = +1 \; , \tag{3.141}$$

and

$$\alpha_\nu = -\frac{3}{5} g_1^2 - 3 g_2^2 + {\rm Tr}\left[3(Y_{\rm u} Y_{\rm u}^\dagger) + (Y_\nu Y_\nu^\dagger)\right] \; ,$$
$$\alpha_l = -\frac{9}{5} g_1^2 - 3 g_2^2 + {\rm Tr}\left[(Y_\nu Y_\nu^\dagger) + 3(Y_l Y_l^\dagger)\right] \; ,$$
$$\alpha_{\rm u} = -\frac{13}{15} g_1^2 - 3 g_2^2 - \frac{16}{3} g_3^2 + {\rm Tr}\left[3(Y_{\rm u} Y_{\rm u}^\dagger) + (Y_\nu Y_\nu^\dagger)\right] \; ,$$
$$\alpha_{\rm d} = -\frac{7}{15} g_1^2 - 3 g_2^2 - \frac{16}{3} g_3^2 + {\rm Tr}\left[3(Y_{\rm d} Y_{\rm d}^\dagger) + (Y_l Y_l^\dagger)\right] \; . \tag{3.142}$$

The RGEs of three gauge couplings g_1, g_2 and g_3 remain to be those given in Eq. (3.136).

The above RGEs allow us to evaluate the running behavior of κ or Y_ν, together with those of Y_l, $Y_{\rm u}$ and $Y_{\rm d}$, from the seesaw scale to the electroweak scale or vice versa. We shall examine the evolution of neutrino masses, lepton flavor mixing angles and CP-violating phases in the subsequent sections.

3.6.2 Evolution of Majorana Neutrino Mass Parameters

Without loss of generality, we choose the flavor basis where Y_l is diagonal: $Y_l = D_l \equiv {\rm Diag}\{y_e, y_\mu, y_\tau\}$ with y_α being the eigenvalues of Y_l. In this case the effective Majorana neutrino coupling matrix κ can be diagonalized by the MNS matrix V; i.e., $V^\dagger \kappa V^* = \widehat{\kappa} \equiv {\rm Diag}\{\kappa_1, \kappa_2, \kappa_3\}$ with κ_i being the eigenvalues of κ. Then

$$\frac{\mathrm{d}\kappa}{\mathrm{d}t} = \frac{\mathrm{d}}{\mathrm{d}t}\left(V\widehat{\kappa}V^T\right) = \dot{V}\widehat{\kappa}V^T + V\dot{\widehat{\kappa}}V^T + V\widehat{\kappa}\dot{V}^T$$
$$= \frac{1}{16\pi^2}\left[\alpha_\kappa V\widehat{\kappa}V^T + C_\kappa\left(D_l^2 V\widehat{\kappa}V^T + V\widehat{\kappa}V^T D_l^2\right)\right] , \qquad (3.143)$$

with the help of Eq. (3.130). After a definition of the Hermitian matrix $S \equiv V^\dagger D_l^2 V$ and the anti-Hermitian matrix $T \equiv V^\dagger \dot{V}$, Eq. (3.143) leads us to

$$\dot{\widehat{\kappa}} = \frac{1}{16\pi^2}\left[\alpha_\kappa\widehat{\kappa} + C_\kappa\left(S\widehat{\kappa} + \widehat{\kappa}S^*\right)\right] - T\widehat{\kappa} + \widehat{\kappa}T^* . \qquad (3.144)$$

Because $\widehat{\kappa}$ is by definition diagonal and real, the left- and right-hand sides of Eq. (3.144) must be diagonal and real. We can therefore arrive at

$$\dot{\kappa}_i = \frac{1}{16\pi^2}\left(\alpha_\kappa + 2C_\kappa \mathrm{Re}S_{ii}\right)\kappa_i , \qquad (3.145)$$

together with $\mathrm{Im}T_{ii} = \mathrm{Re}T_{ii} = \mathrm{Im}S_{ii} = 0$ (for $i = 1, 2, 3$). Since the off-diagonal parts of Eq. (3.144) are vanishing, we have

$$T_{ij}\kappa_j - \kappa_i T_{ij}^* = \frac{C_\kappa}{16\pi^2}\left(S_{ij}\kappa_j + \kappa_i S_{ij}^*\right) \qquad (3.146)$$

with $i \neq j$. Therefore,

$$\mathrm{Re}T_{ij} = -\frac{C_\kappa}{16\pi^2}\cdot\frac{\kappa_i + \kappa_j}{\kappa_i - \kappa_j}\mathrm{Re}S_{ij} ,$$
$$\mathrm{Im}T_{ij} = -\frac{C_\kappa}{16\pi^2}\cdot\frac{\kappa_i - \kappa_j}{\kappa_i + \kappa_j}\mathrm{Im}S_{ij} . \qquad (3.147)$$

Due to $\dot{V} = VT$, Eq. (3.147) actually governs the evolution of V with energies.

We proceed to define $V \equiv PUP'$, in which $P \equiv \mathrm{Diag}\{\mathrm{e}^{\mathrm{i}\phi_e}, \mathrm{e}^{\mathrm{i}\phi_\mu}, \mathrm{e}^{\mathrm{i}\phi_\tau}\}$, $P' \equiv \mathrm{Diag}\{\mathrm{e}^{\mathrm{i}\rho}, \mathrm{e}^{\mathrm{i}\sigma}, 1\}$, and U is the CKM-like matrix containing three neutrino mixing angles and one CP-violating phase. Although P does not have any physical meaning, its phases have their own RGEs (Casas *et al.*, 2000). In contrast, P' serves for the Majorana phase matrix. We find

$$T' \equiv P'TP'^\dagger = P'V^\dagger\dot{V}P'^\dagger = \dot{P}'P'^\dagger + U^\dagger\dot{U} + U^\dagger P^\dagger\dot{P}U , \qquad (3.148)$$

from which we can obtain six independent constraint equations:

$$T'_{11} = T_{11} = \mathrm{i}\dot{\rho} + \sum_\alpha\left[U_{\alpha 1}^*\left(\dot{U}_{\alpha 1} + \mathrm{i}U_{\alpha 1}\dot{\phi}_\alpha\right)\right] ,$$
$$T'_{22} = T_{22} = \mathrm{i}\dot{\sigma} + \sum_\alpha\left[U_{\alpha 2}^*\left(\dot{U}_{\alpha 2} + \mathrm{i}U_{\alpha 2}\dot{\phi}_\alpha\right)\right] ,$$
$$T'_{33} = T_{33} = \sum_\alpha\left[U_{\alpha 3}^*\left(\dot{U}_{\alpha 3} + \mathrm{i}U_{\alpha 3}\dot{\phi}_\alpha\right)\right] ;$$

$$T'_{12} = T_{12}\mathrm{e}^{\mathrm{i}(\rho-\sigma)} = \sum_\alpha \left[U^*_{\alpha 1}\left(\dot{U}_{\alpha 2} + \mathrm{i}U_{\alpha 2}\dot{\phi}_\alpha\right)\right] ,$$
$$T'_{13} = T_{13}\mathrm{e}^{\mathrm{i}\rho} = \sum_\alpha \left[U^*_{\alpha 1}\left(\dot{U}_{\alpha 3} + \mathrm{i}U_{\alpha 3}\dot{\phi}_\alpha\right)\right] ,$$
$$T'_{23} = T_{23}\mathrm{e}^{\mathrm{i}\sigma} = \sum_\alpha \left[U^*_{\alpha 2}\left(\dot{U}_{\alpha 3} + \mathrm{i}U_{\alpha 3}\dot{\phi}_\alpha\right)\right] , \tag{3.149}$$

where α runs over e, μ and τ. Note that $T_{ii} = 0$ holds and T_{ij} is given by Eq. (3.147). In view of $y_e \ll y_\mu \ll y_\tau$, we take $D_l^2 \approx \mathrm{Diag}\{0, 0, y_\tau^2\}$ as an excellent approximation. Then S_{ij}, T_{ij} and T'_{ij} can all be expressed in terms of y_τ^2 and the parameters of U and P'. After a straightforward calculation, we obtain the explicit expressions of Eqs. (3.145) and (3.149) as follows:

$$\dot{\kappa}_i = \frac{\kappa_i}{16\pi^2}\left(\alpha_\kappa + 2C_\kappa y_\tau^2 |U_{\tau i}|^2\right) , \tag{3.150}$$

and

$$\sum_\alpha \left[U^*_{\alpha 1}\left(\mathrm{i}\dot{U}_{\alpha 1} - U_{\alpha 1}\dot{\phi}_\alpha\right)\right] = \dot{\rho} ,$$
$$\sum_\alpha \left[U^*_{\alpha 2}\left(\mathrm{i}\dot{U}_{\alpha 2} - U_{\alpha 2}\dot{\phi}_\alpha\right)\right] = \dot{\sigma} ,$$
$$\sum_\alpha \left[U^*_{\alpha 3}\left(\mathrm{i}\dot{U}_{\alpha 3} - U_{\alpha 3}\dot{\phi}_\alpha\right)\right] = 0 ,$$
$$\sum_\alpha \left[U^*_{\alpha 1}\left(\dot{U}_{\alpha 2} + \mathrm{i}U_{\alpha 2}\dot{\phi}_\alpha\right)\right] = -\frac{C_\kappa y_\tau^2}{16\pi^2}\mathrm{e}^{\mathrm{i}(\rho-\sigma)}\left[\zeta_{12}^{-1}\mathrm{Re}\left(U^*_{\tau 1}U_{\tau 2}\mathrm{e}^{\mathrm{i}(\sigma-\rho)}\right)\right.$$
$$\left. + \mathrm{i}\zeta_{12}\mathrm{Im}\left(U^*_{\tau 1}U_{\tau 2}\mathrm{e}^{\mathrm{i}(\sigma-\rho)}\right)\right] ,$$
$$\sum_\alpha \left[U^*_{\alpha 1}\left(\dot{U}_{\alpha 3} + \mathrm{i}U_{\alpha 3}\dot{\phi}_\alpha\right)\right] = -\frac{C_\kappa y_\tau^2}{16\pi^2}\mathrm{e}^{\mathrm{i}\rho}\left[\zeta_{13}^{-1}\mathrm{Re}\left(U^*_{\tau 1}U_{\tau 3}\mathrm{e}^{-\mathrm{i}\rho}\right)\right.$$
$$\left. + \mathrm{i}\zeta_{13}\mathrm{Im}\left(U^*_{\tau 1}U_{\tau 3}\mathrm{e}^{-\mathrm{i}\rho}\right)\right] ,$$
$$\sum_\alpha \left[U^*_{\alpha 2}\left(\dot{U}_{\alpha 3} + \mathrm{i}U_{\alpha 3}\dot{\phi}_\alpha\right)\right] = -\frac{C_\kappa y_\tau^2}{16\pi^2}\mathrm{e}^{\mathrm{i}\sigma}\left[\zeta_{23}^{-1}\mathrm{Re}\left(U^*_{\tau 2}U_{\tau 3}\mathrm{e}^{-\mathrm{i}\sigma}\right)\right.$$
$$\left. + \mathrm{i}\zeta_{23}\mathrm{Im}\left(U^*_{\tau 2}U_{\tau 3}\mathrm{e}^{-\mathrm{i}\sigma}\right)\right] , \tag{3.151}$$

where $\zeta_{ij} \equiv (\kappa_i - \kappa_j)/(\kappa_i + \kappa_j)$ with $i \neq j$. One can see that those y_τ^2-associated terms only consist of the matrix elements $U_{\tau i}$ (for $i = 1, 2, 3$). If a parametrization of U assures $U_{\tau i}$ to be as simple as possible, the resultant RGEs of neutrino mixing angles and CP-violating phases will be very concise. We find that the FX parametrization advocated in Eq. (3.108) with

$$U = \begin{pmatrix} s_l s_\nu c + c_l c_\nu \mathrm{e}^{-\mathrm{i}\phi} & s_l c_\nu c - c_l s_\nu \mathrm{e}^{-\mathrm{i}\phi} & s_l s \\ c_l s_\nu c - s_l c_\nu \mathrm{e}^{-\mathrm{i}\phi} & c_l c_\nu c + s_l s_\nu \mathrm{e}^{-\mathrm{i}\phi} & c_l s \\ -s_\nu s & -c_\nu s & c \end{pmatrix} \tag{3.152}$$

accords with the above observation, while the "standard" parametrization in Eq. (3.107) does not. That is why the RGEs of neutrino mixing angles and CP-violating phases in the standard parametrization are rather complicated (Casas *et al.*, 2000; Antusch *et al.*, 2003; Mei, 2005; Luo *et al.*, 2005).

Here we take the FX form of U to derive the RGEs of neutrino mass and mixing parameters (Xing, 2006). Combining Eqs. (3.150), (3.151) and (3.152), we arrive at

$$\begin{aligned}
\dot{\kappa}_1 &= \frac{\kappa_1}{16\pi^2}\left(\alpha_\kappa + 2C_\kappa y_\tau^2 s_\nu^2 s^2\right) \; , \\
\dot{\kappa}_2 &= \frac{\kappa_2}{16\pi^2}\left(\alpha_\kappa + 2C_\kappa y_\tau^2 c_\nu^2 s^2\right) \; , \\
\dot{\kappa}_3 &= \frac{\kappa_3}{16\pi^2}\left(\alpha_\kappa + 2C_\kappa y_\tau^2 c^2\right) \; ,
\end{aligned} \tag{3.153}$$

where $\alpha_\kappa \approx -3g_2^2 + 6y_t^2 + \lambda$ (SM) or $\alpha_\kappa \approx -1.2g_1^2 - 6g_2^2 + 6y_t^2$ (MSSM); and

$$\begin{aligned}
\dot{\theta}_l &= \frac{C_\kappa y_\tau^2}{16\pi^2}\, c_\nu s_\nu c \left[\left(\zeta_{13}^{-1} c_\rho c_{(\rho-\phi)} + \zeta_{13} s_\rho s_{(\rho-\phi)}\right)\right. \\
&\quad \left. - \left(\zeta_{23}^{-1} c_\sigma c_{(\sigma-\phi)} + \zeta_{23} s_\sigma s_{(\sigma-\phi)}\right)\right] \; , \\
\dot{\theta}_\nu &= \frac{C_\kappa y_\tau^2}{16\pi^2}\, c_\nu s_\nu \left[s^2\left(\zeta_{12}^{-1} c_{(\sigma-\rho)}^2 + \zeta_{12} s_{(\sigma-\rho)}^2\right) + c^2\left(\zeta_{13}^{-1} c_\rho^2 + \zeta_{13} s_\rho^2\right)\right. \\
&\quad \left. - c^2\left(\zeta_{23}^{-1} c_\sigma^2 + \zeta_{23} s_\sigma^2\right)\right] \; , \\
\dot{\theta} &= \frac{C_\kappa y_\tau^2}{16\pi^2}\, cs \left[s_\nu^2\left(\zeta_{13}^{-1} c_\rho^2 + \zeta_{13} s_\rho^2\right) + c_\nu^2\left(\zeta_{23}^{-1} c_\sigma^2 + \zeta_{23} s_\sigma^2\right)\right] \; ;
\end{aligned} \tag{3.154}$$

as well as

$$\begin{aligned}
\dot{\rho} &= \frac{C_\kappa y_\tau^2}{16\pi^2}\left[\widehat{\zeta}_{12} c_\nu^2 s^2 c_{(\sigma-\rho)} s_{(\sigma-\rho)} + \widehat{\zeta}_{13}\left(s_\nu^2 s^2 - c^2\right) c_\rho s_\rho + \widehat{\zeta}_{23} c_\nu^2 s^2 c_\sigma s_\sigma\right] \; , \\
\dot{\sigma} &= \frac{C_\kappa y_\tau^2}{16\pi^2}\left[\widehat{\zeta}_{12} s_\nu^2 s^2 c_{(\sigma-\rho)} s_{(\sigma-\rho)} + \widehat{\zeta}_{13} s_\nu^2 s^2 c_\rho s_\rho + \widehat{\zeta}_{23}\left(c_\nu^2 s^2 - c^2\right) c_\sigma s_\sigma\right] \; , \\
\dot{\phi} &= \frac{C_\kappa y_\tau^2}{16\pi^2}\left[\left(c_l^2 - s_l^2\right) c_l^{-1} s_l^{-1} c_\nu s_\nu c \left(\zeta_{13}^{-1} c_\rho s_{(\rho-\phi)} - \zeta_{13} s_\rho c_{(\rho-\phi)}\right.\right. \\
&\quad \left. - \zeta_{23}^{-1} c_\sigma s_{(\sigma-\phi)} + \zeta_{23} s_\sigma c_{(\sigma-\phi)}\right) + \widehat{\zeta}_{12} s^2 c_{(\sigma-\rho)} s_{(\sigma-\rho)} \\
&\quad \left. + \widehat{\zeta}_{13}\left(s_\nu^2 - c_\nu^2 c^2\right) c_\rho s_\rho + \widehat{\zeta}_{23}\left(c_\nu^2 - s_\nu^2 c^2\right) c_\sigma s_\sigma\right] \; ,
\end{aligned} \tag{3.155}$$

where $\widehat{\zeta}_{ij} \equiv \zeta_{ij}^{-1} - \zeta_{ij} = 4\kappa_i\kappa_j / \left(\kappa_i^2 - \kappa_j^2\right)$, $c_a \equiv \cos a$ and $s_a \equiv \sin a$ (for $a = \rho$, σ, $\sigma-\rho$, $\rho-\phi$ or $\sigma-\phi$). As a byproduct, the RGEs of three unphysical phases ϕ_α are listed below:

$$\begin{aligned}
\dot{\phi}_e = +\frac{C_\kappa y_\tau^2}{16\pi^2}\left[c_l s_l^{-1} c_\nu s_\nu c \left(\zeta_{13}^{-1} c_\rho s_{(\rho-\phi)} - \zeta_{13} s_\rho c_{(\rho-\phi)} - \zeta_{23}^{-1} c_\sigma s_{(\sigma-\phi)}\right.\right. \\
\left. + \zeta_{23} s_\sigma c_{(\sigma-\phi)}\right) + c^2\left(\widehat{\zeta}_{13} s_\nu^2 c_\rho s_\rho + \widehat{\zeta}_{23} c_\nu^2 c_\sigma s_\sigma\right)\Big] \; ,
\end{aligned}$$

$$\dot{\phi}_\mu = -\frac{C_\kappa y_\tau^2}{16\pi^2}\left[c_l^{-1}s_l c_\nu s_\nu c\left(\zeta_{13}^{-1}c_\rho s_{(\rho-\phi)} - \zeta_{13}s_\rho c_{(\rho-\phi)} - \zeta_{23}^{-1}c_\sigma s_{(\sigma-\phi)} + \zeta_{23}s_\sigma c_{(\sigma-\phi)}\right) - c^2\left(\widehat{\zeta}_{13}s_\nu^2 c_\rho s_\rho + \widehat{\zeta}_{23}c_\nu^2 c_\sigma s_\sigma\right)\right] ,$$

$$\dot{\phi}_\tau = -\frac{C_\kappa y_\tau^2}{16\pi^2}\left[s^2\left(\widehat{\zeta}_{13}s_\nu^2 c_\rho s_\rho + \widehat{\zeta}_{23}c_\nu^2 c_\sigma s_\sigma\right)\right] . \tag{3.156}$$

It is easy to check that the relationship $\dot{\phi} = \dot{\rho} + \dot{\sigma} + \dot{\phi}_e + \dot{\phi}_\mu + \dot{\phi}_\tau$ holds. That is why ϕ_α should not be ignored in deriving the RGEs of those physical parameters, although these three phases can finally be rotated away by rephasing the charged-lepton fields.

Some discussions on the basic features of RGEs of three neutrino masses, three flavor mixing angles and three CP-violating phases are in order.

(a) The running behaviors of three neutrino masses m_i (or equivalently κ_i) are essentially identical and determined by α_κ, unless $\tan\beta$ is large enough in the MSSM to make the y_τ^2-associated term competitive with the α_κ term. In our phase convention, $\dot{\kappa}_i$ or $\dot{m}_i$ (for $i = 1, 2, 3$) are independent of the CP-violating phase ϕ.

(b) Among three neutrino mixing angles, only the derivative of θ_ν contains a term proportional to ζ_{12}^{-1}. Note that $\zeta_{ij}^{-1} = (m_i + m_j)^2/\Delta m_{ij}^2$ with $\Delta m_{ij}^2 \equiv m_i^2 - m_j^2$ holds. Current solar and atmospheric neutrino oscillation data yield $\Delta m_{21}^2 \approx 7.7 \times 10^{-5}$ eV^2 and $|\Delta m_{32}^2| \approx |\Delta m_{31}^2| \approx 2.4 \times 10^{-3}$ eV^2. So θ_ν is in general more sensitive to radiative corrections than θ_l and θ. The evolution of θ_ν can be suppressed through the fine-tuning of $(\sigma - \rho)$. The smallest neutrino mixing angle θ_l may get radiative corrections even if its initial value is zero, and thus it can be radiatively generated from other neutrino mixing angles and CP-violating phases (Antusch *et al.*, 2003; Mei and Xing, 2004; Luo *et al.*, 2005; Luo and Xing, 2006a).

(c) The running behavior of ϕ is quite different from those of ρ and σ, because it includes a peculiar term proportional to s_l^{-1}. This term, which dominates $\dot{\phi}$ when θ_l is sufficiently small, becomes divergent in the limit $\theta_l \to 0$. Indeed, ϕ is not well-defined if θ_l is exactly vanishing. But both θ_l and ϕ can be radiatively generated. We may require that $\dot{\phi}$ remain finite when θ_l approaches zero, implying that the following necessary condition can be extracted from the expression of $\dot{\phi}$ in Eq. (3.155):

$$\zeta_{13}^{-1}c_\rho s_{(\rho-\phi)} - \zeta_{13}s_\rho c_{(\rho-\phi)} - \zeta_{23}^{-1}c_\sigma s_{(\sigma-\phi)} + \zeta_{23}s_\sigma c_{(\sigma-\phi)} = 0 . \tag{3.157}$$

It turns out that

$$\tan\phi = \frac{\widehat{\zeta}_{13}\sin 2\rho - \widehat{\zeta}_{23}\sin 2\sigma}{\left(\zeta_{13}^{-1} + \zeta_{13} + \widehat{\zeta}_{13}\cos 2\rho\right) - \left(\zeta_{23}^{-1} + \zeta_{23} + \widehat{\zeta}_{23}\cos 2\sigma\right)} \tag{3.158}$$

holds. Note that the initial value of θ_l, if it is exactly zero or extremely small, may immediately drive ϕ to its *quasi-fixed point* (Luo and Xing, 2006b). In

this interesting case Eq. (3.158) can be used to understand the relationship between ϕ and two Majorana phases ρ and σ at the quasi-fixed point.

(d) The running behaviors of ρ and σ are relatively mild in comparison with that of ϕ. A remarkable feature of $\dot{\rho}$ and $\dot{\sigma}$ is that they will vanish, if both ρ and σ are initially vanishing. This observation indicates that ρ and σ cannot simultaneously be generated from ϕ via the one-loop RGEs.

(e) The unphysical phases ϕ_μ and ϕ_τ only have relatively mild running effects, while the running behavior of ϕ_e may be violent for sufficiently small θ_l. A quasi-fixed point of ϕ_e is also expected in the limit $\theta_l \to 0$ and under the circumstance given by Eq. (3.157) or Eq. (3.158).

3.6.3 Evolution of Dirac Neutrino Mass Parameters

The Yukawa coupling matrix of Dirac neutrinos Y_ν obeys the RGE given in Eq. (3.138). Because neutrino masses are extremely smaller than charged-lepton masses, the $(Y_\nu Y_\nu^\dagger)$ term can be safely neglected from Eq. (3.138). We are then left with

$$\begin{aligned} 16\pi^2 \frac{{\rm d}Y_\nu}{{\rm d}t} &= \left[\alpha_\nu + C_\nu^l (Y_l Y_l^\dagger)\right] Y_\nu \; , \\ 16\pi^2 \frac{{\rm d}Y_\nu^\dagger}{{\rm d}t} &= Y_\nu^\dagger \left[\alpha_\nu + C_\nu^l (Y_l Y_l^\dagger)\right] \; . \end{aligned} \tag{3.159}$$

Defining the Hermitian quantity $\kappa' \equiv Y_\nu Y_\nu^\dagger$, we obtain

$$16\pi^2 \frac{{\rm d}\kappa'}{{\rm d}t} = 2\alpha_\nu \kappa' + C_\kappa \left[(Y_l Y_l^\dagger)\kappa' + \kappa'(Y_l Y_l^\dagger)\right] \; , \tag{3.160}$$

where $\alpha_\nu \approx -0.45 g_1^2 - 2.25 g_2^2 + 3 y_t^2$ (SM) or $\alpha_\nu \approx -0.6 g_1^2 - 3 g_2^2 + 3 y_t^2$ (MSSM), and $C_\kappa = C_\nu^l$. This RGE is rather similar to the one given in Eq. (3.130) for Majorana neutrinos. Without loss of generality, we choose the flavor basis where $Y_l = D_l \equiv {\rm Diag}\{y_e, y_\mu, y_\tau\}$ holds. In this basis κ' can be diagonalized by the unitary transformation $V^\dagger \kappa' V = \widehat{\kappa}' \equiv {\rm Diag}\{y_1^2, y_2^2, y_3^2\}$ with V being the MNS matrix and y_i being the eigenvalues of Y_ν. Let us denote $V \equiv PUP'$, in which $P = {\rm Diag}\{{\rm e}^{{\rm i}\phi_e}, {\rm e}^{{\rm i}\phi_\mu}, {\rm e}^{{\rm i}\phi_\tau}\}$, $P' \equiv {\rm Diag}\{{\rm e}^{{\rm i}\rho}, {\rm e}^{{\rm i}\sigma}, 1\}$, and U is the CKM-like matrix containing three neutrino mixing angles and one CP-violating phase. Note that P does not take part in the RGEs because it can be removed from Eq. (3.160) in the chosen basis. The phases in P' are also unphysical, but they have their own RGEs. Following a straightforward procedure analogous to the one from Eq. (3.143) to Eq. (3.151) in Section 3.6.2, one may easily figure out the constraint equations for $\widehat{\kappa}'$, U, P' and their derivatives. In the τ-dominance approximation (i.e., $D_l^2 \approx {\rm Diag}\{0, 0, y_\tau^2\}$), we obtain (Xing, 2006)

$$\dot{y}_i \; = \; \frac{y_i}{16\pi^2} \left(\alpha_\nu + C_\kappa y_\tau^2 \left|U_{\tau i}\right|^2\right) \; , \tag{3.161}$$

and

$$\sum_{\alpha}\left(U^*_{\alpha 1}\dot{U}_{\alpha 2}\right)+\mathrm{i}\left(\dot{\rho}U^*_{e1}U_{e2}+\dot{\sigma}U^*_{\mu 1}U_{\mu 2}\right)=-\frac{C_\kappa y_\tau^2}{16\pi^2}\xi_{12}U^*_{\tau 1}U_{\tau 2}\;,$$
$$\sum_{\alpha}\left(U^*_{\alpha 1}\dot{U}_{\alpha 3}\right)+\mathrm{i}\left(\dot{\rho}U^*_{e1}U_{e3}+\dot{\sigma}U^*_{\mu 1}U_{\mu 3}\right)=-\frac{C_\kappa y_\tau^2}{16\pi^2}\xi_{13}U^*_{\tau 1}U_{\tau 3}\;,$$
$$\sum_{\alpha}\left(U^*_{\alpha 2}\dot{U}_{\alpha 3}\right)+\mathrm{i}\left(\dot{\rho}U^*_{e2}U_{e3}+\dot{\sigma}U^*_{\mu 2}U_{\mu 3}\right)=-\frac{C_\kappa y_\tau^2}{16\pi^2}\xi_{23}U^*_{\tau 2}U_{\tau 3}\;, \quad (3.162)$$

where α runs over e, μ and τ, and $\xi_{ij}\equiv\left(y_i^2+y_j^2\right)/\left(y_i^2-y_j^2\right)$ with $i\neq j$.

Given the FX form of U in Eq. (3.152), the Yukawa coupling eigenvalues of three Dirac neutrinos satisfy the following one-loop RGEs:

$$\dot{y}_1=\frac{y_1}{16\pi^2}\left(\alpha_\nu+C_\kappa y_\tau^2 s_\nu^2 s^2\right)\;,$$
$$\dot{y}_2=\frac{y_2}{16\pi^2}\left(\alpha_\nu+C_\kappa y_\tau^2 c_\nu^2 s^2\right)\;,$$
$$\dot{y}_3=\frac{y_3}{16\pi^2}\left(\alpha_\nu+2C_\kappa y_\tau^2 c^2\right)\;. \quad (3.163)$$

The RGEs of three neutrino mixing angles and one (physical) CP-violating phase are given by

$$\dot{\theta}_l=+\frac{C_\kappa y_\tau^2}{16\pi^2}\;c_\nu s_\nu c c_\phi\left(\xi_{13}-\xi_{23}\right)\;,$$
$$\dot{\theta}_\nu=+\frac{C_\kappa y_\tau^2}{16\pi^2}\;c_\nu s_\nu\left[s^2\xi_{12}+c^2\left(\xi_{13}-\xi_{23}\right)\right]\;,$$
$$\dot{\theta}=+\frac{C_\kappa y_\tau^2}{16\pi^2}\;cs\left(s_\nu^2\xi_{13}+c_\nu^2\xi_{23}\right)\;,$$
$$\dot{\phi}=-\frac{C_\kappa y_\tau^2}{16\pi^2}\left(c_l^2-s_l^2\right)c_l^{-1}s_l^{-1}c_\nu s_\nu c s_\phi\left(\xi_{13}-\xi_{23}\right)\;, \quad (3.164)$$

where $c_\phi\equiv\cos\phi$ and $s_\phi\equiv\sin\phi$. The RGEs of unphysical ρ and σ read

$$\dot{\rho}=-\frac{C_\kappa y_\tau^2}{16\pi^2}\;c_l s_l^{-1}c_\nu s_\nu c s_\phi\left(\xi_{13}-\xi_{23}\right)\;,$$
$$\dot{\sigma}=+\frac{C_\kappa y_\tau^2}{16\pi^2}\;c_l^{-1}s_l c_\nu s_\nu c s_\phi\left(\xi_{13}-\xi_{23}\right)\;. \quad (3.165)$$

It is obvious that $\dot{\phi}=\dot{\rho}+\dot{\sigma}$ holds. These RGEs are much more concise than those obtained in the standard parametrization of U (Lindner *et al.*, 2005). Some qualitative discussions about the main features of Eqs. (3.163), (3.164) and (3.165) are in order.

(a) Like the Majorana case, the running behaviors of three Dirac neutrino masses m_i (or equivalently y_i) are nearly identical and determined by α_ν, unless $\tan\beta$ is sufficiently large in the MSSM. It is also worth mentioning that $\dot{y}_i$ or $\dot{m}_i$ (for $i=1,2,3$) are independent of both the CP-violating phase ϕ and the smallest mixing angle θ_l in the chosen parametrization of U.

(b) $\dot{\theta}_\nu$ consists of a term proportional to $\xi_{12} = -(m_1^2 + m_2^2)/\Delta m_{21}^2$. Hence θ_ν is in general more sensitive to radiative corrections than θ_l and θ, whose derivatives depend on $\xi_{13} = -(m_1^2 + m_3^2)/\Delta m_{31}^2$ and $\xi_{23} = -(m_2^2 + m_3^2)/\Delta m_{32}^2$. Given θ_ν and θ at an energy scale, θ_l can be radiatively generated at another energy scale. In this case, however, it is impossible to simultaneously generate the CP-violating phase ϕ. The reason is simply that ϕ can always be rotated away when θ_l is vanishing, and the proportionality relationship between $\dot{\phi}$ and $\sin\phi$ forbids ϕ to be generated even when θ_l becomes non-vanishing.

(c) Different from the Majorana case, there is no nontrivial *quasi-fixed point* in the RGE of ϕ for Dirac neutrinos. If $\dot{\phi}$ is required to keep finite when θ_l approaches zero, then ϕ itself must approach zero or π. On the other hand, $\dot{\theta}_l \propto \cos\phi$ implies that the evolution of θ_l has a turning point characterized by $\phi = \pi/2$ (i.e., $\dot{\theta}_l$ flips its sign at this point). Hence two interesting conclusions can be drawn: first, θ_l can never cross zero if $\theta_l \neq 0$ and $\sin\phi \neq 0$ hold at a certain energy scale; second, CP will always be a good symmetry if $\theta_l = 0$ or $\sin\phi = 0$ holds at a certain energy scale.

(d) The running behavior of ρ is quite similar to that of ϕ, simply because $\dot{\phi} = \dot{\rho}\left(1 - \tan^2\theta_l\right)$ holds. In addition, $\dot{\sigma} = -\dot{\rho}\tan^2\theta_l$ implies that σ only gets some mild radiative corrections.

As defined in Eq. (3.116), the Jarlskog parameter $\mathcal{J}$ is a rephasing invariant of the MNS matrix V and measures the strength of CP and T violation in neutrino oscillations. One has $\mathcal{J} = c_l s_l c_\nu s_\nu c s^2 \sin\phi$ in the FX parametrization, no matter whether three neutrinos are Dirac or Majorana particles. We obtain the one-loop RGE

$$\dot{\mathcal{J}}_{\rm D} = \frac{C_\kappa y_\tau^2}{16\pi^2}\, \mathcal{J}_{\rm D}\left[\left(c_\nu^2 - s_\nu^2\right) s^2 \xi_{12} + \left(c^2 - s_\nu^2 s^2\right)\xi_{13} + \left(c^2 - c_\nu^2 s^2\right)\xi_{23}\right] \tag{3.166}$$

for Dirac neutrinos. So $\mathcal{J}_{\rm D} = 0$ will be a stable result independent of the renormalization scales, provided θ_l or $\sin\phi$ initially vanishes at a given scale. In comparison, we have

$$\begin{aligned}\dot{\mathcal{J}}_{\rm M} = \frac{C_\kappa y_\tau^2}{16\pi^2}\Big\{ & \mathcal{J}_{\rm M}\Big[\left(c_\nu^2 - s_\nu^2\right) s^2 \left(\zeta_{12}^{-1} c_{(\sigma-\rho)}^2 + \zeta_{12} s_{(\sigma-\rho)}^2\right) \\ & + \left(c^2 - s_\nu^2 s^2\right)\left(\zeta_{13}^{-1} c_\rho^2 + \zeta_{13} s_\rho^2\right) + \left(c^2 - c_\nu^2 s^2\right)\left(\zeta_{23}^{-1} c_\sigma^2 + \zeta_{23} s_\sigma^2\right)\Big] \\ & + c_\nu s_\nu c s^2 \left(C_{12}\widehat{\zeta}_{12} + C_{13}\widehat{\zeta}_{13} + C_{23}\widehat{\zeta}_{23}\right)\Big\}\end{aligned} \tag{3.167}$$

for Majorana neutrinos, where

$$\begin{aligned} C_{12} &= c_l s_l s^2 c_\phi c_{(\sigma-\rho)} s_{(\sigma-\rho)} \; , \\ C_{13} &= \left[c_l s_l c_\phi \left(s_\nu^2 - c_\nu^2 c^2\right) + \left(c_l^2 - s_l^2\right) c_\nu s_\nu c\right] c_\rho s_\rho \; , \\ C_{23} &= \left[c_l s_l c_\phi \left(c_\nu^2 - s_\nu^2 c^2\right) - \left(c_l^2 - s_l^2\right) c_\nu s_\nu c\right] c_\sigma s_\sigma \; . \end{aligned} \tag{3.168}$$

This result shows that $\mathcal{J}_{\rm M}$ can be radiatively generated from two nontrivial Majorana phases ρ and σ, even if it is initially vanishing at a given scale.

Taking $\rho = \sigma = 0$, we arrive at $C_{12} = C_{13} = C_{23} = 0$ as well as $\dot{\rho} = \dot{\sigma} = 0$. But it is impossible to obtain the equality $\mathcal{J}_{\rm M}(\rho = \sigma = 0) = \mathcal{J}_{\rm D}$, because $\zeta_{12}^{-1} = \xi_{12}$, $\zeta_{13}^{-1} = \xi_{13}$ and $\zeta_{23}^{-1} = \xi_{23}$ (or equivalently $m_1 m_2 = m_1 m_3 = m_2 m_3 = 0$) cannot simultaneously hold. This observation demonstrates that the running behavior of $\mathcal{J}_{\rm M}$ is essentially different from that of $\mathcal{J}_{\rm D}$ even if one switches off two Majorana phases (Xing and Zhang, 2007).

So far a lot of numerical exercises have been done to illustrate the running behaviors of neutrino mass and mixing parameters from the seesaw scale to the electroweak scale, or vice versa. Some particular attention has been paid to the possibility of generating the smallest neutrino mixing angle θ_{13} (or θ_l) via the effect of its RGE evolution, and to the radiative corrections to a few typical neutrino mixing patterns including the "tri-bimaximal" and "democratic" patterns (see, e.g., Antusch *et al.*, 2002c; Antusch and Ratz, 2002; Mei and Xing, 2004; Plentinger and Rodejohann, 2005; Mei and Xing, 2005; Luo and Xing, 2006a; Lin *et al.*, 2010). To achieve appreciable running effects, however, one usually has to make at least one of the following assumptions: (a) three neutrino masses are nearly degenerate to enhance the magnitudes of ζ_{ij}^{-1} or ξ_{ij}, (b) the value of $\tan\beta$ is sufficiently large to enhance the magnitude of $y_\tau^2 = m_\tau^2(1 + \tan^2\beta)/v^2$ in the MSSM case, and (c) significant threshold effects of heavy particles above the seesaw scale of Majorana neutrinos. We do not elaborate those numerical results in this book.

Let us make two final remarks. First, the chosen flavor basis (i.e., $Y_l = D_l$) is stable against radiative corrections. This point can be seen from Eq. (3.131) or from Eq. (3.138) in the neglect of the $(Y_\nu Y_\nu^\dagger)$ term:

$$16\pi^2 \frac{{\rm d}D_l}{{\rm d}t} = \left(\alpha_l + C_l^l D_l^2\right) D_l \; , \tag{3.169}$$

whose left- and right-hand sides are both diagonal. Hence D_l itself keeps diagonal between the seesaw scale and the electroweak scale, although its three eigenvalues get modified at different energy scales. If D_l were unstable against quantum corrections, the RGEs of neutrino mass and mixing parameters obtained above would no more make sense. Second, the running behaviors of leptons are more or less related to those of quarks because their RGEs are essentially entangled with each other. Even though three light neutrinos impose little influence on the evolution of nine charged fermions, the opposite is not true. That is why one has to use a full set of RGEs of lepton Yukawa couplings, quark Yukawa couplings and gauge couplings to do a complete numerical analysis of the evolution of neutrino masses, flavor mixing angles and CP-violating phases with energy scales.

References

Abachi, S., *et al.* (D0 Collaboration), 1995, Phys. Rev. Lett. **74**, 2422.
Abdurashitov, J. N., *et al.* (SAGE Collaboration), 2002, JETP **95**, 181.
Abe, F., *et al.* (CDF Collaboration), 1995, Phys. Rev. Lett. **74**, 2626.

Abe, K., *et al.* (Belle Collaboration), 2001, Phys. Rev. Lett. **87**, 091802.
Abe, S., *et al.* (Super-Kamiokande Collaboration), 2006, Phys. Rev. Lett. **97**, 171801.
Abe, S., *et al.* (KamLAND Collaboration), 2008, Phys. Rev. Lett. **100**, 221803.
Abrams, G. S., *et al.* (SLAC-SP-017 Collaboration), 1974, Phys. Rev. Lett. **33**, 1406.
Acquafredda, R., *et al.* (OPERA Collaboration), 2006, New J. Phys. **8**, 303.
Adamson, P., *et al.* (MINOS Collaboration), 2008, Phys. Rev. Lett. **101**, 131802.
Aharmim, B., *et al.* (SNO Collaboration), 2005, Phys. Rev. C **72**, 055502.
Ahmad, Q. R., *et al.* (SNO Collaboration), 2002, Phys. Rev. Lett. **89**, 011301.
Ahn, M. H., *et al.* (K2K Collaboration), 2003, Phys. Rev. Lett. **90**, 041801.
Altarelli, G., and Feruglio, F., 2005, Nucl. Phys. B **720**, 64.
Altmann, M., *et al.* (GNO Collaboration), 2000, Phys. Lett. B **490**, 16.
Anderson, C. D., 1933, Phys. Rev. **43**, 491.
Antusch, S., and Ratz, M., 2002, JHEP **0211**, 010.
Antusch, S., *et al.*, 2001, Phys. Lett. B **519**, 238.
Antusch, S., *et al.*, 2002a, Phys. Lett. B **538**, 87.
Antusch, S., *et al.*, 2002b, Phys. Lett. B **525**, 130.
Antusch, S., *et al.*, 2002c, Phys. Lett. B **544**, 1.
Antusch, S., *et al.*, 2003, Nucl. Phys. B **658**, 203.
Antusch, S., *et al.*, 2005, JHEP **0503**, 024.
Apollonio, M., *et al.* (CHOOZ Collaboration), 1998, Phys. Lett. B **420**, 397.
Arpesella, C., *et al.* (Borexino Collaboration), 2008a, Phys. Lett. B **658**, 101.
Arpesella, C., *et al.* (Borexino Collaboration), 2008b, Phys. Rev. Lett. **101**, 091302.
Ashie, Y., *et al.* (Super-Kamiokande Collaboration), 2004, Phys. Rev. Lett. **93**, 101801.
Ashie, Y., *et al.* (Super-Kamiokande Collaboration), 2005, Phys. Rev. D **71**, 112005.
Aubert, B., *et al.* (BABAR Collaboration), 2001; Phys. Rev. Lett. **87**, 091801.
Aubert, J. J., *et al.* (E598 Collaboration), 1974, Phys. Rev. Lett. **33**, 1404.
Babu, K. S., Leung, C. N., and Pantaleone, J., 1993, Phys. Lett. B **319**, 191.
Bahcall, J. N., Pinsonneault, M. H., and Basu, S., 2001, Astrophys. J. **555**, 990.
Bahcall, J. N., Serenelli, A. M., and Basu, S., 2005, Astrophys. J. **621**, L85.
Bardin, D. Yu., Bilenky, S. M., and Pontecorvo, B., 1970, Phys. Lett. B **32**, 68.
Beacom, J. F., and Vogel, P., 1999, Phys. Rev. Lett. **83**, 5222.
Beda, A. G., *et al.* (GEMMA Collaboration), 2007, Phys. Atom. Nucl. **70**, 1873.
Bigi, I. I., and Sanda, A. I., 2000, *CP Violation* (Cambridge University Press).
Bilenky, S. M., and Petcov, S. T., 1987, Rev. Mod. Phys. **59**, 671.
Boehm, F., *et al.* (Palo Verde Collaboration), 2000, Phys. Rev. Lett. **84**, 3764.
Botella, F. J., and Chau, L. L., 1986, Phys. Lett. B **168**, 97.
Branco, G. C., Lavoura, L. and Silva, J. P., 1999, *CP Violation* (Oxford University Press).
Cabibbo, N., 1963, Phys. Rev. Lett. **10**, 531.
Cabibbo, N., 1978, Phys. Lett. B **72**, 333.
Cabral-Rosetti, L. G., *et al.*, 2000, Eur. Phys. J. C **12**, 633.
Casas, J. A., *et al.*, 2000, Nucl. Phys. B **573**, 652.
Chadwick, J., 1932, Nature **129**, 312.

Chakrabortty, J., *et al.*, 2009, Nucl. Phys. B **820**, 116.
Chan, A. H., Low, H. B., and Xing, Z. Z., 2009, Phys. Rev. D **80**, 073006.
Chankowski, P. H., and Pluciennik, Z., 1993, Phys. Lett. B **316**, 312.
Chao, W., and Zhang, H., 2007, Phys. Rev. D **75**, 033003.
Cheng, T. P., and L. F. Li, 1980, Phys. Rev. D **22**, 2860.
Cheng, T. P., Eichten, E., and Li, L. F., 1974, Phys. Rev. D **9**, 225.
Chkareuli, J. L., and Froggatt, C. D., 1999, Phys. Lett. B **450**, 158.
Christenson, *et al.*, 1964, Phys. Rev. Lett. **13**, 138.
Cleveland, B. T., *et al.* (Homestake Collaboration), 1998, Astrophys. J. **496**, 505.
Cowan, C. L., Jr., *et al.*, 1956, Science **124**, 103.
Czakon, M., Gluza, J., and Zralek, M., 1999, Phys. Rev. D **59**, 013010.
Danby, G., *et al.*, 1962, Phys. Rev. Lett. **9**, 36.
Daraktchieva, Z., *et al.* (MUNU Collaboration), 2005, Phys. Lett. B **615**, 153.
Dreiner, H. K., Haber, H. E., and Martin, S. P., 2008, arXiv:0812.1594.
Dvornikov, M., and Studenikin, A., 2004, Phys. Rev. D **69**, 073001.
Eguchi, K., *et al.* (KamLAND Collaboration), 2003, Phys. Rev. Lett. **90**, 021802.
Fogli, G. L., *et al.*, 2008a, Phys. Rev. D **78**, 033010.
Fogli, G. L., *et al.*, 2008b, Phys. Rev. Lett. **101**, 141801.
Friedberg, R., and Lee, T. D., 2006, High Energy Phys. Nucl. Phys. **30**, 591.
Friedberg, R., and Lee, T. D., 2008, Annals Phys. **323**, 1087.
Friedberg, R., and Lee, T. D., 2010, Chin. Phys. C **34**, 1547.
Fritzsch, H., Gell-Mann, M., and Minkowski, P., 1975, Phys. Lett. B **59**, 256.
Fritzsch, H., and Minkowski, P., 1975, Annals Phys. **93**, 193.
Fritzsch, H., and Xing, Z. Z., 1996, Phys. Lett. B **372**, 265.
Fritzsch, H., and Xing, Z. Z., 1997, Phys. Lett. B **413**, 396.
Fritzsch, H., and Xing, Z. Z., 1998a, Phys. Rev. D **57**, 594.
Fritzsch, H., and Xing, Z. Z., 1998b, Phys. Lett. B **440**, 313.
Fritzsch, H., and Xing, Z. Z., 2000a, Phys. Rev. D **61**, 073016.
Fritzsch, H., and Xing, Z. Z., 2000b, Prog. Part. Nucl. Phys. **45**, 1.
Fritzsch, H., and Xing, Z. Z., 2001, Phys. Lett. B **517**, 363.
Fritzsch, H., and Xing, Z. Z., 2004, Phys. Lett. B **598**, 237.
Fritzsch, H., and Xing, Z. Z., 2006, Phys. Lett. B **634**, 514.
Fritzsch, H., and Xing, Z. Z., 2009, Phys. Lett. B **682**, 220.
Fujikawa, K., and Shrock, R. E., 1980, Phys. Rev. Lett. **45**, 963.
Fukuda, Y., *et al.* (Super-Kamiokande Collaboration), 1998a, Phys. Rev. Lett. **81**, 1158.
Fukuda, Y., *et al.* (Super-Kamiokande Collaboration), 1998b, Phys. Rev. Lett. **81**, 1562.
Gell-Mann, M., Ramond, P., and Slansky, R., 1979, in *Supergravity*, edited by van Nieuwenhuizen, P., and Freedman, D. Z. (North-Holland, Amsterdam), p. 315.
Georgi, H., 1975, in *Particles and Fields*, edited by Carlson, C. E. (AIP, New York), p. 575.
Giunti, C., and Studenikin, A., 2009, Phys. Atom. Nucl. **72**, 2089.
Glashow, S. L., 1980, in *Quarks and Leptons*, edited by Lévy, M., *et al.* (Plenum, New York), p. 707.
Gonzalez-Garcia, M. C., Maltoni, M., and Salvado, J., 2010, JHEP **1004**, 056.

Gribov, V., and Pontecorvo, B., 1969, Phys. Lett. B **28**, 463.
Grimus, W., and Stockinger, P., 1998, Phys. Rev. D **57**, 1762.
Hampel, W., *et al.* (GALLEX Collaboration), 1999, Phys. Lett. B **447**, 127.
Hamzaoui, C., 1988, Phys. Rev. Lett. **61**, 35.
Harrison, P. F., Perkins, D. H., and Scott, W. G., 2002, Phys. Lett. B **530**, 167.
Haxton, W. C., and Stephenson, J., 1984, Prog. Part. Nucl. Phys. **12**, 409.
He, X. G., Keum, Y. Y., and Volkas, R. R., 2006, JHEP **0604**, 039.
He, X. G., and Zee, A., 2003, Phys. Lett. B **560**, 87.
Herb, S. W., *et al.*, 1977, Phys. Rev. Lett. **39**, 252.
Jarlskog, C., 1985, Phys. Rev. Lett. **55**, 1039.
Jarlskog, C., 1989, in *Proceedings of the 16th International Meeting on Fundamental Physics: CP Non-conservation and B Physics*, edited by Bernabéu, J., *et al.* (World Scientific, Singapore), p. 40.
Kayser, B., 1982, Phys. Rev. D **26**, 1662.
Kayser, B., 1984, Phys. Rev. D **30**, 1023.
Kayser, B., 2008, arXiv:0804.1497.
Kim, J. E., 1976, Phys. Rev. D **14**, 3000.
King, S. F., and Luhn, C., 2009, JHEP **0910**, 093.
King, S. F., and Singh, N. N., 2000, Nucl. Phys. B **591**, 3.
Kobayashi, M., and Maskawa, T., 1973, Prog. Theor. Phys. **49**, 652.
Kodama, K., *et al.* (DONUT Collaboration), 2001, Phys. Lett. B **504**, 218.
Koide, Y., 1983, Phys. Rev. D **28**, 252.
Konetschny, W., and Kummer, W., 1977, Phys. Lett. B **70**, 433.
Kyuldjiev, A. V., 1984, Nucl. Phys. B **243**, 387.
Lazarides, G., Shafi, Q., and Wetterich, C., 1981, Nucl. Phys. B **181**, 287.
Lee, B. W., and Shrock, R. E., 1977, Phys. Rev. D **16**, 1444.
Li, Y. F., and Xing, Z. Z., 2010, arXiv:1009.5870.
Lin, Y., Merlo, L., and Paris, A., 2010, Nucl. Phys. B **835**, 238.
Lindner, M., Ratz, M., and Schmidt, M. A., 2005, JHEP **0509**, 081.
Liu, D. W., *et al.* (Super-Kamiokande Collaboration), 2004, Phys. Rev. Lett. **93**, 021802.
Lüders, G., 1954, Kgl. Dansk. Vidensk. Selsk. Mat. Fys. Medd. **28**, 1.
Luo, S., Mei, J., and Xing, Z. Z., 2005, Phys. Rev. D **72**, 053014.
Luo, S., and Xing, Z. Z., 2006a, Phys. Lett. B **632**, 341.
Luo, S., and Xing, Z. Z., 2006b, Phys. Lett. B **637**, 279.
Ma, E., 2004, Phys. Rev. D **70**, 031901.
Ma, E., 2007, arXiv:0705.0327.
Machacek, M. E., and Vaughn, M. T., 1984, Nucl. Phys. B **236**, 221.
Magg, M., and Wetterich, C., 1980, Phys. Lett. B **94**, 61.
Majorana, E., 1937, Nuovo Cim. **14**, 171.
Maki, Z., Nakagawa, M., and Sakata, S., 1962, Prog. Theor. Phys. **28**, 870.
Marciano, W. J., and Sanda, A. I., 1977, Phys. Lett. B **67**, 303.
Marciano, W. J., and Parsa, Z., 2003, J. Phys. G **29**, 2629.
Mei, J., 2005, Phys. Rev. D **71**, 073012.
Mei, J., and Xing, Z. Z., 2004, Phys. Rev. D **70**, 053002.
Mei, J., and Xing, Z. Z., 2005, Phys. Lett. B **623**, 227.
Michael, D., *et al.* (MINOS Collaboration), 2006, Phys. Rev. Lett. **97**, 191801.
Mikheyev, S. P., and Smirnov, A. Yu., 1985, Sov. J. Nucl. Phys. **42**, 913.

Minkowski, P., 1977, Phys. Lett. B **67**, 421.
Mohapatra, R. N., Ng, S. P., and Yu, H., 2004, Phys. Rev. D **70**, 057301.
Mohapatra, R. N., and Pal, P. B., 2004, *Massive Neutrinos in Physics and Astrophysics* (3rd Edition) (World Scientific, Singapore), p. 257.
Mohapatra, R. N., and Senjanovic, G., 1980, Phys. Rev. Lett. **44**, 912.
Mohapatra, R. N., and Senjanovic, G., 1981, Phys. Rev. D **23**, 165.
Nakamura, K., *et al.* (Particle Data Group), 2010, J. Phys. G **37**, 075021.
Neddermeyer, S. H., and Anderson, C. D., 1937, Phys. Rev. **51**, 884.
Nieves, J. F., 1982, Phys. Rev. D **26**, 3152.
Nowakowski, M., Paschos, E. A., and Rodriguez, J. M., 2005, Eur. J. Phys. **26**, 545.
Pal, P., and Wolfenstein, L., 1982, Phys. Rev. D **25**, 766.
Pauli, W., 1955, in *Niels Bohr and the Development of Physics* (Pergamon Press, New York), p. 30.
Perl, M. L., *et al.*, 1975, Phys. Rev. Lett. **35**, 1489.
Peskin, M. E., and Schroeder, D. V., 1995, *An Introduction to Quantum Field Theory* (Westview Press, Boulder).
Plentinger, F., and Rodejohann, W., 2005, Phys. Lett. B **625**, 264.
Raffelt, G. G., 1996, *Stars as Laboratories for Fundamental Physics* (The University of Chicago Press).
Raffelt, G. G., 1999, Phys. Rept. **320**, 319.
Rochester, G. D., and Butler, C. C., 1947, Nature **106**, 885.
Rutherford, E., 1919, Phil. Mag. **37**, 581.
Sasaki, K., 1986, Z. Phys. C **32**, 149.
Schechter, J., and Valle, J. W. F., 1980, Phys. Rev. D **22**, 2227.
Schechter, J., and Valle, J. W. F., 1981, Phys. Rev. D **24**, 1883.
Schmidt, M. A., 2007, Phys. Rev. D **76**, 073010.
Schwetz, T., Tortola, M. A., and Valle, J. W. F., 2008, New J. Phys. **10**, 113011.
Schwinger, J., 1951, Phys. Rev. **82**, 914.
Seljak, U., Slosar, A., and McDonald, P., 2006, JCAP **0610**, 014.
Shrock, R., 1982, Nucl. Phys. B **206**, 359.
Strumia, A., and Vissani, F., 2006, arXiv:hep-ph/0606054.
't Hooft, G., 1971, Phys. Lett. B **37**, 195.
't Hooft, G., 1980, in *Proceedings of 1979 Cargèse Institute on Recent Developments in Gauge Theories*, edited by G. 't Hooft *et al.* (Plenum Press, New York), p. 135.
Thomson, J. J., 1897, Phil. Mag. **44**, 293.
Vogel, P., and Engel, J., 1989, Phys. Rev. D **39**, 3378.
Weinberg, S., 1979, Phys. Rev. Lett. **43**, 1566.
Witten, E., 2001, Nucl. Phys. B (Proc. Suppl.) **91**, 3.
Wolfenstein, L., 1978, Phys. Rev. D **17**, 2369.
Wong, H., and Li, H. B., 2005, Mod. Phys. Lett. A **20**, 1103.
Wong, H., *et al.* (TEXONO Collaboration), 2007, Phys. Rev. D **75**, 012001.
Wu, D. D., 1986, Phys. Rev. D **33**, 860.
Xing, Z. Z., 1996a, Nuovo Cim. A **109**, 115.
Xing, Z. Z., 1996b, Nucl. Phys. B (Proc. Suppl.) **50**, 24.
Xing, Z. Z., 2002a, Phys. Lett. B **533**, 85.
Xing, Z. Z., 2002b, Phys. Rev. D **65**, 113010.

Xing, Z. Z., 2004, Int. J. Mod. Phys. A **19**, 1.
Xing, Z. Z., 2005, Phys. Lett. B **618**, 141.
Xing, Z. Z., 2006, Phys. Lett. B **633**, 550.
Xing, Z. Z., 2007, Int. J. Mod. Phys. E **16**, 1361.
Xing, Z. Z., 2008a, Int. J. Mod. Phys. A **23**, 4255.
Xing, Z. Z., 2008b, Phys. Lett. B **660**, 515.
Xing, Z. Z., 2008c, Phys. Rev. D **78**, 011301.
Xing, Z. Z., 2009a, Phys. Lett. B **679**, 111.
Xing, Z. Z., 2009b, Phys. Lett. B **679**, 255.
Xing, Z. Z., and Zhang, H., 2006, Phys. Lett. B **635**, 107.
Xing, Z. Z., and Zhang, H., 2007, Commun. Theor. Phys. **48**, 525.
Xing, Z. Z., and Zhou, S., 2006, High Energy Phys. Nucl. Phys. **30**, 828.
Xing, Z. Z., Yang, D., and Zhou, S., 2010, Phys. Lett. B **690**, 304.
Xing, Z. Z., Zhang, H., and Zhou, S., 2006, Phys. Lett. B **641**, 189.
Xing, Z. Z., Zhang, H., and Zhou, S., 2008, Phys. Rev. D **77**, 113016.
Yanagida, T., 1979, in *Proceedings of the Workshop on Unified Theory and the Baryon Number of the Universe*, edited by O. Sawada and A. Sugamoto (KEK, Tsukuba), p. 95.
Zee, A., 2006, Phys. Lett. B **630**, 58.

4

Seesaw Mechanisms of Neutrino Masses

The origin of nonzero but tiny neutrino masses has been a big puzzle in particle physics. Among various scenarios of neutrino mass generation which are surviving today, the seesaw mechanisms are most popular for model building. In this chapter we shall first outline a few possible ways to go beyond the standard model (SM) and generate finite neutrino masses, and then focus on several typical seesaw mechanisms and discuss how to get a balance between their theoretical naturalness and experimental testability. Possible collider signatures of TeV seesaw mechanisms and their consequences on non-unitary neutrino mixing and CP violation will also be discussed.

4.1 How to Generate Tiny Neutrino Masses

Neutrinos are massless in the SM, just because the structure of the SM itself is too simple to accommodate massive neutrinos.

- Two fundamentals of the SM are the $SU(2)_{\rm L} \times U(1)_{\rm Y}$ gauge symmetry and the Lorentz invariance. Both of them are mandatory to guarantee that the SM is a consistent quantum field theory.
- The particle content of the SM is economical. There are no right-handed neutrinos, so a Dirac neutrino mass term is not allowed. There is only one Higgs doublet, so a gauge-invariant Majorana mass term is forbidden.
- The SM is a renormalizable theory, in which there does not exist a dimension-5 operator that may give each neutrino a Majorana mass.

In other words, the SM accidently possesses the $B-L$ symmetry which assures three neutrinos to be exactly massless. Unlike the masslessness of the photon, which is naturally guaranteed by the electromagnetic $U(1)_{\rm Q}$ gauge symmetry, the masslessness of three neutrinos in the SM is not an immediate consequence of any fundamental law or symmetry principle. But today's neutrino experiments have convincingly indicated the existence of neutrino oscillations (Nakamura *et al.*, 2010). This quantum phenomenon can appear

if and only if neutrinos are massive and lepton flavors are mixed, and thus it is a kind of new physics beyond the SM. To generate nonzero but tiny neutrino masses, one or more of the above-mentioned constraints on the SM must be abandoned or relaxed. It is certainly intolerable to abandon the gauge symmetry and Lorentz invariance; otherwise, one would be led astray. Given the framework of the SM as a consistent field theory, its particle content can be modified and (or) its renormalizability can be abandoned to accommodate massive neutrinos. There are several ways to this goal. For simplicity, we roughly classify the viable ideas about neutrino mass generation into non-seesaw mechanisms and seesaw mechanisms.

4.1.1 Non-seesaw Mechanisms

Among many non-seesaw mechanisms of neutrino masses proposed in the literature, three of them are particularly interesting and have attracted a lot of attention in recent years.

(1) *Non-renormalizable neutrino mass operators.* In 1979, Steven Weinberg extended the SM by introducing some higher-dimension operators in terms of the fields of the SM itself (Weinberg, 1979):

$$\mathcal{L}_{\rm eff} \; = \; \mathcal{L}_{\rm SM} + \frac{\mathcal{L}_{\rm d=5}}{\Lambda} + \frac{\mathcal{L}_{\rm d=6}}{\Lambda^2} + \cdots \; , \tag{4.1}$$

where Λ denotes the cutoff scale of this effective theory. Within such a framework, the lowest-dimension operator that violates the lepton number (L) is the unique dimension-5 operator $HHLL/\Lambda$. After spontaneous gauge symmetry breaking, this Weinberg operator yields $m_i \sim \langle H \rangle^2/\Lambda$ for neutrino masses, which can be sufficiently small ($\lesssim 1$ eV) if Λ is not far away from the scales of possible grand unified theories (i.e., $\Lambda \gtrsim 10^{13}$ GeV for $\langle H \rangle \sim 10^2$ GeV). In this sense, people argue that neutrino masses can serve as a low-energy window onto new physics at superhigh-energy scales.

(2) *Pure Dirac neutrino masses with $B-L$ symmetry.* Given three right-handed neutrinos, the gauge-invariant and lepton-number-conserving mass terms of charged leptons and neutrinos are

$$-\mathcal{L}_{\rm lepton} = \overline{\ell_{\rm L}} Y_l H E_{\rm R} + \overline{\ell_{\rm L}} Y_\nu \tilde{H} N_{\rm R} + {\rm h.c.} \; , \tag{4.2}$$

where $\tilde{H} \equiv {\rm i}\sigma_2 H^*$ is defined and $\ell_{\rm L}$ denotes the left-handed lepton doublet. After spontaneous gauge symmetry breaking, we arrive at the charged-lepton mass matrix $M_l = Y_l v/\sqrt{2}$ and the Dirac neutrino mass matrix $M_\nu = Y_\nu v/\sqrt{2}$ with $v \simeq 246$ GeV. In this case, the smallness of three neutrino masses m_i (for $i = 1, 2, 3$) is attributed to the smallness of three eigenvalues of Y_ν (denoted as y_i for $i = 1, 2, 3$). Then we encounter a transparent hierarchy problem: $y_i/y_e = m_i/m_e \lesssim 0.5$ eV/0.5 MeV $\sim 10^{-6}$. Why is y_i so small? There is no explanation at all in this Dirac-mass picture.

A speculative way out is to invoke extra dimensions; namely, the smallness of Dirac neutrino masses is ascribed to the assumption that three right-handed neutrinos have access to one or more extra spatial dimensions (Dienes *et al.*, 1999; Arkani-Hamed *et al.*, 2002). The idea is simply to confine the SM particles onto a brane and to allow $N_{\rm R}$ to travel in the bulk. For example, the wave function of $N_{\rm R}$ spreads out over the extra dimension y, giving rise to a suppressed Yukawa interaction at $y = 0$ (i.e., the location of the brane):

$$\left[\overline{\ell_{\rm L}} Y_\nu \tilde{H} N_{\rm R}\right]_{y=0} \sim \frac{1}{\sqrt{L}} \left[\overline{\ell_{\rm L}} Y_\nu \tilde{H} N_{\rm R}\right]_{y=L} . \tag{4.3}$$

The magnitude of $1/\sqrt{L}$ is measured by $\Lambda/\Lambda_{\rm Planck}$ and can naturally be small, because the fundamental scale Λ of a full theory with extra dimensions may be much lower than the Planck mass scale $\Lambda_{\rm Planck}$ of the effective four-dimensional theory (e.g., $\Lambda \sim 1$ TeV and $\Lambda_{\rm Planck} \sim 10^{19}$ GeV).

(3) *Radiative generation of tiny neutrino masses.* In a seminal paper published in 1972, Weinberg pointed out that "in theories with spontaneously broken gauge symmetries, various masses or mass differences may vanish in zeroth order as a consequence of the representation content of the fields appearing in the Lagrangian. These masses or mass differences can then be calculated as finite higher-order effects." (Weinberg, 1972). Such a mechanism may allow us to slightly go beyond the SM and radiatively generate tiny neutrino masses. A typical example is the well-known Zee model (Zee, 1980),

$$-\mathcal{L}_{\rm lepton} = \overline{\ell_{\rm L}} Y_l H E_{\rm R} + \overline{\ell_{\rm L}} Y_S S^- {\rm i}\sigma_2 \ell_{\rm L}^c + \tilde{\Phi}^T F S^+ {\rm i}\sigma_2 \tilde{H} + {\rm h.c.} , \tag{4.4}$$

where S^+ and S^- are charged $SU(2)_{\rm L}$ singlet scalars, Φ denotes a new $SU(2)_{\rm L}$ doublet scalar which has the same quantum number as the SM Higgs doublet H, Y_S is an antisymmetric matrix, and F represents a coupling constant and has the dimension of mass. Without loss of generality, we choose the basis of $M_l = Y_l \langle H \rangle = {\rm Diag}\{m_e, m_\mu, m_\tau\}$. In this model neutrinos are massless at the tree level, but their masses can be generated via the one-loop corrections. Given $M_S \gg M_h \sim M_\Phi \sim F$ and $\langle \Phi \rangle \sim \langle H \rangle$, the elements of the effective mass matrix of three light Majorana neutrinos turns out to be

$$(M_\nu)_{\alpha\beta} \sim \frac{M_h}{16\pi^2} \cdot \frac{m_\alpha^2 - m_\beta^2}{M_S^2} (Y_S)_{\alpha\beta} , \tag{4.5}$$

where α and β run over e, μ and τ. The smallness of M_ν is therefore ascribed to the smallness of Y_S and $(m_\alpha^2 - m_\beta^2)/M_S^2$. Although the original version of the Zee model is disfavored by current experimental data on neutrino oscillations, its extensions or variations at the one-loop or two-loop level can survive (Babu, 1988; Ma, 1998).

4.1.2 Seesaw Mechanisms

Without loss of the gauge symmetry and Lorentz invariance, the essential spirit of seesaw mechanisms is to add a few new particles into the SM and allow $B-L$ violation — tiny masses of three known neutrinos are attributed to the existence of heavy degrees of freedom and lepton number violation. There are three typical seesaw mechanisms on the market, and their properties have been extensively studied.

(1) Type-I seesaw — three heavy right-handed neutrinos are added into the SM and the lepton number is violated by their Majorana mass term (Fritzsch *et al.*, 1975; Minkowski, 1977; Yanagida, 1979; Gell-Mann *et al.*, 1979; Glashow, 1980; Mohapatra and Senjanovic, 1980):

$$-\mathcal{L}_{\rm lepton} \; = \; \overline{\ell_{\rm L}} Y_l H E_{\rm R} + \overline{\ell_{\rm L}} Y_\nu \tilde{H} N_{\rm R} + \frac{1}{2} \overline{N_{\rm R}^c} M_{\rm R} N_{\rm R} + {\rm h.c.} \; , \tag{4.6}$$

where $M_{\rm R}$ is the symmetric Majorana mass matrix.

(2) Type-II seesaw — one heavy Higgs triplet is added into the SM and the lepton number is violated by its interactions with both the lepton doublet and the Higgs doublet (Konetschny and Kummer, 1977, Magg and Wetterich, 1980; Schechter and Valle, 1980; Cheng and Li, 1980; Lazarides *et al.*, 1981; Mohapatra and Senjanovic, 1981):

$$-\mathcal{L}_{\rm lepton} \; = \; \overline{\ell_{\rm L}} Y_l H E_{\rm R} + \frac{1}{2} \overline{\ell_{\rm L}} Y_\Delta \Delta {\rm i}\sigma_2 \ell_{\rm L}^c - \lambda_\Delta M_\Delta H^T {\rm i}\sigma_2 \Delta H + {\rm h.c.} \; , \tag{4.7}$$

where

$$\Delta \; \equiv \; \begin{pmatrix} \Delta^- & -\sqrt{2}\, \Delta^0 \\ \sqrt{2}\, \Delta^{--} & -\Delta^- \end{pmatrix} \tag{4.8}$$

denotes the $SU(2)_{\rm L}$ Higgs triplet.

(3) Type-III seesaw — three heavy triplet fermions are added into the SM and the lepton number is violated by their Majorana mass term (Foot *et al.*, 1989; Ma, 1998):

$$-\mathcal{L}_{\rm lepton} \; = \; \overline{\ell_{\rm L}} Y_l H E_{\rm R} + \overline{\ell_{\rm L}} \sqrt{2} Y_\Sigma \Sigma^c \tilde{H} + \frac{1}{2} {\rm Tr} \left(\overline{\Sigma} M_\Sigma \Sigma^c \right) + {\rm h.c.} \; , \tag{4.9}$$

where

$$\Sigma \; = \; \begin{pmatrix} \Sigma^0/\sqrt{2} & \Sigma^+ \\ \Sigma^- & -\Sigma^0/\sqrt{2} \end{pmatrix} \tag{4.10}$$

denotes the $SU(2)_{\rm L}$ fermion triplet.

Of course, there are a number of variations or combinations of these three typical seesaw mechanisms in the literature. Some of them will be introduced in Sections 4.3 and 4.4. For each of the above seesaw pictures, one may get the unique dimension-5 Weinberg operator of neutrino masses after integrating out the corresponding heavy degrees of freedom:

$$\frac{\mathcal{L}_{\rm d=5}}{\Lambda} = \begin{cases} \dfrac{1}{2}\left(Y_\nu M_{\rm R}^{-1} Y_\nu^T\right)_{\alpha\beta} \overline{\ell_{\alpha\rm L}} \tilde{H} \tilde{H}^T \ell^c_{\beta\rm L} + \text{h.c.} & \text{(Type I)} , \\ -\dfrac{\lambda_\Delta}{M_\Delta} \left(Y_\Delta\right)_{\alpha\beta} \overline{\ell_{\alpha\rm L}} \tilde{H} \tilde{H}^T \ell^c_{\beta\rm L} + \text{h.c.} & \text{(Type II)} , \\ \dfrac{1}{2}\left(Y_\Sigma M_\Sigma^{-1} Y_\Sigma^T\right)_{\alpha\beta} \overline{\ell_{\alpha\rm L}} \tilde{H} \tilde{H}^T \ell^c_{\beta\rm L} + \text{h.c.} & \text{(Type III)} . \end{cases} \tag{4.11}$$

After spontaneous gauge symmetry breaking, $\tilde{H}$ achieves its vacuum expectation value $\langle \tilde{H} \rangle = v/\sqrt{2}$ with $v \simeq 246$ GeV. Then we are left with the effective Majorana neutrino mass term for three light neutrinos,

$$-\mathcal{L}_{\rm mass} = \frac{1}{2} \overline{\nu_{\rm L}} M_\nu \nu^c_{\rm L} + \text{h.c.} , \tag{4.12}$$

where the symmetric Majorana mass matrix M_ν is given by

$$M_\nu = \begin{cases} -\dfrac{1}{2} Y_\nu \dfrac{v^2}{M_{\rm R}} Y_\nu^T & \text{(Type I)} , \\ \lambda_\Delta Y_\Delta \dfrac{v^2}{M_\Delta} & \text{(Type II)} , \\ -\dfrac{1}{2} Y_\Sigma \dfrac{v^2}{M_\Sigma} Y_\Sigma^T & \text{(Type III)} . \end{cases} \tag{4.13}$$

It becomes obvious that the smallness of M_ν can be attributed to the largeness of $M_{\rm R}$, M_Δ or M_Σ in the seesaw mechanism.

4.1.3 The Weinberg Operator

Now let us derive the dimension-5 Weinberg operator of neutrino masses $\mathcal{L}_{\rm d=5}/\Lambda$ given in Eq. (4.11). The cutoff scale Λ is roughly characterized by the masses of heavy particles in a seesaw mechanism, and thus it is naturally expected to be much higher than the electroweak scale. At low energies one may integrate out the heavy degrees of freedom and obtain an effective field theory, which only contains the light degrees of freedom, to describe the finite masses of three known neutrinos.

Without loss of generality, we illustrate the approach by considering a field theory consisting of two real scalars $\phi(x)$ and $\Phi(x)$, whose masses are denoted respectively by m_ϕ and M_Φ. We assume $m_\phi \ll M_\Phi$ in this theory. Its Lagrangian can be schematically written as

$$\mathcal{L}_{\rm full}[\phi; \Phi] = \mathcal{L}_{\rm free}[\phi] + \mathcal{L}_{\rm free}[\Phi] + \mathcal{L}_{\rm int}[\phi, \Phi] , \tag{4.14}$$

where $\mathcal{L}_{\rm free}$ denotes the kinetic and mass terms, and $\mathcal{L}_{\rm int}$ represents the interaction term. At an energy scale far below M_Φ, it should be good enough to describe physical phenomena by means of an effective theory which only

involves the field ϕ. The action of this effective theory can accordingly be derived as follows (Weinberg, 1980; Bilenky and Santamaria, 1994):

$$\begin{aligned}\exp\{\mathrm{i}\mathcal{S}_{\rm eff}\} &= \exp\left\{\mathrm{i}\int \mathcal{L}_{\rm eff}[\phi(x)]\mathrm{d}^4x\right\} \\ &= \int [\mathrm{D}\Phi][\mathrm{D}\Phi^\dagger]\exp\left\{\mathrm{i}\int \mathcal{L}_{\rm full}[\phi(x);\Phi(x)]\right\} \\ &= \exp\left\{\mathrm{i}\int [\mathcal{L}_{\rm full}[\phi(x);\Phi(x)=0]+\mathcal{O}[\phi(x)]]\,\mathrm{d}^4x\right\}\ , \quad (4.15)\end{aligned}$$

in which the effective operator arising from the path-integration is denoted as $\mathcal{O}[\phi(x)]$. This operator only depends on the field $\phi(x)$ and may not necessarily be of dimension-four. The effective Lagrangian at low energies is therefore a sum of the Lagrangian without the heavy degrees of freedom and the operator obtained from integrating out the heavy degrees of freedom; i.e., $\mathcal{L}_{\rm eff}[\phi(x)] = \mathcal{L}_{\rm full}[\phi(x);\Phi(x)=0]+\mathcal{O}[\phi(x)]$. Taking the type-I seesaw mechanism for example, we shall subsequently derive the Weinberg operator by integrating out the heavy Majorana neutrinos.

The type-I seesaw model is a simple extension of the SM with three heavy Majorana neutrinos. The full Lagrangian of this model reads

$$\mathcal{L} = \mathcal{L}_{\rm SM} + \overline{N_{\rm R}}\mathrm{i}\not{\partial}N_{\rm R} - \left[\frac{1}{2}\overline{N_{\rm R}^c}M_{\rm R}N_{\rm R} + \overline{\ell_{\rm L}}Y_\nu\tilde{H}N_{\rm R} + \text{h.c.}\right]\ , \quad (4.16)$$

where $\mathcal{L}_{\rm SM}$ stands for the SM Lagrangian. The Majorana mass matrix $M_{\rm R}$ is symmetric and can be diagonalized by a unitary matrix U via the transformation $U^\dagger M_{\rm R}U^* = \widehat{M} = \mathrm{Diag}\,\{M_1, M_2, M_3\}$. In the mass basis of heavy Majorana neutrinos, the Lagrangian involving the heavy degrees of freedom can be rewritten as

$$\mathcal{L}_N = \frac{1}{2}\overline{N_i}\mathrm{i}\not{\partial}N_i - \frac{1}{2}M_i\overline{N_i}N_i - \left[\overline{\ell_{\alpha\rm L}}(\tilde{Y}_\nu)_{\alpha i}\tilde{H}N_i + \text{h.c.}\right]\ , \quad (4.17)$$

where $\widehat{N}_{\rm R} \equiv U^T N_{\rm R}$, $\tilde{Y}_\nu \equiv Y_\nu U^*$ and $N \equiv \widehat{N}_{\rm R} + \widehat{N}_{\rm R}^c$ have been defined, and the relevant family indices have been omitted. Because

$$\left[\overline{\ell_{\rm L}}\tilde{Y}_\nu\tilde{H}N\right]^T = \overline{N}\tilde{Y}_\nu^T\tilde{H}^T\ell_{\rm L}^c\ , \quad \left[\overline{N}\tilde{Y}_\nu^\dagger\tilde{H}^\dagger\ell_{\rm L}\right]^T = \overline{\ell_{\rm L}^c}\tilde{Y}_\nu^*\tilde{H}^*N\ , \quad (4.18)$$

where $\ell_{\rm L}^c \equiv \mathcal{C}\overline{\ell_{\rm L}}^T$ similar to the definitions made in Eq. (3.6), we have

$$\begin{aligned}\overline{\ell_{\alpha\rm L}}(\tilde{Y}_\nu)_{\alpha i}\tilde{H}N_i + \text{h.c.} = \frac{1}{2}\Big[&\overline{N}\left(\tilde{Y}_\nu^T\tilde{H}^T\ell_{\rm L}^c + \tilde{Y}_\nu^\dagger\tilde{H}^\dagger\ell_{\rm L}\right) \\ &+ \left(\overline{\ell_{\rm L}}\tilde{Y}_\nu\tilde{H} + \overline{\ell_{\rm L}^c}\tilde{Y}_\nu^*\tilde{H}^*\right)N\Big]\ , \quad (4.19)\end{aligned}$$

which will be useful in the integration over the heavy Majorana fields. Substituting Eq. (4.19) into Eq. (4.17), we immediately arrive at

$$\mathcal{L}_N = \frac{1}{2}\overline{N}KN - \frac{1}{2}\overline{N}\chi - \frac{1}{2}\overline{\chi}N \; , \tag{4.20}$$

where $K \equiv \mathrm{i}\partial\!\!\!/ - \widehat{M}$, $\overline{\chi} \equiv \chi^\dagger\gamma^0$ and $\chi \equiv \tilde{Y}_\nu^T \tilde{H}^T \ell_{\rm L}^c + \tilde{Y}_\nu^\dagger \tilde{H}^\dagger \ell_{\rm L}$ have been defined. We proceed to apply the formulism in Eqs. (4.14) and (4.15) to the full Lagrangian of the type-I seesaw model in Eq. (4.16), so as to obtain the effective Lagrangian of three light neutrinos at low energies. First of all, we integrate $\mathcal{L}_N$ in Eq. (4.20) over the heavy Majorana neutrino fields; viz.,

$$\int [\mathrm{D}N][\mathrm{D}\overline{N}] \exp\left\{ \mathrm{i} \int \frac{1}{2} \left[\overline{N}KN - \overline{N}\chi - \overline{\chi}N \right] \mathrm{d}^4x \right\} \; , \tag{4.21}$$

which is typically Gaussian. In general, the Gaussian integrals can be expressed in the following way (Weinberg, 1995):

$$\mathscr{I} = \int_{-\infty}^{+\infty} \prod_r \mathrm{d}\xi_r \mathrm{e}^{-Q(\xi)} \; , \tag{4.22}$$

in which

$$Q(\xi) \equiv \frac{1}{2} \sum_{r,s} K_{rs} \xi_r \xi_s + \sum_r L_r \xi_r + M \; . \tag{4.23}$$

Note that K is a nonsingular, positive-definite and symmetric matrix, and the variables ξ_r are real. Hence K can be diagonalized via the orthogonal transformation $\mathscr{S}^T K \mathscr{S} = \kappa$, or equivalently $\mathscr{S}_{rp} \mathscr{S}_{sq} K_{rs} = \kappa_p \delta_{pq}$ with $\mathscr{S}^T \mathscr{S} = \mathscr{S}\mathscr{S}^T = \mathbf{1}$. Given the definition $\tilde{\xi}_r \equiv \mathscr{S}_{sr} \xi_s$, Eq. (4.23) becomes

$$Q(\tilde{\xi}) = \frac{1}{2} \sum_r \kappa_r \tilde{\xi}_r^2 + \sum_r (L\mathscr{S})_r \tilde{\xi}_r + M \; , \tag{4.24}$$

and the integration in Eq. (4.22) turns out to be

$$\begin{aligned} \mathscr{I} &= \mathrm{e}^{-M} \prod_r \int_{-\infty}^{+\infty} \mathrm{d}\tilde{\xi}_r \exp\left\{ -\frac{1}{2}\kappa_r \tilde{\xi}_r^2 - (L\mathscr{S})_r \, \tilde{\xi}_r \right\} \\ &= \mathrm{e}^{-M} \prod_r \left(\frac{1}{2\pi\kappa_r} \right)^{1/2} \exp\left\{ \frac{1}{2} \kappa_r^{-1} \, (L\mathscr{S})_r^2 \right\} \\ &= (2\pi \mathrm{Det}K)^{-1/2} \exp\left\{ \frac{1}{2} L K^{-1} L^T - M \right\} \; , \end{aligned} \tag{4.25}$$

where $\mathrm{Det}K$ is the determinant of K. It is instructive to rewrite the result in Eq. (4.25) by evaluating the extremum of $Q(\xi)$ through $\dfrac{\partial Q(\xi)}{\partial \xi_r} = 0$. After a straightforward calculation, we find the extremum at $\hat{\xi} = -K^{-1} L^T$. Therefore,

$$\begin{aligned}\mathscr{I} &= (2\pi \mathrm{Det}K)^{-1/2} \exp\left\{\frac{1}{2} L K^{-1} L^T - M\right\} \\ &= (2\pi \mathrm{Det}K)^{-1/2} \exp\left\{-Q(\hat{\xi})\right\} \; . \end{aligned} \tag{4.26}$$

This result can be generalized to the complex variables and to a field theory with infinite dimensions. The important point indicated by Eq. (4.26) is that the integral can be obtained by solving the equation of motion, if the variables ξ_r are replaced by the relevant fields. For the complex scalar fields, we have the functional integration

$$\begin{aligned}&\int [\mathrm{D}\phi][\mathrm{D}\phi^\dagger] \exp\left\{\mathrm{i}\int \phi^\dagger(x) K(x,y)\phi(y) - \mathrm{i}\int \left[J^\dagger(z)\phi(z) + \mathrm{h.c.}\right]\right\} \\ &= (\mathrm{Det}K)^{-1} \exp\left\{-\mathrm{i}\int \mathrm{d}^4x \mathrm{d}^4y J^\dagger(x) K^{-1}(x,y) J(y)\right\} \; ; \end{aligned} \tag{4.27}$$

and for the fermion fields, we have

$$\begin{aligned}&\int [\mathrm{D}\psi][\mathrm{D}\overline{\psi}] \exp\left\{\mathrm{i}\int \overline{\psi}(x) K(x,y)\psi(y) - \mathrm{i}\int \left[\overline{J}(z)\psi(z) + \mathrm{h.c.}\right]\right\} \\ &= \mathrm{Det}K \exp\left\{-\mathrm{i}\int \mathrm{d}^4x \mathrm{d}^4y \overline{J}(x) K^{-1}(x,y) J(y)\right\} \; . \end{aligned} \tag{4.28}$$

Note that the integration over the spacetime arguments in the first line of Eq. (4.27) or Eq. (4.28) is implied. Note also that the factors appearing in the bosonic and fermionic integrations (i.e., $(\mathrm{Det}K)^{-1}$ and $\mathrm{Det}K$) are different. Now we apply the result in Eq. (4.28) to Eq. (4.21):

$$\begin{aligned}&\int [\mathrm{D}N][\mathrm{D}\overline{N}] \exp\left\{\mathrm{i}\int \frac{1}{2}\left[\overline{N} K N - \overline{N}\chi - \overline{\chi} N\right] \mathrm{d}^4x\right\} \\ &= \mathrm{Det}K \exp\left\{-\frac{\mathrm{i}}{2}\int \overline{\chi} K^{-1} \chi \mathrm{d}^4x\right\} \\ &= \exp\left\{\frac{\mathrm{i}}{2}\int \mathrm{d}^4x \left(\overline{\ell_\mathrm{L}}\tilde{Y}_\nu \tilde{H} + \overline{\ell_\mathrm{L}^c}\tilde{Y}_\nu^* \tilde{H}^*\right) \widehat{M}^{-1} \left(\tilde{Y}_\nu^T \tilde{H}^T \ell_\mathrm{L}^c + \tilde{Y}_\nu^\dagger \tilde{H}^\dagger \ell_\mathrm{L}\right)\right\} \; , \end{aligned} \tag{4.29}$$

where the field-independent factor $\mathrm{Det}K$ contributes a constant to the action and thus can be omitted, and the operator $(\mathrm{i}\partial\!\!\!/ - \widehat{M})^{-1}$ has been expanded in powers of $\widehat{M}^{-1}$. In the leading-order approximation we can therefore arrive at the Weinberg operator in the type-I seesaw model:

$$\begin{aligned}\frac{\mathcal{L}_{\mathrm{d}=5}}{\Lambda} &= \frac{1}{2}\overline{\ell_\mathrm{L}} \tilde{H} \tilde{Y}_\nu \widehat{M}^{-1} \tilde{Y}_\nu^T \tilde{H}^T \ell_\mathrm{L}^c + \mathrm{h.c.} \\ &= \frac{1}{2}\overline{\ell_\mathrm{L}} \tilde{H} Y_\nu U^* \widehat{M}^{-1} U^\dagger Y_\nu^T \tilde{H}^T \ell_\mathrm{L}^c + \mathrm{h.c.} \\ &= \frac{1}{2}\left(Y_\nu M_\mathrm{R}^{-1} Y_\nu^T\right)_{\alpha\beta} \overline{\ell_{\alpha\mathrm{L}}} \tilde{H} \tilde{H}^T \ell_{\beta\mathrm{L}}^c + \mathrm{h.c.} \; , \end{aligned} \tag{4.30}$$

where $\tilde{Y}_\nu = Y_\nu U^*$ and $M_{\rm R} = U\widehat{M}U^T$ have been used. This result is valid in any flavor basis of heavy Majorana neutrinos. After spontaneous gauge symmetry breaking, the Weinberg operator gives rise to the effective neutrino mass term in Eq. (4.12) with $M_\nu = -M_{\rm D}M_{\rm R}^{-1}M_{\rm D}^T$ and $M_{\rm D} = Y_\nu v/\sqrt{2}$. The dimension-5 operators in the type-II and type-III seesaw models, which have been summarized in Eq. (4.11), can be derived in an analogous way.

4.2 On the Scales of Seesaw Mechanisms

As we have seen, the key point of a seesaw mechanism is to ascribe the smallness of neutrino masses to the existence of some new degrees of freedom heavier than the Fermi scale $v \simeq 246$ GeV. The energy scale where a seesaw mechanism works is crucial, as it is relevant to whether this mechanism is theoretically natural and experimentally testable (Xing, 2009). Between Fermi and Planck scales, there might exist two other fundamental scales: one is the scale of a grand unified theory (GUT) at which strong, weak and electromagnetic forces can be unified, and the other is the TeV scale at which the unnatural gauge hierarchy problem of the SM can be solved or at least softened by a kind of new physics.

4.2.1 Seesaw-induced Hierarchy Problem

Many theorists argue that the conventional seesaw scenarios are natural because their scales (i.e., the masses of heavy degrees of freedom) are close to the GUT scale. This argument is reasonable on the one hand, but it reflects the drawbacks of the conventional seesaw models on the other hand. In other words, the conventional seesaw models have no direct experimental testability and involve a potential hierarchy problem. The latter is usually spoke of when two largely different energy scales exist in a model, but there is no symmetry to stabilize the low-scale physics suffering from large corrections coming from the high-scale physics.

Such a seesaw-induced fine-tuning problem means that the SM Higgs mass M_h is very sensitive to quantum corrections from the heavy degrees of freedom in a seesaw mechanism. For example (Vissani, 1998; Casas *et al.*, 2004; Abada *et al.*, 2007),

$$\delta M_h^2 = \begin{cases} -\dfrac{y_i^2}{8\pi^2}\left(\Lambda^2 + M_i^2 \ln\dfrac{M_i^2}{\Lambda^2}\right) & \text{(Type I)} \\ \dfrac{3}{16\pi^2}\left[\lambda_3\left(\Lambda^2 + M_\Delta^2 \ln\dfrac{M_\Delta^2}{\Lambda^2}\right) + 4\lambda_\Delta^2 M_\Delta^2 \ln\dfrac{M_\Delta^2}{\Lambda^2}\right] & \text{(Type II)} \\ -\dfrac{3y_i^2}{8\pi^2}\left(\Lambda^2 + M_i^2 \ln\dfrac{M_i^2}{\Lambda^2}\right) & \text{(Type III)} \end{cases} \quad (4.31)$$

in three typical seesaw scenarios, where Λ is the regulator cutoff, y_i and M_i (for $i = 1, 2, 3$) stand respectively for the eigenvalues of Y_ν (or Y_Σ) and

$M_{\rm R}$ (or M_Σ), and the contributions proportional to v^2 and M_h^2 have been omitted. Eq. (4.31) shows a quadratic sensitivity to the new scale which is characteristic of the seesaw model, implying that a high degree of fine-tuning would be necessary to accommodate the experimental data on M_h if the seesaw scale is much larger than v (or the Yukawa couplings are not extremely fine-tuned in type-I and type-III seesaws) (Abada *et al.*, 2007).

Taking the type-I seesaw scenario for illustration, we assume $\Lambda \sim M_i$ and require $|\delta M_h^2| \lesssim 0.1$ TeV^2. Then Eq. (4.31) leads us to the rough estimate

$$M_i \sim \left[\frac{(2\pi v)^2 |\delta M_h^2|}{m_i}\right]^{1/3} \lesssim 10^7 {\rm GeV} \left[\frac{0.2 \text{ eV}}{m_i}\right]^{1/3} \left[\frac{|\delta M_h^2|}{0.1 \text{ TeV}^2}\right]^{1/3} . \quad (4.32)$$

This naive result indicates that a hierarchy problem will arise if $M_i \gg 10^7$ GeV in the type-I seesaw scheme. Because of $m_i \sim y_i^2 v^2/(2M_i)$, the bound $M_i \lesssim 10^7$ GeV implies $y_i \sim \sqrt{2m_i M_i}/v \lesssim 2.6 \times 10^{-4}$ for $m_i \sim 0.2$ eV. Such a small magnitude of y_i seems to be a bit unnatural in the sense that the conventional seesaw idea attributes the smallness of m_i to the largeness of M_i other than the smallness of y_i.

There are two possible ways out of this impasse: one is to appeal for the supersymmetry, and the other is to lower the seesaw scale. In the following discussions we shall focus on whether a seesaw mechanism at low energies is theoretically natural and interesting.

4.2.2 Seesaw-induced Naturalness Problem

In reality, there is no direct evidence for a high or extremely high seesaw scale. So eV-, keV-, MeV- and GeV-scale seesaw mechanisms are all possible, at least in principle; and they are technically natural in the sense that their lepton-number-violating mass terms are naturally small according to Gerardus 't Hooft's naturalness criterion ('t Hooft, 1980) — "At any energy scale μ, a set of parameters $\alpha_i(\mu)$ describing a system can be small, if and only if, in the limit $\alpha_i(\mu) \to 0$ for each of these parameters, the system exhibits an enhanced symmetry." But there are several potential problems associated with the seesaw ideas at a very low energy scale (de Gouvea *et al.*, 2007): (a) a low-scale seesaw picture does not give any obvious connection to a theoretically well-justified fundamental physical scale (such as the Fermi scale, the TeV scale, the GUT scale or the Planck scale); (b) the neutrino Yukawa couplings in a low-scale seesaw model turn out to be tiny, giving no actual explanation of why the masses of three known neutrinos are so small; and (c) in general, a very low seesaw scale does not allow the "canonical" thermal leptogenesis mechanism (Fukugita and Yanagida, 1986) to work, although there might be an exotic way out.

It is therefore more natural to consider the possibility of realizing a seesaw mechanism above the electroweak scale but far below $\Lambda \sim 10^7$ GeV. That is just the TeV energy region which is being explored by the Large Hadron

Collider (LHC). There are several reasons for possible existence of new physics at the TeV scale. This kind of new physics should be able to stabilize the Higgs-boson mass and hence the electroweak scale; in other words, it should be able to solve or soften the unnatural gauge hierarchy problem. It has also been argued that the weakly-interacting particle candidates for dark matter should weigh about one TeV or less (Dimopoulos, 1990). If the TeV scale is really a fundamental scale, we shall be reasonably motivated to speculate that possible new physics existing at the TeV scale and responsible for the electroweak symmetry breaking might also be responsible for the origin of neutrino masses (Xing, 2008a). It is interesting and meaningful in this sense to investigate and balance the naturalness and testability of TeV seesaw mechanisms at the energy frontier set by the LHC.

As a big bonus of the conventional (type-I) seesaw mechanism, the thermal leptogenesis mechanism (Fukugita and Yanagida, 1986) provides us with an elegant dynamic picture to interpret the cosmological matter-antimatter asymmetry characterized by the observed ratio of the baryon number density to the photon number density, $\eta_{\rm B} \equiv n_{\rm B}/n_\gamma = (6.1 \pm 0.2) \times 10^{10}$. When heavy Majorana neutrino masses are down to the TeV scale, the Yukawa couplings should be reduced by more than six orders of magnitude so as to generate tiny neutrino masses via the type-I seesaw mechanism and satisfy the out-of-equilibrium condition, but the CP-violating asymmetries of heavy Majorana neutrino decays can still be enhanced by the resonant effects in order to account for $\eta_{\rm B}$. This "resonant leptogenesis" scenario might work in a specific TeV seesaw model (Pilaftsis and Underwood, 2004, 2005; Xing and Zhou, 2007), but its naturalness is certainly questionable. Other seesaw mechanisms might have similar problems at the TeV scale to realize the successful baryogenesis via leptogenesis.

Is there a TeV Noah's Ark which can naturally and simultaneously accommodate the seesaw idea, the leptogenesis picture and the collider signatures? We are most likely not so lucky and should not be too ambitious at present.

4.3 Seesaw Mechanisms at the TeV Scale

The neutrino mass terms in three typical seesaw mechanisms have been given in Section 4.1.2. Without loss of generality, we choose the basis in which the mass eigenstates of three charged leptons are identified with their flavor eigenstates. Let us discuss a few typical TeV seesaw mechanisms.

4.3.1 Type-I Seesaw Mechanism

Given $M_{\rm D} = Y_\nu v/\sqrt{2}$, the approximate type-I seesaw formula in Eq. (4.13) can be rewritten as $M_\nu = -M_{\rm D} M_{\rm R}^{-1} M_{\rm D}^T$. Note that the 3×3 light neutrino mixing matrix V is not exactly unitary in this seesaw scheme, as one can see

more clearly in Section 4.5, and its deviation from unitarity is of $\mathcal{O}(M_{\rm D}^2/M_{\rm R}^2)$. We consider two interesting possibilities:

- $M_{\rm D} \sim \mathcal{O}(10^2)$ GeV and $M_{\rm R} \sim \mathcal{O}(10^{15})$ GeV to get $M_\nu \sim \mathcal{O}(10^{-2})$ eV. In this conventional and *natural* case, $M_{\rm D}/M_{\rm R} \sim \mathcal{O}(10^{-13})$ holds. Hence the non-unitarity of V is only at the $\mathcal{O}(10^{-26})$ level, too small to be observed.
- $M_{\rm D} \sim \mathcal{O}(10^2)$ GeV and $M_{\rm R} \sim \mathcal{O}(10^3)$ GeV to get $M_\nu \sim \mathcal{O}(10^{-2})$ eV. In this *unnatural* case, a significant "structural cancellation" has to be imposed on the textures of $M_{\rm D}$ and $M_{\rm R}$. Because of $M_{\rm D}/M_{\rm R} \sim \mathcal{O}(0.1)$, the non-unitarity of V can reach the percent level and may lead to some observable effects at low energies.

Now we discuss how to realize the above "structural cancellation" for the type-I seesaw mechanism at the TeV scale. For the sake of simplicity, we take the basis of $M_{\rm R} = {\rm Diag}\{M_1, M_2, M_3\}$ for three heavy Majorana neutrinos (N_1, N_2, N_3). It is well known that M_ν vanishes if

$$M_{\rm D} \; = \; m \begin{pmatrix} y_1 & y_2 & y_3 \\ \alpha y_1 & \alpha y_2 & \alpha y_3 \\ \beta y_1 & \beta y_2 & \beta y_3 \end{pmatrix} \qquad \text{and} \qquad \sum_{i=1}^{3} \frac{y_i^2}{M_i} \; = \; 0 \tag{4.33}$$

simultaneously hold (Kersten and Smirnov, 2007). Tiny neutrino masses can be generated from tiny corrections to the texture of $M_{\rm D}$ in Eq. (4.33). For example, $M'_{\rm D} = M_{\rm D} - \epsilon X_{\rm D}$ with $M_{\rm D}$ given above and ϵ being a small dimensionless parameter (i.e., $|\epsilon| \ll 1$) yields

$$M'_\nu \; = \; -M'_{\rm D} M_{\rm R}^{-1} M'^T_{\rm D} \; \simeq \; \epsilon \left(M_{\rm D} M_{\rm R}^{-1} X_{\rm D}^T + X_{\rm D} M_{\rm R}^{-1} M_{\rm D}^T \right) \; , \tag{4.34}$$

from which $M'_\nu \sim \mathcal{O}(10^{-2})$ eV can be obtained by adjusting the size of ϵ.

A lot of attention has recently been paid to a viable type-I seesaw model and its collider signatures at the TeV scale (Xing, 2008a; 2009). At least the following lessons can be learnt:

- Two necessary conditions must be satisfied in order to test a type-I seesaw model at the LHC: (a) M_i are of $\mathcal{O}(1)$ TeV or smaller; and (b) the strength of light-heavy neutrino mixing (i.e., $M_{\rm D}/M_{\rm R}$) is large enough. Otherwise, it would be impossible to produce and detect N_i at the LHC.
- The collider signatures of N_i are essentially decoupled from the mass and mixing parameters of three light neutrinos ν_i. For instance, the small parameter ϵ in Eq. (4.34) has nothing to do with the ratio $M_{\rm D}/M_{\rm R}$.
- The non-unitarity of V might lead to some observable effects in long-baseline neutrino oscillations and some other lepton-flavor-violating or lepton-number-violating processes, if $M_{\rm D}/M_{\rm R}$ is of $\mathcal{O}(0.1)$. More discussions will be given in Section 4.5.
- The clean LHC signatures of heavy Majorana neutrinos are the $\Delta L = 2$ like-sign dilepton events (Keung and Senjanovic, 1983), such as $pp \to W^{*\pm} W^{*\pm} \to \mu^\pm \mu^\pm jj$ (a collider analogue to the neutrinoless double-beta decay) and $pp \to W^{*\pm} \to \mu^\pm N_i \to \mu^\pm \mu^\pm jj$ (a dominant channel due to the resonant production of N_i).

Some instructive and comprehensive analyses of possible LHC events for a single heavy Majorana neutrino have recently been done (Han and Zhang, 2006; del Aguila and Aguilar-Saavedra, 2009a; Atre *et al.*, 2009), but they only serve for illustration because such a simplified type-I seesaw scenario is actually unrealistic.

4.3.2 Type-II Seesaw Mechanism

The type-II seesaw formula $M_\nu = Y_\Delta v_\Delta = \lambda_\Delta Y_\Delta v^2/M_\Delta$ has already been given in Eq. (4.13). Note that the third term in Eq. (4.7) violates both L and $B-L$, so the smallness of λ_Δ is naturally allowed according to 't Hooft's naturalness criterion; i.e., setting $\lambda_\Delta = 0$ will increase the symmetry of $\mathcal{L}_{\rm lepton}$ ('t Hooft, 1980). Given $M_\Delta \sim \mathcal{O}(1)$ TeV, for example, this seesaw mechanism works to generate $M_\nu \sim \mathcal{O}(10^{-2})$ eV provided $\lambda_\Delta Y_\Delta \sim \mathcal{O}(10^{-12})$ holds. Note also that the neutrino mixing matrix V is exactly unitary in the type-II seesaw mechanism, simply because the heavy degrees of freedom do not mix with the light ones.

There are totally seven physical Higgs bosons in the type-II seesaw scheme: doubly-charged H^{++} and H^{--}, singly-charged H^+ and H^-, neutral A^0 (CP-odd), and neutral h and H^0 (CP-even), where h is the SM-like Higgs boson. Except for M_h^2, we get a quasi-degenerate mass spectrum for other scalars (Fileviez Pérez *et al.*, 2008; del Aguila and Aguilar-Saavedra, 2009a): $M^2_{H^{\pm\pm}} = M^2_\Delta \approx M^2_{H^0} \approx M^2_{H^\pm} \approx M^2_{A^0}$. As a consequence, the decay channels $H^{\pm\pm} \to W^\pm H^\pm$ and $H^{\pm\pm} \to H^\pm H^\pm$ are kinematically forbidden. The production of $H^{\pm\pm}$ at the LHC is mainly through $q\bar{q} \to \gamma^*, Z^* \to H^{++}H^{--}$ and $q\bar{q}' \to W^* \to H^{\pm\pm}H^\mp$ processes, which do not depend on the small Yukawa couplings and thus may not be suppressed.

The typical collider signatures in this seesaw scenario are the lepton-number-violating $H^{\pm\pm} \to l^\pm_\alpha l^\pm_\beta$ decays as well as $H^+ \to l^+_\alpha \overline{\nu}$ and $H^- \to l^-_\alpha \nu$ decays (for $\alpha, \beta = e, \mu, \tau$). Their branching ratios

$$\begin{aligned} \mathcal{B}(H^{\pm\pm} \to l^\pm_\alpha l^\pm_\beta) &= \frac{|(M_\nu)_{\alpha\beta}|^2}{\sum\limits_{\rho,\sigma} |(M_\nu)_{\rho\sigma}|^2} \left(2 - \delta_{\alpha\beta}\right) , \\ \mathcal{B}(H^+ \to l^+_\alpha \overline{\nu}) &= \frac{\sum\limits_\beta |(M_\nu)_{\alpha\beta}|^2}{\sum\limits_{\rho,\sigma} |(M_\nu)_{\rho\sigma}|^2} \end{aligned} \tag{4.35}$$

are closely related to the masses, flavor mixing angles and CP-violating phases of three light neutrinos, because $M_\nu = V \widehat{M}_\nu V^T$ with $\widehat{M}_\nu = {\rm Diag}\{m_1, m_2, m_3\}$ holds. Some detailed analyses of such decay modes together with the LHC signatures of $H^{\pm\pm}$ and $H^\pm$ bosons have been done in the literature (see, for example, Fileviez Pérez *et al.*, 2008).

It is worth pointing out that the following dimension-6 operator can easily be derived from the type-II seesaw mechanism:

$$\frac{\mathcal{L}_{\rm d=6}}{\Lambda^2} \; = \; -\frac{(Y_\Delta)_{\alpha\beta}\,(Y_\Delta)^\dagger_{\rho\sigma}}{4M^2_\Delta} \; \left(\overline{\ell_{\alpha\rm L}}\gamma^\mu \ell_{\sigma\rm L}\right) \left(\overline{\ell_{\beta\rm L}}\gamma_\mu \ell_{\rho\rm L}\right) \; , \tag{4.36}$$

which has two immediate low-energy effects: the non-standard interactions of neutrinos and the lepton-flavor-violating interactions of charged leptons. An analysis of such effects provides us with some preliminary information (Malinsky *et al.*, 2009): (a) the magnitudes of non-standard interactions of neutrinos and the widths of lepton-flavor-violating tree-level decays of charged leptons are dependent on the neutrino masses m_i and flavor mixing parameters of V; (b) for a long-baseline neutrino oscillation experiment, the neutrino beam encounters the Earth matter and the electron-type non-standard interaction contributes to the matter potential; and (c) at a neutrino factory, the lepton-flavor-violating processes $\mu^- \to e^- \nu_e \overline{\nu}_\mu$ and $\mu^+ \to e^+ \overline{\nu}_e \nu_\mu$ could cause some wrong-sign muons at a near detector. Current experimental constraints tell us that such low-energy effects are very small, but they might be experimentally accessible in the future precision measurements.

4.3.3 Type-(I+II) Seesaw Mechanism

The type-(I+II) seesaw mechanism can be achieved by combining the neutrino mass terms in Eqs. (4.6) and (4.7). After spontaneous gauge symmetry breaking, we are left with the overall neutrino mass term

$$-\mathcal{L}_{\rm mass} \; = \; \frac{1}{2} \; \overline{\left(\nu_{\rm L} \;\; N^c_{\rm R}\right)} \; \begin{pmatrix} M_{\rm L} & M_{\rm D} \\ M^T_{\rm D} & M_{\rm R} \end{pmatrix} \begin{pmatrix} \nu^c_{\rm L} \\ N_{\rm R} \end{pmatrix} + {\rm h.c.} \; , \tag{4.37}$$

where $M_{\rm D} = Y_\nu v/\sqrt{2}$ and $M_{\rm L} = Y_\Delta v_\Delta$ with $\langle H \rangle \equiv v/\sqrt{2}$ and $\langle \Delta \rangle \equiv v_\Delta$ corresponding to the vacuum expectation values of the neutral components of the Higgs doublet H and the Higgs triplet Δ. This mass term is equivalent to the one given in Eq. (3.30). The 6×6 neutrino mass matrix in Eq. (4.37) is symmetric and can be diagonalized by the unitary transformation

$$\begin{pmatrix} V & R \\ S & U \end{pmatrix}^\dagger \begin{pmatrix} M_{\rm L} & M_{\rm D} \\ M^T_{\rm D} & M_{\rm R} \end{pmatrix} \begin{pmatrix} V & R \\ S & U \end{pmatrix}^* = \begin{pmatrix} \widehat{M}_\nu & \mathbf{0} \\ \mathbf{0} & \widehat{M}_N \end{pmatrix} \; , \tag{4.38}$$

where $\widehat{M}_\nu = {\rm Diag}\{m_1, m_2, m_3\}$ and $\widehat{M}_N = {\rm Diag}\{M_1, M_2, M_3\}$. Needless to say, $V^\dagger V + S^\dagger S = V V^\dagger + R R^\dagger = \mathbf{1}$ holds as a consequence of the unitarity of the above transformation. Hence V, the flavor mixing matrix of three light Majorana neutrinos, must be non-unitary if R and S are nonzero.

In the leading-order approximation, the type-(I+II) seesaw formula reads

$$M_\nu \; = \; M_{\rm L} - M_{\rm D} M^{-1}_{\rm R} M^T_{\rm D} \; . \tag{4.39}$$

Hence type-I and type-II seesaws can be regarded as two extreme cases of the type-(I+II) seesaw. Note that the two mass terms in Eq. (4.39) are possibly comparable in magnitude. If both of them are small, their contributions to M_ν may have significant interference effects which make it practically impossible to distinguish between type-II and type-(I+II) seesaws (Ren and Xing, 2008); but if both of them are large, their contributions to M_ν must be destructive. The latter case unnaturally requires a significant cancellation between two big quantities in order to obtain a small quantity (Chao *et al.*, 2008a), but it is interesting in the sense that it might give rise to some observable collider signatures of heavy Majorana neutrinos.

Let us briefly describe a particular type-(I+II) seesaw model and comment on its possible LHC signatures. First, we assume that both M_i and M_Δ are of $\mathcal{O}(1)$ TeV. Then the production of $H^{\pm\pm}$ and $H^\pm$ bosons at the LHC is guaranteed, and their lepton-number-violating signatures will probe the Higgs triplet sector of the type-(I+II) seesaw mechanism. On the other hand, $\mathcal{O}(M_{\rm D}/M_{\rm R}) \lesssim \mathcal{O}(0.1)$ is possible as a result of $\mathcal{O}(M_{\rm R}) \sim \mathcal{O}(1)$ TeV and $\mathcal{O}(M_{\rm D}) \lesssim \mathcal{O}(v)$, such that appreciable signatures of N_i can be achieved at the LHC. Second, the small mass scale of M_ν implies that the relation $\mathcal{O}(M_{\rm L}) \sim \mathcal{O}(M_{\rm D} M_{\rm R}^{-1} M_{\rm D}^T)$ must hold. In other words, it is the significant but incomplete cancellation between $M_{\rm L}$ and $M_{\rm D} M_{\rm R}^{-1} M_{\rm D}^T$ terms that results in the non-vanishing but tiny masses for three light neutrinos. We admit that dangerous radiative corrections to two mass terms of M_ν require a delicate fine-tuning of the cancellation at the loop level (Chao *et al.*, 2008b). But this scenario allows us to reconstruct $M_{\rm L}$ via the excellent approximation $M_{\rm L} = V \widehat{M}_\nu V^T + R \widehat{M}_N R^T \approx R \widehat{M}_N R^T$, such that the elements of Y_Δ read

$$(Y_\Delta)_{\alpha\beta} = \frac{(M_{\rm L})_{\alpha\beta}}{v_\Delta} \approx \sum_{i=1}^{3} \frac{R_{\alpha i} R_{\beta i} M_i}{v_\Delta} \; , \tag{4.40}$$

where α and β run over e, μ and τ. This result implies that the leptonic decays of $H^{\pm\pm}$ and $H^\pm$ bosons depend on both R and M_i, which determine the production and decays of N_i. Thus we have established an interesting correlation between the singly- or doubly-charged Higgs bosons and the heavy Majorana neutrinos. If the correlative signatures of $H^\pm$, $H^{\pm\pm}$ and N_i can be observed at the LHC, they will serve for a direct experimental test of this type-(I+II) seesaw model.

To illustrate, here we focus on the *minimal* type-(I+II) seesaw model with a single heavy Majorana neutrino, where R can be parametrized in terms of three rotation angles θ_{i4} and three phase angles δ_{i4} (for $i = 1, 2, 3$) (Xing, 2008b). In this case we have

$$\begin{aligned} \omega_1 &\equiv \frac{\sigma(pp \to \mu^+\mu^+ W^- X)|_{N_1}}{\sigma(pp \to \mu^+\mu^+ H^- X)|_{H^{++}}} \approx \frac{\sigma_N}{\sigma_H} \cdot \frac{s_{14}^2 + s_{24}^2 + s_{34}^2}{4} \; , \\ \omega_2 &\equiv \frac{\sigma(pp \to \mu^+\mu^+ W^- X)|_{N_1}}{\sigma(pp \to \mu^+\mu^+ H^{--} X)|_{H^{++}}} \approx \frac{\sigma_N}{\sigma_{\rm pair}} \cdot \frac{s_{14}^2 + s_{24}^2 + s_{34}^2}{4} \end{aligned} \tag{4.41}$$

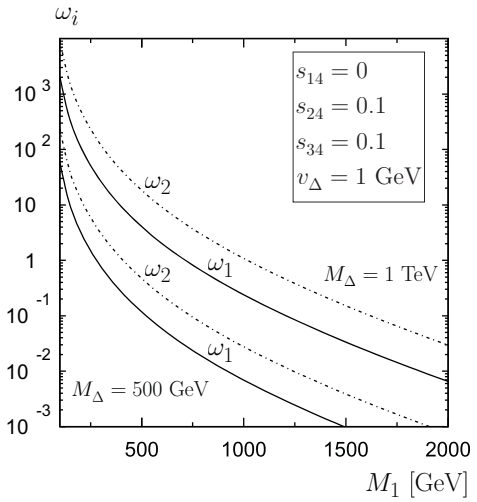

Fig. 4.1 An illustration of the correlative signatures of N_1 and $H^{\pm\pm}$ at the LHC with an integrated luminosity of 300 fb^{-1} (Chao *et al.*, 2008b. With permission from the Elsevier)

for $s_{i4} \equiv \sin\theta_{i4} \lesssim \mathcal{O}(0.1)$, where $\sigma_N \equiv \sigma(pp \to l^+_\alpha N_1 X)/|R_{\alpha 1}|^2$, $\sigma_H \equiv \sigma(pp \to H^{++}H^- X)$ and $\sigma_{\rm pair} \equiv \sigma(pp \to H^{++}H^{--}X)$ are three reduced cross sections (Chao *et al.*, 2008b). Fig. 4.1 shows a numerical illustration of ω_1 and ω_2 changing with M_1 at the LHC with an integrated luminosity of 300 fb^{-1}, and it may give one a ball-park feeling of possible collider signatures of N_1 and $H^{\pm\pm}$ and their correlation.

If an additional heavy Majorana neutrino with a nearly equal mass is introduced into the above scenario, the collider signatures can be resonantly enhanced due to the constructive interference between the contributions from two heavy Majorana neutrinos (Chao *et al.*, 2010). If two heavy Majorana neutrinos with nearly degenerate masses form a pseudo-Dirac particle, however, the lepton-number-violating signatures will be highly suppressed and the trilepton signatures arising from the processes $pp \to l^+_\alpha l^+_\beta l^-_\gamma \nu$ and $pp \to l^-_\alpha l^-_\beta l^+_\gamma \overline{\nu}$ (for $\alpha, \beta, \gamma = e, \mu, \tau$) should be most promising. This case has been discussed in the minimal type-I seesaw model with a softly-broken global $U(1)$ symmetry (Zhang and Zhou, 2010).

4.3.4 Type-III Seesaw Mechanism

The lepton mass terms in the type-III seesaw scheme have already been given in Eq. (4.9). After spontaneous gauge symmetry breaking, we are left with

$$-\mathcal{L}_{\rm mass} = \frac{1}{2}\,\overline{(\nu_{\rm L}\ \ \Sigma^0)} \begin{pmatrix} \mathbf{0} & M_{\rm D} \\ M^T_{\rm D} & M_\Sigma \end{pmatrix} \begin{pmatrix} \nu^c_{\rm L} \\ \Sigma^{0c} \end{pmatrix} + {\rm h.c.}\ ,$$

$$-\mathcal{L}'_{\rm mass} = \overline{(e_{\rm L}\ \Psi_{\rm L})} \begin{pmatrix} M_l & \sqrt{2}M_{\rm D} \\ \mathbf{0} & M_{\Sigma} \end{pmatrix} \begin{pmatrix} E_{\rm R} \\ \Psi_{\rm R} \end{pmatrix} + {\rm h.c.}\ , \tag{4.42}$$

respectively, for neutral and charged fermions, where $M_l = Y_l v/\sqrt{2}$, $M_{\rm D} = Y_{\Sigma} v/\sqrt{2}$, and $\Psi = \Sigma^- + \Sigma^{+c}$. The symmetric 6×6 neutrino mass matrix can be diagonalized by the following unitary transformation:

$$\begin{pmatrix} V & R \\ S & U \end{pmatrix}^{\dagger} \begin{pmatrix} \mathbf{0} & M_{\rm D} \\ M^T_{\rm D} & M_{\Sigma} \end{pmatrix} \begin{pmatrix} V & R \\ S & U \end{pmatrix}^{*} = \begin{pmatrix} \widehat{M}_{\nu} & \mathbf{0} \\ \mathbf{0} & \widehat{M}_{\Sigma} \end{pmatrix} , \tag{4.43}$$

in which $\widehat{M}_{\nu} = {\rm Diag}\{m_1, m_2, m_3\}$ and $\widehat{M}_{\Sigma} = {\rm Diag}\{M_1, M_2, M_3\}$. In the leading-order approximation, this diagonalization yields the type-III seesaw formula $M_{\nu} = -M_{\rm D} M^{-1}_{\Sigma} M^T_{\rm D}$, which is equivalent to the one derived from the effective dimension-5 operator in Eq. (4.13). Let us use one sentence to comment on the similarities and differences between type-I and type-III seesaw mechanisms (Abada *et al.*, 2007): the non-unitarity of the 3×3 neutrino mixing matrix V has appeared in both cases, although the modified couplings between the Z^0 boson and three light neutrinos differ and the non-unitary flavor mixing is also present in the couplings between the Z^0 boson and three charged leptons in the type-III seesaw scenario.

At the LHC, the typical lepton-number-violating signatures of the type-III seesaw mechanism can be $pp \to \Sigma^+ \Sigma^0 \to l^+_{\alpha} l^+_{\beta} + Z^0 W^-(\to 4j)$ and $pp \to \Sigma^- \Sigma^0 \to l^-_{\alpha} l^-_{\beta} + Z^0 W^+(\to 4j)$ processes. A detailed analysis of such collider signatures have been done in the literature (Franceschini *et al.*, 2008; del Aguila and Aguilar-Saavedra, 2009a). As for the low-energy phenomenology, a consequence of this seesaw scenario is the non-unitarity of the 3×3 flavor mixing matrix $\tilde{V}$ ($\approx V$) in both charged- and neutral-current interactions (Abada *et al.*, 2007). Current experimental bounds on the deviation of $\tilde{V}\tilde{V}^{\dagger}$ from the identity matrix are at the 0.1% level, much stronger than those obtained in the type-I seesaw scheme, just because the flavor-changing processes with charged leptons are allowed at the tree level in the type-III seesaw mechanism.

It is worth mentioning that an interesting type-(I+III) seesaw model has recently been proposed (Bajc and Senjanovic, 2007), and its phenomenological and cosmological consequences together with its possible collider signatures have also been explored (Bajc *et al.*, 2007; Arhrib *et al.*, 2010).

4.3.5 Inverse Seesaw Mechanism

Given the naturalness and testability as two prerequisites, the so-called inverse or double seesaw mechanism (Wyler and Wolfenstein, 1983; Mohapatra and Valle, 1986; Ma, 1987) is another interesting possibility of generating tiny neutrino masses at the TeV scale. The idea of this seesaw picture is to add three heavy right-handed neutrinos $N_{\rm R}$, three SM gauge-singlet neutrinos $S_{\rm R}$

and one Higgs singlet Φ into the SM, such that the gauge-invariant lepton mass terms can be written as

$$-\mathcal{L}_{\rm lepton} \; = \; \overline{\ell_{\rm L}} Y_l H E_{\rm R} + \overline{\ell_{\rm L}} Y_\nu \tilde{H} N_{\rm R} + \overline{N^c_{\rm R}} Y_S \Phi S_{\rm R} + \frac{1}{2} \overline{S^c_{\rm R}} M_\mu S_{\rm R} + {\rm h.c.} \; , \tag{4.44}$$

where M_μ is naturally small according to 't Hooft's naturalness criterion ('t Hooft, 1980), because its corresponding mass term violates the lepton number. After spontaneous gauge symmetry breaking, the overall neutrino mass term turns out to be

$$-\mathcal{L}_{\rm mass} \; = \; \frac{1}{2} \, \overline{(\nu_{\rm L} \; N^c_{\rm R} \; S^c_{\rm R})} \begin{pmatrix} \mathbf{0} & M_{\rm D} & \mathbf{0} \\ M^T_{\rm D} & \mathbf{0} & M_S \\ \mathbf{0} & M^T_S & M_\mu \end{pmatrix} \begin{pmatrix} \nu^c_{\rm L} \\ N_{\rm R} \\ S_{\rm R} \end{pmatrix} \; , \tag{4.45}$$

where $M_{\rm D} = Y_\nu \langle H \rangle$ and $M_S = Y_S \langle \Phi \rangle$. A diagonalization of the symmetric 9×9 matrix in Eq. (4.45) leads us to the effective light neutrino mass matrix

$$M_\nu \; = \; M_{\rm D} \left(M^T_S \right)^{-1} M_\mu \left(M_S \right)^{-1} M^T_{\rm D} \tag{4.46}$$

in the leading-order approximation (Chan *et al.*, 2009). Hence the smallness of M_ν is attributed to both the smallness of M_μ itself and the doubly-suppressed $M_{\rm D}/M_S$ term for $M_{\rm D} \ll M_S$. For example, $M_\mu \sim \mathcal{O}(1)$ keV and $M_{\rm D}/M_S \sim \mathcal{O}(10^{-2})$ naturally yield a sub-eV M_ν. One has $M_\nu = \mathbf{0}$ in the limit $M_\mu \to \mathbf{0}$, reflecting the restoration of the slightly-broken lepton number. The heavy sector consists of three pairs of pseudo-Dirac neutrinos, whose CP-conjugated Majorana components have a tiny mass splitting characterized by $\mathcal{O}(M_\mu)$.

4.4 Multiple Seesaw Mechanisms

We have mentioned that a test of the type-I seesaw mechanism at the TeV scale necessitates an appreciable magnitude of $M_{\rm D}/M_{\rm R}$ so as to make it possible to produce and detect heavy Majorana neutrinos at the LHC. This prerequisite unavoidably requires a terrible fine-tuning of $M_{\rm D}$ and $M_{\rm R}$, because one has to impose $M_{\rm R} \sim 1$ TeV, $M_{\rm D}/M_{\rm R} \sim 10^{-3}$ to 10^{-1} and $M_\nu \sim 0.1$ eV simultaneously on the seesaw relation $M_\nu = -M_{\rm D} M^{-1}_{\rm R} M^T_{\rm D}$ (Xing, 2009). It is therefore desirable to invoke new ideas to resolve this *unnaturalness* problem built in the TeV seesaw mechanism.

A *multiple* seesaw mechanism at the TeV scale may satisfy both *naturalness* and *testability* requirements (Xing and Zhou, 2009; Liao, 2010a). To illustrate, we assume that the small mass scale of three light neutrinos arises from a naive seesaw relation $m \sim (\lambda \Lambda_{\rm EW})^{n+1} / \Lambda^n_{\rm SS}$, where λ is a dimensionless Yukawa coupling coefficient and n is an arbitrary integer larger than one. Without any terrible fine-tuning, the seesaw scale can be estimated from

$$\Lambda_{\rm SS} \; \sim \; \lambda^{\frac{n+1}{n}} \left[\frac{\Lambda_{\rm EW}}{100 \; {\rm GeV}} \right]^{\frac{n+1}{n}} \left[\frac{0.1 \; {\rm eV}}{m} \right]^{\frac{1}{n}} 10^{\frac{2(n+6)}{n}} \; {\rm GeV} \; . \tag{4.47}$$

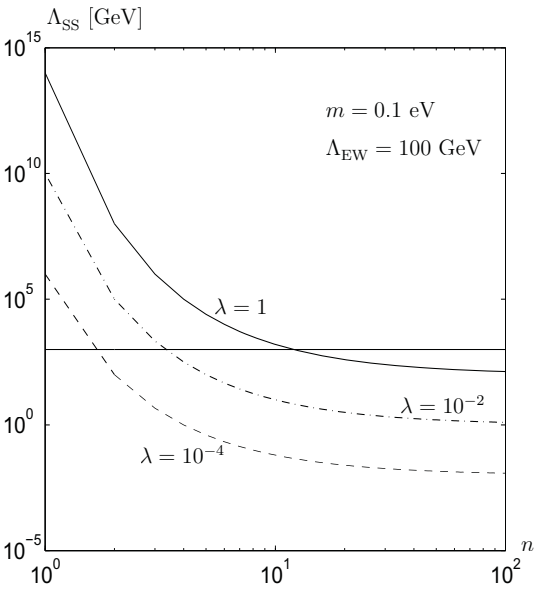

Fig. 4.2 A numerical illustration of the seesaw scale $\Lambda_{\rm SS}$ changing with n and λ as specified in Eq. (4.47). Here the horizontal line stands for the TeV scale

A numerical change of $\Lambda_{\rm SS}$ with n and λ is shown in Fig. 4.2, where $\Lambda_{\rm SS} \sim 1$ TeV may naturally result from $n \geqslant 2$ and $\lambda \geqslant 10^{-3}$. Hence the multiple seesaw idea is expected to work at the TeV scale and provide us with a novel approach to bridge the gap between theoretical naturalness and experimental testability of the canonical seesaw mechanism.

The simplest way to build a multiple seesaw model at the TeV scale is to extend the canonical seesaw mechanism by introducing a number of gauge-singlet fermions $S^i_{n\rm R}$ and scalars Φ_n (for $i = 1, 2, 3$ and $n = 1, 2, \cdots$). We find that a proper implementation of the global $U(1) \times \mathbb{Z}_{2N}$ symmetry leads us to two classes of multiple seesaw mechanisms with the nearest-neighbor-interaction pattern — an interesting form of the overall $3\,(n+2) \times 3\,(n+2)$ neutrino mass matrix in which every 3×3 sub-matrix only interacts with its nearest neighbor. The first class contains an even number of $S^i_{n\rm R}$ and Φ_n and corresponds to an appealing extension of the canonical seesaw mechanism, while the second class has an odd number of $S^i_{n\rm R}$ and Φ_n and is actually a straightforward extension of the inverse seesaw mechanism.

4.4.1 Two Classes of Multiple Seesaw Mechanisms

The spirit of multiple seesaw mechanisms is to make a harmless extension of the SM by adding three right-handed neutrinos $N^i_{\rm R}$ together with some gauge-singlet fermions $S^i_{n\rm R}$ and scalars Φ_n (for $i = 1, 2, 3$ and $n = 1, 2, \cdots$).

Allowing for lepton number violation to a certain extent, we can write the gauge-invariant Lagrangian for neutrino masses as (Xing and Zhou, 2009)

$$-\mathcal{L}_\nu = \overline{\ell_{\rm L}} Y_\nu \tilde{H} N_{\rm R} + \overline{N_{\rm R}^c} Y_{S_1} S_{1{\rm R}} \Phi_1 + \sum_{i=2}^{n} \overline{S_{(i-1){\rm R}}^c} Y_{S_i} S_{i{\rm R}} \Phi_i + \frac{1}{2} \overline{S_{n{\rm R}}^c} M_\mu S_{n{\rm R}} + {\rm h.c.} \; , \tag{4.48}$$

where Y_ν and Y_{S_i} (for $i = 1, 2, \cdots, n$) are the 3×3 Yukawa coupling matrices, and M_μ is a symmetric Majorana mass matrix. After spontaneous gauge symmetry breaking, we arrive at the overall $3\,(n+2) \times 3\,(n+2)$ neutrino mass matrix $\mathcal{M}$ in the flavor basis defined by $(\nu_{\rm L}, N_{\rm R}^c, S_{1{\rm R}}^c, \cdots, S_{n{\rm R}}^c)$ and their charge-conjugate states:

$$\mathcal{M} = \begin{pmatrix} \mathbf{0} & M_{\rm D} & \mathbf{0} & \mathbf{0} & \mathbf{0} & \cdots & \mathbf{0} \\ M_{\rm D}^T & \mathbf{0} & M_{S_1} & \mathbf{0} & \mathbf{0} & \cdots & \mathbf{0} \\ \mathbf{0} & M_{S_1}^T & \mathbf{0} & M_{S_2} & \mathbf{0} & \cdots & \mathbf{0} \\ \mathbf{0} & \mathbf{0} & M_{S_2}^T & \mathbf{0} & \ddots & \ddots & \vdots \\ \mathbf{0} & \mathbf{0} & \mathbf{0} & \ddots & \ddots & M_{S_{n-1}} & \mathbf{0} \\ \vdots & \vdots & \vdots & \ddots & M_{S_{n-1}}^T & \mathbf{0} & M_{S_n} \\ \mathbf{0} & \mathbf{0} & \mathbf{0} & \cdots & \mathbf{0} & M_{S_n}^T & M_\mu \end{pmatrix} , \tag{4.49}$$

where $M_{\rm D} \equiv Y_\nu \langle H \rangle$ and $M_{S_i} = Y_{S_i} \langle \Phi_i \rangle$ (for $i = 1, 2, \cdots, n$) are the 3×3 mass matrices. Setting $N_{\rm R} = S_{0{\rm R}}$ for simplicity, one can observe that the Yukawa interactions between $S_{i{\rm R}}$ and $S_{j{\rm R}}$ exist if and only if their subscripts satisfy the selection rule $|i - j| = 1$ (for $i, j = 0, 1, 2, \cdots, n$). Note that $\mathcal{M}$ manifests a very suggestive nearest-neighbor-interaction (NNI) pattern, which has attracted a lot of attention in the quark sector to understand the observed hierarchies of quark masses and flavor mixing angles (Fritzsch, 1978, 1979; Branco *et al.*, 1989). Such a special structure of $\mathcal{M}$ may arise from a proper implementation of the global $U(1) \times \mathbb{Z}_{2N}$ symmetry. The unique generator of the cyclic group $\mathbb{Z}_{2N}$ is $\varpi = {\rm e}^{{\rm i}\pi/N}$, which produces all the group elements $\mathbb{Z}_{2N} = \{1, \varpi, \varpi^2, \varpi^3, \cdots, \varpi^{2N-1}\}$. By definition, a field Ψ with the charge q transforms as $\Psi \to {\rm e}^{{\rm i}\pi q/N} \Psi$ under $\mathbb{Z}_{2N}$ (for $q = 0, 1, 2, \cdots, 2N-1$). Hence we assign the $U(1)$ and $\mathbb{Z}_{2N}$ charges of the relevant fields in $\mathcal{L}_\nu$ as below:

(1) The global $U(1)$ symmetry can be identified with the lepton number L, namely $L(\ell_{\rm L}) = L(E_{\rm R}) = +1$, where $E_{\rm R}$ represents the charged-lepton singlets in the SM. We arrange the lepton numbers of gauge-singlet fermions and scalars to be $L(N_{\rm R}) = +1$, $L(S_{k{\rm R}}) = (-1)^k$ and $L(\Phi_k) = 0$ (for $k = 1, 2, \cdots, n$). It turns out that only the Majorana mass term $\overline{S_{n{\rm R}}^c} M_\mu S_{n{\rm R}}$ in $\mathcal{L}_\nu$ explicitly violates the $U(1)$ symmetry. After this assignment, other lepton-number-violating mass terms (e.g., $\overline{N_{\rm R}^c} M_{\rm R} N_{\rm R}$ in

the canonical seesaw mechanism) may also appear in the Lagrangian, but they can be eliminated by invoking the discrete $\mathbb{Z}_{2N}$ symmetry.

(2) We assign the $\mathbb{Z}_{2N}$ charge of $S_{n\rm R}$ as $q(S_{n\rm R}) = N$. Then it is easy to verify that the Majorana mass term $\overline{S^c_{n\rm R}} M_\mu S_{n\rm R}$ is invariant under the $\mathbb{Z}_{2N}$ transformation. If all the other gauge-singlet fermions $S_{k\rm R}$ (for $k = 1, 2, \cdots, n-1$) take any charges in $\{1, 2, \cdots, 2N-1\}$ other than N, their corresponding Majorana mass terms are accordingly forbidden. Given $q(\ell_{\rm L}) = q(E_{\rm R}) = q(N_{\rm R}) = 1$, both the charges of $S_{k\rm R}$ (for $k = 1, 2, \cdots, n-1$) and those of Φ_i (for $i = 1, 2, \cdots, n$) can be properly chosen so as to achieve the NNI form of $\mathcal{L}_\nu$ as shown in Eq. (4.48). But the solution to this kind of charge assignment may not be unique, because for a given value of n one can always take $N \gg n$ to fulfill all the above-mentioned requirements. Simple examples (with $n = 1, 2, 3$) will be presented below.

This multiple seesaw picture should be the simplest extension of the canonical seesaw mechanism, since it does not invoke the help of either additional $SU(2)_{\rm L}$ fermion doublets (Dudas and Savoy, 2002) or a new isospin 3/2 Higgs multiplet (Babu *et al.*, 2009; Liao, 2010b). In addition, the inverse seesaw scenario is merely the simplest example in one class of the multiple seesaw mechanisms under discussion (with an odd number of $S^i_{n\rm R}$ or Φ_n).

Now let us diagonalize $\mathcal{M}$ in Eq. (4.49) to achieve the effective mass matrix of three light neutrinos M_ν. Note that $\mathcal{M}$ can be rewritten as

$$\mathcal{M} = \begin{pmatrix} \mathbf{0} & \tilde{M}_{\rm D} \\ \tilde{M}^T_{\rm D} & \tilde{M}_\mu \end{pmatrix} , \tag{4.50}$$

where $\tilde{M}_{\rm D} = (M_{\rm D} \;\; \mathbf{0})$ denotes a $3 \times 3\,(n+1)$ matrix and $\tilde{M}_\mu$ is a symmetric $3\,(n+1) \times 3\,(n+1)$ matrix. Taking $\mathcal{O}(\tilde{M}_\mu) \gg \mathcal{O}(\tilde{M}_{\rm D})$, one can easily obtain $M_\nu = -\tilde{M}_{\rm D} \tilde{M}^{-1}_\mu \tilde{M}^T_{\rm D}$ for three light Majorana neutrinos in the leading-order approximation. As the elements in the fourth to $3n$-th columns of $\tilde{M}_{\rm D}$ are exactly zero, only the 3×3 top left block of $\tilde{M}^{-1}_\mu$ is relevant to the calculation of M_ν. Without loss of generality, the inverse of $\tilde{M}_\mu$ can be figured out by assuming all the non-zero 3×3 sub-matrices of $\mathcal{M}$ to be of rank three. We find two types of solutions, depending on whether n is even or odd, and thus arrive at two classes of multiple seesaw mechanisms:

Class A of multiple seesaw mechanisms — they contain an even number of gauge-singlet fermions $S^i_{n\rm R}$ and scalars Φ_n (i.e., $n = 2k$ with $k = 0, 1, 2, \cdots$) and correspond to a novel extension of the canonical seesaw picture. The effective mass matrix of three light Majorana neutrinos is given by

$$M_\nu = -M_{\rm D} \left[\prod_{i=1}^{k} \left(M^T_{S_{2i-1}} \right)^{-1} M_{S_{2i}} \right] M^{-1}_\mu \left[\prod_{i=1}^{k} \left(M^T_{S_{2i-1}} \right)^{-1} M_{S_{2i}} \right]^T M^T_{\rm D} \tag{4.51}$$

in the leading-order approximation. The $k = 0$ case is obviously equivalent to the canonical seesaw mechanism (i.e., $M_\nu = -M_{\rm D} M^{-1}_{\rm R} M^T_{\rm D}$ by setting $S_{0\rm R} =$

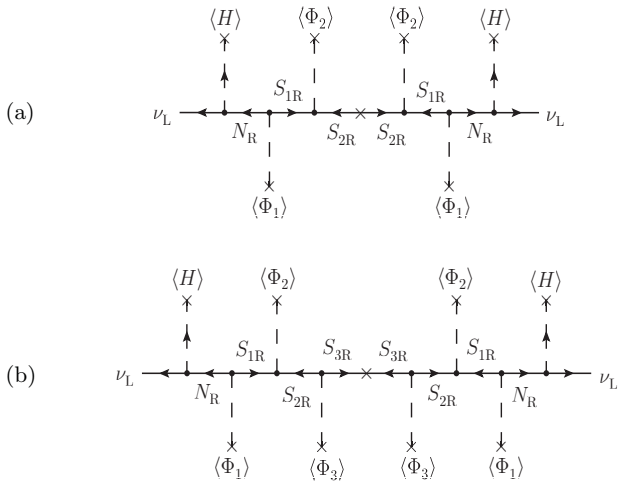

Fig. 4.3 The origin of light Majorana neutrino masses in multiple seesaw mechanisms: (a) the minimal extension of the canonical seesaw mechanism (with $n = 2$); and (b) the minimal extension of the inverse seesaw mechanism (with $n = 3$)

$N_{\rm R}$ and $M_\mu = M_{\rm R}$). If $M_{S_{2i}} \sim M_{\rm D} \sim \mathcal{O}(\Lambda_{\rm EW})$ and $M_{S_{2i-1}} \sim M_\mu \sim \mathcal{O}(\Lambda_{\rm SS})$ hold (for $i = 1, 2, \cdots, k$), then Eq. (4.51) leads to $M_\nu \sim \Lambda_{\rm EW}^{2(k+1)}/\Lambda_{\rm SS}^{2k+1}$, which can effectively lower the conventional seesaw scale $\Lambda_{\rm SS} \sim 10^{14}$ GeV down to the TeV scale as illustrated in Fig. 4.2.

Taking $n = 2$ (i.e., $k = 1$) for example, we simply arrive at

$$M_\nu = -M_{\rm D} \left(M_{S_1}^T\right)^{-1} M_{S_2} M_\mu^{-1} M_{S_2}^T \left(M_{S_1}\right)^{-1} M_{\rm D}^T \; . \tag{4.52}$$

This effective multiple seesaw mass term is illustrated in Fig. 4.3(a). The NNI pattern of $\mathcal{M}$ with $n = 2$ can be obtained by imposing the global $U(1) \times \mathbb{Z}_6$ symmetry on $\mathcal{L}_\nu$, where the proper charge assignment is listed in Table 4.1.

Table 4.1 The charges of relevant fermion and scalar fields under the $U(1) \times \mathbb{Z}_6$ symmetry in the multiple seesaw mechanism with $n = 2$

	$\ell_{\rm L}$	H	$E_{\rm R}$	$N_{\rm R}$	$S_{1\rm R}$	$S_{2\rm R}$	Φ_1	Φ_2
L	$+1$	0	$+1$	$+1$	-1	$+1$	0	0
q	$+1$	0	$+1$	$+1$	$+2$	$+3$	$+3$	$+1$

Class B of multiple seesaw mechanisms — they contain an odd number of gauge-singlet fermions $S_{n\rm R}^i$ and scalars Φ_n (i.e., $n = 2k + 1$ with $k =$

$0, 1, 2, \cdots$) and correspond to an interesting extension of the inverse seesaw picture. The effective mass matrix of three light Majorana neutrinos reads

$$M_\nu = M_{\rm D} \left[\prod_{i=1}^{k} \left(M_{S_{2i-1}}^T \right)^{-1} M_{S_{2i}} \right] \left(M_{S_{2k+1}}^T \right)^{-1} \times M_\mu \left(M_{S_{2k+1}} \right)^{-1} \left[\prod_{i=1}^{k} \left(M_{S_{2i-1}}^T \right)^{-1} M_{S_{2i}} \right]^T M_{\rm D}^T \tag{4.53}$$

in the leading-order approximation. The $k = 0$ case just corresponds to the inverse seesaw scenario with a rather low mass scale of M_μ: $M_\nu = M_{\rm D}(M_{S_1}^T)^{-1} M_\mu (M_{S_1})^{-1} M_{\rm D}^T$. Note that the NNI pattern of $\mathcal{M}$ in the double seesaw mechanism is guaranteed by an implementation of the global $U(1) \times \mathbb{Z}_4$ symmetry with the following charge assignment: $L(\ell_{\rm L}) = L(E_{\rm R}) = L(N_{\rm R}) = +1$, $L(S_{1{\rm R}}) = -1$, $L(H) = L(\Phi_1) = 0$, $q(\ell_{\rm L}) = q(E_{\rm R}) = q(N_{\rm R}) = q(\Phi_1) = +1$, $q(H) = 0$ and $q(S_{1{\rm R}}) = +2$.

If $M_{S_{2i}} \sim M_{\rm D} \sim \mathcal{O}(\Lambda_{\rm EW})$ and $M_{S_{2i-1}} \sim \mathcal{O}(\Lambda_{\rm SS})$ hold (for $i = 1, 2, \cdots, k$), the mass scale of M_μ is in general unnecessary to be as small as that given by the inverse seesaw mechanism. To be more specific, let us consider the minimal extension of the inverse seesaw picture by taking $n = 3$. In this case, we impose the $U(1) \times \mathbb{Z}_{10}$ symmetry on $\mathcal{L}_\nu$ with a proper charge assignment listed in Table 4.2 to assure the NNI form of $\mathcal{M}$. The corresponding formula of M_ν is

$$M_\nu = M_{\rm D} \left(M_{S_1}^T \right)^{-1} M_{S_2} \left(M_{S_3}^T \right)^{-1} M_\mu \left(M_{S_3} \right)^{-1} M_{S_2}^T \left(M_{S_1} \right)^{-1} M_{\rm D}^T \ . \tag{4.54}$$

This effective multiple seesaw mass term is illustrated in Fig. 4.3(b). It becomes obvious that the proportionality of M_ν to M_μ in Eq. (4.54) is doubly suppressed not only by the ratio $M_{\rm D}/M_{S_1} \sim \Lambda_{\rm EW}/\Lambda_{\rm SS}$ but also by the ratio $M_{S_2}/M_{S_3} \sim \Lambda_{\rm EW}/\Lambda_{\rm SS}$, and thus $M_\nu \sim 0.1$ eV can naturally result from $Y_\nu \sim Y_{S_1} \sim Y_{S_2} \sim Y_{S_3} \sim \mathcal{O}(1)$ and $M_\mu \sim 1$ keV at $\Lambda_{\rm SS} \sim 1$ TeV.

Table 4.2 The charges of relevant fermion and scalar fields under the $U(1) \times \mathbb{Z}_{10}$ symmetry in the multiple seesaw mechanism with $n = 3$

	$\ell_{\rm L}$	H	$E_{\rm R}$	$N_{\rm R}$	$S_{1{\rm R}}$	$S_{2{\rm R}}$	$S_{3{\rm R}}$	Φ_1	Φ_2	Φ_3
L	$+1$	0	$+1$	$+1$	-1	$+1$	-1	0	0	0
q	$+1$	0	$+1$	$+1$	$+2$	$+3$	$+5$	$+7$	$+5$	$+2$

4.4.2 Charged-current Interactions

The strength of charged-current interactions is important for both production and detection of light and heavy Majorana neutrinos in a realistic experiment

(e.g., at the LHC and in neutrino oscillations). To define the neutrino mass eigenstates, we diagonalize the overall mass matrix $\mathcal{M}$ in Eq. (4.50) by means of the following unitary transformation:

$$\begin{pmatrix} V & \tilde{R} \\ \tilde{S} & \tilde{U} \end{pmatrix}^{\dagger} \begin{pmatrix} \mathbf{0} & \tilde{M}_{\rm D} \\ \tilde{M}_{\rm D}^{T} & \tilde{M}_{\mu} \end{pmatrix} \begin{pmatrix} V & \tilde{R} \\ \tilde{S} & \tilde{U} \end{pmatrix}^{*} = \begin{pmatrix} \widehat{M}_{\nu} & \mathbf{0} \\ \mathbf{0} & \widehat{M}_{N+S} \end{pmatrix} , \tag{4.55}$$

where $\widehat{M}_{\nu} \equiv {\rm Diag}\{m_1, m_2, m_3\}$ contains the masses of three light Majorana neutrinos (ν_1, ν_2, ν_3), and $\widehat{M}_{N+S}$ denotes a diagonal matrix whose eigenvalues are the masses of $3\,(n+1)$ heavy Majorana neutrinos ($\hat{N}$, $\hat{S}_1$, $\cdots$, $\hat{S}_n$; and each of them consists of three components). The SM charged-current interactions of ν_e, ν_μ and ν_τ can therefore be expressed as

$$\mathcal{L}_{\rm cc} = \frac{g}{\sqrt{2}} \overline{\left(e\ \mu\ \tau\right)_{\rm L}}\, \gamma^{\mu} \left[V \begin{pmatrix} \nu_1 \\ \nu_2 \\ \nu_3 \end{pmatrix}_{\rm L} + \tilde{R} \begin{pmatrix} \hat{N} \\ \hat{S}_1 \\ \vdots \\ \hat{S}_n \end{pmatrix}_{\rm L} \right] W_{\mu}^{-} + {\rm h.c.} \tag{4.56}$$

in the basis where the mass eigenstates of three charged leptons are identified with their flavor eigenstates. Note that V is the 3×3 neutrino mixing matrix responsible for neutrino oscillations, while the $3 \times 3\,(n+1)$ matrix $\tilde{R}$ governs the strength of charged-current interactions of heavy Majorana neutrinos. Note also that both $V V^{\dagger} + \tilde{R} \tilde{R}^{\dagger} = \mathbf{1}$ and $V \widehat{M}_{\nu} V^{T} + \tilde{R} \widehat{M}_{N+S} \tilde{R}^{T} = \mathbf{0}$ hold, and thus V must be non-unitary. It is $\tilde{R}$ that measures the deviation of V from unitarity in neutrino oscillations and determines the collider signatures of heavy Majorana neutrinos at the LHC.

The multiple seesaw idea may lead to rich phenomenology at both the TeV scale and lower energies. For simplicity, here we only mention a few aspects of the phenomenological consequences of multiple seesaw mechanisms.

- *Non-unitary neutrino mixing and CP violation.* Since V is non-unitary, it generally involves a number of new flavor mixing angles and new CP-violating phases (Xing, 2008b). Novel CP-violating effects in the medium-baseline $\nu_\mu \to \nu_\tau$ and $\overline{\nu}_\mu \to \overline{\nu}_\tau$ oscillations may therefore show up and provide a promising signature of the unitarity violation of V, which could be measured at a neutrino factory (Fernandez-Martinez *et al.*, 2007).
- *Collider signatures of heavy Majorana neutrinos.* Given $\tilde{M}_{\rm D} \sim \mathcal{O}(\Lambda_{\rm EW})$ and $\tilde{M}_{\mu} \sim \mathcal{O}(\Lambda_{\rm SS}) \sim \mathcal{O}(1)$ TeV, it is easy to obtain $\tilde{R} \approx \tilde{M}_{\rm D} \tilde{M}_{\mu}^{-1} \tilde{U} \sim \mathcal{O}(0.1)$, which actually saturates the present experimental upper bound on $|\tilde{R}|$ (Antusch *et al.*, 2006). For *Class A* of multiple seesaw mechanisms, their clear LHC signatures are expected to be the like-sign dilepton events arising from the lepton-number-violating processes $pp \to l_{\alpha}^{\pm} l_{\beta}^{\pm} X$ (for $\alpha, \beta = e, \mu, \tau$) mediated by heavy Majorana neutrinos (Atre *et al.*, 2009). For *Class B* of multiple seesaw mechanisms with $M_{\mu} \ll \Lambda_{\rm EW}$, the

mass spectrum of heavy Majorana neutrinos generally exhibits a pairing phenomenon in which the nearest-neighbor Majorana neutrinos have nearly degenerate masses and can be combined to form pseudo-Dirac particles. This feature has already been observed in the inverse seesaw model (Mohapatra and Valle, 1986). Therefore, the discriminating collider signatures at the LHC are expected to be the trilepton events coming from the $pp \to l^{\pm}_{\alpha} l^{\pm}_{\beta} l^{\mp}_{\gamma} X$ processes (for $\alpha, \beta, \gamma = e, \mu, \tau$) (del Aguila and Aguilar-Saavedra, 2009b).

- *Possible candidates for dark matter.* One or more of the heavy Majorana neutrinos and gauge-singlet scalars in our multiple seesaw mechanisms could be arranged to have a sufficiently long lifetime. Such weakly-interacting and massive particles might therefore be a plausible candidate for cold dark matter (Ponton and Randall, 2009).

One may explore more low-energy effects of multiple seesaw mechanisms, such as their contributions to the lepton-flavor-violating processes $\mu \to e\gamma$ and so on. It should also be interesting to explore possible baryogenesis via leptogenesis (Fukugita and Yanagida, 1986), based on a multiple seesaw picture, to interpret the cosmological matter-antimatter asymmetry.

As a flexible and testable TeV seesaw scheme, the multiple seesaw mechanisms can also provide us with plenty of room for model building. But the latter requires further inputs or assumptions. Here we present a simple but instructive example, in which all the textures of 3×3 sub-matrices in the overall neutrino mass matrix $\mathcal{M}$ are symmetric and have the well-known Fritzsch pattern (Fritzsch, 1978),

$$M_a = \begin{pmatrix} 0 & x_a & 0 \\ x_a & 0 & y_a \\ 0 & y_a & z_a \end{pmatrix} \tag{4.57}$$

with $a = \mathrm{D}, S_1, \cdots, S_n$ or μ, for illustration. Choosing the Fritzsch texture makes sense because it coincides with the NNI form of $\mathcal{M}$ itself. We make an additional assumption that the ratio x_a/y_a is a constant independent of the subscript a. Then it is easy to show that the effective mass matrix of three light Majorana neutrinos M_ν has the same Fritzsch texture in the leading-order approximation:

$$\begin{aligned} (M_\nu)_{12} &= -\frac{x^2_{\rm D}}{x_\mu} \left[\prod_{i=1}^{k} \frac{x^2_{S_{2i}}}{x^2_{S_{2i-1}}} \right] , \\ (M_\nu)_{23} &= -\frac{y^2_{\rm D}}{y_\mu} \left[\prod_{i=1}^{k} \frac{y^2_{S_{2i}}}{y^2_{S_{2i-1}}} \right] , \\ (M_\nu)_{33} &= -\frac{z^2_{\rm D}}{z_\mu} \left[\prod_{i=1}^{k} \frac{z^2_{S_{2i}}}{z^2_{S_{2i-1}}} \right] , \end{aligned} \tag{4.58}$$

and $(M_\nu)_{11} = (M_\nu)_{13} = (M_\nu)_{22} = 0$ derived from Eq. (4.51) for *Class A* of multiple seesaw mechanisms (with $n = 2k$ for $k = 0, 1, 2, \cdots$); and

$$(M_\nu)_{12} = \frac{x_{\rm D}^2}{x_{S_{2k+1}}^2} \left[\prod_{i=1}^{k} \frac{x_{S_{2i}}^2}{x_{S_{2i-1}}^2} \right] x_\mu \; ,$$
$$(M_\nu)_{23} = \frac{y_{\rm D}^2}{y_{S_{2k+1}}^2} \left[\prod_{i=1}^{k} \frac{y_{S_{2i}}^2}{y_{S_{2i-1}}^2} \right] y_\mu \; ,$$
$$(M_\nu)_{33} = \frac{z_{\rm D}^2}{z_{S_{2k+1}}^2} \left[\prod_{i=1}^{k} \frac{z_{S_{2i}}^2}{z_{S_{2i-1}}^2} \right] z_\mu \; , \tag{4.59}$$

and $(M_\nu)_{11} = (M_\nu)_{13} = (M_\nu)_{22} = 0$ derived from Eq. (4.53) for *Class B* of multiple seesaw mechanisms (with $n = 2k + 1$ for $k = 0, 1, 2, \cdots$). This seesaw-invariant property of M_ν is interesting since it exactly reflects how two classes of multiple seesaw mechanisms work for every element of M_ν. Note that it is possible to interpret current experimental data on small neutrino masses and large flavor mixing angles by taking both the texture of the light neutrino mass matrix M_ν and that of the charged-lepton mass matrix M_l to be of the Fritzsch form (Xing, 2002; Xing and Zhou, 2004; Zhou and Xing, 2005). Hence the above examples are phenomenologically viable. Once the texture of M_ν is fully reconstructed from more accurate neutrino oscillation data, one may then consider to quantitatively explore the textures of those 3×3 sub-matrices of $\mathcal{M}$ in such a multiple seesaw model.

To conclude, new ideas are eagerly wanted in the LHC era to achieve a proper balance between theoretical naturalness and experimental testability of the elegant seesaw pictures, which ascribe the small masses of three known neutrinos to the existence of some heavy degrees of freedom. We have extended the canonical and inverse seesaw scenarios and proposed two classes of multiple seesaw mechanisms at the TeV scale by introducing an arbitrary number of gauge-singlet fermions and scalars into the SM and by implementing the global $U(1) \times \mathbb{Z}_{2N}$ symmetry in the neutrino sector. These new TeV-scale seesaw mechanisms are expected to lead to rich phenomenology at low energies and open some new prospects for understanding the origin of tiny neutrino masses and lepton number violation.

4.5 Non-unitary Neutrino Mixing and CP Violation

It is worth remarking that the charged-current interactions of light and heavy Majorana neutrinos are not completely independent of each other in type-I, type-(I+II), type-III or multiple seesaw mechanisms. This point can clearly be seen from Eq. (4.56), in which $V V^\dagger + \tilde{R} \tilde{R}^\dagger = \mathbf{1}$ holds. Regardless of the details of each seesaw scheme, one may approximately parametrize the 3×3 mixing matrix of three light Majorana neutrinos as

$$V \approx (\mathbf{1} - \xi)\, V_0 \quad \text{with} \quad \xi = \frac{1}{2}\tilde{R}\tilde{R}^\dagger \; , \tag{4.60}$$

where V_0 is a unitary matrix and ξ measures the deviation of V from V_0. In view of current experimental data on the invisible width of the Z^0 boson, universality tests of electroweak interactions, rare leptonic decays and neutrino oscillations, one may find the following constraints on the elements of ξ at the 90% confidence level (Antusch *et al.*, 2006):

$$|\xi| = \begin{bmatrix} |\xi_{ee}| < 5.5 \times 10^{-3} & |\xi_{e\mu}| < 3.5 \times 10^{-5} & |\xi_{e\tau}| < 8.0 \times 10^{-3} \\ |\xi_{\mu e}| < 3.5 \times 10^{-5} & |\xi_{\mu\mu}| < 5.0 \times 10^{-3} & |\xi_{\mu\tau}| < 5.0 \times 10^{-3} \\ |\xi_{\tau e}| < 8.0 \times 10^{-3} & |\xi_{\tau\mu}| < 5.0 \times 10^{-3} & |\xi_{\tau\tau}| < 5.0 \times 10^{-3} \end{bmatrix} . \tag{4.61}$$

This result implies that the unitarity of V has been tested at the percent level and possible non-unitarity of V can at most reach the same level [1]. Note that the phases of ξ are entirely unrestricted, and thus new CP-violating effects of $\mathcal{O}(10^{-2})$ or smaller may be induced by the non-unitarity of V and are likely to show up in neutrino oscillations (Fernandez-Martinez *et al.*, 2007; Xing, 2008b; Luo, 2008; Goswami and Ota, 2008; Altarelli and Meloni, 2009; Antusch *et al.*, 2009; Malinsky *et al.*, 2009).

4.5.1 Jarlskog Invariants of CP Violation

The strength of CP violation in neutrino oscillations is characterized by the Jarlskog invariants (Jarlskog, 1985; Wu, 1986)

$$J^{ij}_{\alpha\beta} \equiv \mathrm{Im}\left(V_{\alpha i} V_{\beta j} V^*_{\alpha j} V^*_{\beta i}\right) \; , \tag{4.62}$$

where Greek and Latin indices run over (e, μ, τ) and $(1, 2, 3)$, respectively. Without loss of generality, the unitary matrix V_0 in Eq. (4.60) can be parametrized as a product of three rotation matrices in the complex plane:

$$\begin{aligned} V_0 &= \begin{pmatrix} 1 & 0 & 0 \\ 0 & c_{23} & \hat{s}^*_{23} \\ 0 & -\hat{s}_{23} & c_{23} \end{pmatrix} \begin{pmatrix} c_{13} & 0 & \hat{s}^*_{13} \\ 0 & 1 & 0 \\ -\hat{s}_{13} & 0 & c_{13} \end{pmatrix} \begin{pmatrix} c_{12} & \hat{s}^*_{12} & 0 \\ -\hat{s}_{12} & c_{12} & 0 \\ 0 & 0 & 1 \end{pmatrix} \\ &= \begin{pmatrix} c_{12}c_{13} & \hat{s}^*_{12}c_{13} & \hat{s}^*_{13} \\ -\hat{s}_{12}c_{23} - c_{12}\hat{s}_{13}\hat{s}^*_{23} & c_{12}c_{23} - \hat{s}^*_{12}\hat{s}_{13}\hat{s}^*_{23} & c_{13}\hat{s}^*_{23} \\ \hat{s}_{12}\hat{s}_{23} - c_{12}\hat{s}_{13}c_{23} & -c_{12}\hat{s}_{23} - \hat{s}^*_{12}\hat{s}_{13}c_{23} & c_{13}c_{23} \end{pmatrix} , \end{aligned} \tag{4.63}$$

where $c_{ij} \equiv \cos\theta_{ij}$, $s_{ij} \equiv \sin\theta_{ij}$ and $\hat{s}_{ij} \equiv s_{ij} \mathrm{e}^{\mathrm{i}\delta_{ij}}$ with θ_{ij} and δ_{ij} being the rotation and phase angles, respectively. After a proper phase rearrangement,

[1] When the type-III seesaw mechanism is concerned, the experimental bounds on the elements of ξ are slightly stronger than those given above for type-I, type-(I+II) or multiple seesaw mechanisms (Abada *et al.*, 2007). The reason is simply that in the type-III seesaw case the flavor-changing processes with charged leptons are allowed at the tree level and can get stringent experimental constraints.

Eq. (4.63) is actually the standard parametrization advocated by the Particle Data Group (Fritzsch and Xing, 2001; Nakamura *et al.*, 2010). The universal Jarlskog invariant of V_0 reads $J_0 = c_{12}s_{12}c_{13}^2 s_{13}c_{23}s_{23}\sin(\delta_{13}-\delta_{12}-\delta_{23})$ in the above parametrization. Combining Eqs. (4.60) and (4.63), one may calculate $J^{ij}_{\alpha\beta}$ defined in Eq. (4.62). Since both s_{13} and $\xi_{\alpha\beta}$ are small quantities, we neglect the terms of $\mathcal{O}(s_{13}^2)$, $\mathcal{O}(|\xi_{\alpha\beta}|^2)$ and $\mathcal{O}(s_{13}|\xi_{\alpha\beta}|)$ in the calculation. Then it is straightforward to obtain

$$\begin{aligned}
J^{12}_{e\mu} &= J_0 - c_{12}s_{12}c_{23}\left(1+c_{23}^2\right)|\xi_{e\mu}|\sin(\delta_{12}+\delta_{e\mu}) \\
&\quad + c_{12}s_{12}c_{23}^2 s_{23}|\xi_{e\tau}|\sin(\delta_{12}+\delta_{23}+\delta_{e\tau}) \; , \\
J^{23}_{e\mu} &= J_0 + c_{12}s_{12}c_{23}s_{23}^2|\xi_{e\mu}|\sin(\delta_{12}+\delta_{e\mu}) \\
&\quad + c_{12}s_{12}c_{23}^2 s_{23}|\xi_{e\tau}|\sin(\delta_{12}+\delta_{23}+\delta_{e\tau}) \; , \\
J^{12}_{\mu\tau} &= J_0 - c_{12}s_{12}c_{23}s_{23}^2|\xi_{e\mu}|\sin(\delta_{12}+\delta_{e\mu}) \\
&\quad - c_{12}s_{12}c_{23}^2 s_{23}|\xi_{e\tau}|\sin(\delta_{12}+\delta_{23}+\delta_{e\tau}) \; , \\
J^{23}_{\mu\tau} &= J^{12}_{\mu\tau} - 2c_{12}^2 c_{23}s_{23}|\xi_{\mu\tau}|\sin(\delta_{23}+\delta_{\mu\tau}) \; , \\
J^{31}_{\mu\tau} &= J^{12}_{\mu\tau} + 2s_{12}^2 c_{23}s_{23}|\xi_{\mu\tau}|\sin(\delta_{23}+\delta_{\mu\tau}) \; , \\
J^{12}_{\tau e} &= J_0 + c_{12}s_{12}c_{23}s_{23}^2|\xi_{e\mu}|\sin(\delta_{12}+\delta_{e\mu}) \\
&\quad - c_{12}s_{12}s_{23}\left(1+s_{23}^2\right)|\xi_{e\tau}|\sin(\delta_{12}+\delta_{23}+\delta_{e\tau}) \; , \qquad (4.64)
\end{aligned}$$

together with the equality $J^{23}_{\tau e} = J^{31}_{\tau e} = J^{31}_{e\mu} = J^{23}_{e\mu}$ as good approximations. This equality holds simply because the relevant Jarlskog invariants involve the smallest matrix element $V_{e3} \sim s_{13}$ (Malinsky *et al.*, 2009).

Eq. (4.64) shows that the deviation of $J^{ij}_{\alpha\beta}$ from J_0 is governed by the magnitude of $|\xi_{\alpha\beta}|$ and may reach the $\mathcal{O}(10^{-3})$ level. Hence the non-unitary CP-violating effects are possible to be comparable with or even larger than the unitary CP-violating effect characterized by J_0 itself, in particular when θ_{13} is very small. In the $\theta_{13} \to 0$ limit we have $J_0 \to 0$ but $J^{ij}_{\alpha\beta} \neq 0$. It is therefore important to detect CP violation in the future precision neutrino oscillation experiments, so as to probe possible non-unitarity of V as one striking consequence of the TeV-scale seesaw mechanisms.

4.5.2 Mixing Angles and CP-violating Phases

Although the parametrization of V in Eq. (4.60) is valid for an arbitrary number of heavy Majorana neutrinos, its unitarity-conserving part (V_0) and unitarity-violating part (ξ) consist of two sets of different parameters (i.e., θ_{ij} and δ_{ij} versus $\xi_{\alpha\beta}$). Here we concentrate on the type-I and type-(I+II) seesaw mechanisms with three heavy Majorana neutrinos and propose a "standard" parametrization of V in terms of only rotation angles and phase angles (Xing, 2008b). This parametrization is phenomenologically useful because it may reveal the correlation between the charged-current interactions of light and heavy Majorana neutrinos in a much more transparent manner.

When only three heavy Majorana neutrinos are concerned, the standard charged-current interactions of ν_i and N_i in Eq. (4.56) are simplified to

$$\mathcal{L}_{\rm cc} = \frac{g}{\sqrt{2}} \overline{(e\ \mu\ \tau)_{\rm L}}\ \gamma^\mu \left[V \begin{pmatrix} \nu_1 \\ \nu_2 \\ \nu_3 \end{pmatrix}_{\rm L} + R \begin{pmatrix} N_1 \\ N_2 \\ N_3 \end{pmatrix}_{\rm L} \right] W^-_\mu + {\rm h.c.}\ , \tag{4.65}$$

where $VV^\dagger + RR^\dagger = \mathbf{1}$ holds. Note that V and R belong to the same 6×6 unitary matrix, which can be parametrized in terms of 15 rotation angles θ_{ij} and 15 phase angles δ_{ij} (for $1 \leqslant i < j \leqslant 6$). Then the common parameters of V and R characterize their correlation. Let us define the 2-dimensional (1,2), (1,3) and (2,3) rotation matrices in a 6-dimensional complex space:

$$O_{12} = \begin{pmatrix} c_{12} & \hat{s}^*_{12} & 0 & 0 & 0 & 0 \\ -\hat{s}_{12} & c_{12} & 0 & 0 & 0 & 0 \\ 0 & 0 & 1 & 0 & 0 & 0 \\ 0 & 0 & 0 & 1 & 0 & 0 \\ 0 & 0 & 0 & 0 & 1 & 0 \\ 0 & 0 & 0 & 0 & 0 & 1 \end{pmatrix} ,$$

$$O_{13} = \begin{pmatrix} c_{13} & 0 & \hat{s}^*_{13} & 0 & 0 & 0 \\ 0 & 1 & 0 & 0 & 0 & 0 \\ -\hat{s}_{13} & 0 & c_{13} & 0 & 0 & 0 \\ 0 & 0 & 0 & 1 & 0 & 0 \\ 0 & 0 & 0 & 0 & 1 & 0 \\ 0 & 0 & 0 & 0 & 0 & 1 \end{pmatrix} ,$$

$$O_{23} = \begin{pmatrix} 1 & 0 & 0 & 0 & 0 & 0 \\ 0 & c_{23} & \hat{s}^*_{23} & 0 & 0 & 0 \\ 0 & -\hat{s}_{23} & c_{23} & 0 & 0 & 0 \\ 0 & 0 & 0 & 1 & 0 & 0 \\ 0 & 0 & 0 & 0 & 1 & 0 \\ 0 & 0 & 0 & 0 & 0 & 1 \end{pmatrix} , \tag{4.66}$$

where c_{ij}, s_{ij} and $\hat{s}_{ij}$ are defined in the same way as done in Eq. (4.63). Other 2-dimensional rotation matrices O_{ij} (for $1 \leqslant i < j \leqslant 6$) can analogously be defined (Harari and Leuer, 1980; Fritzsch and Plankl, 1987). We parametrize the 6×6 unitary transformation as

$$\begin{pmatrix} A & R \\ B & U \end{pmatrix} \otimes \begin{pmatrix} V_0 & \mathbf{0} \\ \mathbf{0} & \mathbf{1} \end{pmatrix} = [O_{56} O_{46} O_{36} O_{26} O_{16} O_{45} O_{35} O_{25} O_{15} O_{34} O_{24} O_{14}] \otimes [O_{23} O_{13} O_{12}]\ , \tag{4.67}$$

where the explicit form of V_0 has been presented in Eq. (4.63). Comparing Eq. (4.67) with Eq. (4.38) or Eq. (4.55), we immediately get $V = AV_0$. It is obvious that $V \to V_0$ in the limit of $A \to \mathbf{1}$ (or equivalently, $R \to \mathbf{0}$). Thus A signifies the non-unitarity of V. After a lengthy but straightforward calculation, we obtain the expressions of A and R as follows:

$$A = \begin{pmatrix} c_{14}c_{15}c_{16} & 0 & 0 \\ -c_{14}c_{15}\hat{s}_{16}\hat{s}^*_{26} \\ -c_{14}\hat{s}_{15}\hat{s}^*_{25}c_{26} & c_{24}c_{25}c_{26} & 0 \\ -\hat{s}_{14}\hat{s}^*_{24}c_{25}c_{26} \\ -c_{14}c_{15}\hat{s}_{16}c_{26}\hat{s}^*_{36} \\ +c_{14}\hat{s}_{15}\hat{s}^*_{25}\hat{s}_{26}\hat{s}^*_{36} & -c_{24}c_{25}\hat{s}_{26}\hat{s}^*_{36} \\ -c_{14}\hat{s}_{15}c_{25}\hat{s}^*_{35}c_{36} & -c_{24}\hat{s}_{25}\hat{s}^*_{35}c_{36} & c_{34}c_{35}c_{36} \\ +\hat{s}_{14}\hat{s}^*_{24}c_{25}\hat{s}_{26}\hat{s}^*_{36} & -\hat{s}_{24}\hat{s}^*_{34}c_{35}c_{36} \\ +\hat{s}_{14}\hat{s}^*_{24}\hat{s}_{25}\hat{s}^*_{35}c_{36} \\ -\hat{s}_{14}c_{24}\hat{s}^*_{34}c_{35}c_{36} \end{pmatrix},$$

$$R = \begin{pmatrix} \hat{s}^*_{14}c_{15}c_{16} & \hat{s}^*_{15}c_{16} & \hat{s}^*_{16} \\ -\hat{s}^*_{14}c_{15}\hat{s}_{16}\hat{s}^*_{26} \\ -\hat{s}^*_{14}\hat{s}_{15}\hat{s}^*_{25}c_{26} & -\hat{s}^*_{15}\hat{s}_{16}\hat{s}^*_{26} & c_{16}\hat{s}^*_{26} \\ +c_{14}\hat{s}^*_{24}c_{25}c_{26} & +c_{15}\hat{s}^*_{25}c_{26} \\ -\hat{s}^*_{14}c_{15}\hat{s}_{16}c_{26}\hat{s}^*_{36} \\ +\hat{s}^*_{14}\hat{s}_{15}\hat{s}^*_{25}\hat{s}_{26}\hat{s}^*_{36} & -\hat{s}^*_{15}\hat{s}_{16}c_{26}\hat{s}^*_{36} \\ -\hat{s}^*_{14}\hat{s}_{15}c_{25}\hat{s}^*_{35}c_{36} & -c_{15}\hat{s}^*_{25}\hat{s}_{26}\hat{s}^*_{36} & c_{16}c_{26}\hat{s}^*_{36} \\ -c_{14}\hat{s}^*_{24}c_{25}\hat{s}_{26}\hat{s}^*_{36} & +c_{15}c_{25}\hat{s}^*_{35}c_{36} \\ -c_{14}\hat{s}^*_{24}\hat{s}_{25}\hat{s}^*_{35}c_{36} \\ +c_{14}c_{24}\hat{s}^*_{34}c_{35}c_{36} \end{pmatrix}. \quad (4.68)$$

One can see that A and R involve the same parameters: 9 rotation angles and 9 phase angles, which signify non-unitary neutrino mixing and CP violation. Nontrivial A is therefore the bridge between $V = AV_0$ and R.

Note that the triangular form of A is a salient feature of our parametrization. Some interesting consequences of $V = AV_0$ can immediately be drawn from Eqs. (4.63) and (4.68).

- $V_{e3} = c_{14}c_{15}c_{16}\hat{s}^*_{13}$ holds. Given $\theta_{13} = 0$ for V_0, which might result from certain flavor symmetries, V_{e3} turns out to vanish.
- The ratio $|V_{e2}/V_{e1}| = \tan\theta_{12}$ is completely irrelevant to the parameters of A or R. This result implies that the extraction of θ_{12} from solar neutrino oscillation data should be independent of the non-unitarity of V.
- $|V_{e1}|^2 + |V_{e2}|^2 + |V_{e3}|^2 = c^2_{14}c^2_{15}c^2_{16}$ holds. Hence non-vanishing θ_{14}, θ_{15} and θ_{16} violate the normalization condition of three matrix elements in the first row of V.
- $\langle m\rangle_{ee} = c^2_{14}c^2_{15}c^2_{16}|m_1(c_{12}c_{13})^2 + m_2(\hat{s}^*_{12}c_{13})^2 + m_3(\hat{s}^*_{13})^2|$ holds for the effective mass term of the neutrinoless double-beta decay.
- $\langle m\rangle_e = c_{14}c_{15}c_{16}\sqrt{m^2_1c^2_{12}c^2_{13} + m^2_2s^2_{12}c^2_{13} + m^2_3s^2_{13}}$ holds for the effective mass term of the tritium beta decay.

If θ_{14}, θ_{15} and θ_{16} are small, their effects on $\langle m\rangle_e$ and $\langle m\rangle_{ee}$ will be negligible.

In view of the fact that the non-unitarity of V must be small effects (at most at the percent level), we expect $s_{ij} \lesssim \mathcal{O}(0.1)$ (for $i = 1, 2, 3$ and $j = 4, 5, 6$) to hold. Then we obtain (Xing, 2008b)

$$A = \mathbf{1} - \begin{pmatrix} \frac{1}{2}\sum\limits_{i=4}^{6} s_{1i}^2 & 0 & 0 \\ \sum\limits_{i=4}^{6} \hat{s}_{1i}\hat{s}_{2i}^* & \frac{1}{2}\sum\limits_{i=4}^{6} s_{2i}^2 & 0 \\ \sum\limits_{i=4}^{6} \hat{s}_{1i}\hat{s}_{3i}^* & \sum\limits_{i=4}^{6} \hat{s}_{2i}\hat{s}_{3i}^* & \frac{1}{2}\sum\limits_{i=4}^{6} s_{3i}^2 \end{pmatrix} + \mathcal{O}(s_{ij}^4) \; ,$$

$$R = \mathbf{0} + \begin{pmatrix} \hat{s}_{14}^* & \hat{s}_{15}^* & \hat{s}_{16}^* \\ \hat{s}_{24}^* & \hat{s}_{25}^* & \hat{s}_{26}^* \\ \hat{s}_{34}^* & \hat{s}_{35}^* & \hat{s}_{36}^* \end{pmatrix} + \mathcal{O}(s_{ij}^3) \tag{4.69}$$

as two excellent approximations. A striking consequence of the non-unitarity of V is the loss of universality for the Jarlskog invariants of CP violation, as we have shown in Section 4.5.1. Taking account of $\xi = RR^\dagger/2$, we arrive at

$$\xi_{ee} = \frac{1}{2}\sum_{i=4}^{6} s_{1i}^2 \; , \quad \xi_{\mu\mu} = \frac{1}{2}\sum_{i=4}^{6} s_{2i}^2 \; , \quad \xi_{\tau\tau} = \frac{1}{2}\sum_{i=4}^{6} s_{3i}^2 \; ;$$

$$\xi_{e\mu} = \frac{1}{2}\sum_{i=4}^{6} s_{1i} s_{2i} \sin\left(\delta_{2i} - \delta_{1i}\right) \; ,$$

$$\xi_{e\tau} = \frac{1}{2}\sum_{i=4}^{6} s_{1i} s_{3i} \sin\left(\delta_{3i} - \delta_{1i}\right) \; ,$$

$$\xi_{\mu\tau} = \frac{1}{2}\sum_{i=4}^{6} s_{2i} s_{3i} \sin\left(\delta_{3i} - \delta_{2i}\right) \; . \tag{4.70}$$

The deviation of the Jarlskog invariants $J_{\alpha\beta}^{ij}$ from J_0 can also be given in terms of those non-unitary neutrino mixing angles and CP-violating phases.

Finally, it worth mentioning that one may simplify the above results to some extent when discussing either the *minimal* type-I seesaw mechanism with two heavy Majorana neutrinos (Frampton *et al.*, 2002; Guo *et al.*, 2007) or the *minimal* type-(I+II) seesaw mechanism with only one heavy Majorana neutrino (Gu *et al.*, 2006; Chan *et al.*, 2007).

References

Abada, A., *et al.*, 2007, JHEP **0712**, 061.
Altarelli, G., and Meloni, D., 2009, Nucl. Phys. B **809**, 158.
Antusch, S., *et al.*, 2006, JHEP **0610**, 084.

Antusch, S., *et al.*, 2009, Phys. Rev. D **80**, 033002.
Arhrib, A., *et al.*, 2010, Phys. Rev. D **82**, 053004.
Arkani-Hamed, N., *et al.*, 2002, Phys. Rev. D **65**, 024032.
Atre, A., *et al.*, 2009, JHEP **0905**, 030.
Babu, K. S., 1988, Phys. Lett. B **203**, 132.
Babu, K. S., Nandi, S., and Tavartkiladze, Z., 2009, Phys. Rev. D **80**, 071702.
Bajc, B., Nemevsek, M., and Senjanovic, G., 2007, Phys. Rev. D **76**, 055011.
Bajc, B., and Senjanovic, G., 2007, JHEP **0708**, 014.
Branco, G. C., Lavoura, L., and Mota, F., 1989, Phys. Rev. D **39**, 3443.
Bilenky, M., and Santamaria, A., 1994, Nucl. Phys. B **420**, 47.
Casas, J. A., Espinosa, J. R., and Hidalgo, I., 2004, JHEP **0411**, 057.
Chan, A. H., Low, H. B., and Xing, Z. Z., 2009, Phys. Rev. D **80**, 073006.
Chan, A. H., *et al.*, 2007, Phys. Rev. D **76**, 073009.
Chao, W., *et al.*, 2008a, Phys. Rev. D **77**, 016001.
Chao, W., *et al.*, 2008b, Phys. Lett. B **666**, 451.
Chao, W., *et al.*, 2010, Phys. Lett. B **683**, 26.
Cheng, T. P., and Li, L. F., 1980, Phys. Rev. D **22**, 2860.
de Gouvea, A., Jenkins, J., and Vasudevan, N., 2007, Phys. Rev. D **75**, 013003.
del Aguila, F., and Aguilar-Saavedra, J. A., 2009a, Nucl. Phys. B **813**, 22.
del Aguila, F., and Aguilar-Saavedra, J. A., 2009b, Phys. Lett. B **672**, 158.
Dienes, K. R., Dudas, E., and Gherghetta, T., 1999, Nucl. Phys. B **557**, 25.
Dimopoulos, S., 1990, Phys. Lett. B **246**, 347.
Dudas, E., and Savoy, C. A., 2002, Acta Phys. Polon. B **33**, 2547.
Fernandez-Martinez, E., *et al.*, 2007, Phys. Lett. B **649**, 427.
Fileviez Pérez, P., *et al.*, 2008, Phys. Rev. D **78**, 015018.
Foot, R., *et al.*, 1989, Z. Phys. C **44**, 441.
Frampton, P., Glashow, S. L., and Yanagida, T., 2002, Phys. Lett. B **548**, 119.
Franceschini, R., Hambye, T., and Strumia, A., 2008, Phys. Rev. D **78**, 033002.
Fritzsch, H., 1978, Phys. Lett. B **73**, 317.
Fritzsch, H., 1979, Nucl. Phys. B **155**, 189.
Fritzsch, H., Gell-Mann, M., and Minkowski, P., 1975, Phys. Lett. B **59**, 256.
Fritzsch, H., and Plankl, J., 1987, Phys. Rev. D **35**, 1732.
Fritzsch, H., and Xing, Z. Z., 2001, Phys. Lett. B **517**, 363.
Fukugita, M., and Yanagida, T., 1986, Phys. Lett. B **174**, 45.
Gell-Mann, M., Ramond, P., and Slansky, R. 1979, in *Supergravity*, edited by van Nieuwenhuizen, P., and Freedman, D. Z. (North-Holland, Amsterdam), p. 315.
Glashow, S. L., 1980, in *Quarks and Leptons*, edited by Lévy, M., *et al.* (Plenum, New York), p. 707.
Goswami, S., and Ota, T., 2008, Phys. Rev. D **78**, 033012.
Gu, P. H., Zhang, H., and Zhou, S., 2006, Phys. Rev. D **74**, 076002.
Guo, W. L., Xing, Z. Z., and Zhou, S., 2007, Int. J. Mod. Phys. E **16**, 1.
Han, T., and Zhang, B., 2006, Phys. Rev. Lett. **97**, 171804.
Harari, H., and Leuer, M., 1980, Phys. Lett. B **181**, 123.
Jarlskog, C., 1985, Phys. Rev. Lett. **55**, 1039.
Kersten, J., and Smirnov, A. Yu., 2007, Phys. Rev. D **76**, 073005.
Keung, W. Y., and Senjanovic, G., 1983, Phys. Rev. Lett. **50**, 1427.
Konetschny, W., and Kummer, W., 1977, Phys. Lett. B **70**, 433.

Lazarides, G., Shafi, Q., and Wetterich, C., 1981, Nucl. Phys. B **181**, 287.
Liao, Y., 2010a, arXiv:1009.1692.
Liao, Y., 2010b, arXiv:1011.3633.
Luo, S., 2008, Phys. Rev. D **78**, 016006.
Ma, E., 1987, Phys. Lett. B **191**, 287.
Ma, E., 1998, Phys. Rev. Lett. **81**, 1171.
Magg, M., and Wetterich, C., 1980, Phys. Lett. B **94**, 61.
Malinsky, M., *et al.*, 2009a, Phys. Rev. D **79**, 011301.
Malinsky, M., *et al.*, 2009b, Phys. Lett. B **679**, 242.
Minkowski, P., 1977, Phys. Lett. B **67**, 421.
Mohapatra, R. N., and Senjanovic, G., 1980, Phys. Rev. Lett. **44**, 912.
Mohapatra, R. N., and Senjanovic, G., 1981, Phys. Rev. D **23**, 165.
Mohapatra, R. N., and Valle, J. W. F., 1986, Phys. Rev. D **34**, 1642.
Nakamura, K., *et al.* (Particle Data Group), 2010, J. Phys. G **37**, 075021.
Pilaftsis, A., and Underwood, T. E. J., 2004, Nucl. Phys. B **692**, 303.
Pilaftsis, A., and Underwood, T. E. J., 2005, Phys. Rev. D **72**, 113001.
Ponton, E., and Randall, L., 2009, JHEP **0904**, 080.
Ren, P., and Xing, Z. Z., 2008, Phys. Lett. B **666**, 48.
Schechter, J., and Valle, J. W. F., 1980, Phys. Rev. D **22**, 2227.
't Hooft, G., 1980, in *Proceedings of 1979 Cargèse Institute on Recent Developments in Gauge Theories*, edited by 't Hooft, G., *et al.* (Plenum Press, New York), p. 135.
Vissani, F., 1998, Phys. Rev. D **57**, 7027.
Weinberg, S., 1972, Phys. Rev. Lett. **29**, 388.
Weinberg, S., 1979, Phys. Rev. Lett. **43**, 1566.
Weinberg, S., 1980, Phys. Lett. B **91**, 51.
Weinberg, S., 1995, *The Quantum Theory of Fields* (Cambridge University Press).
Wu, D. D., 1986, Phys. Rev. D **33**, 860.
Wyler, D., and Wolfenstein, L., 1983, Nucl. Phys. B **218**, 205.
Xing, Z. Z., 2002, Phys. Lett. B **550**, 178.
Xing, Z. Z., 2004, Int. J. Mod. Phys. A **19**, 1.
Xing, Z. Z., 2008a, Int. J. Mod. Phys. A **23**, 4255.
Xing, Z. Z., 2008b, Phys. Lett. B **660**, 515.
Xing, Z. Z., 2009, Prog. Theor. Phys. Suppl. **180**, 112.
Xing, Z. Z., and Zhou, S., 2004, Phys. Lett. B **593**, 156.
Xing, Z. Z., and Zhou, S., 2007, Phys. Lett. B **653**, 278.
Xing, Z. Z., and Zhou, S., 2009, Phys. Lett. B **679**, 249.
Yanagida, T., 1979, in *Proceedings of the Workshop on Unified Theory and the Baryon Number of the Universe*, edited by Sawada, O., and Sugamoto, A. (KEK, Tsukuba), p. 95.
Zee, A., 1980, Phys. Lett. B **93**, 389.
Zhang, H., and Zhou, S., 2010, Phys. Lett. B **685**, 297.
Zhou, S., and Xing, Z. Z., 2005, Eur. Phys. J. C **38**, 495.

5

Phenomenology of Neutrino Oscillations

So far a number of different neutrino experiments have convincingly observed the phenomena of neutrino oscillations, indicating that neutrinos have rest masses and lepton flavors are mixed. This is the first compelling experimental evidence for new physics beyond the standard model (SM) of elementary particle physics. In this chapter we shall first describe the basic properties of neutrino oscillations in vacuum and then explain the Mikheyev-Smirnov-Wolfenstein (MSW) mechanism for neutrino flavor conversions in matter. Section 5.2 is devoted to an analysis of quantum coherence in neutrino oscillations. We shall reformulate neutrino oscillations by means of the language of the density matrix and flavor polarization vector in Section 5.3. Some ongoing and future accelerator- and reactor-based neutrino oscillation experiments will be briefly introduced in Section 5.4.

5.1 Neutrino Oscillations and Matter Effects

Soon after the discovery of electron antineutrinos in 1956, Bruno Pontecorvo postulated that there might exist the phenomenon of neutrino-antineutrino oscillations by analogy with the phenomenon of K^0-$\overline{K}^0$ mixing (Pontecorvo, 1958). Shortly after the discovery of muon neutrinos in 1962, Ziro Maki, Masami Nakagawa and Shoichi Sakata proposed that two different neutrino flavors could mix with each other and thus the phenomenon of $\nu_e \leftrightarrow \nu_\mu$ or $\overline{\nu}_e \leftrightarrow \overline{\nu}_\mu$ transitions might take place (Maki *et al.*, 1962). Their ideas point to the concept of neutrino (flavor) oscillations: given a beam of neutrinos in a definite flavor state at the source, one may find them in another flavor state at the detector which is at a certain distance from the source. This kind of quantum phenomenon can naturally occur if three known neutrinos have non-degenerate masses and lepton flavors are mixed. Neutrino oscillations have been well established in the past twelve years, thanks to a number of solar, atmospheric, reactor and accelerator neutrino experiments. Both the

longstanding solar neutrino puzzle and the observed deficit of atmospheric muon neutrinos are actually attributed to neutrino oscillations. In this section we first outline the basic properties of neutrino oscillations in vacuum and then describe the phenomenology of neutrino oscillations in matter.

5.1.1 Neutrino Oscillations in Vacuum

Three neutrinos $(\nu_e, \nu_\mu, \nu_\tau)$ are defined as the flavor eigenstates, which accord with three charged leptons (e, μ, τ), in their production processes via the weak charged-current interactions. Since neutrinos are assumed to be massless in the SM, their flavor and mass eigenstates coincide with each other and thus lepton flavors are conserved. But current neutrino oscillation experiments have demonstrated that neutrinos are massive and the SM is incomplete. Beyond the SM we define the mass eigenstates of three neutrinos as (ν_1, ν_2, ν_3), whose eigenvalues are denoted by (m_1, m_2, m_3). In the basis where the mass eigenstates of charged leptons are identified with their flavor eigenstates, the phenomenon of neutrino mixing can be described by a 3×3 unitary matrix V, the so-called Maki-Nakagawa-Sakata (MNS) matrix (Maki *et al.*, 1962):

$$\begin{pmatrix} \nu_e \\ \nu_\mu \\ \nu_\tau \end{pmatrix} = \begin{pmatrix} V_{e1} & V_{e2} & V_{e3} \\ V_{\mu 1} & V_{\mu 2} & V_{\mu 3} \\ V_{\tau 1} & V_{\tau 2} & V_{\tau 3} \end{pmatrix} \begin{pmatrix} \nu_1 \\ \nu_2 \\ \nu_3 \end{pmatrix} \; . \tag{5.1}$$

Different parametrizations of V have been presented in Section 3.5.1.

Now we explain how neutrinos change their flavors when propagating in vacuum. A freely propagating neutrino should be on the mass-shell, or equivalently in the mass eigenstate $\nu_k(t, \mathbf{x})$ (for $k = 1, 2, 3$). Therefore, they must obey the Dirac equation $\left(\mathrm{i}\partial\!\!\!/ - m_k\right) \nu_k(t, \mathbf{x}) = 0$ and the Klein-Gordon equation $\left(\partial^2 + m_k^2\right) \nu_k(t, \mathbf{x}) = 0$ (in the neglect of the spinor structure of the neutrino field which is essentially irrelevant to neutrino oscillations). For a stationary neutrino source, which is the case for all the existing neutrino oscillation experiments, the energy spectrum of neutrinos is fixed and one actually measures their propagation in space rather than in time [1]. To be specific, let us assume that a neutrino beam with energy E is propagating in the one-dimensional space x. In this case the corresponding Klein-Gordon equation can be rewritten as $\left[-(E + \mathrm{i}\partial_x)(E - \mathrm{i}\partial_x) + m_k^2\right] \nu_k(t, x) = 0$. In view of $-\mathrm{i}\partial_x \nu_k(t, x) = p_k \nu_k(t, x)$ due to $\nu_k(t, x) \propto \mathrm{e}^{-\mathrm{i}(Et - p_k x)}$ for free neutrinos, we further obtain

[1] For neutrinos from the conventional sources, their oscillations have been treated in three different ways: the evolution of neutrino states in time, in space, or in space and time. They all lead to the same oscillation probabilities in the relativistic approximation $t \approx x$, as given in Eq. (5.5). However, the scheme of evolution in space is exclusively appropriate to understand the recent proposal of Mössbauer neutrino oscillations (Akhmedov *et al.*, 2008, 2009).

$$\mathrm{i}\partial_x \nu_k(x) = \frac{m_k^2}{2E}\nu_k(x) \;, \tag{5.2}$$

where the approximation $p_k = \sqrt{E^2 - m_k^2} \approx E$ has been made and the terms of $\mathcal{O}(m_k^2/E^2)$ have been omitted. Integrating Eq. (5.2), one may figure out the evolution of the mass eigenstates: $\nu_k(x) = \mathrm{e}^{-\mathrm{i}m_k^2 x/(2E)}\nu_k(0)$. Then the evolution of the flavor eigenstates reads

$$\nu_\alpha(x) = \sum_{k=1}^{3} V_{\alpha k} \exp\left\{-\mathrm{i}\frac{m_k^2}{2E}x\right\} \nu_k(0) \;. \tag{5.3}$$

Note that it is more convenient to work with the neutrino wave functions or state vectors when calculating the neutrino oscillation probabilities. The one-neutrino state $|\nu_k\rangle$ is generated by the Hermitian-conjugate field operator $\nu_k^\dagger(x)$ acting on the vacuum state, and likewise for the flavor states. Hence the evolution of the state vectors is governed by

$$|\nu_\alpha(x)\rangle = \sum_{k=1}^{3} V_{\alpha k}^* \exp\left\{-\mathrm{i}\frac{m_k^2}{2E}x\right\} |\nu_k(0)\rangle \;. \tag{5.4}$$

For a neutrino beam in the flavor state $|\nu_\alpha\rangle$ at the source, the probability of observing it in the state $|\nu_\beta\rangle$ at a distance $x = L$ from the source is

$$\begin{aligned} P(\nu_\alpha \to \nu_\beta) &= |\langle\nu_\beta|\nu_\alpha(L)\rangle|^2 = \sum_{j=1}^{3}\sum_{k=1}^{3} V_{\alpha j}V_{\beta k}V_{\alpha k}^* V_{\beta j}^* \exp\left\{-\mathrm{i}\frac{\Delta m_{kj}^2}{2E}L\right\} \\ &= \sum_{j=1}^{3} |V_{\alpha j}|^2 |V_{\beta j}|^2 + 2\mathrm{Re}\sum_{j<k} V_{\alpha j}V_{\beta k}V_{\alpha k}^* V_{\beta j}^* \exp\left\{-\mathrm{i}\frac{2\pi L}{\lambda_{kj}}\right\} \end{aligned} \tag{5.5}$$

with $\Delta m_{kj}^2 \equiv m_k^2 - m_j^2$ being the neutrino mass-squared differences and $\lambda_{kj} \equiv 4\pi E/\Delta m_{kj}^2$ being the neutrino oscillation lengths. A comparison between L and λ_{ji} is sometimes helpful for a rough estimation of the oscillation probabilities. For instance, the neutrinos from some astrophysical sources travel a very long distance ($L \sim$ Mpc) before arriving at the detector on the Earth. In this case the oscillation lengths λ_{kj} are much smaller than the propagation distance L even for very high neutrino-beam energies $E \gtrsim$ TeV and very small neutrino mass-squared differences $|\Delta m_{kj}^2| \sim 10^{-5}$ eV^2. Hence the oscillatory terms in Eq. (5.5) should be averaged over many circles of oscillations, so that the resultant probabilities are rather simple:

$$\langle P(\nu_\alpha \to \nu_\beta)\rangle = \sum_{i=1}^{3} |V_{\alpha i}|^2 |V_{\beta i}|^2 . \tag{5.6}$$

We see that the phenomenon of neutrino oscillations is due to the coherence among three neutrino mass eigenstates. Eq. (5.6) is always applicable to the

case in which quantum coherence is completely lost. More discussions about the issues of quantum coherence and decoherence in neutrino oscillations will be presented in Section 5.2.

The probabilities of neutrino oscillations in Eq. (5.5) can be rewritten as

$$\begin{aligned} P(\nu_\alpha \to \nu_\beta) &= \sum_{i=1}^{3} \left| V_{\alpha i} V^*_{\beta i} \right|^2 + 2 \sum_{i<j}^{3} {\rm Re}(V_{\alpha i} V_{\beta j} V^*_{\alpha j} V^*_{\beta i}) \cos \frac{\Delta m^2_{ji} L}{2E} \\ &\quad + 2 \sum_{i<j}^{3} {\rm Im}(V_{\alpha i} V_{\beta j} V^*_{\alpha j} V^*_{\beta i}) \sin \frac{\Delta m^2_{ji} L}{2E} \\ &= \left| \sum_{i=1}^{3} V_{\alpha i} V^*_{\beta i} \right|^2 - 4 \sum_{i<j}^{3} {\rm Re}(V_{\alpha i} V_{\beta j} V^*_{\alpha j} V^*_{\beta i}) \sin^2 \frac{\Delta m^2_{ji} L}{4E} \\ &\quad + 2 \sum_{i<j}^{3} {\rm Im}(V_{\alpha i} V_{\beta j} V^*_{\alpha j} V^*_{\beta i}) \sin \frac{\Delta m^2_{ji} L}{2E} \\ &= \delta_{\alpha\beta} - 4 \sum_{i<j}^{3} {\rm Re}(V_{\alpha i} V_{\beta j} V^*_{\alpha j} V^*_{\beta i}) \sin^2 \frac{\Delta m^2_{ji} L}{4E} \\ &\quad + 8 \mathcal{J} \sum_{\gamma} \epsilon_{\alpha\beta\gamma} \sin \frac{\Delta m^2_{21} L}{4E} \sin \frac{\Delta m^2_{31} L}{4E} \sin \frac{\Delta m^2_{32} L}{4E} \; , \end{aligned} \tag{5.7}$$

where the Jarlskog parameter $\mathcal{J}$ has been defined in Eq. (3.116). The survival probabilities of neutrino oscillations (i.e., $\beta = \alpha$) turn out to be

$$P(\nu_\alpha \to \nu_\alpha) = 1 - 4 \sum_{i<j} |V_{\alpha j}|^2 |V_{\beta i}|^2 \sin^2 \frac{\Delta m^2_{ji} L}{4E} \; . \tag{5.8}$$

In the case of two-flavor neutrino oscillations, Eq. (5.8) is simplified to

$$P(\nu_\alpha \to \nu_\alpha) = 1 - \sin^2 2\theta \sin^2 \left(1.27 \frac{\Delta m^2}{{\rm eV}^2} \cdot \frac{L}{\rm km} \cdot \frac{\rm GeV}{E} \right) \; , \tag{5.9}$$

where θ and Δm^2 represent the neutrino mixing angle and mass-squared difference, respectively. Current experimental data on neutrino oscillations can all be interpreted by means of Eq. (5.9) as a good approximation, simply because $|\Delta m^2_{32}| \approx |\Delta m^2_{31}| \gg \Delta m^2_{21}$ and $|V_{e3}|^2 \ll 1$ hold (see Section 3.1 for details). For illustration, Table 5.1 lists six known neutrino oscillation experiments together with their survival probabilities and neutrino mixing angles in the two-flavor neutrino mixing scheme.

Recall that the one-particle state $|\overline{\nu}_i\rangle$ is generated by the neutrino field operator $\nu_i(x)$ rather than its Hermitian conjugate. Hence one may easily read off the probabilities of antineutrino oscillations from Eq. (5.7) through the replacements $V \to V^*$ and $\mathcal{J} \to -\mathcal{J}$:

Table 5.1 Survival probabilities and mixing factors of neutrino oscillations for six known experiments in the two-flavor approximation

Experiment	Survival probability	Mixing factors
Solar $\nu_e \to \nu_e$	$1 - \sin^2 2\theta_{12} \sin^2 \dfrac{\Delta m^2_{21} L}{4E}$	$\sin^2 2\theta_{12} = 4\lvert V_{e1}\rvert^2 \lvert V_{e2}\rvert^2$
KamLAND $\overline{\nu}_e \to \overline{\nu}_e$	$1 - \sin^2 2\theta_{12} \sin^2 \dfrac{\Delta m^2_{21} L}{4E}$	$\sin^2 2\theta_{12} = 4\lvert V_{e1}\rvert^2 \lvert V_{e2}\rvert^2$
Atmospheric $\nu_\mu \to \nu_\mu$	$1 - \sin^2 2\theta_{23} \sin^2 \dfrac{\Delta m^2_{32} L}{4E}$	$\sin^2 2\theta_{23} = 4\lvert V_{\mu 3}\rvert^2 \left(1 - \lvert V_{\mu 3}\rvert^2\right)$
K2K $\nu_\mu \to \nu_\mu$	$1 - \sin^2 2\theta_{23} \sin^2 \dfrac{\Delta m^2_{32} L}{4E}$	$\sin^2 2\theta_{23} = 4\lvert V_{\mu 3}\rvert^2 \left(1 - \lvert V_{\mu 3}\rvert^2\right)$
MINOS $\nu_\mu \to \nu_\mu$	$1 - \sin^2 2\theta_{23} \sin^2 \dfrac{\Delta m^2_{32} L}{4E}$	$\sin^2 2\theta_{23} = 4\lvert V_{\mu 3}\rvert^2 \left(1 - \lvert V_{\mu 3}\rvert^2\right)$
CHOOZ $\overline{\nu}_e \to \overline{\nu}_e$	$1 - \sin^2 2\theta_{13} \sin^2 \dfrac{\Delta m^2_{31} L}{4E}$	$\sin^2 2\theta_{13} = 4\lvert V_{e3}\rvert^2 \left(1 - \lvert V_{e3}\rvert^2\right)$

$$P(\overline{\nu}_\alpha \to \overline{\nu}_\beta) = \delta_{\alpha\beta} - 4 \sum_{i<j}^{3} \mathrm{Re}(V_{\alpha i} V_{\beta j} V^*_{\alpha j} V^*_{\beta i}) \sin^2 \frac{\Delta m^2_{ji} L}{4E} - 8\mathcal{J} \sum_\gamma \epsilon_{\alpha\beta\gamma} \sin \frac{\Delta m^2_{21} L}{4E} \sin \frac{\Delta m^2_{31} L}{4E} \sin \frac{\Delta m^2_{32} L}{4E} \ . \quad (5.10)$$

On the other hand, the probabilities of $\nu_\beta \to \nu_\alpha$ oscillations can also be read off from Eq. (5.7) through the interchange of α and β:

$$P(\nu_\beta \to \nu_\alpha) = \delta_{\alpha\beta} - 4 \sum_{i<j}^{3} \mathrm{Re}(V_{\alpha i} V_{\beta j} V^*_{\alpha j} V^*_{\beta i}) \sin^2 \frac{\Delta m^2_{ji} L}{4E} - 8\mathcal{J} \sum_\gamma \epsilon_{\alpha\beta\gamma} \sin \frac{\Delta m^2_{21} L}{4E} \sin \frac{\Delta m^2_{31} L}{4E} \sin \frac{\Delta m^2_{32} L}{4E} \ . \quad (5.11)$$

A difference between $P(\overline{\nu}_\alpha \to \overline{\nu}_\beta)$ and $P(\nu_\alpha \to \nu_\beta)$ signifies CP violation, while that between $P(\nu_\beta \to \nu_\alpha)$ and $P(\nu_\alpha \to \nu_\beta)$ measures T violation (Cabibbo, 1978). They must be equal to each other (Xing, 2004),

$$\begin{aligned} \Delta P &\equiv P(\nu_\alpha \to \nu_\beta) - P(\overline{\nu}_\alpha \to \overline{\nu}_\beta) \\ &= P(\nu_\alpha \to \nu_\beta) - P(\nu_\beta \to \nu_\alpha) \\ &= 16\mathcal{J} \sum_\gamma \epsilon_{\alpha\beta\gamma} \sin \frac{\Delta m^2_{21} L}{4E} \sin \frac{\Delta m^2_{31} L}{4E} \sin \frac{\Delta m^2_{32} L}{4E} \ , \end{aligned} \quad (5.12)$$

as dictated by CPT invariance. The CPT theorem also ensures that there is no difference between the probabilities of $\nu_\alpha \to \nu_\alpha$ and $\overline{\nu}_\alpha \to \overline{\nu}_\alpha$ oscillations.

Hence it is possible to discover CP or T violation only in the "appearance" neutrino oscillation experiments. A geometric description of CP violation in the language of leptonic unitarity triangles has been given in Section 3.5.3.

So far we have only calculated the probabilities of neutrino-neutrino and antineutrino-antineutrino oscillations. Here let us explain why it is extremely difficult to realize Pontecorvo's original idea and do a neutrino-antineutrino oscillation experiment. We consider a beam of $\overline{\nu}_\alpha$ antineutrinos produced from the vertex of standard charged-current interactions $\alpha^+ + W^- \to \overline{\nu}_\alpha$. After traveling a distance L it will be detected at a detector via the vertex of standard charged-current interactions $\nu_\beta \to \beta^- + W^+$. The amplitude of $\overline{\nu}_\alpha \to \nu_\beta$ oscillations can then be written as

$$A(\overline{\nu}_\alpha \to \nu_\beta) = K \sum_{j=1}^{3} V_{\alpha j} V_{\beta j} \frac{m_j}{E} \exp\left\{ -\mathrm{i} \frac{m_j^2}{2E} L \right\} , \tag{5.13}$$

where E is the beam energy and K denotes a kinematic factor (Schechter and Valle, 1981; de Gouvea *et al.*, 2003). Different from normal $\nu_\alpha \to \nu_\beta$ or $\overline{\nu}_\alpha \to \overline{\nu}_\beta$ oscillations, the $\overline{\nu}_\alpha \to \nu_\beta$ oscillations involve a suppression factor m_j/E in their amplitude. It reflects the fact that the incoming α^+ leads to an antineutrino $\overline{\nu}_\alpha$ in a dominantly right-handed helicity state, whereas the standard charged-current interactions that produce the outgoing β^- would prefer the incident neutrino ν_β being in a left-handed state (Kayser, 2005). Because of $m_j \lesssim 1$ eV and $E \gtrsim 1$ MeV in a realistic experiment, this helicity suppression factor (i.e., $m_j/E \lesssim 10^{-6}$) makes it impossible to observe the phenomenon of neutrino-antineutrino oscillations.

5.1.2 Adiabatic Neutrino Oscillations in Matter

In 1978, Lincoln Wolfenstein pointed out that the coherent forward scattering of neutrinos off matter could significantly change the neutrino flavor content (Wolfenstein, 1978, 1979). It was later on realized that the effective neutrino mixing factor $\sin^2 2\theta_{\rm m}$ in matter could even be maximal no matter how small its counterpart $\sin^2 2\theta$ in vacuum was, provided the resonance condition was satisfied (Barger *et al.*, 1980). In 1985, Stanislav Mikheyev and Alexei Smirnov found that the adiabatic evolution of massive neutrinos in matter could provide an elegant solution to the longstanding solar neutrino puzzle (i.e., the observed flux of solar ν_e neutrinos was much lower than the one predicted by the standard solar model) (Mikheyev and Smirnov, 1985). Today we know that the MSW matter effects on neutrino flavor conversions are also important in the long-baseline neutrino oscillation experiments and crucial for the supernova neutrino detection.

As discussed in Section 2.3, the coherent forward scattering of neutrinos in ordinary matter can be described by the neutrino refractive index, or equivalently the effective potential $\mathcal{V} = \sqrt{2}\, G_{\rm F} n_e$ with n_e being the number density

of electrons. In the two-flavor mixing scheme the state vector of the neutrino system can be written as $|\Psi(t)\rangle = a_e(t)|\nu_e\rangle + a_\mu(t)|\nu_\mu\rangle$, so the corresponding Schrödinger-like equation reads

$$\mathrm{i}\frac{\mathrm{d}}{\mathrm{d}t}\begin{pmatrix} a_e(t) \\ a_\mu(t) \end{pmatrix} = \frac{1}{2E}\left[U\begin{pmatrix} m_1^2 & 0 \\ 0 & m_2^2 \end{pmatrix}U^\dagger + \begin{pmatrix} A & 0 \\ 0 & 0 \end{pmatrix}\right]\begin{pmatrix} a_e(t) \\ a_\mu(t) \end{pmatrix} , \tag{5.14}$$

where $A \equiv 2\sqrt{2}\, G_{\rm F} n_e E$ arises from the effective potential $\mathcal{V}$, and U is the 2×2 neutrino mixing matrix linking the flavor eigenstates to the mass eigenstates:

$$\begin{pmatrix} |\nu_e\rangle \\ |\nu_\mu\rangle \end{pmatrix} = \begin{pmatrix} \cos\theta & \sin\theta \\ -\sin\theta & \cos\theta \end{pmatrix}\begin{pmatrix} |\nu_1\rangle \\ |\nu_2\rangle \end{pmatrix} \tag{5.15}$$

with θ being the mixing angle in vacuum. Let us recast the effective Hamiltonian in Eq. (5.14) into a more instructive form:

$$\mathcal{H}_{\rm m} = \frac{1}{4E}\left[(\Sigma + A)\,\mathbf{1} + \begin{pmatrix} A - \Delta m^2\cos 2\theta & \Delta m^2 \sin 2\theta \\ \Delta m^2 \sin 2\theta & -A + \Delta m^2 \cos 2\theta \end{pmatrix}\right] , \tag{5.16}$$

where $\Delta m^2 \equiv m_2^2 - m_1^2$ and $\Sigma \equiv m_1^2 + m_2^2$ with m_i (for $i = 1, 2$) being the neutrino mass eigenvalues. Note that the $(\Sigma + A)$ term, which is proportional to the identity matrix and thus irrelevant to the neutrino flavor conversion, can actually be neglected in calculating the physical quantities of matter effects. For simplicity, we first consider the case of $n_e =$ constant; namely, the matter density is independent of time and space. Analogous to the treatment of neutrino oscillations in vacuum, the effective Hamiltonian $\mathcal{H}_{\rm m}$ should be diagonalized so as to figure out both the effective neutrino masses and the effective neutrino mixing angle in matter:

$$\begin{aligned} \tilde{m}_1^2 &= \frac{1}{2}\left[\Sigma + A - \sqrt{(A - \Delta m^2\cos 2\theta)^2 + (\Delta m^2 \sin 2\theta)^2}\right] , \\ \tilde{m}_2^2 &= \frac{1}{2}\left[\Sigma + A + \sqrt{(A - \Delta m^2\cos 2\theta)^2 + (\Delta m^2 \sin 2\theta)^2}\right] ; \end{aligned} \tag{5.17}$$

and

$$\tan 2\theta_{\rm m} = \frac{\Delta m^2 \sin 2\theta}{\Delta m^2 \cos 2\theta - A} . \tag{5.18}$$

Note that only $\Delta\tilde{m}^2 \equiv \tilde{m}_2^2 - \tilde{m}_1^2$, which is independent of $(\Sigma + A)$, affects the probabilities of neutrino oscillations in matter:

$$\begin{aligned} \tilde{P}(\nu_e \to \nu_\mu) &= \tilde{P}(\nu_\mu \to \nu_e) = \sin^2 2\theta_{\rm m} \sin^2\left(1.27\frac{\Delta\tilde{m}^2 L}{E}\right) , \\ \tilde{P}(\nu_e \to \nu_e) &= \tilde{P}(\nu_\mu \to \nu_\mu) = 1 - \sin^2 2\theta_{\rm m} \sin^2\left(1.27\frac{\Delta\tilde{m}^2 L}{E}\right) , \end{aligned} \tag{5.19}$$

where $\Delta\tilde{m}^2$, L and E are in units of eV^2, km and GeV, respectively. Note also that there exist two equivalent parameter-space conventions in vacuum: (1)

$0 \leqslant \theta \leqslant \pi/4$ together with positive or negative Δm^2; (2) $0 \leqslant \theta \leqslant \pi/2$ together with positive Δm^2. We shall take the second one, as commonly taken in the literature, because it is also consistent with $\Delta m^2_{21} > 0$ extracted from current experimental data on solar neutrino oscillations. Then Eq. (5.18) leads us to $\theta_{\rm m} \to \theta$ when the matter effect is negligible (i.e., $A \to 0$), or $\theta_{\rm m} \to \pi/2$ when the matter effect is overwhelming (i.e., $A \to \infty$). If the matter density happens to satisfy $A = \Delta m^2 \cos 2\theta$, one will simply arrive at $\theta_{\rm m} = \pi/4$ from Eq. (5.18). This resonant effect is particularly striking because it gives rise to $\sin^2 2\theta_{\rm m} = 1$ in matter even for a very small value of $\sin^2 2\theta$ in vacuum (Barger *et al.*, 1980).

A more interesting and realistic case is the slowly-varying matter density; i.e., the electron density under consideration is time-dependent. For a specific neutrino source, such as the Sun, the time dependence of n_e should be understood as the distance dependence of n_e in the assumption that solar neutrinos are relativistic. Note that the instantaneous neutrino mass eigenstates in matter are linked to the neutrino flavor eigenstates as follows:

$$\begin{pmatrix} |\nu_e\rangle \\ |\nu_\mu\rangle \end{pmatrix} = U_{\rm m} \begin{pmatrix} |\tilde{\nu}_1\rangle \\ |\tilde{\nu}_2\rangle \end{pmatrix} \equiv \begin{pmatrix} \cos\theta_{\rm m} & \sin\theta_{\rm m} \\ -\sin\theta_{\rm m} & \cos\theta_{\rm m} \end{pmatrix} \begin{pmatrix} |\tilde{\nu}_1\rangle \\ |\tilde{\nu}_2\rangle \end{pmatrix} , \tag{5.20}$$

where $U_{\rm m}$ denotes the effective 2×2 neutrino mixing matrix in matter, and its mixing angle $\theta_{\rm m}$ varies with time. Expressing the state vector in the instantaneous mass basis as $|\Psi(t)\rangle = a_1(t)|\tilde{\nu}_1\rangle + a_2(t)|\tilde{\nu}_2\rangle$ and in the flavor basis as $|\Psi(t)\rangle = a_e(t)|\nu_e\rangle + a_\mu(t)|\nu_\mu\rangle$, we are then able to establish the following relationship:

$$\begin{pmatrix} a_e(t) \\ a_\mu(t) \end{pmatrix} = \begin{pmatrix} \cos\theta_{\rm m} & \sin\theta_{\rm m} \\ -\sin\theta_{\rm m} & \cos\theta_{\rm m} \end{pmatrix} \begin{pmatrix} a_1(t) \\ a_2(t) \end{pmatrix} . \tag{5.21}$$

On the other hand, the Schrödinger-like equation in Eq. (5.14) can be put into a simpler form:

$$\mathrm{i}\frac{\mathrm{d}}{\mathrm{d}t} \begin{pmatrix} a_e(t) \\ a_\mu(t) \end{pmatrix} = \frac{1}{2E} \left[U_{\rm m} \begin{pmatrix} \tilde{m}_1^2 & 0 \\ 0 & \tilde{m}_2^2 \end{pmatrix} U_{\rm m}^\dagger \right] \begin{pmatrix} a_e(t) \\ a_\mu(t) \end{pmatrix} . \tag{5.22}$$

With the help of Eq. (5.21), one may convert Eq. (5.22) into

$$\mathrm{i}\frac{\mathrm{d}}{\mathrm{d}t} \begin{pmatrix} a_1(t) \\ a_2(t) \end{pmatrix} = \frac{1}{4E} \begin{pmatrix} -\Delta\tilde{m}^2 & -\mathrm{i}4E\dot{\theta}_{\rm m}(t) \\ \mathrm{i}4E\dot{\theta}_{\rm m}(t) & \Delta\tilde{m}^2 \end{pmatrix} \begin{pmatrix} a_1(t) \\ a_2(t) \end{pmatrix} \tag{5.23}$$

in the instantaneous mass basis, where $\dot{\theta}_{\rm m}(t) \equiv \dfrac{\mathrm{d}\theta_{\rm m}(t)}{\mathrm{d}t}$ is defined, and $\Delta\tilde{m}^2 \equiv \tilde{m}_2^2 - \tilde{m}_1^2$ depends on t too. The evolution equations of two instantaneous mass eigenstates are therefore entangled with each other, unless the adiabatic condition $|\dot{\theta}_{\rm m}(t)| \ll |\Delta\tilde{m}^2|/(4E)$ is satisfied. In such an adiabatic approximation we simply neglect the off-diagonal terms and then integrate Eq. (5.23). The solutions are

$$a_1(t) = a_1(t_0) \exp\left\{ +\mathrm{i} \int_{t_0}^{t} \frac{\Delta\tilde{m}^2(t')}{4E} \mathrm{d}t' \right\} ,$$
$$a_2(t) = a_2(t_0) \exp\left\{ -\mathrm{i} \int_{t_0}^{t} \frac{\Delta\tilde{m}^2(t')}{4E} \mathrm{d}t' \right\} , \tag{5.24}$$

where $\Delta\tilde{m}^2(t) = \sqrt{[A(t) - \Delta m^2 \cos 2\theta]^2 + (\Delta m^2 \sin 2\theta)^2}$ is time-dependent because of $A(t) = 2\sqrt{2}\ G_{\rm F} E n_e(t)$. As a result, the amplitude for the final state to be electron (muon) neutrinos is given by

$$a_e(t) = \cos\theta_{\rm m}(t)\ a_1(t) + \sin\theta_{\rm m}(t)\ a_2(t) ,$$
$$a_\mu(t) = \cos\theta_{\rm m}(t)\ a_2(t) - \sin\theta_{\rm m}(t)\ a_1(t) . \tag{5.25}$$

If there are only the electron neutrinos at $t = t_0$, then we have $a_e(t_0) = 1$ and $a_\mu(t_0) = 0$, leading to $a_1(t_0) = \cos\theta_{\rm m}(t_0)$ and $a_2(t_0) = \sin\theta_{\rm m}(t_0)$. These initial conditions allow us to work out the survival probability of electron neutrinos as follows:

$$P(\nu_e \to \nu_e) = \frac{1}{2} \left[1 + \cos 2\theta_{\rm m}(t) \cos 2\theta_{\rm m}(t_0)\right] + \frac{1}{2} \sin 2\theta_{\rm m}(t) \sin 2\theta_{\rm m}(t_0) \cos\left[\int_{t_0}^{t} \frac{\Delta\tilde{m}^2(t')}{2E} \mathrm{d}t' \right] . \tag{5.26}$$

If neutrinos are produced in a very dense medium, where $n_e(t_0) \to \infty$ is a good approximation, the initial neutrino mixing angle should be $\theta_{\rm m}(t_0) = \pi/2$. Because the detection of neutrinos is usually performed by means of an underground detector below the Earth's surface, the final neutrino mixing angle should take its value in vacuum: $\theta_{\rm m}(t) = \theta$. Furthermore, only the probability averaged over the energy spectrum and detection time is relevant for a realistic experiment. Hence one should drop the last term in Eq. (5.26) and then arrive at the averaged probability

$$\langle P(\nu_e \to \nu_e) \rangle = \frac{1}{2} (1 - \cos 2\theta) = \sin^2\theta . \tag{5.27}$$

This result can be intuitively understood. The electron neutrino ν_e is initially produced almost in the mass eigenstate $\tilde{\nu}_2$ because of $\theta_{\rm m}(t_0) = \pi/2$ arising from the high matter density. As the matter density decreases in an extremely slow way and the adiabatic condition is satisfied, the evolution of the neutrino state will keep in the same mass eigenstate. So we end up with the mass eigenstate ν_2 in vacuum, implying that the probability of finding it as the electron neutrino is just $\sin^2\theta$. The key point here is the validity of the adiabatic condition $|\dot{\theta}_{\rm m}(t)| \ll |\Delta\tilde{m}^2|/(4E)$. Taking account of Eq. (5.18) together with the expression of $\Delta\tilde{m}^2$ given below Eq. (5.24), we obtain

$$\dot{\theta}_{\rm m}(t) = \frac{\Delta m^2 \sin 2\theta}{2\left(\Delta\tilde{m}^2\right)^2} \dot{A}(t) = \sqrt{2}\ G_{\rm F} \frac{\Delta m^2 E \sin 2\theta}{\left(\Delta\tilde{m}^2\right)^2} \dot{n}_e(t) . \tag{5.28}$$

The adiabatic condition can then be written as (Kuo and Pantaleone, 1989a)

$$\sqrt{2}\, G_{\rm F} \left| \frac{{\rm d}n_e(t)}{{\rm d}t} \right| \ll \frac{4\pi^2 \lambda}{\lambda_{\rm m}^3 \sin 2\theta} \,, \tag{5.29}$$

where $\lambda_{\rm m} \equiv 4\pi E/\Delta\tilde{m}^2$ and $\lambda \equiv 4\pi E/\Delta m^2$ are the neutrino oscillation lengths in matter and in vacuum, respectively. Note that the mass-squared difference $\Delta\tilde{m}^2$ reaches its minimum at the resonant point $A = \Delta m^2 \cos 2\theta$, at which the oscillation length $\lambda_{\rm m}$ becomes maximal, so the adiabatic condition might probably be violated at this point. On the resonance one may define the adiabaticity parameter (Kuo and Pantaleone, 1989a)

$$\gamma \equiv \frac{1}{4E} \left[\left| \frac{\Delta\tilde{m}^2}{\dot{\theta}_{\rm m}(t)} \right| \right]_{t=t_r} = \frac{\Delta m^2 \sin^2 2\theta}{2E \cos 2\theta} \left[\frac{1}{n_e(t)} \left| \frac{{\rm d}n_e(t)}{{\rm d}t} \right| \right]^{-1}_{t=t_r} \,, \tag{5.30}$$

where t_r is the resonant point; i.e., $A(t_r) = \Delta m^2 \cos 2\theta$. The adiabatic condition given in Eq. (5.29) can now be expressed as $\gamma \gg 1$. When the adiabaticity parameter γ is of $\mathcal{O}(1)$, the off-diagonal matrix elements in Eq. (5.23) will no longer be negligible. In this non-adiabatic case a transition between the instantaneous mass eigenstates $|\tilde{\nu}_1\rangle$ and $\tilde{\nu}_2\rangle$ must take place, so the oscillation probabilities will inevitably receive very significant corrections.

5.1.3 Non-adiabatic Neutrino Oscillations in Matter

As we have shown above, the electron neutrino ν_e produced in an extremely dense medium stays in the instantaneous mass eigenstate $\tilde{\nu}_2$. It remains in this state if the adiabatic condition $\gamma \gg 1$ is fulfilled. If this condition is violated, however, the neutrino state after crossing the resonant point should be a linear combination of $\tilde{\nu}_1$ and $\tilde{\nu}_2$. In such a case one has to deal with the transition between the instantaneous mass eigenstates. This is typically one of the level-crossing problems (Landau, 1932; Stückelberg, 1932; Zener, 1932) and has been extensively discussed in connection with solar neutrino oscillations (Bethe, 1986; Barger *et al.*, 1986; Parke, 1986; Rosen and Gelb, 1986; Haxton, 1986, 1987; Nötzold, 1987; Toshev, 1987; Kim *et al.*, 1987; Dar *et al.*, 1987; Petcov, 1988; Kuo and Pantaleone, 1989a, 1989b; Bruggen *et al.*, 1995; Friedland, 2001; Kachelrieß and Tomàs, 2001).

Here let us consider a monotonically decreasing matter density profile. The electron neutrinos are produced at $t = t_0$ in the highest density region, and then they pass through the resonant point around $t = t_r$ and come to the vacuum at $t = t_f$. In a region far above ($t = t_- \ll t_r$) or below ($t = t_+ \gg t_r$) the resonant point, the adiabatic approximation should be valid. In between these two adiabatic regions one may introduce the following transition probability between the instantaneous mass eigenstates (Kuo and Pantaleone, 1989a, 1989b):

$$P_c \equiv \left| \langle \tilde{\nu}_1(t_+) | \tilde{\nu}_2(t_-) \rangle \right|^2 \,. \tag{5.31}$$

The survival probabilities for the eigenstates $|\tilde{\nu}_i\rangle$ after crossing the resonant region are $1 - P_c$. As a result, one obtains the averaged survival probability of electron neutrinos (Parke, 1986):

$$\langle P(\nu_e \to \nu_e)\rangle = \left(\cos^2\theta_{\rm m}(t_0) \;\; \sin^2\theta_{\rm m}(t_0)\right) \begin{pmatrix} 1-P_c & P_c \\ P_c & 1-P_c \end{pmatrix} \begin{pmatrix} \cos^2\theta_{\rm m}(t_f) \\ \sin^2\theta_{\rm m}(t_f) \end{pmatrix}$$
$$= \frac{1}{2}\left[1 + (1-2P_c)\cos 2\theta_{\rm m}(t_0)\cos 2\theta_{\rm m}(t_f)\right] \; . \tag{5.32}$$

This result can reproduce Eq. (5.27) in the adiabatic limit with $P_c = 0$, if the initial and final neutrino mixing angles are identified as $\theta_{\rm m}(t_0) = \pi/2$ and $\theta_{\rm m}(t_f) = \theta$. Note that we have used the classical probabilities for finding the electron neutrinos in the mass eigenstates, or vice versa, in the adiabatic regions. The reason is simply that a finite change of the matter density occurs in the distance much longer than the neutrino oscillation length.

In order to calculate the probability P_c, one may solve the coupled first-order differential equations in Eq. (5.14) with a given time-dependent matter density profile. The strategy is to convert the equation array into one second-order differential equation of the amplitude $a_e(t)$. For some special matter density profiles, such as the exponential and linear functions, the exact solutions can be obtained (Kuo and Pantaleone, 1989b). Then one should expand the solutions around the production and detection points, and average them over the phase factor. A different method based on the integration in the complex-time plane was pointed out by Lev Landau, who suggested that one could find the approximate solutions to such differential equations in the quasi-classical limit (Landau, 1932; Dykhne, 1962; Landau and Lifshitz, 1977). Note that the level-crossing point should be at $\Delta\tilde{m}^2 = 0$, where the mass eigenvalues $\tilde{m}_1^2$ and $\tilde{m}_2^2$ are exactly equal. This is possible only if the following condition is satisfied:

$$A(t) = \Delta m^2\left(\cos 2\theta \pm {\rm i}\sin 2\theta\right) = \Delta m^2 {\rm e}^{\pm 2{\rm i}\theta} \; . \tag{5.33}$$

The time variables corresponding to these two possibilities are denoted as t_c^+ and t_c^-, which are located respectively in the upper and lower half-planes of the complex time. Eq. (5.33) indicates that the levels never cross for the real time, and the level-crossing problem in question is definitely of the quantum nature. After extending the Hamiltonian to the complex-time plane analytically, one may choose a continuous path in the upper or lower half-plane. This path, which connects the real-time points (t_-, t_+) and circles around the singular point t_c^+ or t_c^-, can be chosen far away from $t_c^\pm$ such that the adiabatic condition is always valid along it. It has been generally proved that the adiabatic evolution along the path in the complex-time plane determines the non-adiabatic transition probability along the real-time axis (Hwang and Pechukas, 1977). For non-adiabatic neutrino oscillations in matter, one has (Kuo and Pantanleone, 1989a)

$$P_c = \exp\left\{-\mathrm{Im}\left[\int_{t_r}^{t_c^{\pm}} \frac{\Delta\tilde{m}^2(t')}{E}\mathrm{d}t'\right]\right\} , \tag{5.34}$$

where t_c^+ and t_c^- correspond to the increasing and decreasing density profiles, respectively. Given a linear matter density profile, the well-known Landau-Zener formula $P_c^{\mathrm{LZ}} = \exp\{-\pi\gamma/2\}$ with γ being the adiabaticity parameter defined in Eq. (5.30) can be obtained (Parke, 1986).

To explain the complex integration in Eq. (5.34), let us examine the analytical properties of the integrand in the neighborhood of the singular points $t_c^{\pm}$. Here the relevant function is the effective mass-squared difference $\Delta\tilde{m}^2(t)$ given below Eq. (5.24). Redefining $\Delta\tilde{m}^2(t) \equiv \sqrt{f(t)}$, we have

$$f(t) = [A(t) - \Delta m^2 \cos 2\theta]^2 + (\Delta m^2 \sin 2\theta)^2 . \tag{5.35}$$

Combining Eq. (5.35) with Eq. (5.33), we find that $f(t_c^{\pm}) = 0$ holds. But the first derivative of $f(t)$ is in general nonzero at the crossing point; i.e., $\dot{f}(t_c^{\pm}) \neq 0$. With the help of the Taylor expansion of $f(t)$ with respect to $t_c^{\pm}$, one can obtain (Davis and Pechukas, 1976)

$$\Delta\tilde{m}^2(t) = \sqrt{\dot{f}(t_c^{\pm})}\sqrt{t - t_c^{\pm}}\left[1 + \beta(t)(t - t_c^{\pm})\right] , \tag{5.36}$$

where $\beta(t)$ is analytic and single-valued around $t_c^{\pm}$. Because of the square-root function, it is straightforward to observe that $t_c^{\pm}$ are actually the branch points of $\Delta\tilde{m}^2(t)$. Along the circle around $t_c^{\pm}$, the function $\Delta\tilde{m}^2(t)$ will change its sign, implying an exchange of the mass eigenvalues $\tilde{m}_1^2$ and $\tilde{m}_2^2$. To be explicit, we consider a circle around $t_c^{\pm}$ and parametrize it as $t - t_c^{\pm} = \rho \mathrm{e}^{\mathrm{i}\phi}$. It then follows from Eq. (5.36) that $\Delta\tilde{m}^2(\rho, \phi) = -\Delta\tilde{m}^2(\rho, \phi + 2\pi)$. Hence the square-root branch points are essential for the level crossing, and the integration path along the branch cut from t_r to t_c^+ (or t_c^-) should be chosen to keep the imaginary part in Eq. (5.34) positive.

The matter density profile of the Sun, which can significantly affect the behaviors of solar neutrino oscillations, is expected to be exponential: $n_e(t) = n_0 \exp(-t/r_s)$ with $0.23\ R_\odot < r < R_\odot$, where n_0 is a normalization constant, $R_\odot$ denotes the radius of the Sun, and $r_s = 0.092\ R_\odot$ represents the scale height (Pizzochero, 1987; Bahcall, 1989). In this case the zero points of $f(t)$ can be explicitly determined from Eq. (5.33):

$$t_c^{\pm} = -r_s \ln\left(\frac{\Delta m^2}{2\sqrt{2}\ G_{\mathrm{F}} E n_0}\right) \mp 2\mathrm{i} r_s(\theta + k\pi) , \tag{5.37}$$

where k is an arbitrary integer (Pizzochero, 1987) [2]. Then the non-adiabatic transition probability is given by

[2] If there exist several level-crossing points in the complex-time plane, one should choose the one nearest to the real-time axis (Landau and Lifshitz, 1977).

$$\ln P_c = -\frac{1}{E}\mathrm{Im}\int_{t_r}^{t_r+2\mathrm{i}\theta r_s} \sqrt{[A(t') - \Delta m^2\cos 2\theta]^2 + (\Delta m^2 \sin 2\theta)^2}\ \mathrm{d}t' \ . \quad (5.38)$$

The above integration can be simplified by changing the variable in this way: $t' = t_r + \mathrm{i}y$ and $x = -\Delta m^2 \exp(-\mathrm{i}y/r_s)/(2E)$. The final result is found to be (Pizzochero, 1987; Kuo and Pantaleone, 1989a)

$$P_c = \exp\left[-\frac{\pi}{2}\gamma\left(1 - \tan^2\theta\right)\right] \ , \quad (5.39)$$

where $\gamma = r_s \Delta m^2 \sin^2 2\theta/(2E\cos 2\theta)$ is derived from Eq. (5.30) by taking the exponential density profile $n_e(t) = n_0 \exp(-t/r_s)$. Note that Eq. (5.39) reduces to the standard Landau-Zener formula in the $\theta \to 0$ limit, because the corresponding resonance is so narrow that the linear and exponential profiles are essentially identical. The analytical results of the transition probability P_c for a variety of interesting matter density profiles can be found in the literature (Kuo and Pantaleone, 1989a).

5.1.4 The 3 × 3 Neutrino Mixing Matrix in Matter

Now we concentrate on terrestrial matter effects on long-baseline neutrino oscillations. For simplicity, we assume a constant matter density profile (i.e., n_e = constant). This assumption is reasonably good for most of the ongoing or proposed long-baseline neutrino oscillation experiments. Note, however, that the changes of n_e should be carefully taken into account when a neutrino beam travels through the Earth's core (Mocioiu and Shrock, 2000; Akhmedov *et al.*, 2008; Liao, 2008).

In matter we define the effective neutrino masses as $\tilde{m}_i$ (for $i = 1, 2, 3$) and the effective 3×3 neutrino mixing matrix as $\tilde{V}$. The effective Hamiltonians responsible for the propagations of neutrinos in vacuum and in matter are

$$\mathcal{H}_{\mathrm{v}} = \frac{1}{2E} V \begin{pmatrix} m_1^2 & 0 & 0 \\ 0 & m_2^2 & 0 \\ 0 & 0 & m_3^2 \end{pmatrix} V^\dagger \ ,$$

$$\mathcal{H}_{\mathrm{m}} = \frac{1}{2E} \tilde{V} \begin{pmatrix} \tilde{m}_1^2 & 0 & 0 \\ 0 & \tilde{m}_2^2 & 0 \\ 0 & 0 & \tilde{m}_3^2 \end{pmatrix} \tilde{V}^\dagger = \frac{1}{2E} V \begin{pmatrix} m_1^2 & 0 & 0 \\ 0 & m_2^2 & 0 \\ 0 & 0 & m_3^2 \end{pmatrix} V^\dagger + \begin{pmatrix} a & 0 & 0 \\ 0 & 0 & 0 \\ 0 & 0 & 0 \end{pmatrix} \ . \quad (5.40)$$

where E is the neutrino beam energy, and $a = \sqrt{2} G_{\mathrm{F}} n_e$ stands for the terrestrial matter effect. Analogous to Eq. (5.7), the probabilities of neutrino oscillations in matter are given by

$$\tilde{P}(\nu_\alpha \to \nu_\beta) = \delta_{\alpha\beta} - 4\sum_{i<j}^{3} \mathrm{Re}(\tilde{V}_{\alpha i}\tilde{V}_{\beta j}\tilde{V}^*_{\alpha j}\tilde{V}^*_{\beta i}) \sin^2 \frac{\Delta\tilde{m}^2_{ji} L}{4E}$$
$$+ 8\tilde{\mathcal{J}} \sum_{\gamma} \epsilon_{\alpha\beta\gamma} \sin\frac{\Delta\tilde{m}^2_{21} L}{4E} \sin\frac{\Delta\tilde{m}^2_{31} L}{4E} \sin\frac{\Delta\tilde{m}^2_{32} L}{4E} \ , \quad (5.41)$$

where $\Delta\tilde{m}^2_{ji} \equiv \tilde{m}^2_j - \tilde{m}^2_i$ are the effective neutrino mass-squared differences, and $\tilde{\mathcal{J}}$ is the effective Jarlskog parameter defined through

$$\mathrm{Im}(\tilde{V}_{\alpha i}\tilde{V}_{\beta j}\tilde{V}^*_{\alpha j}\tilde{V}^*_{\beta i}) = \tilde{J}\sum_{\gamma}\epsilon_{\alpha\beta\gamma}\sum_{k}\epsilon_{ijk}\; . \tag{5.42}$$

To reveal the behaviors of neutrino oscillations in matter, one needs to work out the relations between $(\tilde{m}^2_i, \tilde{V}, \tilde{\mathcal{J}})$ and $(m^2_i, V, \mathcal{J})$. This can be done by comparing between $\mathcal{H}_{\rm m}$ and $\mathcal{H}_{\rm v}$ in Eq. (5.40). A straightforward calculation yields (Barger *et al.*, 1980; Zaglauer and Schwarzer, 1988; Xing, 2000)

$$\begin{aligned}
\tilde{m}^2_1 &= m^2_1 + \frac{1}{3}x - \frac{1}{3}\sqrt{x^2-3y}\left[z + \sqrt{3\left(1-z^2\right)}\right] \; , \\
\tilde{m}^2_2 &= m^2_1 + \frac{1}{3}x - \frac{1}{3}\sqrt{x^2-3y}\left[z - \sqrt{3\left(1-z^2\right)}\right] \; , \\
\tilde{m}^2_3 &= m^2_1 + \frac{1}{3}x + \frac{2}{3}z\sqrt{x^2-3y} \; ,
\end{aligned} \tag{5.43}$$

where

$$\begin{aligned}
x &= \Delta m^2_{21} + \Delta m^2_{31} + A \; , \\
y &= \Delta m^2_{21}\Delta m^2_{31} + A\left[\Delta m^2_{21}\left(1-|V_{e2}|^2\right) + \Delta m^2_{31}\left(1-|V_{e3}|^2\right)\right] \; , \\
z &= \cos\left[\frac{1}{3}\arccos\frac{2x^3 - 9xy + 27A\Delta m^2_{21}\Delta m^2_{31}|V_{e1}|^2}{2\left(x^2-3y\right)^{3/2}}\right]
\end{aligned} \tag{5.44}$$

with $A = 2aE = 2\sqrt{2}G_{\rm F}En_e$ and $\Delta m^2_{ji} \equiv m^2_j - m^2_i$. It is easy to observe the following sum rule:

$$\sum_{i=1}^{3}\tilde{m}^2_i = \sum_{i=1}^{3} m^2_i + A \; . \tag{5.45}$$

On the other hand, the matrix elements of $\tilde{V}$ and V are related to each other through (Xing, 2000)

$$\tilde{V}_{\alpha i} = \frac{N_i}{D_i}V_{\alpha i} + \frac{A}{D_i}V_{ei}\left[\left(\tilde{m}^2_i - m^2_j\right)V^*_{ek}V_{\alpha k} + \left(\tilde{m}^2_i - m^2_k\right)V^*_{ej}V_{\alpha j}\right] \; , \tag{5.46}$$

where the Greek subscript α runs over (e,μ,τ), the Latin subscripts $i \neq j \neq k$ run over $(1,2,3)$, and

$$\begin{aligned}
N_i &= \left(\tilde{m}^2_i - m^2_j\right)\left(\tilde{m}^2_i - m^2_k\right) - A\left[\left(\tilde{m}^2_i - m^2_j\right)|V_{ek}|^2 + \left(\tilde{m}^2_i - m^2_k\right)|V_{ej}|^2\right] \; , \\
D^2_i &= N^2_i + A^2|V_{ei}|^2\left[\left(\tilde{m}^2_i - m^2_j\right)^2|V_{ek}|^2 + \left(\tilde{m}^2_i - m^2_k\right)^2|V_{ej}|^2\right] \; .
\end{aligned} \tag{5.47}$$

Of course, $A = 0$ immediately leads to $\tilde{m}^2_i = m^2_i$ and $\tilde{V}_{\alpha i} = V_{\alpha i}$. The above exact formulas clearly show how the neutrino mixing matrix and neutrino masses get corrected in the presence of terrestrial matter effects.

The relationship between $\tilde{\mathcal{J}}$ and $\mathcal{J}$ can be established by means of a much more interesting sum rule (Xing, 2001a, 2001b):

$$\sum_{i=1}^{3} \tilde{m}_i^2 \tilde{V}_{\alpha i} \tilde{V}_{\beta i}^* = \sum_{i=1}^{3} m_i^2 V_{\alpha i} V_{\beta i}^* \; , \tag{5.48}$$

which can be derived from the equality between the off-diagonal elements of $\mathcal{H}_{\rm m}$ and $\mathcal{H}_{\rm v}$ in Eq. (5.40). For $\alpha = e$, μ and τ, three equalities can be obtained from Eq. (5.48) and their product is also an equality. Therefore,

$$\begin{aligned} &\sum_{i=1}^{3} \sum_{j=1}^{3} \sum_{k=1}^{3} \tilde{m}_i^2 \tilde{m}_j^2 \tilde{m}_k^2 \; {\rm Im}(\tilde{V}_{ei} \tilde{V}_{\mu j} \tilde{V}_{\tau k} \tilde{V}_{ek}^* \tilde{V}_{\mu i}^* \tilde{V}_{\tau j}^*) \\ &= \sum_{i=1}^{3} \sum_{j=1}^{3} \sum_{k=1}^{3} m_i^2 m_j^2 m_k^2 \; {\rm Im}(V_{ei} V_{\mu j} V_{\tau k} V_{ek}^* V_{\mu i}^* V_{\tau j}^*) \; . \end{aligned} \tag{5.49}$$

This relation can be simplified by using the definitions of $\mathcal{J}$ and $\tilde{\mathcal{J}}$ together with the unitarity conditions of V and $\tilde{V}$. After a straightforward algebraic exercise, we are left with (Xing, 2001a, 2001b)

$$\tilde{\mathcal{J}} \Delta\tilde{m}_{21}^2 \Delta\tilde{m}_{31}^2 \Delta\tilde{m}_{32}^2 = \mathcal{J} \Delta m_{21}^2 \Delta m_{31}^2 \Delta m_{32}^2 \; . \tag{5.50}$$

The same result can also be obtained in different ways (Naumov, 1992; Harrison and Scott, 2000). We observe that $\tilde{\mathcal{J}} = \mathcal{J}$ holds if $A = 0$, and $\tilde{\mathcal{J}} = 0$ holds if $\mathcal{J} = 0$. In other words, CP or T violation in neutrino oscillations in matter is governed by $\mathcal{J}$ via $\tilde{\mathcal{J}}$.

In many cases it is more convenient to parametrize $\tilde{V}$ in terms of the effective neutrino mixing angles and CP-violating phases. Analogous to the standard parametrization of V in vacuum, as given in Eq. (3.107),

$$\begin{aligned} \tilde{V} &= \begin{pmatrix} 1 & 0 & 0 \\ 0 & \tilde{c}_{23} & \tilde{s}_{23} \\ 0 & -\tilde{s}_{23} & \tilde{c}_{23} \end{pmatrix} P \begin{pmatrix} \tilde{c}_{13} & 0 & \tilde{s}_{13} \\ 0 & 1 & 0 \\ -\tilde{s}_{13} & 0 & \tilde{c}_{13} \end{pmatrix} P^\dagger \begin{pmatrix} \tilde{c}_{12} & \tilde{s}_{12} & 0 \\ -\tilde{s}_{12} & \tilde{c}_{12} & 0 \\ 0 & 0 & 1 \end{pmatrix} P' \\ &= \begin{pmatrix} \tilde{c}_{12}\tilde{c}_{13} & \tilde{s}_{12}\tilde{c}_{13} & \tilde{s}_{13} {\rm e}^{-{\rm i}\tilde{\delta}} \\ -\tilde{s}_{12}\tilde{c}_{23} - \tilde{c}_{12}\tilde{s}_{23}\tilde{s}_{13}{\rm e}^{{\rm i}\tilde{\delta}} & \tilde{c}_{12}\tilde{c}_{23} - \tilde{s}_{12}\tilde{s}_{23}\tilde{s}_{13}{\rm e}^{{\rm i}\tilde{\delta}} & \tilde{s}_{23}\tilde{c}_{13} \\ \tilde{s}_{12}\tilde{s}_{23} - \tilde{c}_{12}\tilde{c}_{23}\tilde{s}_{13}{\rm e}^{{\rm i}\tilde{\delta}} & -\tilde{c}_{12}\tilde{s}_{23} - \tilde{s}_{12}\tilde{c}_{23}\tilde{s}_{13}{\rm e}^{{\rm i}\tilde{\delta}} & \tilde{c}_{23}\tilde{c}_{13} \end{pmatrix} P' \; , \end{aligned} \tag{5.51}$$

where $\tilde{c}_{ij} \equiv \cos\tilde{\theta}_{ij}$ and $\tilde{s}_{ij} \equiv \sin\tilde{\theta}_{ij}$ (for $ij = 12, 13, 23$) together with the phase matrices $P = {\rm Diag}\{1, 1, {\rm e}^{{\rm i}\tilde{\delta}}\}$ and $P' = {\rm Diag}\{{\rm e}^{{\rm i}\rho}, {\rm e}^{{\rm i}\sigma}, 1\}$. Since P' itself plays no role in neutrino oscillations, its two Majorana phases ρ and σ are completely insensitive to matter effects. Substituting Eqs. (3.107) and (5.51) into Eqs. (5.46) and (5.47), one may get the relations between $(\tilde{\theta}_{12}, \tilde{\theta}_{13}, \tilde{\theta}_{23}, \tilde{\delta})$ and $(\theta_{12}, \theta_{13}, \theta_{23}, \delta)$. But the exact analytical results are not simple (Zaglauer and Schwarzer, 1988; Xing, 2001c; Freund, 2001). For example [3],

[3] Here we only present the next-to-leading order expression for $\tan\tilde{\theta}_{23}/\tan\theta_{23}$, because the exact result is too complicated to be instructive.

$$\frac{\tan\tilde{\theta}_{12}}{\tan\theta_{12}} = \frac{D_1}{D_2}\cdot\frac{N_2 + A\left[\left(\tilde{m}_2^2 - m_1^2\right)s_{13}^2 + \left(\tilde{m}_2^2 - m_3^2\right)c_{12}^2 c_{13}^2\right]}{N_1 + A\left[\left(\tilde{m}_1^2 - m_2^2\right)s_{13}^2 + \left(\tilde{m}_1^2 - m_3^2\right)s_{12}^2 c_{13}^2\right]} ,$$
$$\frac{\tan\tilde{\theta}_{23}}{\tan\theta_{23}} = 1 + \frac{A\Delta m_{21}^2 s_{12} c_{12} s_{13}\cos\delta}{s_{23}c_{23}\left\{N_3 - A\left[\left(\tilde{m}_3^2 - m_1^2\right)s_{12}^2 + \left(\tilde{m}_3^2 - m_2^2\right)c_{12}^2\right]s_{13}^2\right\}} ,$$
$$\frac{\sin\tilde{\theta}_{13}}{\sin\theta_{13}} = \frac{N_3}{D_3} + \frac{A}{D_3}\left[\left(\tilde{m}_3^2 - m_1^2\right)s_{12}^2 + \left(\tilde{m}_3^2 - m_2^2\right)c_{12}^2\right]c_{13}^2 , \tag{5.52}$$

where D_i and N_i can be read off from Eq. (5.47). In addition, one may relate $\sin\tilde{\delta}$ to $\sin\delta$ by using Eq. (5.50) together with $\tilde{\mathcal{J}} = \tilde{c}_{12}\tilde{s}_{12}\tilde{c}_{13}^2\tilde{s}_{13}\tilde{c}_{23}\tilde{s}_{23}\sin\tilde{\delta}$ and the similar expression of $\mathcal{J}$. Note, however, that both the (2,3) rotation matrix in Eq. (5.51) and the phase matrix P commute with the matter-induced matrix in Eq. (5.40). This observation allows one to derive an exact relationship between $(\tilde{\theta}_{23}, \tilde{\delta})$ and (θ_{23}, δ) (Toshev, 1991):

$$\sin 2\tilde{\theta}_{23}\sin\tilde{\delta} = \sin 2\theta_{23}\sin\delta . \tag{5.53}$$

So $\tilde{\delta} \approx \delta$ holds as a result of $\tilde{\theta}_{23} \approx \theta_{23}$ in the leading-order approximation. Hence both θ_{23} and δ are essentially insensitive to matter effects.

The results obtained above are only valid for neutrinos propagating in matter. For the case of antineutrinos propagating in matter, the corresponding expressions can be easily obtained through the replacements $\delta \Longrightarrow -\delta$ (or $\mathcal{J} \Longrightarrow -\mathcal{J}$) and $A \Longrightarrow -A$. Such formulas should be very useful for the purpose of recasting the fundamental parameters of lepton flavor mixing from the matter-corrected ones, which can be extracted from a variety of long- and medium-baseline neutrino oscillation experiments in the near future.

5.1.5 Leptonic Unitarity Triangles in Matter

We proceed to explore some more properties of lepton flavor mixing and CP violation in matter. For simplicity, we are again subject to a constant matter density profile. The effective Hamiltonians $\mathcal{H}_{\rm v}$ and $\mathcal{H}_{\rm m}$ in Eq. (5.40) are related to each other via

$$\mathcal{H}_{\rm m} = \mathcal{H}_{\rm v} + \begin{pmatrix} a & 0 & 0 \\ 0 & 0 & 0 \\ 0 & 0 & 0 \end{pmatrix} , \tag{5.54}$$

where $a = A/(2E) = \sqrt{2}G_{\rm F}n_e$. This equality actually allows us to obtain a sum rule which is more general than the one given in Eq. (5.48):

$$\sum_{i=1}^{3}\tilde{m}_i^2\tilde{V}_{\alpha i}\tilde{V}_{\beta i}^* = \sum_{i=1}^{3}m_i^2 V_{\alpha i}V_{\beta i}^* + A\delta_{\alpha e}\delta_{e\beta} . \tag{5.55}$$

On the other hand,

$$\mathcal{H}_{\rm m}\mathcal{H}_{\rm m}^\dagger = \mathcal{H}_{\rm v}\mathcal{H}_{\rm v}^\dagger + \mathcal{H}_{\rm v}\begin{pmatrix} a & 0 & 0 \\ 0 & 0 & 0 \\ 0 & 0 & 0 \end{pmatrix} + \begin{pmatrix} a & 0 & 0 \\ 0 & 0 & 0 \\ 0 & 0 & 0 \end{pmatrix}\mathcal{H}_{\rm v}^\dagger + \begin{pmatrix} a^2 & 0 & 0 \\ 0 & 0 & 0 \\ 0 & 0 & 0 \end{pmatrix} , \tag{5.56}$$

which leads us to a new sum rule (Xing and Zhang, 2005)

$$\sum_{i=1}^{3} \tilde{m}_i^4 \tilde{V}_{\alpha i}\tilde{V}_{\beta i}^* = \sum_{i=1}^{3} \left[m_i^4 + A m_i^2 \left(\delta_{\alpha e} + \delta_{e\beta}\right)\right] V_{\alpha i} V_{\beta i}^* + A^2 \delta_{\alpha e}\delta_{e\beta} \; . \tag{5.57}$$

Eqs. (5.55) and (5.57), together with the unitarity conditions

$$\sum_{i=1}^{3} \tilde{V}_{\alpha i}\tilde{V}_{\beta i}^* = \sum_{i=1}^{3} V_{\alpha i} V_{\beta i}^* = \delta_{\alpha\beta} \; , \tag{5.58}$$

constitute a full set of linear equations of $\tilde{V}_{\alpha i}\tilde{V}_{\beta i}^*$ (for $i = 1, 2, 3$). One may make use of these equations to derive the concrete expressions of $\tilde{V}_{\alpha i}\tilde{V}_{\beta i}^*$ in terms of m_i^2, $\tilde{m}_i^2$ and $V_{\alpha i}V_{\beta i}^*$.

Let us first calculate the moduli of $\tilde{V}_{\alpha i}$ by using Eqs. (5.55), (5.57) and (5.58). Those equations are rewritten, in the $\alpha = \beta$ case, as follows:

$$\tilde{X}\begin{pmatrix} |\tilde{V}_{\alpha 1}|^2 \\ |\tilde{V}_{\alpha 2}|^2 \\ |\tilde{V}_{\alpha 3}|^2 \end{pmatrix} = \left(X + 2A\delta_{\alpha e} Y\right)\begin{pmatrix} |V_{\alpha 1}|^2 \\ |V_{\alpha 2}|^2 \\ |V_{\alpha 3}|^2 \end{pmatrix} + \begin{pmatrix} 0 \\ A \\ A^2 \end{pmatrix}\delta_{\alpha e} \; , \tag{5.59}$$

where

$$X = \begin{pmatrix} 1 & 1 & 1 \\ m_1^2 & m_2^2 & m_3^2 \\ m_1^4 & m_2^4 & m_3^4 \end{pmatrix} \; , \qquad Y = \begin{pmatrix} 0 & 0 & 0 \\ 0 & 0 & 0 \\ m_1^2 & m_2^2 & m_3^2 \end{pmatrix} \; ,$$
$$\tilde{X} = \begin{pmatrix} 1 & 1 & 1 \\ \tilde{m}_1^2 & \tilde{m}_2^2 & \tilde{m}_3^2 \\ \tilde{m}_1^4 & \tilde{m}_2^4 & \tilde{m}_3^4 \end{pmatrix} \; . \tag{5.60}$$

With the help of Eq. (5.45), we solve Eq. (5.59) and obtain the following exact results (Xing and Zhang, 2005):

$$\begin{aligned} |\tilde{V}_{e1}|^2 &= \frac{\hat{\Delta}_{21}\hat{\Delta}_{31}}{\tilde{\Delta}_{21}\tilde{\Delta}_{31}}|V_{e1}|^2 + \frac{\hat{\Delta}_{11}\hat{\Delta}_{31}}{\tilde{\Delta}_{21}\tilde{\Delta}_{31}}|V_{e2}|^2 + \frac{\hat{\Delta}_{11}\hat{\Delta}_{21}}{\tilde{\Delta}_{21}\tilde{\Delta}_{31}}|V_{e3}|^2 \; , \\ |\tilde{V}_{e2}|^2 &= \frac{\hat{\Delta}_{22}\hat{\Delta}_{32}}{\tilde{\Delta}_{12}\tilde{\Delta}_{32}}|V_{e1}|^2 + \frac{\hat{\Delta}_{12}\hat{\Delta}_{32}}{\tilde{\Delta}_{12}\tilde{\Delta}_{32}}|V_{e2}|^2 + \frac{\hat{\Delta}_{12}\hat{\Delta}_{22}}{\tilde{\Delta}_{12}\tilde{\Delta}_{32}}|V_{e3}|^2 \; , \\ |\tilde{V}_{e3}|^2 &= \frac{\hat{\Delta}_{23}\hat{\Delta}_{33}}{\tilde{\Delta}_{13}\tilde{\Delta}_{23}}|V_{e1}|^2 + \frac{\hat{\Delta}_{13}\hat{\Delta}_{33}}{\tilde{\Delta}_{13}\tilde{\Delta}_{23}}|V_{e2}|^2 + \frac{\hat{\Delta}_{13}\hat{\Delta}_{23}}{\tilde{\Delta}_{13}\tilde{\Delta}_{23}}|V_{e3}|^2 \; ; \end{aligned} \tag{5.61}$$

and

$$
\begin{aligned}
|\tilde{V}_{\mu 1}|^2 &= \frac{\hat{\Delta}_{12}\hat{\Delta}_{13}}{\tilde{\Delta}_{12}\tilde{\Delta}_{13}}|V_{\mu 1}|^2 + \frac{\hat{\Delta}_{22}\hat{\Delta}_{23}}{\tilde{\Delta}_{12}\tilde{\Delta}_{13}}|V_{\mu 2}|^2 + \frac{\hat{\Delta}_{32}\hat{\Delta}_{33}}{\tilde{\Delta}_{12}\tilde{\Delta}_{13}}|V_{\mu 3}|^2 \; , \\
|\tilde{V}_{\mu 2}|^2 &= \frac{\hat{\Delta}_{11}\hat{\Delta}_{13}}{\tilde{\Delta}_{21}\tilde{\Delta}_{23}}|V_{\mu 1}|^2 + \frac{\hat{\Delta}_{21}\hat{\Delta}_{23}}{\tilde{\Delta}_{21}\tilde{\Delta}_{23}}|V_{\mu 2}|^2 + \frac{\hat{\Delta}_{31}\hat{\Delta}_{33}}{\tilde{\Delta}_{21}\tilde{\Delta}_{23}}|V_{\mu 3}|^2 \; , \\
|\tilde{V}_{\mu 3}|^2 &= \frac{\hat{\Delta}_{11}\hat{\Delta}_{12}}{\tilde{\Delta}_{31}\tilde{\Delta}_{32}}|V_{\mu 1}|^2 + \frac{\hat{\Delta}_{21}\hat{\Delta}_{22}}{\tilde{\Delta}_{31}\tilde{\Delta}_{32}}|V_{\mu 2}|^2 + \frac{\hat{\Delta}_{31}\hat{\Delta}_{32}}{\tilde{\Delta}_{31}\tilde{\Delta}_{32}}|V_{\mu 3}|^2 \; ; \qquad (5.62)
\end{aligned}
$$

and

$$
\begin{aligned}
|\tilde{V}_{\tau 1}|^2 &= \frac{\hat{\Delta}_{12}\hat{\Delta}_{13}}{\tilde{\Delta}_{12}\tilde{\Delta}_{13}}|V_{\tau 1}|^2 + \frac{\hat{\Delta}_{22}\hat{\Delta}_{23}}{\tilde{\Delta}_{12}\tilde{\Delta}_{13}}|V_{\tau 2}|^2 + \frac{\hat{\Delta}_{32}\hat{\Delta}_{33}}{\tilde{\Delta}_{12}\tilde{\Delta}_{13}}|V_{\tau 3}|^2 \; , \\
|\tilde{V}_{\tau 2}|^2 &= \frac{\hat{\Delta}_{11}\hat{\Delta}_{13}}{\tilde{\Delta}_{21}\tilde{\Delta}_{23}}|V_{\tau 1}|^2 + \frac{\hat{\Delta}_{21}\hat{\Delta}_{23}}{\tilde{\Delta}_{21}\tilde{\Delta}_{23}}|V_{\tau 2}|^2 + \frac{\hat{\Delta}_{31}\hat{\Delta}_{33}}{\tilde{\Delta}_{21}\tilde{\Delta}_{23}}|V_{\tau 3}|^2 \; , \\
|\tilde{V}_{\tau 3}|^2 &= \frac{\hat{\Delta}_{11}\hat{\Delta}_{12}}{\tilde{\Delta}_{31}\tilde{\Delta}_{32}}|V_{\tau 1}|^2 + \frac{\hat{\Delta}_{21}\hat{\Delta}_{22}}{\tilde{\Delta}_{31}\tilde{\Delta}_{32}}|V_{\tau 2}|^2 + \frac{\hat{\Delta}_{31}\hat{\Delta}_{32}}{\tilde{\Delta}_{31}\tilde{\Delta}_{32}}|V_{\tau 3}|^2 \; , \qquad (5.63)
\end{aligned}
$$

where $\hat{\Delta}_{ji} \equiv m_j^2 - \tilde{m}_i^2$ and $\tilde{\Delta}_{ji} \equiv \Delta\tilde{m}_{ji}^2 = \tilde{m}_j^2 - \tilde{m}_i^2$ have been defined. Note that $\hat{\Delta}_{ji} = \hat{\Delta}_{jj} + \tilde{\Delta}_{ji}$ holds, and both $\hat{\Delta}_{jj}$ and $\tilde{\Delta}_{ji}$ can be directly read off from Eq. (5.43). Of course, we have $|\tilde{V}_{\alpha i}|^2 = |V_{\alpha i}|^2$ in the $A \to 0$ limit.

We continue to calculate $\tilde{V}_{\alpha i}\tilde{V}^*_{\beta i}$ in terms of $V_{\alpha i}V^*_{\beta i}$ (for $\alpha \neq \beta$). The latter can form three unitarity triangles, which are named as $\triangle_e$ for $(\alpha, \beta) = (\mu, \tau)$, $\triangle_\mu$ for $(\alpha, \beta) = (\tau, e)$ and $\triangle_\tau$ for $(\alpha, \beta) = (e, \mu)$ in Fig. 3.10, in the complex plane in vacuum. Their effective counterparts in matter are then referred to as $\tilde{\triangle}_e$, $\tilde{\triangle}_\mu$ and $\tilde{\triangle}_\tau$. Taking account of Eqs. (5.55), (5.57) and (5.58), one may easily write down a full set of equations of $\tilde{V}_{\alpha i}\tilde{V}^*_{\beta i}$ (for $\alpha \neq \beta$):

$$
\tilde{X} \begin{pmatrix} \tilde{V}_{\alpha 1}\tilde{V}^*_{\beta 1} \\ \tilde{V}_{\alpha 2}\tilde{V}^*_{\beta 2} \\ \tilde{V}_{\alpha 3}\tilde{V}^*_{\beta 3} \end{pmatrix} = \left[X + A\left(\delta_{\alpha e} + \delta_{e\beta}\right) Y \right] \begin{pmatrix} V_{\alpha 1}V^*_{\beta 1} \\ V_{\alpha 2}V^*_{\beta 2} \\ V_{\alpha 3}V^*_{\beta 3} \end{pmatrix} \; , \qquad (5.64)
$$

where $\tilde{X}$, X and Y have been given in Eq. (5.60). The solutions to Eq. (5.64) are (Xing and Zhang, 2005; Zhang and Xing, 2005)

$$
\begin{aligned}
\tilde{V}_{\mu 1}\tilde{V}^*_{\tau 1} &= \frac{(\hat{\Delta}_{21} + A)\Delta_{31}}{\tilde{\Delta}_{21}\tilde{\Delta}_{31}} V_{\mu 1}V^*_{\tau 1} + \frac{(\hat{\Delta}_{11} + A)\Delta_{32}}{\tilde{\Delta}_{21}\tilde{\Delta}_{31}} V_{\mu 2}V^*_{\tau 2} \; , \\
\tilde{V}_{\mu 2}\tilde{V}^*_{\tau 2} &= \frac{(\hat{\Delta}_{32} + A)\Delta_{21}}{\tilde{\Delta}_{32}\tilde{\Delta}_{21}} V_{\mu 2}V^*_{\tau 2} + \frac{(\hat{\Delta}_{22} + A)\Delta_{31}}{\tilde{\Delta}_{32}\tilde{\Delta}_{21}} V_{\mu 3}V^*_{\tau 3} \; , \\
\tilde{V}_{\mu 3}\tilde{V}^*_{\tau 3} &= \frac{(\hat{\Delta}_{13} + A)\Delta_{23}}{\tilde{\Delta}_{13}\tilde{\Delta}_{23}} V_{\mu 3}V^*_{\tau 3} + \frac{(\hat{\Delta}_{33} + A)\Delta_{21}}{\tilde{\Delta}_{13}\tilde{\Delta}_{23}} V_{\mu 1}V^*_{\tau 1} \; , \qquad (5.65)
\end{aligned}
$$

for the effective triangle $\tilde{\triangle}_e$; and

$$\tilde{V}_{\tau 1}\tilde{V}^*_{e1} = \frac{\hat{\Delta}_{21}\Delta_{31}}{\tilde{\Delta}_{21}\tilde{\Delta}_{31}} V_{\tau 1}V^*_{e1} + \frac{\hat{\Delta}_{11}\Delta_{32}}{\tilde{\Delta}_{21}\tilde{\Delta}_{31}} V_{\tau 2}V^*_{e2} \; ,$$
$$\tilde{V}_{\tau 2}\tilde{V}^*_{e2} = \frac{\hat{\Delta}_{32}\Delta_{21}}{\tilde{\Delta}_{32}\tilde{\Delta}_{21}} V_{\tau 2}V^*_{e2} + \frac{\hat{\Delta}_{22}\Delta_{31}}{\tilde{\Delta}_{32}\tilde{\Delta}_{21}} V_{\tau 3}V^*_{e3} \; ,$$
$$\tilde{V}_{\tau 3}\tilde{V}^*_{e3} = \frac{\hat{\Delta}_{13}\Delta_{23}}{\tilde{\Delta}_{13}\tilde{\Delta}_{23}} V_{\tau 3}V^*_{e3} + \frac{\hat{\Delta}_{33}\Delta_{21}}{\tilde{\Delta}_{13}\tilde{\Delta}_{23}} V_{\tau 1}V^*_{e1} \; , \tag{5.66}$$

for the effective triangle $\tilde{\triangle}_\mu$; and

$$\tilde{V}_{e1}\tilde{V}^*_{\mu 1} = \frac{\hat{\Delta}_{21}\Delta_{31}}{\tilde{\Delta}_{21}\tilde{\Delta}_{31}} V_{e1}V^*_{\mu 1} + \frac{\hat{\Delta}_{11}\Delta_{32}}{\tilde{\Delta}_{21}\tilde{\Delta}_{31}} V_{e2}V^*_{\mu 2} \; ,$$
$$\tilde{V}_{e2}\tilde{V}^*_{\mu 2} = \frac{\hat{\Delta}_{32}\Delta_{21}}{\tilde{\Delta}_{32}\tilde{\Delta}_{21}} V_{e2}V^*_{\mu 2} + \frac{\hat{\Delta}_{22}\Delta_{31}}{\tilde{\Delta}_{32}\tilde{\Delta}_{21}} V_{e3}V^*_{\mu 3} \; ,$$
$$\tilde{V}_{e3}\tilde{V}^*_{\mu 3} = \frac{\hat{\Delta}_{13}\Delta_{23}}{\tilde{\Delta}_{13}\tilde{\Delta}_{23}} V_{e3}V^*_{\mu 3} + \frac{\hat{\Delta}_{33}\Delta_{21}}{\tilde{\Delta}_{13}\tilde{\Delta}_{23}} V_{e1}V^*_{\mu 1} \; , \tag{5.67}$$

for the effective triangle $\tilde{\triangle}_\tau$, where $\Delta_{ji} \equiv \Delta m^2_{ji} = m^2_j - m^2_i$ has been defined. One may use the sides of $\tilde{\triangle}_\alpha$ (for $\alpha = e, \mu, \tau$) to calculate the effective Jarlskog invariant $\tilde{\mathcal{J}}$ and then obtain the relationship between $\tilde{\mathcal{J}}$ and $\mathcal{J}$ as given in Eq. (5.50). The areas of $\tilde{\triangle}_e$, $\tilde{\triangle}_\mu$ and $\tilde{\triangle}_\tau$ are all equal to $\tilde{\mathcal{J}}/2$.

We remark that the results obtained above are only valid for neutrinos propagating in matter. As for antineutrinos propagating in matter, the relevant formulas can be directly written out through the replacements $V \Longrightarrow V^*$ (or $\mathcal{J} \Longrightarrow -\mathcal{J}$) and $A \Longrightarrow -A$. For a neutrino oscillation experiment with $L \lesssim 1000$ km, the dependence of terrestrial matter effects on the neutrino beam energy is approximately $A \approx 2.28 \times 10^{-4}$ eV$^2 E/[\text{GeV}]$ (Mocioiu and Shrock, 2000). Typically taking $\Delta_{21} \approx 8 \times 10^{-5}$ eV^2, $\Delta_{32} \approx 2.3 \times 10^{-3}$ eV^2, $\theta_{12} \approx 33^\circ$, $\theta_{13} \approx 3^\circ$, $\theta_{23} \approx 45^\circ$ and $\delta \approx 90^\circ$ in vacuum, we show the numerical dependence of $\tilde{\mathcal{J}}/\mathcal{J}$ on E in Fig. 5.1 for both neutrinos and antineutrinos. We see that $\tilde{\mathcal{J}}$ is in most cases smaller than $\mathcal{J}$. This unfortunate feature makes it hard to directly measure leptonic CP or T violation in any realistic long-baseline neutrino oscillation experiments. If the neutrino beam energy is small (e.g., $E \sim 1$ GeV or smaller), the matter-induced suppression of $\tilde{\mathcal{J}}$ is not significant. In this case a study of CP violation and unitarity triangles in a medium-baseline neutrino oscillation experiment might be more feasible (Minakata and Nunokawa, 2000; Xing, 2001a).

5.2 Neutrino Oscillations and Quantum Coherence

Although the phenomenology of neutrino oscillations has been established, a number of basic issues associated with the theory of neutrino oscillations

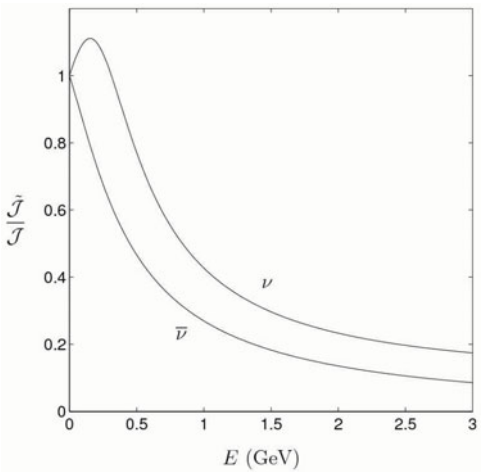

Fig. 5.1 Terrestrial matter effects on the Jarlskog invariant of CP violation for neutrinos (ν with $+A$ and V) and antineutrinos ($\overline{\nu}$ with $-A$ and V^*) in a realistic long-baseline oscillation experiment (Zhang and Xing, 2005. With permission from Springer Science+Business Media)

are still under debate. In this section we introduce the wave-packet approach for describing neutrino oscillations and analyze the conditions of quantum coherence under which neutrino oscillations can take place.

5.2.1 A Paradox of Neutrino Oscillations

The treatment of neutrino oscillations in Section 5.1 is actually oversimple, although it can lead to the correct results. Now let us clarify the same energy or same momentum assumption for neutrino mass eigenstates composing a given neutrino flavor state, because it has often been used in the calculation of neutrino oscillation probabilities.

If the same energy E is assumed for three neutrino mass eigenstates, they must possess different momenta $p_k = \sqrt{E^2 - m_k^2}$ (for $k = 1, 2, 3$) which can approximate to $p_k = E - m_k^2/(2E)$ in the relativistic limit. Then a given neutrino flavor state propagates in the one-dimensional space x as follows:

$$|\nu_\alpha(x)\rangle = \sum_{k=1}^{3} V_{\alpha k}^* \mathrm{e}^{\mathrm{i}p_k x} |\nu_k\rangle \; . \tag{5.68}$$

One may obtain the amplitude of $\nu_\alpha \to \nu_\beta$ oscillations by projecting this state onto $|\nu_\beta\rangle$ at the detector with $x = L$. The oscillation probabilities are

$$P(\nu_\alpha \to \nu_\beta) = \sum_{j=1}^{3} \sum_{k=1}^{3} V_{\alpha j} V_{\beta k} V_{\alpha k}^* V_{\beta j}^* \; \mathrm{e}^{\mathrm{i}(p_k - p_j)L}$$

$$= \sum_{j=1}^{3}\sum_{k=1}^{3} V_{\alpha j}V_{\beta k}V_{\alpha k}^{*}V_{\beta j}^{*} \exp\left\{-\mathrm{i}\frac{\Delta m_{kj}^{2}}{2E}L\right\} . \qquad (5.69)$$

This result is the same as the one given in Eq. (5.5). If the same momentum p is assumed for three neutrino mass eigenstates, nevertheless, they must have different energies $E_k = \sqrt{p^2 + m_k^2}$ (for $k = 1, 2, 3$) which can approximate to $E_k = p + m_k^2/(2p)$ in the relativistic limit. In this case a given neutrino flavor state evolves only in time,

$$|\nu_\alpha(t)\rangle = \sum_{k=1}^{3} V_{\alpha k}^{*}\mathrm{e}^{-\mathrm{i}E_k t}|\nu_k\rangle , \qquad (5.70)$$

and the probabilities of $\nu_\alpha \to \nu_\beta$ oscillations turn out to be

$$\begin{aligned} P(\nu_\alpha \to \nu_\beta) &= \sum_{j=1}^{3}\sum_{k=1}^{3} V_{\alpha j}V_{\beta k}V_{\alpha k}^{*}V_{\beta j}^{*}\mathrm{e}^{-\mathrm{i}(E_k - E_j)t} \\ &= \sum_{j=1}^{3}\sum_{k=1}^{3} V_{\alpha j}V_{\beta k}V_{\alpha k}^{*}V_{\beta j}^{*} \exp\left\{-\mathrm{i}\frac{\Delta m_{kj}^{2}}{2p}t\right\} . \end{aligned} \qquad (5.71)$$

Taking account of $p \approx E \gg m_k$ and $t \approx L$ in the natural unit system, we find that the results obtain in Eqs. (5.69) and (5.71) are identical. An immediate question is why these two totally different assumptions lead to the same result. In fact, these two assumptions contradict each other and neither of them is correct. One may consider the decay mode $\pi^+ \to \mu^+ + \nu_\mu$ and analyze its kinematics in the rest frame of the pion to demonstrate that the same energy or momentum assumption must be wrong. Suppose a neutrino mass eigenstate $|\nu_k\rangle$ with the eigenvalue m_k is produced in this decay, then its momentum and energy are given by

$$\begin{aligned} p_k^2 &= \frac{\left(m_\pi^2 - m_\mu^2 - m_k^2\right)^2 - 4m_k^2 m_\mu^2}{4m_\pi^2} , \\ E_k^2 &= \frac{\left(m_\pi^2 - m_\mu^2 + m_k^2\right)^2}{4m_\pi^2} , \end{aligned} \qquad (5.72)$$

which satisfy $E_k^2 = p_k^2 + m_k^2$. It is straightforward to verify that neither the energies nor the momenta are equal for three neutrino mass eigenstates with non-degenerate masses.

The above paradox originates from the naive treatment of neutrino mass eigenstates as the plane waves. The reason is simply that particles are all generated via the production processes occurring in a finite space volume and a finite time interval, which exclude the plane-wave description. As a matter of fact, particles in the production, propagation and detection are the wave packets. In the wave-packet language the momenta of three neutrino

mass eigenstates are continuously distributed and highly peaked around the averaged values, so are the corresponding energies. After the elapsed time t and at the distance L from the source, the phase difference between the mass eigenstates $|\nu_k\rangle$ and $|\nu_j\rangle$ reads (Akhmedov and Smirnov, 2009)

$$\Delta\phi_{kj} = \left(E_k - E_j\right) t - \left(p_k - p_j\right) L \,, \tag{5.73}$$

where $E_j = \sqrt{p_j^2 + m_j^2}$ and $E_k = \sqrt{p_k^2 + m_k^2}$ hold. Expanding the energy difference in Eq. (5.73) in terms of the neutrino momentum and mass-squared differences, we have

$$\Delta E_{kj} \equiv E_k - E_j = v_g \Delta p_{kj} + \frac{\Delta m_{kj}^2}{2E} \,, \tag{5.74}$$

where v_g is the average group velocity, $E \equiv (E_k + E_j)/2$ denotes the average energy, and $\Delta p_{kj} \equiv p_k - p_j$ represents the momentum difference. Substituting Eq. (5.74) into Eq. (5.73), we obtain the phase difference

$$\Delta\phi_{kj} = \frac{\Delta m_{kj}^2}{2E} t - (L - v_g t) \Delta p_{kj} \,. \tag{5.75}$$

Alternatively, one may expand the momentum difference in Eq. (5.73) in terms of the energy and mass-squared differences:

$$\Delta p_{kj} = \frac{1}{v_g} \Delta E_{kj} - \frac{\Delta m_{kj}^2}{2p} \,, \tag{5.76}$$

where $p \equiv (p_k + p_j)/2$ is the average momentum. Inserting Eq. (5.76) into Eq. (5.73), one arrives at the phase difference

$$\Delta\phi_{kj} = \frac{\Delta m_{kj}^2}{2p} L - \frac{1}{v_g} (L - v_g t) \Delta E_{kj} \,. \tag{5.77}$$

It becomes evident that the phase difference in Eq. (5.75) can reduce to the conventional result $\Delta\phi_{kj} = \Delta m_{kj}^2 t/(2E)$ in Eq. (5.71) in the same momentum assumption. Likewise, $\Delta\phi_{kj}$ in Eq. (5.77) can reproduce the one in Eq. (5.69) in the same energy assumption. These two assumptions are unnecessary because the phase differences in Eq. (5.75) and (5.77) turn into the conventional ones if the condition $L = v_g t$ is fulfilled (Akhmedov and Smirnov, 2009). The interpretation of this condition is as follows: the center of the wave packet should be located around the detector at the distance L; namely, $|L - v_g t|$ should be smaller than the effective width of the wave packet σ_x, which depends on the production and detection of neutrinos. Beyond this range (i.e., $|L - v_g t| \gtrsim \sigma_x$) the neutrino wave functions will be highly suppressed, causing the oscillatory terms in $P(\nu_\alpha \to \nu_\beta)$ to disappear. One may therefore draw two conclusions: (1) the same energy and same momentum assumptions are

unnecessary; (2) the conventional formulas of neutrino oscillation probabilities are valid for relativistic neutrinos if the loss of quantum coherence, due to either the wave-packet separation or the localization of the source and detector, is negligible (Cohen *et al.*, 2009; Akhmedov and Smirnov, 2009).

Before discussing the quantum coherence in neutrino oscillations, we briefly review the interference phenomena and the concept of coherence in optics (Bonn and Wolf, 1980). In the famous Young's double-slit experiment, the light from a monochromatic source passes through two neighboring slits and finally arrives at the screen. It turns out that the light intensity on the screen varies between the minimum and maximum from point to point. The interference occurs due to the phase difference which develops for the two light beams from the slits with different optical paths. This is an elegant experiment to demonstrate the wave nature of light. However, any realistic light source is not exactly monochromatic. For instance, the excited gas can emit light whose spectrum consists of bright sharp lines. If one of these lines is input into the Michelson interferometer, one may observe the circular fringes. It has been found that the visibility of the fringes decreases as the optical path difference between two interfering beams increases. Suppose the real light is actually composed of wave trains, whose frequencies vary in the range of $\Delta\nu$ around the average value ν_0. It can be shown that the duration of the wave trains Δt and the frequency range $\Delta\nu$ fulfill the reciprocity relation $\Delta t \Delta\nu \gg 1/(4\pi)$, which is rather analogous to the Heisenberg uncertainty relation in quantum mechanics. Let us define the coherence length as (Bonn and Wolf, 1980)

$$l_{\rm coh} \equiv c\Delta t \sim \frac{c}{\Delta\nu} = \frac{\overline{\lambda}^2}{\Delta\lambda} \,, \tag{5.78}$$

where c is the speed of light in vacuum and $\overline{\lambda}$ is the average wave length. Hence the circular fringes disappear if the difference of the optical paths becomes much larger than the coherence length.

The quantum coherence in neutrino oscillations seems more complicated than the classical coherence in optics. It is still being debated that under which conditions the coherence of neutrino mass eigenstates is lost, for example, in the analysis of the GSI anomaly (Ivanov *el al.*, 2008; Giunti, 2008; Lipkin, 2008) or the Mössbauer neutrino oscillations (Akhmedov *et al.*, 2009; Bilenky *et al.*, 2009). But it becomes clear that the wave-packet approach is helpful and probably unavoidable in solving such problems (Kayser, 1981; Kiers *et al.*, 1996; Grimus and Stockinger, 1996; Campagne, 1997; Grimus *et al.*, 1998; Shtanov, 1998; Giunti, 2004) and other paradoxes (Akhmedov and Smirnov, 2009). A formal treatment of neutrino oscillations has also been performed in the framework of quantum field theories (Cardall and Chung, 1999; Ioannisian and Pilaftsis, 1999; Cardall, 2000; Beuthe, 2002; Giunti, 2002; Blasone *et al.*, 2002).

5.2.2 The Wave-packet Approach

Now we use the wave-packet language to describe neutrino oscillations. Let us suppose that neutrinos are initially produced via the weak charged-current interactions at the source. After propagating a distance L during the time T, they arrive at the detector and are detected via the weak charged-current interactions. Analogous to the spectral line of the real light, the neutrino mass eigenstates should be represented by the wave packets. For simplicity, we only consider the one-dimensional space x in the direction from the source to the detector. Since both the production and detection of neutrinos are localized in a finite space-time volume, we expect that a neutrino flavor eigenstate is a linear superposition of the wave packets of neutrino mass eigenstates. More explicitly, a neutrino flavor state at any time t can be written as (Giunti and Kim, 1998; Giunti *et al.*, 1993, 1998)

$$|\nu_\alpha(t)\rangle = \sum_{k=1}^{3} V_{\alpha k}^{*} \int \mathrm{d}p \; g_k^{\mathrm{s}}(p) \; \mathrm{e}^{-\mathrm{i}E_k(p)t} |\nu_k(p)\rangle \; , \tag{5.79}$$

where $E_k(p) = \sqrt{p^2 + m_k^2}$ is the neutrino energy for each momentum mode in the wave packet. The distribution function in the momentum space can be taken to be Gaussian:

$$g_k^{\mathrm{s}}(p) = \left[\frac{1}{2\pi(\sigma_p^{\mathrm{s}})^2}\right]^{1/4} \exp\left[-\frac{(p-p_k)^2}{4(\sigma_p^{\mathrm{s}})^2}\right] \; , \tag{5.80}$$

where p_k is the average momentum for the mass eigenstate $|\nu_k\rangle$, and σ_p^{s} is the momentum width of the wave packet. The superscript "s" reminds us of the wave packet at the source. Note that the neutrino mass eigenstates can have different average momenta p_k and energies $E_k \equiv E_k(p_k)$ in this wave-packet formulation. In the coordinate space $|\nu_k(p)\rangle = \mathrm{e}^{\mathrm{i}px}|\nu_k\rangle$ holds, and thus the neutrino wave function of the initial state reads

$$|\nu_\alpha(x,t)\rangle = \left[\frac{1}{2\pi(\sigma_x^{\mathrm{s}})^2}\right]^{1/4} \sum_{k=1}^{3} V_{\alpha k}^{*} \exp\left[\mathrm{i}\,(p_k x - E_k t) - \frac{(x-v_k t)^2}{4(\sigma_x^{\mathrm{s}})^2}\right] |\nu_k\rangle \tag{5.81}$$

with σ_x^{s} being the wave-packet width in the coordinate space. σ_x^{s} and σ_p^{s} are associated with each other via the uncertainty relation $\sigma_x^{\mathrm{s}}\sigma_p^{\mathrm{s}} = 1/2$. In addition, the group velocity of the wave packet is defined as

$$v_k \equiv \left.\frac{\mathrm{d}E_k(p)}{\mathrm{d}p}\right|_{p=p_k} = \frac{p_k}{E_k} \; . \tag{5.82}$$

So $E_k(p) \approx E_k + v_k(p-p_k)$ holds if the distribution function $g_k^{\mathrm{s}}(p)$ is sharply peaked at $p = p_k$ (i.e., $\sigma_p^{\mathrm{s}} \ll E_k^2/m_k$ is satisfied). The neutrino flavor state $|\nu_\beta\rangle$ at the detector is also a superposition of the wave packets of neutrino mass eigenstates:

$$|\nu_\beta\rangle = \sum_{j=1}^{3} V_{\beta j}^{*} \int \mathrm{d}p \; g_j^{\mathrm{d}}(p) |\nu_j(p)\rangle \; . \tag{5.83}$$

Here the distribution function $g_j^{\mathrm{d}}(p)$ can also be taken to be Gaussian, and it corresponds to the wave-packet width σ_p^{d} at the detector. Note that the flavor state $|\nu_\beta\rangle$ is to be experimentally identified at the detector, so we ignore its evolution in time. The corresponding wave function in the coordinate space can be figured out in a similar way:

$$|\nu_\beta(x-L)\rangle = \left[\frac{1}{2\pi(\sigma_x^{\mathrm{d}})^2}\right]^{1/4} \sum_{j=1}^{3} V_{\alpha j}^{*} \exp\left[\mathrm{i}p_j(x-L) - \frac{(x-L)^2}{4(\sigma_x^{\mathrm{d}})^2}\right] |\nu_j\rangle \; , \tag{5.84}$$

where L is the distance between the source and detector, and $\sigma_x^{\mathrm{d}} = 1/(2\sigma_p^{\mathrm{d}})$ denotes the wave-packet width in the coordinate space. The amplitude of $\nu_\alpha \to \nu_\beta$ transition is then given by the integration of $\langle \nu_\beta(x-L)|\nu_\alpha(x,T)\rangle$ over the coordinate x. We obtain

$$A_{\alpha\beta}(L,T) = \sqrt{\frac{2\sigma_x^{\mathrm{s}}\sigma_x^{\mathrm{d}}}{\sigma_x^2}} \sum_{j=1}^{3} V_{\alpha j}^{*} V_{\beta j} \exp\left[\mathrm{i}\left(p_j L - E_j T\right) - \frac{(L - v_j T)^2}{4\sigma_x^2}\right] \tag{5.85}$$

with $\sigma_x^2 = (\sigma_x^{\mathrm{s}})^2 + (\sigma_x^{\mathrm{d}})^2$. The oscillation probability $P_{\alpha\beta}(L,T) = |A_{\alpha\beta}(L,T)|^2$ turns out to be

$$\begin{aligned} P_{\alpha\beta}(L,T) \propto \sum_{j=1}^{3}\sum_{k=1}^{3} V_{\alpha j} V_{\beta k} V_{\alpha k}^{*} V_{\beta j}^{*} \exp\Big\{\mathrm{i}\left[(p_k - p_j)L - (E_k - E_j)T\right] \\ - \frac{1}{4\sigma_x^2}\left[(L - v_k T)^2 + (L - v_j T)^2\right]\Big\} \; . \end{aligned} \tag{5.86}$$

However, the arrival time of neutrinos at the detector has never been measured in current neutrino oscillation experiments. So one should average the oscillation probability over T. The integration over T is Gaussian too, and it can be performed by finding the minimum of the argument of the exponential function. The minimum is achieved at the point

$$T = \frac{(v_k + v_j)L}{v_k^2 + v_j^2} - \frac{2\mathrm{i}(E_k - E_j)\sigma_x^2}{v_k^2 + v_j^2} \; . \tag{5.87}$$

Substituting Eq. (5.87) into Eq. (5.86) and imposing the normalization condition $P_{\alpha e}(L) + P_{\alpha\mu}(L) + P_{\alpha\tau}(L) = 1$, we can get the oscillation probability (Giunti and Kim, 1998; Giunti, 2002; Giunti and Kim, 2007)

$$P_{\alpha\beta}(L) = \sum_{j=1}^{3} |V_{\alpha j}|^2 |V_{\beta j}|^2 + 2\mathrm{Re}\sum_{j<k} V_{\alpha j} V_{\beta k} V_{\alpha k}^{*} V_{\beta j}^{*} \exp\left[-\mathrm{i}\frac{2\pi L}{\lambda_{kj}} - \left(\frac{L}{L_{kj}^{\mathrm{coh}}}\right)^2\right.$$

$$-2\pi^2(1-\xi)\left(\frac{\sigma_x}{\lambda_{kj}}\right)^2\Bigg] \; , \tag{5.88}$$

where ξ is defined via $E_j = E + \xi m_j^2/(2E)$ with E being the average energy of neutrinos in the production process (when $m_j^2 \to 0$), $\lambda_{kj} \equiv 4\pi E/\Delta m_{kj}^2$ denote the neutrino oscillation lengths, and $L_{kj}^{\rm coh} \equiv 4\sqrt{2}\,\sigma_x E^2/|\Delta m_{kj}^2|$ stand for the coherence lengths. Comparing between Eq. (5.88) and Eq. (5.5), we observe that there are two additional terms in the exponential in the wave-packet approach. When the conditions $\sigma_x \ll \lambda_{kj}$ and $L \ll L_{kj}^{\rm coh}$ are satisfied, however, Eq. (5.88) can reproduce Eq. (5.5). Let us give some comments on the physical implications of these two extra terms (Giunti and Kim, 2007).

(1) The coherence of neutrino mass eigenstates is determined by the sizes of $L/L_{kj}^{\rm coh}$ and σ_x/λ_{kj}. All the current neutrino oscillation experiments satisfy the conditions $\sigma_x \ll \lambda_{kj}$ and $L \ll L_{kj}^{\rm coh}$, so the plane-wave treatment of neutrino oscillations is accurate enough and can lead to the correct result.

(2) If $L \gg L_{kj}^{\rm coh}$ holds, the separation between different neutrino wave packets is larger than the effective wave-packet width σ_x. In this case the interference among neutrino mass eigenstates disappears and the oscillatory terms in Eq. (5.88) are exponentially suppressed, so the probabilities of neutrino oscillations are just given by the first term in Eq. (5.88). A similar result has been obtained in Eq. (5.6), where the probabilities are averaged over the neutrino energy spectrum and propagation distances.

(3) If $\sigma_x \gg \lambda_{kj}$ is satisfied, we have $\sigma_x^{\rm s} \gg \lambda_{kj}$ or $\sigma_x^{\rm d} \gg \lambda_{kj}$ or both. In each case neutrino oscillations have already taken place within the source or the detector. As a result, the oscillatory phenomena cannot be observed because of the exponential suppression.

(4) It has been pointed out that the detection may restore the coherence of neutrino mass eigenstates (Kiers *et al.*, 1996). This observation comes from the last term in the exponential in Eq. (5.88). Suppose the energy resolution becomes more accurate, then the momentum uncertainty $\sigma_p^{\rm d}$ becomes smaller. In this case σ_x gets larger, so does the coherence lengths $L_{kj}^{\rm coh} \propto \sigma_x$. It is in practice difficult to observe such a restoration of coherence because of an average over the energy resolution and detection position.

5.2.3 Coherence of Cosmic Neutrinos

If neutrino mass eigenstates are incoherent at the detector, or if the detection of neutrinos has to average the oscillation probabilities over the neutrino energy spectra and propagation distances, the neutrino flavor conversion is just described by the classical probabilities as given in Eq. (5.6). The detection of neutrino oscillations depends both on the coherence of neutrinos and on the experimental setup. Concerning the first condition, one ought to carefully examine the production processes and properties of neutrino sources, and then

determine the widths of neutrino wave packets. The experimental setup for neutrino detection is also important. As we have mentioned, the arrival time of neutrinos at the detector is not measured in current neutrino oscillation experiments. If the energy resolution is so accurate that the neutrino mass eigenstate arriving at the detector can be determined, one will be unable to observe neutrino oscillations (Kayser, 1981). In the following let us examine the coherence of neutrinos from various sources. Such an analysis is very crucial in the discussion of ultrahigh-energy cosmic neutrino oscillations.

In the coordinate space the wave-packet width of neutrinos is σ_x, which is related to the momentum width σ_p through the uncertainty relation $\sigma_x \sim \sigma_p^{-1}$. On the other hand, the group velocity of the wave packet corresponding to the neutrino mass eigenstate $|\nu_k\rangle$ is given by $v_k = p_k/E_k$. Thus a difference between two group velocities of neutrino mass eigenstates reads

$$\Delta v_{kj} = \frac{p_k}{E_k} - \frac{p_j}{E_j} = \frac{\Delta m_{jk}^2}{2E^2} \; , \tag{5.89}$$

where $\Delta m_{jk} \equiv m_j^2 - m_k^2$ and $E \equiv (E_k + E_j)/2$. For simplicity, we only concentrate on the order-of-magnitude estimation by considering two neutrino flavors and omitting all the subscripts. Then Eq. (5.89) can be written as $\Delta v = \Delta m^2/(2E^2)$. After a propagation distance L, the separation between two wave packets is

$$d_L = \frac{L}{v}\Delta v = \frac{\Delta m^2}{2E^2} L \; , \tag{5.90}$$

where v is the average group velocity. If this separation significantly exceeds the wave-packet width (i.e., $d_L \gg \sigma_x$), there will be no overlap between the wave packets of two neutrino mass eigenstates, implying that the coherence will be lost. With the help of Eq. (5.90), one may convert the condition $d_L \gg \sigma_x$ into the following form:

$$L \gg \frac{2E^2\sigma_x}{\Delta m^2} \sim L_{\rm coh} \; , \tag{5.91}$$

where the coherence length is defined as $L_{\rm coh} \equiv 4\pi E^2\sigma_x/\Delta m^2$. Note that the coherence lengths defined in Eq. (5.88) are subject to the case of Gaussian wave packets. The condition for the coherence loss in Eq. (5.91) is consistent with the discussions below Eq. (5.88), where $L \gg L_{\rm coh}$ leads to a high suppression of the oscillatory terms. For simplicity, we ignore the spread of the wave packet caused by the presence of different momentum modes. Note also that the wave-packet width σ_x in question is actually $\sigma_x^{\rm s}$, the width associated with the production mechanism at the source. Although the coherence may be restored at the detector with an excellent energy resolution, an average over the location of the source erases the oscillations. Hence we focus on the production of neutrinos and the wave-packet width at the source.

Let us consider muon neutrinos and antineutrinos from $\pi^+ \to \mu^+ + \nu_\mu$ and $\pi^- \to \mu^- + \overline{\nu}_\mu$ decays, which might be the dominant production mechanism of cosmic neutrinos at a variety of astrophysical sources. In the rest frame of the pion, the neutrino energy has been given in Eq. (5.72). Neglecting small neutrino masses, one may obtain $E^0_\nu = (m^2_\pi - m^2_\mu)/(2m_\pi)$. In such decay modes the wave-packet width of the final-state particle can be estimated from the lifetime of the decaying particle (Nussinov, 1976; Kayser, 1981). For the neutrinos emitted from $\pi^\pm$ decays in the forward direction, we have (Farzan and Smirnov, 2008)

$$\sigma^\pi_x = \frac{\tau_\pi}{\gamma} \approx \frac{E^0_\nu}{E_\nu}\tau_\pi \sim \frac{(m^2_\pi - m^2_\mu)}{2m_\pi E_\nu}\tau_\pi \,, \tag{5.92}$$

where $\tau_\pi = 2.6 \times 10^{-8}$ s is the lifetime of the pion at rest, E_ν is the neutrino energy in the observer's frame, and γ denotes the Lorentz boost factor for a transformation from the rest frame of the decaying pion to the observer's frame. One may follow a similar way to estimate the wave-packet width σ^μ_x for the neutrinos emitted from $\mu^\pm$ decays: $\mu^+ \to e^+ + \overline{\nu}_\mu + \nu_e$ and $\mu^- \to e^- + \nu_\mu + \overline{\nu}_e$. Compared with the width in Eq. (5.92), σ^μ_x is enhanced by a factor $\tau_\mu/\tau_\pi \sim 10^2$, where $\tau_\mu = 2.2 \times 10^{-6}$ s is the lifetime of the muon at rest. The ratio of the wave-packet separation to the wave-packet width turns out to be (Farzan and Smirnov, 2008)

$$\frac{d_L}{\sigma^\pi_x} = \frac{\Delta m^2 m_\pi L}{(m^2_\pi - m^2_\mu)E_\nu \tau_\pi} \,, \tag{5.93}$$

which can be further expressed as

$$\frac{d_L}{\sigma^\pi_x} \sim 0.1 \times \frac{\Delta m^2}{8 \times 10^{-5}\ \mathrm{eV}^2} \cdot \frac{L}{100\ \mathrm{Mpc}} \cdot \frac{10\ \mathrm{TeV}}{E_\nu} \cdot \frac{2.6 \times 10^{-8}\ \mathrm{s}}{\tau_\pi} \,. \tag{5.94}$$

Given the cosmic neutrinos with energies $E \sim 10$ TeV and from certain astrophysical sources at the distances $L \sim 100$ Mpc, the quantum coherence is maintained because the condition $d_L \sim \sigma^\pi_x$ holds as shown in Eq. (5.94). This is always the case for the neutrinos from $\mu^\pm$ decays, whose wave-packet width σ^μ_x is much larger than σ^π_x. Although the coherence is not lost, the oscillatory pattern of ultrahigh-energy cosmic neutrinos from a very distant astrophysical source must disappear. The reason is simply that the distance L between the source and the detector is much longer than the neutrino oscillation length λ_{kj}, so the probabilities of neutrino oscillations have to be averaged over many circles of oscillations and finally take the classical form as given in Eq. (5.6).

However, the simple picture of free particle decays cannot be realized in most astrophysical environments. In a realistic case the pions and muons must interact with the ambient matter, such as photons. The wave-packet widths are then determined by the distance or the time between two successive collisions. Furthermore, it is found that the magnetic fields can significantly affect

the wave-packet widths of neutrinos (Farzan and Smirnov, 2008). The size of a wave packet is in principle possible to be measured by using the time information for a non-stationary beam (Stodolsky, 1998).

5.3 Density Matrix Formulation

In this section we introduce an instructive and useful language, the density matrix and flavor polarization vector, to describe neutrino oscillations. In particular, the phenomenon of two-flavor neutrino oscillations can be visualized as the motion of a magnetic moment precessing about an external magnetic field. The terms of neutrino masses and matter effects correspond to different kinds of external magnetic fields in this formulation, in which the decoherence effects arising from the interactions of neutrinos with media can be easily incorporated.

Let us start with a brief review of the density matrix formalism in quantum mechanics. One may in general encounter two types of physical systems: (1) its state is perfectly known from the wave function $\Psi(t)$; (2) it is the subsystem of a larger one, and in principle does not have a wave function (Landau and Lifshitz, 1977). In the first case we can expand the state vector $|\Psi(t)\rangle$ in terms of a complete series of eigenvectors of the Hamiltonian:

$$|\Psi(t)\rangle = \sum_n C_n(t)|n\rangle \ , \tag{5.95}$$

where the eigenstates $|n\rangle$ are orthogonal, and the coefficients $C_n(t)$ satisfy the normalization condition $|C_1(t)|^2 + \cdots + |C_n(t)|^2 = 1$. The expectation value of an operator $\hat{O}$ reads

$$\langle \hat{O} \rangle = \langle \Psi(t)|\hat{O}|\Psi(t)\rangle = \sum_m \sum_n C_n(t) C_m^*(t) \langle m|\hat{O}|n\rangle \ , \tag{5.96}$$

where $\langle m|\hat{O}|n\rangle \equiv \hat{O}_{mn}$ is the matrix element of the operator. The evolution of this system is governed by the Schrödinger equation

$$\mathrm{i}\frac{\partial}{\partial t}|\Psi(t)\rangle = \mathcal{H}|\Psi(t)\rangle \ . \tag{5.97}$$

Now we define the density operator as follows:

$$\rho(t) \equiv |\Psi(t)\rangle\langle\Psi(t)| = \sum_m \sum_n C_n(t) C_m^*(t) |n\rangle\langle m| \ . \tag{5.98}$$

It is easy to verify that the density matrix ρ is Hermitian, and its elements are given as $\rho_{nm} = C_n(t) C_m^*(t)$. Combining Eqs. (5.96) and (5.98), we obtain

$$\langle \hat{O} \rangle = \sum_m \sum_n \rho_{nm} \hat{O}_{mn} = \mathrm{Tr}\left[\rho \hat{O}\right] \ . \tag{5.99}$$

Furthermore, the evolution equation of the density operator can be derived from the Schrödinger equation

$$\mathrm{i}\frac{\partial\rho}{\partial t} = \left[\mathrm{i}\frac{\partial}{\partial t}|\Psi(t)\rangle\right]\langle\Psi(t)| + |\Psi(t)\rangle\left[\mathrm{i}\frac{\partial}{\partial t}\langle\Psi(t)|\right] = [\mathcal{H},\rho] \ . \tag{5.100}$$

Hence the density matrix description is equivalent to the wave function language for a system with pure states. Two basic properties of ρ are $\mathrm{Tr}[\rho] = 1$ and $\rho^2 = \rho$. For an ensemble with mixed states, the probability for it to be in the state $\Psi^i(t)$ is P_i and the corresponding density operator is defined by

$$\rho \equiv \sum_i P_i|\Psi^i(t)\rangle\langle\Psi^i(t)| = \sum_i\sum_m\sum_n P_i C_n^i C_m^{i*}|n\rangle\langle m| \ . \tag{5.101}$$

In this case the density matrix satisfies $\mathrm{Tr}[\rho^2] < 1$. An application of the density matrix formulation to neutrino oscillations will be discussed in the two- and three-flavor mixing schemes, respectively.

5.3.1 Two-flavor Neutrino Oscillations

With the help of the density matrix formulation, the phenomenon of two-flavor neutrino oscillations can be understood in a pictorial way which is very analogous to the magnetic moment precessing in a magnetic field. Let us first consider the propagation of a stationary neutrino beam in vacuum. The flavor eigenstates $|\nu_e\rangle$ and $|\nu_\mu\rangle$ are related to the mass eigenstates $|\nu_1\rangle$ and $|\nu_2\rangle$ via the following unitary transformation:

$$\begin{pmatrix}|\nu_e\rangle\\ |\nu_\mu\rangle\end{pmatrix} = U\begin{pmatrix}|\nu_1\rangle\\ |\nu_2\rangle\end{pmatrix} \equiv \begin{pmatrix}\cos\theta & \sin\theta\\ -\sin\theta & \cos\theta\end{pmatrix}\begin{pmatrix}|\nu_1\rangle\\ |\nu_2\rangle\end{pmatrix} \ . \tag{5.102}$$

Since two free neutrinos propagate in their mass eigenstates $|\nu_i\rangle$ with definite masses m_i (for $i = 1, 2$), the evolution equation of $|\nu_i(t)\rangle$ can simply be derived from Eq. (5.97):

$$\mathrm{i}\frac{\mathrm{d}}{\mathrm{d}t}\begin{pmatrix}|\nu_1(t)\rangle\\ |\nu_2(t)\rangle\end{pmatrix} = \frac{1}{2E}\begin{pmatrix}m_1^2 & 0\\ 0 & m_2^2\end{pmatrix}\begin{pmatrix}|\nu_1(t)\rangle\\ |\nu_2(t)\rangle\end{pmatrix} \ , \tag{5.103}$$

where the excellent approximation $E_i \approx p + m_i^2/(2p)$ due to $p \approx E \gg m_i$ has been taken for relativistic neutrinos. Multiplying the left- and right-hand sides of Eq. (5.103) by U, we obtain

$$\mathrm{i}\frac{\mathrm{d}}{\mathrm{d}t}\begin{pmatrix}|\nu_e(t)\rangle\\ |\nu_\mu(t)\rangle\end{pmatrix} = \frac{1}{2E}U\begin{pmatrix}m_1^2 & 0\\ 0 & m_2^2\end{pmatrix}U^\dagger\begin{pmatrix}|\nu_e(t)\rangle\\ |\nu_\mu(t)\rangle\end{pmatrix} \ . \tag{5.104}$$

Then the effective Hamiltonian in the flavor basis can be written as

$$\mathcal{H}_\mathrm{v} = \frac{1}{2E}U\begin{pmatrix}m_1^2 & 0\\ 0 & m_2^2\end{pmatrix}U^\dagger = \frac{m_1^2+m_2^2}{4E}\mathbf{1} + \frac{\Delta m^2}{4E}\begin{pmatrix}-\cos 2\theta & \sin 2\theta\\ \sin 2\theta & \cos 2\theta\end{pmatrix} \tag{5.105}$$

with $\Delta m^2 \equiv m_2^2 - m_1^2$. Without loss of generality, we take $\Delta m^2 > 0$ and allow θ to vary in the range $0 \leqslant \theta \leqslant \pi/2$.

Note that the term proportional to the identity matrix in $\mathcal{H}_{\rm v}$ can always be omitted, because it does not affect flavor conversions. After discarding this term, we may further expand $\mathcal{H}_{\rm v}$ in terms of the Pauli matrices:

$$\mathcal{H}_{\rm v} = \frac{\omega_p}{2} \mathbf{B} \cdot \boldsymbol{\sigma} \; , \tag{5.106}$$

where $\omega_p \equiv \Delta m^2/(2E)$, $\mathbf{B} \equiv (\sin 2\theta, 0, -\cos 2\theta)$ and $\boldsymbol{\sigma} \equiv (\sigma_x, \sigma_y, \sigma_z)$. Given the state vector $|\Psi(t)\rangle = a_e(t)|\nu_e\rangle + a_\mu(t)|\nu_\mu\rangle$, the density matrix defined in Eq. (5.98) turns out to be

$$\rho = \begin{pmatrix} |a_e|^2 & a_e a_\mu^* \\ a_\mu a_e^* & |a_\mu|^2 \end{pmatrix} \; . \tag{5.107}$$

The diagonal elements $|a_e|^2$ and $|a_\mu|^2$ give the probabilities for the system to be in the flavor states $|\nu_e\rangle$ and $|\nu_\mu\rangle$, respectively. The off-diagonal elements encode the information on quantum coherence between two flavor states. Because an arbitrary 2×2 Hermitian matrix can always be expanded in terms of the identity matrix and three Pauli matrices, we rewrite the expression of ρ in Eq. (5.107) as (Fano, 1957)

$$\rho = \frac{1}{2} \left(1 + \mathbf{P} \cdot \boldsymbol{\sigma} \right) \; , \tag{5.108}$$

where $\mathbf{P}$ is the so-called flavor polarization vector. Now that the diagonal elements of ρ give the probabilities, the physical meaning of $\mathbf{P}$ is then transparent: its z-component P_z is related to the probabilities through [4]

$$|a_e|^2 = \frac{1}{2} \left(1 + P_z \right) \; , \qquad |a_\mu|^2 = \frac{1}{2} \left(1 - P_z \right) \; . \tag{5.109}$$

Prepared with the new formulation of $\mathcal{H}_{\rm v}$ in Eq. (5.106) and ρ in Eq. (5.108), we recast the evolution equation in Eq. (5.100) into a more suggestive form:

$$\mathrm{i}\dot{\rho}(t) = [\mathcal{H}_{\rm v}, \rho(t)] = \frac{\omega_p}{4} \sum_j \sum_k \left[\sigma_j, \sigma_k \right] B_j P_k(t) = \mathrm{i} \frac{\omega_p}{2} \left[\mathbf{B} \times \mathbf{P}(t) \right] \cdot \boldsymbol{\sigma} \; , \tag{5.110}$$

where the commutation relation $[\sigma_j, \sigma_k] = 2\mathrm{i}\sigma_l$ (for j, k, l to run over $1, 2, 3$ cyclically) has been used. Then Eqs. (5.108) and (5.110) lead us to the desired form of the evolution equation of $\mathbf{P}(t)$ (Fano, 1957; Raffelt, 1996):

$$\frac{\mathrm{d}}{\mathrm{d}t} \mathbf{P}(t) = \omega_p \mathbf{B} \times \mathbf{P}(t) \; . \tag{5.111}$$

[4] We have defined $\mathbf{P} = (P_x, P_y, P_z)$ and $\boldsymbol{\sigma} = (\sigma_x, \sigma_y, \sigma_z)$. Sometimes it is more convenient to denote the Pauli matrices as $(\sigma_1, \sigma_2, \sigma_3)$. These two notations are equivalent and will be alternatively used in this section.

Hence neutrino oscillations can be described by the evolution of the flavor polarization vector. To make the physical meaning of $\mathbf{P}(t)$ clearer, we assume the initial state of a neutrino beam to be purely composed of electron neutrinos; namely, $a_e(0) = 1$ and $a_\mu(0) = 0$. Eqs. (5.107) and (5.108) allow one to determine the initial value of the polarization vector: $\mathbf{P}(0) = (0, 0, 1)$. If the polarization vector points upward (downward), the state is purely an electron (muon) neutrino. On the other hand, Eq. (5.111) means that the length of $\mathbf{P}(t)$ keeps unchanged in the evolution; i.e., $|\mathbf{P}(t)|^2 = 1$. To solve Eq. (5.111), we write out the evolution equation for each component of $\mathbf{P}(t)$:

$$\frac{\mathrm{d}}{\mathrm{d}t}(P_x, P_y, P_z) = \omega_p(P_y \cos 2\theta, -P_z \sin 2\theta - P_x \cos 2\theta, P_y \sin 2\theta) \ . \quad (5.112)$$

Given the initial conditions $\mathbf{P}(0) = (0, 0, 1)$ and $\dot{\mathbf{P}}(0) = (0, -\omega_p \sin 2\theta, 0)$, the above equation can be exactly solved. For example, we obtain

$$P_z(t) = 1 - 2\sin^2 2\theta \sin^2 \frac{\omega_p t}{2} \quad (5.113)$$

for the z-component. This result, together with Eq. (5.109), leads to the survival probability of the electron neutrinos:

$$P(\nu_e \to \nu_e) = |a_e(t)|^2 = 1 - \sin^2 2\theta \sin^2 \frac{\omega_p t}{2} \ . \quad (5.114)$$

Taking $t = L$ in the natural unit system, we see that Eq. (5.114) is consistent with Eq. (5.9). The evolution of the polarization vector is shown in Fig. 5.2. At the beginning $\mathbf{P}$ is located along the z-axis with $\mathbf{P}(0) = (0, 0, 1)$. Then it rotates about the axis in the direction of $\mathbf{B} = (\sin 2\theta, 0, -\cos 2\theta)$, and its angular velocity is simply ω_p. The projection of $\mathbf{P}(t)$ on the z-axis gives rise to the survival probability, as indicated in Eqs. (5.113) and (5.114).

So far we have dealt with the case of $\Delta m^2 > 0$ and $0 \leqslant \theta \leqslant \pi/4$ (the the normal neutrino mass hierarchy). Note that the case of $\Delta m^2 < 0$ and $0 \leqslant \theta \leqslant \pi/4$ (the inverted neutrino mass hierarchy) is equivalent to the case of $\Delta m^2 > 0$ and $\pi/4 \leqslant \theta \leqslant \pi/2$. For the latter case, one may define $\theta' \equiv \pi/2 - \theta$ and replace θ with $\pi/2 - \theta'$ in the effective Hamiltonian. As a consequence, the direction of the magnetic field becomes $\mathbf{B} = (\sin 2\theta', 0, \cos 2\theta')$ which is now lying in the first quadrant of the (x, z) plane. The survival probability in Eq. (5.114) keeps unchanged, as it should be. All the above discussions are applicable for antineutrino-antineutrino oscillations.

We proceed to include the matter effects in the density matrix formulation. The Schrödinger-like equation for neutrinos propagating in ordinary matter has been given in Section 5.1. The matter effects can be described by the effective potential $\mathcal{V} = \sqrt{2} G_{\rm F} n_e$, which linearly contributes to the effective Hamiltonian $\mathcal{H}_{\rm m}$ in matter:

$$\mathcal{H}_{\rm m} - \mathcal{H}_{\rm v} = \sqrt{2}\, G_{\rm F} n_e \begin{pmatrix} 1 & 0 \\ 0 & 0 \end{pmatrix} = \frac{G_{\rm F} n_e}{\sqrt{2}} \mathbf{1} + \frac{G_{\rm F} n_e}{\sqrt{2}} \begin{pmatrix} 1 & 0 \\ 0 & -1 \end{pmatrix} \ . \quad (5.115)$$

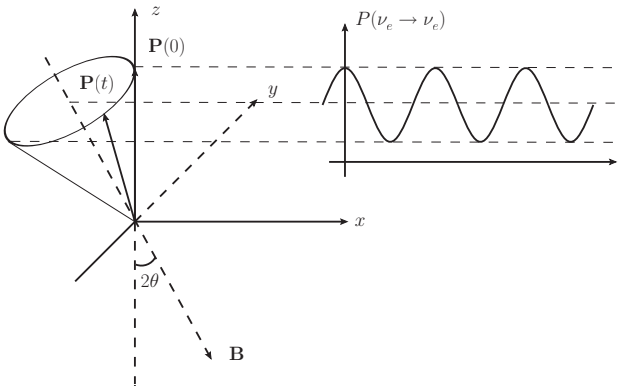

Fig. 5.2 The evolution of the polarization vector $\mathbf{P}(t)$ in the flavor space, where $\mathbf{P}(0) = (0, 0, 1)$ is the initial condition and the magnetic field is in the direction of $\mathbf{B} = (\sin 2\theta, 0, -\cos 2\theta)$ with θ being the neutrino mixing angle in vacuum

The first term on the right-hand side of Eq. (5.115) can be omitted because it is irrelevant to neutrino flavor conversions. Then we rewrite the above equation in terms of the Pauli matrices as

$$\mathcal{H}_{\rm m} - \mathcal{H}_{\rm v} = \frac{\lambda}{2} \mathbf{L} \cdot \boldsymbol{\sigma} \; , \tag{5.116}$$

where $\lambda \equiv \sqrt{2} G_{\rm F} n_e$, and $\mathbf{L} = (0, 0, 1)$ is the unit vector along the positive z-axis. In a way similar to the derivation of Eq. (5.111), the evolution equation of the polarization vector in matter is found to be

$$\frac{\mathrm{d}}{\mathrm{d}t} \mathbf{P}(t) = \left(\omega_p \mathbf{B} + \lambda \mathbf{L} \right) \times \mathbf{P}(t) \; . \tag{5.117}$$

We see that matter effects are equivalent to a new magnetic field in the direction of the z-axis. If the matter density is a constant, the behavior of neutrino flavor conversions turns out to be very similar to that in vacuum. In this case the matter-corrected neutrino mixing angle and frequency are denoted as $\theta_{\rm m}$ and $\omega_p^{\rm m}$, respectively. They are related to their counterparts in vacuum through $\omega_p \mathbf{B} + \lambda \mathbf{L} \equiv \omega_p^{\rm m} \mathbf{B}^{\rm m}$ with $\mathbf{B}^{\rm m} \equiv (\sin 2\theta_{\rm m}, 0, -\cos 2\theta_{\rm m})$. A straightforward calculation yields

$$\omega_p^{\rm m} = \sqrt{\omega_p^2 + \lambda^2 - 2\lambda \omega_p \cos 2\theta} \; , \quad \tan 2\theta_{\rm m} = \frac{\omega_p \sin 2\theta}{\omega_p \cos 2\theta - \lambda} \; . \tag{5.118}$$

Note that $\omega_p^{\rm m}$ can be defined as $\omega_p^{\rm m} \equiv \Delta \tilde{m}^2 / (2E)$ with $\Delta \tilde{m}^2$ being the effective neutrino mass-squared difference in matter. Note also that Eq. (5.117) can be rewritten as $\dot{\mathbf{P}}(t) = \omega_p^{\rm m} \mathbf{B}^{\rm m} \times \mathbf{P}(t)$. If the matter density is extremely small (i.e., $\lambda \to 0$), one may easily reproduce neutrino oscillations in vacuum from Eqs. (5.117) and (5.118). In the $\lambda \to +\infty$ limit we can obtain

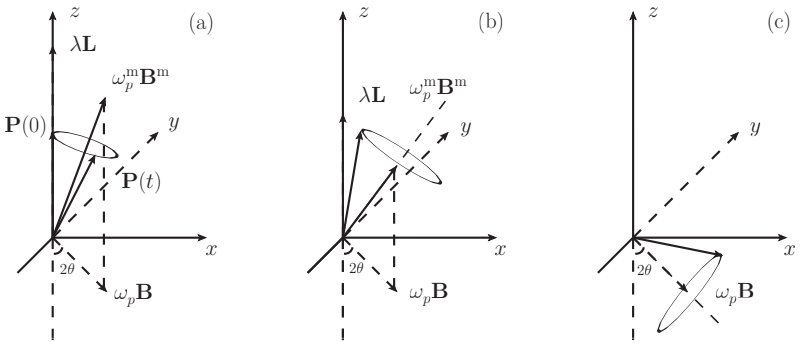

Fig. 5.3 The visualization of two-flavor neutrino oscillations in matter: (a) at the beginning the matter density is very large and $\mathbf{P}(0) = (0, 0, 1)$ holds, so the polarization vector $\mathbf{P}(t)$ rotates around the effective magnetic field $\mathbf{B}^{\rm m} = (\sin 2\theta_{\rm m}, 0, -\cos 2\theta_{\rm m})$; (b) as the matter density decreases, $\mathbf{P}(t)$ turns to rotate around the new magnetic field $\mathbf{B}^{\rm m}$; (c) after the matter density approaches zero, $\mathbf{B}^{\rm m}$ approaches $\mathbf{B}$ and $\mathbf{P}(t)$ rotates around $\mathbf{B}$ but spins down

$\tan 2\theta_{\rm m} \to 0^-$, or equivalently $\theta_{\rm m} \to \pi/2$, from Eq. (5.118). This limit implies that the heavier mass eigenstate $\tilde{\nu}_2$ dominates in the electron flavor state ν_e. In the $\cos 2\theta > 0$ case, which corresponds to the normal neutrino mass hierarchy, one has $\theta_{\rm m} = \pi/4$ if the resonant condition $\lambda = \omega_p \cos 2\theta$ is satisfied. In the $\cos 2\theta < 0$ case, which is equivalent to the inverted neutrino mass hierarchy, there is no resonance associated with $\tan 2\theta_{\rm m}$. Hence we anticipate that matter effects should be helpful in fixing the mass ordering of neutrinos. This is actually the case in solar neutrino oscillation experiments.

In many astrophysical environments the matter densities are not constant. For simplicity, we consider a slowly-varying matter density profile which finds proper applications both in the Sun and in some supernovae. Such a density profile allows us to make the adiabatic approximation. In this approximation the effective magnetic field $\mathbf{B}^{\rm m}$ changes its direction very slowly, as compared with the rotation of $\mathbf{P}(t)$ around $\mathbf{B}^{\rm m}$. Fig. 5.3 illustrates three typical stages of this process, which actually takes place for neutrinos propagating in the Sun. The situation is quite different from the case of a constant matter density profile, because the initial neutrino flavor can be significantly changed and this change is represented by the polarization vector pointing to the negative z-axis as shown in Fig. 5.3(c). One may exactly solve P_z from the evolution equation in Eq. (5.117), but its solution involves a time-dependent coefficient $\lambda(t)$. An intuitive interpretation of matter effects is as follows. If the matter density and the corresponding magnetic field change slowly in comparison with the rotation of the polarization vector, then the latter has enough time to catch up with the magnetic field and keeps the open angle intact. Initially, the polarization vector $\mathbf{P}$ is almost aligned with $\mathbf{B}^{\rm m}$ because

of the high matter density at the production point. It will be aligned with **B** after the matter density decreases to zero. So $P_z = -\cos 2\theta$ holds and the survival probability is the same as that given in Eq. (5.27). The non-adiabatic case, which has been discussed in Section 5.1.3, can also be treated in this geometrical representation (Kim *et al.*, 1988).

5.3.2 Three-flavor Neutrino Oscillations

One may generalize the above density matrix formulation to describe three-flavor neutrino oscillations. In this more realistic case the neutrino flavor eigenstates $(\nu_e, \nu_\mu, \nu_\tau)$ are linked to their mass eigenstates (ν_1, ν_2, ν_3) via a 3×3 unitary matrix V, which has been parametrized in Eq. (3.107). The Majorana phases of V are irrelevant to neutrino oscillations and thus can be omitted in our discussions. Then we have

$$\begin{pmatrix} \nu_e \\ \nu_\mu \\ \nu_\tau \end{pmatrix} = \begin{pmatrix} 1 & 0 & 0 \\ 0 & c_{23} & s_{23} \\ 0 & -s_{23} & c_{23} \end{pmatrix} \begin{pmatrix} c_{13} & 0 & s_{13}\mathrm{e}^{-\mathrm{i}\delta} \\ 0 & 1 & 0 \\ -s_{13}\mathrm{e}^{\mathrm{i}\delta} & 0 & c_{13} \end{pmatrix} \begin{pmatrix} c_{12} & s_{12} & 0 \\ -s_{12} & c_{12} & 0 \\ 0 & 0 & 1 \end{pmatrix} \begin{pmatrix} \nu_1 \\ \nu_2 \\ \nu_3 \end{pmatrix} \; . \tag{5.119}$$

Since the CP-violating phase δ is entirely unrestricted, we may tentatively switch it off. Furthermore, we define a convenient flavor basis:

$$\begin{pmatrix} \nu_e \\ \nu_x \\ \nu_y \end{pmatrix} = \begin{pmatrix} 1 & 0 & 0 \\ 0 & c_{23} & -s_{23} \\ 0 & s_{23} & c_{23} \end{pmatrix} \begin{pmatrix} \nu_e \\ \nu_\mu \\ \nu_\tau \end{pmatrix} \; . \tag{5.120}$$

This basis is also convenient for discussing three-flavor neutrino oscillations in matter, because muon and tau neutrinos have the same interactions with ordinary matter. In this basis we can write the effective Hamiltonian $\mathcal{H}_\mathrm{v}$ as

$$\omega_p^\mathrm{L} \begin{pmatrix} s_{12}^2 c_{13}^2 & s_{12} c_{12} c_{13} & -s_{12}^2 c_{13} s_{13} \\ s_{12} c_{12} c_{13} & c_{12}^2 & -s_{12} c_{12} s_{13} \\ -s_{12}^2 s_{13} c_{13} & -s_{12} c_{12} s_{13} & s_{12}^2 s_{13}^2 \end{pmatrix} + \omega_p^\mathrm{H} \begin{pmatrix} s_{13}^2 & 0 & c_{13} s_{13} \\ 0 & 0 & 0 \\ c_{13} s_{13} & 0 & c_{13}^2 \end{pmatrix} \; , \tag{5.121}$$

where $\omega_p^\mathrm{H} \equiv \Delta m_{31}^2/(2p)$ and $\omega_p^\mathrm{L} \equiv \Delta m_{21}^2/(2p)$ are the high- and low-level oscillation frequencies, respectively. Current experimental data yield $\Delta m_{31}^2 \approx 2.4 \times 10^{-3}$ eV^2 and $\Delta m_{21}^2 \approx 7.9 \times 10^{-5}$ eV^2, and thus $\omega_p^\mathrm{H} \gg \omega_p^\mathrm{L}$ for a given momentum mode. In other words, the term associated with ω_p^H is expected to be dominant in Eq. (5.121). In this case the three-flavor neutrino oscillations can approximate to the two-flavor neutrino oscillations with the high-level frequency ω_p^H and the mixing angle θ_{13}. Such an approximation has been extensively adopted in the study of flavor conversions of supernova neutrinos (Hannestad *et al.*, 2006; Duan *et al.*, 2006; Fogli *et al.*, 2007).

In the case of three-flavor neutrino mixing we have to deal with some 3×3 Hermitian matrices, such as the density matrix and the effective Hamiltonian. It is well known that an arbitrary 3×3 Hermitian matrix can be expanded in terms of the identity matrix and eight Gell-Mann matrices:

$$\Lambda_0 = \begin{pmatrix} 1 & 0 & 0 \\ 0 & 1 & 0 \\ 0 & 0 & 1 \end{pmatrix} , \quad \Lambda_1 = \begin{pmatrix} 0 & 1 & 0 \\ 1 & 0 & 0 \\ 0 & 0 & 0 \end{pmatrix} , \quad \Lambda_2 = \begin{pmatrix} 0 & -\mathrm{i} & 0 \\ \mathrm{i} & 0 & 0 \\ 0 & 0 & 0 \end{pmatrix} ,$$
$$\Lambda_3 = \begin{pmatrix} 1 & 0 & 0 \\ 0 & -1 & 0 \\ 0 & 0 & 0 \end{pmatrix} , \quad \Lambda_4 = \begin{pmatrix} 0 & 0 & 1 \\ 0 & 0 & 0 \\ 1 & 0 & 0 \end{pmatrix} , \quad \Lambda_5 = \begin{pmatrix} 0 & 0 & -\mathrm{i} \\ 0 & 0 & 0 \\ \mathrm{i} & 0 & 0 \end{pmatrix} ,$$
$$\Lambda_6 = \begin{pmatrix} 0 & 0 & 0 \\ 0 & 0 & 1 \\ 0 & 1 & 0 \end{pmatrix} , \quad \Lambda_7 = \begin{pmatrix} 0 & 0 & 0 \\ 0 & 0 & -\mathrm{i} \\ 0 & \mathrm{i} & 0 \end{pmatrix} , \quad \Lambda_8 = \frac{1}{\sqrt{3}} \begin{pmatrix} 1 & 0 & 0 \\ 0 & 1 & 0 \\ 0 & 0 & -2 \end{pmatrix} , \quad (5.122)$$

where the normalization of the Gell-Mann matrices is taken to be $\mathrm{Tr}\left[\Lambda_a \Lambda_b\right] = 2\delta_{ab}$ (for $a, b = 1, 2, \cdots, 8$). Note that the Gell-Mann matrices satisfy the $SU(3)$ Lie algebra; i.e., $[\Lambda_a, \Lambda_b] = \sum_c \mathrm{i} f_{abc} \Lambda_c$. Here the structure constants f_{abc} are antisymmetric with respect to any two indices, and those nonzero ones are given by

$$\frac{f_{123}}{2} = f_{147} = f_{165} = f_{246} = f_{257} = f_{345} = f_{376} = \frac{f_{458}}{\sqrt{3}} = \frac{f_{678}}{\sqrt{3}} = 1 \; . \quad (5.123)$$

An arbitrary 3×3 Hermitian matrix M can then be expanded as

$$M = \frac{1}{3} M_0 \Lambda_0 + \frac{1}{2} \mathbf{M} \cdot \boldsymbol{\Lambda} \equiv \frac{1}{3} M_0 \Lambda_0 + \frac{1}{2} \sum_{a=1}^{8} M_a \Lambda_a \; , \quad (5.124)$$

where $M_0 = \mathrm{Tr}\left[M \Lambda_0\right]$ and $M_a = \mathrm{Tr}\left[M \Lambda_a\right]$ (for $a = 1, 2, \cdots, 8$). Now we work in an eight-dimensional vector space spanned by eight unit vectors $\mathbf{e}_a$, so any vector $\mathbf{M}$ can be represented by its components M_a (i.e., $\mathbf{M} = M_1 \mathbf{e}_1 + \cdots + M_8 \mathbf{e}_8$). By means of this language, we have

$$\mathcal{H}_{\rm v} = \omega_p \left(\frac{1}{3} B_0 \Lambda_0 + \frac{1}{2} \mathbf{B} \cdot \boldsymbol{\Lambda} \right) \; , \quad (5.125)$$

where $\omega_p \equiv |\Delta m^2_{31}|/(2p) > 0$; and the "magnetic field $\mathbf{B}$" is given by

$$\mathbf{B} = 2\varepsilon s_{12} c_{12} c_{13} \mathbf{e}_1 + \left[s^2_{13} - \varepsilon (c^2_{12} - s^2_{12} c^2_{13}) \right] \mathbf{e}_2 + 2(1 - \varepsilon s^2_{12}) s_{13} c_{13} \mathbf{e}_4$$
$$- 2\varepsilon s_{12} c_{12} s_{13} \mathbf{e}_6 + \frac{1}{2\sqrt{3}} \left[(\varepsilon - 2)(3 c^2_{13} - 1) + 3\varepsilon s^2_{13} (2 c^2_{13} - 1) \right] \mathbf{e}_8 \quad (5.126)$$

with $\varepsilon \equiv \Delta m^2_{21} / \Delta m^2_{31}$. One has $\varepsilon > 0$ for $\Delta m^2_{31} > 0$ and $\varepsilon < 0$ for $\Delta m^2_{31} < 0$. In the latter case an overall minus sign should be introduced into the expression of $\mathbf{B}$. The three-flavor density matrix ρ can be written as

$$\rho(t) = \frac{1}{3} \Lambda_0 + \frac{1}{2} \mathbf{P}(t) \cdot \boldsymbol{\Lambda} \; , \quad (5.127)$$

where $\mathrm{Tr}[\rho] = 1$ holds as the normalization condition. Eqs. (5.125) and (5.127) allow one to work out the evolution equation of the polarization vector $\mathbf{P}(t)$:

$$\frac{\mathrm{d}}{\mathrm{d}t}\mathbf{P}(t) = \omega_p \mathbf{B} \times \mathbf{P}(t) \equiv \omega_p \sum_{a=1}^{8} \sum_{b=1}^{8} f_{abc} B_a P_b(t) \mathbf{e}_c \; , \tag{5.128}$$

which is a direct generalization of Eq. (5.111) to the three-flavor case. In order to understand the physical meaning of $\mathbf{P}(t)$, we consider a beam of ν_α neutrinos in the pure flavor state propagating in vacuum. The state vector of this system can be written as $|\Psi(t)\rangle = a_e(t)|\nu_e\rangle + a_\mu(t)|\nu_\mu\rangle + a_\tau(t)|\nu_\tau\rangle$, and the density matrix is defined as $\rho(t) = |\Psi(t)\rangle\langle\Psi(t)|$. The diagonal matrix elements of $\rho(t)$ are given by $\rho_{\beta\beta} = |a_\beta|^2$ (for $\beta = e, \mu, \tau$). They are just the probabilities of $\nu_\alpha \to \nu_\beta$ oscillations. More explicitly, we obtain

$$\begin{aligned} P(\nu_\alpha \to \nu_e) &= \frac{1}{3} + \frac{1}{2}\left(P_3 + \frac{1}{\sqrt{3}} P_8\right) \; , \\ P(\nu_\alpha \to \nu_\mu) &= \frac{1}{3} - \frac{1}{2}\left(P_3 - \frac{1}{\sqrt{3}} P_8\right) \; , \\ P(\nu_\alpha \to \nu_\tau) &= \frac{1}{3} - \frac{1}{\sqrt{3}} P_8 \; . \end{aligned} \tag{5.129}$$

Note that different initial flavors correspond to different initial conditions of the polarization vector. If the initial state is an electron neutrino, for instance, the nonzero components of $\mathbf{P}(0)$ will be $P_3(0) = 1$ and $P_8(0) = 1/\sqrt{3}$. We remark that Eq. (5.129) has been written in the $(\nu_e, \nu_\mu, \nu_\tau)$ basis, but the relations obtained therein are actually independent of the flavor bases. The point is that the equation of motion in Eq. (5.128) should be solved with the corresponding magnetic field $\mathbf{B}$ in a specific basis. A pictorial presentation of the evolution of $\mathbf{P}(t)$ can be done in the eight-dimensional space, but it is too complicated to be intuitive and instructive. Nonetheless, it is straightforward to include matter effects into this picture and calculate the probabilities of neutrino oscillations by solving the evolution equation of the polarization vector. The density matrix formulation has been used to analyze the three-flavor conversions of supernova neutrinos (Duan *et al.*, 2008; Dasgupta and Dighe, 2008; Dasgupta *et al.*, 2008; Fogli *et al.*, 2009).

5.3.3 Non-linear Evolution Equations

The density matrix formulation of neutrino oscillations is extremely useful in some astrophysical and cosmological circumstances, such as in the core-collapse supernovae or in the early Universe, where neutrinos oscillate and frequently interact with the ambient particles. But it is improper to treat neutrinos as a beam of particles in these cases, as we have mentioned in Chapter 2. For instance, neutrinos from the core of a supernova have to traverse a region where the number densities of neutrinos and antineutrinos are much higher than the number density of electrons. Hence two crucial points should be noted: (1) one has to take account of the neutrino-neutrino

coherent scattering effects, which may dominate over the usual MSW matter effects on neutrino flavor conversions; (2) there is no distinction between the test and background neutrinos, since both of them contribute to the total flux of supernova neutrinos which will be experimentally detected. A reasonable way out is to consider the number densities of neutrinos for different flavors in a thermal ensemble. Such a picture is particularly suitable for the description of neutrinos in the early Universe (Dolgov, 2002).

For unmixed neutrinos and antineutrinos, it is sufficient to consider the evolution of their occupation numbers $f_{\mathbf{p}}$ and $\overline{f}_{\mathbf{p}}$ for each momentum mode $\mathbf{p}$. As shown in Chapter 2, the occupation number of a scalar boson ϕ is given by the ensemble average of the corresponding occupation number operator $a^\dagger_{\mathbf{p}} a_{\mathbf{p}}$; i.e., $f_{\mathbf{p}} = \langle a^\dagger_{\mathbf{p}} a_{\mathbf{p}} \rangle$, where $a^\dagger_{\mathbf{p}}$ and $a_{\mathbf{p}}$ are the creation and annihilation operators respectively. For mixed neutrinos and antineutrinos, their flavors should be taken into account. In an analogous way one may define the density matrices (Sigl and Raffelt, 1993)

$$\begin{aligned} \langle b^\dagger_j(\mathbf{p}) b_i(\mathbf{q}) \rangle &= (2\pi)^3 \delta^3(\mathbf{p}-\mathbf{q}) \left(\rho_{\mathbf{p}}\right)_{ij} \; , \\ \langle d^\dagger_i(\mathbf{p}) d_j(\mathbf{q}) \rangle &= (2\pi)^3 \delta^3(\mathbf{p}-\mathbf{q}) \left(\overline{\rho}_{\mathbf{p}}\right)_{ij} \; , \end{aligned} \tag{5.130}$$

where $b^\dagger_i$ and b_i (or $d^\dagger_i$ and d_i) denote the creation and annihilation operators of neutrinos ν_i (or antineutrinos $\overline{\nu}_i$). The diagonal matrix elements of $\rho_{\mathbf{p}}$ are just the occupation number densities $f^i_{\mathbf{p}}$ for neutrinos ν_i, and the neutrino number density n_{ν_i} is given by the integration of $f^i_{\mathbf{p}}$ over the momentum space. Likewise for the case of antineutrinos $\overline{\nu}_i$. Note that the family indices on the left-hand sides of two identities in Eq. (5.130) are in the opposite order, which ensures the transformation in the flavor space to be the same for $\rho_{\mathbf{p}}$ and $\overline{\rho}_{\mathbf{p}}$. This point can be understood by noting that $b_i(\mathbf{p})$ and $d^\dagger_i(\mathbf{p})$ are present in the quantization of the neutrino field $\nu_i(x)$, on which the flavor transformation is acting. On the other hand, we remark that Eq. (5.130) is defined for the neutrino mass eigenstates, because the neutrino flavor states have no definite masses and a construction of the Fock space for them is problematic (Giunti *et al.*, 1992).

For free neutrinos, the time evolution of their creation and annihilation operators is simple: $b_k(\mathbf{p},t) = b_k(\mathbf{p},0) \mathrm{e}^{-\mathrm{i}E_k t}$ and $d_k(\mathbf{p},t) = d_k(\mathbf{p},0) \mathrm{e}^{-\mathrm{i}E_k t}$, where $E_k = \sqrt{|\mathbf{p}|^2 + m^2_k}$ is the neutrino energy. Hence the free Hamiltonian operator can be written as

$$\hat{\mathcal{H}}_0 = \int \frac{\mathrm{d}^3\mathbf{p}}{(2\pi)^3} \sum_{k=1}^{3} \left[b^\dagger_k(\mathbf{p}) b_k(\mathbf{p}) + d^\dagger_k(\mathbf{p}) d_k(\mathbf{p}) \right] E_k \; . \tag{5.131}$$

Let us define the operators (Sigl and Raffelt, 1993)

$$D_{jk}(\mathbf{p},t) \equiv b^\dagger_k(\mathbf{p},t) b_j(\mathbf{p},t) \; , \quad \overline{D}_{jk}(\mathbf{p},t) \equiv d^\dagger_j(\mathbf{p},t) d_k(\mathbf{p},t) \; . \tag{5.132}$$

As a result, the density matrices can be expressed as $\langle D_{jk}(\mathbf{p},t)\rangle = \rho_{\mathbf{p}}$ and $\langle \overline{D}_{jk}(\mathbf{p},t)\rangle = \overline{\rho}_{\mathbf{p}}$, where Eq. (5.130) has been used and the factor $(2\pi)^3\delta^3(0)$ has been consistently set to unity. Now we look at the time evolution of the density matrices. The evolution of the operators defined in Eq. (5.132) is determined by the Heisenberg equations

$$\dot{D}_{jk}(\mathbf{p},t) = \mathrm{i}\left[\hat{\mathcal{H}}, D_{jk}(\mathbf{p},t)\right] \; , \quad \dot{\overline{D}}_{jk}(\mathbf{p},t) = \mathrm{i}\left[\hat{\mathcal{H}}, \overline{D}_{jk}(\mathbf{p},t)\right] \; , \tag{5.133}$$

where $\hat{\mathcal{H}} = \hat{\mathcal{H}}_0 + \hat{\mathcal{H}}_{\rm int}$ is the total Hamiltonian operator. The evolution equations of $\rho_{\mathbf{p}}$ and $\overline{\rho}_{\mathbf{p}}$ can be obtained by taking the expectation values on both sides of Eq. (5.133). These equations will be closed if their right-hand sides can be reduced to $\rho_{\mathbf{p}}$ and $\overline{\rho}_{\mathbf{p}}$ themselves. In the absence of any interactions (i.e., $\hat{\mathcal{H}} = \hat{\mathcal{H}}_0$), we substitute the Hamiltonian operator in Eq. (5.131) into Eq. (5.133) and then calculate its first identity as follows:

$$\begin{aligned} \dot{D}_{jk}(\mathbf{p},t) &= \mathrm{i}\int \frac{\mathrm{d}^3\mathbf{q}}{(2\pi)^3} \sum_{l=1}^{3} E_l \left[b_l^\dagger(\mathbf{q}) b_l(\mathbf{q}), b_k^\dagger(\mathbf{p},t) b_j(\mathbf{p},t)\right] \\ &= \mathrm{i}\left(E_k - E_j\right) D_{jk}(\mathbf{p},t) \; , \end{aligned} \tag{5.134}$$

where the anti-commutation relations $\{b_j(\mathbf{p},t), b_k^\dagger(\mathbf{q},t)\} = (2\pi)^3\delta^3(\mathbf{p}-\mathbf{q})$ and $\{b_j(\mathbf{p},t), b_k(\mathbf{q},t)\} = \{b_j^\dagger(\mathbf{p},t), b_k^\dagger(\mathbf{q},t)\} = 0$ have been used. Given the relations $b_k(\mathbf{p},t) = b_k(\mathbf{p},0)\mathrm{e}^{-\mathrm{i}E_k t}$ and $d_k(\mathbf{p},t) = d_k(\mathbf{p},0)\mathrm{e}^{-\mathrm{i}E_k t}$, it is easy to obtain the result in Eq. (5.134). This treatment is instructive for dealing with the case where $\hat{\mathcal{H}}_{\rm int}$ is present. Taking the expectation values on both sides of Eq. (5.134), we get the equation of motion

$$\dot{\rho}_{jk}(\mathbf{p},t) = \mathrm{i}\left(E_k - E_j\right) \rho_{jk}(\mathbf{p},t) \tag{5.135}$$

for the density matrices of neutrinos. In a similar way we can obtain

$$\dot{\overline{\rho}}_{jk}(\mathbf{p},t) = \mathrm{i}\left(E_j - E_k\right) \overline{\rho}_{jk}(\mathbf{p},t) \tag{5.136}$$

for the density matrices of antineutrinos. Let us translate the above results from the mass basis into the flavor basis, where it is more convenient to account for neutrino interactions. Because of $\nu_\alpha = V_{\alpha 1}\nu_1 + V_{\alpha 2}\nu_2 + V_{\alpha 3}\nu_3$ (for $\alpha = e, \mu, \tau$), the elements of the density matrices $\rho_{\mathbf{p}}(t)$ and $\overline{\rho}_{\mathbf{p}}(t)$ turn out to be

$$\begin{aligned} \rho_{\alpha\beta}(\mathbf{p},t) &= \sum_j \sum_k V_{\alpha j} \rho_{jk}(\mathbf{p},t) V^*_{\beta k} \; , \\ \overline{\rho}_{\alpha\beta}(\mathbf{p},t) &= \sum_j \sum_k V_{\alpha j} \overline{\rho}_{jk}(\mathbf{p},t) V^*_{\beta k} \; . \end{aligned} \tag{5.137}$$

In the flavor basis we make use of Eq. (5.135) to derive the equation of motion for the density matrix elements $\rho_{\alpha\beta}(\mathbf{p},t)$:

$$\dot{\rho}_{\alpha\beta} = \mathrm{i}\sum_j \sum_k \left[V_{\alpha j}\rho_{jk}E_k V^*_{\beta k} - V_{\alpha j}E_j\rho_{jk}V^*_{\beta k}\right]$$
$$= \mathrm{i}\sum_j \sum_k \sum_l \sum_\gamma \left[(V_{\alpha j}\rho_{jl}V^*_{\gamma l})(V_{\gamma k}E_k V^*_{\beta k}) - (V_{\alpha j}E_j V^*_{\gamma j})(V_{\gamma l}\rho_{lk}V^*_{\beta k})\right]$$
$$= \mathrm{i}\sum_\gamma \left[\rho_{\alpha\gamma}\Omega^0_{\gamma\beta} - \Omega^0_{\alpha\gamma}\rho_{\gamma\beta}\right] = -\mathrm{i}\left[\Omega^0, \rho\right]_{\alpha\beta} \ , \tag{5.138}$$

where

$$\Omega^0_{\alpha\beta}(\mathbf{p}) \equiv \left[|\mathbf{p}|^2\delta_{\alpha\beta} + \sum_{i=1}^{3} V_{\alpha i}m_i^2 V^*_{\beta i}\right]^{1/2} \approx E\delta_{\alpha\beta} + (\mathcal{H}_{\rm v})_{\alpha\beta} \tag{5.139}$$

in the approximation $|\mathbf{p}| \approx E \gg m_i$, and $\mathcal{H}_{\rm v}$ has been given in Eq. (5.40). The approximation made in Eq. (5.139) allows us to rewrite Eq. (5.138) as [5]

$$\dot{\rho}_{\mathbf{p}}(t) = -\mathrm{i}\left[\mathcal{H}_{\rm v}, \rho_{\mathbf{p}}(t)\right] \ , \tag{5.140}$$

which is formally the same as that given in Eq. (5.100). As far as antineutrinos are concerned, one may analogously obtain

$$\dot{\overline{\rho}}_{\mathbf{p}}(t) = +\mathrm{i}\left[\mathcal{H}_{\rm v}, \overline{\rho}_{\mathbf{p}}(t)\right] \ . \tag{5.141}$$

Thanks to these equations of motion, a geometrical representation of neutrino oscillations is also applicable. The difference between the density matrices introduced in Section 5.3.2 and discussed here is that they work separately for the one-particle state and an ensemble of neutrinos. In the two-flavor scheme one may expand $\rho_{\mathbf{p}}$, $\overline{\rho}_{\mathbf{p}}$ and $\mathcal{H}_{\rm v}$ in terms of the Pauli matrices as

$$\rho_{\mathbf{p}} = \frac{1}{2}\left(f_{\mathbf{p}} + \mathbf{P}_{\mathbf{p}}\cdot\boldsymbol{\sigma}\right) \ , \qquad \overline{\rho}_{\mathbf{p}} = \frac{1}{2}\left(\overline{f}_{\mathbf{p}} + \overline{\mathbf{P}}_{\mathbf{p}}\cdot\boldsymbol{\sigma}\right) \ , \tag{5.142}$$

and

$$\mathcal{H}_{\rm v} = \frac{1}{2}\left(\Sigma + \omega_{\mathbf{p}}\mathbf{B}\cdot\boldsymbol{\sigma}\right) \ . \tag{5.143}$$

Of course, neutrino flavor conversions can also be described by the evolution of the polarization vectors $\mathbf{P}_{\mathbf{p}}(t)$ and $\overline{\mathbf{P}}_{\mathbf{p}}(t)$. The above four equations yield

$$\dot{\mathbf{P}}_{\mathbf{p}}(t) = +\omega_{\mathbf{p}}\mathbf{B}\times\mathbf{P}_{\mathbf{p}}(t) \ ,$$
$$\dot{\overline{\mathbf{P}}}_{\mathbf{p}}(t) = -\omega_{\mathbf{p}}\mathbf{B}\times\overline{\mathbf{P}}_{\mathbf{p}}(t) \ , \tag{5.144}$$

where $\omega_{\mathbf{p}} \equiv \Delta m^2/(2|\mathbf{p}|)$ and $\mathbf{B} = (\sin 2\theta, 0, -\cos 2\theta)$ with θ being the neutrino mixing angle in vacuum. This result indicates that $\mathbf{P}_{\mathbf{p}}(t)$ and $\overline{\mathbf{P}}_{\mathbf{p}}(t)$ rotate around $\mathbf{B}$ at the same speed but in the opposite directions.

[5] Note that we have used $\rho_{ij}(\mathbf{p}, t)$ and $\rho_{\alpha\beta}(\mathbf{p}, t)$ to denote the elements of the density matrix $\rho_{\mathbf{p}}(t)$ in the mass and flavor bases, respectively.

In the presence of neutrino interactions, we take the expectation values on both sides of Eq. (5.133) and then obtain

$$\dot{\rho}_{\mathbf{p}}(t) = -\mathrm{i}\left[\Omega^0_{\mathbf{p}}, \rho_{\mathbf{p}}(t)\right] + \mathrm{i}\langle\left[\hat{\mathcal{H}}_{\rm int}(t), D_{\mathbf{p}}(t)\right]\rangle \; , \tag{5.145}$$

and a similar equation for $\overline{\rho}_{\mathbf{p}}(t)$. In the assumption that neutrinos are not correlated with the background, it is possible to decompose the expectation value into a medium part and a neutrino part. In this case Eq. (5.145) and its counterpart for antineutrinos can be reduced to the equations including only $\rho_{\mathbf{p}}(t)$ and $\overline{\rho}_{\mathbf{p}}(t)$. Taking account of the neutrino interactions in the SM, one may work out the non-linear evolution equations in the leading-order approximation (Sigl and Raffelt, 1993; Hannestad *et al.*, 2006):

$$\begin{aligned}
\dot{\mathbf{P}}_{\mathbf{p}} &= +\left[\omega_{\mathbf{p}}\mathbf{B} + \lambda\mathbf{L} + \sqrt{2}\, G_{\rm F} \int \frac{{\rm d}^3\mathbf{q}}{(2\pi)^3}(\mathbf{P}_{\mathbf{q}} - \overline{\mathbf{P}}_{\mathbf{q}}) g(\theta_{\mathbf{pq}})\right] \times \mathbf{P}_{\mathbf{p}} \; , \\
\dot{\overline{\mathbf{P}}}_{\mathbf{p}} &= -\left[\omega_{\mathbf{p}}\mathbf{B} - \lambda\mathbf{L} - \sqrt{2}\, G_{\rm F} \int \frac{{\rm d}^3\mathbf{q}}{(2\pi)^3}(\mathbf{P}_{\mathbf{q}} - \overline{\mathbf{P}}_{\mathbf{q}}) g(\theta_{\mathbf{pq}})\right] \times \overline{\mathbf{P}}_{\mathbf{p}} \; ,
\end{aligned} \tag{5.146}$$

where $g(\theta_{\mathbf{pq}}) \equiv 1 - \cos\theta_{\mathbf{pq}}$ with $\theta_{\mathbf{pq}}$ being the angle between the neutrino momenta $\mathbf{p}$ and $\mathbf{q}$. The ordinary matter effects are represented by the term $\lambda\mathbf{L}$ with $\lambda = \sqrt{2}G_{\rm F}n_e$. The integral terms in the brackets of Eq. (5.146) come from the neutrino-neutrino coherent scattering, which makes the evolution equations of the polarization vectors non-linear.

To illustrate the non-linear effects induced by the neutrino-neutrino coherent scattering, we consider a simple ensemble which initially contains pure electron neutrinos and antineutrinos. Their number densities are assumed to be equal ($n_{\nu_e} = n_{\overline{\nu}_e}$), and the flavor polarization vector can be normalized to unity. Hence Eq. (5.146) is simplified to

$$\begin{aligned}
\dot{\mathbf{P}} &= \left[+\omega\mathbf{B} + \lambda\mathbf{L} + \mu(\mathbf{P} - \overline{\mathbf{P}})\right] \times \mathbf{P} \; , \\
\dot{\overline{\mathbf{P}}} &= \left[-\omega\mathbf{B} + \lambda\mathbf{L} + \mu(\mathbf{P} - \overline{\mathbf{P}})\right] \times \overline{\mathbf{P}} \; ,
\end{aligned} \tag{5.147}$$

where $\mu \equiv \sqrt{2}G_{\rm F}n_{\nu_e}$ is the strength of neutrino-neutrino interactions. Two additional assumptions will be made: (1) only one single momentum mode is considered, so the vacuum oscillation frequency ω is universal for both neutrinos and antineutrinos; (2) the neutrino density dominates over the electron density $n_{\nu_e} \gg n_e$, so the matter-effect term in Eq. (5.147) can be neglected. We focus on the non-linear effects governed by the equations

$$\begin{aligned}
\dot{\mathbf{P}} &= \left[+\omega\mathbf{B} + \mu(\mathbf{P} - \overline{\mathbf{P}})\right] \times \mathbf{P} \; , \\
\dot{\overline{\mathbf{P}}} &= \left[-\omega\mathbf{B} + \mu(\mathbf{P} - \overline{\mathbf{P}})\right] \times \overline{\mathbf{P}} \; .
\end{aligned} \tag{5.148}$$

Three-flavor oscillations can well approximate to the two-flavor ones due to the strong hierarchy $|\Delta m^2_{32}| \approx |\Delta m^2_{31}| \gg \Delta m^2_{21}$, as shown in Eq. (5.121). In

this approximation only the smallest neutrino mixing angle θ_{13} is relevant. For the normal neutrino mass hierarchy, we have $\mathbf{B} = (\sin 2\theta_{13}, 0, -\cos 2\theta_{13})$. For the inverted neutrino mass hierarchy, θ_{13} is close to $\pi/2$ and thus a tiny angle $\theta'_{13} \equiv \pi/2 - \theta_{13}$ can be defined. In this case the z-component of the magnetic field becomes positive, $\mathbf{B} = (\sin 2\theta'_{13}, 0, \cos 2\theta'_{13})$. Defining the difference between the polarization vectors as $\mathbf{D} \equiv \mathbf{P} - \overline{\mathbf{P}}$ and the sum of them as $\mathbf{S} \equiv \mathbf{P} + \overline{\mathbf{P}}$, we transform Eq. (5.148) into

$$\dot{\mathbf{S}} = \omega \mathbf{B} \times \mathbf{D} + \mu \mathbf{D} \times \mathbf{S} \; , \qquad \dot{\mathbf{D}} = \omega \mathbf{B} \times \mathbf{S} \; . \tag{5.149}$$

In view of $\dot{\mathbf{B}} = 0$ and $\mathbf{B} \times \mathbf{B} = 0$, we further define $\mathbf{Q} = \mathbf{S} - \omega \mathbf{B}/\mu$ and then rewrite Eq. (5.149) as the differential equations of $\mathbf{Q}$ and $\mathbf{D}$:

$$\dot{\mathbf{Q}} = \mu \mathbf{D} \times \mathbf{Q} \; , \qquad \dot{\mathbf{D}} = \omega \mathbf{B} \times \mathbf{Q} \; . \tag{5.150}$$

Given the initial conditions $\mathbf{P}(0) = \overline{\mathbf{P}}(0) = (0, 0, 1)$, which lead to $\mathbf{D}(0) = 0$ and $\mathbf{S}(0) = (0, 0, 2)$, Eq. (5.150) can be solved for the z-components of $\mathbf{Q}$ and $\mathbf{D}$. As a consequence, we find

$$\begin{aligned} P_z &= \frac{S_z + D_z}{2} = \frac{1}{2} \left(Q_z + \frac{\omega}{\mu} B_z + D_z \right) \; , \\ \overline{P}_z &= \frac{S_z - D_z}{2} = \frac{1}{2} \left(Q_z + \frac{\omega}{\mu} B_z - D_z \right) \; . \end{aligned} \tag{5.151}$$

The numerical results for P_z and $\overline{P}_z$ in the case of the inverted neutrino mass hierarchy are shown in Fig. 5.4, where $\theta'_{13} = 0.01$ has been input. Assuming the neutrino-neutrino interaction strength μ to be much larger than the vacuum oscillation frequency ω, we can observe that P_z and $\overline{P}_z$ keep their initial values (i.e., $P_z(0) = \overline{P}_z(0) = +1$) unchanged for some time, and then rapidly fall down to about -1. This behavior implies that the initial electron neutrinos can almost completely transform into the muon or tau neutrinos. For the normal neutrino mass hierarchy, P_z and $\overline{P}_z$ slightly fluctuate around their initial values as a result of the tiny value of θ_{13}. This interesting evolution of P_z and $\overline{P}_z$, which is sometimes called the "bipolar flavor conversion", can be understood by converting the equation of motion in Eq. (5.150) into that for the pendulum in a vertical plane (Hannestad *et al.*, 2006). In the small-mixing-angle limit, the evolution associated with the normal neutrino mass hierarchy corresponds to the pendulum swinging around the stable point where the potential energy is minimal. As far as the inverted neutrino mass hierarchy is concerned, however, the pendulum is initially placed at the highest point which is unstable. Hence it is ready to fall down to the lowest point, causing the complete neutrino flavor conversion.

In a realistic case for supernova neutrino oscillations, one should carefully take into account the neutrino energy spectra, the asymmetry between the number densities of neutrinos and antineutrinos, the matter effects and the neutrino trajectories (Duan and Kneller, 2009). We shall discuss the flavor conversions of supernova neutrinos in more detail in Chapter 7.

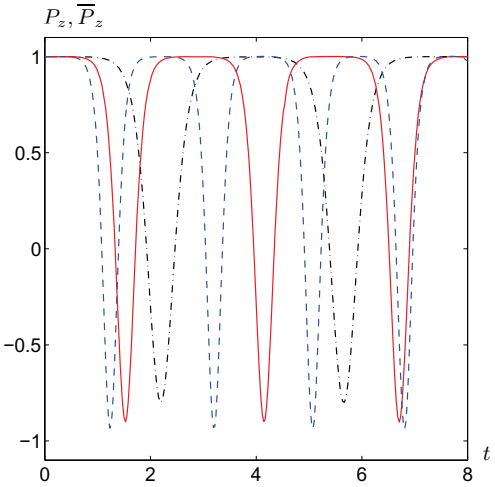

Fig. 5.4 The evolution of P_z and $\overline{P}_z$ for the inverted neutrino mass hierarchy, where $\theta'_{13} = 0.01$ and $\omega = 1$ together with $\mu = 5$ (dot-dashed line), $\mu = 10$ (solid line) and $\mu = 15$ (dashed line) have been input (Hannestad *et al.*, 2006. With permission from the American Physical Society)

5.4 Future Long-baseline Neutrino Oscillation Facilities

Current solar, atmospheric, accelerator and reactor neutrino experiments have provided us with very compelling evidence for neutrino oscillations, from which Δm^2_{21}, $|\Delta m^2_{32}|$, θ_{12} and θ_{23} are determined to a reasonably good degree of accuracy. The ongoing and future neutrino oscillation experiments are expected to answer the following three questions: (a) what is the sign of Δm^2_{32}? (b) how small is the smallest neutrino mixing angle θ_{13}? (c) how large is the CP-violating phase δ? In this section we shall first give a brief overview of the prospects of some high-intensity long-baseline neutrino oscillation experiments, and then give a slightly detailed introduction about the Daya Bay reactor antineutrino oscillation experiment in China.

5.4.1 Prospects of Accelerator Neutrino Experiments

Three types of facilities have so far been proposed to provide high-intensity neutrino beams: the super-beam facility, the beta-beam facility and the neutrino factory (Gonzalez-Garcia and Maltoni, 2008; Bandyopadhyay *et al.*, 2009). The physics performance of each facility can be evaluated by a set of observables, including the number of degrees of freedom which are used to describe the experimental outputs as well as the sensitivities to θ_{13}, δ, the sign of Δm^2_{32}, and a deviation of θ_{23} from $\pi/4$. Such precision measurements are extremely important to pin down the hierarchy of the neutrino mass

spectrum, the accurate pattern of the 3×3 neutrino mixing matrix and the strength of leptonic CP violation in neutrino oscillations.

(1) *The super-beam facilities.* Conventional accelerator-based neutrino beams are produced from the primary decays of charged pions and have been used to do either $\nu_\mu \to \nu_\mu$ and $\overline{\nu}_\mu \to \overline{\nu}_\mu$ disappearance experiments, such as the K2K and MINOS experiments (Ahn *et al.*, 2006; Michael *et al.*, 2006), or $\nu_\mu \to \nu_\tau$ and $\overline{\nu}_\mu \to \overline{\nu}_\tau$ appearance experiments, such as the OPERA experiment (Kodama *et al.*, 1999). They can be optimized by designing a high-power proton accelerator which delivers more intense proton beams to the target, so as to produce high-intensity but low-energy ν_μ and $\overline{\nu}_\mu$ beams for $\nu_\mu \to \nu_e$ and $\overline{\nu}_\mu \to \overline{\nu}_e$ appearance experiments. A super-beam is usually referred to as a conventional neutrino beam driven by the proton driver with a beam power in the range of 2 MW to 5 MW (Bandyopadhyay *et al.*, 2009).

The technology required for a super-beam facility is well known. But the sensitivity of a super-beam experiment to $\nu_\mu \to \nu_e$ and $\overline{\nu}_\mu \to \overline{\nu}_e$ oscillations is limited by the fact that the primary $\pi^\pm$ decays, the subsequent $\mu^\pm$ decays and the kaon decays in the decay pipe of the facility can produce a small fraction of ν_e and $\overline{\nu}_e$ events. This intrinsic contamination increases with the beam energy and thus has to be kept as low as possible. One may design an appropriate beam line configuration to suppress the ν_e or $\overline{\nu}_e$ background from the kaon decays. One may also produce an off-axis neutrino beam, which is arranged to be tilted by a few degrees with respect to the vector pointing from the source to the far detector (McDonald, 2001), to suppress the ν_e or $\overline{\nu}_e$ background induced by $\pi^\pm$ decays. The kinematics of a two-body pion decay assures that all the pions above a given momentum produce neutrinos of almost the same energy at a given angle $\theta \neq 0$ with respect to the axis. So the off-axis technique can yield a low-energy neutrino beam with a small energy spread, which has several advantages over the broad-band on-axis neutrino beam. For example, the off-axis neutrino beam allows energy cuts to be applied to reduce backgrounds and allows the L/E parameter of an experiment to be tuned to the oscillation maximum, although its flux is much smaller than the on-axis neutrino flux.

The ongoing T2K experiment is just an off-axis experiment (Itow *et al.*, 2001). Its facility consists of a conventional neutrino beam driven by the protons of 30 GeV from the J-PARC proton synchrotron at a beam power of 0.75 MW, two near detectors (one on-axis and the other off-axis) located 280 m away from the neutrino source, and the far detector which is just the Super-Kamiokande (SK) neutrino detector. Its main goal is to observe the appearance of ν_e events in an almost pure ν_μ neutrino beam after traveling a distance of 295 km from the J-PARC accelerator center to the SK detector. The off-axis beam angle of this experiment has been chosen to maximize the sensitivity to θ_{13}. An upgrade to the power of the J-PARC proton synchrotron is under consideration in order to provide a 50 GeV proton beam at the power of 4 MW. In this case the construction of a Mton-scale water Cherenkov

detector (the so-called Hyper-Kamiokande detector) at a distance of about 1000 km away from the J-PARC accelerator center would allow one to do a high-intensity off-axis long-baseline neutrino oscillation experiment, which is expected to be sensitive to both the sign of Δm^2_{32} and the CP-violating phase δ (Ishitsuka *et al.*, 2005; Kajita *et al.*, 2007; Hagiwara *et al.*, 2007).

The NOνA facility, which is now under construction, will also do an off-axis neutrino experiment optimized for searching for $\nu_\mu \to \nu_e$ oscillations with a sensitivity ten times better than the ongoing MINOS experiment (Ayres *et al.*, 2005). It employs an upgraded version of the already existing NuMI beamline at a power of 0.7 MW in the Fermilab. The neutrino beam energy is about 2 GeV, and the baseline length is in the range of 700 km to 900 km (from the Fermilab to northern Minnesota) with a far detector sited 12 km (equivalent to $\theta \sim 0.85^\circ$) off-axis. Both the near and far detectors are the "totally active" liquid scintillator detectors. Given a 15-kton far detector and a 5-year run, the NOνA experiment is likely to achieve a sensitivity to $\sin^2 2\theta_{13}$ comparable to that of the T2K experiment. In particular, the long baseline of the NOνA experiment will allow one to probe the sign of Δm^2_{32} with the help of terrestrial matter effects.

T2K and NOνA belong to the first-generation super-beam experiments. The second-generation ones, such as T2HK and CERN-SPL, are under consideration (Gonzalez-Garcia and Maltoni, 2008; Bandyopadhyay *et al.*, 2009).

(2) *The beta-beam facilities.* A beta-beam is produced from the boosted radioactive-ion decays and thus is a pure ν_e or $\overline{\nu}_e$ beam (Zucchelli, 2002). It can be used to do either $\nu_e \to \nu_e$ and $\overline{\nu}_e \to \overline{\nu}_e$ disappearance experiments or $\nu_e \to \nu_\mu$ (or ν_τ) and $\overline{\nu}_e \to \overline{\nu}_\mu$ (or $\overline{\nu}_\tau$) appearance experiments. There are three variables that determine the properties of a beta-beam facility (Bandyopadhyay *et al.*, 2009): the type of ions to be used (especially the endpoint kinetic energy of the electron in the beta decay, E_0); the relativistic γ factor (equal to energy divided by mass) of the ion; and the baseline length L. Once these parameters are fixed, the neutrino flux can be precisely calculated because the kinematics of the beta decay is well known (Burguet-Castell *et al.*, 2004). To set up a proper beta-beam, the isotope should be sufficiently long-lived to avoid strong losses in the acceleration phase, but it must decay fast enough to produce an intensive neutrino beam. Two ion species, whose lifetimes are both around 1 s, have been identified as the optimal candidates (Zucchelli, 2002): ^{6}He with $E_0 = 3506.7$ keV for generating $\overline{\nu}_e$ events and ^{18}Ne with $E_0 = 3423.7$ keV for producing ν_e events. Some other ions with larger E_0, which are able to produce more energetic neutrino beams at the same γ/L, have also been considered (Donini and Fernandez-Martinez, 2006; Rubbia *et al.*, 2006).

On the other hand, an optimization of the γ factor and the baseline length L should take account of several physics requirements (Bandyopadhyay *et al.*, 2009): (a) the value of $L/\langle E_\nu \rangle$ should satisfy $\sin^2(1.27\Delta m^2_{32} L/E_\nu) \sim 1$ (the first oscillation maximum) such that the oscillation signatures can be as

large as possible; (b) the neutrino beam energy E_ν should be above the muon production threshold such that the ν_μ or $\overline{\nu}_\mu$ appearance can be searched for in the far detector; (c) E_ν should be large enough for a measurement of the spectral distortion to be used to resolve the intrinsic parameter degeneracy problem; (d) L should be as long as possible to determine the sign of Δm^2_{32} with the help of terrestrial matter effects; and (e) the event rate should be as large as possible — increasing the value of γ for a fixed ion flux can enhance E_ν and thus the number of events because the cross sections of neutrino-nucleon interactions increase with E_ν. All these requirements point to the conclusion that the γ factor should be enhanced as much as possible and the baseline length L should be tuned to sit near an oscillation peak.

The beta-beams can roughly be classified into the low- and high-energy ones. A low-energy beta-beam with $\langle E_\nu \rangle$ in the sub-GeV range matches the distance $L = 130$ km from CERN to the Modane laboratory in the Frejus tunnel (Autin *et al.*, 2003). In comparison, a high-energy beta-beam with $\langle E_\nu \rangle$ in the range of 1 GeV to 1.5 GeV matches the distance $L \sim 700$ km between CERN and Canfranc, CERN and Gran Sasso, or Fermilab and Soudan (Bandyopadhyay *et al.*, 2009). A higher-energy beta-beam experiment would require the Large Hadron Collider at CERN to accelerate the ions to produce ν_e events of $\langle E_\nu \rangle \sim 5$ GeV and $\overline{\nu}_e$ events of $\langle E_\nu \rangle \sim 7.5$ GeV together with a very long baseline $L \sim 3000$ km (Gonzalez-Garcia and Maltoni, 2008).

(3) *The neutrino factory.* The technology for producing an intensive muon beam was initially explored for the purpose of building a muon collider at the TeV energy scale. This technology is more feasible for building the neutrino factory at much lower energies. In a neutrino factory muons are accelerated from a high-intensity source to energies of several tens of GeV and then injected into a storage ring with long straight sections (Geer, 1998; De Rujula *et al.*, 1999). Therefore, both ν_μ (or $\overline{\nu}_\mu$) and ν_e (or $\overline{\nu}_e$) events can be produced from the well-known muon decay modes $\mu^- \to e^- + \overline{\nu}_e + \nu_\mu$ and $\mu^+ \to e^+ + \nu_e + \overline{\nu}_\mu$. These neutrino beams, whose energies are up to the muon energy itself, allow one to do the following neutrino oscillation experiments:

(1)	$\nu_e \to \nu_e$	$\overline{\nu}_e \to \overline{\nu}_e$	Disappearance
(2)	$\nu_e \to \nu_\mu$	$\overline{\nu}_e \to \overline{\nu}_\mu$	Appearance (golden channel)
(3)	$\nu_e \to \nu_\tau$	$\overline{\nu}_e \to \overline{\nu}_\tau$	Appearance (silver channel)
(4)	$\nu_\mu \to \nu_\mu$	$\overline{\nu}_\mu \to \overline{\nu}_\mu$	Disappearance
(5)	$\nu_\mu \to \nu_e$	$\overline{\nu}_\mu \to \overline{\nu}_e$	Appearance (challenging)
(6)	$\nu_\mu \to \nu_\tau$	$\overline{\nu}_\mu \to \overline{\nu}_\tau$	Appearance (interesting)

Some careful studies about the design of a neutrino factory have been carried out in Europe, Japan and the USA (Bandyopadhyay *et al.*, 2009). The conclusion is that an accelerator complex capable of providing about 10^{21} muon decays per year can be built, and the optimal detector should better be able to perform both appearance and disappearance experiments. The detection of ν_α (or $\overline{\nu}_\alpha$) neutrinos (for $\alpha = e, \mu, \tau$) is to look for the α^- (or α^+) events

produced from the charged-current interactions of ν_α (or $\overline{\nu}_\alpha$) neutrinos with the medium of the far detector.

Among twelve neutrino oscillation processes that can be measured at a neutrino factory, the "golden" channel is the $\nu_e \to \nu_\mu$ transition [6]. Because ν_e neutrinos are produced from the decays of positive muons while ν_μ neutrinos produce negative muons via the charged-current interactions in the detector, the ν_μ appearance can simply be detected by looking for the "wrong-sign" muons which are unable to get contaminated in the dominant background (i.e., "right-sign" muons). The full statistical sensitivity can therefore be exploited to probe very small values of θ_{13} and δ (Huber and Winter, 2003).

The so-called "silver" channel at a neutrino factory is the $\nu_e \to \nu_\tau$ transition signified by the ν_τ appearance (or equivalently, the τ^- events) in the far detector. A careful comparison between the CP- or T-violating effects in golden and silver channels would allow one to test whether leptonic CP violation arises from the unique phase δ, because the genuine CP- and T-violating terms in these two channels should have the opposite signs (Strumia and Vissani, 2006).

In fact, a determination of (θ_{13}, δ) from the measurement of a single neutrino oscillation channel suffers from an eight-fold ambiguity; i.e., there are in general eight different regions of the parameter space which can fit the same experimental data in the (θ_{13}, δ) plane (Bandyopadhyay *et al.*, 2009). One may speculate two possible ways to resolve this parameter degeneracy problem: one is to measure the golden neutrino oscillation channel at different baselines (i.e., different values of L/E); and the other is to make use of the rich flavor content of neutrino beams by combining the measurements of different channels at a neutrino factory.

It is very challenging to observe the $\nu_\mu \to \nu_e$ transition, because the e^- signals associated with the ν_e appearance can easily get contaminated in the far detector. In this sense it might be a bit easier, at least not hopeless, to search for the e^+ signals associated with the $\overline{\nu}_e$ appearance arising from the $\overline{\nu}_\mu \to \overline{\nu}_e$ transition in the detector with a delicate detection technique. We stress that the study of CP violation in $\nu_\mu \to \nu_\tau$ and $\overline{\nu}_\mu \to \overline{\nu}_\tau$ oscillations at a neutrino factory is particularly interesting, since they are insensitive to the standard CP-violating effect characterized by the phase δ but sensitive to some new CP-violating effects induced by either the non-unitarity of the 3×3 neutrino mixing matrix or the non-standard neutrino interactions (Meloni *et al.*, 2010). In the presence of terrestrial matter effects and (or) new physics, it is also useful to combine the measurements of both appearance and disappearance neutrino oscillation channels so as to pin down the wanted parameters with much smaller uncertainties or ambiguities.

[6] Its CP-conjugate process $\overline{\nu}_e \to \overline{\nu}_\mu$ can also be regarded as a golden channel, but one should keep in mind that the rate of μ^+ signals associated with the appearance of $\overline{\nu}_\mu$ events is about two times lower than that of μ^- signals associated with the appearance of ν_μ events in the far detector (Strumia and Vissani, 2006).

A detailed description of the "standard" neutrino factory setup, together with its physics potential, has been presented by the ISS Physics Working Group (Bandyopadhyay *et al.*, 2009). We hope that a neutrino factory, if it can be built in the future, will deepen our understanding of the dynamics of neutrino oscillations and open a promising window towards some new physics which might be relevant to the origin of neutrino masses or to the unrevealed interactions between neutrinos and matter.

5.4.2 Prospects of Reactor Antineutrino Experiments

It is well known that Wolfgang Pauli's neutrino hypothesis was first verified in 1956 thanks to the Savannah River reactor antineutrino experiment (Cowan *et al.*, 1956). It is also known that very convincing evidence for the electron antineutrino oscillations was first achieved in 2003 thanks to the KamLAND reactor antineutrino experiment (Eguchi *et al.*, 2003). These two examples are sufficient for illustration of the importance of reactor antineutrino experiments in the study of neutrino properties and neutrino interactions. Hence one expects that a high-intensity reactor antineutrino oscillation experiment can help pin down the smallest neutrino mixing angle θ_{13} in the near future.

The present upper bound on θ_{13} was actually obtained from the CHOOZ reactor antineutrino experiment (Apollonio *et al.*, 1998). A lot of attention has recently been paid to the next generation of reactor antineutrino experiments based on the observation that the performance of the CHOOZ experiment can be remarkably improved if the systematics is better controlled and the statistics is significantly enhanced (Anderson *et al.*, 2004). Different from the accelerator neutrino oscillation experiments, the reactor antineutrino oscillation experiments are free of the parameter degeneracy problem and able to determine or constrain the magnitude of θ_{13} in a direct and clean way. In the three-flavor neutrino mixing scheme, the probability of reactor $\overline{\nu}_e \to \overline{\nu}_e$ oscillations at a baseline range of 1 km to 2 km can be simplified to a two-flavor oscillation pattern to a good degree of accuracy:

$$\begin{aligned} P(\overline{\nu}_e \to \overline{\nu}_e) &= 1 - 4 \sum_{i<j} |V_{ei}|^2 |V_{ej}|^2 \sin^2 \left(1.27 \frac{\Delta m^2_{ji} L}{E} \right) \\ &\approx 1 - 4 |V_{e3}|^2 \left(1 - |V_{e3}|^2 \right) \sin^2 \left(1.27 \frac{\Delta m^2_{31} L}{E} \right) \\ &= 1 - \sin^2 2\theta_{13} \sin^2 \left(1.27 \frac{\Delta m^2_{31} L}{E} \right) , \end{aligned} \tag{5.152}$$

where $|\Delta m^2_{32}| \approx |\Delta m^2_{31}| \gg \Delta m^2_{21}$ and $|V_{e3}|^2 = \sin^2 \theta_{13} \ll 1$ have been used. So far a number of projects, including Double Chooz in France (Ardellier *et al.*, 2006) and Daya Bay in China (Guo *et al.*, 2007), have been proposed to probe how small θ_{13} could be (Goodman, 2009).

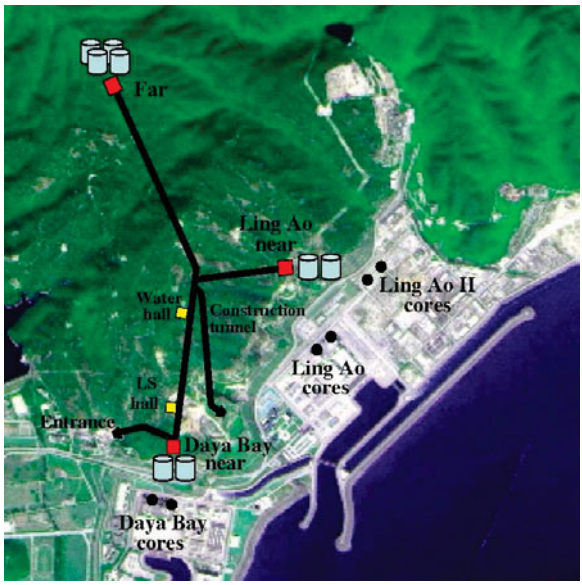

Fig. 5.5 The layout of the Day Bay reactor antineutrino experiment. Two pairs of reactor cores (Daya Bay and Ling Ao) are running and the third one (Ling Ao II) will run soon. Four detector modules are deployed at the far site, and two detector modules are deployed at each of the two near sites (Guo *et al.*, 2007)

Of the currently-proposed reactor antineutrino experiments, the Double Chooz experiment has the opportunity to obtain physical results first. This experiment employs two almost identical medium-size detectors. The near detector is located 280 m from the Chooz nuclear cores and can be used to control the systematics. The far detector, which is situated in the same cavern as the CHOOZ detector (i.e., 1.05 km from the Chooz nuclear cores), will be able to detect 5×10^5 $\overline{\nu}_e$ events in three years of operation with a relative systematic error of 0.6%. Hence the Double Chooz experiment is likely to determine or limit $\sin^2 2\theta_{13}$ to the range of 0.022 to 0.030 (for $|\Delta m^2_{31}|$ varying from 3.5×10^{-3} eV^2 down to 2.5×10^{-3} eV^2) within an unrivaled time scale and a modest cost (Ardellier *et al.*, 2006).

The Daya Bay experiment is the first neutrino oscillation experiment being done in China. In this experiment the electron antineutrino beam takes its source at the Daya Bay nuclear power complex which is currently composed of two pairs of reactor cores (Daya Bay and Ling Ao) separated by about 1.1 km, as illustrated in Fig. 5.5. The complex can now generate 11.6 GW of thermal power, which will increase to 17.4 GW by early 2011 after the third pair of reactor cores (Ling Ao II) is put into operation (Guo *et al.*, 2007). The location of this complex is adjacent to a mountainous terrain in

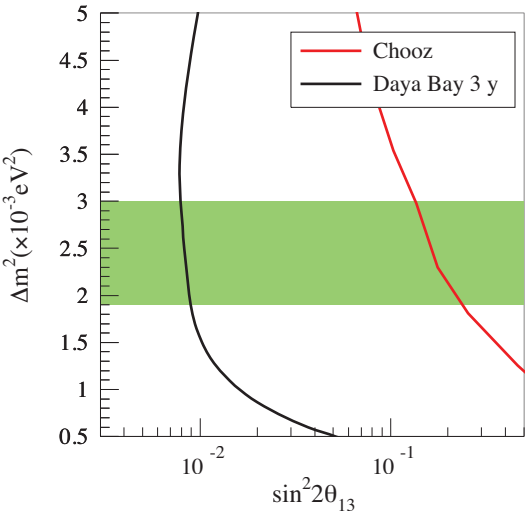

Fig. 5.6 The expected sensitivity of the Daya Bay experiment to $\sin^2 2\theta_{13}$ at the 90% confidence level with three years of data, in comparison with the present CHOOZ limit on $\sin^2 2\theta_{13}$ (Wang, 2010. With permission from the American Institute of Physics). The shaded region corresponds to the allowed interval of $\Delta m^2 \equiv |\Delta m^2_{31}|$ at the 90% confidence level

Shenzhen, southern China, and thus it is ideal for sitting underground detectors that are well shielded from the cosmogenic contamination. The basic layout of the Daya Bay experiment consists of three underground laboratories with a tetrad of far detector modules and two pairs of near detector modules, which are linked through a few horizontal tunnels. Fig. 5.5 shows the detector deployment at these sites. The Daya Bay near detector is 363 m from the Daya Bay reactor cores, while the Ling Ao near detector is 481 m from the Ling Ao reactor cores and 526 m from the Ling Ao II reactor cores. They can monitor the rate and energy distribution of $\overline{\nu}_e$ events and reduce the systematic uncertainties in detecting $\sin^2 2\theta_{13}$. The distances of the far detector from the Daya Bay, Ling Ao and Ling Ao II reactor cores are 1985 m, 1618 m and 1613 m, respectively. Therefore, the first $\overline{\nu}_e \to \overline{\nu}_e$ oscillation maximum can be observed at the far detector to ensure the maximal experimental sensitivity to $\sin^2 2\theta_{13}$.

The sensitivity of the Daya Bay experiment to $\sin^2 2\theta_{13}$ has been analyzed by using the single parameter raster scan method (Guo *et al.*, 2007). Fig. 5.6 shows the sensitivity contours in the $\sin^2 2\theta_{13}$ versus $\Delta m^2 \equiv |\Delta m^2_{31}|$ plane for three years of operation. One can see that the sensitivity of this experiment is able to reach the challenging goal of $\sin^2 2\theta_{13} \sim 1\%$, provided both systematic and statistic uncertainties are well under control (Wang, 2006; Wang, 2010).

The Daya Bay experiment is smoothly going on. Its civil construction is now underway, so is the deployment of the near detectors. After the far detector is deployed in 2011 or 2012, the Daya Bay Collaboration will start to take data. A determination of the smallest neutrino mixing angle θ_{13}, or at least a stringent constraint on θ_{13} if it is too small to be experimentally accessible, is highly expected from this experiment [7].

It is finally worth mentioning the RENO experiment located on the site of the Yonggwang power plant in the southwest of Korea (Ahn *et al.*, 2010). This plant, which spans about 1.3 km, consists of six reactors lined up in roughly equal distances and has a total thermal power of 16.4 GW. There are two identical detectors in the RENO experiment: they are at about 290 m (near) and 1380 m (far), respectively, from the reactor array. The design of the RENO detectors is quite similar to that of the Double Chooz detectors. One expects that the RENO experiment may start data taking in the near future and reach the sensitivity $\sin^2 2\theta_{13} = 0.019$ after five years of running (Mezzetto and Schwetz, 2010).

References

Ahn, J. K., *et al.* (RENO Collaboration), 2010, arXiv:1003.1391.
Ahn, M. H., *et al.* (K2K Collaboration), 2006, Phys. Rev. D **74**, 072003.
Akhmedov, E. K., and Smirnov, A. Yu., 2009, Phys. Atom. Nucl. **72**, 1363.
Akhmedov, E. K., Kopp, J., and Lindner, M., 2008a, JHEP **0805**, 005.
Akhmedov, E. K., Kopp, J., and Lindner, M., 2009, J. Phys. G. **36**, 078001.
Akhmedov, E. K., Maltoni, M., and Smirnov, A. Yu., 2008b, JHEP **0806**, 072.
Anderson, K., *et al.*, 2004, arXiv:hep-ex/0402041.
Apollonio, M., *et al.* (CHOOZ Collaboration), 1998, Phys. Lett. B **420**, 397.
Ardellier, F., *et al.* (Double Chooz Collaboration), 2006, arXiv:hep-ex/0606025.
Autin, B., *et al.*, 2003, J. Phys. G. **29**, 1637.
Ayres, D. S., *et al.* (NOνA Collaboration), 2005, arXiv:hep-ex/0503053.
Bahcall, J. N., 1989, *Neutrino Astrophysics* (Cambridge University Press).
Bandyopadhyay, A., *et al.* (ISS Physics Working Group), 2009, Rept. Prog. Phys. **72**, 106201.
Barger, V., *et al.*, 1980, Phys. Rev. D **22**, 2718.
Barger, V., *et al.*, 2000, Phys. Rev. D **62**, 013004.
Barger, V., Phillips, R. J. N., and Whisnant, K., 1986, Phys. Rev. D **34**, 980.
Bethe, H. A., 1986, Phys. Rev. Lett. **56**, 1305.
Beuthe, M., 2002, Phys. Rev. D **66**, 013003.
Bilenky, S. M., von Feilitzsch, F., and Potzel, W., 2009, J. Phys. G **36**, 078002.
Blasone, M., Capolupo, A., and Vitiello, G., 2002, Phys. Rev. D **66**, 025033.

[7] Here let us mention a possible follow-up project of the Daya Bay experiment (Zhan *et al.*, 2008, 2009): to measure the sign of Δm^2_{31} and determine the neutrino mass hierarchy by doing a longer baseline reactor antineutrino oscillation experiment. The feasibility of such a precision measurement, which makes use of the Daya Bay nuclear power complex and a sufficiently large far detector located about 58 km from the reactor site, is now under discussion.

Bonn, M., and Wolf, E., 1980, *Principles of Optics* (Pergamon Press).
Bruggen, M., Haxton, W. C., and Qian, Y. Z., 1995, Phys. Rev. D **51**, 4028.
Burguet-Castell, J., *et al.*, 2004, Nucl. Phys. B **695**, 217.
Cabibbo, N., 1978, Phys. Lett. B **72**, 333.
Campagne, J. E., 1997, Phys. Lett. B **400**, 135.
Cardall, C. Y., 2000, Phys. Rev. D **61**, 073006.
Cardall, C. Y., and Chung, D. J. H., 1999, Phys. Rev. D **60**, 073012.
Cohen, A. G., Glashow, S. L. and Ligeti, Z., 2009, Phys. Lett. B **678**, 191.
Cowan, C. L., Jr., *et al.*, 1956, Science **124**, 103.
Dar A., *et al.*, 1987, Phys. Rev. D **35**, 3607.
Dasgupta, B., and Dighe, A., 2008, Phys. Rev. D **77**, 113002.
Dasgupta, B., *et al.*, 2008, Phys. Rev. D **77**, 113007.
Davis, J. P., and Pechukas, P., 1976, J. Chem. Phys. **64**, 3129.
de Gouvea, A., Kayser, B., and Mohapatra, R., 2003, Phys. Rev. D **67**, 053004.
De Rujula, A., Gavela, M. B., and Hernandez, P., 1999, Nucl. Phys. B **547**, 21.
Dolgov, A. D., 2002, Phys. Rept. **370**, 333.
Donini, A., and Fernandez-Martinez, E., 2006, Phys. Lett. B **641**, 432.
Duan, H., Fuller, G. M., and Qian, Y. Z., 2008, Phys. Rev. D **77**, 085016.
Duan, H., and Kneller, J., 2009, J. Phys. G **36**, 113201.
Duan, H., *et al.*, 2006, Phys. Rev. D **74**, 105014.
Dykhne, A. M., 1962, Sov. Phys. JETP **14**, 941.
Eguchi, K., *et al.* (KamLAND Collaboration), 2003, Phys. Rev. Lett. **90**, 021802.
Fano, U., 1957, Rev. Mod. Phys. **29**, 74.
Farzan, Y., and Smirnov, A. Yu., 2008, Nucl. Phys. B **805**, 356.
Fogli, G., *et al.*, 2007, JCAP **0712**, 010.
Fogli, G., *et al.*, 2009, JCAP **0904**, 030.
Freund, M., 2001, Phys. Rev. D **64**, 053003.
Freund, M., *et al.*, 2000, Nucl. Phys. B **578**, 27.
Friedland, A., 2001, Phys. Rev. D **64**, 013008.
Geer, S., 1998, Phys. Rev. D **57**, 6989.
Giunti, C., 2002, JHEP **0211**, 017.
Giunti, C., 2004, Found. Phys. Lett. **17**, 103.
Giunti, C., 2008, Phys. Lett. B **665**, 92.
Giunti, C., and Kim, C. W., 1998, Phys. Rev. D **58**, 017301.
Giunti, C., and Kim, C. W., 2007, *Fundamentals of Neutrino Physics and Astrophysics* (Oxford University Press).
Giunti, C., Kim, C. W., and Lee, U. W., 1992, Phys. Rev. D **45**, 2414.
Giunti, C., Kim, C. W., and Lee, U. W., 1998, Phys. Lett. B **421**, 237.
Giunti, C., *et al.*, 1993, Phys. Rev. D **48**, 4310.
Gonzalez-Garcia, M. C., and Maltoni, M., 2008, Phys. Rept. **460**, 1.
Goodman, M., 2009, Nucl. Phys. A **827**, 518C.
Grimus, W., and Stockinger, P., 1996, Phys. Rev. D **54**, 3414.
Grimus, W., Stockinger, P., and Mohanty, S., 1998, Phys. Rev. D **59**, 013001.
Guo, X., *et al.* (Daya Bay Collaboration), 2007, arXiv:hep-ex/0701029.
Hagiwara, K., Okamura, N., and Senda, K. I., 2007, Phys. Rev. D **76**, 093002.
Hannestad, S., *et al.*, 2006, Phys. Rev. D **74**, 105010.
Harrison, P. F., and Scott, W. G., 2000, Phys. Lett. B **476**, 349.
Haxton, W. C., 1986, Phys. Rev. Lett. **57**, 1271.

Haxton, W. C., 1987, Phys. Rev. D **35**, 2352.
Huber, P., and Winter, W., 2003, Phys. Rev. D **68**, 037301.
Hwang, J. T., and Pechukas, P., 1977, J. Chem. Phys. **67**, 4640.
Ioannisian, A., and Pilaftsis, A., 1999, Phys. Rev. D **59**, 053003.
Ishitsuka, M., *et al.*, 2005, Phys. Rev. D **72**, 033003.
Itow, Y., *et al.* (T2K Collaboration), 2001, arXiv:hep-ex/0106019.
Ivanov, A. N., Reda, R., and Kienle, P., 2008, arXiv:0801.2121.
Kachelrieß, M., and Tomàs, R., 2001, Phys. Rev. D **64**, 073002.
Kajita, T., *et al.*, 2007, Phys. Rev. D **75**, 013006.
Kayser, B., 1981, Phys. Rev. D **24**, 110.
Kayser, B., 2005, Phys. Scripta **T121**, 156.
Kiers, K., Nussinov, S., and Weiss, N., 1996, Phys. Rev. D **53**, 537.
Kim, C. W., Kim, J., and Sze, W. K., 1988, Phys. Rev. D **37**, 1072.
Kim, C. W., Nussinov, S., and Sze, W. K., 1987, Phys. Lett. B **184**, 403.
Kim, C. W., Sze, W. K., and Nussinov, S., 1987, Phys. Rev. D **35**, 4014.
Kodama, K., *et al.* (OPERA Collaboration), 1999, CERN-SPSC-99-20.
Kuo, T. K., and Pantaleone, J., 1989a, Phys. Rev. D **39**, 1930.
Kuo, T. K., and Pantaleone, J., 1989b, Rev. Mod. Phys. **61**, 937.
Landau, L. D., 1932, Phys. Z. Sowjetunion **2**, 46.
Landau, L. D., and Lifshitz, E. M., 1977, *Quantum Mechnics: Non-relativistic Theory* (Pergamon Press).
Liao, W., 2008, Phys. Rev. D **77**, 053002.
Lipkin, H. J., 2008, arXiv:0805.0435.
Maki, Z., Nakagawa, M., and Sakata, S., 1962, Prog. Theor. Phys. **28**, 870.
McDonald, K. T., 2001, arXiv:hep-ex/0111033.
Meloni, D., *et al.*, 2010, JHEP **1004**, 041.
Mezzetto, M., and Schwetz, T., 2010, J. Phys. G **37**, 103001.
Michael, D. G., *et al.* (MINOS Collaboration), 2006, Phys. Rev. Lett. **97**, 191801.
Mikheyev, S. P., and Smirnov, A. Yu., 1985, Sov. J. Nucl. Phys. **42**, 913.
Minakata, H., and Nunokawa, H., 2000, Nucl. Instrum. Meth. A **472**, 421.
Mocioiu, I., and Shrock, R., 2000, Phys. Rev. D **62**, 053017.
Naumov, V. A., 1992, Int. J. Mod. Phys. D **1**, 379.
Nötzold, D., 1987, Phys. Rev. D **36**, 1625.
Nussinov, S., 1976, Phys. Lett. B **63**, 201.
Parke, S. J., 1986, Phys. Rev. Lett. **57**, 1275.
Petcov, S. T., 1988, Phys. Lett. B **200**, 373.
Pizzochero, P., 1987, Phys. Rev. D **36**, 2293.
Pontecorvo, B., 1958, Sov. Phys. JETP **7**, 172.
Raffelt, G. G., 1996, *Stars as Laboratories for Fundamental Physics* (The University of Chicago Press).
Rich, J., 1993, Phys. Rev. D **48**, 4318.
Rosen, S. P., and Gelb, J. M., 1986, Phys. Rev. D **34**, 969.
Rubbia, C., *et al.*, 2006, Nucl. Instrum. Meth. A **568**, 475.
Schechter, J., and Valle, J. W. F., 1981, Phys. Rev. D **23**, 1666.
Shtanov, Yu. V., 1998, Phys. Rev. D **57**, 4418.
Sigl, G., and Raffelt, G. G., 1993, Nucl. Phys. B **406**, 423.
Stodolsky, L., 1998, Phys. Rev. D **58**, 036006.

Strumia, A., and Vissani, F., 2006, arXiv:hep-ph/0606054.
Stückelberg, E. C. G., 1932, Helv. Phys. Acta. **5**, 369.
Toshev, S., 1987, Phys. Lett. B **196**, 170.
Toshev, S., 1991, Mod. Phys. Lett. A **6**, 455.
Wang, W., 2010, AIP Conf. Proc. **1222**, 494.
Wang, Y. F., 2006, arXiv:hep-ex/0610024.
Wolfenstein, L., 1978, Phys. Rev. D **17**, 2369.
Wolfenstein, L., 1979, Phys. Rev. D **20**, 2634.
Xing, Z. Z., 2000, Phys. Lett. B **487**, 327.
Xing, Z. Z., 2001a, Phys. Rev. D **63**, 073012.
Xing, Z. Z., 2001b, Phys. Rev. D **64**, 033005.
Xing, Z. Z., 2001c, Phys. Rev. D **64**, 073014.
Xing, Z. Z., 2004, Int. J. Mod. Phys. A **19**, 1.
Xing, Z. Z., and Zhang, H., 2005, Phys. Lett. B **618**, 131.
Zaglauer, H. W., and Schwarzer, K. H., 1988, Z. Phys. C **40**, 273.
Zener, C., 1932, Proc. R. Soc. London A **137**, 697.
Zhan, L., *et al.*, 2008, Phys. Rev. D **78**, 111103.
Zhan, L., *et al.*, 2009, Phys. Rev. D **79**, 073007.
Zhang, H., and Xing, Z. Z., 2005, Eur. Phys. J. C **41**, 143.
Zucchelli, P., 2002, Phys. Lett. B **532**, 166.

6

Neutrinos from Stars

Stars represent an important source of astrophysical neutrinos, and the study of stellar neutrinos is an important branch of neutrino astronomy. In this chapter we shall first introduce the basic theory of stellar evolution and then describe the basic properties of stellar neutrinos. To be explicit, we shall concentrate on the neutrinos generated from thermal nuclear reactions in the solar core. The production processes, experimental detection and flavor conversions of solar neutrinos will be discussed in detail.

6.1 Stellar Evolution in a Nutshell

Although there does not exist a complete theory of star formation, it is commonly believed that stars were formed from the clouds of the primordial gases bounded by the gravity. A star can in general be defined as an astrophysical object bounded by the gravity of itself and radiating energy from its internal thermal nuclear reactions (Prialnik, 2000). In this section we outline the quantities describing a star and the equations governing its evolution.

6.1.1 Distance, Luminosity and Mass

The Sun is a typical main-sequence star best known to us. Let us first summarize the observational characteristics of the Sun so as to get a ballpark feeling of the main-sequence stars, which represent a long and static period in the evolution of stars. The average distance between the Sun and the Earth is defined as an astronomical unit: 1 AU $= 1.496 \times 10^{13}$ cm. The total mass of the Sun is $\mathcal{M}_\odot = 1.989 \times 10^{33}$ g, and its radius is $R_\odot = 6.955 \times 10^{10}$ cm. In comparison, the mass and radius of the Earth are $\mathcal{M}_\oplus = 5.974 \times 10^{27}$ g and $R_\oplus = 6.378 \times 10^8$ cm. Note that $R_\odot$ (or AU) serves as a standard scale in determining the distances of planets (or stars) from the Earth within (or beyond) the solar system. A common method for the distance determination is the stellar parallax (Prialnik, 2000; Carroll and Ostlie, 2007). The

parallax is one half of the angle between the lines of sight of a star from two different positions of the observers. By a measurement of the parallax p, the distance of a star from the solar system can be determined as $d = (1\ \text{AU})/\tan p \approx (1\ \text{AU})/p$, where p is assumed to be very small and its unit is radian. In view of 1 radian $= 57.2958^\circ = 206265''$, one may define the distance unit as parallax second (i.e., parsec or pc for short). Then an astrophysical distance can be written as $d = (1/p)$ pc with 1 pc $= 3.086 \times 10^{18}$ cm, where the unit of p is arc second. Another conventional unit is light year (i.e., ly for short), defined as the distance travelled by the light in a Julian year. Namely, 1 ly $= 9.461 \times 10^{17}$ cm and then 1 pc ≈ 3.262 ly. The stellar parallax is always smaller than $1''$. For instance, Proxima Centauri (the nearest star other than the Sun) has a parallax angle $\sim 0.77''$ (Carroll and Ostlie, 2007). The Earth's atmosphere makes a ground-based telescope difficult to reach a precision better than $0.03''$, implying that it is impossible to measure a distance farther than 30 pc. To overcome such an obstacle, the European Space Agency launched the satellite Hipparcos in 1989. This mission was able to measure the parallax angles with an accuracy in the range $(0.7 \sim 0.9) \times 10^{-3}$ arc seconds for more than 10^5 stars (Perrymann *et al.*, 1997).

The observation of a star is to measure its apparent luminosity l, which depends on the absolute luminosity L and the distance d. The values of L and l characterize the energies emitted from the star per second and received by the detector per second per square centimeter, respectively. If the energy released by a star is isotropic and not absorbed on the way to the detector, we have $l \equiv L/(4\pi d^2)$ (Carroll and Ostlie, 2007). Historically, the apparent magnitude m is used to describe the brightness of stars. The Greek astronomer Hipparchus was the first to assign $m = 1$ to the brightest star and $m = 6$ to the dimmest one in the sky (Krisciunas, 2001). It was later realized that the human eye actually responded to a difference in the logarithm of the brightness. For instance, a difference of 5 magnitudes corresponds to a factor of 100 in brightness; i.e., one magnitude difference is equivalent to a factor of $100^{1/5}$ in the apparent luminosity. One may therefore obtain $l \propto 10^{-2m/5}$, implying

$$\frac{l_2}{l_1} = 10^{2(m_1 - m_2)/5} \ . \tag{6.1}$$

The absolute magnitude M is defined as the apparent magnitude that a star would have if it were located at 10 pc from the Earth. So one may express the distance of a star in terms of its apparent and absolute magnitudes:

$$d = 10^{(m - M + 5)/5} \ , \tag{6.2}$$

where d is measured in parsecs, and $m - M = 5 \log[d/(10\ \text{pc})]$ is called the star's radius modulus. The absolute luminosity of the Sun is $L_\odot = 3.839 \times 10^{33}$ erg s^{-1}. The apparent luminosity of the Sun can then be given by

$$l_\odot = \frac{L_\odot}{4\pi (1\ \text{AU})^2} = 1.365 \times 10^6\ \text{erg cm}^{-2}\ \text{s}^{-1} \ , \tag{6.3}$$

which is known as the solar constant [1]. The constant of proportionality of $l \propto 10^{-2m/5}$ has been experimentally determined to be 2.52×10^{-5} erg cm^{-2} s^{-1} (Weinberg, 2008). Given the value of $l_\odot$ in Eq. (6.3), the apparent magnitude of the Sun is found to be $m_{\rm Sun} = -26.83$. In view of the Earth-Sun distance $d = 1$ AU $= 4.848 \times 10^{-6}$ pc, we obtain the absolute magnitude of the Sun

$$M_{\rm Sun} = m_{\rm Sun} - 5 \log \left(\frac{d}{10 \ {\rm pc}} \right) = +4.74 \ . \tag{6.4}$$

Since the absolute magnitude is defined at the fixed distance 10 pc, the ratio of two different absolute magnitudes is the same as that of the corresponding absolute luminosities. The absolute magnitude M of a star is therefore related to its absolute luminosity L as follows:

$$M = M_{\rm Sun} - 2.5 \log \left(\frac{L}{L_\odot} \right) \ . \tag{6.5}$$

It seems natural for an observer to first measure the apparent magnitude m and then use the distance d to probe the intrinsic properties of a star, such as M via Eq. (6.2) or L through Eq. (6.5). If a star belongs to a special class (e.g., the pulsating variable stars), however, its L and M can be determined in a way independent of d (Carroll and Ostlie, 2007). In this case one may use Eq. (6.2) to work out the star's distance.

Note that both M and L have been defined for all the wavelengths of the light from a star. Astronomers usually introduce the color magnitudes M_U, M_B and M_V for the ultraviolet (U), blue (B) and visual (V) wavelength regions. The reason is simply that a measurement can only be carried out in a finite wavelength range. For a star with known d, its absolute color magnitude can be fixed by the radius modulus $m - M = 5 \log[d/(10 \ {\rm pc})]$. The color index defined as $B - V \equiv M_B - M_V$ is obviously independent of the distance d. Fig. 6.1 shows the color-magnitude diagram for more than 3700 stars from the Hipparchos catalog. The main feature of this diagram is that the stars are not uniformly distributed but concentrate on the band denoted as the main sequence, implying that it is the longest and most static period in the whole lifetime of stars.

On the other hand, it has been found that the spectra of starlight are well consistent with that of the blackbody radiation. Hence the spectrum is peaked at a wavelength $\lambda_{\rm max}$, corresponding to an effective temperature T via Wien's displacement law $b = \lambda_{\rm max} T = 0.29$ cm K. The luminosity L of a blackbody of area A and temperature T is given by $L = A \sigma_{\rm SB} T^4$, where $\sigma_{\rm SB}$ is the Stefan-Boltzmann constant given in Table 6.1. For a spherical star with

[1] Here we adopt the centimeter-gram-second (cgs) unit system instead of the International System of units (abbreviated to SI from its French name). For example, 1 Joule $= 10^7$ erg and $L_\odot = 3.839 \times 10^{26}$ W. Some frequently-used fundamental constants in the SI units are listed in Table 6.1, and the conversion factors between the SI and cgs unit systems are given in Table 6.2.

Table 6.1 Fundamental physical constants in the SI units, where the figures in the parentheses after the values denote the 1σ uncertainties in the last digits (Mohr *et al.*, 2007, 2008; Nakamura *et al.*, 2010)

Quantity	Symbol	Value
speed of light in vacuum	c	$2.99\ 792\ 458 \times 10^{8}$ m s^{-1}
Planck constant	h	$6.626\ 068\ 96(33) \times 10^{-34}$ J s
reduced Planck constant	$\hbar$	$1.054\ 571\ 628(53) \times 10^{-34}$ J s
Boltzmann constant	$k_{\rm B}$	$1.380\ 6504(24) \times 10^{-23}$ J K^{-1}
Newton constant	$G_{\rm N}$	$6.674\ 28(67) \times 10^{-11}$ m^3 kg^{-1} s^{-2}
Stefan-Boltzmann constant	$\sigma_{\rm SB}$	$5.670\ 400(40) \times 10^{-8}$ W m^{-2} K^{-4}
Wien constant	b	$2.897\ 7685(51) \times 10^{-3}$ m K
Avogadro constant	$\mathcal{N}_{\rm A}$	$6.022\ 141\ 79(30) \times 10^{-23}$ mol^{-1}
electron charge magnitude	e	$1.602\ 176\ 487(40) \times 10^{-19}$ C
electron mass	m_e	$9.109\ 382\ 15(45) \times 10^{-31}$ kg
proton mass	m_p	$1.672\ 621\ 637(83) \times 10^{-27}$ kg
neutron mass	m_n	$1.674\ 927\ 211(84) \times 10^{-27}$ kg
atomic mass unit	$m_{\rm H}$	$1.660\ 538\ 782(83) \times 10^{-27}$ kg

Table 6.2 Conversion factors from the SI units to the cgs units, or vice versa (Carroll and Ostlie, 2007. With permission from Pearson Education, Inc.)

Quantity	SI unit	cgs unit	Conversion factor
length	m	cm	10^{-2}
mass	kg	g	10^{-3}
time	s	s	1
charge	C	esu	$3.335\ 640\ 952 \times 10^{-10}$
force	N (kg m s^{-2})	dyne (g cm s^{-2})	10^{-5}
energy	J (N m)	erg (dyne cm)	10^{-7}
power	W (J s^{-1})	erg s^{-1}	10^{-7}
pressure	Pa (N m^{-2})	dyne cm^{-2}	10^{-1}

radius R, one may define the effective temperature $T_{\rm eff}$ via $L = 4\pi R^2 \sigma_{\rm SB} T_{\rm eff}^4$, implying that the surface flux is given by $F = L/(4\pi R^2) = \sigma_{\rm SB} T_{\rm eff}^4$. Taking the Sun for example, we can estimate the temperature at its surface:

$$T_\odot = \left(\frac{L_\odot}{4\pi \sigma_{\rm SB} R_\odot^2} \right)^{1/4} \approx 5777 \text{ K} . \tag{6.6}$$

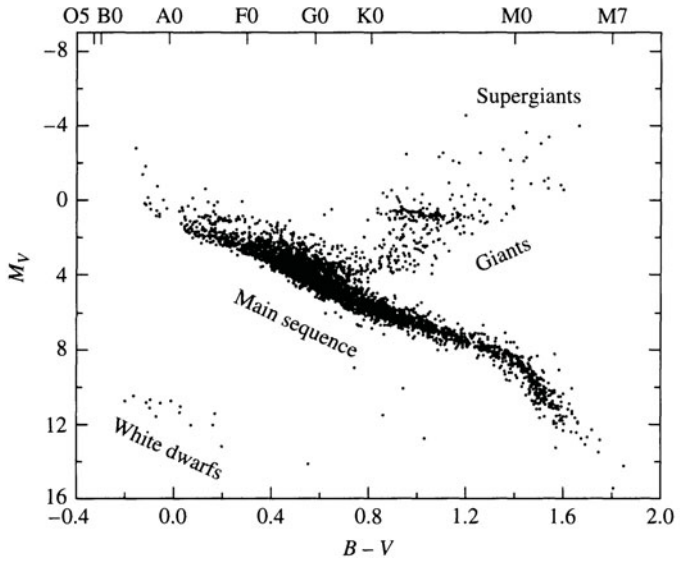

Fig. 6.1 The color-magnitude diagram for the stars from the Hipparchos catalog, where the spectral types are given at the top border (Carroll and Ostlie, 2007. With permission from Pearson Education, Inc.)

This result means that the spectrum of sunlight is peaked at $\lambda_{\rm max} \approx 502$ nm. The color-magnitude diagram can also be represented as a relationship between $T_{\rm eff}$ and L. The stars having the same luminosity may appear different colors because of their different radii. Furthermore, the initial masses of stars are crucial for their later evolution and account for the distinct branches in Fig. 6.1. A successful theory of stellar evolution should predict the correlation among the mass, luminosity and radius of a star.

A common method to exactly measure the masses of stars has been lacking. The mass of the Sun can be determined from Kepler's third law, $P^2 = 4\pi^2 d^3/(G_{\rm N}\mathcal{M}_\odot)$, where P and d stand respectively for the period of a planet and its average distance from the Sun. Note that a planet's mass is negligible as compared with the solar mass. Taking the planet as the Earth, one can derive the solar mass by inputting the relevant properties of the Earth and the precisely-measured Newton constant $G_{\rm N}$. Another case, in which the stellar mass can be determined, is that the star happens to be a binary star. Given the distance d of a binary star and its orbital plane perpendicular to the line of sight of an observer, one may figure out the mass ratio of the primary star to its companion star: $\mathcal{M}_1/\mathcal{M}_2 = \theta_2/\theta_1$, where θ_1 and θ_2 are the angles spanned by the corresponding semimajor axes a_1 and a_2. On the other hand, the total mass of a binary star can be extracted by using Kepler's third law. The realistic situation may of course be complicated by the motion of the center of mass of a binary star (Carroll and Ostlie, 2007).

6.1.2 Basic Equations of Stellar Evolution

A star and its dynamics can well be understood in some reasonable approximations. In fact, the spherical symmetry is quite a good approximation due to the isotropic self-gravity of the system. It is also reasonable to assume hydrodynamic and thermal equilibrium, at least for the main-sequence stars. In order to make clear these points, we estimate the timescales of some important processes in stars. First, the typical velocity of a mass point in the gravity of a star with mass $\mathcal{M}$ and radius R is the escape velocity $v = \sqrt{G_{\rm N}\mathcal{M}/R}$. The dynamical timescale is defined as the time during which the mass point can travel from the surface to the center of a star at the speed v,

$$\tau_{\rm dyn} \approx \frac{R}{v} = \sqrt{\frac{R^3}{G_{\rm N}\mathcal{M}}} \approx 10^3 \sqrt{\left(\frac{R}{R_\odot}\right)^3 \left(\frac{\mathcal{M}_\odot}{\mathcal{M}}\right)} \ \ {\rm s} \ . \tag{6.7}$$

Note that $\tau_{\rm dyn} \approx 10^3$ s is much shorter than the age of the Sun, which is about 1.5×10^{17} s. This observation implies that the star will collapse in such a short time, if there is no pressure force to balance the gravity. If the pressure exceeds the gravity, however, the dynamical process may be a violent explosion. In this sense a stable star should be assumed to be in the hydrostatic equilibrium state. Second, we introduce the gravitational (or Kelvin-Helmholtz) timescale $\tau_{\rm gra}$. The total gravitational potential energy is $U \sim G_{\rm N}\mathcal{M}^2/R$, so the time for a star to radiate all this energy is given by

$$\tau_{\rm gra} \approx \frac{U}{L} = \frac{G_{\rm N}\mathcal{M}^2}{RL} \approx 10^{15} \left(\frac{\mathcal{M}}{\mathcal{M}_\odot}\right)^2 \left(\frac{R_\odot}{R}\right) \left(\frac{L_\odot}{L}\right) \ \ {\rm s} \ , \tag{6.8}$$

where L is the stellar luminosity. This timescale is shorter than one percent of the age of the Sun, implying that the Sun would have burnt out if it were only powered by the gravitational potential energy. Finally, the nuclear timescale is set by the total mass of a star and the released energy from its nuclear reactions. The ratio of nuclear binding energies to the rest mass of nucleons is about $\varepsilon \approx 10^{-3}$, so the total nuclear energy is characterized by $\varepsilon\mathcal{M}$. The nuclear timescale is therefore given as

$$\tau_{\rm nuc} \approx \frac{\varepsilon\mathcal{M}}{L} \approx 5 \times 10^{17} \left(\frac{\mathcal{M}}{\mathcal{M}_\odot}\right) \left(\frac{L_\odot}{L}\right) \ \ {\rm s} \ , \tag{6.9}$$

which is several times longer than the age of the Sun and exceeds that of the Universe. Hence only the initial composition in a fraction rather than all of the stellar mass has been changed by thermal nuclear reactions. The above discussions indicate that the pressure, gravity and nuclear reactions are the most important ingredients in a theory of stellar evolution. In the following we shall present a brief summary of the fundamental principles and basic equations of stellar evolution (Chandrasekhar, 1938; Bahcall, 1989; Prialnik, 2000; Salaris and Cassisi, 2005).

(1) *Hydrostatic equilibrium.* The pressure is needed to balance the gravity, and thus it makes the star in hydrostatic equilibrium. Consider a thin spherical shell at the radius r. Its mass is given by $\Delta\mathcal{M} = 4\pi\rho(r)r^2\Delta r$, where $\rho(r)$ is the local matter density and Δr denotes the thickness of the shell. The gravity between the sphere with radius r and the mass shell reads

$$f_{\rm gra} = -\frac{G_{\rm N}\mathcal{M}(r)\Delta\mathcal{M}}{r^2} \,, \tag{6.10}$$

while the force caused by the pressure $P(r)$ is $f_{\rm p} = 4\pi r^2\,[-P(r+\Delta r) + P(r)]$. By requiring the balance $f_{\rm gra} + f_{\rm p} = 0$ and setting $\Delta r \to 0$, one obtains

$$\frac{{\rm d}P(r)}{{\rm d}r} = -\frac{G_{\rm N}\mathcal{M}(r)\rho(r)}{r^2} \,, \tag{6.11}$$

where the total mass $\mathcal{M}(r)$ contained in the sphere with radius r is given by $\mathcal{M}(r) = \int_0^r 4\pi r'^2\rho(r'){\rm d}r'$. The latter can also be expressed in the differential form as $\dfrac{{\rm d}\mathcal{M}(r)}{{\rm d}r} = 4\pi r^2\rho(r)$, which is just the equation of mass continuity. Since the right-hand side of Eq. (6.11) is always negative, the pressure should decrease as the radius increases. A rough estimate of the pressure in the center of the Sun leads us to

$$\frac{{\rm d}P(r)}{{\rm d}r} \sim \frac{P_{\rm s} - P_{\rm c}}{R_\odot} \sim -\frac{P_{\rm c}}{R_\odot} \,, \tag{6.12}$$

where $P_{\rm s} \approx 0$ and $P_{\rm c}$ stand respectively for the pressure at the surface and in the center of the Sun. Comparing between Eqs. (6.11) and (6.12), we get

$$P_{\rm c} \sim G_{\rm N}\frac{\mathcal{M}_\odot\overline{\rho}_\odot}{R_\odot} \sim 2.7\times10^{15}\ {\rm dyne\ cm^{-2}} \,, \tag{6.13}$$

where $\overline{\rho}_\odot = \mathcal{M}_\odot/(4\pi R_\odot^3/3) \sim 1.41\ {\rm g\ cm^{-3}}$ is the average density of the Sun. A more accurate calculation yields $P_{\rm c} = 2.34\times10^{17}\ {\rm dyne\ cm^{-2}}$, which should be compared with the standard atmospheric pressure $1\ {\rm atm} = 1.013\times10^6\ {\rm dyne\ cm^{-2}}$. We see that the central pressure of the Sun is very high, so are its temperature and density to be shown below.

(2) *Equation of state.* There are essentially two kinds of contributions to the pressure: one is from the ideal gas consisting of electrons and ionized atoms, and the other is from radiation or photons. More importantly, the pressure may come from the degenerate electrons and neutrons such as in the white dwarfs and neutron stars. The pressure of the ideal gas is given by $P_{\rm gas} = nk_{\rm B}T$ with $k_{\rm B}$ being the Boltzmann constant and n being the particle number density. One may also express this pressure as $P_{\rm gas} = \rho k_{\rm B}T/(\mu m_{\rm H})$, where $\mu \equiv \overline{m}/m_{\rm H}$ denotes the mean molecular weight, $m_{\rm H}$ is the atomic mass unit, and $\overline{m} \equiv \rho/n$ represents the average mass of a gas particle. The pressure of radiation is related to the energy density through $P_{\rm rad} = u/3$ with

$u = aT^4$, where $a = 4\sigma_{\rm SB}/c = 7.56 \times 10^{-15}$ erg cm^{-3} K^{-4} is the radiation constant. The total pressure turns out to be

$$P = P_{\rm gas} + P_{\rm rad} = \frac{\rho kT}{\mu m_{\rm H}} + \frac{1}{3}aT^4 \; . \tag{6.14}$$

In order to determine the mean molecular weight, one has to know the chemical composition of the gas. For the ionized gas, we have

$$\frac{1}{\mu m_{\rm H}} = \frac{1}{\overline{m}} = \frac{n}{\rho} = \frac{\sum\limits_j N_j(1+z_j)}{\sum\limits_j N_j m_j} \; , \tag{6.15}$$

where N_j is the number of the "j" atoms, z_j denotes the number of free electrons in the "j" atom and m_j is its mass. We define the atomic number $A_j = m_j/m_{\rm H}$ and the mass fraction X_j, which is the ratio of the total mass of the "j" atoms to that of the gas. Then Eq. (6.15) can be rewritten as

$$\frac{1}{\mu m_{\rm H}} = \sum_j \frac{N_j(1+z_j)}{N_j m_j} \cdot \frac{N_j m_j}{\sum\limits_j N_j m_j} = \sum_j \frac{N_j(1+z_j)}{N_j A_j m_{\rm H}} X_j \; . \tag{6.16}$$

To illustrate, we assume a completely ionized gas and denote the mass fractions of hydrogen, helium and other heavier elements as X, Y and Z with $X + Y + Z = 1$. So the mean molecular weight is given by

$$\frac{1}{\mu} = 2X + \frac{3}{4}Y + \left\langle \frac{1+z_j}{A_j} \right\rangle Z \approx 2X + \frac{3}{4}Y + \frac{1}{2}Z \; . \tag{6.17}$$

Note that $1 + z_j \approx z_j$ and $A_j \approx 2z_j$ hold for the elements much heavier than helium. For a neutral gas, one may set $z_j = 0$ in Eq. (6.16) and then obtain $\mu^{-1} \approx X + Y/4 + \langle A_j^{-1} \rangle Z$. For young stars with the typical composition $X = 0.71$, $Y = 0.27$ and $Z = 0.02$, one may get $\mu = 1.29$ for a neutral gas or $\mu = 0.61$ for a completely ionized gas. Omitting the pressure of radiation, we can estimate the temperature of the solar core by using Eq. (6.14):

$$T_{\rm c} \sim \frac{\mu m_{\rm H} P_{\rm c}}{\overline{\rho}_\odot k_{\rm B}} \sim 1.44 \times 10^7 \ {\rm K} \; , \tag{6.18}$$

where Eq. (6.13) and $\mu = 0.61$ for an ionized gas have been used. This rough estimate is in good agreement with the result $T_{\rm c} = 1.57 \times 10^7$ K from a more detailed analysis. In fact, the chemical composition in the Sun is slightly different from $X = 0.71$, $Y = 0.27$ and $Z = 0.02$ because a fraction of hydrogen has been converted into helium.

(3) *Chemical composition.* Hydrogen and helium dominate the initial chemical composition of stars, but nuclear reactions taking place in the stars will change the element abundances. Consider a two-body nuclear reaction

$$I(Z_i, A_i) + J(Z_j, A_j) \rightleftharpoons K(Z_k, A_k) + L(Z_l, A_l) \ , \tag{6.19}$$

where Z_m and A_m (for $m = i, j, k, l$) denote the atomic and mass numbers of the element I, J, K or L. To figure out the number density n_i, we need to know the cross section of this reaction σ_{ijk} and the relative velocity v between I and J. Because of $Z_i + Z_j = Z_k + Z_l$ and $A_i + A_j = A_k + A_l$, the index "l" can be omitted in denoting σ_{ijk}. The effective target area is $n_i\sigma_{ijk}$, and the number of the "J" particles crossing this area in unit time is $n_j v$. So the number of reactions occurring in unit time and unit volume is given by $n_i n_j \sigma_{ijk} v$ or $n_i n_j R_{ijk}$ with $R_{ijk} = \sigma_{ijk} v$ being the interaction rate. As a result, the evolution of n_i reads

$$\dot{n}_i = -n_i \sum_{j,k} n_j R_{ijk} + \sum_{k,l} \frac{n_k n_l}{1 + \delta_{kl}} R_{kli} \ , \tag{6.20}$$

where the factor $1/(1+\delta_{kl})$ takes account of the identical particles with $k = l$. For the initial states with $i = j$, the factor $1/2$ will be cancelled because the reaction reduces the number of the "I" particles by two units. In terms of the mass fraction X_j of the "J" particles, Eq. (6.20) can be recast into

$$\frac{\dot{X}_i}{A_i} = \frac{\rho}{m_{\rm H}} \left[-\frac{X_i}{A_i} \sum_{j,k} \frac{X_j}{A_j} R_{ijk} + \sum_{k,l} \frac{X_k X_l}{A_k A_l} \cdot \frac{R_{kli}}{1 + \delta_{kl}} \right] \ , \tag{6.21}$$

where R_{ijk} relies on the matter density, temperature and chemical elements.

(4) *Energy conservation.* For a spherical shell at the radius r with a thickness $\mathrm{d}r$, its local or interior luminosity is defined as $\mathrm{d}L_r = 4\pi r^2 \rho(r) \epsilon \mathrm{d}r$ with ϵ being the coefficient of energy generation per unit time and unit mass. The energy conservation means

$$\frac{\mathrm{d}L_r}{\mathrm{d}r} = 4\pi r^2 \epsilon \rho(r) \ , \tag{6.22}$$

where $\epsilon = \epsilon_{\rm gra} + \epsilon_{\rm nuc} - \epsilon_\nu$ including the gravitational potential energy, the energy released from nuclear reactions and that carried away by neutrinos.

(5) *Energy transfer.* There are three different ways of energy transport in stars: radiation, convection and conduction. Radiation means that energies produced by the gravitational potential and nuclear reactions are carried away by photons from the core to the surface of a star. Although convection is important in the stellar evolution, thermal radiation and conduction are dominant in the Sun. Convection in the Sun is rather complicated and only relevant in its outer layer with a thickness of about $0.3R_\odot$ (Basu and Antia, 2008). Let us first discuss radiation. Consider a flux of photons $F_{\rm rad}$ traversing

a slab with thickness $\mathrm{d}r$. The photons will be absorbed by matter in the slab, and its energy loss is given by $\mathrm{d}F_{\rm rad} = -\kappa_\gamma \rho F_{\rm rad}\mathrm{d}r$, where κ_γ denotes the opacity coefficient and ρ is the matter density. Note that κ_γ itself depends on the matter density, chemical composition, and temperature of the slab. The radiation flux is then given by

$$F_{\rm rad} = F_0 \mathrm{e}^{-\kappa_\gamma \rho r} = F_0 \mathrm{e}^{-r/\lambda_\gamma} \ , \tag{6.23}$$

where F_0 is the initial flux and $\lambda_\gamma \equiv (\kappa_\gamma \rho)^{-1}$ can be regarded as the mean free path of photons. Since $\mathrm{d}F_{\rm rad}/c$ measures a change of the momentum of radiation which is equivalent to a change of the pressure of radiation $\mathrm{d}P_{\rm rad}$, we have $\dfrac{\mathrm{d}P_{\rm rad}}{\mathrm{d}r} = -\kappa_\gamma \rho F_{\rm rad}/c$. Given $P_{\rm rad} = aT^4/3$, the local luminosity $L_r = 4\pi r^2 F_{\rm rad}$ can be related to the temperature gradient as follows:

$$L_r = -4\pi r^2 \frac{4acT^3}{3\kappa_\gamma \rho} \cdot \frac{\mathrm{d}T}{\mathrm{d}r} \ . \tag{6.24}$$

We proceed to discuss conduction, the energy transported by the particles except photons. The energy flux of non-degenerate electrons can be written as $F_e = n_e E_e v$, where n_e denotes the average number density of electrons, $E_e = 3k_{\rm B}T/2$ is the thermal energy, and v is the average velocity of electrons. Note that the absorption of electrons leads to a decrease of the energy flux: $\mathrm{d}F_e = -\lambda_e^{-1} F_e \mathrm{d}r$ with λ_e being the mean free path of electrons. Therefore,

$$F_e = -\frac{3}{2}\lambda_e n_e k_{\rm B} v \frac{\mathrm{d}T}{\mathrm{d}r} \ . \tag{6.25}$$

This result has a form similar to that of $F_{\rm rad} = L_r/(4\pi r^2)$ as one can see from Eq. (6.24). Combining the radiation and conduction contributions, we define the total energy flux as $F \equiv F_{\rm rad} + F_e$ and rewrite the local luminosity as $L_r = 4\pi r^2 F$. Then the overall energy transport can be expressed as

$$L_r = -4\pi r^2 \frac{4acT^3}{3\kappa \rho} \cdot \frac{\mathrm{d}T}{\mathrm{d}r} \ , \tag{6.26}$$

where $\kappa^{-1} \equiv \kappa_\gamma^{-1} + \kappa_e^{-1}$ is defined, and $\kappa_e = 8acT^3/(9\lambda_e n_e k_{\rm B} v \rho)$ is the opacity coefficient of electrons. Finally, we mention that convection as a mechanism of the energy and chemical element transport is involved in the large-scale motion of matter in stars (Salaris and Cassisi, 2005). Since there is no satisfactory theory of convection at present, the convective flux is usually calculated in some approximations (Biermann, 1951; Vitense, 1953; Böhm-Vitense, 1958). It is expected that the convective transport is insignificant in the stellar core where neutrinos are produced (Bahcall, 1989).

In summary, the local luminosity $L_r(r)$, pressure $P(r)$, temperature $T(r)$, density $\rho(r)$ and chemical elements X_i (for $i = 1, 2, \cdots, n$) of a star are governed by a set of differential equations. Because of the equation of state,

we are left with $n+3$ independent quantities (i.e., P, T, L_r and X_i) which are described by the following $n+3$ differential equations:

$$\begin{aligned}\frac{\mathrm{d}P(r)}{\mathrm{d}r} &= -\frac{G_{\mathrm{N}}\mathcal{M}(r)\rho(r)}{r^2}\ ,\\ \frac{\mathrm{d}T(r)}{\mathrm{d}r} &= -\frac{3\kappa\rho}{4acT^3(r)}\cdot\frac{L_r(r)}{4\pi r^2}\ ,\\ \frac{\mathrm{d}L_r(r)}{\mathrm{d}r} &= 4\pi^2 r^2\epsilon\rho(r)\ ,\end{aligned} \tag{6.27}$$

and $\dfrac{\mathrm{d}X_i}{\mathrm{d}t} = f_i[X_i, \rho(r), T(r)]$ with f_i being definable through Eq. (6.21). To solve these equations, one has to impose the initial conditions and calculate the energy production coefficient ϵ, the opacity coefficient κ and the interaction rates R_{ijk} by means of particle physics.

6.1.3 Energy Sources of Stars

The gravitational potential energy and thermal nuclear reactions are two important energy sources of stars. First, let us present the virial theorem and apply it to the stars in hydrostatic equilibrium. With the help of $\mathrm{d}\mathcal{M} = 4\pi\rho r^2\mathrm{d}r$, one may rewrite Eq. (6.11) as $\dfrac{\mathrm{d}P}{\mathrm{d}\mathcal{M}} = -G_{\mathrm{N}}\mathcal{M}/(4\pi r^4)$. Then

$$\int_0^{\mathcal{M}_{\mathrm{s}}} 4\pi r^3\frac{\mathrm{d}P}{\mathrm{d}\mathcal{M}}\mathrm{d}\mathcal{M} = -\int_0^{\mathcal{M}_{\mathrm{s}}}\frac{G_{\mathrm{N}}\mathcal{M}}{r}\mathrm{d}\mathcal{M}\ , \tag{6.28}$$

where $\mathcal{M}_{\mathrm{s}}$ is the total mass of the star. The right-hand side of Eq. (6.28) represents the gravitational potential energy Ω, while an integration by parts on its left-hand side leads to

$$\int_0^{\mathcal{M}_{\mathrm{s}}} 12\pi r^2 P\frac{\mathrm{d}r}{\mathrm{d}\mathcal{M}}\mathrm{d}\mathcal{M} = 3\int_0^{\mathcal{M}_{\mathrm{s}}}\frac{P}{\rho}\mathrm{d}\mathcal{M}\ , \tag{6.29}$$

where we have used $P = P_{\mathrm{s}} = 0$ at the surface and the mass conservation $\dfrac{\mathrm{d}r}{\mathrm{d}\mathcal{M}} = 1/(4\pi r^2\rho)$. For an ideal gas, the internal energy per unit mass is $u = 3k_{\mathrm{B}}T/(2\mu m_{\mathrm{H}})$ and the equation of state reads $P/\rho = k_{\mathrm{B}}T/(\mu m_{\mathrm{H}})$. So Eqs. (6.28) and (6.29) establish a relationship between the internal energy U and the gravitational potential energy Ω:

$$U \equiv \int_0^{\mathcal{M}_{\mathrm{s}}} u\ \mathrm{d}\mathcal{M} = -\frac{\Omega}{2}\ , \tag{6.30}$$

known as the virial theorem. The total energy is $E = U + \Omega = \Omega/2 < 0$, as it should be for a bound system. Consider a star without nuclear reactions but radiating energies from its surface. Its luminosity is $L = -\dfrac{\mathrm{d}E}{\mathrm{d}t}$. The

virial theorem yields $L \propto -\dfrac{\mathrm{d}\Omega}{\mathrm{d}t}$, implying that the gravitational potential energy decreases so as to give a positive luminosity. Hence the star has to contract when it radiates energies, and it has a negative specific heat. The virial theorem can also be used to estimate the average temperature. Taking account of $\Omega \propto -G_{\rm N}\mathcal{M}_{\rm s}^2/R$ and $U = 3k_{\rm B}\overline{T}\mathcal{M}_{\rm s}/(2\mu m_{\rm H})$, one may get the average temperature $\overline{T} \propto \mathcal{M}_{\rm s}/R \propto \mathcal{M}_{\rm s}^{2/3}\overline{\rho}^{1/3}$, where the average density is defined as $\overline{\rho} \propto \mathcal{M}_{\rm s}/R^3$. For two stars with the same mass, the one with a larger matter density must have a higher average temperature.

Table 6.3 Conversion factors of five frequently-used units in the system of natural units with $\hbar = k_{\rm B} = c = 1$ (Raffelt, 1996, with permission from the University of Chicago Press; Raffelt and Rodejohann, 1999)

	s^{-1}	cm^{-1}	K	eV	g
s^{-1}	1	$0.334 \cdot 10^{-10}$	0.764×10^{-11}	0.658×10^{-15}	1.173×10^{-48}
cm^{-1}	2.998×10^{10}	1	0.2289	1.973×10^{-5}	0.352×10^{-37}
K	1.310×10^{11}	4.369	1	0.862×10^{-4}	1.537×10^{-37}
eV	1.519×10^{15}	0.507×10^{5}	1.160×10^{4}	1	1.783×10^{-33}
g	0.852×10^{48}	2.843×10^{37}	0.651×10^{37}	0.561×10^{33}	1

Second, let us calculate the energy production from nuclear reactions. If a sum of the masses of initial nuclei is larger than that of final nuclei in a specific reaction (i.e., $M_{\rm initial} > M_{\rm final}$), the energy released from this reaction is then given by $\Delta E = M_{\rm initial} - M_{\rm final}$. Such a mass difference comes from the binding energy of a nucleus. Given a nucleus $X(Z, A)$ with mass M_X, for example, its binding energy is $E_{\rm bind} = Zm_p + (A - Z)m_n - M_X$ with $m_p = 938.272$ MeV and $m_n = 939.565$ MeV being the proton and neutron masses [2]. The nucleus of ^{56}Fe possesses the maximal binding energy per nucleon: $(E_{\rm B}/A)(^{56}\mathrm{Fe}) = 8.79$ MeV. That is why the elements lighter (or heavier) than ^{56}Fe can produce energies via thermonuclear fusion (or nuclear fission). Consider the energy release from the nuclear reaction in Eq. (6.19):

$$Q_{ijk} = M_I + M_J - M_K - M_L \ . \tag{6.31}$$

As discussed in Section 6.1.2, the number of reactions occurring in unit time and unit volume is $n_i n_j R_{ijk}$ with $R_{ijk} = \sigma_{ijk} v$ being the reaction rate. With the help of Eq. (6.21), the rate of energy production in unit mass is given as

[2] The natural units with $\hbar = c = k_{\rm B} = 1$ are commonly adopted in particle physics. In this case the units of length, mass, time and temperature can be expressed in the unit of energy (1 eV $= 1.602 \times 10^{-19}$ J $= 1.602 \times 10^{-12}$ erg). The conversion factors of these units are listed in Table 6.3.

$$\epsilon_{\rm nuc} = \frac{\rho}{m_{\rm H}^2} \sum_{i,j,k} \frac{1}{1+\delta_{ij}} \cdot \frac{X_i X_j}{A_i A_j} R_{ijk} Q_{ijk} \ . \tag{6.32}$$

Note that the initial nuclei have to overcome the Coulomb repulsive force between them, in order for the nuclear reactions to take place. The thermal energies of the nuclei are around keV $\sim 10^7$ K, but the barrier at nuclear distances is as high as several MeV. Nevertheless, these reactions can still happen via quantum tunneling effects. George Gamow pointed out that the penetration probability or the cross section must be proportional to $\exp[-2\pi Z_i Z_j e^2/(\hbar v)]$ (Gamow, 1928). In addition, the Maxwell-Boltzmann distribution of the velocity is proportional to $\exp[-M_{\rm g} v^2/(2k_{\rm B}T)]$, where the reduced mass of the gas particle is defined as $M_{\rm g} \equiv M_I M_J/(M_I+M_J)$. As the velocity v increases, the first exponential function increases but the second one decreases. Hence the product $\exp[-2\pi Z_i Z_j e^2/(\hbar v)] \exp[-M_{\rm g} v^2/(2k_{\rm B}T)]$ possesses a maximum, the so-called Gamow peak. The cross section is conventionally defined as

$$\sigma_{ijk}(E) = \frac{S_{ij}(E)}{E} \exp(-2\pi\eta) \ , \tag{6.33}$$

where $\eta \equiv Z_i Z_j e^2/(\hbar v)$. The exponential factor $\exp(-2\pi\eta)$ in Eq. (6.33) comes from quantum tunneling and is known as the Gamow penetration factor. A dimensional analysis yields $\sigma_{ijk}(E) \sim \pi\lambda_{\rm de}^2 \sim \pi h^2/p^2 \propto E^{-1}$, where $\lambda_{\rm de} = h/p$ is the de Broglie wavelength and $E = p^2/2M_{\rm g}$ has been used. The astrophysical factor $S_{ij}(E)$ is energy-dependent and contains the information of nuclear structure. In practice, one may extrapolate the experimental data on $S_{ij}(E)$ at high energies to the low-energy regime relevant to stellar environments. Because the typical temperature in stars is in the range of $(1 \sim 100)$ keV and much smaller than nuclear masses, the velocity distribution is well described by the Maxwell-Boltzmann function:

$$R_{ijk} = \frac{2}{\pi^{1/2}(k_{\rm B}T)^{3/2}} \int_0^\infty E^{1/2} {\rm e}^{-E/k_{\rm B}T} v\sigma(v) {\rm d}E \ , \tag{6.34}$$

where the relative velocity v and the kinetic energy E satisfy $E = M_{\rm g} v^2/2$. A combination of Eqs. (6.33) and (6.34) leads us to (Cox and Giuli, 1968)

$$R_{ijk} = \sqrt{\frac{8}{\pi M_{\rm g} k_{\rm B} T}} S_{ij} \int_0^\infty {\rm e}^{-\left(y + C/\sqrt{y}\right)} {\rm d}y \ , \tag{6.35}$$

where $y \equiv E/(k_{\rm B}T)$, $C = (2\pi M_{\rm g})^{1/2} Z_i Z_j e^2/[\hbar (k_{\rm B}T)^{1/2}]$, and S_{ij} is assumed to be a constant. As a matter of fact, $S_{ij}(E)$ takes the value at the Gamow peak if its energy dependence is non-negligible (Bahcall, 1989).

Astronomical observations have established that all the main-sequence stars are predominantly composed of hydrogen. Hence the energy source of

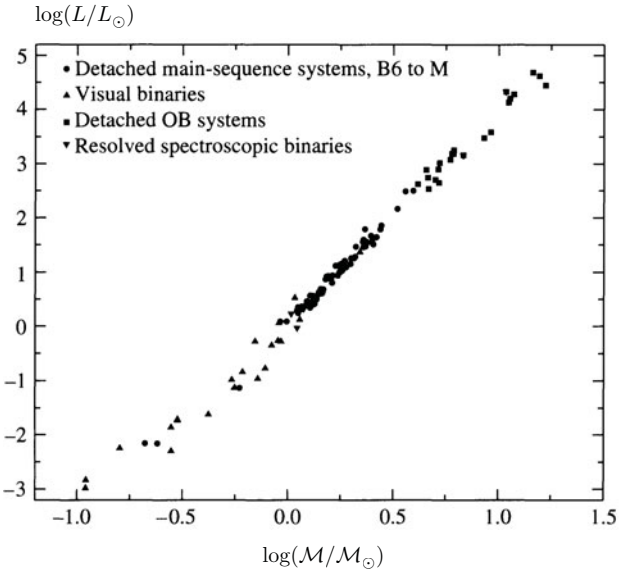

Fig. 6.2 The observational data on the mass-luminosity relation for the main-sequence stars (Carroll and Ostlie, 2007. With permission from Pearson Education, Inc.)

these stars is most likely to be the fusion of four hydrogen nuclei into one ^{4}He nucleus. To be specific, we write out the reaction

$$4p + 2e^- \rightarrow {}^4\mathrm{He} + 2\nu_e + Q \,, \tag{6.36}$$

where $Q \approx 4m_p + 2m_e - m_{^4\mathrm{He}} \approx 26.73$ MeV is just 0.7% of the sum of initial proton masses. If the Sun were composed entirely of hydrogen and all the hydrogen were converted into helium via the above reaction, the time for this process to be completed would be $\tau \sim 0.7\% \times m_p \times (\mathcal{M}_\odot/m_p)/L_\odot \approx 10^{11}$ yr, where the present solar luminosity is assumed. If only 10% of the hydrogen in the Sun is consumed, the solar lifetime will be of the right order of magnitude $\tau \sim 10^{10}$ yr, consistent with the nuclear timescale τ_{nuc} given in Eq. (6.9). The hydrogen burning proceeds in two different ways: the proton-proton (pp) chain and the carbon-nitrogen-oxygen (CNO) circle, which are also the main sources of stellar neutrinos. The advanced nuclear fusions, such as the carbon and silicon burning, require much higher temperatures $\sim 10^9$ K. Hence we shall only consider the hydrogen-burning stage, which is relevant to the Sun and thus the production of solar neutrinos (Bahcall, 1989).

6.1.4 The Mass-Luminosity Relation

The color-magnitude diagram has been shown in Fig. 6.1, from which one can see a clear correlation between the effective temperature and luminosity. For

the main-sequence stars, there exists an empirical mass-luminosity relation shown in Fig. 6.2. More explicitly (Cox and Giuli, 1968; Prialnik, 2000),

$$\frac{L}{L_\odot} \propto \left(\frac{\mathcal{M}}{\mathcal{M}_\odot}\right)^\nu , \tag{6.37}$$

where $\nu = 3 \sim 5$ denotes the power index for the main-sequence stars. Given a chemical composition similar to the Sun, it has been found that $\nu \approx 3.6$ holds for the stars with their masses lying in the range $20\mathcal{M}_\odot > \mathcal{M} > 2\mathcal{M}_\odot$, $\nu \approx 4.5$ for $2\mathcal{M}_\odot > \mathcal{M} > 0.5\mathcal{M}_\odot$ and $\nu \approx 2.6$ for $0.5\mathcal{M}_\odot > \mathcal{M} > 0.2\mathcal{M}_\odot$ (Salaris and Cassisi, 2005). Let us use the basic equations to understand such an elegant relation. With the help of the condition of hydrostatic equilibrium in Eq. (6.11), we approximately obtain $P \sim \mathcal{M}^2/R^4$ by equating the left-hand side of Eq. (6.11) with P/R and taking the average density $\rho \sim \mathcal{M}/R^3$. Assuming the equation of state of the ideal gas (i.e., $P \propto \rho T$), we get the temperature $T \propto P/\rho \sim \mathcal{M}/R$. These relations, together with Eq. (6.24), allow us to derive an empirical mass-luminosity relation for $\nu = 3$:

$$L \propto \frac{R^4}{\mathcal{M}} T^4 \propto \frac{R^4}{\mathcal{M}} \left(\frac{\mathcal{M}}{R}\right)^4 = \mathcal{M}^3 . \tag{6.38}$$

For massive stars with $\mathcal{M} > 10\mathcal{M}_\odot$, the mass-luminosity relation becomes less steep. The reason for this difference is simply that the radiation pressure is dominant in the massive stars, so the pressure is given by $P \propto T^4$ and $T \propto \mathcal{M}^{1/2}/R$ arises from $P \sim \mathcal{M}^2/R^4$. After inserting $T \propto \mathcal{M}^{1/2}/R$ into Eq. (6.38), we can arrive at a linear mass-luminosity relation $L \propto \mathcal{M}$. These simple arguments help us understand the observed correlation between stellar masses and luminosities, at least to some extent. It is worth mentioning that the mass-luminosity relation is not applicable to the other branches of stars shown in Fig. 6.1. Those kinds of stars may have the cores with degenerate electrons, and hence the above simple arguments are invalid.

6.2 Neutrinos from the Sun

Although how stars formed in the first place remains an open question, it is believed that they originated from a gravitationally bound system of the primordial gas. The theory of Big Bang nucleosynthesis tells us that the mass fraction of helium in the primordial gas is about 25%, and the rest is almost hydrogen. The bound gas contracts due to the energy loss via electromagnetic radiation, but the temperature of this system increases because of the negative specific heat. When the temperature is high enough to ignite hydrogen, the energy released from hydrogen fusion makes the gas expanding. As a result, the gravity is balanced by the pressure force and the system achieves hydrostatic equilibrium. This is the case for the main-sequence stars, like the

Sun. When all the hydrogen at the stellar core is consumed, further evolution of the star depends on its initial mass. For a mass below $(2 \sim 3)\mathcal{M}_{\odot}$, the helium as a product of hydrogen fusion accumulates at the center and there is a hydrogen-burning shell around the dense helium core. Meanwhile, matter around the core starts to expand and hence the temperature of the surface decreases. In other words, the star becomes redder and is called a red giant. The core of a red giant is so hot and dense that helium fusion becomes possible. The stage with a helium-burning core and a hydrogen-burning shell is known as a horizontal-branch star. For a mass up to $(6 \sim 8)\mathcal{M}_{\odot}$, carbon and oxygen can be produced in the stellar core, but further fusion processes are not allowed. Since all the fuels are burnt out, these stars with a degenerate core will cool down by emitting neutrinos and photons until they disappear from view. Such a star is referred to as a white dwarf. For more massive stars with $\mathcal{M} > (6 \sim 8)\mathcal{M}_{\odot}$, nuclear fusion at the center can continue to the formation of the most stable element — iron. When the degenerate iron core reaches the Chandrasekhar limit and there are no more energies released from nuclear reactions, the core becomes unstable. Further contraction allows photons to disassociate the nuclei, and this process will consume energies and further reduce the pressure. In addition, electrons are captured by the nuclei and converted into electron neutrinos. The latter will escape and carry away more energies. So the unstable core must continue to collapse. A collapsed star and its subsequent evolution may lead to a type-II supernova. Neutrinos emitted from the type-II supernova explosion will be discussed in Chapter 7.

We shall subsequently focus our interest on the Sun, a typical main-sequence star, by introducing the standard solar model (SSM). We shall also pay particular attention to the production of solar neutrinos.

6.2.1 The Standard Solar Model

The answer to why the Sun shines was first given by Hans Bethe, who worked out the solar nuclear fusion chains in 1939 (Bethe, 1939). Neutrinos produced from these nuclear reactions were completely ignored, because the existence of neutrinos had not been experimentally established by that time (Bethe and Peierls, 1934). In 1940, George Gamow and Mario Schoenberg pointed out that neutrinos could take away a large amount of energies and should be very important in a collapsing star (Gamow and Schoenberg, 1940, 1941). Neutrinos were first discovered by Clyde Cowan and Frederick Reines in 1956 (Cowan *et al.*, 1956). A theoretical calculation of solar neutrino fluxes was carried out by John Bahcall in 1964, and a proposal for detecting solar neutrinos was put forward by Raymond Davis in the same year (Bahcall, 1964; Davis, 1964). The SSM was originally built and continuously refined by Bahcall and his collaborators (Bahcall *et al.*, 1982, 2001, 2006; Bahcall and Ulrich, 1988; Bahcall and Pinsonneault, 1995).

Let us summarize the main approximations made in the SSM, or more generally in a theory of the main-sequence stars (Bahcall, 1989). (1) The

Sun is spherically symmetric and its intrinsic properties only depend on its radius. As a consequence, the rotation and magnetic fields can be neglected. (2) Hydrostatic equilibrium is always assumed in the SSM. Any significant deviation from hydrostatic equilibrium would have already led the Sun to a global contraction or expansion in about one hour (i.e., the dynamical timescale $\tau_{\rm dyn} \sim 10^3$ s). (3) The energy transport is induced by photons or convection. The radiative energy transport is dominant in the solar core, while the convective energy transport becomes important near the solar surface. (4) The energy production is attributed to thermal nuclear reactions, and the energy gain or loss induced by the local contraction or expansion should be taken into account. (5) The chemical composition is changed only through nuclear reactions, and thermal or gravitational diffusion of nuclear elements should be included. Based on these approximations, the basic equations given in Section 6.1 can then be applied to the Sun.

We proceed to outline the input parameters in the SSM. They include the primordial chemical abundances, radiative opacity, equation of state and nuclear reaction rates. The primordial chemical composition is usually given by the helium mass fraction Y and the metal-to-hydrogen ratio Z/X. The latter can be extracted from a measurement of the chemical abundances of the solar surface. Note that the metal here stands for the elements heavier than helium. Since the surface temperature is relatively low, nuclear reactions cannot be initiated and thus the abundance at the surface can represent the primordial one. We are able to measure the chemical abundance of the solar surface in two different ways. The first is the mass spectroscopy of meteorites at terrestrial laboratories. However, the volatile elements including hydrogen, helium, carbon, nitrogen, oxygen and neon might have been depleted in the pristine meteorites. In this case silicon is usually chosen to measure the relative abundances of other elements. Hence some prior knowledge of silicon at the solar surface is needed to determine the chemical composition. The other way is to analyze the solar spectrum and atomic lines. It depends on the model of the solar atmosphere and spectrum formation. These two methods are consistent with and complementary to each other, and the latest results with widely-used compilations are listed in Table 6.4 (Asplund *et al.*, 2009). It is worth remarking that the initial chemical composition can significantly affect the radiative opacity of the solar core, which has a great impact on the central temperature and thus solar neutrino fluxes.

Building the SSM may begin with the so-called zero-age-main-sequence star of $1\mathcal{M}_\odot$ (Prialnik, 2000). Since the age $\tau_\odot$, luminosity $L_\odot$ and radius $R_\odot$ of the Sun have been precisely measured, they must be reproduced by the SSM. These important parameters of the Sun are listed in Table 6.5. The density and sound velocity profiles of the Sun, from its surface to the deep core, can be determined from the study of the solar acoustic oscillations (i.e., the so-called helioseismology). They also provide strict constraints on the SSM (Basu and Antia, 2008).

Table 6.4 The latest and widely-used mass fractions of hydrogen (X), helium (Y) and metals (Z) in the present-day solar photosphere (Asplund *et al.*, 2009. With permission from Annual Reviews)

References	X	Y	Z	Z/X
Anders and Grevesse, 1989	0.7314	0.2485	0.0201	0.0274
Grevesse and Noels, 1993	0.7336	0.2485	0.0179	0.0244
Grevesse and Sauval, 1998	0.7345	0.2485	0.0169	0.0231
Lodders, 2003	0.7491	0.2377	0.0133	0.0177
Asplund *et al.*, 2005	0.7392	0.2485	0.0122	0.0165
Lodders *et al.*, 2009	0.7390	0.2469	0.0141	0.0191
Asplund *et al.*, 2009	0.7381	0.2485	0.0134	0.0181

Table 6.5 Some important parameters of the Sun (Bahcall, 1989. With permission from the Cambridge University Press)

Parameter	Value
Luminosity ($L_\odot$)	3.86×10^{33} erg s^{-1}
Mass ($\mathcal{M}_\odot$)	1.99×10^{33} g
Radius ($R_\odot$)	6.96×10^{10} cm
Age ($\tau_\odot$)	4.57×10^{9} yr
Central density ($\rho_{\rm C}$)	148 g cm^{-3}
Central hydrogen abundance ($X_{\rm C}$)	0.34

6.2.2 Proton-proton Chain and CNO Cycle

As shown in Eq. (6.36), the main energy source in the Sun is the nuclear fusion reaction which converts four protons into a helium nucleus and releases the energy $Q \approx 26.73$ MeV. Two neutrinos are emitted from this reaction and carry away only 2% of the total energy. The burning of hydrogen proceeds via the *pp* chain and CNO cycle.

(1) *The pp chain.* The first process is $p + p \to {\rm D} + e^+ + \nu_e$. The positron may immediately annihilate with an ambient electron and thus it contributes to the energy production. The electron neutrinos produced from this reaction are referred to as the *pp* neutrinos. They have a continuous energy spectrum and a maximal energy $E_\nu^{\rm max} = 0.420$ MeV. The rate of *pp* reactions can be calculated by using the standard theory of weak interactions together with the experimental data on the proton-proton scattering and properties of the deuteron (Bahcall *et al.*, 1982). The second process is the electron-capture reaction $p + e^- + p \to {\rm D} + \nu_e$, where the energy of the electron neutrino is

$E_\nu = 1.442$ MeV. The energy spectrum of such *pep* neutrinos is in principle discrete, but the broadening effects due to the thermal motion actually make the spectrum continuous. Note that the nuclear matrix elements relevant to the *pp* and *pep* reactions are the same, so the ratio of these two reaction rates is independent of the SSM. The *pep* reaction rate can be accurately calculated by means of the electroweak theory and with the help of the *pp* reaction rate. The next step in the *pp* chain is the production of ^{3}He in the proton-capture reaction $\mathrm{D} + p \rightarrow {}^3\mathrm{He} + \gamma$. This is the only reaction for the deuteron burning in the Sun, and there are no neutrinos produced from this process. The termination of the *pp* chain is mainly via the process $^3\mathrm{He} + {}^3\mathrm{He} \rightarrow {}^4\mathrm{He} + 2p$ (i.e., the *pp*-I chain). There is also another termination with the probability 2×10^{-7} via the reaction $p + {}^3\mathrm{He} \rightarrow {}^4\mathrm{He} + e^+ + \nu_e$, where neutrinos with energies up to $E_\nu^{\max} = 18.77$ MeV are generated. Although these *hep* neutrinos have sufficiently high energies, their flux is unfortunately too small to be detected. The remaining two possibilities for the termination of the *pp* chain are related to the production of beryllium ^{7}Be through $^3\mathrm{He} + {}^4\mathrm{He} \rightarrow {}^7\mathrm{Be} + \gamma$ and its subsequent interactions: (a) the *pp*-II chain characterized by $^7\mathrm{Be} + e^- \rightarrow {}^7\mathrm{Li} + \nu_e$ and $^7\mathrm{Li} + p \rightarrow 2\ {}^4\mathrm{He}$ with a branching fraction 99.87%, producing ^{7}Be neutrinos with either $E_\nu = 0.862$ MeV (with the probability 89.7%) or $E_\nu = 0.384$ MeV due to the excited state of lithium (with the probability 10.3%); (b) the *pp*-III chain characterized by $^7\mathrm{Be} + p \rightarrow {}^8\mathrm{B} + \gamma$, $^8\mathrm{B} \rightarrow {}^8\mathrm{Be}^* + e^+ + \nu_e$ and $^8\mathrm{Be}^* \rightarrow 2\ {}^4\mathrm{He}$ with a branching fraction 0.13%, producing ^{8}B neutrinos with a maximal energy $E_\nu^{\max} = 15$ MeV. Although the reaction rate of $^7\mathrm{Be} + p \rightarrow {}^8\mathrm{B} + \gamma$ is highly suppressed, it is practically easier to detect ^{8}B neutrinos because their energies are much higher than those of the more abundant *pp*, *pep* and ^{7}Be neutrinos. In fact, all the solar neutrino experiments are sensitive to ^{8}B neutrinos.

(2) *The CNO cycle.* Since carbon is most abundant among the heavy elements in stars, the CNO cycle offers another important way to realize hydrogen fusion. More explicitly, we have $^{12}\mathrm{C} + p \rightarrow {}^{13}\mathrm{N} + \gamma$, $^{13}\mathrm{N} \rightarrow {}^{13}\mathrm{C} + e^+ + \nu_e$ and $^{13}\mathrm{C} + p \rightarrow {}^{14}\mathrm{N} + \gamma$, where electron neutrinos arise from the β^+ decays of ^{13}N and thus are known as ^{13}N neutrinos. The further proton-capture process $^{14}\mathrm{N} + p \rightarrow {}^{15}\mathrm{O} + \gamma$ rarely occurs, but it gives birth to ^{15}O neutrinos and terminates one of the CNO cycles via $^{15}\mathrm{O} \rightarrow {}^{15}\mathrm{N} + e^+ + \nu_e$ and $^{15}\mathrm{N} + p \rightarrow {}^{12}\mathrm{C} + {}^4\mathrm{He}$. There exists a slim chance ($\sim 0.1\%$) for the production of ^{16}O in the proton-capture reaction of ^{15}N (i.e., $^{15}\mathrm{N} + p \rightarrow {}^{16}\mathrm{O} + \gamma$), which initiates another CNO cycle and produces ^{17}F neutrinos via $^{16}\mathrm{O} + p \rightarrow {}^{17}\mathrm{F} + \gamma$ and $^{17}\mathrm{F} \rightarrow {}^{17}\mathrm{O} + e^+ + \nu_e$. This cycle is terminated by the production of helium via $^{17}\mathrm{O} + p \rightarrow {}^{14}\mathrm{N} + {}^4\mathrm{He}$. All the CNO neutrinos result from the β^+ decays, so the corresponding neutrino energy spectra are continuous. The experimental detection of CNO neutrinos seems very difficult because their energies and fluxes are not sufficiently high.

6.2.3 Solar Neutrino Fluxes

Nuclear energies and neutrinos are released from the *pp* chain and CNO cycle. The energies are mostly carried away by photons, which diffuse from the solar core until they reach the photosphere where the medium becomes transparent. The diffusion time of photons is about 10^4 yr. In comparison, neutrinos almost freely escape from the Sun after they are produced. Hence the detection of solar neutrinos can offer direct evidence for thermonuclear reactions in the center of the Sun. We summarize various sources of solar neutrinos together with their average and maximal energies in Table 6.6. Note that ^{7}Be and *pep* neutrinos have discrete line spectra.

Table 6.6 Various sources of solar neutrinos together with their average energies $\langle E_\nu \rangle$ and maximal energies $E_\nu^{\max}$ as compared with the average thermal energies E (in units of MeV) (Giunti and Kim, 2007. With permission from the Oxford University Press)

Source	Reaction	$\langle E_\nu \rangle$	$E_\nu^{\max}$	E
pp	$p + p \to \mathrm{D} + e^+ + \nu_e$	0.2668	0.423	13.0987
pep	$p + e^- + p \to \mathrm{D} + \nu_e$	1.455	1.455	11.9193
hep	$^3\mathrm{He} + p \to {}^4\mathrm{H} + e^+ + \nu_e$	9.628	18.778	3.7370
^{7}Be	$^7\mathrm{Be} + e^- \to {}^7\mathrm{Li} + \nu_e$	0.8631	0.8631	12.6008
^{7}Be	$^7\mathrm{Be} + e^- \to {}^7\mathrm{Li}^* + \nu_e$	0.3855	0.3855	12.6008
^{8}B	$^8\mathrm{B} \to {}^8\mathrm{Be}^* + e^+ + \nu_e$	6.735	~ 15	6.6305
^{13}N	$^{13}\mathrm{N} \to {}^{13}\mathrm{C} + e^+ + \nu_e$	0.7063	1.1982	3.4577
^{15}O	$^{15}\mathrm{O} \to {}^{15}\mathrm{N} + e^+ + \nu_e$	0.9964	1.7317	21.5706
^{17}F	$^{17}\mathrm{F} \to {}^{17}\mathrm{O} + e^+ + \nu_e$	0.9977	1.7364	2.363

Since nuclear reactions in the *pp* chain and CNO cycle are already known, one may directly calculate solar neutrino fluxes for all the sources listed in Table 6.6. The most relevant quantity for the reaction rate R_{ij} is the astrophysical factor S_{ij} defined in Eq. (6.33). A neutrino flux is actually computed by integrating the local production rate over the volume of the Sun,

$$\Phi_i = \int_0^{\mathcal{M}_\odot} R_i \left[\rho(\mathcal{M}), T(\mathcal{M}), \{X_j\}\right] \mathrm{d}\mathcal{M} \,, \tag{6.39}$$

where the subscript i denotes the neutrino source type, and R_i describes the corresponding production rate per unit mass. The latter apparently depends on the matter density, local temperature and chemical composition. Now that both the thermal energy and neutrinos are generated from the hydrogen

fusion reaction $4p + 2e^- \rightarrow {}^4\mathrm{He} + 2\nu_e + Q$ with $Q = 26.73$ MeV, we can roughly estimate the total neutrino flux:

$$\Phi_\nu \equiv \sum_i \Phi_i \approx 2 \times \frac{L_\odot}{4\pi(1\ \mathrm{AU})^2} \cdot \frac{1}{Q} \approx 6.4 \times 10^{10}\ \mathrm{cm}^{-2}\ \mathrm{s}^{-1}\ , \qquad (6.40)$$

where the factor 2 takes account of the fact that two neutrinos are produced from hydrogen fusion, and $L_\odot$ is the solar luminosity. A recent revision of the abundances of heavy elements at the solar surface yields $(Z/X)_\odot = 0.0165$ (Asplund *et al.*, 2005) as compared with the previous result $(Z/X)_\odot = 0.0229$ (Grevesse and Sauval, 1998). This new determination of solar metallicity is in contradiction with the helioseismological measurements (Chaplin *et al.*, 2007; Basu *et al.*, 2007). In contrast, the earlier and larger value of metallicity agrees very well with the solar density and pressure profiles extracted from the helioseismological observations (Serenelli *et al.*, 2009). Two SSMs have been constructed by using the previous (larger) and recent (smaller) results of heavy-element abundances, so they are referred to as BPS(GS98) and BPS(AGS05), respectively (Pena-Garay and Serenelli, 2008).

Fig. 6.3 illustrates the distribution of solar neutrino fluxes as a function of the solar radius fraction $r/R_\odot$. Note that solar neutrinos are actually produced in the core region with $r < 0.35\ R_\odot$. In particular, almost all the ^{8}B neutrinos are produced from the core ($r \lesssim 0.1 R_\odot$), so their total flux depends sensitively on the central temperature T. It has been found that $\Phi_{^8\mathrm{B}} \propto T^{18}$, $\Phi_{^7\mathrm{Be}} \propto T^8$ and $\Phi_{pp} \propto T^{-1.2}$ hold approximately. The *pp* neutrinos are generated in the region from which most of the solar luminosity arises. Hence the above temperature dependence of *pp* neutrinos is mainly ascribed to the constraint coming from the solar luminosity (Bahcall, 1989). Theoretical predictions for the energy spectra of solar neutrinos from the SSM of BPS(GS98) 2008 are shown in Fig. 6.4. In addition, solar neutrino fluxes predicted by the SSMs of BPS(GS98) 2008 and BPS(AGS05) 2008 are listed in Table 6.7. A difference between the predictions of these two models for every neutrino flux is given in the last column of Table 6.7.

6.3 Experimental Detection of Solar Neutrinos

Solar neutrinos can be detected by means of radiochemical reactions, water Cherenkov detectors and (or) liquid scintillators. Some typical and important experiments on solar neutrinos will be briefly introduced in this section, from which one can see why there was the well-known solar neutrino problem.

6.3.1 Radiochemical Methods

It was Bruno Pontecorvo who first suggested detecting electron neutrinos via the inverse beta decay (Pontecorvo, 1946; Alvarez, 1948)

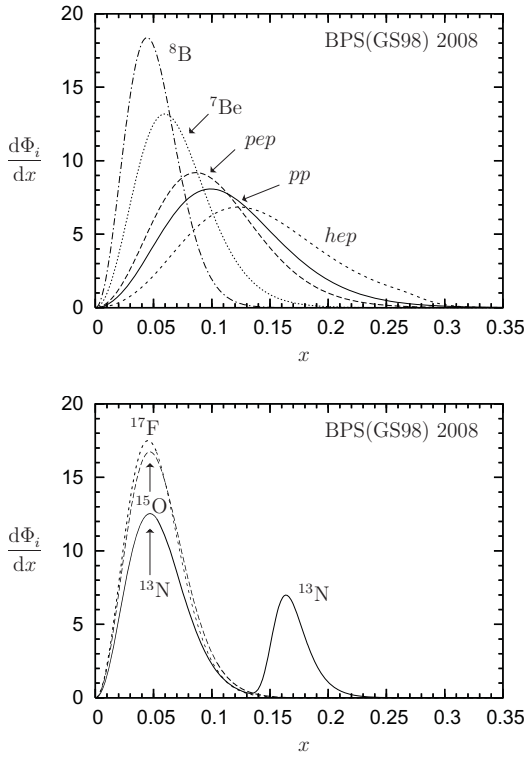

Fig. 6.3 The distribution of solar neutrino fluxes $\frac{d\Phi_i}{dx}$ with respect to the solar radius fraction $x \equiv r/R_\odot$, where the SSM of BPS(GS98) 2008 has been assumed (Pena-Garay and Serenelli, 2008)

$$\nu_e + {}^{37}\mathrm{Cl} \rightarrow {}^{37}\mathrm{Ar} + e^- \ . \tag{6.41}$$

This method was later used by Davis in the pioneering Homestake solar neutrino experiment (Davis, 1964). The energy threshold for the Cl-Ar reaction in Eq. (6.41) is $E_\nu^{\mathrm{th}} = 0.814$ MeV, so the Homestake experiment can only detect those solar neutrinos with medium and high energies. This experiment was located in the Homestake Gold Mine at Lead in South Dakota. Its detector was a single horizontal steel tank and contained a volume of 615 tons of liquid perchloroethylene C_2Cl_4, and hence the neutrino target was about 2.16×10^{30} atoms (130 tons) of ^{37}Cl. The key problem of a chlorine experiment is to extract and count the resultant argon atoms. First, a small amount of isotopically pure ^{36}Ar or ^{38}Ar carrier gas is placed in the tank of liquid perchloroethylene. Then the detector is exposed to solar neutrinos for about two months. This time interval is chosen such that the number of ^{37}Ar atoms can nearly grow to the saturation value (i.e., the production rate is equal to the decay rate). After the exposure, the argon atoms are extracted by purging

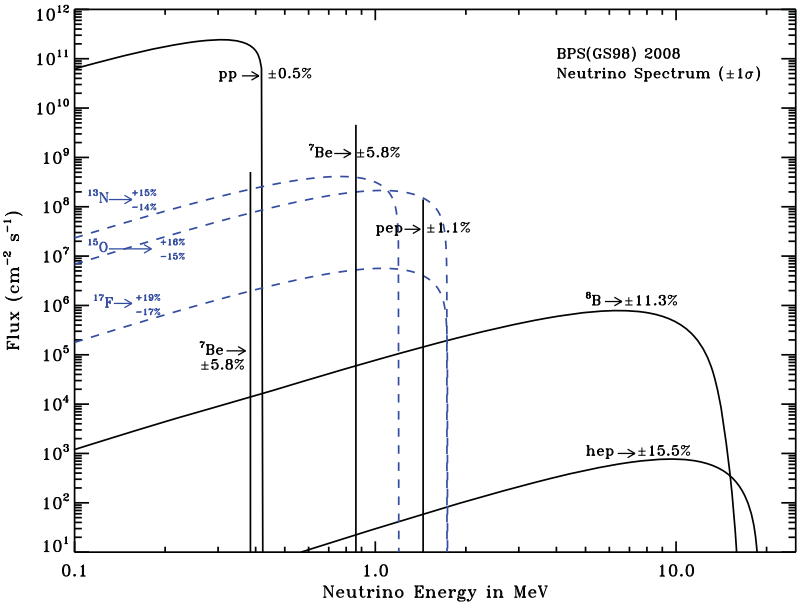

Fig. 6.4 The energy spectra of solar neutrinos from the SSM of BPS(GS98) 2008, where the 1σ theoretical uncertainties are given (Pena-Garay and Serenelli, 2008)

Table 6.7 Solar neutrino fluxes predicted by the SSMs of BPS(GS98) 2008 and BPS(AGS05) 2008. Note that the fluxes are given in units of 10^{10} (*pp*), 10^{9} (^{7}Be), 10^{8} (*pep*, ^{13}N and ^{15}O), 10^{6} (^{8}B and ^{17}F) and 10^{3} (*hep*) cm^{-2} s^{-1}, respectively (Pena-Garay and Serenelli, 2008)

Source	BPS(GS98) 2008	BPS(AGS05) 2008	Difference
pp	$5.97(1 \pm 0.006)$	$6.04(1 \pm 0.005)$	1.2%
pep	$1.41(1 \pm 0.011)$	$1.45(1 \pm 0.010)$	2.8%
hep	$7.90(1 \pm 0.15)$	$8.22(1 \pm 0.15)$	4.1%
^{7}Be	$5.07(1 \pm 0.06)$	$4.55(1 \pm 0.06)$	10%
^{8}B	$5.94(1 \pm 0.11)$	$4.72(1 \pm 0.11)$	21%
^{13}N	$2.88(1 \pm 0.15)$	$1.89(1^{+0.14}_{-0.13})$	34%
^{15}O	$2.15(1^{+0.17}_{-0.16})$	$1.34(1^{+0.16}_{-0.15})$	31%
^{17}F	$5.82(1^{+0.19}_{-0.17})$	$3.25(1^{+0.16}_{-0.15})$	44%

with the helium gas. The recovery efficiency of ^{37}Ar is determined by comparing the measured isotopic composition of the extracted argon atoms with the amount of isotopically pure carrier gas at the beginning of each run. Finally, the extracted ^{37}Ar atoms are counted by observing the 2.82 keV Auger elec-

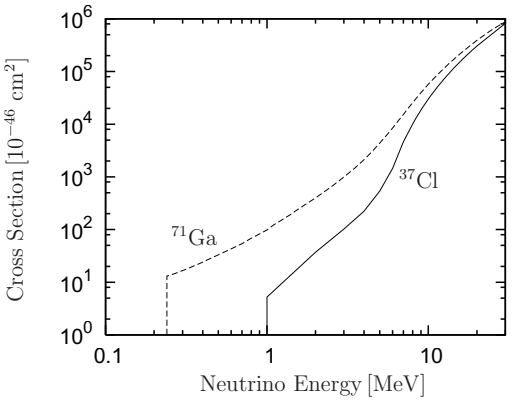

Fig. 6.5 The neutrino absorption cross sections on ^{37}Cl and ^{71}Ga as functions of the energies of incident neutrinos (Bahcall *et al.*, 1996; Bahcall, 1997. With permission from the American Physical Society)

trons from the electron-capture decay of ^{37}Ar (i.e., $^{37}\mathrm{Ar} + e^- \rightarrow {}^{37}\mathrm{Cl} + \nu_e$). The main background is induced by the cascades of energetic muons from cosmic rays. The cascade particles, including pions, protons and neutrons, may interact with ^{37}Cl and produce ^{37}Ar. The background is estimated to be (0.08 ± 0.03) atoms of ^{37}Ar per day (Bahcall, 1989).

Fig. 6.5 shows the neutrino absorption cross section on the chlorine. It is easy to see that the chlorine experiment is most sensitive to the high-energy part of ^{8}B neutrinos. The solar neutrino unit (SNU) has often been used to express the neutrino capture rate (Bahcall, 1969, 1989):

$$R = \sum_i \Phi_i \sigma \sim \left[10^{10}\ \mathrm{cm}^{-2}\ \mathrm{s}^{-1}\right] \times \left[10^{-46}\ \mathrm{cm}^2\right] = 10^{-36}\ \mathrm{s}^{-1}\ , \qquad (6.42)$$

so 1 SNU corresponds to 10^{-36} interactions per target atom per second. After 25 years of measurements (from March 1970 to February 1994), the Homestake experiment reported the following average solar neutrino rate (Cleveland *et al.*, 1998): $R_{\mathrm{Cl}}^{\mathrm{exp}} = 2.56 \pm 0.16$ (stat.) $\pm\, 0.16$ (syst.) SNU $= 2.56 \pm 0.23$ SNU, which was only about 1/3 of the theoretical prediction made by Bahcall (Bahcall, 1989; 1997). Current theoretical predictions are $R_{\mathrm{Cl}}^{\mathrm{th}} = 8.46^{+0.87}_{-0.88}$ SNU based on the SSM of BPS(GS98) and $R_{\mathrm{Cl}}^{\mathrm{th}} = 6.86^{+0.69}_{-0.70}$ SNU according to the SSM of BPS(AGS05) (Pena-Garay and Serenelli, 2008). Therefore, we conclude that the observed neutrino rate given above remains about one third of the expected one.

There were three other solar neutrino experiments using the radiochemical method: GALLEX, GNO and SAGE, which detected solar neutrinos via the inverse beta decay of ^{71}Ga (Kuzmin, 1966)

$$\nu_e + {}^{71}\mathrm{Ga} \rightarrow {}^{71}\mathrm{Ge} + e^-\ , \qquad (6.43)$$

where the neutrino energy threshold is $E_\nu^{\rm th} = 0.233$ MeV. Such a low value of $E_\nu^{\rm th}$ makes it possible to detect solar neutrinos almost in the whole energy range as shown in Fig. 6.4. In particular, a measurement of *pp* neutrinos from the *pp* chain reactions is of great importance because the *pp* neutrino flux is closely related to the solar luminosity. The neutrino absorption cross section on ^{71}Ga is shown in Fig. 6.5 as a function of the neutrino energy (from 0.24 MeV to 30 MeV). Let us briefly summarize the main results of GALLEX, GNO and SAGE experiments.

(1) The GALLium EXperiment (GALLEX) was done at the Laboratori Nazionali del Gran Sasso (LNGS) in Italy. Its detector contained 30.3 tons of ^{71}Ga in the form of a concentrated $GaCl_3$-HCl solution, and was exposed to solar neutrinos for a time period between three and four weeks. The GALLEX experiment ran from May 1991 to January 1997, with a break in 1997 (Hampel *et al.*, 1999), and was then followed by the Gallium Neutrino Observatory (GNO) experiment. The GNO experiment used the same detector of the GALLEX experiment but improved its extraction equipment (Altmann *et al.*, 2000, 2005). A recent reanalysis of the data accumulated in the GALLEX experiment yields the solar neutrino rate $R_{\rm Ga}^{\rm exp}({\rm GALLEX}) = 73.4^{+7.1}_{-7.3}$ SNU (Kaether *et al.*, 2010). The two gallium experiments at LNGS totally lasted 12 years, and their joint result has been found to be $R_{\rm Ga}^{\rm exp}({\rm GALLEX + GNO}) = 69.3^{+5.5}_{-5.5}$ SNU (Altmann *et al.*, 2005).

(2) The Soviet-American Gallium Experiment (SAGE) was located in the Baksan Neutrino Observatory of the Russian Academy of Sciences in the northern Caucasus mountains (Abazov *et al.*, 1991; Abdurashitov *et al.*, 1994, 2002, 2006). The detection method used in the SAGE experiment is the same as that used in the GALLEX and GNO experiments. After running from January 1990 to December 2001, the SAGE experiment reported the average solar neutrino rate $R_{\rm Ga}^{\rm exp}({\rm SAGE}) = 70.8^{+6.5}_{-6.1}$ SNU (Abdurashitov *et al.*, 2002). This result is in good agreement with the one obtained from the GALLEX and GNO experiments.

Theoretical predictions for the neutrino capture rate on ^{71}Ga are $R_{\rm Ga}^{\rm th} = 127.9^{+8.1}_{-8.2}$ SNU based on the SSM of BPS(GS98) and $R_{\rm Ga}^{\rm th} = 120.5^{+6.9}_{-7.1}$ SNU according to the SSM of BPS(AGS05) (Pena-Garay and Serenelli, 2008). Either of them is nearly twice the result obtained from the GALLEX/GNO or SAGE experiment. In other words, there is a discrepancy of more than 5σ between theoretical predictions and experimental data in this respect.

6.3.2 Water Cherenkov Detectors

If the velocities of charged particles exceed the speed of light in a medium, they can radiate photons. This phenomenon is known as Cherenkov radiation (Landau and Lifshitz, 1984). So an important neutrino detection method is to measure Cherenkov radiation emitted from ultra-relativistic charged leptons which are produced from neutral- and charged-current neutrino interactions. The Cherenkov detector allows a real-time measurement of the direction of

charged leptons, and thus it can determine the direction of incident neutrinos. Since the refractive index of light in water is $n \approx 1.33$, the Cherenkov radiation forms a light cone with an open angle given by $\cos\theta = 1/(nv)$. Taking the velocity $v \approx c$ for ultra-relativistic charged leptons, one obtains $\theta \approx 41^\circ$. The axis of the light cone is just the track of the running charged lepton. A water Cherenkov detector usually consists of many photomultiplier tubes (PMTs) used to measure Cherenkov radiation. Both the energy and direction of incident neutrinos can in principle be reconstructed.

All the Cherenkov detectors used to detect solar neutrinos make use of water as the medium. Let us briefly summarize the main results of a few important solar neutrino experiments of this type.

(1) The Kamioka Nucleon Decay Experiment (Kamiokande), which originally aimed for the detection of nucleon decays, was completed in 1983. Its detector was placed 1000 m underground in the Kamioka mine, about 200 km west of Tokyo. It had a cylindrical water tank containing 3000 tons of pure water. About 1000 PMTs were attached to the inner surface of the tank. In 1985, the detector was upgraded to Kamiokande-II in order to observe solar ^{8}B neutrinos. The relevant process is the neutrino-electron elastic scattering

$$\nu_\alpha + e^- \to \nu_\alpha + e^- \ , \tag{6.44}$$

where $\alpha = e$, μ or τ. Since the cross section for electron neutrinos is about six times larger than those for muon and tau neutrinos, as shown in Eq. (2.79), the reaction in Eq. (6.44) is most sensitive to electron neutrinos. The energy threshold for recoil electrons was lowered from 7.5 MeV in Kamiokande-II to 7.0 MeV in Kamiokande-III (Fukuda *et al.*, 1996), implying that the neutrino energy threshold decreased from $E_\nu = 7.2$ MeV to $E_\nu = 6.7$ MeV. The measurements made by the Kamiokande experiment from January 1987 to February 1995 led us to the flux of ^{8}B neutrinos $\Phi_{^8\mathrm{B}}(\mathrm{Kamiokande}) = (2.80 \pm 0.19 \pm 0.33) \times 10^6$ cm^{-2} s^{-1} (Fukuda *et al.*, 1996). This result is only about 1/2 of the ^{8}B neutrino flux predicted by the SSM in Table 6.7.

(2) The Super-Kamiokande (SK) experiment has a 50 kiloton water Cherenkov detector, which is also located in the Kamioka mine, about 500 m from the cavity occupied by the Kamiokande detector. The SK detector consists of a stainless steel cylindrical water tank with about 11000 PMTs in the inner detector and about 1900 PMTs in the outer detector (Fukuda *et al.*, 2003). The first phase of the SK experiment started in 1996 and ended in 2001. The energy threshold for recoil electrons is 6.5 MeV for the first 280 days and 5.0 MeV for the remaining time. The corresponding neutrino energy thresholds are $E_\nu = 6.2$ MeV and $E_\nu = 4.7$ MeV, respectively. The detected ^{8}B neutrino flux was $\Phi_{^8\mathrm{B}}(\mathrm{SK}) = (2.35 \pm 0.02 \pm 0.08) \times 10^6$ cm^{-2} s^{-1} (Hosaka *et al.*, 2006). In particular, the angular distribution of neutrino events was measured in the SK experiment. It provided a convincing evidence that the observed neutrinos really came from the Sun. Although the SK experiment searched for the time variation of solar neutrino events, the data were consistent with a null day-night asymmetry and the measured seasonal variation

was compatible with the change in the Sun-Earth distance. After an unfortunate accident, the second phase of the SK experiment ran from December 2002 to October 2005 with a reduced PMT coverage and a higher energy threshold (Cravens *et al.*, 2008). Some efforts were made in the third phase of this experiment, which ran from August 2006 to August 2008, to cut the systematic errors by a factor of two, to reduce the low-energy background and to achieve a low energy threshold $E_\nu = 4.5$ MeV (Yang *et al.*, 2009).

(3) The Sudbury Neutrino Observatory (SNO) has a Cherenkov detector located in the Creighton mine, near Sudbury, Ontario (Boger *et al.*, 2000). The detector consists of a transparent acrylic sphere filled with 1000 tons of heavy water D_2O. The Cherenkov light is detected by about 9500 inward-looking PMTs. The SNO experiment can measure solar neutrinos via charged-current (CC), neutral-current (NC) and elastic scattering (ES) reactions:

$$\begin{aligned} \text{CC}: &\quad \nu_e + \text{D} \to p + p + e^- \ , \\ \text{NC}: &\quad \nu_\alpha + \text{D} \to p + n + \nu_\alpha \ , \\ \text{ES}: &\quad \nu_\alpha + e^- \to \nu_\alpha + e^- \ , \end{aligned} \tag{6.45}$$

where $\alpha = e$, μ or τ. The CC reaction in the SNO experiment has a threshold of 5.5 MeV for the recoil energy of the final-state electron, corresponding to a neutrino energy threshold $E_\nu = 6.9$ MeV. Hence it is sensitive to solar ^{8}B neutrinos. The NC reaction is sensitive to all three neutrino flavors with an energy threshold $E_\nu = 2.224$ MeV, so it is very important to measure the total flux of ^{8}B neutrinos via this process. The ES reaction has a neutrino energy threshold $E_\nu = 5.7$ MeV in the SNO experiment, and thus it is only sensitive to ^{8}B neutrinos.

The SNO experiment underwent three phases: (a) the D_2O phase ran from November 1999 to May 2001, and the neutron produced in the NC reaction was detected via the process $n + \text{D} \to {}^3\text{He} + \gamma$; (b) the NaCl phase operated from July 2001 to August 2003, during which time about 2 tons of NaCl were added into heavy water to enhance the neutron detection efficiency (via $n + {}^{35}\text{Cl} \to {}^{36}\text{Cl} + \gamma$'s) and the ability to statistically separate the NC and CC signals, leading to a significant improvement in the accuracy of the measured ν_e and ν_x (for $x = \mu$ or τ) fluxes; (c) the final phase used ^{3}He to capture the neutron, yielding a proton-tritium pair and thus an electronic pulse in the counter wire (Aharmim *et al.*, 2008). The fluxes of solar ^{8}B neutrinos obtained from different reactions in the NaCl phase of the SNO experiment are (Aharmim *et al.*, 2005)

$$\begin{aligned} \Phi_{\text{CC}}^{\text{SNO}} &= \left(1.68\ {}^{+0.06}_{-0.06}\ {}^{+0.08}_{-0.09}\right) \times 10^6\ \text{cm}^{-2}\ \text{s}^{-1} \ , \\ \Phi_{\text{EC}}^{\text{SNO}} &= \left(2.35\ {}^{+0.22}_{-0.22}\ {}^{+0.15}_{-0.15}\right) \times 10^6\ \text{cm}^{-2}\ \text{s}^{-1} \ , \\ \Phi_{\text{NC}}^{\text{SNO}} &= \left(4.94\ {}^{+0.21}_{-0.21}\ {}^{+0.38}_{-0.34}\right) \times 10^6\ \text{cm}^{-2}\ \text{s}^{-1} \ . \end{aligned} \tag{6.46}$$

The ratio $\Phi_{\rm CC}^{\rm SNO}/\Phi_{\rm NC}^{\rm SNO} = 0.340 \pm 0.023^{+0.029}_{-0.031}$ differs from unity by 17σ. These results are crucial in establishing neutrino oscillations as the best solution to the solar neutrino problem, as one can see in Section 6.4.

6.3.3 Future Solar Neutrino Experiments

We have summarized some solar neutrino experiments based on the radiochemical methods and Cherenkov detectors. There is another ongoing experiment, Borexino, which uses the liquid scintillator detector and aims to observe the low-energy components of solar neutrinos (Alimonti *et al.*, 2009a, 2009b). The Borexino detector is located at the underground LNGS in central Italy. Solar neutrinos are detected via elastic ν_e-e^- scattering, and the scintillator light induced by the recoil electrons is observed by the PMTs. The Borexino Collaboration has recently reported the first result of ^{8}B solar neutrinos with an energy threshold $E_\nu = 3$ MeV (Bellini *et al.*, 2010a): $\Phi_{^8\rm B}({\rm Borexino}) = (2.4 \pm 0.4 \pm 0.1) \times 10^6$ cm^{-2} s^{-1}, which is in good agreement with the results of the SNO and SK experiments. In addition, a direct measurement of ^{7}Be neutrinos ($E_\nu = 0.862$ MeV) in the Borexino experiment yields the neutrino interaction rate $49 \pm 3({\rm stat.}) \pm 4({\rm syst.})$ counts per day per 100 tons from an analysis of the data accumulated during the period between May 2007 and April 2008, while the prediction given by the high-metallicity SSM is 74 ± 4 counts per day per 100 tons (Arpesella *et al.*, 2008). The observation of such low-energy neutrinos is very important in testing nuclear reactions in the Sun and matter effects on solar neutrinos with different energies. It is worth mentioning that the Borexino Collaboration has also observed geoneutrinos — the electron antineutrinos produced in the beta decays of radioactive isotopes in the Earth (Bellini *et al.*, 2010b).

The future solar neutrino experiments will extensively make use of the scintillator detectors, and nearly all of them have other scientific purposes such as a search for dark matter, neutrinoless double-beta decays and proton decays (Klein, 2008). The main goal is to measure low-energy *pp*, *pep*, ^{7}Be and CNO neutrinos by lowering the relevant backgrounds. The Borexino experiment has made an important step forward in measuring ^{7}Be neutrinos, which are crucial for understanding neutrino oscillations in matter and physics in the solar core. The KamLAND experiment plans to reduce its backgrounds by means of scintillator purification, such that ^{7}Be neutrinos can be observed via the elastic neutrino-electron scattering reaction. The SNO+ experiment is also based on the scintillator detector and the elastic ν_e-e^- scattering process, and it will be sensitive to *pep* and CNO neutrinos. The proposed LENS experiment uses the indium-doped scintillator and thus is sensitive to the charged-current interaction $\nu_e + {}^{115}{\rm In} \to e^- + {}^{115}{\rm Sn} + 2\gamma$. The full LENS detector is expected to measure the energy spectrum of *pp* neutrinos and to detect the signals of ^{7}Be, CNO and *pep* neutrinos (Raghavan, 2002). The CLEAN and XMASS experiments use the liquid neon and xenon, respectively, to observe the scintillator light in order to detect dark matter. The

low-energy thresholds of these experiments allow a measurement of solar *pp* neutrinos (McKinsey and Coakley, 2005).

6.4 Solar Neutrino Oscillations

It has been seen that all the solar neutrino experiments pointed to a very significant discrepancy between the measured neutrino flux and the expected one from the SSM. This is the well-known solar neutrino problem (Davis, 1994). In this section we first describe this problem and then show that its best solution comes from neutrino oscillations together with the Mikheyev-Smirnov-Wolfenstein (MSW) matter effects (Wolfenstein, 1978; Mikheyev and Smirnov, 1985, 1986). It is also possible to place strict constraints on the lifetimes and electromagnetic properties of neutrinos from solar neutrino oscillation experiments.

6.4.1 The Solar Neutrino Problem

Fig. 6.6 offers a comparison between the rates of solar neutrinos predicted by the SSM of BPS(GS98) 2008 [3] and measured in the solar neutrino experiments (Pena-Garay and Serenelli, 2008). To examine whether the solar neutrino problem is real or not, one should first of all make the theoretical uncertainties of the SSM itself as small as possible. Note that the SSM is constructed based on some important input parameters (e.g., the chemical composition, radiative opacity and nuclear reaction rates) which may affect its predictions for solar neutrino fluxes (Bahcall, 1989). Some comments on these parameters are in order (Pena-Garay and Serenelli, 2008).

(1) The abundances of heavy elements have a great impact on the calculations of the CNO neutrino fluxes. Hence the solar composition dominates the uncertainties in the fluxes of ^{13}N (13%), ^{15}O (12%) and ^{17}F (17%) neutrinos (as one can see in Table 6.7), but it is not dominant for other neutrinos.

(2) For ^{8}B and ^{7}Be neutrinos, the main uncertainties (6.8% and 3.2%) come from the opacity, which is closely related to solar metallicity (especially the abundance of iron). The reason is that the fluxes of ^{8}B and ^{7}Be neutrinos are highly sensitive to the temperature, determined mainly by the opacity.

(3) The astrophysical S factors cause some subleading uncertainties in evaluating the solar neutrino fluxes. For example, S_{33} and S_{34} corresponding to $^{3}\mathrm{He} + {}^{3}\mathrm{He} \rightarrow {}^{4}\mathrm{He} + 2p$ and $^{3}\mathrm{He} + {}^{4}\mathrm{He} \rightarrow {}^{7}\mathrm{Be} + \gamma$ reactions give rise to 2.5% and 2.8% uncertainties for ^{7}Be neutrinos; and the factor S_{17} from the reaction $^{7}\mathrm{Be} + p \rightarrow {}^{8}\mathrm{B} + \gamma$ induces a 3.8% uncertainty. Thermal and gravitational diffusion effects may lead to comparable uncertainties.

[3] Useful numerical tables and plots based on the SSM can be found from the website http://www.mpa-garching.mpg.de/∼aldos/.

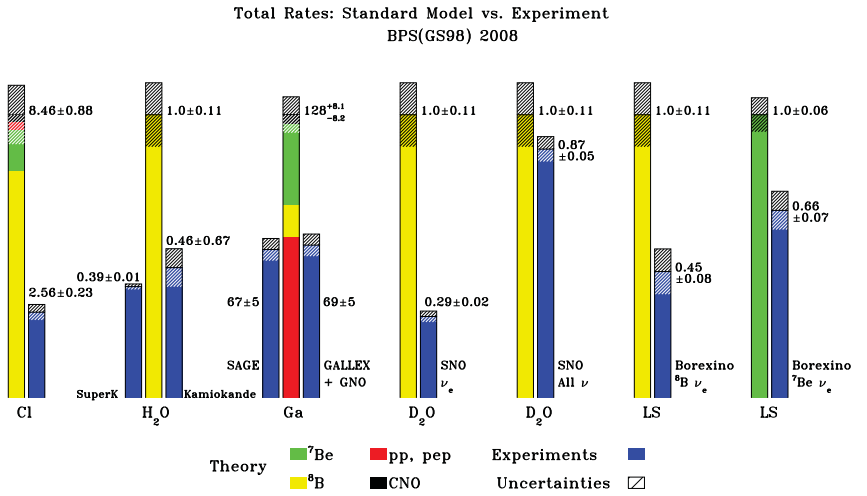

Fig. 6.6 The rates of solar neutrinos from theoretical predictions and experimental data (Pena-Garay and Serenelli, 2008)

It is obvious that the uncertainties given in Table 6.7 and Fig. 6.6 cannot accommodate the remarkable discrepancy between theoretical predictions and experimental results. In particular, the NC events (sensitive to all three neutrino flavors) measured in the SNO experiment show that the total flux of ^{8}B neutrinos is consistent with that predicted by the SSM. So the solar neutrino problem should be resolved by reexamining the basic properties of neutrinos themselves instead of modifying the SSM. The most convincing solution to this problem turns out to be neutrino oscillations. On the other hand, solar neutrino oscillation experiments are now able to make important contributions to the theory of stars (Serenelli, 2010; Basu and Antia, 2008).

6.4.2 The MSW Matter Effects

The experimental results illustrated in Fig. 6.6 indicate that the fluxes of solar electron neutrinos must have changed during their journey from the solar core to the detector, and a proper solution to the observed deficit must have an energy-dependent feature. The standard solution to this problem is the oscillation of solar neutrinos, a pure quantum phenomenon which allows electron neutrinos to transform into muon and (or) tau neutrinos when they travel from the solar core to the Earth. Let us explain the key points by taking the two-flavor $\nu_e \leftrightarrow \nu_\mu$ oscillations for example. The survival probability of initial electron neutrinos is given by

$$P(\nu_e \to \nu_e) = 1 - \sin^2 2\theta \sin^2 \left(\frac{\Delta m^2 L}{4E} \right) , \tag{6.47}$$

where θ is the neutrino mixing angle in vacuum, and $\Delta m^2 \equiv m_2^2 - m_1^2$ denotes the mass-squared difference between two neutrino mass eigenstates ν_1 and ν_2. Since the energy spectrum of solar neutrinos is continuous, the probability $P(\nu_e \to \nu_e)$ should be averaged over the spectrum. This treatment leads us to the averaged probability $\langle P(\nu_e \to \nu_e)\rangle = 1 - 0.5 \sin^2 2\theta$ (Gribov and Pontecorvo, 1969). Hence the minimal value of this survival probability is 1/2 when $\theta = \pi/4$ holds. Considering the SNO measurements of solar ^{8}B neutrinos (i.e., the measured neutrino flux is only about one third of the total neutrino flux), one immediately observes that the above treatment is not applicable. A correct interpretation of all the solar neutrino experiments has to take into account the matter effects on neutrino oscillations.

Neutrino oscillations in matter have been described in Chapter 5. Here we apply the main results to the case of solar neutrino oscillations. First, we estimate the effective potential relevant to $\nu_e \to \nu_\mu$ oscillations in the solar core, where the matter density is about $\rho_{\rm C} = 150$ g cm^{-3} and the electron number density is $n_e = 100\ \mathcal{N}_{\rm A}$ cm^{-3} with $\mathcal{N}_{\rm A} = 6.022 \times 10^{23}$ being the Avogadro constant (Bahcall, 1989). So the effective potential reads

$$\mathcal{V} = \sqrt{2}\, G_{\rm F} n_e \approx 7.6 \times 10^{-12}\ {\rm eV}\ . \tag{6.48}$$

For the electron neutrinos with a typical energy $E \sim 10$ MeV, the resonance condition $A = 2\mathcal{V}E = \Delta m^2 \cos 2\theta$ can be satisfied if $\Delta m^2 \cos 2\theta = 1.5 \times 10^{-4}$ eV^2 holds. In fact, the electron number density of the Sun decreases from its core to its surface. One has an approximate exponential law $n_e(r) = n_0 {\rm e}^{-r/r_0}$, where $n_0 = 245\ \mathcal{N}_{\rm A}$ cm^{-3} and $r_0 = 0.1 R_\odot$ in the range of $0.1 < r/R_\odot < 0.9$. Therefore, whether the neutrinos can encounter the resonance point depends on their energy and mixing parameters (Mikheyev and Smirnov, 1985; Kuo and Pantaleone, 1989).

Next, we assume $\tan^2\theta \sim 0.5$ and $\Delta m^2 \sim 8 \times 10^{-5}$ eV^2. In this case one can see that the resonance energy at the solar core is given by

$$E_{\rm res} = \frac{\Delta m^2 \cos 2\theta}{2\mathcal{V}} \approx 1.75\ {\rm MeV}\ , \tag{6.49}$$

where the value of $\mathcal{V}$ obtained in Eq. (6.48) has been input. This estimate implies that matter effects are insignificant for those solar neutrinos with energies below $E_{\rm res}$; in other words, such low-energy neutrinos mainly undergo vacuum oscillations. The Borexino experiment has measured the flux of ^{7}Be neutrinos, whose energies are well below the resonance energy $E_{\rm res}$. So it is more appropriate to use $\nu_e \to \nu_e$ oscillations in vacuum to interpret the experimental data of ^{7}Be neutrinos (i.e., the observed neutrino flux is about 0.6 of the expected one, as shown in Fig. 6.6). Given $\langle P(\nu_e \to \nu_e)\rangle = 1 - 0.5 \sin^2 2\theta \approx 0.6$, a straightforward calculation leads us to $\theta \approx 32^\circ$, which is consistent with the values extracted from other solar neutrino oscillation data. If the energies of solar neutrinos are above $E_{\rm res}$, the resonant flavor conversion may take place at $r = r_{\rm res}$, where the resonance condition $A = \Delta m^2 \cos 2\theta$ is

satisfied. In this case the adiabaticity parameter defined in Eq. (5.30) can be estimated as follows:

$$\gamma \equiv \frac{\Delta m^2 \sin^2 2\theta}{2E \cos 2\theta} \left[\frac{1}{n_e(r)} \left| \frac{\mathrm{d}n_e(r)}{\mathrm{d}r} \right| \right]^{-1}_{r=r_{\rm res}} \sim \left(\frac{2 \text{ MeV}}{E} \right) \times 10^5 \ , \quad (6.50)$$

where $\tan^2\theta \sim 0.5$ and $\Delta m^2 \sim 8 \times 10^{-5}$ eV^2 have been input. This result implies that the resonance point is adiabatically crossed. Hence the averaged survival probability is determined by Eq. (5.32) with the vanishing Laudau-Zener probability $P_{\rm c} = 0$:

$$\langle P(\nu_e \to \nu_e) \rangle = \frac{1}{2} \left[1 + \cos 2\theta_{\rm m}(r_i) \cos 2\theta \right] \ , \quad (6.51)$$

where $\theta_{\rm m}(r_i)$ is the effective neutrino mixing angle in matter at the neutrino production point r_i. For ^{8}B neutrinos with energies far above $E_{\rm res}$, one has $A \gg \Delta m^2 \cos 2\theta$ and thus $\theta_{\rm m}(r_i) \approx \pi/2$ as indicated by Eq. (5.18). We are simply left with $\langle P(\nu_e \to \nu_e) \rangle \approx \sin^2\theta \sim 1/3$ (for $\tan^2\theta \sim 0.5$), which is just the observed rate of ^{8}B neutrinos in the SNO experiment.

Now that matter effects depend on both the neutrino energies and flavor mixing parameters, a full determination of the solar neutrino mixing angle and mass-squared difference requires a global analysis of all the available experimental data on solar neutrino oscillations (with different energy thresholds). The earlier data from chlorine, gallium, Kamiokande and SK experiments indicated four possible regions in the $(\tan^2\theta, \Delta m^2)$ parameter space, but only the large-mixing-angle MSW solution was singled out by the SNO experiment and confirmed by the KamLAND experiment (Eguchi *et al.*, 2003). In the three-flavor framework it is possible to determine or constrain three neutrino mixing angles (θ_{12}, θ_{13} and θ_{23}) and two mass-squared differences (Δm^2_{21} and Δm^2_{32}) from a global analysis of current data on solar, atmospheric, reactor and accelerator neutrino oscillations (Gonzalez-Garcia and Maltoni, 2008). A brief summary of the present values of these five parameters has been given in Tables 3.1 and 3.2.

6.4.3 Constraints on Neutrino Properties

In the early days some interesting ideas other than neutrino oscillations, such as the spin-flavor oscillation (Voloshin and Vysotskii, 1986; Voloshin *et al.*, 1986a, 1986b) and neutrino decays (Bahcall *et al.*, 1972; Acker *et al.*, 1991; Acker and Pakvasa, 1994), were proposed to solve the solar neutrino problem. Today we believe that the spin-flavor oscillation or neutrino decays can at most belong to the subleading effects as compared with solar neutrino oscillations. One may constrain the magnetic dipole moments or lifetimes of neutrinos by using more accurate solar neutrino oscillation data.

If neutrinos have finite magnetic dipole moments, their spins may be flipped in strong magnetic fields. As a consequence, the left-handed neutrino $\nu_{\rm L}$ with negative helicity can be converted into the right-handed neutrino $\nu_{\rm R}$ with positive helicity. The latter does not take part in the standard weak interactions and thus escapes the experimental detection. Hence it was proposed that the solar neutrino deficit could be ascribed to the spin procession effects (Cisneros, 1971; Pulido, 1992). But the conversion rate for $\nu_{\rm L} \to \nu_{\rm R}$ in the solar core was highly suppressed by matter effects (Voloshin and Vysotskii, 1986; Voloshin *et al.*, 1986a, 1986b). It was later realized that the spin-flavor oscillation $\nu_{\alpha{\rm L}} \to \nu_{\beta{\rm R}}$ might be resonantly enhanced in the Sun if neutrinos had finite transition dipole moments (Akhmedov, 1988; Lim and Marciano, 1988). If neutrinos are Majorana particles, the solar neutrino fluxes are likely to contain electron antineutrinos which may result from the spin-flavor oscillation $\nu_e \to \overline{\nu}_\mu$ and the standard oscillation $\overline{\nu}_\mu \to \overline{\nu}_e$. By measuring the antineutrino component of a solar neutrino flux via the inverse beta reaction $\overline{\nu}_e + p \to n + e^+$, the Kamiokande experiment has set some restrictive limits on the solar $\overline{\nu}_e$ flux (Barbieri *et al.*, 1991). More recently, the KamLAND experiment yields $\Phi_{\overline{\nu}_e} < 3.7 \times 10^2$ cm^{-2} s^{-1} for solar electron antineutrinos at the 90% confidence level (Eguchi *et al.*, 2004). In the case of random magnetic fields inside the Sun, the above constraint on $\Phi_{\overline{\nu}_e}$ can be translated into a limit on the magnetic dipole moment of neutrinos: $\mu_\nu <$ a few $\times 10^{-12}$ $\mu_{\rm B}$ (Miranda *et al.*, 2004).

If neutrinos are unstable, a heavier neutrino may decay into the lightest one plus a photon or an invisible new particle. In this case the neutrino flux with an energy E over a distance L will be diminished by a factor $\exp(-t/\tau_{\rm lab}) = \exp[-(L/E)(m_i/\tau_i)]$, where m_i and τ_i are the mass and lifetime of the neutrino mass eigenstate ν_i in the rest frame (Beacom and Bell, 2002). Since radiative neutrino decays and their experimental constraints have been discussed in Chapter 3, here we only consider the $\nu_i \to \nu_j + \phi$ decay with ϕ being the Majoron (Chikashige *et al.*, 1981; Gelmini and Roncadelli, 1981). Then the relevant mass eigenstate of solar neutrinos is ν_2 and $\tau_2/m_2 > 10^{-4}$ s eV^{-1} can be extracted from the experimental data (Beacom and Bell, 2002; Joshipura *et al.*, 2002; Bandyopadhyay *et al.*, 2003). For invisible neutrino decays, the best direct limit is $\tau_1/m_1 > 10^5$ s eV^{-1} obtained from the Supernova 1987A explosion. The future refinement of the SSM itself and the precision measurement of solar neutrinos will definitely improve the constraints on the intrinsic properties of neutrinos.

References

Abazov, A. I., *et al.* (SAGE Collaboration), 1991, Phys. Rev. Lett. **67**, 3332.

Abdurashitov, J. N., *et al.* (SAGE Collaboration), 1994, Phys. Lett. B **328**, 234.

Abdurashitov, J. N., *et al.* (SAGE Collaboration), 2002, JETP **95**, 181.

Abdurashitov, J. N., *et al.* (SAGE Collaboration), 2006, Astropart. Phys. **25**, 349.

Acker, A., and Pakvasa, S., 1994, Phys. Lett. B **320**, 320.
Acker, A., Pakvasa, S., and Pantaleone, J., 1991, Phys. Rev. D **43**, 1754.
Aharmim, B., *et al.* (SNO Collaboration), 2005, Phys. Rev. C **72**, 055502.
Aharmim, B., *et al.* (SNO Collaboration), 2008, Phys. Rev. Lett. **101**, 111301.
Akhmedov, E. Kh., 1988, Sov. J. Nucl. Phys. **48**, 382.
Alimonti, G., *et al.* (Borexino Collaboration), 2009a, Nucl. Instrum. Meth. A **600**, 568.
Alimonti, G., *et al.* (Borexino Collaboration), 2009b, Nucl. Instrum. Meth. A **609**, 58.
Altmann, M., *et al.* (GNO Collaboration), 2000, Phys. Lett. B **490**, 16.
Altmann, M., *et al.* (GNO Collaboration), 2005, Phys. Lett. B **616**, 174.
Alvarez, L. W., 1949, UC Radiation Laboratory Report UCRL-328.
Anders, E., and Grevesse, N., 1989, Geochim. Cosmochim. Acta **53**, 197.
Arpesella, C., *et al.* (Borexino Collaboration), 2008, Phys. Rev. Lett. **101**, 091302.
Asplund, M., Grevesse, N., and Sauval, A. J., 2005, ASP Conf. Ser. **336**, 25.
Asplund, M., *et al.*, 2009, Ann. Rev. Astron. Astrophys. **47**, 481.
Bahcall, J. N., 1964, Phys. Rev. Lett. **12**, 300.
Bahcall, J. N., 1969, Phys. Rev. Lett. **23**, 251.
Bahcall, J. N., 1989, *Neutrino Astrophysics* (Cambridge University Press).
Bahcall, J. N., 1997, Phys. Rev. C **56**, 3391.
Bahcall, J. N., and Pinsonneault, M. H., 1995, Rev. Mod. Phys. **67**, 781.
Bahcall, J. N., and Ulrich, R. K., 1988, Rev. Mod. Phys. **60**, 297.
Bahcall, J. N., Cabibbo, N., and Yahil, A., 1972, Phys. Rev. Lett. **28**, 316.
Bahcall, J. N., *et al.*, 1982, Rev. Mod. Phys. **54**, 767.
Bahcall, J. N., *et al.*, 1996, Phys. Rev. C **54**, 411.
Bahcall, J. N., Pinsonneault, M. H., and Basu, S., 2001, Astrophys. J. **555**, 990.
Bahcall, J. N., Serenelli, A. M., and Basu, S., 2006, Astrophys. J. Suppl., **165**, 400.
Bandyopadhyay, A., Choubey, S., and Goswami, S., 2003, Phys. Lett. B **555**, 33.
Barbieri, R., *et al.*, 1991, Phys. Lett. B **259**, 119.
Basu, S., and Antia, H. M., 2008, Phys. Rept. **457**, 217.
Basu, S., *et al.*, 2007, Astrophys. J. **655**, 660.
Beacom, J. F., and Bell, N. F., 2002, Phys. Rev. D **65**, 113009.
Bellini, G., *et al.* (Borexino Collaboration), 2010a, Phys. Rev. D **82**, 033006.
Bellini, G., *et al.* (Borexino Collaboration), 2010b, Phys. Lett. B **687**, 299.
Bethe, H. A., 1939, Phys. Rev. **55**, 434.
Bethe, H., and Peierls, R., 1934, Nature **133**, 532.
Biermann, L., 1951, Z. Astrophys. **28**, 304.
Boger, J., *et al.* (SNO Collaboration), 2000, Nucl. Instrum. Meth. A **449**, 172.
Böhm-Vitense, E., 1958, Z. Astrophys. **46**, 108.
Carroll, B. W., and Ostlie, D. A., 2007, *An Introduction to Modern Astrophysics* (Pearson Education, Inc.).
Chandrasekhar, S., 1938, *An Introduction to the Study of Stellar Structure* (The University of Chicago Press).
Chaplin, W. J., *et al.*, 2007, Astrophys. J. **670**, 872.

Chikashige, Y., Mohapatra, R. N., and Peccei, R. D., 1981, Phys. Lett. B **98**, 265.
Cisneros, A., 1971, Astrophys. Space Sci. **10**, 87.
Cleveland, B. T., *et al.* (Homestake Collaboration), 1998, Astrophys. J. **496**, 505.
Cowan, C. L., Jr., *et al.*, 1956, Science **124**, 103.
Cox, J. P., and Giuli, R. T., 1968, *Principles of Stellar Structure: Physical Principles* (Gordon and Breach, Science Publishers, Inc.).
Cravens, J. P., *et al.* (Super-Kamiokande Collaboration), 2008, Phys. Rev. D **78**, 032002.
Davis, R. Jr., 1964, Phys. Rev. Lett. **12**, 303.
Davis, R. Jr., 1994, Prog. Part. Nucl. Phys. **32**, 13.
Eguchi, K., *et al.* (KamLAND Collaboration), 2003, Phys. Rev. Lett. **90**, 021802.
Eguchi, K., *et al.* (KamLAND Collaboration), 2004, Phys. Rev. Lett. **92**, 071301.
Fukuda, Y., *et al.* (Kamiokande Collaboration), 1996, Phys. Rev. Lett. **77**, 1683.
Fukuda, S., *et al.* (Super-Kamiokande Collaboration), 2003, Nucl. Instrum. Meth. A **501**, 418.
Gamow, G., 1928, Z. Phys. **51**, 204.
Gamow, G., and Schoenberg, M., 1940, Phys. Rev. **58**, 1117.
Gamow, G., and Schoenberg, M., 1941, Phys. Rev. **59**, 339.
Gelmini, G. B., and Roncadelli, M., 1981, Phys. Lett. B **99**, 411.
Giunti, C., and Kim, C. W., 2007, *Fundamentals of Neutrino Physics and Astrophysics* (Oxford University Press).
Gonzalez-Garcia, M. C., and Maltoni, M., 2008, Phys. Rept. **460**, 1.
Grevesse, N., and Noels, A., 1993, in *Origin and Evolution of the Elements* (edited by Prantzos, N., Vangioni-Flam, E., and Casse, M.), p. 14.
Grevesse, N., and Sauval, A. J., 1998, Space Sci. Rev. **85**, 161.
Gribov, V. N., and Pontecorvo, B., 1969, Phys. Lett. B **28**, 493.
Hampel, W., *et al.* (GALLEX Collaboration), 1999, Phys. Lett. B **447**, 127.
Hosaka, J., *et al.* (Super-Kamiokande Collaboration), 2006, Phys. Rev. D **73**, 112001.
Joshipura, A. S., Masso, E., and Mohanty, S., 2002, Phys. Rev. D **66**, 113008.
Kaether, F., *et al.*, 2010, Phys. Lett. B **685**, 47.
Klein, J. R., 2008, J. Phys Conf. Ser. **136**, 022004.
Krisciunas, K., 2001, arXiv:astro-ph/0106313.
Kuo, T. K., and Pantaleone, J., 1989, Rev. Mod. Phys. **61**, 937.
Kuzmin, V. A., 1966, Sov. Phys. JETP **22**, 1051.
Landau, L. D., and Lifshitz, E. M., 1984, *Electrodynamics of Continuous Media* (Pergamon Press).
Lim, C. S., and Marciano, W. J., 1988, Phys. Rev. D **37**, 1368.
Lodders, K., 2003, Astrophys. J. **591**, 1220.
Lodders, K., Palme, H., and Gail, H. P., 2009, arXiv:0901.1149.
McKinsey, D. N., and Coakley, K. J., 2005, Astropart. Phys. **22**, 355.
Mikheyev, S., and Smirnov, A. Yu., 1985, Sov. J. Nucl. Phys. **42**, 913.
Mikheyev, S., and Smirnov, A. Yu., 1986, Nuovo Cim. C **9**, 17.
Miranda, O. G., *et al.*, 2004, Phys. Rev. Lett. **93**, 051304.
Mohr, P. J., Taylor, B. N., and Newell, D. B., 2007, Phys. Today **60**, 52.
Mohr, P. J., Taylor, B. N., and Newell, D. B., 2008, Rev. Mod. Phys. **80**, 633.

Nakamura, K., *et al.* (Particle Data Group), 2010, J. Phys. G **37**, 075021.
Pena-Garay, C., and Serenelli, A. M., 2008, arXiv:0811.2424.
Perryman, M. A. C., *et al.*, 1997, Astron. Astrophys. **323**, L49.
Pontecorvo, B., 1946, Chalk River Report PD-205.
Prialnik, D., 2000, *An Introduction to the Theory of Stellar Structure and Evolution* (Cambridge University Press).
Pulido, J., 1992, Phys. Rept. **211**, 167.
Raffelt, G. G., 1996, *Stars as Laboratories for Fundamental Physics* (The University of Chicago Press).
Raffelt, G. G., and Rodejohann, W., 1999, arXiv:hep-ph/9912397.
Salaris, M., and Cassisi, S., 2005, *Evolution of Stars and Stellar Populations* (John Wiley & Sons, Ltd.).
Serenelli, A. M., 2010, Astrophys. Space Sci. **328**, 13.
Serenelli, A. M., *et al.*, 2009, Astrophys. J. **705**, L123.
Vitense, E., 1953, Z. Astrophys. **32**, 135.
Voloshin, M. B., and Vysotskii, M. I., 1986, Sov. J. Nucl. Phys. **44**, 544.
Voloshin, M. B., Vysotskii, M. I., and Okun, L. B., 1986a, Sov. J. Nucl. Phys. **44**, 440.
Voloshin, M. B., Vysotskii, M. I., and Okun, L. B., 1986b, Sov. Phys. JETP **64**, 446.
Weinberg, S., 1972, *Gravitation and Cosmology: Principles and Applications of the General Theory of Relativity* (John Wiley & Sons, Inc.).
Weinberg, S., 2008, *Cosmology* (Oxford University Press).
Wolfenstein, L., 1978, Phys. Rev. D **17**, 2369.
Yang, S. B., *et al.* (Super-Kamiokande Collaboration), 2009, arXiv:0909.5469.

7

Neutrinos from Supernovae

The discovery of neutrinos emitted from the Supernova 1987A (SN 1987A) explosion is an outstanding milestone in both neutrino physics and neutrino astronomy. On the one hand, this fortunate observation of supernova neutrinos provides a strong support for the modern theory of supernova explosions. On the other hand, it implies that there exists another class of astrophysical neutrino sources or astrophysical laboratories. A part of this chapter is to introduce the standard picture of core-collapse supernovae and production mechanisms of supernova neutrinos. After a brief account of the experimental detection of the neutrino burst from the SN 1987A, we shall explore its implications on neutrino masses and neutrino lifetimes. The flavor conversions of supernova neutrinos, including the effects of collective neutrino oscillations, will be discussed in detail.

7.1 Stellar Core Collapses and Supernova Neutrinos

The evolution and fate of stars depend crucially on their initial masses. The reason is simply that the self-gravity of stars should be balanced by the pressure force to maintain hydrostatic equilibrium. For main-sequence stars, thermal nuclear reactions serve as the energy source and offer the desired pressure force. In this section we shall consider the thermal pressure from degenerate electrons or neutrons. This is the case for white dwarfs and neutron stars, which have burnt out nuclear fuels at the final stage of stellar evolution. After discussing the electron degeneracy pressure, we shall show that the degenerate stellar core becomes unstable and collapses when its mass exceeds the Chandrasekhar limit $\mathcal{M}_{\rm Ch} \sim 1.4\mathcal{M}_{\odot}$ (Chandrasekhar, 1931a, 1931b, 1935). We shall pay particular attention to the core-collapse supernovae which first experience the collapse and then rebounce, ejecting the stellar mantle and envelope and leaving neutron stars or black holes at the center. The role played by neutrinos in the core-collapse supernovae, together with possible mechanisms of supernova explosions, will also be discussed.

7.1.1 Degenerate Stars

For a massive star with $\mathcal{M} \gtrsim 8\mathcal{M}_\odot$, nuclear fusion reactions in the core will continue until the iron-group nuclei (e.g., ^{56}Fe and ^{56}Ni) are abundantly produced. At this moment the massive star takes on the onion-like structure with an iron core surrounded by the shells of silicon, sulfur, oxygen, neon, carbon and helium from inner layers to outer layers. Since iron is the most tightly bound nucleus, no fusion reactions can take place. So the thermal pressure from fusion reactions is not available and the core will contract under its self-gravity. This contraction ceases if the iron core becomes degenerate and the degeneracy pressure of electrons is high enough to support the weight of the core. White dwarfs result from the stars that are not sufficiently massive to ignite carbon and oxygen in the core, and the gravity is balanced by the pressure from degenerate electrons (Liebert, 1980; Chandrasekhar, 1984; Koester and Chanmugan, 1990; Hansen and Liebert, 2003).

Now let us consider a degenerate gas of electrons at the temperature of absolute zero (i.e., $T = 0$). Due to the Pauli exclusion principle, all the states with momenta ranging from zero to the Fermi momentum $p_{\rm F}$ are occupied. Since the density of quantum states in the momentum space is $\mathrm{d}^3\mathbf{p}/(2\pi)^3$, the total number of electrons in these states reads

$$N_e = 2V \int_0^{p_{\rm F}} \frac{4\pi p^2 \mathrm{d}p}{(2\pi)^3} = \frac{V p_{\rm F}^3}{3\pi^2} \ , \tag{7.1}$$

where the factor 2 takes account of the spin states and V is the volume of the system. Hence $p_{\rm F}$ is determined by the number density of electrons $n_e \equiv N_e/V$; i.e., $p_{\rm F} = (3\pi^2 n_e)^{1/3}$. The corresponding Fermi energy $\varepsilon_{\rm F} \equiv p_{\rm F}^2/(2m_e)$ for non-relativistic electrons is given by $\varepsilon_{\rm F} = (3\pi^2 n_e)^{2/3}/(2m_e)$. Multiplying the integrand in Eq. (7.1) by $p^2/(2m_e)$ and performing the integration over the momentum, we can obtain the total energy E of this system. The latter is related to the pressure as follows (Landau and Lifshitz, 1980):

$$P = \frac{2E}{3V} = \frac{(3\pi^2)^{2/3}}{5m_e} n_e^{5/3} \ . \tag{7.2}$$

This equation of state is also valid for nonzero temperatures, but the condition for strong degeneracy $T \ll \varepsilon_{\rm F}$ should be satisfied. As the gas of degenerate electrons is compressed, the density increases, so does the mean energy. In this case one should consider the relativistic effects if $\varepsilon_{\rm F}$ becomes much larger than m_e. The Fermi energy of relativistic electrons is given as $\varepsilon_{\rm F} = p_{\rm F} = (3\pi^2 n_e)^{1/3}$. Multiplying the integrand in Eq. (7.1) by $\varepsilon = p$ and integrating over the momentum, we arrive at (Landau and Lifshitz, 1980)

$$P = \frac{E}{3V} = \frac{(3\pi)^{2/3}}{4} n_e^{4/3} \ . \tag{7.3}$$

The system consisting of only degenerate electrons is actually unstable, so the positively charged nuclei must be present to balance the negative charges of

electrons. However, the degeneracy pressure from electrons is dominant over the thermal pressure of the nuclei. The latter is henceforth assumed to have no impact on the equation of state of the whole system. The number density of electrons is given by $n_e = \rho/(\tilde{\mu}_e m_{\rm H})$, where $\tilde{\mu}_e$ and $m_{\rm H}$ stand respectively for the mean molecular weight per electron and the atomic mass unit. With the help of Eqs. (7.2) and (7.3), we may rewrite the equation of state as

$$P = K_i \rho^\gamma \qquad (\text{for } i = 1, 2) \,, \tag{7.4}$$

in which $K_1 = (3\pi^2)^{2/3}/[5m_e(\tilde{\mu}_e m_{\rm H})^{5/3}]$ with $\gamma = 5/3$ for non-relativistic electrons, and $K_2 = (3\pi^2)^{2/3}/[4(\tilde{\mu}_e m_{\rm H})^{4/3}]$ with $\gamma = 4/3$ for extremely relativistic electrons. One always has $\tilde{\mu}_e \approx 2$ for heavy nuclei, and thus the corresponding K_1 and K_2 are independent of the density. Note that Eq. (7.4) is just the equation of state for the polytropic process with the index n defined by $\gamma = 1 + 1/n$. So one may solve Eq. (6.12) for hydrostatic equilibrium with the help of Eqs. (6.13) and (7.4). The resultant second-order differential equation for the density is (Prialnik, 2000)

$$\frac{(n+1)K}{4\pi G_{\rm N} n} \cdot \frac{1}{r^2} \cdot \frac{\mathrm{d}}{\mathrm{d}r}\left[\frac{r^2}{\rho^{(n-1)/n}} \cdot \frac{\mathrm{d}\rho}{\mathrm{d}r}\right] = -\rho \,, \tag{7.5}$$

where $K = K_1$ for $n = 3/2$ and $K = K_2$ for $n = 3$. The density distribution $\rho(r)$ for $0 \leqslant r \leqslant R$ should fulfill the initial conditions $\rho(R) = 0$ (with R being the radius of the star) and $\dfrac{\mathrm{d}\rho}{\mathrm{d}r} = 0$ at the center. These conditions follow from the equation of state and the pressure profile with $P(R) = 0$ and $\dfrac{\mathrm{d}P}{\mathrm{d}r} = 0$ at $r = 0$. After a change of variables $\rho = \rho_{\rm c}\Theta^n$ and $r = \alpha\xi$, where $\alpha \equiv \{(n+1)K/4\pi G_{\rm N}\rho_{\rm c}^{(n-1)/n}\}^{1/2}$ and $\rho_{\rm c}$ is the central density, we obtain the Lane-Emden equation of index n (Chandrasekhar, 1938; Prialnik, 2000):

$$\frac{1}{\xi^2} \cdot \frac{\mathrm{d}}{\mathrm{d}\xi}\left(\xi^2 \frac{\mathrm{d}\Theta}{\mathrm{d}\xi}\right) = -\Theta^n \tag{7.6}$$

with the corresponding initial conditions $\Theta = 1$ and $\dfrac{\mathrm{d}\Theta}{\mathrm{d}\xi} = 0$ at $\xi = 0$. In general, Eq. (7.6) can be numerically solved. It has been found that Θ decreases monotonically to zero at a finite $\xi = \xi_R$ for $n < 5$ (Shapiro and Teukolsky, 1983). Note that $\Theta(\xi_R) = 0$ corresponds to $\rho = 0$ at the surface of the star. Hence the radius and the mass of the star are given by (Shapiro and Teukolsky, 1983)

$$R = \alpha\xi_R = \rho_{\rm c}^{(1-n)/2n}\xi_R\left[\frac{(n+1)K}{4\pi G_{\rm N}}\right]^{1/2} \,, \tag{7.7}$$

and

$$\mathcal{M} = \int_0^R 4\pi r^2 \rho(r) \mathrm{d}r = 4\pi \rho_{\rm c}^{(3-n)/2n} \xi_R^2 \left[\frac{(n+1)K}{4\pi G_{\rm N}}\right]^{3/2} \left|\frac{\mathrm{d}\Theta}{\mathrm{d}\xi}\right|_{\xi=\xi_R} , \quad (7.8)$$

where Eq. (7.6) has been used to evaluate the integration. Eliminating $\rho_{\rm c}$ in Eqs. (7.7) and (7.8), we get an interesting mass-radius relation

$$\mathcal{M} \propto R^{(3-n)/(1-n)} , \quad (7.9)$$

implying that $\mathcal{M} \propto R^{-3}$ for $n = 3/2$. More interestingly, the mass $\mathcal{M}$ is independent of R and $\rho_{\rm c}$ for $n = 3$. In this case a mass limit must exist as $\rho_{\rm c} \to \infty$ and $R \to 0$. Substituting $n = 3$, $K = K_2$, $\xi_R \approx 6.897$ and $\left|\frac{\mathrm{d}\Theta}{\mathrm{d}\xi}\right|_{\xi=\xi_R} = 0.0424$ into Eq. (7.8), one gets the Chandrasekhar mass limit $\mathcal{M}_{\rm Ch} \approx 5.7\tilde{\mu}_e^{-2}\mathcal{M}_\odot \approx 1.4\mathcal{M}_\odot$ for $\tilde{\mu}_e = 2$ (Chandrasekhar, 1931a, 1931b, 1935). The existence of such a mass limit can be understood in an intuitive way, which was first presented by Lev Landau (Landau, 1932; Shapiro and Teukolsky, 1983). For a star with the total baryon number $N_{\rm b}$, its gravitational potential energy is given by $E_{\rm g} \propto -G_{\rm N} N_{\rm b} R^{-1}$. On the other hand, the Fermi energy of relativistic degenerate electrons is $E_{\rm F} \propto N_{\rm b}^{1/3} R^{-1}$. If $N_{\rm b}$ is very large (i.e., the star is very massive), the total energy $E = E_{\rm g} + E_{\rm F}$ can be negative and thus decrease without bound as the radius R decreases. As a result, a limit of $N_{\rm b}$ or $\mathcal{M} = N_{\rm b} m_p$ exists for $E = 0$ (i.e., the balance between the gravity and the degeneracy pressure of electrons).

7.1.2 Core-collapse Supernovae

Supernovae are exploding stars that emit a large amount of thermal energy in a relatively short time (e.g., from one year to several days) and overshine all the other stars in the host galaxies. They are in general classified as type-I and type-II supernovae, which can be further divided into subclasses (e.g., type-Ia, b, c) according to the existence of hydrogen, helium or silicon spectral lines (Bethe, 1990). Although the explosion mechanism for type-Ia supernovae remains an open question, it is commonly assumed that the energy from nuclear fusion reactions accounts for the explosion. In this case neutrinos are not as important as in the core-collapse type-Ib, type-Ic and type-II supernovae, where the explosion is powered by the gravitational potential energy and nearly all the energy is released in the form of neutrinos. We shall concentrate on type-II supernovae in the following.

As mentioned before, a massive star ($\mathcal{M} \gtrsim 8\ \mathcal{M}_\odot$) will develop a degenerate iron core at the final stage of its evolution. Moreover, the silicon-burning shell will continuously contribute mass to the core and eventually lead to an excess over the Chandrasekhar mass limit and thus the gravitational collapse. Two other microscopic processes at this moment make the situation worse. As the iron core contracts, the temperature will slightly increase. Hence the

photodissociation of heavy nuclei (e.g., $\gamma + {}^{56}\mathrm{Fe} \to 13\ {}^{4}\mathrm{He} + 4\ n - 124$ MeV) becomes more efficient. This endothermic reaction consumes thermal energies and thus reduces the thermal pressure. On the other hand, the degenerate electrons will be captured by heavy nuclei or free nucleons via $e^- + A(Z,N) \to A(Z-1,N+1) + \nu_e$. Since neutrinos are weakly interacting with matter, they will escape from the core immediately after production and take away enormous thermal energies. Furthermore, the number of electrons has been diminished such that the degeneracy pressure is accordingly reduced. Both the photodissociation of nuclei and the electron-capture process can further reduce the thermal pressure and aggravate the collapse (Bethe, 1990; Janka, *et al.*, 2007).

The collapse is obviously determined by the gravity and hydrodynamics. Interestingly, it has been discovered that the inner part of the iron core collapses in a homologous way; i.e., the distribution of temperature and density is similar and only scales with respect to time (Goldreich and Weber, 1980). For the inner core, the velocity of infalling matter is proportional to the radius but smaller than the velocity of sound, while the outer core falls inward supersonically (Yahil and Lattimer, 1982; Yahil, 1983). The critical (or sonic) point can be taken as the position where the infall velocity equals the sound velocity. Thus the inner core is in good contact with itself, whereas the outer one is not. As the core collapses, the matter density in the center reaches and exceeds the nuclear density $\rho_0 \sim 3 \times 10^{14}$ g cm^{-3}. The nuclear matter is less compressible and the pressure builds up gradually, so the gravitational collapse of the inner core will be hindered. However, the freely-falling outer part cannot immediately feel the pressure, so the matter still falls inward. If the infall velocity ultimately goes to zero, the pressure wave will become a shock at the large radius just beyond the sonic point (Cooperstein and Baron, 1990; Bethe, 1990). It is expected that such a shock wave will traverse the whole star and be able to expel the mantle and envelope, giving rise to a supernova (Colgate and Johnson, 1960). Meanwhile, a neutron star or black hole remains at the center. But most of the detailed numerical simulations have not confirmed this prompt-shock explosion picture. When the shock wave propagates outward, it will disassociate heavy nuclei into nucleons at the energy expense of 9 MeV per nucleon. It turns out that the shock wave stalls typically at a radius about 400 km. Whether the prompt shock can succeed or not depends sensitively on the pre-supernova evolution, such as the equation of state and the mass of the core (Baron *et al.*, 1985a, 1985b). Usually the prompt shock will fail if the mass of the iron core is greater than $1.25\mathcal{M}_\odot$ (Arnett, 1983; Hillebrandt, 1982a, 1982b, 1984; Cooperstein *et al.*, 1984; Baron and Cooperstein, 1990).

Because of the failure of the prompt-shock model, the neutrino transport model was proposed (Colgate and White, 1966) and the delayed-shock model was developed (Bowers and Wilson, 1982a, 1982b; Wilson, 1985; Bethe and Wilson, 1985). Neutrinos play a crucial role in this mechanism. When the

matter density of the inner core increases to about 10^{12} g cm^{-3}, electron neutrinos (with energies around 10 MeV) resulting from the electron-capture processes will be trapped due to coherent scattering of neutrinos on heavy nuclei via the neutral-current interactions. The trapped electron neutrinos form a degenerate Fermi sea through the beta equilibrium reaction $e^- + p \leftrightarrow n + \nu_e$. Hence the gravitational potential energy during the collapse has been converted into the chemical potentials of electrons and neutrinos. Neutrinos diffuse out of the core and heat the materials in the region below the stalled shock, and ultimately revive the shock and lead to a successful explosion (Colgate and White, 1966; Bethe and Wilson, 1985). A simulation including the neutrino transport actually demonstrates that a proper fraction of the neutrino energy could successfully revive the stalled shock (Janka and Müller, 1993). However, it is still unclear how neutrinos deposit the right amount of energies and whether the convection and rotation effects are inevitable for a successful explosion (Janka *et al.*, 2007).

7.1.3 Supernova Neutrinos

As pointed out by George Gamow and Mario Schoenberg, neutrinos may play a crucial role in a collapsing star (Gamow and Schoenberg, 1940, 1941). In the supernova context neutrinos can be trapped in the core via coherent neutrino-nucleon scattering (Freedman, 1974; Mazurek, 1975; Sato, 1975). The interactions of neutrinos with the background nucleons and electrons have been systematically studied (Tubbs and Schramm, 1975; Lamb and Pethick, 1976; Bethe *et al.*, 1979). The mean free path of neutrinos for elastic scattering is given by (Bethe *et al.*, 1979)

$$\lambda_\nu = 1.0 \times 10^8 \text{ cm} \left(\frac{\rho}{10^{12} \text{ g cm}^{-3}} \right) \left(\frac{\text{MeV}}{E_\nu} \right)^2 \left[\left(\frac{N^2}{6A} \right) X_\text{h} + X_n \right]^{-1} , \quad (7.10)$$

where ρ is the matter density, E_ν denotes the neutrino energy, X_h and X_n represent the mass fractions of heavy nuclei and nucleons, N and A are the numbers of neutrons and nucleons in an average nucleus. We have taken $\sin^2 \theta_\text{w} = 1/4$ in obtaining Eq. (7.10). The contribution from neutral-current interactions of neutrinos with protons, which is proportional to $(1 - 4 \sin^2 \theta_\text{w})$, is therefore vanishing. Taking $X_\text{h} \approx 1$ and $X_n \approx 0$ during the infall phase, one obtains $\lambda_\nu \approx 2$ km for $E_\nu = 10$ MeV, $\rho = 10^{12}$ g cm^{-3}, $N \approx 50$ and $N/A = 0.6$ (Bethe, 1990). The radius of the core corresponding to $\rho = 10^{12}$ g cm^{-3} is about $R = 30$ km, and hence neutrinos are essentially trapped in the core and can only get out of it by diffusion (Cooperstein, 1988a, 1988b).

After being trapped, the electron neutrinos come into chemical equilibrium with the degenerate electrons and nucleons through the beta process $e^- + p \leftrightarrow \nu_e + n$. Therefore, a degenerate Fermi sea of neutrinos builds up, and the corresponding chemical potential is determined by $\mu_{\nu_e} = \mu_e - \hat{\mu}$ with $\hat{\mu} \equiv \mu_n - \mu_p \approx 100$ MeV. The chemical potential of degenerate electrons

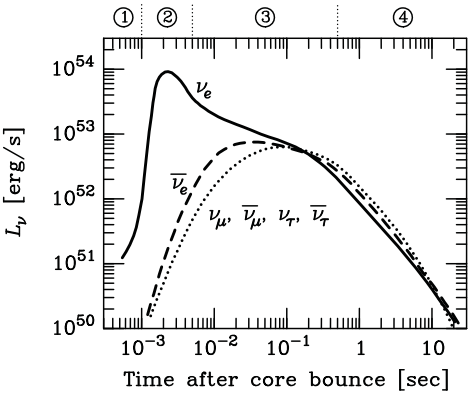

Fig. 7.1 Luminosities of neutrinos ν_α and antineutrinos $\overline{\nu}_\alpha$ (for $\alpha = e, \mu, \tau$) versus the time after the core bounce. Four stages of the delayed-explosion scenario are shown (Raffelt, 1996. With permission from the University of Chicago Press): (1) the collapse and bounce; (2) the shock propagation and prompt neutrino burst; (3) the matter accretion and mantle cooling while the shock stalls; (4) the Kelvin-Helmholtz cooling of the neutron star after explosion

is $\mu_e \approx 111$ MeV$(\rho_{13} Y_e)^{1/3}$, where ρ_{13} denotes the matter density in units of 10^{13} g cm^{-3} and Y_e is the number fraction of electrons. For the nuclear density $\rho_0 = 3 \times 10^{14}$ g cm^{-3} and a typical electron fraction $Y_e = 0.4$, we have $\mu_e \approx 250$ MeV and $\mu_{\nu_e} \approx 150$ MeV (Bethe, 1990). Hence the gravitational potential energy released during the collapse has been largely converted into the chemical potentials of degenerate electrons and neutrinos. Shortly after the bounce, the shock wave disassociates the infalling heavy nuclei into free nucleons, on which the electron-capture rate is much larger. On the other hand, the matter density in the region just below the shock wave has been dramatically reduced, allowing the electron neutrinos to freely escape. This is the so-called prompt neutronization or deleptonization burst of neutrinos. The electron capture and the neutrino burst lead to a moderate reduction of the lepton number in the iron core. As a consequence, the neutrinos of all flavors can now be produced via the electron-positron annihilation $e^+ + e^- \to \nu_\alpha + \overline{\nu}_\alpha$, the plasmon decays $\gamma^* \to \nu_\alpha + \overline{\nu}_\alpha$ and the nucleonic bremsstrahlung $N + N \to N + N + \nu_\alpha + \overline{\nu}_\alpha$ (Suzuki, 1991, 1993). For illustration, the neutrino luminosity from the standard delayed-explosion scenario is shown in Fig. 7.1, where one can see the highly-peaked neutrino burst and the approximate equilibration of neutrino luminosities at later times. Note that the neutrino luminosities are dependent on the time.

Similar to electron neutrinos, muon and tau neutrinos are also trapped and keep in local thermal equilibrium with electrons and nucleons. They diffuse outward to their respective neutrino spheres, from which they may freely escape. Hence the energy spectra of neutrinos can be well described by the

Fermi-Dirac distribution functions with temperatures at the neutrino spheres. Since muon and tau neutrinos only undergo the neutral-current interactions, the corresponding neutrino spheres are located much deeper in the core than that of electron neutrinos. So one obtains the inequality of neutrino average energies $\langle E_{\nu_e}\rangle < \langle E_{\nu_x}\rangle$ (for $\nu_x = \nu_\mu, \overline{\nu}_\mu, \nu_\tau, \overline{\nu}_\tau$). It is worth mentioning that the interaction rate of electron antineutrinos ($\overline{\nu}_e + p \to e^+ + n$) is smaller than that of electron neutrinos ($\nu_e + n \to e^- + p$) because of the neutron-rich core. Therefore, the average energy of $\overline{\nu}_e$ should be larger than that of ν_e but smaller than that of other kinds of neutrinos; i.e., $\langle E_{\nu_e}\rangle < \langle E_{\overline{\nu}_e}\rangle < \langle E_{\nu_x}\rangle$. Their typical values are obtained from a numerical simulation (Raffelt, 1996):

$$\langle E_\nu \rangle = \begin{cases} 10 \sim 12 \text{ MeV} & \nu_e \ , \\ 14 \sim 18 \text{ MeV} & \overline{\nu}_e \ , \\ 18 \sim 24 \text{ MeV} & \nu_x \ , \end{cases} \tag{7.11}$$

where ν_x denotes $\nu_{\mu,\tau}$ and $\overline{\nu}_{\mu,\tau}$. Fig. 7.1 shows that the luminosities of three different neutrino flavors are approximately equilibrated, so the neutrino number fluxes should satisfy $F_{\nu_e} > F_{\overline{\nu}_e} > F_{\nu_x}$, where $\langle E_{\nu_e}\rangle < \langle E_{\overline{\nu}_e}\rangle < \langle E_{\nu_x}\rangle$ has been taken into account. The detailed flavor-dependent fluxes and energy spectra can only be achieved by doing specific numerical simulations (Raffelt, 2001; Keil *et al.*, 2003).

To estimate the total neutrino energy, we calculate the gravitational energy released from the collapse of an iron core with mass $\mathcal{M}_{\rm c} \sim 1.4\mathcal{M}_\odot$ and radius $R_{\rm c} \sim 10^3$ km into the neutron star with the same mass but a much smaller radius $R_{\rm NS} \sim 10$ km. The gravitational binding energy of the neutron star turns out to be (Raffelt, 1996)

$$E_{\rm b} = \frac{3G_{\rm N}\mathcal{M}_{\rm c}^2}{5R_{\rm NS}} \approx 3 \times 10^{53} \left(\frac{\mathcal{M}_{\rm c}}{1.4\ \mathcal{M}_\odot}\right)^2 \left(\frac{10 \text{ km}}{R_{\rm NS}}\right) \text{ erg} \ . \tag{7.12}$$

Assuming the energy equilibration among all kinds of neutrinos, we can then obtain the total neutrino energy $E_\nu = E_{\rm b}/6 \approx 5 \times 10^{52}$ erg for each neutrino or antineutrino species.

7.2 Lessons from the Supernova 1987A

On 24 February 1987, Ian Shelton and Oscar Duhalde at the Las Campanas Observatory in Chile saw a new star in the Large Magellanic Cloud (Shelton *et al.*, 1987). They actually discovered the first supernova since 1604, and it was visible even by the naked eye. This observation was confirmed by some other astronomers at slightly later times. More importantly, the neutrinos emitted from the SN 1987A were detected. In this section we shall first summarize the experimental detection of supernova neutrinos and show that

the observations are essentially compatible with theoretical predictions. Then the lessons that we have learnt from the SN 1987A observations, in particular some constraints on the intrinsic properties of neutrinos, will be discussed. We shall briefly comment on the relic neutrinos from old supernovae (i.e., the diffuse supernova neutrino background) and the future experiments aiming to observe supernova neutrinos.

7.2.1 Discoveries of the Neutrino Burst

Neutrinos emitted from the SN 1987A explosion were independently discovered by two laboratories, Kamiokande-II in Japan (Hirata *et al.*, 1987, 1988) and Irvine-Michigan-Brookhaven (IMB) in Ohio, USA (Bionta *et al.*, 1987; Bratton *et al.*, 1988). The Kamiokande experiment was intended to detect proton decays, and it was upgraded in 1985 to Kamiokande-II so as to observe solar ^{8}B neutrinos. The IMB experiment was originally designed to detect proton decays, too. Both of them utilized water Cherenkov detectors. As discussed above, neutrinos of all flavors are emitted from a supernova explosion. The dominant signals come from the charged-current process $\overline{\nu}_e + p \to n + e^+$ of electron antineutrinos. In comparison, the charged-current process $\nu_e + {}^{16}\mathrm{O} \to e^- + {}^{16}\mathrm{F}$ of electron neutrinos and the elastic neutrino-electron scattering $\nu_\alpha + e^- \to \nu_\alpha + e^-$ contribute at a subdominant level.

The Kamiokande-II detector's energy threshold for $\overline{\nu}_e$ is about 8 MeV. It recorded the first supernova neutrino event at 7 : 35 : 35 UT (Universal Time) on 23 February 1987. In total 12 neutrino events were observed, and the signals lasted about 12 seconds. The probability for these events to be caused by statistical fluctuations or cosmic muon backgrounds was found to be extremely small (Hirata *et al.*, 1987). The output of $\overline{\nu}_e$ with an average energy around 15 MeV is 8×10^{52} erg, well consistent with the theoretical prediction $E_\nu = E_\mathrm{b}/6 \approx 5 \times 10^{52}$ erg. The neutrino signals were first registered by the IMB detector at 7 : 35 : 41.37 UT on the same day, and they lasted about 6 seconds. With a high energy threshold of 20 MeV, the IMB experiment totally recorded 8 neutrino events (Bionta *et al.*, 1987).

The registration time and energies of supernova neutrino events in the Kamiokande-II and IMB experiments are summarized in Tables 7.1 and 7.2. They are compatible with the standard delayed-explosion scenario. First, the duration of neutrino signals was measured to be several seconds, just as expected for the neutrino-cooling time of neutron stars. Second, the total energy taken away by neutrinos from the supernova is essentially equal to the gravitational binding energy given in Eq. (7.12). So 99% of the gravitational binding energy stores in the form of neutrinos, 1% is used for the explosion, and only 0.01% is emitted in the form of photons.

Table 7.1 shows that there were 9 neutrino events within 2 seconds, but the last 3 events arrived about 7 seconds later. However, the IMB detector recorded two neutrino events during this time interval. This discrepancy seems to be a statistical accident, which was observed with an appreciable

Table 7.1 The measured properties of twelve neutrino events in the Kamiokande-II experiment (Hirata *et al.*, 1987. With permission from the American Physical Society). Note that the energy and angular distributions refer to the recoil electrons or positrons. The registration time for the first supernova neutrino event is 7 : 35 : 35 UT

Event number	Time (seconds)	Energy (MeV)	Angle (degrees)
1	0	20.0 ± 2.9	18 ± 18
2	0.107	13.5 ± 3.2	15 ± 27
3	0.303	7.5 ± 2.0	108 ± 32
4	0.324	9.2 ± 2.7	70 ± 30
5	0.507	12.8 ± 2.9	135 ± 23
6	0.686	6.3 ± 1.7	68 ± 77
7	1.541	35.4 ± 8.0	32 ± 16
8	1.728	21.0 ± 4.2	30 ± 18
9	1.915	19.8 ± 3.2	38 ± 22
10	9.219	8.6 ± 2.7	122 ± 30
11	10.433	13.0 ± 2.6	49 ± 26
12	12.439	8.9 ± 1.9	91 ± 39

Table 7.2 The measured properties of eight neutrino events in the IMB experiment (Bionta *et al.*, 1987. With permission from the American Physical Society). Note that the registration time of neutrino events is given in the Universal Time (UT), the uncertainties of the energy and angular distributions are $\pm 15\%$ and $\pm 15^\circ$, respectively

Event number	Time (UT)	Energy (MeV)	Angle (degrees)
1	7 : 35 : 41.37	38	74
2	7 : 35 : 41.79	37	52
3	7 : 35 : 42.02	40	56
4	7 : 35 : 42.52	35	63
5	7 : 35 : 42.94	29	40
6	7 : 35 : 44.06	37	52
7	7 : 35 : 46.38	20	39
8	7 : 35 : 46.96	24	102

frequency in numerical simulations (Bahcall *et al.*, 1988). Two other experiments, Baksan (Alexeyev *et al.*, 1988) and Mont Blanc (Aglietta *et al.*, 1987), reported the supernova neutrino signals too. The Baksan scintillation telescope in the North Caucasus observed 5 neutrino events within 9.1 seconds at

7 : 36 : 11.8 UT on 23 February 1987, but it recorded the first event 25 seconds later than the IMB detector did. The Baksan Collaboration later found that the registration time of the first neutrino event should be $7:36:11.8^{+2}_{-54}$ UT, essentially compatible with that reported by the Kamiokande-II and IMB experiments (Suzuki, 2008). The Mont Blanc Neutrino Observatory reported the neutrino burst of 5 pulses at 2 : 52 : 36 UT on 23 February 1987, about 4.5 hours earlier than the Kamiokande-II detector did. This result has been controversial, and it should have nothing to do with the SN 1987A (de Rujula, 1987; Arnett *et al.*, 1989).

Because of the poor statistics (i.e., totally 20 events obtained from the Kamiokande-II and IMB experiments), it is impossible to determine the energy spectra of supernova neutrinos. Future high-statistics observations of the neutrino burst from a galactic supernova will definitely help us understand the explosion mechanism and probe the intrinsic properties of neutrinos.

7.2.2 Constraints on Neutrino Properties

A measurement of the neutrino burst from the SN 1987A provides a strong support for the standard picture of core-collapse supernovae. One may extract useful information on the intrinsic properties of massive neutrinos, such as their lifetimes, masses and magnetic moments (Bethe, 1990).

(1) *Neutrino lifetimes.* The SN 1987A is situated in the Large Magellanic Cloud, whose distance from the Earth is $D = 50 \pm 5$ kpc $= (160 \pm 16) \times 10^3$ ly (Andreani *et al.*, 1987). If the number of supernova neutrinos or antineutrinos is assumed not to be significantly reduced by neutrino decays, the laboratory neutrino lifetime τ should be much longer than the propagation time (i.e., $\tau > D/c \approx 5 \times 10^{12}$ s). Note that relativistic neutrinos with $E_\nu \gg m_\nu$ travel almost at the speed of light. This is always the case for supernova neutrinos with an average energy $E_\nu \sim 10$ MeV. More accurately, the neutrino velocity v_ν is given by $\beta_\nu \equiv v_\nu/c \approx 1 - m_\nu^2/(2E_\nu^2)$. Hence the neutrino lifetime τ_0 in the rest frame should satisfy

$$\tau_0 = \tau\sqrt{1-\beta_\nu^2} > 5 \times 10^5 \text{ s } \left(\frac{m_\nu}{1 \text{ eV}}\right)\left(\frac{10 \text{ MeV}}{E_\nu}\right) , \tag{7.13}$$

which essentially rules out neutrino decays as a possible solution to the solar neutrino problem (Bethe, 1990).

(2) *Neutrino masses.* Now that neutrinos are massive, their arrival times must be different from the arrival time of massless neutrinos. For a distance of 50 kpc, the time delay Δt of a massive neutrino is determined by

$$\Delta t = \frac{D}{c} - \frac{D}{v_\nu} \approx 2.5 \text{ s} \left(\frac{m_\nu}{10 \text{ eV}}\right)^2 \left(\frac{10 \text{ MeV}}{E_\nu}\right)^2 . \tag{7.14}$$

To constrain m_ν, one may argue that Δt should not exceed the duration of neutrino signals observed in the Kamiokande-II and IMB experiments. Taking

$\Delta t < 10$ s for $E_\nu = 10$ MeV, for example, we obtain $m_\nu < 20$ eV. However, the emission of supernova neutrinos is distributed in time. A more reasonable statistical treatment yields $m_\nu < 16$ eV (Spergel and Bahcall, 1988).

(3) *Neutrino magnetic moments.* The existence of magnetic moments may induce the spin flip of neutrinos in the supernova via some scattering processes (e.g., the neutrino-electron scattering). After the spin flip, the left-handed neutrinos $\nu_{\rm L}$ are converted into the right-handed ones $\nu_{\rm R}$, which have no standard weak interactions with matter and can freely escape from the supernova. The rapid energy loss caused by right-handed neutrinos would significantly reduce the duration of neutrino signals and thus contradict the relevant experimental results. Along this line, the neutrino magnetic moment μ_ν can be strictly constrained as $\mu_\nu < 10^{-12}\ \mu_{\rm B}$ with $\mu_{\rm B}$ being the Bohr magneton (Raffelt and Seckel, 1988; Lattimer and Cooperstein, 1988; Barbieri and Mohapatra, 1988). It is worth mentioning that this energy-loss argument has been widely used to constrain the properties of weakly-interacting particles, such as sterile neutrinos and axions (Raffelt, 1990, 1996).

In addition, the observed neutrino burst from the SN 1987A can also shed light on the neutrino mass spectrum and the flavor mixing pattern. This aspect will be discussed in Section 7.3 and Section 7.4.

7.2.3 The Diffuse Supernova Neutrino Background

A very important lesson learnt from the SN 1987A is that the core-collapse supernovae emit neutrinos. The flux of neutrinos and antineutrinos emitted from all the core-collapse supernovae in the causally-reachable Universe is called the diffuse supernova neutrino background (DSNB). The DSNB provides us with an isotropic and time-independent source of supernova neutrinos. A measurement of the DSNB will be complementary to that of a galactic supernova neutrino burst (Ando and Sato, 2004; Beacom, 2010; Lunardini, 2010). The flavor-dependent flux of the DSNB at the Earth is determined by the neutrino emission from a single supernova explosion, the cosmic supernova rate and neutrino oscillations. Given $R_{\rm SN}(z)$ as the supernova rate per comoving volume at the redshift z, one may write down the number density of supernova neutrinos (e.g., $\overline{\nu}_e$) in the energy interval $[E_\nu, E_\nu + {\rm d}E_\nu]$ (Ando and Sato, 2004):

$$
{\rm d}n_\nu(E_\nu) = \left[R_{\rm SN}(z)(1+z)^3\right] \frac{{\rm d}t}{{\rm d}z} {\rm d}z \left[\frac{{\rm d}N_\nu(E'_\nu)}{{\rm d}E'_\nu} {\rm d}E'_\nu\right] (1+z)^{-3} \; , \tag{7.15}
$$

where $E'_\nu = (1+z)E_\nu$ is the neutrino energy at the redshift z, which is now measured as E_ν. The factors $(1+z)^{\pm 3}$ in Eq. (7.15) take account of the expansion of the Universe, and $\dfrac{{\rm d}N_\nu(E_\nu)}{{\rm d}E_\nu}$ stands for the number spectrum of neutrinos from one supernova explosion. Assuming the standard ΛCDM model with $k = 0$ and neglecting the tiny contribution from $\Omega_{\rm r}$, we have [1]

[1] See Section 9.1.3 for a detailed discussion.

$$\frac{\mathrm{d}z}{\mathrm{d}t} = -H_0(1+z)\sqrt{\Omega_{\rm m}(1+z)^3+\Omega_{\rm v}}\ , \tag{7.16}$$

where H_0 is today's Hubble constant, $\Omega_{\rm m} \approx 0.26$ and $\Omega_{\rm v} \approx 0.74$ measure the dominant energy budget of today's Universe. A combination of Eqs. (7.15) and (7.16) yields the differential number flux of the DSNB:

$$\frac{\mathrm{d}\phi}{\mathrm{d}E_\nu} \equiv c\frac{\mathrm{d}n_\nu}{\mathrm{d}E_\nu} = \frac{c}{H_0}\int_0^{z_{\rm max}} R_{\rm SN}(z)\frac{\mathrm{d}N_\nu(E'_\nu)}{\mathrm{d}E'_\nu}\cdot\frac{\mathrm{d}z}{\sqrt{\Omega_{\rm m}(1+z)^3+\Omega_{\rm v}}}\ , \tag{7.17}$$

where $z_{\rm max} = 5$ denotes the time when the gravitational collapse took place (Ando and Sato, 2004). The theoretical predictions for the DSNB flux are complicated by the supernova rate density $R_{\rm SN}(z)$, which is determined by the star formation rate $R_{\rm SF}(z)$ and the distribution of stellar masses $\psi(\mathcal{M})$. Given the conventional Salpeter function $\psi(\mathcal{M}) = \dfrac{\mathrm{d}n}{\mathrm{d}\mathcal{M}} \propto \mathcal{M}^{-2.35}$ for $0.1\mathcal{M}_\odot \lesssim \mathcal{M} \lesssim 100\mathcal{M}_\odot$, one finds (Beacom, 2010)

$$R_{\rm SN}(z) = R_{\rm SF}(z)\frac{\int_8^{50}\psi(\mathcal{M})\mathrm{d}\mathcal{M}}{\int_{0.1}^{100}\mathcal{M}\psi(\mathcal{M})\mathrm{d}\mathcal{M}} \simeq \frac{R_{\rm SF}(z)}{142\mathcal{M}_\odot}\ , \tag{7.18}$$

where $\mathcal{M}$ is given in units of $\mathcal{M}_\odot$. In Eq. (7.18) we have assumed that the stars with masses between $8\mathcal{M}_\odot$ and $50\mathcal{M}_\odot$ may give rise to the core-collapse supernovae. The model predictions are consistent with the observational data of the star formation rate, yielding $R_{\rm SF}(0) = (0.5 \sim 2.9) \times 10^{-2}\ \mathcal{M}_\odot\ {\rm year}^{-1}\ {\rm Mpc}^{-3}$ (Baldry and Glazebrook, 2003). The rate increases for higher redshifts and the results are quite robust for $0 < z \lesssim 2$, a region which is most relevant to the DSNB. Finally, we have to know the number spectrum of neutrinos from a typical supernova explosion. Since neither the initial neutrino spectra nor the neutrino mixing effects are well understood, it is convenient to take the effective Fermi-Dirac form

$$\frac{\mathrm{d}N_\nu}{\mathrm{d}E_\nu} = E_\nu^{\rm tot}\frac{120}{7\pi^4}\cdot\frac{E_\nu^2}{T^4}\cdot\frac{1}{\mathrm{e}^{E_\nu/T}+1}\ , \tag{7.19}$$

where $E_\nu^{\rm tot}$ denotes the total neutrino energy, and $T = \langle E_\nu\rangle/3.15$ is the temperature at the neutrino sphere. Both $E_\nu^{\rm tot}$ and $\langle E_\nu\rangle$ can be determined from the SN 1987A observations.

Several events of the DSNB per year are expected in the Super-Kamiokande (SK) experiment. However, such events must have been hidden by the detector backgrounds, which can be substantially reduced by adding gadolinium to detect neutrons (Beacom, 2010). The SK experiment has set a limit $\phi(E_\nu > 19.3\ {\rm MeV}) \lesssim 1.2\ {\rm cm}^{-2}\ {\rm s}^{-1}$ at the 99% confidence level (Malek *et al.*, 2003). Fig. 7.2 shows the predicted DSNB signal at the SK detector with a mass of 22.5 kton, together with the backgrounds from reactor and atmospheric neutrinos (Beacom and Vagins, 2004). It is obvious that the discovery prospects for the DSNB are excellent in the future.

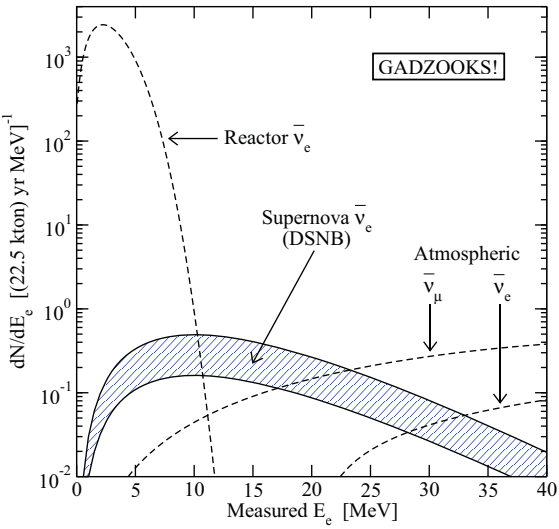

Fig. 7.2 The predicted energy spectrum of the DSNB at the SK experiment, where the backgrounds from reactor and atmospheric neutrinos have also been shown (Beacom and Vagins, 2004. With permission from the American Physical Society)

7.2.4 Future Supernova Neutrino Experiments

We have got only one lucky chance to observe the neutrino burst from the supuernova explosion (i.e., the SN 1987A). A high-statistics neutrino signal from nearby galaxies will shed light both on the mechanism of supernova explosions and on the intrinsic properties of neutrinos. Based on the measurements of supernova neutrino bursts, the observations of the DSNB will help us understand the cosmic supernova rate and variations of the neutrino emission from one supernova to another. Let us briefly summarize a few experimental methods which have been or will be used to observe supernova neutrinos (Scholberg, 2007).

(1) *Inverse beta decays.* The inverse beta decay $\overline{\nu}_e + p \to e^+ + n$ is currently the most promising process to detect supernova neutrinos. The reason is simply that its decay rate is typically two orders of magnitude larger than other interaction rates in any detectors with a large amount of protons. In a water Cherenkov detector (e.g., SK and IceCube), the Cherenkov light of the final-state positron is measured. Since the IceCube detector is intended to detect high-energy or ultrahigh-energy neutrinos, it is unable to record the MeV supernova neutrinos on an event-by-event basis. Such low-energy neutrino events can be identified with a coincident increase in single count rates from many phototubes (Halzen *et al.*, 1994; Ahrens *et al.*, 2002). To reduce the backgrounds in the SK experiment, it has been suggested to spike the

water with gadolinium trichloride so as to enhance the neutron capture rate (Beacom and Vagins, 2004). The inverse beta decay of supernova neutrinos can also be observed in a scintillation detector, such as the Baksan, LVD, KamLAND, Borexino and MiniBooNE detectors.

(2) *Charged-current interactions on nuclei.* The electron neutrinos from core-collapse supernovae (e.g., the prompt ν_e burst) are crucial for probing the dynamics of supernova explosions. They can be detected via the charged-current reactions $\nu_e + A(Z,N) \rightarrow A(Z+1,N-1) + e^-$, although their cross sections are usually small. For example, $\nu_e + {}^{16}\mathrm{O} \rightarrow {}^{16}\mathrm{F} + e^-$ for a water Cherenkov detector; $\nu_e + \mathrm{D} \rightarrow p + p + e^-$ for heavy water; and $\nu_e + {}^{12}\mathrm{C} \rightarrow {}^{12}\mathrm{N} + e^-$ for a scintillation detector. The proposed liquid-argon detectors, such as ICARUS (Hargrove *et al.*, 1996) and LANNDD (Bueno *et al.*, 2003), will make use of the reaction $\nu_e + {}^{40}\mathrm{Ar} \rightarrow {}^{40}\mathrm{K}^* + e^-$ and observe the photons from the deexcitation of ${}^{40}\mathrm{K}^*$. Such experiments are expected to be exclusively sensitive to supernova electron neutrinos.

(3) *Elastic scattering and neutral-current interactions.* In the standard picture of core-collapse supernovae, neutrinos of all three flavors are emitted. Flavor conversions of supernova neutrinos further guarantee the presence of muon and tau neutrinos. The measurements of different neutrino fluxes can therefore provide a strong support for the supernova theory and independent evidence for neutrino oscillations. The elastic scattering $\nu_\alpha + e^- \rightarrow \nu_\alpha + e^-$ (for $\alpha = e, \mu, \tau$) in a water Cherenkov detector is less important than the inverse beta decay of $\overline{\nu}_e$, but it can measure the direction of incident neutrinos which points back to the location of the supernova. For a neutral-current reaction $\nu_x + A \rightarrow \nu_x + A^*$ (for $x = \mu, \tau$), it is possible to tag the ejected nucleons or deexcitation photons from the excited nucleus A^*. Interestingly, the detectors intended to detect dark matter or solar neutrinos may also be sensitive to supernova neutrinos via the coherent neutrino-nucleus scattering.

Some current and future experiments sensitive to supernova neutrinos are listed in Table 7.3, where the neutrino events for a supernova explosion at a distance of 8.5 kpc are roughly estimated (Scholberg, 2010). It is worth mentioning that gravitational waves should be produced from the core collapses. So an analysis of the correlation between gravitational waves and neutrino signals would be very interesting and helpful in the study of supernova physics (Pagliaroli *et al.*, 2009; Halzen and Raffelt, 2009).

7.3 Matter Effects on Supernova Neutrinos

The neutrino spectra of three different flavors at the neutrino spheres can be approximately described by the Fermi-Dirac distributions with different effective temperatures. When neutrinos freely stream from the neutrino spheres to the supernova surface, however, the oscillation effects may change the spectra. In this section we shall discuss the ordinary matter effects on supernova neutrino oscillations, in particular the Mikheyev-Smirnov-Wolfenstein (MSW)

Table 7.3 A summary of current and proposed detectors with sensitivities to supernova neutrinos, where the number of events is estimated for a supernova explosion at a distance of 8.5 kpc (Scholberg, 2010. With permission from the Institute of Physics)

Detector	Type	Mass (kton)	Location	No. of Events	Status
Baksan	C_nH_{2n}	0.33	Caucasus	50	Running
Super-K	H_2O	32	Japan	8000	Running
LVD	C_nH_{2n}	1	Italy	300	Running
KamLAND	C_nH_{2n}	1	Japan	300	Running
MiniBooNE	C_nH_{2n}	0.7	USA	200	Running
Borexino	C_nH_{2n}	0.3	Italy	100	Running
IceCube	Long string	0.4/PMT	South Pole	N/A	Running
SNO+	C_nH_{2n}	0.8	Canada	300	Near Future
HALO	Pb	0.07	Canada	80	Near Future
ICARUS	Ar	0.6	Italy	230	Near Future
NOνA	C_nH_{2n}	15	USA	3000	Near Future
LBNE LAr	Liquid Argon	5	USA	1900	Future
LBNE WC	H_2O	300	USA	78,000	Future
MEMPHYS	H_2O	440	Europe	120,000	Future
Hyper-K	H_2O	500	Japan	130,000	Future
LENA	C_nH_{2n}	50	Europe	15,000	Future
GLACIER	Ar	100	Europe	38,000	Future

resonant conversions (Wolfenstein, 1978, 1979; Mikheyev and Smirnov, 1985). The resonances associated with high ($|\Delta m^2_{31}| \approx 2.4 \times 10^{-3}$ eV^2) and low ($\Delta m^2_{21} \approx 8.0 \times 10^{-5}$ eV^2) neutrino mass-squared differences can take place in the mantle and envelope of a supernova. Accordingly, the initial flavor distribution at the neutrino sphere will be significantly modified, leading to some observable effects. In addition to the resonant conversions inside the supernova, the matter effects inside the Earth may further reprocess the neutrino spectra. A measurement of the neutrino burst from a future galactic supernova explosion could help pin down the smallest neutrino mixing angle θ_{13} and the neutrino mass hierarchy (Dutta *et al.*, 2000; Dighe and Smirnov, 2000). On the other hand, the neutrinos just above the neutrino sphere are so dense that the coherent neutrino-neutrino scattering may dominate over the neutrino interactions with ordinary matter. In this case the collective neutrino flavor conversions can happen, and they may have already changed the neutrino spectra before the ordinary matter effects do their work. This intriguing phenomenon will be discussed in detail in Section 7.4.

7.3.1 Neutrino Fluxes and Energy Spectra

Before discussing neutrino oscillations and matter effects, one should know neutrino fluxes and energy spectra of different flavors. Note that the neutrino sphere is defined for a specific energy, and neutrinos with different energies are actually emitted from different neutrino spheres. More accurately, the cross section of the neutrino-nucleon scattering becomes larger for neutrinos with higher energies, so does the radius of the neutrino sphere. Since the temperature decreases with the increasing radius in a supernova, the neutrinos with higher energies have lower temperatures. This observation implies that the energy spectrum must get pinched at the high energy end. The original neutrino flux from the supernova core can be effectively described by a pinched Fermi-Dirac spectrum (Raffelt, 1996):

$$F^0_{\nu_\alpha}(E_{\nu_\alpha}, T_{\nu_\alpha}, \eta_{\nu_\alpha}, L_{\nu_\alpha}, d) = \frac{L_{\nu_\alpha}}{4\pi d^2} \cdot \frac{1}{T^4_{\nu_\alpha} F_3(\eta_{\nu_\alpha})} \cdot \frac{E^2_{\nu_\alpha}}{\mathrm{e}^{(E_{\nu_\alpha}/T_{\nu_\alpha} - \eta_{\nu_\alpha})} + 1} \; , \tag{7.20}$$

where E_{ν_α} is the energy of ν_α, T_{ν_α} denotes the effective temperature at the neutrino sphere, η_{ν_α} is the pinching parameter, L_{ν_α} stands for the neutrino luminosity, and d represents the distance to the supernova. Note that $F_3(\eta_{\nu_\alpha}) \equiv \int_0^\infty x^3 [\mathrm{e}^{x-\eta_{\nu_\alpha}} + 1]^{-1} \mathrm{d}x$ is a Fermi-Dirac integral, and $F_3(0) = 7\pi^4/120$ holds. We stress that η_{ν_α} should not be identified with $\mu_{\nu_\alpha}/T_{\nu_\alpha}$ in the thermal Fermi-Dirac distribution, where μ_{ν_α} is the chemical potential. Hence the relation $\eta_{\nu_\alpha} = -\eta_{\overline{\nu}_\alpha}$ does not hold for neutrinos ν_α and antineutrinos $\overline{\nu}_\alpha$. In other words, the distribution in Eq. (7.20) is not thermal.

Numerical simulations of the neutrino transport in the supernova core indicate that the average neutrino energies satisfy $\langle E_{\overline{\nu}_e} \rangle = (14 \sim 22)$ MeV, $\langle E_{\nu_e} \rangle = (0.5 \sim 0.8) \langle E_{\overline{\nu}_e} \rangle$ and $\langle E_{\nu_x} \rangle = (1.1 \sim 1.6) \langle E_{\overline{\nu}_e} \rangle$, where ν_x denotes the non-electron flavors ν_μ, $\overline{\nu}_\mu$, ν_τ and $\overline{\nu}_\tau$ (Keil *et al.*, 2003). Moreover, one obtains $0 \lesssim \eta_{\nu_e} \lesssim 3$, $0 \lesssim \eta_{\overline{\nu}_e} \lesssim 3$ and $0 \lesssim \eta_{\nu_x} \lesssim 2$, implying that electron neutrinos and electron antineutrinos might have stronger pinching effects. Given a value of η_{ν_α}, the effective temperature T_{ν_α} for each neutrino flavor can be determined by $\langle E_{\nu_\alpha} \rangle$. The time-integrated neutrino luminosity L_{ν_α} is typically $(1 \sim 5) \times 10^{52}$ erg, and $d \sim 10$ kpc holds for a galactic supernova. The luminosities of different neutrino flavors are expected to be equal within a factor of two or so (Keil *et al.*, 2003).

Note that the neutrino luminosities, temperatures and pinching parameters should be time-dependent as the supernova evolves. Hence the integrated neutrino fluxes may differ from that given by Eq. (7.20). The time-dependent effects (e.g., the propagation of the shock wave) can be imprinted in the final neutrino fluxes and thus observable in experiments (Fogli *et al.*, 2005).

7.3.2 Matter Effects in the Supernova

It is well known that neutrino oscillations with the MSW matter effects can perfectly solve the solar neutrino problem. An immediate question is

whether matter effects play an important role in the flavor conversions of supernova neutrinos. Given two independent neutrino mass-squared differences $|\Delta m^2_{31}| \approx 2.4 \times 10^{-3}$ eV^2 and $\Delta m^2_{21} \approx 8.0 \times 10^{-5}$ eV^2, the question becomes whether the MSW resonance conditions for neutrino oscillations are satisfied in the supernova environment. Considering a generic neutrino mass-squared difference Δm^2 and the flavor mixing angle θ, one finds that the matter density on the MSW resonance is given by (Kuo and Pantaleone, 1989)

$$\rho^* = \frac{m_{\rm H}}{\sqrt{2}\, G_{\rm F} Y_e} \cdot \frac{\Delta m^2}{2E} \cos 2\theta \; , \tag{7.21}$$

where $m_{\rm H}$ is the atomic mass unit, Y_e denotes the electron number fraction, and E represents the neutrino beam energy. As mentioned before, the initial neutrino fluxes of muon and tau flavors are equal. Moreover, the weak interactions of ν_μ and ν_τ neutrinos are almost indistinguishable when the energies are about tens of MeV. Hence the oscillation between ν_μ and ν_τ is irrelevant here, and it is convenient to work in the flavor basis $(\nu_e, \nu'_\mu, \nu'_\tau)$ which renders the effective Hamiltonian to be diagonal in the ν_μ-ν_τ sector (Dighe and Smirnov, 2000). In view of the smallness of the neutrino mixing angle θ_{13}, we may describe the system by two pairs of mixing parameters: $(\theta_{13}, \Delta m^2_{31})$ and $(\theta_{12}, \Delta m^2_{21})$. A global analysis of current neutrino oscillation data actually yields $\theta_{12} \approx 34^\circ$ and $\theta_{13} < 12^\circ$ (Gonzalez-Garcia *et al.*, 2010). For the high neutrino mass-squared difference, the resonance condition is fulfilled at

$$\rho^*_{\rm H} = 3.4 \times 10^3 \text{ g cm}^{-3} \left(\frac{|\Delta m^2_{31}|}{2.4 \times 10^{-3} \text{ eV}^2} \right) \left(\frac{10 \text{ MeV}}{E} \right) \left(\frac{0.5}{Y_e} \right) \; , \tag{7.22}$$

where $\cos 2\theta_{13} \approx 1$ has been taken; and for the low mass-squared difference,

$$\rho^*_{\rm L} = 42 \text{ g cm}^{-3} \left(\frac{\Delta m^2_{21}}{8.0 \times 10^{-5} \text{ eV}^2} \right) \left(\frac{10 \text{ MeV}}{E} \right) \left(\frac{0.5}{Y_e} \right) \; , \tag{7.23}$$

where $\cos 2\theta_{12} \approx 0.37$ has been input. So the MSW resonances may only occur in the outer layers of the mantle or envelope (i.e., the regions far from the supernova core and neutrino spheres). Because of $|\Delta m^2_{31}| \gg \Delta m^2_{21}$, the two resonances are well separated in space. Hence it is reasonable to treat the whole three-flavor system as a two-flavor problem in each resonant region.

As shown in Section 5.1, the resonant flavor conversion may be either adiabatic or non-adiabatic, or in-between, depending on the adiabaticity parameter γ. Given the density profile $\rho(r) = 10^{13}$ g cm^{-3}(10 km/r)$^3 \equiv Ar^{-3}$, which is typical for a supernova during the first few seconds after bounce (Brown *et al.*, 1982; Bethe, 1990), the transition probability between two mass eigenstates can be calculated by using the Landau-Zener formula

$$P_{\rm LZ} = \exp\left[-\frac{\pi}{2} \gamma \right] = \exp\left[-\left(\frac{E_0}{E} \right)^{2/3} \right] \; , \tag{7.24}$$

where the critical energy E_0 is given by (Dighe and Smirnov, 2000)

$$E_0 = \left(\frac{\pi}{12}\right)^{3/2} \frac{\Delta m^2 \sin^3 2\theta}{\cos^2 2\theta} \left(\frac{2\sqrt{2}\, G_{\rm F} Y_e}{m_{\rm H}} A\right)^{1/2} . \tag{7.25}$$

Note that $\Delta m^2 = |\Delta m^2_{31}|$ and $\theta = \theta_{13}$ should be taken in Eq. (7.25) for the high-level resonance. More explicitly, we have (Lunardini and Smirnov, 2003)

$$E_0^{\rm H} \simeq 2.6 \times 10^7 \ {\rm MeV} \left(\frac{|\Delta m^2_{31}|}{2.4 \times 10^{-3} \ {\rm eV}^2}\right) \sin^3 \theta_{13} . \tag{7.26}$$

It is now evident that $\gamma \propto (E_0^{\rm H}/E)^{2/3}$ depends on θ_{13}. For $\sin^2 \theta_{13} \gtrsim 10^{-3}$ and $E \sim 10$ MeV, one has $P_{\rm H} = \exp[-(E_0^{\rm H}/E)^{2/3}] \approx 0$ which implies a pure adiabatic conversion. For $\sin^2 \theta_{13} \lesssim 10^{-5}$ and $E \sim 10$ MeV, one has $P_{\rm H} \approx 1$ which strongly violates the adiabaticity. For an intermediate value of $\sin^2 \theta_{13}$, $P_{\rm H}$ increases with the neutrino energy E. After substituting $\Delta m^2 = \Delta m^2_{21}$ and $\theta = \theta_{12}$ into Eq. (7.25), we find that the low-level resonant conversion is always adiabatic (i.e., $E_0^{\rm L} \gg E$ and thus $P_{\rm L} \approx 0$). As for antineutrinos, one may similarly evaluate the transition probabilities $\overline{P}_{\rm H}$ and $\overline{P}_{\rm L}$ if the resonances exist. Given $\Delta m^2_{31} > 0$, both high- and low-level resonances occur in the neutrino sector. For $\Delta m^2_{31} < 0$, the low-level resonance occurs in the neutrino sector and the high-level one takes place in the antineutrino sector.

Because of the high matter density in a supernova, the effective neutrino mixing angles are suppressed and the flavor states $(\nu_e, \nu'_\mu, \nu'_\tau)$ coincide with the effective mass eigenstates $(\nu_{1{\rm m}}, \nu_{2{\rm m}}, \nu_{3{\rm m}})$ in matter. Hence the flavor conversions can be treated as the propagation of neutrino mass eigenstates and the crossing among them. At the surface of a supernova one arrives at the incoherent fluxes of neutrino mass eigenstates, which will travel to the surface of the Earth without further flavor conversions. Let us consider the flavor conversions in the case of either $m_3 > m_2 > m_1$ (normal hierarchy) or $m_2 > m_1 > m_3$ (inverted hierarchy) for both neutrinos and antineutrinos (Dighe and Smirnov, 2000).

(1) *The normal neutrino mass hierarchy.* In this case the original fluxes of neutrino mass eigenstates are given by $F^0_{\nu_{1{\rm m}}} = F^0_{\nu_x} = F^0_{\nu_{2{\rm m}}}$ and $F^0_{\nu_{3{\rm m}}} = F^0_{\nu_e}$, where $F^0_{\nu_x} = F^0_{\nu_\mu} = F^0_{\nu_\tau}$ holds as an excellent approximation. The probability for $\nu_{3{\rm m}}$ to be ν_1 at the surface is $P_{\rm H} P_{\rm L}$; i.e., this happens through both high- and low-level crossings. The probabilities of $\nu_{1{\rm m}} \to \nu_1$ and $\nu_{2{\rm m}} \to \nu_1$ transitions turn out to be $(1 - P_{\rm L})$ and $P_{\rm L}(1 - P_{\rm H})$, respectively. So the flux of the mass eigenstate ν_1 at the supernova surface reads

$$F^0_{\nu_1} = P_{\rm H} P_{\rm L} F^0_{\nu_e} + (1 - P_{\rm H} P_{\rm L}) F^0_{\nu_x} . \tag{7.27}$$

One may figure out the fluxes of ν_2 and ν_3 in a similar way:

$$F^0_{\nu_2} = P_{\rm H} (1 - P_{\rm L}) F^0_{\nu_e} + (1 - P_{\rm H} + P_{\rm H} P_{\rm L}) F^0_{\nu_x} ,$$

$$F^0_{\nu_3} = (1 - P_{\rm H})\, F^0_{\nu_e} + P_{\rm H} F^0_{\nu_x} \ . \tag{7.28}$$

The flux of electron neutrinos at the Earth is then obtained by projecting the mass eigenstates onto the flavor eigenstates. Up to a factor L^{-2}, where L is the distance to the Earth, we have

$$F^{\rm E}_{\nu_e} = \sum_i |V_{ei}|^2 F^0_{\nu_i} = p F^0_{\nu_e} + (1 - p)\, F^0_{\nu_x} \tag{7.29}$$

together with the survival probability

$$p = |V_{e1}|^2 P_{\rm H} P_{\rm L} + |V_{e2}|^2 P_{\rm H}\,(1 - P_{\rm L}) + |V_{e3}|^2\,(1 - P_{\rm H}) \ , \tag{7.30}$$

where V_{ei} (for $i = 1, 2, 3$) denotes an element of the neutrino mixing matrix V. The total flux of ν_μ and ν_τ can be derived from the conservation of neutrino fluxes: $F^{\rm E}_{\nu_\mu} + F^{\rm E}_{\nu_\tau} = (1 - p) F^0_{\nu_e} + (1 + p) F^0_{\nu_x}$. As for supernova antineutrinos, their mass eigenstates coincide with their flavor eigenstates (i.e., $\overline{\nu}_{1\rm m} = \overline{\nu}_e$, $\overline{\nu}_{2\rm m} = \overline{\nu}_\mu$ and $\overline{\nu}_{3\rm m} = \overline{\nu}_\tau$). As mentioned above, there is no level crossing in the antineutrino sector for the normal mass hierarchy. Hence antineutrinos can always keep in the mass eigenstates until they reach the Earth. It is then straightforward to calculate the flux of electron antineutrinos at the Earth:

$$F^{\rm E}_{\overline{\nu}_e} = \sum_i |V_{ei}|^2 F^0_{\overline{\nu}_i} = \overline{p} F^0_{\overline{\nu}_e} + (1 - \overline{p})\, F^0_{\overline{\nu}_x} \tag{7.31}$$

together with the survival probability $\overline{p} = |V_{e1}|^2$. The sum of $\overline{\nu}_\mu$ and $\overline{\nu}_\tau$ fluxes can similarly be fixed by the conservation of antineutrino fluxes.

(2) *The inverted neutrino mass hierarchy.* In the region of high matter densities, the neutrino mass eigenstates are identified with their flavor eigenstates as follows: $\nu_{1\rm m} = \nu_{\mu'}$, $\nu_{2\rm m} = \nu_e$ and $\nu_{3\rm m} = \nu_{\tau'}$ for neutrinos; $\overline{\nu}_{1\rm m} = \overline{\nu}_{\tau'}$, $\overline{\nu}_{2\rm m} = \overline{\nu}_{\mu'}$ and $\overline{\nu}_{3\rm m} = \overline{\nu}_e$ for antineutrinos (Dighe and Smirnov, 2000). Recall that the high-level resonance exists in the antineutrino sector and the low-level one occurs in the neutrino sector. In view of Eqs. (7.29) and (7.31), we find that it is only needed to calculate the survival probabilities of electron neutrinos (p) and electron antineutrinos ($\overline{p}$). Since the initial electron neutrino ν_e is in the mass eigenstate ν_{2m}, the probabilities of $\nu_{2\rm m} \to \nu_1$ and $\nu_{2\rm m} \to \nu_2$ transitions are $P_{\rm L}$ and $(1 - P_{\rm L})$, respectively. So we have

$$p = |V_{e1}|^2 P_{\rm L} + |V_{e2}|^2\,(1 - P_{\rm L}) \ . \tag{7.32}$$

As for antineutrinos, $\overline{\nu}_e$ initially coincides with $\overline{\nu}_{3\rm m}$. It converts into $\overline{\nu}_1$ via the high-level resonance with the probability $\overline{P}_{\rm H}$, and stays in $\overline{\nu}_3$ with the probability $(1 - \overline{P}_{\rm H})$. The survival probability of electron antineutrinos turns out to be

$$\overline{p} = |V_{e1}|^2 \overline{P}_{\rm H} + |V_{e3}|^2 \left(1 - \overline{P}_{\rm H}\right) \ . \tag{7.33}$$

Eqs. (7.29) and (7.31) together with Eqs. (7.32) and (7.33) give rise to the fluxes of electron neutrinos and electron antineutrinos at the Earth.

Finally, we summarize the matter effects on neutrino oscillations in the supernova mantle and envelope:

$$p = |V_{e2}|^2 P_{\rm H} + |V_{e3}|^2 \left(1 - P_{\rm H}\right) \ , \quad \overline{p} = |V_{e1}|^2 \ , \tag{7.34}$$

for the normal neutrino mass hierarchy; and

$$p = |V_{e2}| \ , \quad \overline{p} = |V_{e1}|^2 P_{\rm H} + |V_{e3}|^2 \left(1 - P_{\rm H}\right) \ , \tag{7.35}$$

for the inverted neutrino mass hierarchy. Note that we have set $P_{\rm L} = 0$ and $P_{\rm H} = \overline{P}_{\rm H}$. Although $P_{\rm H}$ relies on $\sin^2\theta_{13}$, one may simplify Eqs. (7.34) and (7.35) in two interesting scenarios: (A) for $\sin^2\theta_{13} \gtrsim 10^{-3}$ and thus $P_{\rm H} \approx 0$, one arrives at $p = 0$ and $\overline{p} = \sin^2\theta_{12}$ for the normal mass hierarchy or $p = \sin^2\theta_{12}$ and $\overline{p} = 0$ for the inverted mass hierarchy; (B) for $\sin^2\theta_{13} \lesssim 10^{-5}$ and thus $P_{\rm H} \approx 1$, one obtains $p = \sin^2\theta_{12}$ and $\overline{p} = \cos^2\theta_{12}$ for both mass hierarchies. The terms of $\sin^2\theta_{13}$ are omitted in either scenario. We conclude that a measurement of the supernova neutrino fluxes has the great potential to probe the smallest neutrino mixing angle θ_{13} and pin down the neutrino mass hierarchy (Lunardini and Smirnov, 2003; Raffelt, 2005).

7.3.3 Matter Effects in the Earth

We have discussed the supernova neutrino fluxes at the surface of the Earth. Depending on the location of a supernova and the time of a day, supernova neutrinos may traverse the Earth before arriving at the detector. Hence a comparison between the neutrino signals in two detectors located at different places could reveal the matter effects induced by the Earth (Dighe and Smirnov, 2000; Dighe *et al.*, 2003; Mirizzi *et al.*, 2006).

If neutrinos do not cross the core of the Earth, one may assume that the average matter density is a constant. The density profile changes abruptly from the vacuum to the Earth. In this case one has to calculate the transition amplitude of $\nu_i^{(1)} \to \nu_j^{(2)}$, where $\nu_i^{(1)}$ and $\nu_j^{(2)}$ denote the neutrino mass eigenstates in media "1" and "2", respectively. Since the neutrino flavor eigenstates cross the interface continuously, the transition amplitudes are given by (Kuo and Pantaleone, 1989)

$$\begin{aligned} \mathcal{A}(\nu_i^{(1)} \to \nu_j^{(2)}) &= \begin{pmatrix} \cos\theta^{(2)} & -\sin\theta^{(2)} \\ \sin\theta^{(2)} & \cos\theta^{(2)} \end{pmatrix} \begin{pmatrix} \cos\theta^{(1)} & \sin\theta^{(1)} \\ -\sin\theta^{(1)} & \cos\theta^{(1)} \end{pmatrix} \\ &= \begin{pmatrix} \cos\left[\theta^{(1)} - \theta^{(2)}\right] & \sin\left[\theta^{(1)} - \theta^{(2)}\right] \\ -\sin\left[\theta^{(1)} - \theta^{(2)}\right] & \cos\left[\theta^{(1)} - \theta^{(2)}\right] \end{pmatrix} \ , \end{aligned} \tag{7.36}$$

in which the two-flavor oscillation has been assumed, $\theta^{(1)}$ and $\theta^{(2)}$ are the corresponding mixing angles in media. Now we calculate the probability that

a mass eigenstate ν_i entering the Earth arrives at the detector as ν_α. First, ν_i converts into the mass eigenstates $\nu_{1\mathrm{m}}$ and $\nu_{2\mathrm{m}}$ in matter with the amplitudes given in Eq. (7.36). Second, the propagation of mass eigenstates in a constant matter profile induces a phase difference $\Phi_\mathrm{m} = \Delta\tilde{m}^2 L/(2E)$ between $\nu_{1\mathrm{m}}$ and $\nu_{2\mathrm{m}}$, where $\Delta\tilde{m}^2$ stands for the effective neutrino mass-squared difference in matter, L is the distance traveled by neutrinos, and E denotes the neutrino beam energy. Finally, $\nu_{1\mathrm{m}}$ and $\nu_{2\mathrm{m}}$ reach the detector and are measured as ν_α with the amplitudes given by the neutrino mixing matrix. Put all these together, we obtain the probability of $\nu_i \to \nu_\alpha$ as (Dighe *et al.*, 2003)

$$P_{i\alpha} = \left| \left[\begin{pmatrix} \cos\theta_\mathrm{m} & -\sin\theta_\mathrm{m} \\ \sin\theta_\mathrm{m} & \cos\theta_\mathrm{m} \end{pmatrix} \begin{pmatrix} 1 & 0 \\ 0 & \mathrm{e}^{\mathrm{i}\Phi_\mathrm{m}} \end{pmatrix} \begin{pmatrix} \cos\Delta\theta & \sin\Delta\theta \\ -\sin\Delta\theta & \cos\Delta\theta \end{pmatrix} \right]_{\alpha i} \right|^2 , \quad (7.37)$$

where $\Delta\theta \equiv \theta_\mathrm{m} - \theta$ with θ_m (or θ) being the mixing angle in matter (or vacuum). Taking $\nu_1 \to \nu_e$ for example, we explicitly get

$$P_{1e} = \cos^2\theta_{12} - \sin 2\theta_{12}^\mathrm{m} \sin 2\left(\theta_{12}^\mathrm{m} - \theta_{12}\right) \sin^2\left(\frac{\Delta\tilde{m}_{21}^2 L}{4E}\right) . \quad (7.38)$$

In addition, we can obtain $P_{2e} = 1 - P_{1e}$ due to the probability conservation. We proceed to consider the terrestrial matter effects on supernova neutrinos. Given the fluxes of neutrino mass eigenstates $F_{\nu_i}^0$, the flux of ν_e at the detector turns out to be

$$F_{\nu_e}^\mathrm{D} = \sum_i F_{\nu_i}^0 P_{ie} , \quad (7.39)$$

where P_{ie} can be read off from Eq. (7.37). In the case of a normal neutrino mass hierarchy, the fluxes $F_{\nu_i}^0$ have been given in Eqs. (7.27) and (7.28). These equations allow us to rewrite Eq. (7.39) as $F_{\nu_e}^\mathrm{D} = p^\mathrm{D} F_{\nu_e}^0 + (1 - p^\mathrm{D}) F_{\nu_x}^0$, where the probability p^D reads

$$p^\mathrm{D} = P_{1e} P_\mathrm{H} P_\mathrm{L} + P_{2e} P_\mathrm{H} \left(1 - P_\mathrm{L}\right) + P_{3e} \left(1 - P_\mathrm{H}\right) . \quad (7.40)$$

If there are two detectors and only one of them is shadowed by the Earth, then the terrestrial matter effects are characterized by the difference between $F_{\nu_e}^\mathrm{D}$ and $F_{\nu_e}^\mathrm{E}$. More explicitly,

$$F_{\nu_e}^\mathrm{D} - F_{\nu_e}^\mathrm{E} = \left(p^\mathrm{D} - p\right) \left(F_{\nu_e}^0 - F_{\nu_x}^0\right) . \quad (7.41)$$

Note that the matter effects would vanish if $F_{\nu_e}^0 = F_{\nu_x}^0$ exactly held. Since the initial fluxes of supernova neutrinos are energy-dependent, $(F_{\nu_e}^0 - F_{\nu_x}^0)$ is in general positive at low energies and becomes negative at higher energies. So it may change its sign at the critical energy E_C, where $F_{\nu_e}^0(E_\mathrm{C}) = F_{\nu_x}^0(E_\mathrm{C})$ holds. Furthermore, Eqs. (7.30) and (7.40) lead us to

$$p^{\rm D} - p = P_{\rm H} \left(1 - 2P_{\rm L}\right) \left(P_{2e} - |V_{e2}|^2\right) \ , \tag{7.42}$$

where we have neglected the contribution from ν_3 oscillations because it is suppressed by both $\sin^2 \theta_{13}$ and $\sin 2(\theta_{13}^{\rm m} - \theta_{13})$. In the most general case, two different detectors "D1" and "D2" are both shadowed by the Earth. Then we have (Dighe and Smirnov, 2000)

$$F^{\rm D1}_{\nu_e} - F^{\rm D2}_{\nu_e} = P_{\rm H} \left(1 - 2P_{\rm L}\right) \left(P^{\rm D1}_{2e} - P^{\rm D2}_{2e}\right) \left(F^0_{\nu_e} - F^0_{\nu_x}\right) \ , \tag{7.43}$$

where $P^{\rm D1}_{2e}$ and $P^{\rm D2}_{2e}$ denote the probabilities of $\nu_2 \to \nu_e$ for two different detectors. Some comments on Eq. (7.43) are in order: (1) the contributions from the initial supernova neutrino fluxes ($F^0_{\nu_e} - F^0_{\nu_x}$), the flavor conversions in the supernova envelope $P_{\rm H}(1 - 2P_{\rm L})$ and the propagation in the Earth ($P^{\rm D1}_{2e} - P^{\rm D2}_{2e}$) are clearly factorized; (2) a difference between the initial ν_e and ν_x fluxes is required for significant matter effects; (3) the high-level resonance needs to be non-adiabatic (i.e., $P_{\rm H} \approx 1$), otherwise the matter effects would be suppressed by $P_{\rm H}$. One may analogously consider the matter effects on electron antineutrinos and obtain the counterpart of Eq. (7.43) as follows:

$$F^{\rm D1}_{\overline{\nu}_e} - F^{\rm D2}_{\overline{\nu}_e} = \left(1 - 2\overline{P}_{\rm L}\right) \left(\overline{P}^{\rm D1}_{1e} - \overline{P}^{\rm D2}_{1e}\right) \left(F^0_{\overline{\nu}_e} - F^0_{\overline{\nu}_x}\right) \ . \tag{7.44}$$

Note that the factor $\overline{P}_{\rm H}$ does not appear in Eq. (7.44), because the high-level resonance is absent in the antineutrino sector. As for the inverted neutrino mass hierarchy, a straightforward analysis yields (Dighe and Smirnov, 2000)

$$F^{\rm D1}_{\nu_e} - F^{\rm D2}_{\nu_e} = \left(1 - 2P_{\rm L}\right) \left(\overline{P}^{\rm D1}_{2e} - \overline{P}^{\rm D2}_{2e}\right) \left(F^0_{\nu_e} - F^0_{\nu_x}\right) \tag{7.45}$$

for neutrinos; and

$$F^{\rm D1}_{\overline{\nu}_e} - F^{\rm D2}_{\overline{\nu}_e} = \overline{P}_{\rm H} \left(1 - 2\overline{P}_{\rm L}\right) \left(P^{\rm D1}_{1e} - P^{\rm D2}_{1e}\right) \left(F^0_{\overline{\nu}_e} - F^0_{\overline{\nu}_x}\right) \tag{7.46}$$

for antineutrinos. In light of current neutrino oscillation data, the low-level resonance is always adiabatic and thus $P_{\rm L} = \overline{P}_{\rm L} = 0$ holds. So Eq. (7.45) is obtainable from Eq. (7.44) with the replacements $\overline{\nu}_e \to \nu_e$ and $\overline{\nu}_x \to \nu_x$; and Eq. (7.46) can be obtained from Eq. (7.43) with the replacements $\nu_e \to \overline{\nu}_e$, $\nu_x \to \overline{\nu}_x$ and $P_{\rm H} \to \overline{P}_{\rm H}$. Table 7.4 summarizes the matter effects both in the supernova envelope and in the Earth. For the latter, we only list the channels in which the terrestrial matter effects may be significant. Note that the shock wave will pass the dense region, where the high-level resonance takes place, and may break the adiabaticity of the resonance. In this case the survival probabilities have to be modified (Schirato and Fuller, 2002; Fogli *et al.*, 2003, 2005). The channels sensitive to the shock-wave effects are also listed in Table 7.4.

Table 7.4 The survival probabilities p (neutrinos) and $\overline{p}$ (antineutrinos), terrestrial matter effects and shock-wave effects in three scenarios (Raffelt, 2005. With permission from the Institute of Physics)

Mass hierarchy	$\sin^2\theta_{13}$	p	$\overline{p}$	Earth matter	Shock wave
Normal	$\gtrsim 10^{-3}$	0	$\cos^2\theta_{12}$	$\overline{\nu}_e$	ν_e
Inverted	$\gtrsim 10^{-3}$	$\sin^2\theta_{12}$	0	ν_e	$\overline{\nu}_e$
Any	$\lesssim 10^{-5}$	$\sin^2\theta_{12}$	$\cos^2\theta_{12}$	ν_e and $\overline{\nu}_e$	–

7.4 Collective Neutrino Flavor Conversions

Soon after the discovery of the MSW matter effects on solar neutrino flavor conversions, it was realized that the coherent forward scattering of neutrinos on a dense neutrino background should be important in the core-collapse supernovae and in the early Universe (Fuller *et al.*, 1987; Nötzold and Raffelt, 1988). In contrast with the MSW effects in ordinary matter, the neutrino self-interaction potential has the off-diagonal elements in the flavor basis (Pantaleone, 1992a, 1992b). Due to this neutrino self-interaction potential, neutrinos might have undergone collective oscillations in the early Universe (i.e., a large fraction of neutrinos with different energies oscillated coherently) (Samuel, 1993, 1996; Kostelecký *et al.*, 1993; Kostelecký and Samuel, 1993, 1994, 1995, 1996; Pantaleone, 1998; Pastor *et al.*, 2002).

In the context of core-collapse supernovae, the synchronized and bipolar neutrino oscillations are the main features of the collective phenomena (Duan and Kneller, 2009; Duan *et al.*, 2010). Such collective effects may give rise to the almost complete flavor conversions and dramatically affect the neutrino energy spectra. In this section we shall introduce collective neutrino oscillations and try to understand the physics behind them. It should be kept in mind that this topic is now under active studies, and it remains unclear whether collective neutrino oscillations will be significantly changed in a realistic supernova environment including the non-spherical geometry, convective effects and magnetic fields (Duan *et al.*, 2010). Hence we shall concentrate on the generic features of collective neutrino oscillations and some analytical understanding of them by assuming the standard delayed-explosion scenario.

7.4.1 Equations of Motion

In Section 5.3 we have formulated neutrino oscillations in the language of the density matrix, presented the equations of motion for the flavor polarization vectors $\mathbf{P}$ and $\overline{\mathbf{P}}$, and illustrated the nonlinear behavior of flavor conversions in the simplest case with the isotropic neutrino gases, monochromatic neutrino energy spectra and equal number densities of neutrinos and

antineutrinos. To be more realistic, we introduce the so-called neutrino bulb model which accounts for the geometry of the neutrino emission from a proto-neutron star (Duan *et al.*, 2006b, 2010). Fig. 7.3 shows the corresponding geometrical layout. The test neutrinos with different emission angles $\vartheta_{\rm R}$ may experience different flavor conversions, because they have distinct histories of interactions when traveling from the surface of the proto-neutron star to point A with a radius r. The background neutrinos come from a special part of the neutrino sphere, which is within the cone with an open angle $\vartheta_{\rm max} = \arcsin(R_\nu/r)$. Given the geometry in Fig. 7.3, the equations of motion for the polarization vectors $\mathbf{P}_{\mathbf{p}}(t)$ and $\overline{\mathbf{P}}_{\mathbf{p}}(t)$ in Eq. (5.146) can be rewritten as those for $\mathbf{P}_\vartheta(E,t)$ and $\overline{\mathbf{P}}_\vartheta(E,t)$, where ϑ is the polar angle of the neutrino momentum $\mathbf{p}$ and $E = |\mathbf{p}|$ is the neutrino energy:

$$\begin{aligned}
\dot{\mathbf{P}}_\vartheta &= \left[+\omega\mathbf{B} + \lambda\mathrm{L} + 2\sqrt{2}\pi G_{\rm F} \int {\rm d}c_{\vartheta'}{\rm d}E(\mathbf{P}_{\vartheta'} - \overline{\mathbf{P}}_{\vartheta'}) g(\vartheta,\vartheta')\right] \times \mathbf{P}_\vartheta \; , \\
\dot{\overline{\mathbf{P}}}_\vartheta &= \left[-\omega\mathbf{B} + \lambda\mathrm{L} + 2\sqrt{2}\pi G_{\rm F} \int {\rm d}c_{\vartheta'}{\rm d}E(\mathbf{P}_{\vartheta'} - \overline{\mathbf{P}}_{\vartheta'}) g(\vartheta,\vartheta')\right] \times \overline{\mathbf{P}}_\vartheta \; , \quad (7.47)
\end{aligned}$$

where $g(\vartheta,\vartheta') \equiv 1 - c_\vartheta c_{\vartheta'}$, $c_\vartheta \equiv \cos\vartheta$ and $c_{\vartheta'} \equiv \cos\vartheta'$ with ϑ' being the polar angle of the momentum $\mathbf{q}$ of the background neutrinos. Note that $\vartheta' \in [0, \vartheta_{\rm max}]$ and thus $\cos\vartheta' \in [\cos\vartheta_{\rm max}, 1]$. In view of Fig. 7.3, one finds

$$r\sin\vartheta = R_\nu \sin\vartheta_{\rm R} \; , \qquad t = \sqrt{r^2 - R_\nu^2 \sin^2\vartheta_{\rm R}} - R_\nu\cos\vartheta_{\rm R} \; , \qquad (7.48)$$

and thus there exists a one-to-one correspondence between (t,ϑ) and $(r,\vartheta_{\rm R})$. With the help of the second expression in Eq. (7.48), we get ${\rm d}t = {\rm d}r/\cos\vartheta$. So the polarization vectors can also be expressed as $\mathbf{P}_{\vartheta_{\rm R}}(E,r)$ and $\overline{\mathbf{P}}_{\vartheta_{\rm R}}(E,r)$. These observations imply that the evolution of the polarization vectors with t is equivalent to that with r. The latter is more convenient to study the flavor conversions of supernova neutrinos.

In the multi-angle calculations, the equations of motion are numerically solved for $\vartheta_{\rm R}$ and E (Duan *et al.*, 2006b; Fogli *et al.*, 2007). Since such simulations are very time-consuming and too complicated to make the underlying physics transparent, it makes sense to resort to some analytical approximations in the single-angle limit by assuming all the polarization vectors to behave as the ones at $\vartheta_{\rm R} = 0$. The corresponding equations of motion can be derived from Eq. (7.47) by setting $\vartheta = \vartheta_{\rm R} = 0$ and discarding the angular dependence of the polarization vectors. In this case the integration over the polar angle ϑ' yields a geometrical function

$$D(r) \equiv \int_{\cos\vartheta_{\rm max}}^1 {\rm d}c_{\vartheta'}(1 - c_{\vartheta'}) = \frac{1}{2}\left[1 - \sqrt{1 - \left(\frac{R_\nu}{r}\right)^2}\right]^2 \; . \qquad (7.49)$$

We have $D(r) \propto r^{-4}$ for $r \gg R_\nu$. In the following discussions, we shall only consider the single-angle approximation in order to analytically reveal

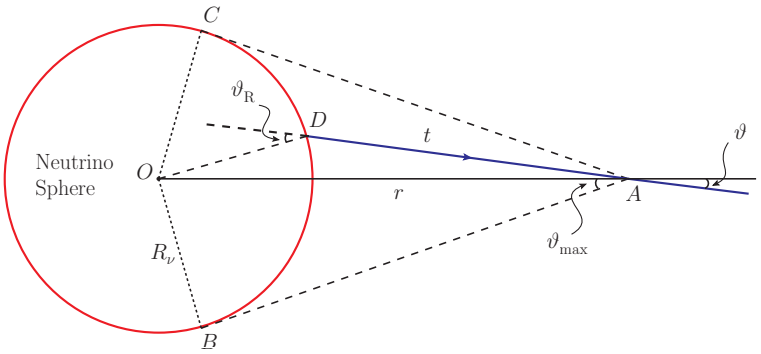

Fig. 7.3 A sketch of the neutrino emission from the neutrino sphere in the neutrino bulb model (Duan *et al.*, 2006b, 2010. With permission from the American Physical Society). The test neutrinos emitted from the neutrino sphere at point D with the emission angle $\vartheta_{\rm R}$ arrive at point A, and the elapsed time is $t = \overline{DA}$. The distance from A to the center of the proto-neutron star is $r = \overline{OA}$, and the polar angle of the neutrino trajectory is ϑ, which also characterizes the direction of the neutrino momentum $\hat{\mathbf{p}} \equiv \mathbf{p}/|\mathbf{p}|$. The background neutrinos come from the special part of the neutrino sphere lying in the cone with an open angle $\vartheta_{\rm max} \equiv \arcsin(R_\nu/r)$, where R_ν denotes the radius of the neutrino sphere

the salient features of collective neutrino oscillations. This approximation is reasonably good, although the multi-angle effects may cause the kinematic decoherence among the flavor conversions of neutrinos with different emission angles (Esteban-Pretel *et al.*, 2007; Fogli *et al.*, 2007).

As mentioned in Chapter 5, the three-flavor oscillations may approximate to the two-flavor oscillations $\nu_e \leftrightarrow \nu_x$ and $\overline{\nu}_e \leftrightarrow \overline{\nu}_x$ due to $|\Delta m^2_{31}| \gg \Delta m^2_{21}$, where ν_x (or $\overline{\nu}_x$) stands for the superposition of ν_μ and ν_τ (or $\overline{\nu}_\mu$ and $\overline{\nu}_\tau$) and the relevant mixing parameters are Δm^2_{31} and θ_{13}. Some comments on the conventions in the equations of motion are in order.

(1) Taking account of the definitions of the flavor polarization vectors in Eq. (5.142), we have $\mathrm{Tr}\left[\rho_{\mathbf{p}}\right] = f_{\nu_e}(\mathbf{p}) + f_{\nu_x}(\mathbf{p})$ and $P^z_{\mathbf{p}} = f_{\nu_e}(\mathbf{p}) - f_{\nu_x}(\mathbf{p})$ with $f_{\nu_e}(\mathbf{p})$ and $f_{\nu_x}(\mathbf{p})$ being the distribution functions of ν_e and ν_x, respectively. Similar relations for $\overline{\rho}_{\mathbf{p}}$, $\overline{\mathbf{P}}_{\mathbf{p}}$, $f_{\overline{\nu}_e}(\mathbf{p})$ and $f_{\overline{\nu}_x}(\mathbf{p})$ can be obtained for antineutrinos. One may redefine $\mathbf{P}_{\mathbf{p}}$ and $\overline{\mathbf{P}}_{\mathbf{p}}$ by factoring out the distribution functions such that they only measure the flavor composition of the system:

$$\rho_{\mathbf{p}} = \frac{1}{2} f_\nu(\mathbf{p}) \left(1 + \mathbf{P}_{\mathbf{p}} \cdot \boldsymbol{\sigma}\right) \ , \qquad \overline{\rho}_{\mathbf{p}} = \frac{1}{2} f_{\overline{\nu}}(\mathbf{p}) \left(1 + \overline{\mathbf{P}}_{\mathbf{p}} \cdot \boldsymbol{\sigma}\right) \ , \tag{7.50}$$

where $f_\nu = f_{\nu_e} + f_{\nu_x}$ and $f_{\overline{\nu}} = f_{\overline{\nu}_e} + f_{\overline{\nu}_x}$. Thus we have $P^z = [f_{\nu_e} - f_{\nu_x}]/f_\nu$ and $\overline{P}^z = [f_{\overline{\nu}_e} - f_{\overline{\nu}_x}]/f_{\overline{\nu}}$, where the momentum dependence is implied. For a system which initially has pure ν_e and $\overline{\nu}_e$, the polarization vectors are therefore normalized to unity (i.e., $|\mathbf{P}_{\mathbf{p}}| = |\overline{\mathbf{P}}_{\mathbf{p}}| = 1$). Note that different

normalization schemes have been used in the literature (Hannestad *et al.*, 2006; Fogli *et al.*, 2007; Duan *et al.*, 2010).

(2) The neutrino-antineutrino system under discussion is often assumed to be isotropic, so the direction of the neutrino momentum is irrelevant. In this case the flavor polarization vectors depend on the neutrino energy $E \approx p = |\mathbf{p}|$. If the frequency $\omega = |\Delta m^2_{31}|/(2E)$ is defined, then the dependence on E can be converted into the one on ω. That is why the flavor polarization vectors are sometimes written as $\mathbf{P}_\omega$ and $\overline{\mathbf{P}}_\omega$ for each energy mode.

(3) If the strength of neutrino-neutrino interactions is defined as $\mu \equiv \sqrt{2}\, G_{\rm F} n_\nu$ with n_ν being the local neutrino number density, then the equations of motion can be rewritten as

$$\mathbf{P}_\omega = [+\omega\mathbf{B} + \lambda\mathbf{L} + \mu\mathbf{D}] \times \mathbf{P}_\omega \; , \quad \overline{\mathbf{P}}_\omega = [-\omega\mathbf{B} + \lambda\mathbf{L} + \mu\mathbf{D}] \times \overline{\mathbf{P}}_\omega \; , \quad (7.51)$$

where $\mathbf{D} \equiv \mathbf{P} - \overline{\mathbf{P}}$ with $\mathbf{P} \equiv \int_0^\infty \mathbf{P}_\omega {\rm d}\omega$ and $\overline{\mathbf{P}} \equiv \int_0^\infty \overline{\mathbf{P}}_\omega {\rm d}\omega$ being the global polarization vectors. Note that $n_\nu \propto D(r) L_\nu / \langle E_\nu \rangle$, where $D(r)$ is the geometrical function given in Eq. (7.49) in the single-angle approximation, L_ν denotes the total neutrino luminosity and $\langle E_\nu \rangle$ is the average neutrino energy. In the region far from the neutrino sphere we have $n_\nu(r) \propto r^{-4}$, and the electron density is approximately $n_e(r) \propto r^{-3}$. Just above the neutrino sphere, the neutrino density is so high that the neutrino-neutrino self-interaction becomes larger than the neutrino interaction with ordinary matter.

Numerical simulations with the general equations of motion have shown three salient features of collective neutrino oscillations (Duan *et al.*, 2006a, 2006b, 2010; Fogli *et al.*, 2007): (1) *synchronized oscillations* — neutrinos with different energies (and thus different intrinsic oscillation frequencies) oscillate coherently; (2) *bipolar oscillations* — neutrinos and antineutrinos oscillate in opposite directions and form two separate groups; (3) *energy spectral splits* — in the final neutrino and antineutrino energy spectra, a critical energy $E_{\rm c}$ splits the spectra sharply into parts of almost pure different flavors. These features will be described in detail in the following subsections.

7.4.2 Synchronized Neutrino Oscillations

Let us recall the neutrino oscillations in vacuum, whose equation of motion reads $\dot{\mathbf{P}} = \omega\mathbf{B} \times \mathbf{P}$ with $\omega = \Delta m^2/(2p)$. This is just the equation of motion for the angular-momentum $\mathbf{P}$ precessing around the magnetic field $\mathbf{B}$, and the corresponding magnetic dipole moment is given by $\mathbf{M} = \omega\mathbf{P}$. So $\omega = |\mathbf{M}|/|\mathbf{P}|$ plays the role of gyromagnetic ratio and determines the rate of precession. Next, we consider an ensemble of homogeneous and isotropic neutrino gas. The total number of neutrinos is N_ν, and the ensemble has a large volume V. Denoting the polarization vector of each neutrino as $\mathbf{P}_j$ and the corresponding momentum as $p_j = |\mathbf{p}_j|$ (for $j = 1, 2, \cdots, N_\nu$), one may define the total polarization vector $\mathbf{J} = \mathbf{P}_1 + \mathbf{P}_2 + \cdots + \mathbf{P}_{N_\nu}$. The equation of motion for the individual polarization vector turns out to be (Pastor *et al.*, 2002)

$$\dot{\mathbf{P}}_j = \omega_j \mathbf{B} \times \mathbf{P}_j + \frac{\sqrt{2}\, G_{\rm F}}{V} \mathbf{J} \times \mathbf{P}_j \; , \tag{7.52}$$

where $\omega_j \equiv \Delta m^2/(2p_j)$. If the vacuum oscillation term is switched off, then $\mathbf{P}_j$ precesses around $\mathbf{J}$. After switching on the vacuum oscillation term and summing over the index j on both sides of Eq. (7.52), we obtain

$$\dot{\mathbf{J}} = \sum_{j=1}^{N_\nu} \omega_j \mathbf{B} \times \mathbf{P}_j \; , \tag{7.53}$$

which is not in the closed form for $\mathbf{J}$. If the neutrino self-interaction dominates over the vacuum oscillation term, then $\mathbf{P}_j$ rotates around $\mathbf{J}$ rapidly and thus its transverse components are averaged to zero. We are finally left with $\mathbf{P}_j = \hat{\mathbf{J}}(\mathbf{P}_j \cdot \hat{\mathbf{J}})$ with $\hat{\mathbf{J}} \equiv \mathbf{J}/|\mathbf{J}|$. So Eq. (7.53) can be rewritten as

$$\dot{\mathbf{J}} = \mathbf{B} \times \hat{\mathbf{J}} \sum_{j=1}^{N_\nu} \omega_j (\mathbf{P}_j \cdot \hat{\mathbf{J}}) \equiv \omega_{\rm syn} \mathbf{B} \times \mathbf{J} \; , \tag{7.54}$$

where the gyromagnetic ratio $\omega_{\rm syn}$ is given by

$$\omega_{\rm syn} = \frac{1}{|\mathbf{J}|} \sum_{j=1}^{N_\nu} \omega_j (\mathbf{P}_j \cdot \hat{\mathbf{J}}) \; . \tag{7.55}$$

If all the initial neutrinos are prepared in a specific flavor state, then the polarization vectors $\mathbf{P}_j$ are aligned with $\mathbf{J}$ and thus $|\mathbf{J}| = N_\nu$ and $\mathbf{P}_j \cdot \hat{\mathbf{J}} = 1$, leading to $\omega_{\rm syn} = (\omega_1 + \omega_2 + \cdots + \omega_{N_\nu})/N_\nu$ (i.e., an average value of the vacuum oscillation frequencies). If the neutrino self-interaction is dominant over the vacuum oscillation term, we conclude that all the polarization vectors $\mathbf{P}_j$ are aligned with $\mathbf{J}$ which precesses around the weak magnetic field $\mathbf{B}$ with the frequency $\omega_{\rm syn}$ given in Eq. (7.55). For neutrino oscillations in vacuum, a broad distribution of neutrino energies will induce the flavor decoherence such that the oscillations will be damped. In contrast, these energy modes will oscillate coherently with a common frequency $\omega_{\rm syn}$ provided the neutrino self-interaction is strong enough. This collective phenomenon is just the so-called synchronized neutrino oscillations (Pastor *et al.*, 2002).

In more realistic cases, one should take into account the effects of antineutrinos. The equations of motion for both neutrinos and antineutrinos are given by (Pastor *et al.*, 2002)

$$\begin{aligned} \dot{\mathbf{P}}_j &= +\omega_j \mathbf{B} \times \mathbf{P}_j + \frac{\sqrt{2}\, G_{\rm F}}{V} \left(\mathbf{J} - \overline{\mathbf{J}} \right) \times \mathbf{P}_j \; , \\ \dot{\overline{\mathbf{P}}}_k &= -\omega_k \mathbf{B} \times \overline{\mathbf{P}}_k + \frac{\sqrt{2}\, G_{\rm F}}{V} \left(\mathbf{J} - \overline{\mathbf{J}} \right) \times \overline{\mathbf{P}}_k \; , \end{aligned} \tag{7.56}$$

where the total polarization vector $\overline{\mathbf{J}}$ is the sum of $\overline{\mathbf{P}}_k$ (for $k = 1, 2, \cdots, N_{\overline{\nu}}$) with $N_{\overline{\nu}}$ being the number of antineutrinos in the ensemble. Analogous to

the case with only neutrinos, both $\mathbf{P}_j$ and $\overline{\mathbf{P}}_k$ will be aligned with the global vector $\mathbf{I} \equiv \mathbf{J} - \overline{\mathbf{J}}$ which precesses around the weak magnetic field $\mathbf{B}$. The relevant equation of motion is $\dot{\mathbf{I}} = \omega_{\rm syn} \mathbf{B} \times \mathbf{I}$, where

$$\omega_{\rm syn} = \frac{1}{|\mathbf{I}|} \left[\sum_{j=1}^{N_\nu} \omega_j \left(\mathbf{P}_j \cdot \hat{\mathbf{I}} \right) + \sum_{k=1}^{N_{\overline{\nu}}} \omega_k \left(\overline{\mathbf{P}}_k \cdot \hat{\mathbf{I}} \right) \right] \tag{7.57}$$

with $\hat{\mathbf{I}} \equiv \mathbf{I}/|\mathbf{I}|$. Therefore, the neutrino-antineutrino system behaves in a way similar to the pure neutrino system. Note that a large asymmetry between neutrinos and antineutrinos is required to assure the synchronized oscillations, otherwise $\mathbf{I} = \mathbf{J} - \overline{\mathbf{J}}$ would vanish and the neutrino self-interaction would be absent. In a supernova environment, however, the synchronized neutrino oscillations are suppressed by either the high matter density or the large neutrino fluxes themselves (Duan *et al.*, 2007).

7.4.3 Bipolar Flavor Conversions

The bipolar flavor conversions may take place when the strength of neutrino-neutrino interactions $\mu \equiv \sqrt{2}\, G_{\rm F} n_\nu$ is comparable with the vacuum oscillation frequency $\omega \equiv \Delta m^2/(2p)$. If $\mu \gg \omega$ holds, the synchronized oscillations will occur, as discussed in the previous subsection. Let us first of all explain the bipolar system, which has already been introduced in Section 5.3. The simplest bipolar system initially consists of pure ν_e and $\overline{\nu}_e$ with equal densities and energies. The corresponding equations of motion for $\mathbf{P}$ and $\overline{\mathbf{P}}$ are given in Eq. (5.148), or equivalently for $\mathbf{D} \equiv \mathbf{P} - \overline{\mathbf{P}}$ and $\mathbf{Q} \equiv \mathbf{S} - \omega \mathbf{B}/\mu$ with $\mathbf{S} \equiv \mathbf{P} + \overline{\mathbf{P}}$ given in Eq. (5.150). The numerical result for the survival probability in the case of the inverted neutrino mass hierarchy has been shown in Fig. 5.4, where one can observe the complete flavor conversions of both neutrinos and antineutrinos. In the case of the normal neutrino mass hierarchy, only the oscillations with extremely small mixing angles are allowed and thus the flavor content is almost unchanged.

This bipolar system can be well understood by analogy with the spherical pendulum (Hannestad *et al.*, 2006). Given the initial conditions $\mathbf{P}(0) = \overline{\mathbf{P}}(0) = (0, 0, 1)$ and thus $\mathbf{D}(0) = 0$ and $\mathbf{S}(0) = (0, 0, 2)$, it is possible to get $\mathbf{Q}(0) = (-\omega \sin 2\theta/\mu, 0, 2 + \omega \cos 2\theta/\mu)$ because of $\mathbf{B} = (\sin 2\theta, 0, -\cos 2\theta)$ with θ being the mixing angle. In view of the equations of motion shown in Eq. (5.150), one may observe that $\mathbf{B}$ and $\mathbf{Q}$ lie in the (x, z)-plane and $\mathbf{D}$ is along the y-axis. In addition, the length of $\mathbf{Q}$ is conserved; i.e.,

$$Q \equiv |\mathbf{Q}| = \left[4 + \left(\frac{\omega}{\mu} \right)^2 + 4 \left(\frac{\omega}{\mu} \right) \cos 2\theta \right]^{1/2} . \tag{7.58}$$

If $\mathbf{Q} = Q(\sin\varphi, 0, \cos\varphi)$ and $\mathbf{D} = D(0, 1, 0)$ with $D \equiv |\mathbf{D}|$ are taken, the equations of motion of $\mathbf{Q}$ and $\mathbf{D}$ in Eq. (5.150) can be simplified to those of φ and D:

$$\dot{\varphi} = \mu D \ , \qquad \dot{D} = -\omega Q \sin\left(\varphi + 2\theta\right) \ . \tag{7.59}$$

Eq. (7.59) allows us to obtain a second-order differential equation of the tilt angle φ (Hannestad *et al.*, 2006):

$$\ddot{\varphi} = -\kappa^2 \sin(\varphi + 2\theta) \ , \tag{7.60}$$

where $\kappa \equiv \sqrt{\omega\mu Q}$ denotes the intrinsic frequency. This result implies that $\mathbf{Q}$ in the flavor space behaves like a spherical pendulum. Note that one may also derive Eq. (7.59) from the Hamiltonian

$$H(\varphi, D) = \frac{\kappa^2}{\mu}\left[1 - \cos(\varphi + 2\theta)\right] + \frac{1}{2}\mu D^2 \ , \tag{7.61}$$

if one identifies φ as a general coordinate and D as the canonically conjugate momentum. Therefore, the first and second terms in Eq. (7.61) stand respectively for the potential and kinetic energies. Let us define the potential energy as (Hannestad *et al.*, 2006)

$$V(\varphi) = \kappa^2\left[1 - \cos(\varphi + 2\theta)\right] \ , \tag{7.62}$$

which determines whether the system is stable or not for a given initial value of φ. In the case of the normal neutrino mass hierarchy, we can expand the potential in terms of small tilt and mixing angles (i.e., $\varphi \ll 1$ and $\theta \ll 1$):

$$V(\varphi) = \frac{\kappa^2}{2}(\varphi + 2\theta)^2 \ . \tag{7.63}$$

Hence the minimum of the potential is reached at $\varphi_{\rm min} = -2\theta$. On the other hand, one may get $\sin\varphi(0) = -[\omega/(\mu Q)]\sin 2\theta$ or $\varphi(0) \approx -2\theta[\omega/(\mu Q)] > -2\theta$ from $\mathbf{Q}(0) = (-\omega\sin 2\theta/\mu, 0, 2+\omega\cos 2\theta/\mu)$. So the initial value $\varphi(0)$ is in the vicinity of the stable point $\varphi_{\rm min}$, and the system will oscillate around $\varphi_{\rm min}$ with the frequency κ and the amplitude $2\theta[1 - \omega/(\mu Q)]$. That is why there is no significant flavor conversion for the normal neutrino mass hierarchy. The inverted neutrino mass hierarchy corresponds to $\theta \sim \pi/2$, and hence the equations of motion are the same as those in the case of the normal mass hierarchy but with θ being replaced by $\theta \equiv \pi/2 - \theta'$. In this case the potential in Eq. (7.62) can be expanded as

$$V(\varphi) = -\frac{\kappa^2}{2}(\varphi - 2\theta')^2 \ , \tag{7.64}$$

whose maximum is achieved at $\varphi_{\rm max} = 2\theta'$. Similarly, the initial value of φ is given by $\sin\varphi(0) = -[\omega/(\mu Q)]\sin 2\theta'$ with $Q \approx |2 - \omega/\mu|$ in the $\theta' \ll 1$ limit. Depending on the value of ω/μ, the initial tilt angle $\varphi(0)$ varies from 0 to $2\theta' - \pi$. Therefore, φ initially lies around the maximum point and it should finally roll down to the minimum $\varphi_{\rm min} = -\pi$. P_z and $\overline{P}_z$ at $\varphi_{\rm min}$ are consequently given by

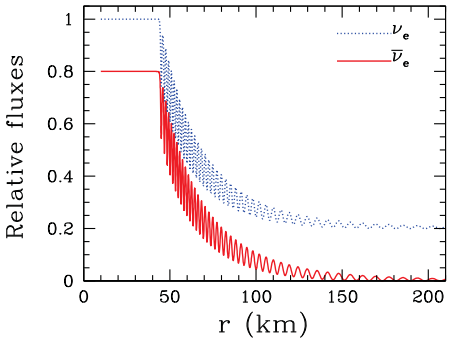

Fig. 7.4 The relative fluxes of ν_e and $\overline{\nu}_e$ events in the neutrino-antineutrino asymmetric scenario (Hannestad *et al.*, 2006. With permission from the American Physical Society): (1) the initial conditions $P_z(0) = 1$ and $\overline{P}_z(0) = 0.8$ are taken; (2) the profile of the neutrino self-interaction strength $\mu(r) \approx 0.3 \times 10^5$ km$^{-1} r_{10}^{-4}$ is assumed, where r_{10} is the radius r in units of 10 km (i.e., the radius of the neutrino sphere); (3) the mixing angle is given by $\sin 2\theta' = 0.001$ in the case of the inverted neutrino mass hierarchy

$$P_z|_{\varphi_{\rm min}} = \overline{P}_z|_{\varphi_{\rm min}} \approx \frac{1}{2}\left(\frac{\omega}{\mu} - \left|2 - \frac{\omega}{\mu}\right|\right) \ . \tag{7.65}$$

So the complete flavor conversions (i.e., $P_z = \overline{P}_z = -1$) are possible only if the neutrino self-interaction strength is large enough (i.e., $\omega/\mu \ll 1$). For intermediate values of ω/μ, the flavor conversions will be partial.

Fig. 5.4 has shown that the complete flavor conversion is periodic, implying that the transformed neutrinos will be converted back into the original flavor state. This is not the case, however, if the variation of the strength of neutrino-neutrino interactions is taken into account. Since $\mu(r) \propto r^{-4}$, the interaction strength decreases as neutrinos propagate outwards. Hence the kinetic energy $\mu D^2/2$ of the pendulum given in Eq. (7.61) becomes smaller after some oscillations such that the pendulum is unable to reach its initial height. Fig. 7.4 illustrates the relative neutrino fluxes in the bipolar system with asymmetric ν_e and $\overline{\nu}_e$ events. These results follow from a numerical solution to the equations of motion with two typical inputs for realistic supernova neutrinos: the neutrino-antineutrino asymmetry with $P_z(0) = 1$ and $\overline{P}_z(0) = 0.8$, and $\mu(r) = 0.3 \times 10^5$ km$^{-1} r_{10}^{-4}$ with r_{10} being the radius r in units of 10 km. Just above the neutrino sphere $r = 10$ km, the neutrino self-interaction strength μ is 10^5 times larger than the vacuum oscillation frequency ω. Significant flavor conversions start around $r \approx 45$ km, and the behavior between $r \approx 10$ km and $r \approx 45$ km is due to the synchronized oscillations which are guaranteed by the large neutrino-antineutrino asymmetry and the large value of μ in this region. However, the flavor conversions in this region are essentially negligible just because the effective mixing angle is highly suppressed.

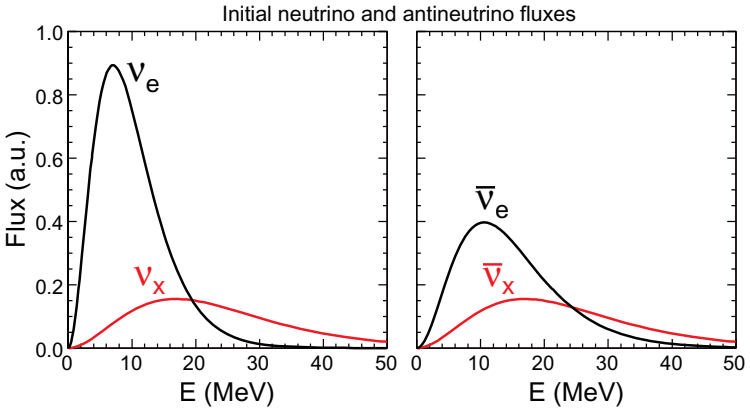

Fig. 7.5 The initial fluxes (in arbitrary units) at the neutrino sphere $r = 10$ km for different neutrino flavors as functions of the neutrino energy (Fogli *et al.*, 2007. With permission from the Institute of Physics)

Fig. 7.4 shows that the synchronized oscillations take place at small r (e.g., 10 km $\lesssim r \lesssim$ 45 km) or for large μ, and the ordinary vacuum oscillations occur at large r (e.g., $r > 200$ km) or for small μ. Thus the bipolar oscillations are expected to happen at intermediate r or for modest μ. In the general case with a neutrino-antineutrino asymmetry $\mathbf{P}(0) = \alpha\overline{\mathbf{P}}(0)$ (for $0 \leqslant \alpha \leqslant 1$), the condition for the bipolar neutrino oscillations turns out to be $\omega \lesssim \mu < 4(1+\alpha)\omega/(1-\alpha)^2$ (Duan *et al.*, 2006a; Hannestad *et al.*, 2006).

7.4.4 Neutrino Spectral Splits

An intriguing phenomenon observed in the numerical simulations of supernova neutrino flavor conversions is the existence of a critical energy $E_{\rm c}$ which splits the transformed neutrino spectra into parts of almost pure but different flavors (Duan *et al.*, 2006b; Fogli *et al.*, 2007). Let us first specify the initial fluxes of neutrinos and antineutrinos. For simplicity, the relevant neutrinos and antineutrinos are assumed to follow the thermal distribution at the neutrino sphere $r = R_\nu = 10$ km; i.e.,

$$\phi_i(E) = \frac{2}{3\zeta(3)T_i^3} \cdot \frac{E^2}{{\rm e}^{E/T_i} + 1} \,, \tag{7.66}$$

where $\zeta(3) \approx 1.202$ is a Riemann zeta function, and the subscript "i" stands for ν_e, $\overline{\nu}_e$, ν_x or $\overline{\nu}_x$. The effective temperature T_i can be determined such that the average neutrino energies are $\langle E_{\nu_e} \rangle = 10$ MeV, $\langle E_{\overline{\nu}_e} \rangle = 15$ MeV and $\langle E_{\nu_x} \rangle = \langle E_{\overline{\nu}_x} \rangle = 24$ MeV. The standard delayed-explosion supernova model indicates that the luminosities of different neutrino species are almost equal, so the number fluxes of neutrinos per unit energy in any direction are

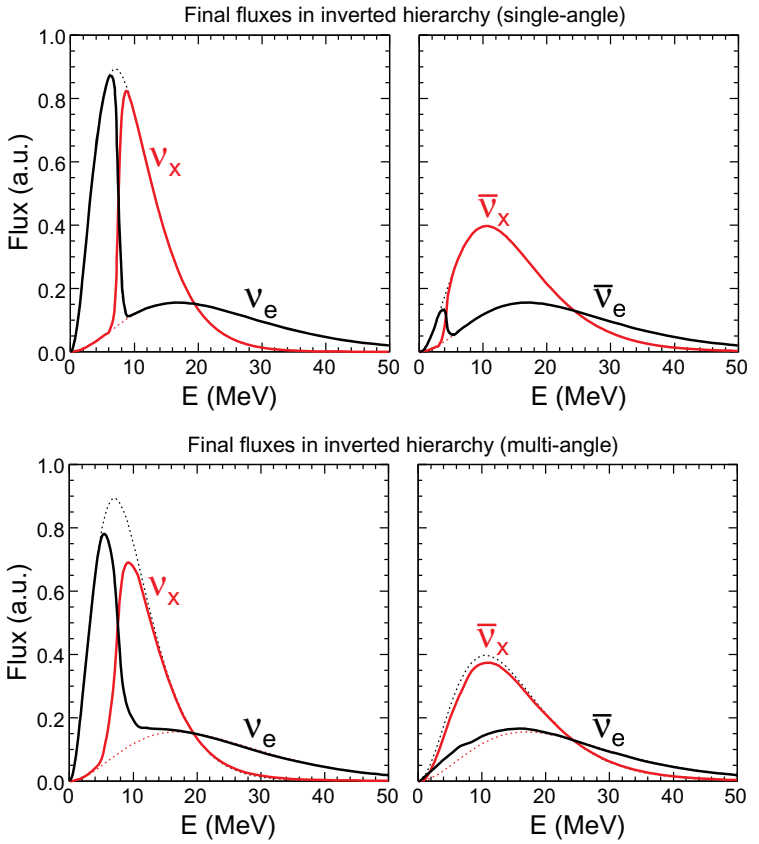

Fig. 7.6 The final fluxes at the radius $r = 200$ km for different neutrino flavors as functions of the neutrino energy, where the dotted lines represent the initial fluxes. The upper and lower panels are for the single- and multi-angle calculations, respectively (Fogli *et al.*, 2007. With permission from the Institute of Physics)

$$j_i(E) = \frac{L_\nu}{4\pi^2 R_\nu^2} \cdot \frac{\phi_i(E)}{\langle E_i \rangle} \,, \tag{7.67}$$

where the common neutrino luminosity is $L_\nu = 10^{51}$ erg s^{-1}. The initial neutrino spectra are plotted in Fig. 7.5, in which the fluxes are proportional to $\phi_i(E)/\langle E_i \rangle$ and properly normalized. In the single-angle approximation, the neutrino distribution functions are given by $f_i(r, E) = 2\pi D(r) j_i(E)$ with $D(r)$ being the geometrical function given in Eq. (7.49). With the help of these initial conditions and the matter density profile, one may solve the equations of motion in Eq. (7.47) in the single- and multi-angle scenarios. The final results of neutrino fluxes at the radius $r = 200$ km are shown in Fig. 7.6 and summarized as follows (Fogli *et al.*, 2007).

(1) In the final neutrino spectra, there exists a critical energy $E_{\rm c} \simeq 7$ MeV. In the energy region below $E_{\rm c}$, the neutrino flavors remain the same; but above $E_{\rm c}$, the complete flavor conversions take place. As for antineutrinos, the critical energy is $\overline{E}_{\rm c} \simeq 4$ MeV.

(2) The split in the antineutrino spectra disappears in the multi-angle calculations, but the one for neutrinos survives. The neutrino spectral splits only occur in the case of the inverted neutrino mass hierarchy.

Note that the matter density profile used in the above calculations is high enough to make sure that the MSW resonances are absent in the region of collective neutrino oscillations (Fogli *et al.*, 2007). If the shallow matter profiles are taken, the spectral splits may exist in both normal and inverted neutrino mass hierarchies (Duan *et al.*, 2006b, 2007). In the following we shall assume the decoupling of collective neutrino oscillations from the MSW resonances and analytically understand the neutrino spectral splits (Raffelt and Smirnov, 2007a, 2007b).

We start with the equations of motion in Eq. (7.51). Instead of using $\overline{\mathbf{P}}_\omega$, one may extend the polarization vector $\mathbf{P}_\omega$ to negative frequencies such that $\overline{\mathbf{P}}_\omega = \mathbf{P}_{-\omega}$ with $\omega > 0$. In this case the equations of motion can be rewritten in terms of only $\mathbf{P}_\omega$; i.e.,

$$\dot{\mathbf{P}}_\omega = (\omega\mathbf{B} + \lambda\mathbf{L} + \mu\mathbf{D}) \times \mathbf{P}_\omega \; , \tag{7.68}$$

where $\mathbf{D} = \int_{-\infty}^{+\infty} s_\omega \mathbf{P}_\omega {\rm d}\omega$ with $s_\omega \equiv {\rm sign}(\omega) = \omega/|\omega|$. Since the absence of the MSW resonances has been assumed, it is possible to eliminate the matter term $\lambda\mathbf{L}$ by going into a rotating frame (Duan *et al.*, 2006a; Hannestad *et al.*, 2006). After the elimination of $\lambda\mathbf{L}$ and the integration of Eq. (7.68) with s_ω, we obtain the equation of motion of $\mathbf{D}$ as

$$\dot{\mathbf{D}} = \mathbf{B} \times \mathbf{M} \; , \tag{7.69}$$

where $\mathbf{M} \equiv \int_{-\infty}^{+\infty} s_\omega \omega \mathbf{P}_\omega$. Eq. (7.69) indicates that $\dfrac{{\rm d}(\mathbf{D}\cdot\mathbf{B})}{{\rm d}t} = 0$ holds and thus $D_z = \mathbf{B}\cdot\mathbf{D}$ is conserved. For the small mixing angle, one approximately has $\mathbf{B} = (0, 0, -1)$ or $\mathbf{B} = (0, 0, 1)$ in the case of the normal or inverted neutrino mass hierarchy. Because D_z denotes the excess of the ν_e flux, the conservation of D_z implies that the collective effects only induce the pair transformation $\nu_e + \overline{\nu}_e \to \nu_x + \overline{\nu}_x$. Therefore, the ν_e excess from deleptonization is conserved.

The equation of motion in Eq. (7.68) can also be written as $\dot{\mathbf{P}}_\omega = \mathbf{H}_\omega \times \mathbf{P}_\omega$ with $\mathbf{H}_\omega \equiv \omega\mathbf{B} + \mu\mathbf{D}$, implying that each polarization vector $\mathbf{P}_\omega$ precesses around $\mathbf{H}_\omega$. In the adiabatic limit each $\mathbf{H}_\omega$ moves slowly as compared with the precession of $\mathbf{P}_\omega$, so the latter will follow the former. We assume that all $\mathbf{P}_\omega$ are initially prepared in a specific flavor and thus aligned with each other. If μ is very large, $\mathbf{P}_\omega$ is essentially aligned with $\mathbf{H}_\omega$. Therefore, $\mathbf{P}_\omega$ keeps aligned with $\mathbf{H}_\omega$ during the entire period of evolution in the adiabatic limit. $\mathbf{P}_\omega(\mu) = \hat{\mathbf{H}}_\omega(\mu) P_\omega$ with $\hat{\mathbf{H}}_\omega = \mathbf{H}_\omega/|\mathbf{H}_\omega|$ and $P_\omega = |\mathbf{P}_\omega|$ is consequently

the solution to the equation of motion. On the other hand, all $\mathbf{H}_\omega$ lie in the so-called corotating plane spanned by $\mathbf{B}$ and $\mathbf{D}$, and thus all $\mathbf{P}_\omega$ and $\mathbf{M}$ stay in the same plane in the adiabatic limit. We can now decompose $\mathbf{M}$ into $\mathbf{M} = b\mathbf{B} + \omega_{\rm c}\mathbf{D}$ and express Eq. (7.69) as

$$\dot{\mathbf{D}} = \omega_{\rm c}\mathbf{B} \times \mathbf{D} \; . \tag{7.70}$$

This result implies that both $\mathbf{D}$ and the corotating plane precess around $\mathbf{B}$ with the common frequency $\omega_{\rm c}$. Hence the system experiences a fast precession around $\mathbf{B}$ with $\omega_{\rm c}(\mu)$ and the drift in the corotating plane due to the variation of $\mu(t)$. A convenient treatment is to go into the corotating frame, where the effective Hamiltonian reads

$$\mathbf{H}_\omega = [\omega - \omega_{\rm c}(\mu)]\,\mathbf{B} + \mu\mathbf{D} \; . \tag{7.71}$$

Initially $\mu \to \infty$, the oscillations are synchronized and have $\omega_{\rm c}(\mu \to \infty) = \omega_{\rm syn}$; i.e., all $\mathbf{P}_\omega$ form a total polarization vector $\mathbf{P}$. As μ decreases, the $\mathbf{P}_\omega$ will spread out but remain in the corotating plane. Finally $\mu \to 0$, Eq. (7.71) implies that all $\mathbf{H}_\omega$ or all $\mathbf{P}_\omega$ with $\omega > \omega_{\rm c}^0 \equiv \omega_{\rm c}(\mu = 0)$ are aligned with $\mathbf{B}$, while the others are antialigned. In other words, the flavor conversions are complete for $\omega < \omega_{\rm c}^0$ and absent for $\omega < \omega_{\rm c}^0$; i.e., the spectral split is inevitable at $\omega = \omega_{\rm c}^0$. Since the length of $\mathbf{P}_\omega$ is conserved and all $\mathbf{P}_\omega$ are finally aligned with either $+\mathbf{B}$ or $-\mathbf{B}$, the lepton number conservation yields (Raffelt and Smirnov, 2007a, 2007b)

$$D_z = \int_{-\infty}^{0} P_\omega {\rm d}\omega - \int_{0}^{\omega_{\rm c}^0} P_\omega {\rm d}\omega + \int_{\omega_{\rm c}^0}^{+\infty} P_\omega {\rm d}\omega \; . \tag{7.72}$$

Hence the critical energy $E_{\rm c} = |\Delta m^2|/(2\omega_{\rm c}^0)$ is determined by the neutrino spectrum P_ω and the initial lepton number D_z. The above arguments clearly explain the existence of neutrino spectral splits and reveal the underlying physics behind them — the lepton number conservation.

Much progress has recently been made in the study of supernova neutrino spectral splits. It is found that there exist multiple spectral splits for both normal and inverted neutrino mass hierarchies if the neutrino fluxes in the cooling phase are considered (Dasgupta *et al.*, 2009). However, the three-flavor effects may smear one of the splits (Friedland, 2010; Dasgupta *et al.*, 2010b). Many open issues, including the kinematical decoherence of different angular modes in the multi-angle scenario and the criteria for adiabaticity, remain to be solved (Duan *et al.*, 2010).

7.4.5 Effects of Three Neutrino Flavors

So far we have discussed collective neutrino oscillations in the two-flavor approximation. This approximation is well justified in the supernova environment: (a) the charged leptons μ and τ are too heavy to be produced in

the supernova core, so ν_μ and ν_τ have only neutral-current interactions which cannot distinguish between the muon and tau flavors; (b) for the same reason, the total fluxes and average energies of ν_μ and ν_τ are equal; (c) because of the strong hierarchy $|\Delta m^2_{31}| \gg \Delta m^2_{21}$, the relevant neutrino mixing parameters for collective neutrino oscillations should be Δm^2_{31} and θ_{13}. However, the three-flavor effects should be taken into account for a few reasons.

(1) For completeness, the analytical and numerical studies of collective neutrino oscillations should be performed in the three-flavor framework including the CP-violating phase (Gava and Volpe, 2008).

(2) The three-flavor effects may trigger collective neutrino oscillations even if the smallest neutrino mixing angle θ_{13} is exactly vanishing (Dasgupta *et al.*, 2010a). As mentioned before, the bipolar system can be viewed as a spherical pendulum. In the case of the inverted neutrino mass hierarchy, the pendulum is initially placed around an unstable point and will rapidly move to a stable point, causing almost complete flavor conversions. This transformation is independent of θ_{13} as long as it is small. If $\theta_{13} = 0$ exactly holds, the system may continue to stay at the unstable point and thus flavor conversions cannot take place. Although quantum fluctuations might trigger the transformation (Hannestad *et al.*, 2006), the three-flavor effects including radiative corrections and small differences between ν_μ and ν_τ fluxes could practically do this job.

(3) We stress that the generic features of collective neutrino oscillations (i.e., synchronized oscillations, bipolar flavor conversions and spectral splits) preserve in the three-flavor case. However, some new features may emerge and quantitatively change the two-flavor predictions. For instance, there exist two different splits in the neutrino spectra, which are determined by two distinct conditions for lepton number conservation (Dasgupta *et al.*, 2008; Duan *et al.*, 2008). To be explicit, let us use the Bloch-vector formalism given in Section 5.3 and decompose the vacuum Hamiltonian term into $\mathbf{H}_\omega = \omega(\mathbf{B}_{\rm H} + \varepsilon \mathbf{B}_{\rm L})$, where $\mathbf{B}_{\rm H}$ (or $\mathbf{B}_{\rm L}$) denotes the magnetic field associated with Δm^2_{31} (or Δm^2_{21}) and $\varepsilon \equiv \Delta m^2_{21}/|\Delta m^2_{31}|$ is defined. With the help of the equation of motion of the polarization vector $\mathbf{P}$, it is straightforward to show $\dfrac{{\rm d}(\mathbf{B}_{\rm H} \cdot \mathbf{P})}{{\rm d}t} = \dfrac{{\rm d}(\mathbf{B}_{\rm L} \cdot \mathbf{P})}{{\rm d}t} = 0$ (i.e., the conditions for lepton number conservation). By virtue of the same arguments leading to Eq. (7.72), one can understand the patterns of spectral splits in the three-flavor case.

Finally, it is worth mentioning that the first multi-angle simulations of neutrino flavor conversions in the three-flavor case have recently been done for an O-Ne-Mg core-collapse supernova (Cherry *et al.*, 2010). Although the results are qualitatively consistent with those in the single-angle limit, it is found that the multi-angle effects reduce the adiabaticity of flavor evolution for the normal neutrino mass hierarchy. Further studies of collective neutrino oscillations are needed in order to understand the underlying physics.

References

Aglietta, M., *et al.*, 1987, Europhys. Lett. **3**, 1315.
Ahrens, J., *et al.*, 2002, Astropart. Phys. **16**, 345.
Alexeyev, E. N., *et al.*, 1988, Phys. Lett. B **205**, 209.
Ando, S., and Sato, K., 2004, New J. Phys. **6**, 170.
Andreani, P., Ferlet, R., and Vidal-Madjar, A., 1987, Nature **326**, 770.
Arnett, W. D., 1983, Astrophys. J. **263**, L55.
Arnett, W. D., *et al.* 1989, Annu. Rev. Astron. Astrophys. **27**, 629.
Bahcall, J. N., Spergel, D. N., and Press, W. H., 1988, in *Supernova 1987A in the Large Magellanic Cloud*, edited by Kafatos, M., and Michalitsianos, A. G. (Cambridge University), p. 172.
Baldry, I. K., and Glazebrook, K., 2003, Astrophys. J. **548**, 522.
Barbieri, R., and Mohapatra, R. N., 1988, Phys. Rev. Lett. **61**, 27.
Baron, E. A., and Cooperstein, J., 1990, Astrophys. J. **353**, 597.
Baron, E. A., Cooperstein, J., and Kahana, S., 1985a, Phys. Rev. Lett. **55**, 126.
Baron, E. A., Cooperstein, J., and Kahana, S., 1985b, Nucl. Phys. A **440**, 744.
Beacom, J. F., 2010, Ann. Rev. Nucl. Part. Sci. **60**, 439.
Beacom, J. F., and Vagins, M. R., 2004, Phys. Rev. Lett. **93**, 171101.
Bethe, H. A., 1990, Rev. Mod. Phys. **62**, 801.
Bethe, H. A., and Wilson, J. R., 1985, Astrophys. J. **295**, 14.
Bethe, H. A., *et al.*, 1979, Nucl. Phys. A **324**, 487.
Bionta, R. M., *et al.*, 1987, Phys. Rev. Lett. **58**, 1494.
Bowers, R. L., and Wilson, J. R., 1982a, Astrophys. J. Suppl. **50**, 115.
Bowers, R. L., and Wilson, J. R., 1982b, Astrophys. J. **263**, 366.
Bratton, C. B., *et al.*, 1988, Phys. Rev. D **37**, 3361.
Brown, G. E., Bethe, H. A., and Baym, G., 1982, Nucl. Phys. A **375**, 481.
Bueno, A., Gil-Botella, I., and Rubbia, A., 2003, arXiv:hep-ph/0307222.
Burrows, A., 1988, Astrophys. J. **334**, 891.
Chandrasekhar, S., 1931a, Astrophys. J. **74**, 81.
Chandrasekhar, S., 1931b, Mon. Not. Roy. Astron. Soc. **91**, 456.
Chandrasekhar, S., 1935, Mon. Not. Roy. Astron. Soc. **95**, 207.
Chandrasekhar, S., 1938, *An Introduction to the Study of Stellar Structure* (The University of Chicago Press).
Chandrasekhar, S., 1984, Rev. Mod. Phys. **56**, 137.
Cherry, J. F., *et al.*, 2010, Phys. Rev. D **82**, 085025.
Colgate, S. A., and Johnson, M. H., 1960, Phys. Rev. Lett. **5**, 235.
Colgate, S. A., and White, R. H., 1966, Astrophys. J. **143**, 626.
Cooperstein, J., 1988a, Phys. Rev. C **37**, 786.
Cooperstein, J., 1988b, Phys. Rept. **163**, 95.
Cooperstein, J., and Baron, E. A., 1990, in *Supernovae*, edited by Petschek, A. (Springer, Berlin), p. 213.
Cooperstein, J., Bethe, H. A., and Brown, G. E., 1984, Nucl. Phys. A **429**, 527.
Dasgupta, B., and Dighe, A., 2008, Phys. Rev. D **77**, 103002.
Dasgupta, B., *et al.*, 2008, Phys. Rev. D **77**, 113007.
Dasgupta, B., *et al.*, 2009, Phys. Rev. Lett. **103**, 051105.
Dasgupta, B., *et al.*, 2010b, Phys. Rev. D **81**, 093008.

Dasgupta, B., Raffelt, G. G., and Tamborra, I., 2010a, Phys. Rev. D **81**, 073004.
de Rujula, A., 1987, Phys. Lett. B **193**, 514.
Dighe, A., and Smirnov, A. Yu., 2000, Phys. Rev. D **62**, 033007.
Dighe, A., Keil, M. T., and Raffelt, G. G., 2003, JCAP **0306**, 005.
Duan, H., and Kneller, J. P., 2009, J. Phys. G **36**, 113201.
Duan, H., *et al.*, 2006b, Phys. Rev. D **74**, 105014.
Duan, H., Fuller, G. M., and Qian, Y. Z., 2006a, Phys. Rev. D **74**, 123004.
Duan, H., Fuller, G. M., and Qian, Y. Z., 2007, Phys. Rev. D **76**, 085013.
Duan, H., Fuller, G. M., and Qian, Y. Z., 2008, Phys. Rev. D **77**, 085016.
Duan, H., Fuller, G. M., and Qian, Y. Z., 2010, arXiv:1001.2799.
Dutta, G., *et al.*, 2000, Phys. Rev. D **61**, 013009.
Esteban-Pretel, A., *et al.*, 2007, Phys. Rev. D **76**, 125018.
Fogli, G., *et al.*, 2003, Phys. Rev. D **68**, 033005.
Fogli, G., *et al.*, 2005, JCAP **0504**, 002.
Fogli, G., *et al.*, 2007, JCAP **0712**, 010.
Freedman, D. Z., 1974, Phys. Rev. D **9**, 1389.
Friedland, A., 2010, Phys. Rev. Lett. **104**, 191102.
Fuller, G. M., *et al.*, 1987, Astrophys. J. **322**, 795.
Gava, J., and Volpe, C., 2008, Phys. Rev. D **78**, 083007.
Goldreich, P., and Weber, S. V., 1980, Astrophys. J. **238**, 991.
Gonzalez-Garcia, M. C., Maltoni, M., and Salvado, J., 2010, JHEP **1004**, 056.
Halzen, F., Jacobsn, J. E., and Zas, E., 1994, Phys. Rev. D **49**, 1758.
Halzen, F., and Raffelt, G. G., 2009, Phys. Rev. D **80**, 087301.
Hannestad, S., *et al.*, 2006, Phys. Rev. D **74**, 105010.
Hansen, B. M. S., and Liebert, J., 2003, Annu. Rev. Astron. Astrophys. **41**, 465.
Hillebrandt, W., 1982a, in *Supernovae: A Survey of Current Research*, edited by Rees, M. J., and Stoneham, R. S. (Reidel, Dordrecht), p. 123.
Hillebrandt, W., 1982b, Astron. Astrophys. **110**, L3.
Hillebrandt, W., 1984, Ann. N.Y. Acade. Sci. **422**, 197.
Hirata, K. S., *et al.*, 1987, Phys. Rev. Lett. **58**, 1490.
Hirata, K. S., *et al.*, 1988, Phys. Rev. D **38**, 448.
Janka, H. T., and Müller, E., 1993, in *Proc. of the IAU Coll. 145*, edited by McCray, R., and Wang, Z. (Cambridge University Press).
Janka, H. T., *et al.*, 2007, Phys. Rept. **442**, 38.
Keil, M. T., Raffelt, G. G., and Janka, H. T., 2003, Astrophys. J. **590**, 971.
Koester, D., and Chanmugam, G., 1990, Rep. Prog. Phys. **53**, 837.
Kostelecký, V. A., Pantaleone, J. T., and Samuel, S., 1993, Phys. Lett. B **315**, 46.
Kostelecký, V. A., and Samuel, S., 1993, Phys. Lett. B **318**, 127.
Kostelecký, V. A., and Samuel, S., 1994, Phys. Rev. D **49**, 1740.
Kostelecký, V. A., and Samuel, S., 1995, Phys. Rev. D **52**, 621.
Kostelecký, V. A., and Samuel, S., 1996, Phys. Lett. B **385**, 159.
Kuo, T. K., and Pantaleone, J., 1989, Rev. Mod. Phys. **61**, 937.
Lamb, D. Q., and Pethick, C. J., 1976, Astrophys. J. **209**, L77.
Lamitter, J. M., and Cooperstein, J., 1988, Phys. Rev. Lett. **61**, 23.
Landau, L. D., 1932, Phys. Z. Sowjetunion **1**, 285.
Landau, L. D., and Lifshitz, E. M., 1980, *Statistical Physics* (Pergamon Press).
Liebert, J., 1980, Annu. Rev. Astron. Astrophys. **18**, 363.

Lunardini, C., 2010, arXiv:1007.3252.
Lunardini, C., and Smirnov, A. Yu., 2003, JCAP **0306**, 009.
Malek, M., *et al.*, 2003, Phys. Rev. Lett. **90**, 061101
Mazurek, T., 1975, Astrophys. Space Sci. **35**, 117.
Mikheyev, S. P., and Smirnov, A. Yu., 1985, Sov. J. Nucl. Phys. **42**, 913.
Mirizzi, A., Raffelt, G. G., and Serpico, P. D., 2006, JCAP **0605**, 012.
Nötzold, D., and Raffelt, G. G., 1988, Nucl. Phys. B **307**, 924.
Pagliaroli, G., *et al.*, 2009, Phys. Rev. Lett. **103**, 031102.
Pantaleone, J. T., 1992a, Phys. Rev. D **46**, 510.
Pantaleone, J. T., 1992b, Phys. Lett. B **287**, 128.
Pantaleone, J. T., 1998, Phys. Rev. D **58**, 073002.
Pastor, S., Raffelt, G. G., and Semikoz, D. V., 2002, Phys. Rev. D **65**, 053011.
Prialnik, D., 2000, *An Introduction to the Theory of Stellar Structure and Evolution* (Cambridge University Press).
Raffelt, G. G., 1990, Phys. Rept. **198**, 1.
Raffelt, G. G., 1996, *Stars as Laboratories for Fundamental Physics* (University of Chicago Press).
Raffelt, G. G., 2001, Astrophys. J. **561**, 890.
Raffelt, G. G., 2005, Phys. Scripta **T121**, 102.
Raffelt, G. G., and Seckel, D., 1988, Phys. Rev. Lett. **60**, 1793.
Raffelt, G. G., and Smirnov, A. Yu., 2007a, Phys. Rev. D **76**, 081301.
Raffelt, G. G., and Smirnov, A. Yu., 2007b, Phys. Rev. D **76**, 125008.
Samuel, S., 1993, Phys. Rev. D **48**, 1462.
Samuel, S., 1996, Phys. Rev. D **53**, 5382.
Sato, K., 1975, Prog. Theor. Phys. **54**, 1352.
Schirato, R. C., and Fuller, G. M., 2002, arXiv:astro-ph/0205390.
Shapiro, S. L., and Teukolsky, S. A., 1983, *Black Holes, White Dwarfs, and Neutron Stars: The physics of Compact Objects* (John Wiley & Sons, Inc.).
Shelton, I., Duhalde, O., and Jones, A., 1987, Int. Astron. Union Circular 4316.
Scholberg, K., 2007, arXiv:astro-ph/0701081.
Scholberg, K., 2010, J. Phys. Conf. Ser. **203**, 012079.
Spergel, D. N., and Bahcall, J. N., 1988, Phys. Lett. B **200**, 366.
Suzuki, A., 2008, J. Phys. Conf. Ser. **120**, 072001.
Suzuki, H., 1991, Num. Astrophys. Japan **2**, 267.
Suzuki, H., 1993, Front. Phys. **5**, 219.
Tubbs, D. L., and Schramm, D. N., 1975, Astrophys. J. **201**, 467.
Wilson, J. R., 1985, in *Numerical Astrophysics*, edited by Centrella, J. M., LeBlanc, J. M., and Bowers, R. L. (Jones & Bartlett, Boston), p. 422.
Wolfenstein, L., 1978, Phys. Rev. D **17**, 2369.
Wolfenstein, L., 1979, Phys. Rev. D **20**, 2634.
Yahil, A., 1983, Astrophys. J. **265**, 1047.
Yahil, A., and Lattimer, J. M., 1982, in *Supernovae: A Survey of Current Research*, edited by Rees, M. J., and Stoneham, R. S. (Reidel, Dordrecht), p. 53.

8

Ultrahigh-energy Cosmic Neutrinos

Many astrophysical objects in the Universe are expected to produce cosmic neutrinos with very high energies (1 TeV $\lesssim E_\nu \lesssim$ 1 PeV), ultrahigh energies ($E_\nu \gtrsim$ 1 PeV) or extremely high energies ($E_\nu \gtrsim$ 100 EeV) [1]. Such energetic neutrinos may serve as a unique cosmic messenger and provide us with useful information about the cosmos that cannot be extracted from the measurements of cosmic rays and gamma rays. The burning questions in neutrino astronomy include where ultrahigh-energy (UHE) cosmic neutrinos originate from and how they can be detected. In this chapter we shall first describe some possible sources of UHE cosmic neutrinos and then outline a few possible ways to detect them. The flavor distribution and oscillations of UHE cosmic neutrinos, together with their sensitivities to new physics, will also be discussed. We shall finally highlight the importance of multi-messenger astronomy by illustrating the interplay between UHE cosmic neutrinos and cosmic rays, gamma rays or gravitational waves.

8.1 Possible Sources of UHE Cosmic Neutrinos

The sources of UHE cosmic neutrinos are presumably related to those of UHE cosmic rays. In fact, most of the models for the origin of UHE cosmic rays predict the existence of UHE cosmic neutrinos. Such models can be classified into two categories: the top-down and bottom-up scenarios. In the top-down scenarios it is assumed that UHE cosmic rays originate from the annihilation or decays of some superheavy particles, which must be the

[1] Note that the terms VHE (very high energy), UHE (ultrahigh energy) and EHE (extremely high energy) are highly relative and taste-dependent. Some useful units of energy in neutrino astronomy are keV = 10^3 eV, MeV = 10^6 eV, GeV = 10^9 eV, TeV = 10^{12} eV, PeV = 10^{15} eV, EeV = 10^{18} eV, ZeV = 10^{21} eV and YeV = 10^{24} eV, where "k", "M", "G", "T", "P", "E", "Z" and "Y" denote kilo, mega, giga, tera, peta, exa, zetta and yotta, respectively.

relics of the Big Bang. In the bottom-up scenarios it is assumed that UHE cosmic rays originate in some cosmic accelerators. One may find a long list of the hitherto-proposed sources of UHE cosmic neutrinos (Halzen and Hooper, 2002). Some of them will be briefly introduced in this section.

8.1.1 The GZK Cutoff and UHE Neutrinos

Charged cosmic rays consist mostly of protons and heavier nuclei with lifetimes of $\mathcal{O}(10^6)$ years or longer. The "primary" cosmic rays are referred to as those particles accelerated at the astrophysical sources, and the "secondary" cosmic rays are those particles produced in the interactions of the primary cosmic rays with the interstellar gas. The existence of cosmic rays was discovered by Victor Hess in 1912, and the extensive air showers initiated by the primary cosmic rays were first observed by Pierre Auger in 1938 (Auger *et al.*, 1938). After about a century of measurements, the energy spectrum of cosmic rays is now determined to a good degree of accuracy. It spans more than ten orders of magnitude and exhibits an approximate power-law shape. Fig. 8.1 shows the "all-particle" spectrum of cosmic rays, in which the differential flux $F(E) \equiv \dfrac{\mathrm{d}\Phi}{\mathrm{d}E}$ has been multiplied by $E^{2.7}$ so as to make the visibility of its steep structure much better (Nakamura *et al.*, 2010). The impressive steepening that occurs between $E = 10^{15}$ eV and $E = 10^{16}$ eV is the so-called "knee" of the spectrum. A structure known as the "ankle" of the spectrum appears around $E = 10^{19}$ eV. If the cosmic rays up to energies of 10^{17} eV to 10^{18} eV originate in our Galaxy, those around and beyond the ankle are most likely to have an extragalactic origin. In fact, the origin of UHE cosmic rays is not known at all, nor are the reasons for either the knee or the ankle of the spectrum of cosmic rays.

Soon after Arno Penzias and Robert Wilson discovered the cosmic microwave background (CMB) radiation (Penzias and Wilson, 1965), it was pointed out by Kenneth Greisen and independently by Georgiy Zatsepin and Vadim Kuzmin that this radiation would have a strong attenuating effect on the propagation of cosmic rays with energies higher than about 10^{20} eV (Greisen, 1966; Zatsepin and Kuzmin, 1966). Today we expect that the Greisen-Zatsepin-Kuzmin (GZK) cutoff takes place in the spectrum of cosmic rays around $E \sim 5 \times 10^{19}$ eV, as a result of the onset of inelastic interactions of UHE cosmic rays with the CMB photons. The dominant reaction leading to the GZK cutoff is the pion photoproduction on the Δ^+ resonance; i.e., $p + \gamma_{\rm CMB} \to \Delta^+(1232) \to p + \pi^0$ or $n + \pi^+$, where the final-state particles roughly have only half of the energy of the initial proton. If the Δ^+ resonance is unavailable, a weakened version of the GZK cutoff may result from the non-resonant photoproduction of one or more pions (Coleman and Glashow, 1998): $p + \gamma_{\rm CMB} \to p + \mathbf{n}\pi$ or $n + \mathbf{n}\pi$, where $\mathbf{n}$ is a positive integer and the total electric charge of $\mathbf{n}\pi$ should be consistent with the conservation of electric charges for this multi-pion channel. A simple kinematic analysis

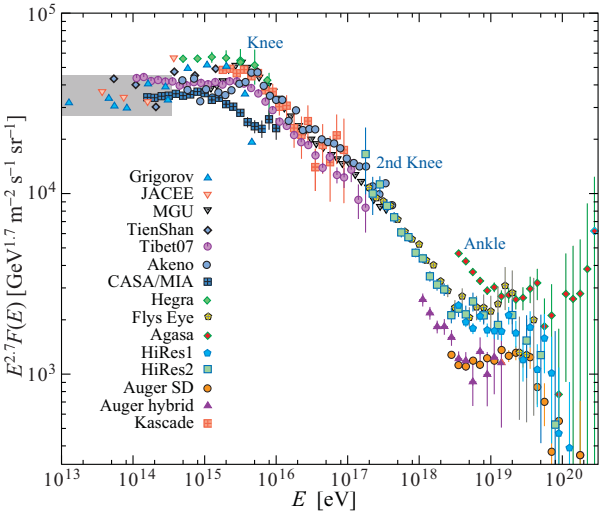

Fig. 8.1 The all-particle spectrum of cosmic rays from the air shower measurements, where the shaded area shows the range covered by the direct measurements (Nakamura *et al.*, 2010. With permission from the Institute of Physics)

yields a threshold energy of the proton in either case:

$$E_{\rm th} = \begin{cases} \dfrac{m_\Delta^2 - m_p^2}{2\langle E_\gamma \rangle} \approx \dfrac{3.19}{\langle E_\gamma \rangle} \times 10^{17}{\rm eV}^2 & \text{(on resonance)}\,, \\ \dfrac{m_\pi \left(2m_p + m_\pi\right)}{2\langle E_\gamma \rangle} \approx \dfrac{1.36}{\langle E_\gamma \rangle} \times 10^{17}{\rm eV}^2 & \text{(no resonance)}\,, \end{cases} \tag{8.1}$$

where $\langle E_\gamma \rangle$ denotes the average CMB photon energy [2], and only a single pion ($\mathbf{n} = 1$) has been taken into account in the non-resonant case. An input of $\langle E_\gamma \rangle \approx 6.35 \times 10^{-4}$ eV leads to $E_{\rm th} \approx 5.0 \times 10^{20}$ GeV (or 2.1×10^{20} GeV) for the resonant (or non-resonant) pion photoproduction. This naive result, which is somewhat larger than $E_{\rm GZK} \sim 5 \times 10^{19}$ eV, implies that Eq. (8.1) can only be used to give a ballpark estimate of the GZK cutoff. The reason is simply that many details of the inelastic photon-proton interactions in the CMB need to be carefully dealt with (Stecker, 1968).

Fig. 8.1 shows that the observed spectrum of cosmic rays has a dip structure at the GZK-cutoff energy $E_{\rm GZK}$. This significant steepening has been revealed mainly in the HiRes and Auger experiments (Abbasi *et al.*, 2008; Abraham *et al.*, 2008), and it is apparently inconsistent with the AGASA measurement (Takeda *et al.*, 2003). Such a cutoff implies that the Universe is opaque to EHE cosmic rays, with an absorption length of $\lambda_{p+\gamma_{\rm CMB}} =$

[2] Given the CMB temperature $T_\gamma = 2.725$ K, it is easy to get the photon energy $E_\gamma = 2.348 \times 10^{-4}$ eV. The average value of E_γ at T_γ is $\langle E_\gamma \rangle_{T_\gamma} \approx 6.35 \times 10^{-4}$ eV.

$n_{\rm CMB}^{-1}\sigma_{p+\gamma_{\rm CMB}}^{-1} \sim 8$ Mpc for $n_{\rm CMB} \approx 411$ cm^{-3} and $\sigma_{p+\gamma_{\rm CMB}} \sim 10^{-28}$ cm^2 (Halzen and Hooper, 2002). In other words, the GZK effect suppresses EHE cosmic rays coming from distances larger than a few tens of Megaparsecs. The Auger experiment is expected to provide a solid observational basis for the existence or non-existence of the GZK cutoff by detecting a sufficiently large number of events at and above $E_{\rm GZK}$ in the coming years.

Associated with the GZK cutoff of cosmic rays, cosmogenic neutrinos can be produced from the decays of charged pions (or neutrons) (Berezinsky and Zatsepin, 1969): $\pi^+ \to \mu^+ + \nu_\mu$ and $\mu^+ \to e^+ + \overline{\nu}_\mu + \nu_e$ (or $n \to p + e^- + \overline{\nu}_e$). The energies of such GZK neutrinos should be close to $E_{\rm GZK}$, because roughly equal energies go into the secondary nucleons and pions in the photoproduction processes discussed above. A measurement of UHE cosmic neutrinos with $E_\nu \sim E_{\rm GZK}$ can therefore serve for a promising way to probe the GZK cutoff of UHE cosmic rays. Of course, the flux of GZK neutrinos is so low ($\lesssim 10^{-26}$ MeV^{-1}cm^{-2}s^{-1}sr^{-1}) that it will be very challenging to observe them even at an unprecedented km^3-scale detector (Spiering, 2009).

8.1.2 Astrophysical Sources of UHE Neutrinos

The expected astrophysical sources of UHE neutrinos include the active galactic nuclei (AGN), gamma ray bursts (GRBs) and other sources associated with compact stellar objects, such as the supernova remnants, X-ray binaries and microquasars (Halzen and Hooper, 2002; Torres and Anchordoqui, 2004). Here we give a brief introduction about two typical examples, AGN and GRBs, together with a rough estimate of the UHE neutrino fluxes from those optically thin sources.

(1) *UHE cosmic neutrinos from AGN.* The AGN should presumably belong to the most promising UHE neutrino sources, but the detailed mechanism of neutrino production in the AGN remains unclear. One may follow a conservative way, which is independent of any specific neutrino-production models, to describe the AGN according to their geometric properties and electromagnetic emission (Achterberg *et al.*, 2006). For instance, the observational differences among a variety of AGN (e.g., blazars, radio galaxies and quasars) can be partially interpreted with the help of a geometrically axisymmetric scheme as the result of their different inclination angles which are defined as the angles between the lines of sight and the AGN axis (Urry and Padovani, 1995). Fig. 8.2 shows some basic ingredients of such an axisymmetric scheme of the AGN. It consists of a rotating supermassive black hole, two jets with matter outflowing along the rotation axis and an accretion disk of matter perpendicular to the rotation axis.

The radio emission of AGN is assumed to originate mostly in relativistic jets; namely, it is caused by the synchrotron radiation of electrons moving along the jet. The energy spectrum of the photons emitted from the AGN and observed on the Earth may range from radio waves to TeV gamma rays.

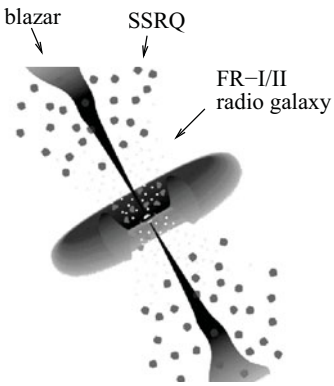

Fig. 8.2 A pictorial scheme of the AGN with a black hole in the center and an accretion disk perpendicular to the direction of two jets along its rotation axis. The different inclination angles of the lines of sight with respect to the jet for blazars, steep spectrum radio quasars (SSRQs) and radio galaxies are indicated by arrows (Urry and Padovani, 1995; Achterberg *et al.*, 2006. With permission from Elsevier)

The luminous energy of the AGN is presumably supplied by the gravitational energy of matter falling into the supermassive black hole in the center of their core. In this case the infalling matter forms an accretion shock at a certain distance from the central black hole, where protons can be accelerated by the first-order Fermi acceleration (Protheroe and Szabo, 1992; Tu, 2004). Protons and other charged primaries can also be accelerated in the relativistic jets or in the hot spots (e.g., of the FR-II radio galaxies) to energies around or above 10^{20} eV (Rachen and Biermann, 1993). Then a large amount of pions can be produced from the interactions of protons with the dense matter surrounding the core of the AGN (in particular, the intense photon field). In this scenario the photons and protons cannot escape from the source region (Stecker and Salamon, 1996), and thus the latter might only be visible by detecting the UHE neutrinos arising from the decays of charged pions.

The accelerated protons may interact with the ambient photons or matter via the reactions $p + \gamma \rightarrow \Delta^+ \rightarrow n + \pi^+$ and $p + X \rightarrow \pi^{\pm} + Y$, leading to the production of UHE neutrinos through $\pi^+ \rightarrow \mu^+ + \nu_\mu$ and $\pi^- \rightarrow \mu^- + \overline{\nu}_\mu$ decays as well as $\mu^+ \rightarrow e^+ + \overline{\nu}_\mu + \nu_e$ and $\mu^- \rightarrow e^- + \nu_\mu + \overline{\nu}_e$ decays. On the other hand, the decays of neutral pions (i.e., $\pi^0 \rightarrow 2\gamma$) can produce high-energy gamma rays. The resultant neutrino and gamma-ray fluxes are expected to be of the same order of magnitude (Achterberg *et al.*, 2006). Since the proton and target photon spectra fall steeply with the increase of energies in most scenarios, the multi-pion production, kaon production and higher resonances only represent a small correction to the single pion production. Given the low plasma density in the AGN jets, the proton-photon interactions are likely to dominate over the proton-proton interactions (or generically, the

proton-X interactions) unless the latter can take place at the inner edge of the accretion disk (Nellen *et al.*, 1993; Stecker and Salamon, 1996).

Blazars, which emit high-energy radiation in collimated jets pointing at the Earth, are a subclass of AGN. They are characterized by a flat radio spectrum (Achterberg *et al.*, 2006), and appear less distant than the GRBs since their lower luminosity makes distant sources difficult to observe (Halzen and Hooper, 2002). Blazars have been identified to be prodigious gamma-ray sources by a number of experiments in different energy regimes: infrared, keV (or X-ray), GeV and TeV. Gamma rays in the multi-TeV range are observed from the most powerful blazars. If the emission of high-energy photons in the blazar jets only involves the electromagnetic processes (i.e., electron acceleration and inverse Compton scattering), it is impossible to produce neutrinos. If highly-shocked protons are present in the blazar jets, however, they may interact with the ambient photons and matter to generate charged and neutral pions which can then decay into UHE neutrinos and photons.

(2) *UHE cosmic neutrinos from GRBs.* GRBs are the brightest gamma ray sources in the Universe during a period of a few seconds or tens of seconds. An enormous amount of energy, typically 10^{51} erg to 10^{54} erg per second, is released from a GRB. It can phenomenologically be described as a fireball expanding with a highly relativistic velocity and powered by the radiation pressure (Waxman, 2003). The delayed low-energy emission or "afterglow" of GRBs has been observed (Kulkarni *et al.*, 2000) and it indicates that GRBs are predominantly generated in host galaxies and are likely the result of a stellar process — e.g., the "collapsar" scenario, where a supermassive star undergoes the core collapse resulting in a failed supernova, is one of the most popular models proposed for the fireball's inner engine (MacFadyen and Woosley, 1999; Halzen and Hooper, 2002). The dynamics of a GRB fireball is quite similar to the physics of the early expanding Universe: (a) a radiation-dominated soup of leptons and photons (and few baryons) is initially present, and it is hot enough to freely produce electron-positron pairs; (b) the optical depth of photons is large enough that it is possible to create a thermal plasma of photons, electrons and positrons — a fireball which can then expand and accelerate to relativistic velocities; (c) the fireball expands with increasing velocity until it becomes optically thin, and then the photons may escape and the radiation is released in the visual display of a GRB (Halzen and Hooper, 2002; Waxman, 2003). The observed hard photon spectra are produced from the synchrotron radiation of electrons accelerated by the shocks in the expanding fireball, because the latter is made up of multiple shocks. The protons present in the fireball can also be accelerated to very high energies in the same region, making the GRBs a good candidate for the source of UHE cosmic rays.

Analogous to the case of AGN, pions can be produced from a GRB via interactions of the accelerated protons with the target photon field which is simply the highly variable radiation formed in the GRB blast wave and

detected as the GRB. The most important pion photoproduction processes are $p+\gamma \to n+\pi^+$ and $p+\gamma \to p+\pi^0$, in which a large fraction of the initial proton energy is lost. In contrast, only a small fraction of the initial proton energy is lost in the e^+e^- pair photoproduction process $p+\gamma \to p+e^++e^-$. For the resonant pion photoproduction (i.e., $p+\gamma \to \Delta^+ \to p+\pi^0$ or $n+\pi^+$), high-energy gamma rays may come from $\pi^0 \to 2\gamma$ decays and high-energy neutrinos can arise from $\pi^+ \to \mu^+ + \nu_\mu$ decays together with $\mu^+ \to e^+ + \overline{\nu}_\mu + \nu_e$ decays. For the non-resonant multi-pion channel $p+\gamma \to p+\mathbf{n}\pi$ or $n+\mathbf{n}\pi$, the production rate of π^+, π^- and π^0 events is possible to approach $1:1:1$ (Dermer and Atoyan, 2006), implying that the ratio of ν_μ, $\overline{\nu}_\mu$, ν_e, $\overline{\nu}_e$ and γ events would be $2:2:1:1:2$. The energies of cosmic neutrinos produced from the interactions of shocked protons with the ambient photons in GRBs may vary from TeV to EeV (Halzen and Hooper, 2002) [3].

(3) *UHE neutrino fluxes from optically thin sources.* Both AGN and GRBs are probably the cosmic accelerators in which UHE cosmic rays may originate. The accelerated electrons lose their energy in the magnetic field as a result of their synchrotron radiation. The resultant photons provide a target field for protons and heavier nuclei to trigger the meson photoproduction and photo-disintegration processes, respectively. A neutron produced in this way may diffuse out of the magnetically confining source before it undergoes the beta decay. Such an astrophysical source is referred to as the optically thin source, as shown in Fig. 8.3 (left). For an optically thick source in Fig. 8.3 (right), however, some neutrons may scatter inelastically off the photon gas before they escape from the region of magnetic confinement (Ahlers, 2007). Focusing on the optically thin source and assuming the resonant photoproduction $p+\gamma \to \Delta^+ \to n+\pi^+$ to be the dominant process for the charged-pion production, we shall estimate the UHE neutrino flux in the following.

In the assumption made above, we obtain ν_μ, $\overline{\nu}_\mu$ and ν_e events from $\pi^+ \to \mu^+ + \nu_\mu$ and $\mu^+ \to e^+ + \overline{\nu}_\mu + \nu_e$ decays. They constitute the flux of UHE neutrinos emitted from an optically thin source. Following the Waxman-Bahcall treatment (Waxman and Bahcall, 1999), we define $\epsilon_\pi \equiv \langle E_\pi \rangle / \langle E_n \rangle$ as a ratio of the average pion energy to the average neutron energy in the reaction $p+\gamma \to \Delta^+(1232) \to n+\pi^+$. The inelasticity of this process is kinematically determined by requiring equal boosts for n and π^+ (Stecker, 1968), giving $\epsilon_\pi \approx 0.28$. The average energies of ν_μ and μ^+ emitted from the π^+ decay are $\langle E_{\nu_\mu} \rangle \approx \gamma_\pi (m_\pi^2 - m_\mu^2)/(2m_\pi) \approx E_\pi (1 - m_\mu^2/m_\pi^2)/2 \approx 0.22 E_\pi$ and $\langle E_\mu \rangle \approx E_\pi - \langle E_{\nu_\mu} \rangle \approx 0.78 E_\pi$. Because μ^+ is much heavier than e^+ and the neutrino masses are negligibly small, we assume that the energy of μ^+ is equally distributed among e^+, $\overline{\nu}_\mu$ and ν_e in the μ^+ decay; i.e.,

[3] Like a supernova, a GRB radiates the vast majority of its initial energy as thermal MeV neutrinos. On the other hand, neutrons may decouple from protons in the expanding fireball. If their relative velocity is sufficiently large, their interactions may produce charged pions (i.e., $p+n \to p+p+\pi^-$ and $p+n \to n+n+\pi^+$) which can then produce GeV neutrinos (Halzen and Hooper, 2002).

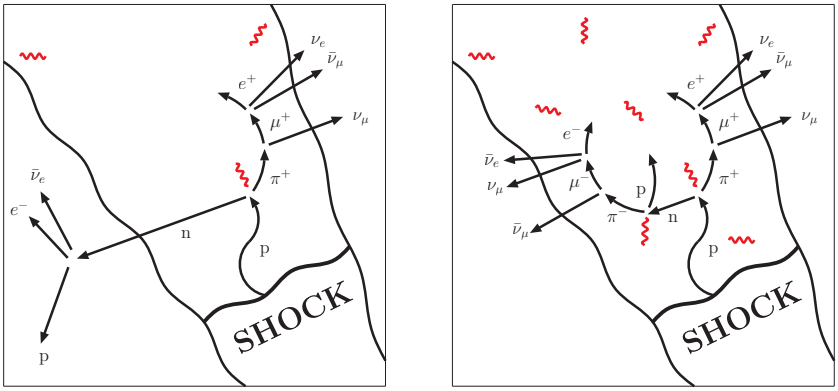

Fig. 8.3 A sketch of the neutrino production in an accelerator of UHE cosmic rays. The relative fluxes depend on the optical thickness of the magnetic confinement region illustrated by the wavy lines. The left and right panels represent the optically thin and thick sources, respectively (Ahlers *et al.*, 2006. With permission from Elsevier)

$\langle E_{\overline{\nu}_\mu} \rangle \approx \langle E_{\nu_e} \rangle \approx 0.26 E_\pi$ (Ahlers, 2007). Roughly speaking, about 1/4 of the pion's energy is taken away by each of ν_μ, $\overline{\nu}_\mu$ and ν_e. So we define a flavor-universal ratio for three relevant neutrinos,

$$\epsilon_\nu \equiv \frac{\langle E_\nu \rangle}{\langle E_n \rangle} = \frac{\langle E_\nu \rangle}{\langle E_\pi \rangle} \cdot \frac{\langle E_\pi \rangle}{\langle E_n \rangle} \approx \frac{\epsilon_\pi}{4} \,, \tag{8.2}$$

which will later on be used in the calculation of the UHE neutrino flux.

For a given optically thin source at the redshift position z, one may consider the differential rate of the neutron flux in an energy interval $[E_1, E_2]$ and that of the neutrino flux in the corresponding energy interval $[\epsilon_\nu E_1, \epsilon_\nu E_2]$:

$$\begin{aligned} \mathcal{N}_\nu &\equiv \int_{\epsilon_\nu E_1}^{\epsilon_\nu E_2} \mathrm{d}E \mathcal{L}_\nu(z, E) \,, \\ \mathcal{N}_n &\equiv \int_{E_1}^{E_2} \mathrm{d}E \mathcal{L}_n(z, E) = \int_{\epsilon_\nu E_1}^{\epsilon_\nu E_2} \mathrm{d}E \frac{1}{\epsilon_\nu} \mathcal{L}_n(z, E/\epsilon_\nu) \,, \end{aligned} \tag{8.3}$$

where $\mathcal{L}_\nu$ (or $\mathcal{L}_n$) denotes the neutrino (or neutron) luminosity per comoving volume. Since the rates of the neutron and neutrino fluxes are 1 : 3 (i.e., $\mathcal{N}_\nu = 3\mathcal{N}_n$), we have (Ahlers *et al.*, 2006; Ahlers, 2007)

$$\mathcal{L}_\nu(z, E) = \frac{3}{\epsilon_\nu} \mathcal{L}_n(z, E/\epsilon_\nu) \,. \tag{8.4}$$

Except for the resonant (Z-burst) interactions in the cosmic neutrino background (Weiler, 1982, 1999; Fargion *et al.*, 1999), the UHE neutrinos may

only undergo the redshift loss once they are emitted from the source. Their propagation function is simply given by a step function: $P_{\nu|\nu}(E; E_i, z) = \Theta(E_i - (1+z)E)$, whose derivative is just the delta function. Then one can arrive at the total flux of UHE neutrinos (Ahlers, 2007):

$$J_\nu(E) = \frac{1}{4\pi}\int_0^\infty \mathrm{d}E_i \int_0^\infty \mathrm{d}z \frac{1}{H(z)(1+z)} \left|\frac{\partial P_{\nu|\nu}(E; E_i, z)}{\partial E}\right| \mathcal{L}_\nu(z, E_i)$$
$$= \frac{1}{4\pi}\cdot\frac{3}{\epsilon_\nu}\int_0^\infty \mathrm{d}z \frac{1}{H(z)}\mathcal{L}_n(z, (1+z)E/\epsilon_\nu) \,, \tag{8.5}$$

where $H(z)$ is the Hubble expansion rate at the redshift position z. Such a UHE neutrino flux, which arises from a transparent source of cosmic rays, is often referred to as the Waxman-Bahcall flux (Waxman and Bahcall, 1999).

8.1.3 Top-down Models and UHE Neutrinos

In the "bottom-up" approach discussed above, it is very difficult to identify an astrophysical source as the wanted "zevatron" accelerator of cosmic rays. A variety of "top-down" models have so far been proposed to avoid this difficulty and attribute the observed UHE cosmic ray primaries to the decay or annihilation products of some supermassive particles. Two classes of the top-down models, the superheavy dark matter (DM) and topological defects (TDs), have attracted some particular interest because they are well motivated even if the origin of UHE cosmic rays is irrelevant. For instance, TDs (e.g., monopoles, cosmic strings, domain walls, etc.) are a generic prediction of some grand unified theories and could be formed in the symmetry-breaking phase transitions in the early Universe. The superheavy DM is an interesting DM candidate, and its stable or metastable particles with masses around 10^{13} GeV could be produced during the inflation era of the Universe. If one of the top-down models is responsible for the origin of UHE cosmic rays, it must be able to produce UHE neutrinos and photons.

Superheavy stable or metastable relic particles can be a good candidate for cold DM. They could be produced in the early Universe in various ways, for example, by gravitational interactions from vacuum fluctuations at the end of inflation (Chung *et al.*, 1999; Kuzmin and Tkachev, 1999). The lifetime of a superheavy DM particle X has to lie in the range $10^{17}\ \mathrm{s} \lesssim \tau_X \lesssim 10^{28}\ \mathrm{s}$ (Kachelrieß, 2008), longer or much longer than the age of the Universe. Such a long-lived particle might be protected by an underlying global symmetry which is broken in a perturbative way by high-dimensional operators suppressed by $1/M^n$ with $n \geqslant 7$, where M is close to the Planck mass scale, or in a non-perturbative way by wormhole or instanton effects (Berezinsky *et al.*, 1997; Kuzmin and Rubakov, 1998; Hamaguchi *et al.*, 1998). The superheavy DM has several clear observational signatures (Kachelrieß, 2008). (1) It does not predict a GZK cutoff for UHE cosmic rays; instead, it yields a

spectrum, which is flatter than that given by an astrophysical source, up to the kinematical cutoff at $E \sim m_X/2$. (2) The decay or annihilation products of the superheavy DM contain a lot of $\pi^{\pm}$ and π^0 events whose decays yield large UHE neutrino and photon fluxes, usually larger than those produced from the shock-accelerated protons at an astrophysical source. (3) The flux of cosmic rays from the superheavy DM should show a galactic anisotropy, as the Sun is not in the center of the Galaxy. (4) There is no correlation between UHE cosmic ray arrival directions and astrophysical sources, since extragalactic cosmic rays are strongly suppressed in a superheavy DM model.

TDs, whose existence was in no conflict with cosmic inflation, could be produced in the non-thermal phase transitions during the preheating stage of the Universe (Vilenkin and Shellard, 1994). They can naturally produce particles with sufficiently high energies, but have problems to produce sufficiently large fluxes of UHE cosmic ray primaries because of the typically large distance between two TDs (Kachelrieß, 2008). So the flux of UHE cosmic rays is either exponentially suppressed or strongly anisotropic if a TD happens to be nearby. Note that the energy spectrum of UHE cosmic rays originating from cosmic strings might have a less pronounced GZK cutoff, simply because it is not so steep as usual and is dominated by photons instead of protons. Since cosmic strings do not cluster, no correlation is expected between the UHE cosmic ray arrival directions and astrophysical sources.

It is worth mentioning that the weakly interacting massive particles (WIMPs), which are regarded as one of the most promising DM candidates, can also produce energetic neutrinos when they annihilate. A typical example of WIMPs is the lightest supersymmetric particle, such as the neutralino. If the masses of WIMPs are around the electroweak scale, their annihilation will produce neutrinos and antineutrinos with energies of $\mathcal{O}(10^2)$ GeV to $\mathcal{O}(1)$ TeV. The detection of such signatures at a neutrino telescope can serve for an indirect search for DM (Bell, 2008; Halzen and Hooper, 2009). In comparison, the detection of UHE neutrinos with $E \gtrsim \mathcal{O}(1)$ PeV will indirectly probe the existence of the superheavy DM or TDs.

8.2 Detection of UHE Cosmic Neutrinos

An important subject of high-energy neutrino astronomy is to search for the point-like neutrino sources, which would help solve a longstanding problem — the origin of UHE cosmic rays. The detection of UHE cosmic neutrinos requires the construction of huge detectors, the so-called neutrino telescopes, which are well motivated by their discovery potential in astronomy, astrophysics, cosmology and particle physics (Halzen, 2006a). Because the fluxes of cosmic rays above the knee are too small to be detected in the satellite or balloon experiments, large ground-based or underground detectors with large effective detection areas have to be built. The most important experimental

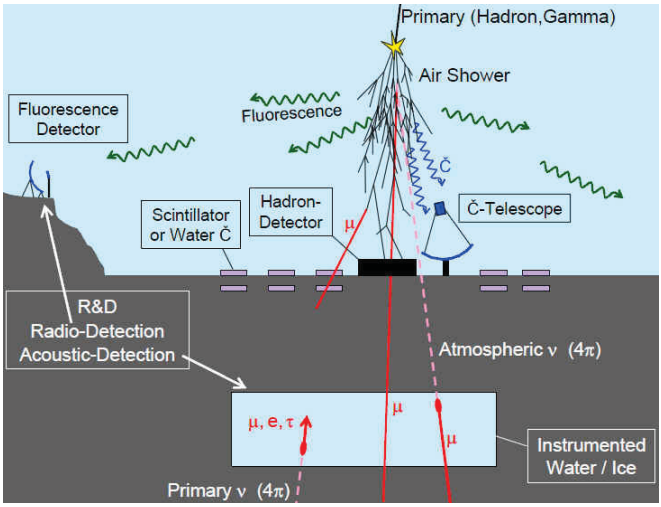

Fig. 8.4 A sketch of the experimental techniques for ground-based or underground detection of high-energy cosmic rays, gamma rays and neutrinos (Lohse, 2005)

techniques for ground-based or underground observation of high-energy cosmic rays, gamma rays and neutrinos are sketched in Fig. 8.4 (Lohse, 2005). To detect UHE cosmic neutrinos, a deep underground ice or water Cherenkov detector is needed. In addition, radio and acoustic detection techniques for the detection of neutrino interactions have been developed.

8.2.1 A km^3-scale UHE Neutrino Telescope

An optical Cherenkov neutrino telescope consists of large arrays of photomultiplier tubes underwater or under ice. It detects the Cherenkov light emitted by charged leptons which have been produced in neutrino interactions with the medium (water or ice). This technique was established by two pioneering detectors, NT200 in Lake Baikal (Balkanov *et al.*, 1998) and AMANDA at the South Pole (Ahrens *et al.*, 2004; Ackermann *et al.*, 2006). At present three underwater neutrino telescope projects, ANTARES (Aslanides *et al.*, 1999), NESTOR (Tzamarias *et al.*, 2003) and NEMO (Piatelli *et al.*, 2005), are being pursued in the Mediterranean sea. The most impressive optical Cherenkov neutrino telescope is IceCube, a km^3-scale successor of AMANDA at the South Pole (Achterberg *et al.*, 2006).

IceCube is a km^3-volume under-ice neutrino detector under construction at the South Pole. Once its deployment is completed in 2011, IceCube will comprise 4800 digital optical modules (DOMs) along 80 vertical strings deployed in the ice at depths from 1450 m to 2450 m. The distance between

two neighboring strings is 125 m. Each string consists of 60 DOMs at a vertical spacing of 16.7 m. Each DOM consists of a 25-cm-diameter Hamamatsu photomultiplier tube, the electronics for waveform digitization and a spherical pressure-resistant glass housing. Half of the array configuration with 40 strings had been finished before April 2008, and it has began operating since May 2008. The IceCube facility is complemented with an air shower array, IceTop, which covers a surface of 1 km^2 above the IceCube detector and is composed of 80 detector stations (Bernardini, 2009). Each station is equipped with two ice Cherenkov tanks. The IceTop facility serves as a veto to cosmic ray showers and as a calibration array, and it can also be used to study some other scientific topics on cosmic rays.

The IceCube detector is optimized to detect cosmic neutrinos of all flavors in the energy range from TeV to EeV. The signal waveforms recorded by individual photomultipliers are digitized in each DOM and transmitted to the surface by twisted-pair cables (Bernardini, 2009). Experimental data can be processed by several hardware and software triggers, which are responsive to different event topologies. A series of reconstruction algorithms and event filters are applied in situ to the calibrated data so as to reduce the trigger rate to a total data volume, which can then be transferred north via a satellite. Such events will later on be fitted to the templates representing different neutrino interaction modes (Bernardini, 2009). The IceCube Collaboration has so far searched for possible point-like sources of cosmic neutrinos in the northern sky by using the data recorded from 2007 to 2008 with 22 strings of the detector and 275.7 days of live time (Abbasi *et al.*, 2009). The final sample of 5114 neutrino candidate events agrees well with the expected background of atmospheric muon neutrinos and a small component of atmospheric muons, and shows no evidence for a point-like source.

To build a km^3-scale neutrino telescope in the northern hemisphere as a counterpart of IceCube is well motivated (Avignone *et al.*, 2008). On the one hand, the candidate sources for high-energy neutrinos are not isotropically distributed in the local Universe. This fact, together with the probably modest number of detectable sources, calls for a complete coverage of the sky. On the other hand, only a telescope in the northern hemisphere is able to see the upward-going neutrinos coming from the galactic center — a place of particular interest. Hence KM3NeT, a km^3-scale UHE neutrino telescope in the Mediterranean sea to complement the IceCube detector at the South Pole, has been proposed (Carr *et al.*, 2007). The KM3NeT design study is currently underway to address many important issues, such as its scientific sensitivity, fast and secure installation, stable operation and maintainability, and long-term deep-sea measurements.

8.2.2 Identification of UHE Neutrino Flavors

For either IceCube or KM3NeT, the detection of all neutrino flavors is important because of the tau neutrino "regeneration" through the Earth and

neutrino oscillations (Halzen, 2006a). A generic cosmic accelerator is expected to produce UHE neutrinos from the decays of charged pions, and thus the ratio of initial $(\nu_e + \overline{\nu}_e)$, $(\nu_\mu + \overline{\nu}_\mu)$ and $(\nu_\tau + \overline{\nu}_\tau)$ fluxes should be $\phi_e : \phi_\mu : \phi_\tau = 1 : 2 : 0$. Thanks to neutrino oscillations, this ratio turns out to be $1 : 1 : 1$ at a neutrino telescope, as one can see in Section 8.3. The appearance of ν_τ (or $\overline{\nu}_\tau$) events is a natural consequence of neutrino oscillations. Unlike UHE ν_e and ν_μ neutrinos, which can be absorbed by their charged-current interactions with matter in the Earth, UHE ν_τ neutrinos cannot be absorbed in the Earth due to the charged-current regeneration effect (Halzen and Saltzberg, 1998). In other words, ν_τ neutrinos with energies larger than 1 PeV can pass through the Earth and then emerge with energies of about 1 PeV. The reason is simple: an UHE ν_τ neutrino interacting in the Earth can produce another ν_τ neutrino, whose energy is somewhat lower, either directly via the neutral-current interaction of ν_τ with matter or indirectly via the decay of a τ lepton produced from the charged-current interaction of ν_τ with matter. UHE ν_τ neutrinos will therefore cascade down to the PeV level at which the Earth is essentially transparent.

A km^3-scale neutrino telescope is in general designed to detect cosmic neutrinos of all possible energies above $\mathcal{O}(10^2)$ GeV. It actually detects the secondary particle showers initiated by neutrinos of all flavors as well as the leading secondary muon tracks initiated only by muon neutrinos (Halzen, 2006b). Let us briefly describe how to identify different neutrino flavors at the IceCube (or KM3NeT) detector.

(1) *Identification of electron neutrinos.* High-energy electron neutrinos can only deposit $\lesssim 1\%$ of their energy into an electromagnetic shower initiated by the leading final-state electrons (e.g., $\nu_e + n \to p + e^-$) (Halzen, 2006a) [4]. The rest of their energy goes into the fragments of the targets which produce a second subdominant shower. The span of the electromagnetic shower is only a few meters in ice or water, much smaller than the horizontal spacing of the DOMs ($\sim$ 125 m). Hence such a shower approximates to a point-like source of Cherenkov photons radiated by its charged particles. These Cherenkov photons trigger the DOM at the single photoelectron level over a spherical volume whose radius scales up with the shower energy (Halzen, 2006a), as illustrated in Fig. 8.5. A measurement of the radius of this sphere in the lattice of DOMs can then be used to determine the energy of the incident electron neutrinos. Because the shower itself and its accompanying Cherenkov lightpool are not completely symmetric but elongated in the direction of the leading electron, the direction of the incident neutrino can then be reconstructed to a reasonable degree of accuracy (with an error bar $\lesssim 10^\circ$) (Halzen, 2006b).

[4] For high-energy electron antineutrinos, $\overline{\nu}_e + p \to n + e^+$ and other similar charged-current interactions take place in the detector. One may therefore identify ν_e and $\overline{\nu}_e$ events by observing e^- and e^+ events, respectively.

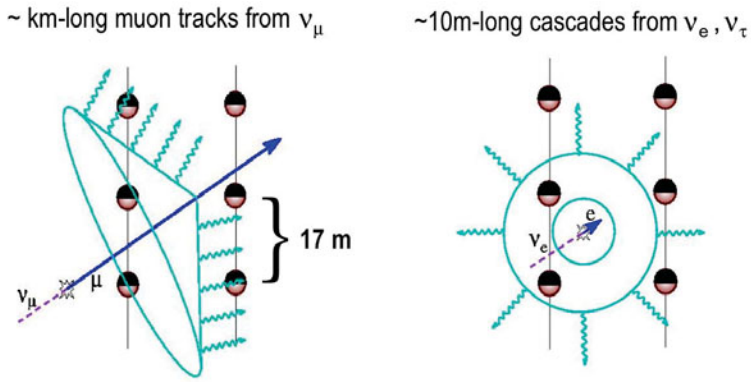

Fig. 8.5 Cherenkov light patterns produced by muons (left) and by secondary showers initiated by electron and tau neutrinos (right) in IceCube (Halzen, 2006b. With permission from Springer Science+Business Media)

(2) *Identification of muon neutrinos.* The secondary muons initiated by the incident muon neutrinos may range over a few kilometers when $E_\nu \sim \mathcal{O}(1)$ TeV and tens of kilometers when $E_\nu \sim \mathcal{O}(1)$ EeV, generating showers along their tracks by bremsstrahlung, pair production and photonuclear interactions (Halzen, 2006a). These are the sources of Cherenkov radiation and can be detected in the same way as that for high-energy electron neutrinos discussed above. Since the energy of the muon degrades along its track, the energy of the secondary showers decreases and thus the distance from the track over which the associated Cherenkov light can trigger a DOM becomes smaller and smaller. The geometric pattern of the Cherenkov lightpool surrounding the muon track is therefore a kilometer-long cone whose radius gradually decreases, as shown in Fig. 8.5. For the first kilometer, a high-energy muon typically loses about one tenth of its initial energy in a couple of showers. Hence the initial size of the cone is the radius of a shower with about 10% of the muon energy (e.g., about 130 m for an 100 TeV muon) (Halzen, 2006b). Near the end of its range the muon becomes minimum ionizing and emits light which creates single photoelectron signals at a distance of just over 10 m from the track. Because of the stochastic nature of muon energy loss, only the logarithm of the muon energy can be measured. Although UHE muons initiated by the incident UHE muon neutrinos have ranges of tens of kilometers, the initial energies of their events cannot always be measured. A muon can be produced at one energy, travel several kilometers and then be detected with another (much lower) energy (Halzen, 2006b).

(3) *Identification of tau neutrinos.* Relative to electron and muon neutrinos, the production rate of tau neutrinos from a cosmic accelerator is suppressed by about five orders of magnitude. But the detection of UHE tau neutrinos at a neutrino telescope makes sense because nearly half of the UHE

muon neutrinos can actually convert over cosmic distances into tau neutrinos as a consequence of neutrino oscillations. On the other hand, an UHE tau neutrino beam is not absorbed by the Earth due to its "regeneration" effect. Hence it can always reach the detector in spite of some energy loss. There are several ways to identify the flavor of UHE tau neutrinos in a km^3-scale neutrino telescope. The most striking signature comes from the characteristic double-bang events, in which the production and decay of a tau are detected as two separated showers inside the detector (Learned and Pakvasa, 1995; Gaisser *et al.*, 1995). It is also possible to identify the "lollipop" events in which a tau neutrino creates a long minimum-ionizing track that penetrates the detector and ends in a high-energy cascade when the tau decays (Halzen, 2006b). The parent tau track can then be identified by the reduced catastrophic energy loss compared with a muon track with the similar energy. To identify a double-bang event in the IceCube or KM3NeT detector, the following conditions have to be satisfied (Halzen, 2006b): (a) the incident tau neutrino has to interact with ice or water via the charged-current interactions, producing a hadronic shower contained inside or close to the instrumented volume; (b) the produced tau must decay inside the detector into a final state which can generate an electromagnetic or hadronic shower contained inside the device; (c) the travel distance of the tau (before it decays) has to be sufficiently long such that the two showers can be clearly separated; and (d) the showers must be sufficiently energetic to trigger the DOMs.

8.2.3 Other Ways to Detect UHE Neutrinos

Besides the optical detection of UHE cosmic neutrinos in ice and water, some other techniques have been developed to measure the low-flux tails of UHE cosmic neutrino spectra (see Fig. 8.4 for illustration).

(1) *Radio detection of neutrino-induced air showers.* Electromagnetic cascades produced by the interactions of high-energy electron neutrinos can emit strong coherent Cherenkov radiation in any dielectric medium, the so-called Askaryan effect (Askaryan, 1962, 1965) which was first observed in 2001 (Saltzberg *et al.*, 2001). The signal strength rises proportionally to E_ν^2, making this method particularly interesting for detecting UHE cosmic neutrinos. In ice or salt domes, attenuation lengths of several kilometers can be reached with the radio detection technique, depending on the frequency band, ice temperature or salt quality (Avignone *et al.*, 2008). This allows large spacing between the individual detectors and a comparatively cheap extension to large volumes. Hence radio detection in ice or salt may be competitive with or superior to optical detection for $E_\nu \gtrsim \mathcal{O}(10)$ PeV. The ANITA Long Duration Balloon experiment was designed specifically to search for cosmic neutrinos above $E_\nu \sim 10^{17}$ eV in an Antarctic circumpolar flight (Barwick *et al.*, 2006). At a typical altitude of about 35 km above the ice surface, the ANITA detector is able to record radio impulses in the thick ice sheet and monitor a huge volume ($\sim 1.6 \times 10^6$ km^3). ANITA's antennas are 32

quad-ridged dual-linear-polarization horns, each with a field of view which averages about 50° angular diameter over their $(0.2 \cdots 1.2) \times 10^9$ Hz working bandwidth. The combined view of all antennas covers the entire lower hemisphere down to angles of about 55°, comprising 99.4% of the area within the horizon (Gorham *et al.*, 2009). Some initial results from ANITA's first 35-day flight have recently been reported, but no evidence for a diffuse flux of cosmic neutrinos above $E_\nu \approx 3 \times 10^{18}$ eV is found (Gorham *et al.*, 2009).

(2) *Acoustic detection of neutrino-induced showers in water, ice or salt.* This promising technique, based on Gurgen Askaryan's observation that an interacting neutrino can emit a thin thermoacoustic pancake normal to the shower axis (Askaryan, 1962, 1965), remains in its R&D phase. It relies on the ionization loss in high-energy particle cascades transforming into heat, and the subsequent fast expansion of the medium leads to a short acoustic pulse (Avignone *et al.*, 2008). The signal power spectrum peaks at 20 kHz, where the attenuation length of sea water or ice is expected to be a few kilometers. Such a large theoretical attenuation length has not been experimentally demonstrated, but it makes this method attractive for the detection of extremely energetic cosmic neutrinos (in the EeV region) because large detector spacing is mandatory in order to achieve a huge detection volume necessary for a low neutrino flux. Open key issues include the signal strength and natural background levels (Podgorski and Ribordy, 2010). Acoustic detectors might be deployed to surround the optical detectors of KM3NeT in the Mediterranean sea and enhance its sensitivity to much higher energies, but radio does not work in salt water. For IceCube, a hybrid scheme consisting of optical, radio and acoustic detection facilities has been proposed (Vandenbroucke *et al.*, 2006; Avignone *et al.*, 2008) and its total volume will be of $\mathcal{O}(10^2)$ km^3.

(3) *Optical detection of neutrino-induced air showers.* This technique can be used to measure horizontal air showers initiated by neutrino interactions deep in the atmosphere. A large air shower detector (e.g., Auger) is able to probe cosmic neutrinos in the energy range 0.1 EeV $\lesssim E_\nu \lesssim$ 1 EeV. If the effective detector mass is sufficiently large (e.g., more than 20 gigatons), it is possible to detect UHE tau neutrinos scratching the Earth and interacting close to the detector array (Avignone *et al.*, 2008). They are known as the Earth-skimming neutrinos (Feng *et al.*, 2002; Fargion, 2002). An extremely energetic tau produced in such interactions may escape the rock, and the particle cascade produced by its decay in the atmosphere above the detector array can then be recorded. When E_ν approaches its maximum, one is led to the space-based detectors monitoring larger volumes than visible from any point on the Earth's surface. The EUSO project has been proposed to launch large mirrors with optical detectors to the height of 500 km on the International Space Station and search for fluorescence and Cherenkov light signals arising from UHE neutrino interactions in the atmosphere (Agnetta, 2006). On the other hand, one may simply consider to apply the techniques

of air shower fluorescence and Cherenkov light detectors with the help of a mountain or the Earth's crust. The CRTNT project has therefore been proposed to detect the Earth-skimming UHE tau neutrinos (Cao *et al.*, 2005). Both projects are at present suspended, unfortunately.

It is finally worth mentioning a Chinese version of the CRTNT (cosmic ray tau neutrino telescope) project (Liu *et al.*, 2009). Such a telescope is assumed to be located at the foothill of Mt Balikun in Xinjiang, China. The site is sufficiently dry throughout the year and the mountain is reasonably thick and sufficiently steep, suitable for detecting the Earth-skimming UHE tau neutrinos by means of air shower fluorescence and Cherenkov light detectors. Because of their charged-current interactions with the rock, the incident UHE cosmic neutrinos may convert into charged leptons inside the mountain. The electrons can quickly shower in the rock, while the muons may travel a very long distance before decaying. Hence both of them are difficult to be detected using this method. The taus produced inside the mountain may have a sufficiently long lifetime to escape from the mountain, and then decay and induce air showers in the air near the mountain. For the time being it remains unclear whether the CRTNT project in China has a bright prospect or not.

8.3 Flavor Distribution of UHE Cosmic Neutrinos

On the way from a distant astrophysical source to a telescope on the Earth, the flavors of UHE cosmic neutrinos must oscillate many times. A measurement of the flavor distribution of UHE cosmic neutrinos at a telescope can therefore probe their initial flavor composition, which is closely associated with the source properties, or examine the effects of neutrino mixing and CP violation in such ultralong-baseline neutrino oscillations. In principle, it is also possible to use the flavor oscillations of UHE neutrinos to test some fundamental symmetries (e.g., CPT invariance) or explore some "exotic" properties of neutrinos (e.g., neutrino decays).

8.3.1 Flavor Issues of UHE Neutrinos

Given the initial UHE cosmic neutrino fluxes $\Phi = \{\phi_e, \phi_\mu, \phi_\tau\}$ at a distant astrophysical source, its flavor components are defined as $\phi_\alpha = \phi_{\nu_\alpha} + \phi_{\overline{\nu}_\alpha}$ (for $\alpha = e, \mu, \tau$), where ϕ_{ν_α} and $\phi_{\overline{\nu}_\alpha}$ denote the ν_α and $\overline{\nu}_\alpha$ fluxes, respectively. At a neutrino telescope one may similarly define the fluxes $\Phi^{\rm T} = \{\phi_e^{\rm T}, \phi_\mu^{\rm T}, \phi_\tau^{\rm T}\}$ with $\phi_\alpha^{\rm T} = \phi_{\nu_\alpha}^{\rm T} + \phi_{\overline{\nu}_\alpha}^{\rm T}$ (for $\alpha = e, \mu, \tau$). The relation between ϕ_{ν_α} (or $\phi_{\overline{\nu}_\alpha}$) and $\phi_{\nu_\alpha}^{\rm T}$ (or $\phi_{\overline{\nu}_\alpha}^{\rm T}$) is given by

$$\begin{aligned} \phi_{\nu_\beta}^{\rm T} &= \sum_\alpha \phi_{\nu_\alpha} P(\nu_\alpha \to \nu_\beta) \; , \\ \phi_{\overline{\nu}_\beta}^{\rm T} &= \sum_\alpha \phi_{\overline{\nu}_\alpha} P(\overline{\nu}_\alpha \to \overline{\nu}_\beta) \; , \end{aligned} \tag{8.6}$$

where $P(\nu_\alpha \to \nu_\beta)$ and $P(\overline{\nu}_\alpha \to \overline{\nu}_\beta)$ stand respectively for the probabilities of $\nu_\alpha \to \nu_\beta$ and $\overline{\nu}_\alpha \to \overline{\nu}_\beta$ oscillations. As the cosmological distances far exceed the observed neutrino oscillation lengths, $P(\nu_\alpha \to \nu_\beta)$ and $P(\overline{\nu}_\alpha \to \overline{\nu}_\beta)$ are actually averaged over many oscillations and take a very simple form:

$$\langle P(\nu_\alpha \to \nu_\beta) \rangle = \langle P(\overline{\nu}_\alpha \to \overline{\nu}_\beta) \rangle = \sum_i |V_{\alpha i}|^2 |V_{\beta i}|^2 \; , \tag{8.7}$$

as already shown in Eq. (5.6), where $V_{\alpha i}$ and $V_{\beta i}$ (for $i = 1, 2, 3$ and $\alpha, \beta = e, \mu, \tau$) denote the elements of the neutrino mixing matrix V. Eqs. (8.6) and (8.7) lead us to a straightforward relation between ϕ_α and $\phi^{\rm T}_\beta$:

$$\phi^{\rm T}_\beta \; = \; \sum_\alpha \sum_i |V_{\alpha i}|^2 |V_{\beta i}|^2 \phi_\alpha \; . \tag{8.8}$$

The unitarity of V assures a sum rule $\phi^{\rm T}_e + \phi^{\rm T}_\mu + \phi^{\rm T}_\tau = \phi_e + \phi_\mu + \phi_\tau \equiv \phi_0$.

For most of the astrophysical sources which are able to produce UHE neutrinos via the decays of charged pions (and kaons) followed by the decays of muons, we expect $\phi_e : \phi_\mu : \phi_\tau = 1 : 2 : 0$ to hold. This flavor ratio is only approximate in practice, not only because the production of ν_τ and $\overline{\nu}_\tau$ events is not purely suppressed but also because the sizes of ϕ_e and ϕ_μ may depend on the very details of a source model (e.g., the energy spectrum of UHE neutrinos at the source). A careful estimate yields $\phi_e : \phi_\mu : \phi_\tau \approx 1 : 1.86 : x$ with $x \lesssim 0.001$ (Lipari *et al.*, 2007; Pakvasa *et al.*, 2008). For the postulated neutron beam source (Anchordoqui *et al.*, 2004; Crocker *et al.*, 2005), however, $\phi_e : \phi_\mu : \phi_\tau = 1 : 0 : 0$ might approximately hold; and for a possible muon-damped source (Rachen and Meszaros, 1998; Kashti and Waxman, 2005), one has $\phi_e : \phi_\mu : \phi_\tau = 0 : 1 : 0$ as a good approximation. As for the "GZK neutrinos" produced via the dominant $p + \gamma_{\rm CMB} \to \Delta^+ \to n + \pi^+$ process, one expects $\phi_e : \phi_\mu : \phi_\tau = 1 : 0 : 0$ when the neutrino energy is below about 100 PeV and the neutron decays dominate the neutrino production; or $\phi_e : \phi_\mu : \phi_\tau = 1 : 2 : 0$ when the neutrino energy is above about 100 PeV and the pion decays dominate the neutrino production (Engel *et al.*, 2001; Pakvasa, 2008). To universally describe the flavor content of UHE cosmic neutrinos at different sources, we propose a simple parametrization of their initial fluxes as (Xing and Zhou, 2006)

$$\phi_e = \phi_0 \sin^2\xi \cos^2\zeta \; , \quad \phi_\mu = \phi_0 \cos^2\xi \cos^2\zeta \; , \quad \phi_\tau = \phi_0 \sin^2\zeta \; , \tag{8.9}$$

where $\xi \in [0, \pi/2]$ and $\zeta \in [0, \pi/2]$, and $\phi_0 = \phi_e + \phi_\mu + \phi_\tau$ denotes the total flux. Then the conventional flux ratio $\phi_e : \phi_\mu : \phi_\tau = 1 : 2 : 0$ corresponds to $\xi = \arctan(1/\sqrt{2}) \approx 35.3^\circ$ and $\zeta = 0^\circ$. Of course, ξ and ζ take different values for other aforementioned sources.

At a neutrino telescope three *working* observables, which are largely free from the systematic uncertainties associated with the measurements of $\phi^{\rm T}_\alpha$

(for $\alpha = e, \mu, \tau$), can be defined as $R_\alpha \equiv \phi_\alpha^{\rm T}/(\phi_\beta^{\rm T} + \phi_\gamma^{\rm T})$, where α, β, γ run over e, μ, τ cyclically. Since R_e, R_μ and R_τ satisfy

$$\frac{R_e}{1+R_e} + \frac{R_\mu}{1+R_\mu} + \frac{R_\tau}{1+R_\tau} \; = \; 1 \; , \tag{8.10}$$

only two of them are independent. Without loss of generality, we choose R_e and R_μ as two typical observables and derive their explicit relations with ξ and ζ. Substituting Eqs. (8.8) and (8.9) into Eq. (8.10), we obtain

$$\begin{aligned} R_e &= \frac{P_{ee} \sin^2\xi + P_{\mu e} \cos^2\xi + P_{\tau e} \tan^2\zeta}{\sec^2\zeta - \left[P_{ee} \sin^2\xi + P_{\mu e} \cos^2\xi + P_{\tau e} \tan^2\zeta\right]} \; , \\ R_\mu &= \frac{P_{e\mu} \sin^2\xi + P_{\mu\mu} \cos^2\xi + P_{\tau\mu} \tan^2\zeta}{\sec^2\zeta - \left[P_{e\mu} \sin^2\xi + P_{\mu\mu} \cos^2\xi + P_{\tau\mu} \tan^2\zeta\right]} \; , \end{aligned} \tag{8.11}$$

where $P_{\alpha\beta} \equiv |V_{\alpha 1}|^2 |V_{\beta 1}|^2 + |V_{\alpha 2}|^2 |V_{\beta 2}|^2 + |V_{\alpha 3}|^2 |V_{\beta 3}|^2$ (for $\alpha, \beta = e, \mu, \tau$). The source flavor parameters ξ and ζ turn out to be (Xing and Zhou, 2006)

$$\begin{aligned} \sin^2\xi &= \frac{r_e (P_{\tau\mu} - P_{\mu\mu}) - r_\mu (P_{\tau e} - P_{\mu e}) + (P_{\mu\mu} P_{\tau e} - P_{\mu e} P_{\tau\mu})}{(r_e - P_{\tau e})(P_{e\mu} - P_{\mu\mu}) - (r_\mu - P_{\tau\mu})(P_{ee} - P_{\mu e})} \; , \\ \tan^2\zeta &= \frac{r_e (P_{\mu\mu} - P_{e\mu}) - r_\mu (P_{\mu e} - P_{ee}) + (P_{e\mu} P_{\mu e} - P_{ee} P_{\mu\mu})}{(r_e - P_{\tau e})(P_{e\mu} - P_{\mu\mu}) - (r_\mu - P_{\tau\mu})(P_{ee} - P_{\mu e})} \; , \end{aligned} \tag{8.12}$$

where $r_e \equiv \phi_e^{\rm T}/\phi_0 = R_e/(1+R_e)$ and $r_\mu \equiv \phi_\mu^{\rm T}/\phi_0 = R_\mu/(1+R_\mu)$ have been used to simplify the expressions. One may in principle choose either (R_e, R_μ) or (r_e, r_μ) as a set of working observables to inversely determine ξ and ζ. In the standard parametrization of V shown in Eq. (3.107), the magnitudes of $P_{\alpha\beta}$ depend on three mixing angles $(\theta_{12}, \theta_{13}, \theta_{23})$ and one CP-violating phase (δ). So R_e and R_μ totally rely on six parameters. One may make two arguments on flavor physics at a neutrino telescope:

- If θ_{12}, θ_{13}, θ_{23} and δ are known to a good degree of accuracy, then a measurement of R_e and R_μ will help determine or constrain the initial flavor composition of UHE cosmic neutrinos for a given astrophysical source (Xing and Zhou, 2006; Choubey and Rodejohann, 2009; Lai *et al.*, 2009).
- If the production mechanism and flavor distribution of UHE neutrinos at an astrophysical source have been understood, then a measurement of R_e and R_μ will help probe the neutrino mixing pattern and CP violation (Serpico and Kachelrieß, 2005; Serpico, 2006; Xing, 2006; Winter, 2006; Rodejohann, 2007; Xing, 2007; Blum *et al.*, 2007; Choubey *et al.*, 2008).

In the following we illustrate the second point by taking a simple example.

Let us focus on a conventional astrophysical source of UHE cosmic neutrinos with the ideal flavor ratio $\phi_e : \phi_\mu : \phi_\tau = 1 : 2 : 0$. Because of neutrino oscillations, the flavor ratio at a neutrino telescope can be calculated by

means of Eq. (8.8). It is easy to show that the flavor distribution at the telescope may have a democratic pattern $\phi_e^{\rm T} : \phi_\mu^{\rm T} : \phi_\tau^{\rm T} = 1 : 1 : 1$, provided the condition $|V_{\mu i}| = |V_{\tau i}|$ (for $i = 1, 2, 3$) or equivalently the μ-τ symmetry is satisfied (Xing and Zhou, 2008). This condition corresponds to either $\theta_{13} = 0$ and $\theta_{23} = \pi/4$ (CP invariance) or $\delta = \pm\pi/2$ and $\theta_{23} = \pi/4$ (CP violation) in the standard parametrization of V. Current neutrino oscillation data indicate that θ_{13} is very small and θ_{23} is close to $\pi/4$, and thus V exhibits an approximate μ-τ symmetry. In this case we use two small parameters θ_{13} and $\varepsilon \equiv \theta_{23} - \pi/4$ to describe the small effects of μ-τ symmetry breaking:

$$\begin{bmatrix} |V_{e1}|^2 & |V_{e2}|^2 & |V_{e3}|^2 \\ |V_{\mu 1}|^2 & |V_{\mu 2}|^2 & |V_{\mu 3}|^2 \\ |V_{\tau 1}|^2 & |V_{\tau 2}|^2 & |V_{\tau 3}|^2 \end{bmatrix} = \frac{1}{2} \begin{bmatrix} 2c_{12}^2 & 2s_{12}^2 & 0 \\ s_{12}^2 & c_{12}^2 & 1 \\ s_{12}^2 & c_{12}^2 & 1 \end{bmatrix} + \varepsilon \begin{bmatrix} 0 & 0 & 0 \\ -s_{12}^2 & -c_{12}^2 & 1 \\ s_{12}^2 & c_{12}^2 & -1 \end{bmatrix} + \frac{\theta_{13}}{2} \sin 2\theta_{12} \cos\delta \begin{bmatrix} 0 & 0 & 0 \\ 1 & -1 & 0 \\ -1 & 1 & 0 \end{bmatrix} + \cdots \; , \tag{8.13}$$

where $c_{12} \equiv \cos\theta_{12}$, $s_{12} \equiv \sin\theta_{12}$, and higher-order terms of θ_{13} and ε have been omitted. Substituting Eq. (8.13) into Eq. (8.8), we arrive at (Xing, 2006)

$$\phi_e^{\rm T} : \phi_\mu^{\rm T} : \phi_\tau^{\rm T} = (1 - 2\Delta) : (1 + \Delta) : (1 + \Delta) \; , \tag{8.14}$$

where $\Delta = (2\varepsilon \sin^2 2\theta_{12} - \theta_{13} \sin 4\theta_{12} \cos\delta)/4$ compatible with the approximation made in Eq. (8.13). It is obvious that the naive flavor democracy is broken as a direct consequence of μ-τ symmetry breaking. Given $30^\circ < \theta_{12} < 38^\circ$, $\theta_{13} < 10^\circ$ (≈ 0.17) and $|\varepsilon| < 9^\circ$ (≈ 0.16) as indicated by current experimental data (see Section 3.1.5), we find $-0.1 \lesssim \Delta \lesssim +0.1$ by allowing δ to vary from 0 to 2π. The working observables R_e, R_μ and R_τ defined above Eq. (8.10) for a neutrino telescope turn out to be

$$R_e \approx \frac{1}{2} - \frac{3}{2}\Delta \; , \quad R_\mu \approx R_\tau \approx \frac{1}{2} + \frac{3}{4}\Delta \; . \tag{8.15}$$

So R_e is most sensitive to the effect of μ-τ symmetry breaking.

One may also consider to probe the breaking of μ-τ symmetry by detecting the $\overline{\nu}_e$ flux from a distant astrophysical source through the Glashow resonance (GR) channel $\overline{\nu}_e + e \to W^- \to$ anything (Glashow, 1960). The latter can actually take place over a narrow energy interval around the $\overline{\nu}_e$ energy $E_{\overline{\nu}_e}^{\rm GR} \approx M_W^2/2m_e \approx 6.3$ PeV. A neutrino telescope is in principle possible to measure both the GR-mediated $\overline{\nu}_e$ events ($N_{\overline{\nu}_e}^{\rm GR}$) and the $\nu_\mu + \overline{\nu}_\mu$ events of charged-current (CC) interactions ($N_{\nu_\mu + \overline{\nu}_\mu}^{\rm CC}$) in the vicinity of $E_{\overline{\nu}_e}^{\rm GR}$. Their ratio, defined as $R_{\rm GR} \equiv N_{\overline{\nu}_e}^{\rm GR}/N_{\nu_\mu + \overline{\nu}_\mu}^{\rm CC}$, can be related to the ratio of $\overline{\nu}_e$ events to ν_μ and $\overline{\nu}_\mu$ events entering the detector, $R_0 \equiv \phi_{\overline{\nu}_e}^{\rm T}/(\phi_{\nu_\mu}^{\rm T} + \phi_{\overline{\nu}_\mu}^{\rm T})$. One obtains $R_{\rm GR} = aR_0$ with $a \approx 30.5$ (Bhattacharjee and Gupta, 2005) by considering the muon events with contained vertices in a water- or ice-based

detector (Beacom *et al.*, 2003a). Provided the neutrinos are initially produced via the decays of charged pions created from high-energy pp or $p\gamma$ collisions at an optically thin source, their flavor composition can be expressed as follows: $\{\phi_{\nu_e},\ \phi_{\overline{\nu}_e},\ \phi_{\nu_\mu},\ \phi_{\overline{\nu}_\mu},\ \phi_{\nu_\tau},\ \phi_{\overline{\nu}_\tau}\} = \{1/6,\ 1/6,\ 1/3,\ 1/3,\ 0,\ 0\}\phi_0$ (for pp collisions) or $\{1/3,\ 0,\ 1/3,\ 1/3,\ 0,\ 0\}\phi_0$ (for $p\gamma$ collisions). In either case $\phi_e : \phi_\mu : \phi_\tau = 1 : 2 : 0$ holds. Due to neutrino oscillations, the $\overline{\nu}_e$ flux detected at a neutrino telescope reads (Xing, 2006, 2008)

$$\phi^{\rm T}_{\overline{\nu}_e}(pp) = \frac{\phi_0}{6}\left(1 - 2\Delta\right) \ , \qquad \phi^{\rm T}_{\overline{\nu}_e}(p\gamma) = \frac{\phi_0}{12}\left(\sin^2 2\theta_{12} - 4\Delta\right) \ , \tag{8.16}$$

where Δ has been given below Eq. (8.14). In addition, we have $\phi^{\rm T}_{\nu_\mu} + \phi^{\rm T}_{\overline{\nu}_\mu} \approx \phi_0(1 + \Delta)/3$. It is then straightforward to obtain

$$R_0(pp) \approx \frac{1}{2} - \frac{3}{2}\Delta \ , \qquad R_0(p\gamma) \approx \frac{\sin^2 2\theta_{12}}{4} - \frac{4 + \sin^2 2\theta_{12}}{4}\Delta \ . \tag{8.17}$$

This result indicates that $R_0(p\gamma)$ is very sensitive to the value of $\sin^2 2\theta_{12}$ (Anchordoqui *et al.*, 2005), and the effect of μ-τ symmetry breaking shows up in both $R_0(p\gamma)$ and $R_0(pp)$.

8.3.2 Flavor Effects in New Physics Scenarios

Some "exotic" scenarios of new physics, such as quantum decoherence, CPT violation, neutrino decays, sterile neutrinos and non-unitarity of the 3×3 neutrino mixing matrix V, may also affect the flavor oscillations of UHE cosmic neutrinos for a given source.

(1) *Quantum decoherence.* In some models of quantum gravity the phenomenon of spacetime "foam" may be incorporated and the singular microscopic fluctuations of the metric give the ground state of quantum gravity the structure of a "stochastic medium" (Barenboim *et al.*, 2006). Such a medium has the profound effect of CPT-violating decoherence of quantum matter as it propagates. A striking consequence of gravitational decoherence on neutrino oscillations is the exponential damping of oscillatory terms with time or distances. In a generic Lindblad decoherence model the probabilities of $\nu_\alpha \to \nu_\beta$ oscillations can be written as (Barenboim *et al.*, 2006)

$$P(\nu_\alpha \to \nu_\beta) = \frac{1}{3} + \sum_i O_i {\rm e}^{-\mathcal{D}_i L} \ , \tag{8.18}$$

where O_i denotes an oscillatory term modified by quantum decoherence, $\mathcal{D}_i$ is the corresponding decoherence parameter which can be either a constant or a function of energy, and L represents the travel distance of neutrinos. For UHE cosmic neutrinos from a very distant source (i.e., $L \to \infty$), one is left with $P(\nu_\alpha \to \nu_\beta) = 1/3$ under complete quantum decoherence and thus

$\phi^{\rm T}_\beta = \phi_0/3$ or $\phi^{\rm T}_e : \phi^{\rm T}_\mu : \phi^{\rm T}_\tau = 1 : 1 : 1$ at a neutrino telescope regardless of their initial flavor composition (Liu *et al.*, 1997; Ahluwalia, 2001; Hooper *et al.*, 2005). This result mimics the one obtained in Section 8.3.1 from a specific astrophysical source with $\phi_e : \phi_\mu : \phi_\tau = 1 : 2 : 0$ and under the exact μ-τ symmetry. To search for possible evidence for quantum decoherence in UHE cosmic neutrino oscillations, one should consider an astrophysical source which has a different flavor content (e.g., $\phi_e : \phi_\mu : \phi_\tau = 1 : 0 : 0$ from the beta decay of neutrons) (Hooper *et al.*, 2005; Pakvasa, 2008).

(2) *CPT violation.* In a theory with spontaneous CPT violation (Colladay and Kostelecký, 1997), its Lagrangian may contain the vector- and pseudovector-like spinor bilinears $\overline{\psi}\gamma_\mu\psi$ and $\overline{\psi}\gamma_\mu\gamma_5\psi$ which are apparently CPT-odd as shown in Table 3.5. An effective CPT- and Lorentz-violating operator contributing to the neutrino sector can be parametrized as $\mathcal{O}_\nu = \overline{\nu}_{\alpha\rm L} C^{\alpha\beta}_\mu \gamma^\mu \nu_{\beta\rm L}$, where α and β run over e, μ and τ, and $C^{\alpha\beta}_\mu$ are real coefficients (Dighe and Ray, 2008). This operator can modify the dispersion relation of neutrinos and the effective Hamiltonian responsible for their propagation. Hence the behaviors of UHE cosmic neutrino oscillations get modified:

$$\langle P(\nu_\alpha \to \nu_\beta)\rangle = \langle P(\overline{\nu}_\alpha \to \overline{\nu}_\beta)\rangle = \sum_i |V'_{\alpha i}|^2 |V'_{\beta i}|^2 \; , \tag{8.19}$$

where V' is the effective neutrino mixing matrix which depends on both V and C_μ (Bustamante *et al.*, 2010). Given a conventional source of UHE cosmic neutrinos with $\phi_e : \phi_\mu : \phi_\tau = 1 : 2 : 0$, CPT violation has a large room to modify the flavor democracy $\phi^{\rm T}_e : \phi^{\rm T}_\mu : \phi^{\rm T}_\tau = 1 : 1 : 1$ at a neutrino telescope (Barenboim and Quigg, 2003; Bustamante *et al.*, 2010).

(3) *Unitarity violation.* In some seesaw models in which there exists the mixing between three light neutrinos and a few heavy degrees of freedom (e.g., heavy Majorana neutrinos) as discussed in Chapter 4, the 3×3 neutrino mixing matrix V must be non-unitary. The strength of unitarity violation can be of $\mathcal{O}(10^{-2})$ if a seesaw model works at the TeV scale (Xing, 2009), and thus it may show up in UHE cosmic neutrino oscillations. Following the parametrization of V given in Section 4.5.2, we consider a simple pattern of V which slightly deviates from the tri-bimaximal neutrino mixing pattern V_0 given in Eq. (3.110) (Xing and Zhou, 2008):

$$V \approx V_0 - \begin{pmatrix} \frac{2}{\sqrt{6}} W_1 & \frac{1}{\sqrt{3}} W_1 & 0 \\ \frac{1}{\sqrt{6}} (2X - W_2) & \frac{1}{\sqrt{3}} (X + W_2) & \frac{1}{\sqrt{2}} W_2 \\ \frac{1}{\sqrt{6}} (2Y - Z + W_3) & \frac{1}{\sqrt{3}} (Y + Z - W_3) & \frac{1}{\sqrt{2}} (Z + W_3) \end{pmatrix} \; , \tag{8.20}$$

where $W_i = (s^2_{i4} + s^2_{i5} + s^2_{i6})/2$ (for $i = 1, 2, 3$), $X = \hat{s}_{14}\hat{s}^*_{24} + \hat{s}_{15}\hat{s}^*_{25} + \hat{s}_{16}\hat{s}^*_{26}$, $Y = \hat{s}_{14}\hat{s}^*_{34} + \hat{s}_{15}\hat{s}^*_{35} + \hat{s}_{16}\hat{s}^*_{36}$ and $Z = \hat{s}_{24}\hat{s}^*_{34} + \hat{s}_{25}\hat{s}^*_{35} + \hat{s}_{26}\hat{s}^*_{36}$ with $s_{ij} \equiv \sin\theta_{ij}$ and $\hat{s}_{ij} \equiv {\rm e}^{{\rm i}\delta_{ij}} s_{ij}$ being defined. The mixing angles θ_{ij} can at most be of $\mathcal{O}(0.1)$, but the CP-violating phases δ_{ij} are entirely unrestricted. Now we look at the oscillations of UHE cosmic neutrinos coming from a conventional

astrophysical source with $\phi_e : \phi_\mu : \phi_\tau = 1 : 2 : 0$. With the help of Eq. (8.8), we arrive at (Xing and Zhou, 2008)

$$\begin{aligned}
\phi_e^{\rm T} &\equiv \frac{\phi_0}{3}\left[1 - \frac{4}{9}\left(7W_1 + 2W_2\right) + \frac{4}{9}{\rm Re}X\right] , \\
\phi_\mu^{\rm T} &\equiv \frac{\phi_0}{3}\left[1 - \frac{4}{9}\left(W_1 + 8W_2\right) - \frac{2}{9}{\rm Re}X\right] , \\
\phi_\tau^{\rm T} &\equiv \frac{\phi_0}{3}\left[1 - \frac{2}{9}\left(2W_1 + 7W_2 + 9W_3\right) - \frac{2}{9}{\rm Re}X\right] ,
\end{aligned} \tag{8.21}$$

at a neutrino telescope. The flavor democracy of $\phi_\alpha^{\rm T}$ (for $\alpha = e, \mu, \tau$) is clearly broken, and the effect of this symmetry breaking can be as large as several percent. Because of the non-unitarity of V, the total flux of UHE cosmic neutrinos at the telescope is not equal to that at the source:

$$\sum_\alpha \phi_\alpha^{\rm T} = \phi_0\left[1 - \frac{2}{3}\left(2W_1 + 3W_2 + W_3\right)\right] . \tag{8.22}$$

This sum approximately amounts to $0.96\phi_0$ if $W_i \sim 0.01$ (for $i = 1, 2, 3$). The non-unitarity of V is very small and certainly difficult to be observed in a realistic experiment, but Eqs. (8.21) and (8.22) can at least illustrate how sensitive a neutrino telescope should be to this kind of new physics.

(4) *Neutrino decays.* Now that neutrinos have finite masses and lepton flavors are mixed, the heavier neutrinos are in general expected to decay into the lighter ones via the flavor-changing channels. But one may wonder (a) whether the lifetimes of neutrinos are short enough to be phenomenologically interesting and (b) what the dominant decay modes are (Pakvasa, 2000). Radiative neutrino decays are less interesting in this sense, whereas the "exotic" decays $\nu_i \to \nu_j + \chi$ with χ being a Majoron (Chikashige *et al.*, 1981; Gelmini and Roncadelli, 1981) or unparticle (Zhou, 2008) might be suggestive and interesting. Regardless of any details of model building and other astrophysical implications, here we focus on the flavor issues of unstable UHE cosmic neutrinos. Given a neutrino mass eigenstate ν_i, a characteristic feature of its decay is the strong energy dependence: $\exp(-t/\tau_{\rm lab})$ with $\tau_{\rm lab} = \tau_0 E/m_i$, where τ_0, m_i, E, t and L denote the rest-frame lifetime of ν_i, its mass, its energy, its travel time and its travel distance, respectively (Beacom *et al.*, 2003b). For simplicity, we only consider the case that the decays are complete (i.e., such exponential factors vanish) for UHE cosmic neutrinos on their way from a distant astrophysical source to a neutrino telescope on the Earth. In this case only the lightest neutrinos arrive at the Earth (Farzan and Smirnov, 2002). If the neutrino mass spectrum has a normal hierarchy, the lightest neutrino is $\nu_1 = V_{e1}^* \nu_e + V_{\mu 1}^* \nu_\mu + V_{\tau 1}^* \nu_\tau$ and thus the flavor ratio at the telescope is

$$\phi_e^{\rm T} : \phi_\mu^{\rm T} : \phi_\tau^{\rm T} = |V_{e1}|^2 : |V_{\mu 1}|^2 : |V_{\tau 1}|^2 , \tag{8.23}$$

independent of the initial flavor composition at the source. Given the inverted neutrino mass hierarchy, the lightest neutrino is $\nu_3 = V^*_{e3}\nu_e + V^*_{\mu 3}\nu_\mu + V^*_{\tau 3}\nu_\tau$ and hence the flavor ratio at the telescope is given by

$$\phi^{\rm T}_e : \phi^{\rm T}_\mu : \phi^{\rm T}_\tau = |V_{e3}|^2 : |V_{\mu 3}|^2 : |V_{\tau 3}|^2 \; . \tag{8.24}$$

Taking $V = V_0$ to be the tri-bimaximal neutrino mixing pattern, for example, we obtain $\phi^{\rm T}_e : \phi^{\rm T}_\mu : \phi^{\rm T}_\tau = 4 : 1 : 1$ (normal hierarchy) or $0 : 1 : 1$ (inverted hierarchy). If $|V_{e3}| \neq 0$, the numerical result will depend on three mixing angles and the CP-violating phase δ (Beacom *et al.*, 2004; Meloni and Ohlsson, 2007; Xing and Zhou, 2008; Maltoni and Winter, 2008). Of course, the flavor ratio of UHE cosmic neutrinos may also get modified in the existence of incomplete decays, magnetic fields and "exotic" new physics (Pakvasa, 2008).

(5) *Sterile neutrinos.* Today one seems not to be well motivated to consider the existence of very light sterile neutrinos [5], which may take part in the oscillations of active neutrinos (i.e., ν_e, ν_μ and ν_τ) and modify the standard interpretation of solar, atmospheric, reactor and accelerator neutrino oscillation data (Xing, 2008). If one or more sterile neutrinos exist, their mixing with active neutrinos has to be sufficiently suppressed; otherwise, neutrino oscillations would bring sterile neutrinos in equilibrium with active neutrinos before neutrino decoupling — the resultant excess in energy density would endanger the standard scheme for the Big Bang nucleosynthesis of light elements (Barbieri and Dolgov, 1990; Kalliomäki *et al.*, 1999). Using $V_{\alpha i}$ and $S_{\alpha j}$ to denote the active-active and active-sterile neutrino mixing matrix elements, respectively, we can express the averaged probabilities of UHE cosmic neutrino oscillations as (Xing and Zhou, 2008)

$$\langle P(\nu_\alpha \to \nu_\beta) \rangle = \langle P(\overline{\nu}_\alpha \to \overline{\nu}_\beta) \rangle = \sum_{i=1}^{3} |V_{\alpha i}|^2 |V_{\beta i}|^2 + \sum_{j=1}^{n} |S_{\alpha j}|^2 |S_{\beta j}|^2 \; , \tag{8.25}$$

where α and β run over e, μ and τ, and

$$\sum_{i=1}^{3} |V_{\alpha i}|^2 + \sum_{j=1}^{n} |S_{\alpha j}|^2 = 1 \; . \tag{8.26}$$

Eq. (8.26) shows the direct unitarity violation of V induced by light sterile neutrinos. Two observations have been achieved in the literature (Athar *et al.*, 2000; Keränen *et al.*, 2003; Awasthi and Choubey, 2007): (a) for small active-sterile neutrino mixing, the effect of non-unitarity of V at neutrino telescopes is very small and quite similar to that obtained in Eq. (8.21); (b) for relatively large hitherto-unconstrained mixing between active and sterile neutrino species, the flavor distribution of UHE cosmic neutrinos at neutrino telescopes might be significantly modified.

[5] A *sterile* neutrino is by definition a hypothetical neutrino that does not interact with other known particles via electroweak or strong interactions except gravity.

We admit that the present versions of neutrino telescopes are mainly designed to be a discovery tool for UHE cosmic neutrinos. A determination of the flavor distribution of UHE cosmic neutrinos actually requires the precision measurements. Using neutrino telescopes to probe new physics is certainly more challenging and could only be done in the long run.

8.4 Neutrinos and Multi-messenger Astronomy

Although most of what we have known about the cosmos derives from the observation of photons, we are learning some further things beyond the solar system by observing cosmic rays and neutrinos. Different astronomical messengers, such as gamma rays, protons, neutrinos and even gravitational waves, are expected to complement one another in probing the high-energy Universe. Hence some longstanding problems in astronomy may finally be solved in the era of multi-messenger astronomy. In this section we shall briefly describe the interplay between UHE cosmic neutrinos and cosmic rays, gamma rays or gravitational waves in a given astrophysical source. The interaction of UHE cosmic neutrinos with the cosmic neutrino background (CνB) via the Z-resonance will also be discussed.

8.4.1 Cosmic Neutrinos and Z-bursts

The existence of the CνB, comprised of relic neutrinos from the epoch of decoupling of weak interactions about one second after the Big Bang, is a robust prediction of the standard Big Bang cosmology (Kolb and Turner, 1990; Peebles, 1993). Today's temperature and number density of cosmic background neutrinos can be calculated in terms of the observed temperature and number density of cosmic background photons:

$$\begin{aligned} T_{\nu_i} = T_{\overline{\nu}_i} &= \left(\frac{4}{11}\right)^{1/3} T_\gamma \approx 1.945 \text{ K} , \\ n_{\nu_i} = n_{\overline{\nu}_i} &= \frac{3}{22} n_\gamma \approx 56 \text{ cm}^{-3} , \end{aligned} \tag{8.27}$$

where ν_i (or $\overline{\nu}_i$) denotes a neutrino (or antineutrino) species with the definite mass m_i (for $i = 1, 2, 3$), $T_\gamma = 2.725$ K and $n_\gamma = 411$ cm^{-3} (Nakamura *et al.*, 2010) have been input. As a result, the average three-momentum of each relic neutrino is rather small: $\langle p_{\nu_i} \rangle = \langle p_{\overline{\nu}_i} \rangle = 3T_{\nu_i} \approx 5.835 \text{ K} \approx 5.028 \times 10^{-4}$ eV, implying that at least two mass eigenstates of the relic neutrinos are non-relativistic today (i.e., $\langle p_{\nu_i} \rangle = \langle p_{\overline{\nu}_i} \rangle \ll m_i$) no matter how the neutrino mass spectrum looks like [6]. These cosmic background neutrinos are subject to the

[6] In view of $\Delta m^2_{21} \approx 7.6 \times 10^{-5}$ eV^2 and $|\Delta m^2_{31}| \approx 2.4 \times 10^{-3}$ eV^2 in Table 3.1, one may have $m_2 \approx 8.7 \times 10^{-3}$ eV and $m_3 \approx 4.9 \times 10^{-2}$ eV (normal mass hierarchy); or $m_1 \approx 4.9 \times 10^{-2}$ eV and $m_2 \approx 5.0 \times 10^{-2}$ eV (inverted mass hierarchy); or $m_1 \sim m_2 \sim m_3 \gtrsim \sqrt{|\Delta m^2_{31}|} \approx 4.9 \times 10^{-2}$ eV (near mass degeneracy).

gravitational clustering on massive structures (e.g., cold dark matter). Hence there may exist some local overdensities in the CνB relative to the standard value given in Eq. (8.27), and the corresponding momentum distribution of relic neutrinos is possible to deviate from the one given by the homogeneous and isotropic relativistic Fermi-Dirac distribution (Ringwald, 2009).

An interesting observation is that UHE cosmic neutrinos, when propagating over cosmological distances, may interact with the CνB via the Z boson and thus get absorbed (Weiler, 1982). Although the cross sections of $\nu_{\rm UHE} + \overline{\nu}_{\rm C\nu B} \to Z^* \to$ hadrons and $\overline{\nu}_{\rm UHE} + \nu_{\rm C\nu B} \to Z^* \to$ hadrons are negligibly small in most cases, they can be significantly enhanced when the reactions take place on the Z resonance. In this special case the energy of an UHE neutrino ν_i has to satisfy $M_Z^2 \approx (E_{\nu_i} + m_i)^2 - E_{\nu_i}^2 \approx 2 m_i E_{\nu_i}$; namely,

$$E_{\nu_i} \approx \frac{M_Z^2}{2 m_i} \approx 4.2 \times \left(\frac{\rm eV}{m_i} \right) \times 10^{21}~{\rm eV} \; . \tag{8.28}$$

Such extremely energetic cosmic neutrinos might originate from the superheavy DM or TDs in the very early Universe. Given the width of the Z boson $\Gamma_Z = (2.4952 \pm 0.0023)$ GeV (Nakamura *et al.*, 2010), the Z-resonance enhancement is more generally achievable for E_{ν_i} or $E_{\overline{\nu}_i}$ to lie in the range $M_Z^2/(2m_i) \pm \Gamma_Z$. The hadrons produced from the Z decay form a highly-collimated final state, because the Z boson in the rest frame of relic neutrinos has a Lorentz boost factor characterized by $E_{\nu_i}/M_Z \sim 10^{11}$ for $m_i \sim \mathcal{O}(0.1)$ eV. If the Z-mediated interaction between $\nu_{\rm UHE}$ (or $\overline{\nu}_{\rm UHE}$) and $\overline{\nu}_{\rm C\nu B}$ (or $\nu_{\rm C\nu B}$) takes place at a distance of less than 50 Mpc from the Earth, the attenuation should be small such that the UHE cosmic rays arising from the Z-bursts may induce air showers in the Earth's atmosphere and give rise to some events above the GZK cutoff (Fargion *et al.*, 1999; Weiler, 1999). Considering that the average multiplicity of the reaction $e^+ e^- \to Z \to$ hadrons is about 30 and its final state is on average composed of about 2 nucleons, 10 neutral pions and 17 charged pions (Bilenky *et al.*, 2003), one may estimate the average energy of protons and pions produced from the Z-burst process: $\langle E_p \rangle \sim \langle E_\pi \rangle \sim E_{\nu_i}/30$. Neutral and charged pions originate photons and neutrinos, respectively, via $\pi^0 \to \gamma + \gamma$ and $\pi^+ \to \mu^+ + \nu_\mu$ followed by $\mu^+ \to e^+ + \overline{\nu}_\mu + \nu_e$ (or $\pi^- \to \mu^- + \overline{\nu}_\mu$ followed by $\mu^- \to e^- + \nu_\mu + \overline{\nu}_e$). As discussed in Section 8.1.3, about 1/4 of the charged pion's energy is taken away by each neutrino or antineutrino. So the average energies of UHE photons and neutrinos emitted from the Z-bursts are [7]

$$\begin{aligned} \langle E_\gamma \rangle &\sim \frac{E_{\nu_i}}{60} \approx 7.0 \times \left(\frac{\rm eV}{m_i} \right) \times 10^{19}~{\rm eV} \; , \\ \langle E_\nu \rangle &\sim \frac{E_{\nu_i}}{120} \approx 3.5 \times \left(\frac{\rm eV}{m_i} \right) \times 10^{19}~{\rm eV} \; . \end{aligned} \tag{8.29}$$

[7] Note that more energetic neutrinos may come from the direct $Z \to \nu_i + \overline{\nu}_i$ decay with an average energy $\langle E_\nu \rangle \approx E_{\nu_i}/2 \approx 2.1 \times ({\rm eV}/m_i) \times 10^{21}$ eV.

In the Z-burst scenario these protons, photons and neutrinos constitute the primaries of UHE cosmic rays. A measurement of such UHE cosmic rays would in principle allow one to determine the neutrino masses (Päs and Weiler, 2001; Fodor *et al.*, 2002).

The Z-burst mechanism provides an appealing opportunity to detect the CνB in two approaches. The first one is to search for the "emission" feature of Z-bursts, characterized by a directional excess of UHE cosmic rays, gamma rays and neutrinos beyond the GZK cutoff. As discussed above, this scenario probes the Universe delimited by the GZK sphere and is sensitive to the local overdensities in the CνB which may result from the gravitational clustering on cold dark matter and baryonic structures (Van Elewyck, 2007). The other approach is to search for the "absorption" feature in the UHE cosmic neutrino flux which would reflect their interactions with the CνB via the Z-resonance along their path (Weiler, 1982; Roulet, 1993; Yoshida, 1994). Such an energetic neutrino flux arriving at the Earth is therefore expected to exhibit absorption dips whose locations in the energy spectrum are determined by the respective redshifted resonance energies of $\nu_{\rm UHE}+\overline{\nu}_{\rm C\nu B}\rightarrow Z\rightarrow$ anything and $\overline{\nu}_{\rm UHE}+\nu_{\rm C\nu B}\rightarrow Z\rightarrow$ anything processes: $E'_{\nu_i}\approx M_Z^2/\left[2m_i\left(1+z\right)\right]$, depending on both the neutrino masses m_i and the source redshift z. The observation of these dips would not only serve as the most direct evidence for the existence of the CνB but also help determine the absolute values of relic neutrino masses and the distribution of UHE cosmic neutrino sources (Eberle *et al.*, 2004; Barenboim *et al.*, 2005; D'Olivo *et al.*, 2006; Ringwald and Schrempp, 2006; Scholten and van Vliet, 2008).

8.4.2 Cosmic Neutrinos and Gamma Rays

Supernova remnants (SNRs) have been conjectured to be the accelerators of galactic cosmic rays for a long time (Baade and Zwicky, 1934; Ginzburg and Syrovatskii, 1964). In the past few years the HESS Collaboration has determined the energy spectra of a few young SNRs, such as RX J1713.7-3946 and RX J0852.0-4622 (Vela Junior), and demonstrated that they emit gamma rays with energies above 10 TeV (Aharonian *et al.*, 2006a, 2007a, 2007b). But it is still impossible to conclusively pinpoint SNRs as the sources of galactic cosmic rays by identifying that the observed gamma rays originate from the decays of neutral pions. Eliminating the possibility of a purely electromagnetic origin of TeV gamma rays is challenging, and hence detecting their accompanying neutrinos would provide incontrovertible evidence for the acceleration of cosmic rays at the sources (Halzen, 2009). The connection between photon and neutrino fluxes in the case of galactic supernova shocks is clear: cosmic rays interact with the ambient matter (e.g., dense molecular clouds in the disk) and then produce equal numbers of π^+, π^- and π^0 in hadronic collisions $p+p\rightarrow\mathbf{n}\left(\pi^+ +\pi^- +\pi^0\right)+X$ with $\mathbf{n}\geqslant 1$ being an integer. One may therefore estimate the neutrino flux expected from the source

by means of the known gamma ray spectrum (Vissani, 2006; Vissani and Villante, 2008; Villante and Vissani, 2008).

Let us assume that equal numbers of π^+, π^- and π^0 events have been produced from a SNR. Then VHE gamma rays can originate from the decay mode $\pi^0 \to \gamma + \gamma$, and their flux $\phi_\gamma(E)$ is related to the flux of neutral pions $\phi_{\pi^0}(E)$ in the following way (Vissani, 2006) [8]:

$$\phi_\gamma(E) = 2\int_E^\infty \mathrm{d}E' \frac{\phi_{\pi^0}(E')}{E'} \; ; \tag{8.30}$$

or equivalently, $\dfrac{\mathrm{d}\phi_\gamma(E)}{\mathrm{d}E} = -2\phi_{\pi^0}(E)/E$, implying that the gamma ray flux has to be strictly decreasing. On the other hand, VHE neutrinos can originate from the decay mode $\pi^+ \to \mu^+ + \nu_\mu$. Similar to Eq. (8.30), the ν_μ and π^+ fluxes are related to each other though

$$\phi_{\nu_\mu}(E) = \kappa \int_{\kappa E}^\infty \mathrm{d}E' \frac{\phi_{\pi^+}(E')}{E'} \; , \tag{8.31}$$

where $\kappa \equiv 1/(1-r)$ with $r \equiv m_\mu^2/m_\pi^2 \approx 0.573$. In the extremely relativistic limit E_{ν_μ} and E_{μ^+} lie in the ranges $0 \leqslant E_{\nu_\mu} \leqslant E_{\pi^+}(1-r)$ and $rE_{\pi^+} \leqslant E_{\mu^+} \leqslant E_{\pi^+}$, respectively. Note that the approximate isospin-invariant distribution of pions implies $\phi_{\pi^0} \approx \phi_{\pi^+} \approx \phi_{\pi^-}$. Then a comparison between Eqs. (8.30) and (8.31) leads us to the relationship $\phi_{\nu_\mu}(E) = \kappa\phi_\gamma(\kappa E)/2$. In addition, ϕ_{μ^+} can be read off from Eq. (8.31) by replacing its integral's interval with $E_{\mu^+} \in [rE_{\pi^+}, E_{\pi^+}]$; namely, $\phi_{\mu^+}(E) = \kappa[\phi_\gamma(E) - \phi_\gamma(E/r)]/2$. The μ^+ decay produces $\overline{\nu}_\mu$ and ν_e, whose flux is given by (Vissani, 2006)

$$\phi_\nu(E_\nu) = \int_0^1 \frac{\mathrm{d}y}{y} \phi_{\mu^+}(E_{\mu^+}) \left[g_0(y) - g_1(y)\overline{\mathcal{P}}_\mu(E_{\mu^+}) \right] \; , \tag{8.32}$$

where the subscript ν denotes ν_e or $\overline{\nu}_\mu$, $y \equiv E_\nu/E_{\mu^+}$, $g_0(y) = 2(1-3y^2+2y^3)$ and $g_1(y) = -2(1-6y+9y^2-4y^3)$ for $\nu = \nu_e$, or $g_0(y) = (5-9y^2+4y^3)/3$ and $g_1(y) = (1-9y^2+8y^3)/3$ for $\nu = \overline{\nu}_\mu$, and $\overline{\mathcal{P}}_{\mu^+}$ describes the μ^+ polarization averaged over the π^+ distribution:

$$\overline{\mathcal{P}}_{\mu^+}(E) \times \phi_{\mu^+}(E) = -\frac{\kappa}{2}\left[\phi_\gamma(E) + \phi_\gamma(E/r)\right] + \kappa^2 r \int_E^{E/r} \mathrm{d}E' \frac{\phi_\gamma(E')}{E'} \; . \tag{8.33}$$

As for $\pi^- \to \mu^- + \overline{\nu}_\mu$ and $\mu^- \to e^- + \nu_\mu + \overline{\nu}_e$ decays, the corresponding $\overline{\nu}_\mu$, ν_μ and $\overline{\nu}_e$ fluxes can similarly be given by Eqs. (8.31) and (8. 32). Thus one

[8] We have assumed that the VHE gamma ray flux is not significantly absorbed by the source. Hence the method described here is not directly applicable to a number of possible galactic sources of VHE photons and neutrinos such as microquasars that are intrinsically non-transparent, or to possible extragalactic sources since the infrared photon background absorbs VHE gamma rays if their energies are above about 10 TeV (Aharonian *et al.*, 2006b; Vissani, 2006).

may obtain the fluxes of VHE neutrinos and antineutrinos in terms of that of VHE gamma rays from a galactic SNR. Two comments are in order.

- One may include the contribution of the $\eta \to \gamma + \gamma$ decay to the VHE photon flux and those of leptonic $K^{\pm}$ decays to the VHE neutrino fluxes in a more careful analysis (Vissani, 2006; Villante and Vissani, 2008).
- One may incorporate neutrino oscillations into the above formulas with the replacement $\phi_{\nu_\mu} \to \phi_{\nu_\mu}\langle P(\nu_\mu \to \nu_\mu)\rangle + \phi_{\nu_e}\langle P(\nu_e \to \nu_\mu)\rangle$, where $\langle P(\nu_\alpha \to \nu_\beta)\rangle$ (for $\alpha, \beta = e, \mu, \tau$) have been given in Eq. (8.7). The same treatment is valid for antineutrinos (Vissani and Villante, 2008).

It is then possible to compute the fluxes of VHE neutrinos and antineutrinos with the help of the observed VHE gamma rays (Vissani, 2006; Villante and Vissani, 2008; Vissani and Villante, 2008; Morlino *et al.*, 2009).

The astrophysical sources of extragalactic cosmic rays include AGN and GRBs. For example, the fireball producing a GRB converts a fraction of a solar mass into the acceleration of electrons which is seen as synchrotron photons (Halzen, 2009). Shocks in the expanding GRB fireball may convert roughly the same amount of energy into the acceleration of protons that are observed as UHE cosmic rays (Waxman, 1995). In this scenario cosmic rays and synchrotron photons coexist before the fireball reaches transparency and produces the observed GRB display. Their interactions via the Δ^+-resonance processes $p + \gamma \to \Delta^+ \to \pi^0 + p$ and $p + \gamma \to \Delta^+ \to \pi^+ + n$ can give rise to neutral and charged pions, respectively, with probabilities 2/3 and 1/3. UHE gamma rays and neutrinos are then produced from $\pi^0 \to \gamma + \gamma$, $\pi^+ \to \mu^+ + \nu_\mu$ and $\mu^+ \to e^+ + \overline{\nu}_\mu + \nu_e$ decays. As discussed in Section 8.1.2, about 1/4 (or 1/2) of the pion's energy is taken away by each neutrino (or photon). Then we have $x_\nu \equiv E_\nu/E_p \approx 0.25\langle E_\pi\rangle/\langle E_p\rangle$ and $x_\gamma \equiv E_\gamma/E_p \approx 0.5\langle E_\pi\rangle/\langle E_p\rangle$, where $\langle E_\pi\rangle/\langle E_p\rangle \approx \epsilon_\pi/(1+\epsilon_\pi) \approx 0.22$ with $\epsilon_\pi \equiv \langle E_\pi\rangle/\langle E_n\rangle \approx 0.28$ measures the average energy transferred from the proton to the pion. The UHE neutrino and photon fluxes produced by a GRB are therefore given by

$$\begin{aligned} \frac{\mathrm{d}\phi_\nu}{\mathrm{d}E} &= 1 \times \frac{1}{3} \times \frac{1}{x_\nu} \frac{\mathrm{d}\phi_p}{\mathrm{d}E_p}\bigg|_{E_p = E/x_\nu} , \\ \frac{\mathrm{d}\phi_\gamma}{\mathrm{d}E} &= 2 \times \frac{2}{3} \times \frac{1}{x_\gamma} \frac{\mathrm{d}\phi_p}{\mathrm{d}E_p}\bigg|_{E_p = E/x_\gamma} , \end{aligned} \tag{8.34}$$

where ϕ_ν $(= \phi_e = \phi_\mu = \phi_\tau)$ stands for the sum of neutrino and antineutrino fluxes of each flavor which will not be distinguished at a neutrino telescope. Provided the energy spectrum of primary protons is taken to be $\dfrac{\mathrm{d}\phi_p}{\mathrm{d}E_p} \propto E_p^{-2}$, then Eq. (8.34) leads us to the relation $\dfrac{\mathrm{d}\phi_\gamma}{\mathrm{d}E} = 8\dfrac{\mathrm{d}\phi_\nu}{\mathrm{d}E}$. It is well known that neutrino oscillations over cosmic distances approximately yield equal fluxes for three flavors. Given some details of the source and the detector, one should

be able to evaluate the flux of UHE neutrinos and the number of events to be detected (Halzen, 2009). It might be impossible to observe the corresponding UHE gamma rays because they would be absorbed by the CMB on their way from an extragalactic source to the Earth.

8.4.3 Neutrinos and Gravitational Waves

As a classical field theory of gravitation, Einstein's general relativity predicts the existence of gravitational waves emitted from massive objects undergoing large accelerations. Typical examples include the binary systems of compact objects like neutron stars and black holes, or ultra-compact binaries such as double white dwarfs and ultra-compact X-ray binaries (Avignone *et al.*, 2008). Many attempts have been made to verify the existence of gravitational waves. In particular, Russell Hulse and Joseph Taylor received the 1993 Nobel Prize for their indirect detection of gravitational waves through the energy loss of the binary pulsar PSR 1913+16 (Hulse and Taylor, 1975). The direct observation of gravitational waves is still a big challenge in astrophysics, although the experimental techniques are becoming more mature than before.

Since supernova explosions are believed to be the sources of long-timescale GRBs, the observation of gravitational waves expected from such violent events may allow us to better understand the dynamical processes giving rise to GRBs. In the forthcoming era of multi-messenger astronomy it will be particularly interesting to detect high-energy neutrinos in coincidence with gravitational waves produced from supernovae and GRBs. Both messengers can escape very dense media and travel over cosmological distances without being absorbed, pointing back to their common sources and carrying information from the innermost regions of those astrophysical engines (Van Elewyck, 2009). They could also reveal possible hidden sources that are unable to be seen by means of high-energy gamma rays. Indeed, neutrino bursts associated with the same source as gravitational waves can lead to some effects in the gravitational wave antennas, but the contrary is not true (Castagnoli *et al.*, 1978). The point is simply that the velocity of a massive neutrino is slightly smaller than that of the massless graviton and hence results in a time delay between their signals to be detected on the Earth. It is therefore meaningful and useful to establish a correlation in time among neutrino and gravitational wave detectors for a given astrophysical source. On the other hand, the detection of gravitational waves and high-energy neutrinos originating from the early Universe will provide a unique source of information about fundamental physics at work in the early Universe.

The feasibility of searching for high-energy neutrinos in coincidence with gravitational waves is under discussion. In principle, a neutrino telescope can accurately determine the time and direction of high-energy neutrino events, while a network of gravitational wave detectors can also provide timing and directional information for gravitational wave bursts (Van Elewyck, 2009). Combining the measurements from these totally independent detectors will

allow one to achieve robust background rejection and much better sensitivities. A typical example is to combine the ANTARES neutrino telescope (Carr, 2008) with the VIRGO and LIGO interferometers for gravitational waves (Acernese *et al.*, 2008; Abbott *et al.*, 2008). They share the challenge to search for faint and rare signals on top of abundant noise or background events, and the observation of coincident triggers would provide strong evidence for a gravitational wave burst and a neutrino burst coming from a common source (Van Elewyck, 2009; Pradier, 2009).

References

Abbasi, R., *et al.* (HiRes Collaboration), 2008, Phys. Rev. Lett. **100**, 101101.

Abbasi, R., *et al.* (IceCube Collaboration), 2009, Astrophys. J. **701**, L47.

Abbott, B., *et al.* (LIGO Collaboration), 2008, Class. Quant. Grav. **25**, 245008.

Abraham, J., *et al.* (Pierre Auger Collaboration), 2008, Phys. Rev. Lett. **101**, 061101.

Acernese, F., *et al.* (VIRGO Collaboration), 2008, Class. Quant. Grav. **25**, 225001.

Achterberg, A., *et al.* (IceCube Collaboration), 2006, Astropart. Phys. **26**, 282.

Ackermann, M., *et al.* (AMANDA Collaboration), 2006, Astropart. Phys. **24**, 459.

Agnetta, G., *et al.* (EUSO Collaboration), 2006, arXiv:astro-ph/0602151.

Aharonian, F., *et al.* (HESS Collaboration), 2006a, Astron. Astrophys. **449**, 223.

Aharonian, F., *et al.* (HESS Collaboration), 2006b, Nature **440**, 1018.

Aharonian, F., *et al.* (HESS Collaboration), 2007a, Astron. Astrophys. **464**, 235.

Aharonian, F., *et al.* (HESS Collaboration), 2007b, Astrophys. J. **661**, 236.

Ahlers, M., 2007, DESY-THESIS-2007-002.

Ahlers, M., Ringwald, A., and Tu, H., 2006, Astropart. Phys. **24**, 438.

Ahluwalia, D. V., 2001, Mod. Phys. Lett. A **16**, 917.

Ahrens, J., *et al.* (AMANDA Collaboration), 2004, Phys. Rev. Lett. **92**, 071102.

Anchordoqui, L. A., *et al.*, 2004, Phys. Lett. B **593**, 42.

Anchordoqui, L. A., *et al.*, 2005, Phys. Lett. B **621**, 18.

Askaryan, G. A., 1962, JETP **14**, 441.

Askaryan, G. A., 1965, JETP **21**, 658.

Aslanides, E., *et al.* (ANTARES Collaboration), 1999, arXiv:astro-ph/9907432.

Athar, H., Jezabek, M., and Yasuda, O., 2000, Phys. Rev. D **62**, 103007.

Auger, P., Maze, R., and Grivet-Meyer, T., 1938, Comptes rendus **206**, 1721.

Avignone, F., *et al.*, 2008, *Status and Perspective of Astroparticle Physics in Europe* (Astroparticle Physics Roadmap Phase I).

Awasthi, R. L., and Choubey, S., 2007, Phys. Rev. D **76**, 113002.

Baade, W., and Zwicky, F., 1934, Phys. Rev. D **46**, 76.

Balkanov, V. A., *et al.* (Baikal Collaboration), 1998, Prog. Part. Nucl. Phys. **40**, 391.

Barbieri, R., and Dolgov, A., 1990, Phys. Lett. B **237**, 440.

Barenboim, G., and Quigg, C., 2003, Phys. Rev. D **67**, 073024.

Barenboim, G., *et al.*, 2005, Phys. Rev. D **71**, 083002.
Barenboim, G., *et al.*, 2006, Nucl. Phys. B **758**, 90.
Barwick, S. W., *et al.* (ANITA Collaboration), 2006, Phys. Rev. Lett. **96**, 171101.
Beacom, J. F., *et al.*, 2003a, Phys. Rev. D **68**, 093005.
Beacom, J. F., *et al.*, 2003b, Phys. Rev. Lett. **90**, 181301.
Beacom, J. F., *et al.*, 2004, Phys. Rev. D **69**, 017303.
Bell, N. F., 2008, J. Phys. Conf. Ser. **136**, 022043.
Berezinsky, V. S., and Zatsepin, G. T., 1969, Phys. Lett. B **28**, 423.
Berezinsky, V. S., Kachelrieß, M., and Vilenkin, A., 1997, Phys. Rev. Lett. **79**, 4302.
Bernardini, E., 2009, AIP Conf. Proc. **1112**, 138.
Bhattacharjee, P., and Gupta, N., 2005, arXiv:hep-ph/0501191.
Bilenky, S. M., *et al.*, 2003, Phys. Rept. **379**, 69.
Blum, K., Nir, Y., and Waxman, E., 2007, arXiv:0706.2070.
Bustamante, M., Gago, A. M., and Peña-Garay, C., 2010, JHEP **1004**, 066.
Cao, Z., *et al.*, 2005, J. Phys. G **31**, 571.
Carr, J., 2008, J. Phys. Conf. Ser. **136**, 022047.
Carr, J., *et al.* (KM3NeT Collaboration), 2007, arXiv:0711.2145.
Castagnoli, C., Galeotti, P., and Saavedra, O., 1978, Astrophys. Space Sci. **55**, 511.
Chikashige, Y., Mohapatra, R. N., and Peccei, R. D., 1981, Phys. Lett. B **98**, 265.
Choubey, S., Niro, V., and Rodejohann, W., 2008, Phys. Rev. D **77**, 113006.
Chung, D. J. H., Kolb, E. W., and Riotto, A., 1999, Phys. Rev. D **59**, 023501.
Coleman, S. R., and Glashow, S. L., 1998, arXiv:hep-ph/9808446.
Colladay, D., and Kostelecký, V. A., 1997, Phys. Rev. D **55**, 6760.
Crocker, R. M., *et al.*, 2005, Astrophys. J. **622**, 892.
Dermer, C. D., and Atoyan, A., 2006, New. J. Phys. **8**, 122.
Dighe, A., and Ray, S., 2008, Phys. Rev. D **78**, 036002.
D'Olivo, J. C., *et al.*, 2006, Astropart. Phys. **25**, 47.
Eberle, B., *et al.*, 2004, Phys. Rev. D **70**, 023007.
Engel, R., Seckel, D., and Stanev, T., 2001, Phys. Rev. D **64**, 093010.
Fargion, D., 2002, Astrophys. J. **570**, 909.
Fargion, D., Mele, B., and Salis, A., 1999, Astrophys. J. **517**, 725.
Farzan, Y., and Smirnov, A. Yu., 2002, Phys. Rev. D. **65**, 113001
Feng, J. L., *et al.*, 2002, Phys. Rev. Lett. **88**, 161102.
Fodor, Z., Katz, S. D., and Ringwald, A., 2002, Phys. Rev. Lett. **88**, 171101.
Gaisser, T. K., Halzen, F., and Stanev, T., 1995, Phys. Rept. **258**, 173.
Gelmini, G. B., and Roncadelli, M., 1981, Phys. Lett. B **99**, 411.
Ginzburg, V. L., and Syrovatskii, S. I., 1964, *Origin of Cosmic Rays* (MacMillan, New York).
Glashow, S. L., 1960, Phys. Rev. **118**, 316.
Gorham, P. W., *et al.* (ANITA Collaboration), 2009, Phys. Rev. Lett. **103**, 051103.
Greisen, K., 1966, Phys. Rev. Lett. **16**, 748.
Halzen, F., 2006a, AIP Conf. Proc. **809**, 130.
Halzen, F., 2006b, Eur. Phys. J. C **46**, 669.

Halzen, F., 2009, arXiv:0911.2676.
Halzen, F., and Hooper, D., 2002, Rep. Prog. Phys. **65**, 1025.
Halzen, F., and Hooper, D., 2009, New J. Phys. **11**, 105019
Halzen, F., and Saltzberg, D., 1998, Phys. Rev. Lett. **81**, 4305.
Hamaguchi, K., Nomura, Y., and Yanagida, T., 1998, Phys. Rev. D **58**, 103503.
Hooper, D., Morgan, D., and Winstanley, E., 2005, Phys. Lett. B **609**, 206.
Hulse, R. A., and Taylor, J. H., 1975, Astrophys. J. **195**, L51.
Kachelrieß, M., 2008, arXiv:0810.3017.
Kalliomäki, A., Maalampi, J., and Tanimoto, M., 1999, Phys. Lett. B **469**, 179.
Kashti, T., and Waxman, E., 2005, Phys. Rev. Lett. **95**, 181101.
Keränen, P., *et al.*, 2003, Phys. Lett. B **574**, 162.
Kolb, E. W., and Turner, M. S., 1990, *The Early Universe* (Addison-Wesley).
Kulkarni, S. R., *et al.*, 2000, SPIE **4005**, 9.
Kuzmin, V. A., and Rubakov, V. A., 1998, Phys. Atom. Nucl. **61**, 1028.
Kuzmin, V. A., and Tkachev, I. I., 1999, Phys. Rev. D **59**, 123006.
Lai, K. C., Lin, G. L., and Liu, T. C., 2009, Phys. Rev. D **80**, 103005.
Learned, J. G., and Pakvasa, S., 1995, Astropart. Phys. **3**, 267.
Lipari, P., Lusignoli, M., and Meloni, D., 2007, Phys. Rev. D **75**, 123005.
Liu, Y., Hu, L., and Ge, M. L., 1997, Phys. Rev. D **56**, 6648.
Liu, J. L., *et al.*, 2009, J. Phys. G. **36**, 075201.
Lohse, T., 2005, POS (HEP2005) **411**, 1.
MacFadyen, A., and Woosley, S. E., 1999, Astrophys. J. **524**, 262.
Maltoni, M., and Winter, W., 2008, JHEP **0807**, 064.
Meloni, D., and Ohlsson, T., 2007, Phys. Rev. D **75**, 125017.
Morlino, G., Blasi, P., and Amato, E., 2009, Astropart. Phys. **31**, 376.
Moshir, M., *et al.*, 1990, BAAS **22**, 1325.
Nakamura, K., *et al.* (Particle Data Group), 2010, J. Phys. G **37**, 075021.
Nellen, L., Mannheim, K., and Biermann, P. L., 1993, Phys. Rev. D **47**, 5270.
Pakvasa, S., 2000, AIP Conf. Proc. **542**, 99.
Pakvasa, S., 2008, Mod. Phys. Lett. A **23**, 1313.
Pakvasa, S., Rodejohann, W., and Weiler, T. J., 2008, JHEP **0802**, 005.
Päs, H., and Weiler, T., 2001, Phys. Rev. D **63**, 113015.
Peebles, P. J. E., 1993, *Principles of Physical Cosmology* (Princeton University Press).
Penzias, A. A., and Wilson, R. W., 1965, Astrophys. J. **142**, 419.
Piatelli, P., *et al.* (NEMO Collaboration), 2005, Nucl. Phys. B (Proc. Suppl.) **143**, 359.
Podgorshi, M., and Ribordy, M., 2010, arXiv:1001.3963
Pradier, T., 2009, Nucl. Instrum. Meth. A **602**, 268.
Protheroe, R. J., and Szabo, A. P., 1992, Phys. Rev. Lett. **69**, 2885.
Rachen, J. P., and Biermann, P. L., 1993, Astron. Astrophys. **272**, 161.
Rachen, J. P., and Meszaros, P., 1998, Phys. Rev. D **58**, 123005.
Ringwald, A., 2009, Nucl. Phys. A **827**, 501c.
Ringwald, A., and Schrempp, L., 2006, JCAP **0610**, 012.
Rodejohann, W., 2007, JCAP **0701**, 029.
Roulet, E., 1993, Phys. Rev. D **47**, 5247.
Saltzberg, D., *et al.*, 2001, Phys. Rev. Lett. **86**, 2802.
Scholten, O., and van Vliet, A., 2008, JCAP **0806**, 015.

Serpico, P. D., 2006, Phys. Rev. D **73**, 047301.
Serpico, P. D., and Kachelrieß, M., 2005, Phys. Rev. Lett. **94**, 211102.
Spiering, C., 2009, AIP Conf. Proc. **1085**, 18.
Stecker, F. W., 1968, Phys. Rev. Lett. **21**, 1016.
Stecker, F. W., and Salamon, M. H., 1996, Space Sci. Rev. **75**, 341.
Takeda, *et al.* (AGASA Collaboration), 2003, Astropart. Phys. **19**, 447.
Torres, D. F., and Anchordoqui, L. A., 2004, Rept. Prog. Phys. **67**, 1663.
Tu, H., 2004, DESY-THESIS-2004-018.
Tzamarias, S. E., *et al.* (NESTOR Collaboration), 2003, Nucl. Instrum. Meth. A **502**, 150.
Urry, C. M., and Padovani, P., 1995, Publ. Astron. Soc. Pac. **107**, 803.
Vandenbroucke, J. A., *et al.*, 2006, Int. J. Mod. Phys. A **21S1**, 259.
Van Elewyck, V., 2007, Nucl. Phys. B (Proc. Suppl.) **165**, 223.
Van Elewyck, V., 2009, arXiv:0908.2454.
Vilenkin, A., and Shellard, E. P. S., 1994, *Cosmic Strings and other Topological Defects* (Cambridge University Press).
Villante, F. L., and Vissani, F., 2008, Phys. Rev. D **78**, 103007.
Vissani, F., 2006, Astropart. Phys. **26**, 310.
Vissani, F., and Villante, F. L., 2008, Nucl. Instrum. Meth. A **588**, 123.
Waxman, E., 1995, Phys. Rev. Lett. **75**, 386.
Waxman, E., 2003, Lect. Notes Phys. **598**, 393.
Waxman, E., and Bahcall, J. N., 1999, Phys. Rev. D **59**, 023002.
Weiler, T. J., 1982, Phys. Rev. Lett. **49**, 234.
Weiler, T. J., 1999, Astropart. Phys. **11**, 303.
Winter, W., 2006, Phys. Rev. D **74**, 033015.
Xing, Z. Z., 2006, Phys. Rev. D **74**, 013009.
Xing, Z. Z., 2007, Nucl. Phys. B (Proc. Suppl.) **168**, 274.
Xing, Z. Z., 2008, Nucl. Phys. B (Proc. Suppl.) **175-176**, 421.
Xing, Z. Z., 2009, Prog. Theor. Phys. Suppl. **180**, 112.
Xing, Z. Z., and Zhou, S., 2006, Phys. Rev. D **74**, 013010.
Xing, Z. Z., and Zhou, S., 2008, Phys. Lett. B **666**, 166.
Yoshida, S., 1994, Astropart. Phys. **2**, 187.
Zatsepin, G. T., and Kuzmin, V. A., 1966, JETP Lett. **4**, 78.
Zhou, S., 2008, Phys. Lett. B **659**, 336.

9

Big Bang Nucleosynthesis and Relic Neutrinos

The concerns of cosmology include the birth of the Universe, its evolution, its structure, and its ultimate fate. At present the most convincing theoretical paradigm in cosmology is the so-called Big Bang model, which attributes the origin of the Universe to an extremely hot and dense plasma that was highly isotropic and homogeneous. In this intriguing picture the evolution of the early Universe underwent a number of crucial events, such as the inflation, quark-baryon transition, neutrino decoupling, nucleosynthesis and photon decoupling. The Big Bang nucleosynthesis (BBN) has so far provided us with the most reliable probe of the early Universe based on the well-established knowledge of particle physics and nuclear physics. In this chapter we shall make use of the standard Big Bang model to describe the irreplaceable role of neutrinos in the history of the Universe. In particular, their contributions to the energy density of the Universe, their effects on the BBN and their properties as the cosmic neutrino background (CνB) will be discussed in some detail. Possible ways and experimental challenges to directly detect these Big Bang relic neutrinos will also be introduced.

9.1 Neutrinos in the Early Universe

The Big Bang model of cosmology, which was first formulated by George Gamow and his collaborators in the 1940's (Gamow, 1946; Alpher *et al.*, 1948), is based on Einstein's general relativity and the cosmological principle. The latter states that the Universe was homogeneous and isotropic at early times and on large scales, implying that all spatial positions in the Universe should be essentially equivalent. Instead of going into details of the standard Big Bang model of cosmology, which has been described in an excellent way in some textbooks (see, e.g., Kolb and Turner, 1990; Weinberg, 2008), we shall briefly introduce some of its key ingredients and consequences relevant to the expansion of the early Universe and the interplay of matter, radiation and vacuum energy up to the time of neutrino decoupling.

9.1.1 Hubble's Law and the Friedmann Equations

One of the seminal discoveries in the history of science is Edwin Hubble's observation that galaxies have been receding from each other at a velocity v which is linearly proportional to their distance D (Hubble, 1929): $v = HD$ with H being the time-dependent Hubble parameter. The present-day value of H, known as the Hubble constant $H_0 \equiv H(t_0)$ at $t = t_0$, has been measured to a good degree of accuracy: $H_0 = 100\, h$ km s^{-1} Mpc^{-1} with $h = 0.72 \pm 0.03$ (Nakamura *et al.*, 2010) [1]. The physical coordinate distance D from the Earth to a distant galaxy at time t can be written as $D(t) = rR(t)$, where r denotes the time-independent comoving coordinate distance measured in a reference frame moving together with the expansion of the Universe, and $R(t)$ is the cosmological scale parameter which determines proper distances in terms of the comoving coordinates. Given the cosmological principle (i.e., homogeneity and isotropy of the early Universe), $R(t)$ is the same over all space and depends only time. The value of $R(t)$ at time t is related to its value today at $t = t_0$ via a redshift factor: $R(t) = R(t_0)/(1 + z)$. Hubble's law on the expansion of the Universe can then be expressed as

$$\dot{R}(t) = HR(t) \,, \tag{9.1}$$

where $\dot{R} \equiv \dfrac{\mathrm{d}R}{\mathrm{d}t}$. One may also define a dimensionless scale parameter $a(t) \equiv R(t)/R(t_0)$ to express Hubble's law: $\dot{a}(t) = Ha(t)$.

The evolution of the Universe is governed by the solution of Einstein's field equations of general relativity. Given a homogeneous and isotropic distribution of matter and radiation behaving like the perfect frictionless fluid, Einstein's equations lead to the Friedmann equations (Friedmann, 1922):

$$H^2 = \left(\frac{\dot{R}}{R}\right)^2 = \frac{8\pi G_{\mathrm{N}}\rho}{3} - \frac{k}{R^2} + \frac{\Lambda}{3} \,, \tag{9.2}$$

$$H^2 + \dot{H} = \frac{\ddot{R}}{R} = -\frac{4\pi G_{\mathrm{N}}}{3}\,(\rho + 3p) + \frac{\Lambda}{3} \,, \tag{9.3}$$

where G_{N} is Newton's gravitational constant, ρ denotes the energy density, p represents the isotropic pressure, k is the curvature constant, and Λ is the cosmological constant. Differentiating Eq. (9.2), we obtain

$$\dot{H} = \frac{4\pi G_{\mathrm{N}}}{3H}\dot{\rho} + \frac{k}{R^2} \tag{9.4}$$

with the help of Eq. (9.1). A combination of Eqs. (9.2), (9.3) and (9.4) yields

[1] Note that 1 Mpc $= 10^3$ kpc $= 10^6$ pc, where pc = parsec is a commonly-used unit of cosmic distances. 1 pc $= 3.0857 \times 10^{13}$ km is defined as the distance that an object has to be for its parallax to equal 1 second of arc (or 1/3600 of a degree).

$$\dot{\rho} = -3H\left(\rho + p\right) \ . \tag{9.5}$$

In some literature the so-called Friedmann equation only refers to Eq. (9.2).

The ultimate fate of the Universe is determined by the curvature constant k, which can only take the discrete values 0 and ± 1. In astrophysics $k = +1$, $k = -1$ and $k = 0$ correspond respectively to closed, open and spatially flat geometries. Let us assume $\Lambda = 0$ in Eq. (9.2) to discuss the cosmological meaning of k. The $k = +1$ case corresponds to a closed Universe which expands and reaches a maximum radius and then recollapses in a finite time, whereas the $k = -1$ case corresponds to an open Universe which expands without any limit. For $k = 0$, the Universe is flat in the sense that it expands forever but the velocity tends asymptotically to zero at sufficiently large t. But these simple observations may change if Λ is nonvanishing. Current observational data indicate that the Universe is extremely close to a flat Universe (i.e., $k \approx 0$) on large scales.

9.1.2 The Energy Density of the Universe

The energy density ρ and the isotropic pressure p in Eq. (9.3) are in general related to each other through the equation of state: $p = w\rho$, where w is a dimensionless parameter. If w is time-independent, then Eq. (9.5) becomes $\dot{\rho} = -3\left(1 + w\right)\rho\dot{R}/R$ and can be easily integrated. The result is

$$\rho \propto R^{-3(1+w)} \ . \tag{9.6}$$

The total energy density of the Universe may consist of three components:

$$\rho = \rho_{\rm m} + \rho_{\rm r} + \rho_{\rm v} \ , \tag{9.7}$$

where $\rho_{\rm m}$, $\rho_{\rm r}$ and $\rho_{\rm v}$ stand respectively for the energy densities of matter, radiation and vacuum. The role of $\rho_{\rm v}$ is equivalent to that of the cosmological constant Λ in the Friedmann equation; i.e., $\Lambda = 8\pi G_{\rm N}\rho_{\rm v}$. Eq. (9.2) can then be rewritten as

$$H^2 = \left(\frac{\dot{R}}{R}\right)^2 = \frac{8\pi G_{\rm N}}{3}\left(\rho_{\rm m} + \rho_{\rm r} + \rho_{\rm v}\right) - \frac{k}{R^2} \ . \tag{9.8}$$

In the following we discuss the simplified solutions to Eq. (9.8) by assuming the energy density ρ to be dominated by one of its three components, and summarize relevant results in Table 9.1.

(1) *A radiation-dominated Universe.* The early Universe was very hot and dense, and thus its energy density was dominated by radiation (or relativistic particles). A gas of radiation can be described by the equation of state $p = \rho_{\rm r}/3$ (i.e., $w = 1/3$). In this case Eq. (9.6) becomes $\rho_{\rm r} \propto R^{-4}$. Neglecting the terms associated with $\rho_{\rm m}$, $\rho_{\rm v}$ and k in Eq. (9.8), we immediately arrive at $\dot{R} \propto 1/R$. As a result, $R(t) \propto t^{1/2}$ and $H = 1/(2t)$.

Table 9.1 The equation of state, energy density and scale parameter of a Universe dominated by radiation, matter or vacuum energy.

Different era	Equation of state	Energy density	Scale parameter
Radiation	$p = \rho/3$	$\rho_{\rm r} \propto R^{-4} \propto t^{-2}$	$R \propto t^{1/2}$
Matter	$p \approx 0$	$\rho_{\rm m} \propto R^{-3} \propto t^{-2}$	$R \propto t^{2/3}$
Vacuum	$p = -\rho$	$\rho_{\rm v} = \text{constant}$	$R \propto \exp(\sqrt{\Lambda/3}\, t)$

(2) *A matter-dominated Universe.* At relatively late times the Universe gradually cooled down, so non-relativistic matter eventually dominated the energy density over radiation. An essentially pressureless gas corresponds to the equation of state $p \approx 0$ (i.e., $w \approx 0$) [2], implying $\rho_{\rm m} \propto R^{-3}$ as one can see from Eq. (9.6). If the terms associated with $\rho_{\rm r}$, $\rho_{\rm v}$ and k in Eq. (9.8) are omitted, we obtain $\dot{R} \propto 1/R^{1/2}$. Therefore, $R(t) \propto t^{2/3}$ and $H = 2/(3t)$ hold.

(3) *A vacuum-dominated Universe.* In quantum field theory the vacuum is defined as the lowest energy state of a system and contains virtual particle-antiparticle pairs which spontaneously appear and disappear. The vacuum energy density $\rho_{\rm v}$, which acts as a cosmological constant Λ, could dominate the energy density of the Universe in an era when $R(t)$ is large enough. In this case the vacuum state is described by the equation of state $p = -\rho_{\rm v}$, and such a negative pressure is equivalent to a gravitational repulsion. It is obvious that $\rho_{\rm v}$ is independent of $R(t)$, as a result of $w = -1$. Neglecting the terms associated with $\rho_{\rm m}$, $\rho_{\rm r}$ and k in Eq. (9.8), we simply obtain $H = \dot{R}/R = \sqrt{\Lambda/3}$ and thus $R(t) \propto \exp(\sqrt{\Lambda/3}\, t)$. This result implies an exponential expansion of the Universe. One may argue that the parameter $w = p/\rho$ might be inconstant and deviate from -1 as a result of the dynamically evolving vacuum energy or "dark energy" (Garnavich *et al.*, 1998; Perlmutter *et al.*, 1999; Maor *et al.*, 2002). If w is a constant, the best current measurement for the equation of state yields $w = -1.006^{+0.067}_{-0.068}$ (Komatsu *et al.*, 2009). So we simply assume that the vacuum energy is equivalent to a cosmological constant with $w = -1$.

One may use the Friedmann equation in Eq. (9.8) to define the critical energy density of the Universe which assures $k = 0$ to hold:

$$\rho_{\rm c} \equiv \frac{3H^2}{8\pi G_{\rm N}} \,. \tag{9.9}$$

To be more explicit, $\rho_{\rm c} \approx 1.05 \times 10^{-5}\ h^2$ GeV cm^{-3} with h being the rescaled Hubble parameter. Today's value of the critical density is expected to be $\rho_{\rm c} \approx 9.6 \times 10^{-27}$ kg m^{-3} $\approx 5.4 \times 10^{-6}$ GeV cm^{-3} with the input $h \approx 0.72$.

[2] In fact, the gas consisting of non-relativistic particles has the equation of state $p = (2\rho/3) \cdot (v^2/c^2)$ (Perkins, 2009). Because $v^2 \ll c^2$ generally holds for cosmic matter, the pressure that it exerts is very small and can be neglected.

The cosmological density parameter Ω, which is also called the closure parameter, is defined as the ratio of the energy density to the critical density:

$$\Omega \equiv \frac{\rho}{\rho_{\rm c}} = 1 + \frac{k}{H^2 R^2} \ , \tag{9.10}$$

where Eqs. (9.7) and (9.8) have been used. One can see that a flat Universe with $k = 0$ must have $\Omega = 1$ for all values of t. When $\Omega > 1$, $k = +1$ holds and the Universe is closed. When $\Omega < 1$, $k = -1$ holds and the Universe is open. Similar definitions $\Omega_{\rm m} \equiv \rho_{\rm m}/\rho_{\rm c}$, $\Omega_{\rm r} \equiv \rho_{\rm r}/\rho_{\rm c}$ and $\Omega_{\rm v} \equiv \rho_{\rm v}/\rho_{\rm c}$ lead to the relationship

$$\Omega = \Omega_{\rm m} + \Omega_{\rm r} + \Omega_{\rm v} \ . \tag{9.11}$$

At the present time ($t = t_0$) the density of the microwave photon radiation is measured by $\Omega_{\rm r}(t_0) \approx 4.84 \times 10^{-5}$ and thus completely negligible in comparison with that of non-relativistic matter $\Omega_{\rm m}(t_0) \approx 0.26$, but the major contribution to Ω comes from the vacuum term $\Omega_{\rm v}(t_0) \approx 0.74$ if $k = 0$ is assumed (Komatsu *et al.*, 2009; Nakamura *et al.*, 2010). Both luminous baryonic matter and dark matter contribute to $\Omega_{\rm m}$, and the latter actually dominates.

9.1.3 The Age and Radius of the Universe

Let us estimate the age of the Universe by means of the Friedmann equation. Note that $R(t) = R(t_0)/(1+z)$ holds, where z denotes the redshift. Eq. (9.9) means $8\pi G_{\rm N}/3 = H^2(t)/\rho_{\rm c}(t) = H_0^2/\rho_{\rm c}(t_0)$, where H_0 is the Hubble constant today at $t = t_0$. Then Eq. (9.8) can be rewritten as

$$\begin{aligned} H^2(t) &= \frac{H_0^2}{\rho_{\rm c}(t_0)} \left[\rho_{\rm m}(t) + \rho_{\rm r}(t) + \rho_{\rm v}(t) - \frac{\rho_{\rm c}(t_0)}{H_0^2} \cdot \frac{k}{R^2(t)} \right] \\ &= \frac{H_0^2}{\rho_{\rm c}(t_0)} \left[\rho_{\rm m}(t_0) \, (1+z)^3 + \rho_{\rm r}(t_0) \, (1+z)^4 + \rho_{\rm v}(t_0) \right. \\ &\quad \left. - \frac{\rho_{\rm c}(t_0)}{H_0^2} \cdot \frac{k}{R^2(t_0)} \, (1+z)^2 \right] \\ &= H_0^2 \left[\Omega_{\rm m}(t_0) \, (1+z)^3 + \Omega_{\rm r}(t_0) \, (1+z)^4 + \Omega_{\rm v}(t_0) \right. \\ &\quad \left. + \left[1 - \Omega_{\rm m}(t_0) - \Omega_{\rm r}(t_0) - \Omega_{\rm v}(t_0) \right] (1+z)^2 \right] \ , \end{aligned} \tag{9.12}$$

where Table 9.1 and Eq. (9.10) have been used. Furthermore, one has

$$H = \frac{\dot{R}}{R} = -\frac{1}{1+z} \cdot \frac{{\rm d}z}{{\rm d}t} \quad \Longrightarrow \quad {\rm d}t = -\frac{1}{(1+z)\, H} {\rm d}z \ , \tag{9.13}$$

with the help of Hubble's law in Eq. (9.1). Given $z = \infty$ at $t = 0$ and $z = 0$ at $t = t_0$, it is possible to determine the age of the Universe (i.e., the value

of t_0) by substituting Eq. (9.12) into Eq. (9.13) and then calculating the integration. For simplicity, here we assume the Universe to be flat with $k = 0$ or $\Omega_{\rm m}(t_0) + \Omega_{\rm r}(t_0) + \Omega_{\rm v}(t_0) = 1$ and neglect the tiny $\Omega_{\rm r}(t_0)$ term. The age of the Universe turns out to be

$$t_0 = \frac{1}{H_0} \int_0^\infty \frac{{\rm d}z}{(1+z)\sqrt{\Omega_{\rm m}(t_0)\,(1+z)^3 + \Omega_{\rm v}(t_0)}} = \frac{1}{3H_0\sqrt{\Omega_{\rm v}(t_0)}} \ln \frac{1+\sqrt{\Omega_{\rm v}(t_0)}}{1-\sqrt{\Omega_{\rm v}(t_0)}} \,, \tag{9.14}$$

where $\Omega_{\rm v}(t_0) = 1 - \Omega_{\rm m}(t_0)$. Taking $\Omega_{\rm m}(t_0) \approx 0.26$, $\Omega_{\rm v}(t_0) \approx 0.74$ and $h \approx 0.72$ for example, we obtain $t_0 \approx 1/H_0 \approx 13.6$ Gyr. This estimate is consistent very well with the age of the Universe deduced from the study of its structure formation by means of the cosmic microwave background (CMB) and large-scale structures: $t_0 = 13.69 \pm 0.13$ Gyr (Komatsu *et al.*, 2009).

The radius of the observable Universe, defined as $D_{\rm H}$, is measured by the distance from the Earth to the optical horizon beyond which no light signals could reach the Earth at the present time (Perkins, 2009). As the Universe expands and time evolves, this distance increases because more parts of the Universe come inside the horizon. Hence $D_{\rm H} > ct_0 \approx 4.2$ Gpc is expected, where $c = 2.99792458 \times 10^8$ m s^{-1} is the speed of light which has been taken to be unity in the system of natural units. Note that the physical coordinate distance from the Earth to any point of the Universe at time t is expressed as $D(t) = rR(t)$ with r being the comoving coordinate distance. Since both r and $R(t)$ are not directly measurable, we need to link them to the Hubble parameter $H(t)$ and the redshift z with the help of the Friedmann-Lemaître-Robertson-Walker metric. The latter is known as

$${\rm d}s^2 = {\rm d}t^2 - R^2(t) \left[\frac{{\rm d}r^2}{1-kr^2} + r^2 \left({\rm d}\theta^2 + \sin^2\theta\ {\rm d}\phi^2 \right) \right] . \tag{9.15}$$

Given a light signal to or from a distant object at fixed (θ, ϕ), ${\rm d}s^2 = 0$ holds and thus

$$\frac{{\rm d}r}{\sqrt{1-kr^2}} = \frac{{\rm d}t}{R(t)} = -\frac{{\rm d}z}{HR(t_0)} \,, \tag{9.16}$$

where Eq. (9.13) and $R(t) = R(t_0)/(1+z)$ have been used. We obtain

$$R(t_0) \int_0^r \frac{{\rm d}r}{\sqrt{1-kr^2}} = -\int_z^0 \frac{{\rm d}z}{H} = \frac{I(z)}{H_0} \,, \tag{9.17}$$

where Eq. (9.12) has been used, and

$$I(z) \equiv \int_0^z \Big[\Omega_{\rm m}(t_0)\,(1+z)^3 + \Omega_{\rm r}(t_0)\,(1+z)^4 + \Omega_{\rm v}(t_0) + [1 - \Omega_{\rm m}(t_0) - \Omega_{\rm r}(t_0) - \Omega_{\rm v}(t_0)]\,(1+z)^2 \Big]^{-1/2} {\rm d}z \,. \tag{9.18}$$

The simplest case is $k = 0$, corresponding to a flat Universe, in which $D(z) = rR(t_0) = I(z)/H_0$ as one can easily see from Eq. (9.17). The horizon distance $D_{\rm H}$ is then obtainable by setting $z = \infty$ for the upper limit of the integration in Eq. (9.18). Typically taking $\Omega_{\rm r}(t_0) = 0$, $\Omega_{\rm m}(t_0) = 0.26$ and $\Omega_{\rm v}(t_0) = 0.74$, we find a numerical solution $I(\infty) \approx 3.5$. The radius of the observable flat Universe turns out to be $D_{\rm H} \sim 3.5\, c/H_0 \approx 3.5\, ct_0 \approx 14.8$ Gpc $\approx 4.8 \times 10^{10}$ ly.

9.1.4 Radiation in the Early Universe

If matter has been conserved in the Universe, its energy density is expected to vary as $\rho_{\rm m} \propto R^{-3}$. In comparison, the energy density of radiation varies as $\rho_{\rm r} \propto T^4 \propto R^{-4}$ if it is in thermal equilibrium (see Table 9.1). The extra R^{-1} in $\rho_{\rm r}$, as compared with $\rho_{\rm m}$ for non-relativistic matter, simply arises from the redshift. So $\rho_{\rm r} \propto R^{-4}$ applies not only to the CMB photons but also to any relativistic particles in the early Universe, provided they have a uniform distribution on the same cosmological scale as the photons (Perkins, 2009). Although $\rho_{\rm m} \gg \rho_{\rm r}$ holds today, we believe that $\rho_{\rm r} \gg \rho_{\rm m}$ and $\rho_{\rm r} \gg \rho_{\rm v}$ must have been true for small values of R in the olden days of the Universe. In that case the Friedmann equation in Eq. (9.8) can be simplified to

$$\left(\frac{\dot{R}}{R}\right)^2 = \frac{8\pi G_{\rm N}}{3}\rho_{\rm r} \ , \tag{9.19}$$

because the term proportional to k/R^2 is also negligible as compared with the term proportional to $\rho_{\rm r} \propto R^{-4}$. Therefore,

$$\frac{\dot{\rho}_{\rm r}}{\rho_{\rm r}} = -4\frac{\dot{R}}{R} = -\frac{8}{3}\sqrt{6\pi G_{\rm N}\rho_{\rm r}} \ , \tag{9.20}$$

leading to the energy density of radiation:

$$\rho_{\rm r} = \frac{3}{32\pi G_{\rm N}} \cdot \frac{1}{t^2} \ . \tag{9.21}$$

For a photon gas in thermal equilibrium, its energy density is given by

$$\rho_{\rm r} = 4\sigma_{\rm SB}T^4 = \frac{g_\gamma \pi^2}{30}T^4 \ , \tag{9.22}$$

where $\sigma_{\rm SB} = \pi^2/60$ is the Stefan-Boltzmann constant and $g_\gamma = 2$ denotes the number of spin substates of the photon. Combining Eqs. (9.21) and (9.22) allows us to obtain a relationship between the temperature of radiation and the time of expansion in the early Universe:

$$T = \left(\frac{45}{16 g_\gamma \pi^3 G_{\rm N}}\right)^{1/4} \frac{1}{\sqrt{t}} \ . \tag{9.23}$$

This result implies $T \approx 1.31\ \mathrm{MeV}/\sqrt{t} \approx 1.52 \times 10^{10}\ \mathrm{K}/\sqrt{t}$ with t being in seconds. In view of $T \to \infty$ as $t \to 0$, we conclude that the Universe must have started out as a hot Big Bang.

Note that the spectrum of blackbody photons of energy $E = p$ is given by the Bose-Einstein distribution. The latter describes the number of photons per unit volume in the momentum interval $p \to p + \mathrm{d}p$. To be explicit [3],

$$\begin{aligned} n_\gamma &= \int_0^\infty \frac{g_\gamma p^2 \mathrm{d}p}{2\pi^2 \left[\exp\left(E/T\right) - 1\right]} \\ &= \frac{2\zeta(3)}{\pi^2} \cdot \frac{g_\gamma}{2} T^3 \approx 411 \left(\frac{T}{2.725\ \mathrm{K}}\right)^3 \mathrm{cm}^{-3}\ , \end{aligned} \tag{9.24}$$

in which $\zeta(3) \approx 1.202$ is a Riemann zeta function. Taking $T = 2.725$ K as today's CMB temperature, one obtains the number density of relic photons $n_\gamma \approx 411\ \mathrm{cm}^{-3}$. The total energy density of photons integrated over their blackbody spectrum turns out to be

$$\rho_\mathrm{r} = \int_0^\infty \frac{g_\gamma E p^2 \mathrm{d}p}{2\pi^2 \left[\exp\left(E/T\right) - 1\right]} = \frac{g_\gamma \pi^2}{30} T^4\ , \tag{9.25}$$

which is already given in Eq. (9.22). Given $T = 2.725$ K today at $t = t_0$, the energy density of radiation is $\rho_\mathrm{r}(t_0) \approx 4.65 \times 10^{-31}\ \mathrm{kg\ m}^{-3} \approx 2.61 \times 10^{-10}\ \mathrm{GeV\ cm}^{-3}$. Hence $\Omega_\mathrm{r}(t_0) = \rho_\mathrm{r}(t_0)/\rho_\mathrm{c} \approx 4.84 \times 10^{-5}$, about four orders of magnitude smaller than $\Omega_\mathrm{m}(t_0) \approx 0.26$.

Relativistic leptons and quarks can also contribute to the energy density of radiation if they are sufficiently stable. A fermion gas obeys the Fermi-Dirac distribution, and the corresponding number density in the relativistic limit (i.e., $T \gg m$ and $E = \sqrt{p^2 + m^2} \to p$ with m being the fermion mass and p being the momentum) reads

$$n_\mathrm{f} = \int_0^\infty \frac{g_\mathrm{f} p^2 \mathrm{d}p}{2\pi^2 \left[\exp\left(E/T\right) + 1\right]} = \frac{3\zeta(3)}{2\pi^2} \cdot \frac{g_\mathrm{f}}{2} T^3 \tag{9.26}$$

with g_f being the number of spin substates of the fermion. Similar to ρ_r in Eq. (9.25), the total energy density of relativistic fermions integrated over their Fermi-Dirac distribution is

$$\rho_\mathrm{f} = \int_0^\infty \frac{g_\mathrm{f} E p^2 \mathrm{d}p}{2\pi^2 \left[\exp\left(E/T\right) + 1\right]} = \frac{7 g_\mathrm{f} \pi^2}{240} T^4\ . \tag{9.27}$$

For a mixture of extremely relativistic bosons and fermions, their total energy density is expected to be

[3] Four integrals are very useful in calculating the Bose-Einstein and Fermi-Dirac distributions: $\int_0^\infty x^2 \left(\mathrm{e}^x - 1\right)^{-1} \mathrm{d}x = 2\zeta(3)$, $\int_0^\infty x^3 \left(\mathrm{e}^x - 1\right)^{-1} \mathrm{d}x = \pi^4/15$, $\int_0^\infty x^2 \left(\mathrm{e}^x + 1\right)^{-1} \mathrm{d}x = 3\zeta(3)/2$ and $\int_0^\infty x^3 \left(\mathrm{e}^x + 1\right)^{-1} \mathrm{d}x = 7\pi^4/120$, where $\zeta(3) \approx 1.202$ is a Riemann zeta function (Broadhurst, 2010).

$$\rho_{\rm b+f} = \sum_{\rm b} \int_0^\infty \frac{g_{\rm b} E p^2 {\rm d}p}{2\pi^2 \left[\exp\left(E/T\right) - 1\right]} + \sum_{\rm f} \int_0^\infty \frac{g_{\rm f} E p^2 {\rm d}p}{2\pi^2 \left[\exp\left(E/T\right) + 1\right]}$$
$$= \frac{g_* \pi^2}{30} T^4 \ , \tag{9.28}$$

where the effective number of degrees of freedom g_* is given by

$$g_* = \sum_{\rm b} g_{\rm b} + \frac{7}{8} \sum_{\rm f} g_{\rm f} \tag{9.29}$$

with the summation over all types of relativistic particles and antiparticles which contribute to the energy density of radiation in the early Universe.

In the radiation-dominated epoch, the relation between T and t obtained in Eq. (9.23) should be modified by replacing g_γ with g_*. As a result,

$$t = \left(\frac{45}{16 g_* \pi^3}\right)^{1/2} \frac{M_{\rm Pl}}{T^2} \approx \frac{0.301}{\sqrt{g_*}} \cdot \frac{M_{\rm Pl}}{T^2} \ , \tag{9.30}$$

where $M_{\rm Pl} = 1/\sqrt{G_{\rm N}} \approx 1.22 \times 10^{19}$ GeV is the Planck mass. To be specific, $tT^2 \approx 2.42/\sqrt{g_*}$ s MeV^2. One may also express the Hubble parameter $H(t)$ in terms of the temperature T in the radiation-dominated epoch of the early Universe. Combining Eqs. (9.20), (9.21) and (9.30), we obtain

$$H(t) = \frac{\dot{R}}{R} = \frac{1}{2t} \approx 1.66 \sqrt{g_*} \frac{T^2}{M_{\rm Pl}} \ . \tag{9.31}$$

When the temperature was high enough, all types of elementary particles and their antiparticles would have been in the thermal bath of the early Universe. In this case g_* equals the number of all available spin and color substates of particles and antiparticles. Given the standard model (SM) of electroweak and strong interactions which contains one photon, eight gluons, three massive gauge bosons, one Higgs boson, six quarks, six antiquarks, three charged leptons, three charged antileptons, three massless neutrinos and three massless antineutrinos [4], the value of g_* turns out to be $g_* = 28 + 7/8 \times 90 = 106.75$. This number would become smaller as the Universe expanded and the temperature fell. For example, the most massive particles (i.e., the top quark, the Higgs boson and the $W^\pm$ and Z^0 bosons) would have been rapidly lost by their decays (in less than 10^{-23} s) and not replenished once the temperature T is significantly below their masses (Perkins, 2009). After T fell below the scale of quantum chromodynamics $\Lambda_{\rm QCD} \sim 200$ MeV, the remaining quarks,

[4] Note that each quark (or antiquark) has three color substates and each massless neutrino (or antineutrino) has one spin substate. Although three known neutrinos should be massive beyond the SM, their masses are so small that the coupling of each neutrino to the additional spin substate is strongly suppressed and its effect on the value of g_* is therefore negligible (Grupen *et al.*, 2005).

antiquarks and gluons would no longer exist as separate components of a plasma but as color-neutral hadrons such as pions and nucleons. However, only protons and neutrons could survive since all the other hadrons would be too short-lived to exist beyond the first few nanoseconds. After $T \lesssim 20$ MeV most of the nucleons and antinucleons would have annihilated into radiation and the number of surviving nucleons was only about one billionth of the number of photons.

Note that Eq. (9.30), or equivalently $tT^2 \approx 2.42/\sqrt{g_*}$ s MeV^2, can be used to estimate what time a typical energy scale of particle physics corresponds to. Given $g_* = 106.75$, the Planck scale $T \sim 10^{19}$ GeV and the Fermi scale $T \sim 10^2$ GeV correspond respectively to $t \sim 10^{-45}$ s and $t \sim 10^{-11}$ s after the Big Bang. The scale of grand unified theories $T \sim 10^{16}$ GeV is associated with $t \sim 10^{-39}$ s. Around the scale $\Lambda_{\rm QCD}$, just before the hadronization of light quarks and gluons, one may take the photon, eight gluons, three light quarks (u, d, s), the electron, the muon, three neutrinos and their antiparticles to be relativistic. In this case $g_* = 18+7/8\times 50 = 61.75$ holds, and thus $T \sim \Lambda_{\rm QCD}$ corresponds to $t \sim 7.7 \times 10^{-6}$ s after the Big Bang.

9.1.5 Neutrino Decoupling

When the temperature went down to a few MeV, the only surviving relativistic particles in the early Universe were photons, electrons, positrons, neutrinos and antineutrinos. In this case the effective number of degrees of freedom g_* took its value $g_* = 2+7/8\times 10 = 10.75$. The relevant photons, leptons and antileptons should have been present in comparable numbers thanks to the equilibrium reactions $\gamma + \gamma \rightleftharpoons e^+ + e^- \rightleftharpoons \nu_\alpha + \overline{\nu}_\alpha$ (for $\alpha = e, \mu, \tau$). The $e^+ + e^- \rightleftharpoons \nu_\alpha + \overline{\nu}_\alpha$ scattering is a weak neutral-current process whose thermally-averaged cross section is roughly $\langle \sigma_{e^\pm} v_{e^\pm} \rangle \sim G_{\rm F}^2 T^2$, in which $v_{e^\pm}$ denotes the relative velocity of electrons and positrons. The collision rate for this reaction is $\Gamma = n_{e^\pm} \langle \sigma_{e^\pm} v_{e^\pm} \rangle$ with $n_{e^\pm}$ being the number density of electrons or positrons. Given $n_{e^\pm} \sim T^3$ at T as one can see from Eq. (9.26), the collision rate turns out to be $\Gamma \sim G_{\rm F}^2 T^5$. In comparison, the expansion rate of the Universe in the radiation-dominated epoch is $H \sim \sqrt{g_*} T^2 / M_{\rm Pl}$ as shown in Eq. (9.31). Hence neutrinos and antineutrinos would become out of equilibrium and decoupled from the thermal bath as soon as $\Gamma < H$ for sufficiently small T. A rough estimate yields the "freeze-out" temperature

$$T_{\rm fr} \sim \left(\frac{\sqrt{g_*}}{G_{\rm F}^2 M_{\rm Pl}} \right)^{1/3} \sim 1 \text{ MeV} \tag{9.32}$$

for neutrinos to go out of equilibrium. We therefore expect that neutrinos and antineutrinos froze out for $T < T_{\rm fr}$ and then evolved in a way independent of other particles and radiation [5]. In other words, the Universe became

[5] Different from muon and tau neutrinos, the electron neutrinos and their antiparticles could interact with the nucleons via the charged-current weak processes

transparent to neutrinos and antineutrinos, whose momenta would simply redshift with the cosmic expansion. So the effective neutrino temperature fell as $T \sim 1/R$, just like the temperature of photons. The number density of the decoupled neutrinos would continue to decrease in proportion to $1/R^3$ and contribute to g_*, if they were stable and relativistic.

Soon after the neutrino decoupling (i.e., when $T \lesssim m_e$), electrons and positions began to annihilate via $e^+ + e^- \to \gamma + \gamma$. The energy released from this annihilation process would heat up the photon gas relative to the neutrino gas, because the latter was already decoupled. The enhancement of the photon temperature can be calculated by means of the entropy conservation. The entropy per unit volume of the particle gas is given by $s = \int \mathrm{d}Q/T$ with Q being the energy content per unit volume of photons, electrons and positrons at temperature T. Considering Eq. (9.28) and taking $Q = \rho_{\rm b+f}$ with $g_* = 2 + 7/8 \times 4 = 11/2$, we have

$$s = \int \frac{2g_*\pi^2}{15} T^2 \mathrm{d}T = \frac{2g_*\pi^2}{45} T^3 = \frac{11}{4} \cdot \frac{2g_\gamma \pi^2}{45} T^3 \,. \tag{9.33}$$

After the annihilation of electrons and positrons the photons must have attained a temperature T_γ with the corresponding entropy density

$$s_\gamma = \int \frac{2g_\gamma\pi^2}{15} T_\gamma^2 \mathrm{d}T_\gamma = \frac{2g_\gamma\pi^2}{45} T_\gamma^3 \,. \tag{9.34}$$

Because the expansion of the Universe keeps adiabatic or isentropic, $s_\gamma = s$ holds. As a result,

$$T_\gamma = \left(\frac{11}{4}\right)^{1/3} T \,. \tag{9.35}$$

In comparison, the relic neutrinos received no boost and their temperature should just be $T_\nu = T$. The relationship between T_ν and T_γ turns out to be

$$T_\nu = \left(\frac{4}{11}\right)^{1/3} T_\gamma \,. \tag{9.36}$$

For photons and relic neutrinos in this epoch, the total relativistic energy density is given by

$$\rho_{\gamma+\nu} = \rho_\gamma + \rho_\nu = \frac{g_\gamma \pi^2}{30} T_\gamma^4 + \frac{7}{8} \cdot \frac{g_\nu \pi^2}{30} T_\nu^4 = \frac{g'_* \pi^2}{30} T_\gamma^4 \,, \tag{9.37}$$

where the effective number of degrees of freedom g'_* is defined as

---

$\nu_e + n \rightleftharpoons e^- + p$, $\overline{\nu}_e + p \rightleftharpoons e^+ + n$ and $\overline{\nu}_e + e^- + p \rightleftharpoons n$. The point where $\Gamma \sim H$ held for these reactions determines the freeze-out temperature, which is approximately the same as that given in Eq. (9.32). So all neutrino flavors were decoupled from other particles below $T_{\rm fr} \sim 1$ MeV.

$$g'_* \equiv g_\gamma + \frac{7}{8} g_\nu \left(\frac{T_\nu}{T_\gamma}\right)^4 = 2 + 6 \times \frac{7}{8} \left(\frac{4}{11}\right)^{4/3} \approx 3.36 \,, \tag{9.38}$$

applying to the region with $T \ll 1$ MeV (Kolb and Turner, 1990). The total entropy density of photons and relic neutrinos is therefore given by

$$\begin{aligned} s_{\gamma+\nu} &= s_\gamma + s_\nu = \frac{2g_\gamma \pi^2}{45} T_\gamma^3 + \frac{7}{8} \cdot \frac{2g_\nu \pi^2}{45} T_\nu^3 \\ &= \frac{2\pi^2}{45} \left[1 + \frac{7}{8} \cdot \frac{g_\nu}{g_\gamma} \left(\frac{T_\nu}{T_\gamma}\right)^3\right] g_\gamma T_\gamma^3 \\ &= \frac{2\pi^2}{45} \cdot \frac{\pi^2}{\zeta(3)} \left(1 + \frac{7}{8} \times \frac{6}{2} \times \frac{4}{11}\right) n_\gamma \approx 7.04 n_\gamma \,, \end{aligned} \tag{9.39}$$

where Eqs. (9.24) and (9.36) have been used. Although the neutrinos and photons have had no more interactions since the neutrino decoupling, they have been suffering from the same redshift as the Universe expands and cools down. Hence their relative number densities today should be the same as those at the time of neutrino decoupling. With the help of Eqs. (9.24) and (9.26), the number density of relic neutrinos and antineutrinos of all three flavors is expected to be

$$\begin{aligned} n_\nu &= \frac{3\zeta(3)}{2\pi^2} \cdot \frac{g_\nu}{2} T_\nu^3 = \frac{3}{4} \cdot \frac{g_\nu}{g_\gamma} \left(\frac{T_\nu}{T_\gamma}\right)^3 n_\gamma = \frac{9}{11} n_\gamma \\ &\approx 336 \left(\frac{T_\gamma}{2.725 \text{ K}}\right)^3 \text{cm}^{-3} \,. \end{aligned} \tag{9.40}$$

Taking $T_\gamma = 2.725$ K for the CMB radiation today, we immediately obtain $T_\nu \approx 1.945$ K and $n_\nu \approx 336$ cm^{-3} for the CνB.

So far we have assumed that neutrinos were fully decoupled at $T_{\rm fr} \sim 1$ MeV and thus did not share any entropy from the $e^\pm$ annihilation after T was below m_e. In practice, such an instantaneous neutrino decoupling approximation should be slightly corrected because neutrinos could still have slight interactions with the electromagnetic plasma at $T < 1$ MeV and hence received a small portion of the entropy from the $e^\pm$ annihilation (Dicus *et al.*, 1982). Those more energetic neutrinos may be more heated, because the weak interactions in the relevant range of energies get stronger with rising energies. This phenomenon results in a momentum-dependent (non-thermal) distortion in the neutrino distribution from the thermal equilibrium case (Mangano *et al.*, 2002). The small effect of a non-instantaneous neutrino decoupling, together with a much smaller effect on T_γ/T_ν induced by finite-temperature quantum electrodynamics corrections to the electromagnetic plasma, can be taken into account by defining an effective number of neutrino species in the effective number of degrees of freedom g'_* given in Eq. (9.38). Namely,

$$g'_* = 2\left[1 + \frac{21}{8}\left(\frac{4}{11}\right)^{4/3}\right] \quad \Longrightarrow \quad g'_* = 2\left[1 + \frac{7}{8}\left(\frac{4}{11}\right)^{4/3} N_\nu^{\rm eff}\right] \,, \tag{9.41}$$

where $N_\nu^{\rm eff} = 3$ has been taken in the limit of an instantaneous neutrino decoupling. A careful numerical analysis shows that $N_\nu^{\rm eff} \approx 3.04$ (Seljak and Zaldarriaga, 1996; Mangano *et al.*, 2002).

Note that we have assumed neutrinos to be extremely relativistic in the above discussions by ignoring their rest masses. Current neutrino oscillation data indicate that at least two neutrinos should be massive. When T_ν was comparable with a neutrino mass, this kind of neutrinos would no more be relativistic. Because both T_ν and T_γ fell as $1/R$ after neutrinos were decoupled from the thermal bath, their relationship obtained in Eq. (9.36) in the relativistic limit should essentially keep valid even if one or all of three neutrino species became non-relativistic. For a similar reason we expect that the relationship between the number densities of relic neutrinos and photons obtained in Eq. (9.40) should essentially keep unchanged even today at $t = t_0$.

Note also that we have neglected the effect of neutrino oscillations on the process of neutrino decoupling in the above discussions. This effect can be taken into account by solving the momentum-dependent kinetic equations for the neutrino spectra (Dolgov *et al.*, 2002; Hannestad, 2002; Mangano *et al.*, 2005). It is found that neutrino oscillations in the early Universe should not have an appreciable impact on the neutrino energy density, so their effect on the BBN should likewise be inappreciable (Mangano *et al.*, 2005).

9.2 Big Bang Nucleosynthesis

One of the major achievements in the standard Big Bang cosmology is the BBN theory which successfully describes how protons and neutrons could fuse together and form the light elements (e.g., D, ^{3}H, ^{3}He, ^{4}He and ^{7}Li) in the first few minutes after the Big Bang. All of the heavier elements were formed much later from the synthesis of nuclei in stars. We shall outline the BBN timeline in this section and emphasize that the predictions of the BBN theory for the abundances of the light elements are in good agreement with the primordial abundances of those elements observed today in the cosmos.

It should be noted that the light element abundances observed today are not all "primordial", because our epoch is certainly much later than the BBN era and the stellar nucleosynthesis has already commenced for a long time. The ejected remains of this stellar processing may alter the light element abundances from their primordial values and produce some heavy elements such as C, N, O and Fe ("metals") (Nakamura *et al.*, 2010). In this case one should look for the astrophysical sites with low metal abundances so as to measure the light element abundances which are much closer to the primordial ones. For all the light elements, the precision with which their primordial abundances can be inferred is mainly limited by systematic errors of the measurements.

9.2.1 The Neutron-to-proton Ratio

In the radiation-dominated epoch of the early Universe, the synthesis of the light elements took place at temperatures varying roughly from about 1 MeV to below 0.1 MeV. During this BBN period the time t and the temperature T are related to each other through the relationship $tT^2 \approx 2.42/\sqrt{g_*}$ s MeV^2, where the effective number of degrees of freedom g_* changes from 10.75 (for relativistic γ, e^-, ν_e, ν_μ, ν_τ and their antiparticles) to 3.36 (as T dropped below the electron mass $m_e \approx 0.511$ MeV). At a higher temperature such as $T \sim 200$ MeV, the gluons, quarks and antiquarks were bound into nucleons and antinucleons. The latter could remain in thermal equilibrium as the temperature dropped to $T \sim 50$ MeV, but their number densities were exponentially suppressed by a factor $\exp(-m_N/T)$ with $m_N \approx 0.94$ GeV (Grupen *et al.*, 2005). At temperatures below about 20 MeV most of the nucleons and antinucleons should have annihilated and thus the resulting nucleon density was unable to make a significant contribution to the total energy density of the Universe. Since there are not any imaginable baryon-number-violating processes that would have occurred at temperatures near and in the BBN era, the baryon number conservation assures the sum of the number densities of non-relativistic protons and neutrons to be constant in a comoving volume and change as $n_p + n_n \sim T^3 \sim R^{-3}$ in a physical coordinate system.

Before the decoupling or freeze-out of electron neutrinos and electron antineutrinos, the following charged-current weak interactions allow the bilateral conversion of neutrons and protons:

$$n + \nu_e \rightleftharpoons p + e^- \ , \quad p + \overline{\nu}_e \rightleftharpoons n + e^+ \ , \quad n \rightleftharpoons p + e^- + \overline{\nu}_e \ . \tag{9.42}$$

Because of $T \ll m_N \approx 0.94$ GeV in the epoch under discussion, the nucleons can be treated as essentially at rest. The initial and final lepton energies in each of the above processes are then related to each other via $E_{e^-} - E_{\nu_e} = Q$ (for $n + \nu_e \rightleftharpoons p + e^-$), $E_{\overline{\nu}_e} - E_{e^+} = Q$ (for $p + \overline{\nu}_e \rightleftharpoons n + e^+$) or $E_{e^-} + E_{\overline{\nu}_e} = Q$ (for $n \rightleftharpoons p + e^- + \overline{\nu}_e$), where $Q = m_n - m_p = 1.293$ MeV. The reactions in Eq. (9.42) were in thermal equilibrium for $T \gtrsim T_{\rm fr}$, because they could proceed faster than the expansion rate of the Universe (i.e., $\Gamma > H$). In this case the ratio of the neutron and proton number densities is given by [6]

$$\frac{n_n}{n_p} = \left(\frac{m_n}{m_p}\right)^{3/2} \mathrm{e}^{-(m_n - m_p)/T} \approx \mathrm{e}^{-Q/T} \ . \tag{9.43}$$

Tentatively ignoring the effect of neutron decays and taking $T_{\rm fr} \approx 0.72$ MeV as the freeze-out temperature of neutrinos from a more careful analysis (Grupen *et al.*, 2005), one may obtain $n_n/n_p \approx 1/6$ at $T_{\rm fr}$ corresponding to

[6] In the non-relativistic limit the number density of either bosons or fermions can be described by $n = g\,(mT)^{3/2}\,/\,(2\pi)^{3/2} \exp(-m/T)$, where g is the number of internal degrees of freedom for the particle in question and m denotes its rest mass. This result is valid in the assumption that the chemical potentials are negligible.

$t \approx 1.4$ s after the Big Bang. Below the freeze-out temperature the neutrons were free to decay via $n \to p + e^- + \overline{\nu}_e$. This process lasted a few minutes before the neutrons were bound up into deuterium and started the chain of nucleosynthesis reactions. During this period the ratio n_n/n_p reads

$$\frac{n_n(t')}{n_p(t')} = \frac{\mathrm{e}^{-Q/T_{\rm fr}}\mathrm{e}^{-t'/\tau_n}}{1+\mathrm{e}^{-Q/T_{\rm fr}}\left(1-\mathrm{e}^{-t'/\tau_n}\right)} \approx \mathrm{e}^{-Q/T_{\rm fr}}\mathrm{e}^{-t'/\tau_n} \ , \tag{9.44}$$

where t' means the time beginning from the freeze-out point to the start of the nucleosynthesis, and $\tau_n = (885.7 \pm 0.8)$ s is the mean lifetime of neutrons. At a time $t \approx 160$ s (i.e., $t' \approx 158.6$ s and $T \approx 0.09$ MeV for $g_* \approx 3.36$), the neutron-to-proton ratio dropped to $n_n/n_p \approx 0.14$. From here on out the Universe should be cold enough that the BBN could start from scratch.

9.2.2 Synthesis of the Light Nuclei

The nucleosynthesis chain began with the formation of deuterium in the reaction $n + p \to \mathrm{D} + \gamma$ with the binding energy $E_{\rm bind} \approx 2.22$ MeV. This is an electromagnetic process which has a cross section much larger than those of the weak processes listed in Eq. (9.42), and thus it could stay in thermal equilibrium for quite a while. In other words, the deuterium would be broken apart as soon as it was produced if there were many photons and their energies were greater than $E_{\rm bind}$. Such a photodissociation process actually delayed the production of deuterium after the temperature T dropped below $E_{\rm bind}$. Defining the ratio of the baryon and photon number densities as $\eta \equiv n_{\rm B}/n_\gamma$, one may use the quantity $1/\eta \exp(-E_{\rm bind}/T)$ to approximately estimate the number of photons per baryon (i.e., per nucleon) above the deuterium photodissociation threshold energy. Note that η is the only free parameter in the BBN theory. Given $\eta \approx 6 \times 10^{-10}$, the number of photons with energies above $E_{\rm bind}$ is found to be roughly equal to that of baryons at $T \sim 0.1$ MeV or $t \sim 132$ s. Somewhat below this temperature the deuterium could begin to form without being immediately photodissociated again.

Over the next few minutes, almost all the neutrons that had survived since the BBN started were processed into the most stable light element ^{4}He via a number of dominant two-body processes such as $\mathrm{D} + n \to {}^3\mathrm{H} + \gamma$, $\mathrm{D} + \mathrm{D} \to {}^3\mathrm{H} + p$, $\mathrm{D} + p \to {}^3\mathrm{He} + \gamma$, $\mathrm{D} + \mathrm{D} \to {}^3\mathrm{He} + n$, and

$$\begin{aligned} &\mathrm{D} + \mathrm{D} \to {}^4\mathrm{He} + \gamma \ , \qquad {}^3\mathrm{H} + p \to {}^4\mathrm{He} + \gamma \ , \\ &\mathrm{D} + {}^3\mathrm{H} \to {}^4\mathrm{He} + n \ , \qquad \mathrm{D} + {}^3\mathrm{He} \to {}^4\mathrm{He} + p \ . \end{aligned} \tag{9.45}$$

Much heavier nuclei could not form in any significant quantity both because of the absence of stable nuclei with the mass number $A = 5$, 6 or 8 and due to the large Coulomb barriers for some relevant reactions (Weinberg, 2008; Perkins, 2009; Nakamura *et al.*, 2010). As an example, ^{7}Li and ^{7}Be could be produced through the processes

$$^3\mathrm{H} + {}^4\mathrm{He} \rightarrow {}^7\mathrm{Li} + \gamma\ , \qquad {}^3\mathrm{He} + {}^4\mathrm{He} \rightarrow {}^7\mathrm{Be} + \gamma\ ,$$
$$^7\mathrm{Be} + e^- \rightarrow {}^7\mathrm{Li} + \nu_e\ , \qquad {}^7\mathrm{Be} + n \rightarrow {}^7\mathrm{Li} + p\ . \tag{9.46}$$

One may therefore estimate the primordial mass fraction of ^{4}He (i.e., the ratio of the masses of all ^{4}He elements to those of all nuclei), conventionally referred to as $Y_{\rm p} = m_{\rm He} n_{\rm He} / \left[m_N \left(n_p + n_n \right) \right]$, by assuming that all of the neutrons ended up in ^{4}He. Namely, we have $n_{\rm He} \approx n_n/2$ and $m_{\rm He} \approx 4 m_N$ together with $m_N \approx m_p \approx m_n \approx 0.94$ GeV. In this approximation,

$$Y_{\rm p} \approx \frac{2 n_n}{n_p + n_n} \approx 0.246\ , \tag{9.47}$$

where $n_n/n_p \approx 0.14$ at $T \approx 0.09$ MeV or $t \approx 160$ s has typically been input. It should be pointed out that the observed ^{4}He abundance in the cosmos as given below is consistent with the above prediction from the BBN theory and far greater than the one which could have been produced from hydrogen burning in main-sequence stars (Perkins, 2009). Hence $Y_{\rm p}$ is truly a measure of the primordial ^{4}He abundance.

A semi-quantitative but more accurate expression of the ^{4}He mass fraction is given by (Cirelli *et al.*, 2005; Strumia and Vissani, 2006)

$$Y_{\rm p} \approx 0.248 + 0.0096 \times \ln \left(\frac{\eta}{6.15 \times 10^{-10}} \right) + 0.013 \times \left(N_\nu^{^4\mathrm{He}} - 3 \right)\ , \tag{9.48}$$

where $N_\nu^{^4\mathrm{He}}$ denotes the effective number of neutrino species relevant to the ^{4}He abundance. If there were a very light sterile neutrino contributing to the effective number of relativistic degrees of freedom during the BBN, the last term in Eq. (9.48) with $N_\nu^{^4\mathrm{He}} = 4$ would not be negligible. Hence the BBN theory allows us to constrain not only the baryon-to-photon ratio but also the number of neutrino species. To determine the value of $Y_{\rm p}$ as accurately as possible, one may measure the ^{4}He abundance in regions of hot ionized gas from "metal-poor" galaxies where only a relatively small amount of heavier elements have been produced through the stellar burning of hydrogen (Grupen *et al.*, 2005). So far a lot of data on ^{4}He and CNO have been accumulated from the most metal-poor (H II) regions in dwarf galaxies, and they confirm that the small stellar contribution to helium is positively correlated with the metal production (Nakamura *et al.*, 2010). Extrapolating a set of measurements of the ^{4}He mass fraction to zero metallicity yields the primordial value of $Y_{\rm p}$ as follows (Olive and Skillman, 2004): $Y_{\rm p} = 0.249 \pm 0.009$. Other recent extrapolations to zero metallicity lead us to $Y_{\rm p} = 0.247 \pm 0.001$ or 0.252 ± 0.001 (Izotov *et al.*, 2007), or $Y_{\rm p} = 0.248 \pm 0.003$ (Peimbert *et al.*, 2007). These results are apparently consistent with one another. Fig. 9.1 shows the numerical dependence of $Y_{\rm p}$ on η, constrained by both the BBN and CMB measurements (Cyburt *et al.*, 2008; Nakamura *et al.*, 2010).

A salient feature of the BBN theory is that it can account not only for the ^{4}He abundance but also for the other light elements (such as D, ^{3}He

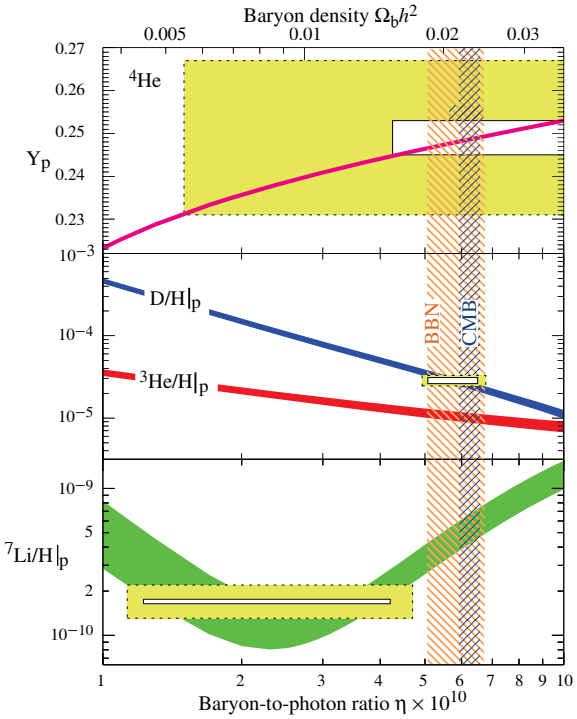

Fig. 9.1 The abundances of D, ^{3}He, ^{4}He and ^{7}Li elements predicted by the BBN theory, where the bands show the ranges at the 95% confidence level (Cyburt *et al.*, 2008). The boxes indicate the observational data with $\pm 2\sigma$ statistical errors (smaller boxes) or with $\pm 2\sigma$ statistical and systematic errors (larger boxes). The narrow vertical band stands for the CMB measurement of the cosmic baryon-to-photon ratio η, while the wider one represents the BBN concordance range. Both of them are given at the 95% confidence level (Nakamura *et al.*, 2010. With permission from the Institute of Physics).

and ^{7}Li) whose primordial abundances are rather small but far larger than the values that would have been if those light elements had only been produced from thermonuclear reactions in stellar interiors. Different from the ^{4}He abundance, which is traditionally given as the mass fraction $Y_{\rm p}$, the primordial abundances of the other light elements are usually presented as the number fractions. For instance, the ^{3}He abundance is described by the ^{3}He-to-hydrogen number density ratio $^3{\rm He/H}|_{\rm p} \equiv n_{^3{\rm He}}/n_{\rm H}$. Of particular importance is the primordial deuterium abundance, which can be estimated by the semi-quantitative formula (Cirelli *et al.*, 2005)

$$\left.\frac{\rm D}{\rm H}\right|_{\rm p} \approx (2.75 \pm 0.13) \times 10^{-5} \left(\frac{6.15 \times 10^{-10}}{\eta}\right)^{1.6} \left[1 + 0.11\left(N_\nu^{\rm D} - 3\right)\right] \quad (9.49)$$

with an uncertainty arising mainly from the nuclear cross sections. Assuming $N_\nu^{\rm D} = N_\nu^{^4{\rm He}} \equiv N_\nu$, one may therefore determine or constrain the magnitudes of η and N_ν by combining the measurements of $Y_{\rm p}$ in Eq. (9.48) and ${\rm D/H}|_{\rm p}$ in Eq. (9.49). This point is clearly illustrated in Fig. 9.1, where $N_\nu = 3$ has been taken to determine the cosmic baryon-to-photon ratio η from the BBN data on the primordial D and ^{4}He abundances.

Although deuterium can be produced via the reaction $p + p \to {\rm D} + e^+ + \nu_e$ in hydrogen-burning stars, it will quickly be fused into helium. Hence one believes that there are no astrophysical sources of deuterium (Epstein *et al.*, 1976). In order to measure the primordial D abundance, one has to detect the high-redshift and low-metallicity gas clouds which are far away and far back in time and thus have never been a part of stars (Grupen *et al.*, 2005). The presence of deuterium has been measured from some quasar absorption systems at high redshifts via its isotope-shifted Lyman-α absorption, and an average of the measurements done by several groups yields ${\rm D/H}|_{\rm p} = (2.82 \pm 0.21) \times 10^{-5}$ (Nakamura *et al.*, 2010). We expect that more accurate measurements of the D abundance might offer the most stringent constraint on the number of neutrino species during the BBN.

The best determination of the primordial ^{7}Li abundance comes from the measurements of hot metal-poor stars in the spheroid (Pop II) of our galaxy. One may extrapolate to zero metallicity to find out the magnitude of the lithium-to-hydrogen ratio ${\rm Li/H}|_{\rm p}$. Current experimental data yield ${\rm Li/H}|_{\rm p} = (1.7 \pm 0.06 \pm 0.44) \times 10^{-10}$, as shown in Fig. 9.1 (Nakamura *et al.*, 2010). But one can see that the stellar Li/H measurements are inconsistent with the CMB and D/H measurements because they apparently point to different values of η. For now this lithium problem is a central unresolved issue in the BBN theory, and its solution might involve new physics beyond the SM of particle physics (Jedamzik and Pospelov, 2009).

It is much more difficult to measure the primordial ^{3}He abundance, since the only available data on ^{3}He are from the solar system and high-metallicity (H II) regions in our galaxy (Bania *et al.*, 2002). But one might use the predicted value of the primordial ^{3}He-to-hydrogen ratio (i.e., ${}^3{\rm He/H}|_{\rm p}$ as shown in Fig. 9.1) to constrain stellar astrophysics.

9.2.3 The Baryon Density and Neutrino Species

Thanks to the BBN theory, it is possible to determine the cosmic baryon-to-photon ratio η and the number of neutrino species N_ν from some reliable measurements of the primordial ^{4}He and D abundances. The value of $\eta \equiv n_{\rm B}/n_\gamma$ allows us to calculate the baryon number density $n_{\rm B}$, since the photon number density $n_\gamma \approx 411\ {\rm cm}^{-3}$ is already known as given in Eq. (9.24) with the CMB temperature $T = 2.725$ K. We have $n_{\rm B} \approx 0.25\ {\rm m}^{-3}$ today for $\eta \approx 6 \times 10^{-10}$. The baryons are non-relativistic today, so their energy density is simply the total mass of nucleons per unit volume:

$$\rho_{\rm B} = m_N n_{\rm B} = m_N n_\gamma \eta \ , \tag{9.50}$$

where $m_N \approx m_p \approx m_n \approx 0.94$ GeV. Then we obtain the ratio of the energy density of baryons to the critical energy density of the Universe:

$$\Omega_{\rm B} \equiv \frac{\rho_{\rm B}}{\rho_{\rm c}} \approx 3.68 \times 10^7 \frac{\eta}{h^2} \ , \tag{9.51}$$

where $\rho_{\rm c}$ has been given in Eq. (9.9). Taking $\eta \approx 6 \times 10^{-10}$ and $h \approx 7.2$ today at $t = t_0$, for example, we arrive at $\Omega_{\rm B}(t_0) \approx 0.043$ together with $\rho_{\rm B}(t_0) \approx 2.32 \times 10^{-7}$ GeV cm^{-3} $\approx 4.12 \times 10^{-28}$ kg m^{-3}. This result is consistent very well with $\Omega_{\rm B}(t_0) = 0.0438 \pm 0.0013$ extracted from the recent measurement of temperature variations in the CMB radiation (Nakamura *et al.*, 2010). In comparison, $\Omega_{\rm r}(t_0) \approx 4.84 \times 10^{-5}$ and $\Omega_{\rm m}(t_0) \approx 0.26$. We see that $\Omega_{\rm B}(t_0) \gg \Omega_{\rm r}(t_0)$ holds but $\Omega_{\rm B}(t_0)$ itself is only about 16.5% of $\Omega_{\rm m}(t_0)$. It is worthwhile to make a remark here: while the relative numbers of photons, baryons and antibaryons would have been comparable in the first nanoseconds after the Big Bang (their difference should only be in spin multiplicity factors), most of the nucleons and antinucleons must have later disappeared due to their mutual annihilation, leaving a tiny — about one part per billion — excess of nucleons as the matter of the everyday world (Perkins, 2009). In other words, there is no primordial antimatter surviving today in the observable Universe. This cosmological matter-antimatter asymmetry will be discussed in detail in Chapter 11.

Once the cosmic baryon-to-photon ratio η is known, the primordial deuterium or helium abundance can be fixed to a quite narrow range by the BBN theory (see Fig. 9.1 for illustration). As shown in Eqs. (9.48) and (9.49), a simple comparison between the predicted and measured values of $Y_{\rm p}$ or $\left.{\rm D/H}\right|_{\rm p}$ allows us to determine or constrain the effective number of neutrino species. Note that the helium and deuterium curves in Fig. 9.1 are plotted by taking $N_\nu^{\rm eff} = 3$ in the limit of an instantaneous neutrino decoupling (Cyburt *et al.*, 2008). If small corrections for non-equilibrium neutrino heating are taken into account in the thermal evolution below $T \sim 1$ MeV, one has $N_\nu^{\rm eff} \approx 3.04$ (Seljak and Zaldarriaga, 1996; Mangano *et al.*, 2002). Note also that $N_\nu^{\rm eff}$ matters in the BBN era (for $T < m_e$) via the effective number of degrees of freedom

$$g_* \approx 2 \left[1.681 + 0.227 \left(N_\nu^{\rm eff} - 3\right)\right] \ , \tag{9.52}$$

which is equivalent to g'_* given in Eq. (9.41). For instance, $g_* \approx 3.82$ would hold if $N_\nu^{\rm eff} = 4$ were taken, as compared with $g_* \approx 3.36$ for $N_\nu^{\rm eff} = 3$. Hence the presence of extra neutrino flavors (or of any other relativistic species) at this time would enhance g_*, leading to a larger freeze-out temperature $T_{\rm fr}$, a larger neutron-to-proton ratio n_n/n_p and a larger ^{4}He mass fraction $Y_{\rm p}$ as one can easily see from Eqs. (9.32), (9.43) and (9.47). This observation was originally used to constrain the number of light neutrino families before the LEP experiment demonstrated $N_\nu = 3$ to a high degree of accuracy for the SM of electroweak interactions (Nakamura *et al.*, 2010).

The above discussions illustrate that the BBN provides us with an interesting playground to enjoy the interplay between particle physics and cosmology. Just as one may use the observed helium and deuterium abundances to probe the effective number of degrees of freedom g_*, any changes in the strong, weak, electromagnetic or gravitational coupling constants can be similarly constrained (Nakamura *et al.*, 2010). Furthermore, the constraints on the effective number of neutrino species can be translated into the limits on other types of particles or particle masses that would affect the expansion rate of the Universe during the BBN. For the sake of simplicity, however, we do not go into details of concrete new physics models and their possible consequences on the BBN in this book.

9.3 Possible Ways to Detect Relic Neutrinos

The Big Bang model of cosmology predicts the existence of a CνB composed of relic neutrinos which were decoupled from matter and radiation at about $T_{\rm fr} \lesssim 1$ MeV or $t \gtrsim 0.74$ s after the Big Bang. It is quite analogous to the well-known CMB, whose formation was at a time of about 3.8×10^5 years after the Big Bang (i.e., when the photons were decoupled from matter at a temperature of about 0.26 eV). At present the observational evidence for this CνB is rather indirect, coming mainly from the measurements of the primordial abundances of light elements, the anisotropies in the CMB and the large-scale structures of the cosmos. Is it possible to directly detect the CνB by means of current experimental technologies?

9.3.1 Cosmic Neutrino Background

In Section 9.1.5 we have shown that the large-scale properties of the CνB are closely related to those of the CMB. In particular, the temperatures or number densities of relic neutrinos and photons are related to each other:

$$T_\nu = \left(\frac{4}{11}\right)^{1/3} T_\gamma \; , \qquad n_\nu = \frac{9}{11} n_\gamma \; . \tag{9.53}$$

Given $T_\gamma \approx 2.725$ K and $n_\gamma \approx 411$ cm^{-3} for the CMB radiation today, the corresponding temperature and number density of the CνB turn out to be $T_\nu \approx 1.945$ K and $n_\nu \approx 336$ cm^{-3}. As a consequence, the average three-momentum of each relic neutrino is very small (Ringward, 2009):

$$\langle p_\nu \rangle = 3 T_\nu \approx 5.8 \text{ K} \approx 5 \times 10^{-4} \text{ eV} \; , \tag{9.54}$$

implying that at least two mass eigenstates of the relic neutrinos are already non-relativistic today no matter whether the neutrino mass spectrum has a normal hierarchy or an inverted hierarchy (see Section 8.4.1 for a similar

discussion). The CνB is naively expected to be homogeneous and isotropic on large scales, but it is somewhat subject to the gravitational clustering effect due to the existence of cold dark matter and baryonic structures. Hence some local overdensities might appear in the CνB as compared with the standard value given above, and the momentum distribution might more or less deviate from the one following from the Fermi-Dirac distribution.

The presence of the CνB can affect the evolution of CMB anisotropies and the growth of matter perturbations. For instance, relativistic relic neutrinos contributed to the energy density of radiation and thus had an impact on the time of matter-radiation equality. The free-streaming massive neutrinos could also suppress the growth of structures on small scales. Similar to CMB anisotropies, CνB anisotropies have been calculated although it is extremely difficult to detect them even in the far future. If neutrinos were massless, the power spectrum of CνB fluctuations would closely resemble the usual CMB spectrum without the baryon-photon acoustic oscillations (Hu *et al.*, 1995). The calculation of the primary CνB spectrum is rather complicated for massive neutrinos, and the CνB anisotropy can be quite sensitive to the absolute values of neutrino masses (Hannestad and Brandbyge, 2009).

9.3.2 Direct Detection of Relic Neutrinos

As indicated in Eq. (9.54), relic neutrinos have little kinetic energies today. It is extremely difficult to detect such low-energy neutrinos because the cross sections of their interactions with matter within a detector are terribly suppressed. Nevertheless, it is very important to directly verify the existence of the CνB in order to test the neutrino aspects of the Big Bang model of cosmology. Here we give a brief overview of a few proposals for the direct detection of the CνB in the present epoch and in our local neighborhood.

(1) *Relic neutrino capture on β-decaying nuclei.* The most promising method for detecting the CνB is to search for a peak, which is related to the capture of a relic electron neutrino, in the energy spectrum of a beta decay. This idea was first proposed by Steven Weinberg a long time ago (Weinberg, 1962; Irvine and Humphreys, 1983), and has recently attracted some interest (Cocco *et al.*, 2007, 2009; Lazauskas *et al.*, 2008; Blennow, 2008; Kaboth *et al.*, 2010; Li *et al.*, 2010). The point can be made clear as follows. Let us consider a nucleus N which can naturally undergo the beta decay $N \to N' + e^- + \overline{\nu}_e$ with an energy release $Q_\beta = m_N - m_{N'} - m_e > 0$ in the limit of vanishing neutrino masses (i.e., $m_i \to 0$ for $i = 1, 2, 3$). Then we see that the neutrino capture reaction

$$\nu_e + N \to N' + e^- \tag{9.55}$$

has a salient feature: it can take place with no threshold on the incident neutrino energy E_{ν_i} (for each mass eigenstate ν_i in ν_e). In contrast, the reaction $\overline{\nu}_e + N' \to N + e^+$ is subject to a threshold on the incoming antineutrino

energy $E_{\overline{\nu}_i}$. The number of events for the neutrino capture in Eq. (9.55) is determined by the product of the cross section of the reaction itself and the flux of relic ν_e neutrinos, which depend respectively on $1/v_{\nu_i}$ and v_{ν_i} with $v_{\nu_i} \sim 3T_\nu/m_i$ being the modulus of the velocity of ν_i (Lazauskas *et al.*, 2008). Hence it converges to a finite value even for $v_{\nu_i} \to 0$ or $E_{\nu_i} \to 0$ and can be reasonably large if a sufficient amount of the β-decaying target material is prepared (Cocco *et al.*, 2007; Lazauskas *et al.*, 2008). In the extreme case with $m_i \to 0$ and $E_{\nu_i} \to 0$, the ν_e neutrino contributes to this reaction via its correct lepton number and the final-state electron exactly possesses the β-decay endpoint energy Q_β. Given finite values of neutrino masses m_i, however, the monoenergetic electron's kinetic energy is $Q_\beta + E_{\nu_i} \gtrsim Q_\beta + m_i$ for each neutrino mass eigenstate ν_i. In comparison, the non-monoenergetic electron emitted from the beta decay $N \to N' + e^- + \overline{\nu}_e$ carries a kinetic energy $Q_\beta - E_{\nu_i} \lesssim Q_\beta - m_i$ for each ν_i if the recoil of the final-state nucleus N' is neglected. So there is a gap equal to or larger than $2m_i$ between the electron's kinetic energy in $\nu_e + N \to N' + e^-$ and that in $N \to N' + e^- + \overline{\nu}_e$ (Cocco *et al.*, 2007) [7]. This observation implies that it is possible, at least in principle, to distinguish the neutrino capture reaction from its corresponding beta decay by measuring the energy spectrum of final-state electrons to an unprecedentedly high degree of accuracy characterized by the neutrino masses. One may therefore has a chance to directly detect the presence of the CνB in this way.

The capture rate of relic electron neutrinos via $\nu_e + N \to N' + e^-$ can be given as (Lazauskas *et al.*, 2008; Blennow, 2008; Li *et al.* 2010)

$$\mathcal{N}^{(i)}_{\mathrm{C}\nu\mathrm{B}} \approx 6.5 |V_{ei}|^2 \frac{n_{\nu_i}}{\bar{n}_{\nu_i}} \ \mathrm{yr}^{-1} \ \mathrm{MCi}^{-1} \ , \tag{9.56}$$

where V_{ei} denotes the neutrino mixing matrix element and $|V_{ei}|^2$ measures the electron neutrino content of ν_i (for $i = 1, 2, 3$), $n_{\nu_i}/\bar{n}_{\nu_i}$ is the ratio of the relic neutrino density on the Earth to the mean relic neutrino density in the Universe for each neutrino mass eigenstate. With the help of Eq. (9.53), we have $\bar{n}_{\nu_i} = n_\nu/6 \approx 56 \ \mathrm{cm}^{-3}$. We expect that $n_{\nu_i}/\bar{n}_{\nu_i} \gtrsim 1$ holds in view of the gravitational clustering of relic neutrinos (Ringwald and Wong, 2004). Taking N to be the tritium (i.e., $\nu_e + {}^3\mathrm{H} \to {}^3\mathrm{He} + e^-$), for example, one has $Q_\beta = 18.6$ keV and 1 MCi source of tritium is about 100 g. In this case the capture rate should be reasonably large for a long running time of the experiment. The main problem is whether the CνB signal would be detectable given the overwhelming rate of the beta decay. Of course, the signal-to-noise ratio critically depends on m_i, $|V_{ei}|$ and the energy resolution

[7] If the mass of the lightest neutrino is below $\langle p_\nu \rangle$ given in Eq. (9.54) (i.e., it remains hot or relativistic today), then its energy can be expressed as $E_{\nu_i} \approx \sqrt{\langle p_\nu \rangle^2 + m_i^2}$, which is of $\mathcal{O}(\langle p_\nu \rangle)$ and hence has little impact on the overall electron energy spectrum under discussion (Li *et al.*, 2010).

of the detection apparatus Δ (Cocco *et al.*, 2007; Lazauskas *et al.*, 2008; Blennow, 2008; Kaboth *et al.*, 2010; Li *et al.*, 2010). But this ratio relies neither on the value of Q_β nor on the nuclear matrix elements for the final-state electrons to lie within the energy resolution interval Δ just below the endpoint. Given $m_i < \Delta$, the corresponding signal-to-noise ratio is expected to be

$$\frac{\mathcal{N}_{\rm C\nu B}^{(i)}}{\mathcal{N}_\beta^{(i)}} \approx 6\pi^2 \frac{n_{\nu_i}}{\Delta^3} \approx 2.5 \times 10^{-11} \frac{n_{\nu_i}}{\bar{n}_{\nu_i}} \left(\frac{1 \ {\rm eV}}{\Delta} \right)^3 . \tag{9.57}$$

This number is hopelessly small, unless it could be significantly enhanced by an extreme gravitational clustering effect.

It is unrealistic to apply the above method to all the presently-developed β-decay experiments, including the KATRIN experiment (Otten and Weinheimer, 2008), for two obvious reasons: (a) the amount of their target material is very small, leading to a tiny total capture rate of relic neutrinos; and (b) their energy resolution is very poor ($\Delta \gtrsim m_i$), such that the signal-to-noise ratio is too small to claim a discovery (Ringwald, 2009).

If the CνB consists of both active neutrinos (ν_1, ν_2, ν_3) and sterile neutrinos (ν_4, ν_5, $\cdots$), the latter may also leave an imprint on the electron energy spectrum in the capture of relic electron neutrinos by means of radioactive beta-decaying nuclei. To be more explicit, let us assume that the masses of sterile neutrinos are of $\mathcal{O}(0.1)$ eV and somewhat larger than the absolute mass scale of three active neutrinos. In this case we have a few very general expectations about the direct laboratory detection of the CνB and its sterile component (Li *et al.*, 2010). First, the signal of the sterile component of the CνB is on the right-hand side of the electron energy spectrum as compared with the signal of the active component of the CνB. Their separation is measured by their mass differences. Second, the rate of events for the signal of relic sterile neutrinos is crucially dependent on the magnitude of their mixing with active neutrinos. Hence a larger value of $|V_{ei}|$ (for $i \geqslant 4$) leads to a higher rate of signal events. Third, whether a signal can be separated from its background depends on the finite energy resolution Δ in a realistic experiment. In general, $\Delta \leqslant m_i/2$ (for $i = 1, 2, \cdots$) is required to detect the CνB via a neutrino capture reaction.

(2) *A Cavendish-type torsion balance for relic neutrinos.* We are not at rest with respect to the almost isotropic CMB, nor to the almost isotropic CνB because the Earth is moving through both of them. The coherent scattering of a relic neutrino flux off the target matter in a terrestrial detector may give rise to a mechanical force (Shvartsman *et al.*, 1982; Smith and Lewin, 1983), which is possibly detectable in a Cavendish-type torsion balance by searching for an annual modulation of the signal (Hagmann, 1999). The point is that relic neutrinos have a macroscopic de Broglie wavelength $\lambda_\nu = 1/T_\nu \approx 0.12$ cm, where $T_\nu \approx 1.945$ K has been input. So a terrestrial detector with a mass density ρ and a linear size $r < \lambda_\nu$ may experience a tiny acceleration induced by the neutrino wind due to the coherent neutrino-nucleon scattering effect.

If neutrinos are Dirac particles, which can have vectorial couplings, this tiny acceleration is described by (Ferreras and Wasserman, 1995; Duda *et al.*, 2001; Gelmini, 2005; Ringwald, 2009) [8]

$$a \approx \sum_{\nu,\bar{\nu}} \frac{4\pi}{3}\, \mathcal{N}_{\rm A}^2\, \rho\, r^3\, \sigma_{\nu N} \underbrace{(n_\nu\, v_{\rm rel})}_{\rm flux} \underbrace{(2\, m_\nu\, v_{\rm rel})}_{\rm mom.\ transfer}$$
$$\approx 2 \times 10^{-28}\ {\rm cm\ s^{-2}} \left(\frac{n_\nu}{\bar{n}_\nu}\right) \left(\frac{10^{-3}\, c}{v_{\rm rel}}\right) \left(\frac{\rho}{\rm g\ cm^{-3}}\right) \left(\frac{r}{\lambda_\nu}\right)^3 , \qquad (9.58)$$

where $\mathcal{N}_{\rm A}$ is Avogadro's number, $\sigma_{\nu N} \approx G_{\rm F}^2 m_\nu^2/\pi$ measures the cross section of elastic neutrino-nucleon scattering, and $v_{\rm rel} \equiv |\langle \mathbf{v} - \mathbf{v}_\oplus \rangle|$ denotes the mean velocity of the relic neutrinos in the rest system of the detector with $|\mathbf{v}_\oplus| \approx 7.7 \times 10^{-4}\, c$ being the velocity of the Earth through the Milky Way. If neutrinos are Majorana particles, which only have axial couplings, the corresponding acceleration involves a further suppression factor $(v_{\rm rel}/c)^2 \sim 10^{-6}$ for an unpolarized target or $v_{\rm rel}/c \sim 10^{-3}$ for a polarized target (Hagmann, 1999). The minimal acceleration that can be detected by current Cavendish-type torsion balances is of $\mathcal{O}(10^{-13})$ cm/s^2 (Adelberger *et al.*, 2009), overwhelmingly larger than the expected signal. Solar neutrinos and dark matter are likely to produce a much larger background (Strumia and Vissani, 2006).

(3) *The Stodolsky effect.* This effect consists of an energy split of the two spin states of non-relativistic electrons in the CνB; i.e., the energy of an electron receives an extra contribution $\Delta E_e \sim G_{\rm F} \mathbf{s} \cdot \mathbf{v} (n_\nu - n_{\overline{\nu}})$ that relies on the direction of its spin $\mathbf{s}$ with respect to the relic neutrino wind $\mathbf{v}$ (Stodolsky, 1974). The magnitude of ΔE_e depends on $G_{\rm F}$ instead of $G_{\rm F}^2$, but it might be suppressed by the asymmetry of relic neutrino and antineutrino number densities. The latter is defined as $\eta_\nu \equiv (n_\nu - n_{\overline{\nu}})/n_\gamma$. The Stodolsky effect is also dependent on the Dirac or Majorana nature of non-relativistic neutrinos (Gelmini, 2005). It practically manifests itself as a torque $\mathcal{T} \sim N_e \Delta E_e$ acting on a magnetized macroscopic object with N_e polarized electrons. In the typical case of one polarized electron per atom, an object with a linear size r and atomic number A may experience a tiny acceleration induced by the relic neutrino wind (Strumia and Vissani, 2006):

$$a \sim \frac{\mathcal{T}}{A N_e m_e r} \sim 10^{-28}\ {\rm cm\ s^{-2}} \left(\frac{100}{A}\right) \left(\frac{\rm cm}{r}\right) \left(\frac{\langle \mathbf{v} \rangle}{10^{-3}}\right) \eta_\nu\ . \qquad (9.59)$$

We see that the estimates in Eqs. (9.58) and (9.59) are comparable in magnitude, far below the present experimental sensitivities.

(4) *Z-bursts of relic and UHE neutrinos.* As discussed in Section 8.4.1, ultrahigh-energy (UHE) cosmic neutrinos may interact with the CνB and get absorbed via the following reactions taking place on the Z resonance:

[8] Since relic neutrinos are mostly non-relativistic today, their effects in question are significantly dependent on their Dirac or Majorana nature (Gelmini, 2005).

$\nu_{\rm UHE} + \overline{\nu}_{\rm C\nu B} \rightarrow Z \rightarrow$ hadrons and $\overline{\nu}_{\rm UHE} + \nu_{\rm C\nu B} \rightarrow Z \rightarrow$ hadrons (Weiler, 1982). In such a Z-burst event the kinetic energy of an UHE neutrino ν_i ought to be $E_{\nu_i} \approx M_Z^2/(2m_i) \approx 4.2 \times ({\rm eV}/m_i) \times 10^{21}$ eV, where m_i stands for the mass of ν_i. One may use the Z-burst mechanism to probe the existence of the CνB in two ways: one is to detect the "emission" feature of Z-bursts characterized by a directional excess of UHE cosmic rays, gamma rays and neutrinos above the well-known GZK cutoff $E_{\rm GZK} \sim 5 \times 10^{19}$ eV (see Section 8.1.1 for a detailed discussion), and the other is to observe the "absorption" feature in the UHE cosmic neutrino flux which is just the consequence of its interactions with the CνB on the Z resonance (Weiler 1982; Roulet, 1993; Yoshida, 1994). But in either case the signal rate is too small to be detected by means of the present technology of UHE neutrino telescopes.

References

Adelberger, E. G., *et al.*, 2009, Prog. Part. Nucl. Phys. **62**, 102.
Alpher, R. A., Bethe, H., and Gamow, G., 1948, Phys. Rev. **73**, 803.
Bania, T. M., *et al.*, 2002, Nature **415**, 54.
Blennow, M., 2008, Phys. Rev. D **77**, 113014.
Broadhurst, D., 2010, arXiv:1004.4238.
Cirelli, M., *et al.*, 2005, Nucl. Phys. B **708**, 215.
Cocco, A. G., Mangano, G., and Messina, M., 2007, JCAP **0706**, 015.
Cocco, A. G., Mangano, G., and Messina, M., 2009, Phys. Rev. D **79**, 053009.
Cyburt, R. H., *et al.*, 2008, JCAP **0811**, 012.
Dicus, D. A., *et al.*, 1982, Phys. Rev. D **26**, 2694.
Dolgov, A. D., *et al.*, 2002, Nucl. Phys. B **632**, 363.
Duda, G., Gelmini, G., and Nussinov, S., 2001, Phys. Rev. D **64**, 122001.
Epstein, R. I., *et al.*, 1976, Nature **263**, 198.
Ferreras, I., and Wasserman, I., 1995, Phys. Rev. D **52**, 5459.
Friedmann, A., 1922, Z. Phys. **10**, 377.
Gamow, G., 1946, Phys. Rev. **70**, 572.
Garnavich, P. M., *et al.* (Supernova Search Team), 1998, Astrophys. J. **509**, 74.
Gelmini, G. B., 2005, Phys. Scr. **T121**, 131.
Grupen, C., *et al.*, 2005, *Astroparticle Physics* (Springer-Verlag).
Hagmann, C., 1999, arXiv:astro-ph/9902102.
Hannestad, S., 2002, Phys. Rev. D **65**, 083006.
Hannestad, S., and Brandbyge, J., 2010, JCAP **1003**, 020.
Hu, W., *et al.*, 1995, Phys. Rev. D **52**, 5498.
Hubble, E., 1929, Proc. Nat. Acad. Sci. **15**, 168.
Irvine, J. M., and Humphreys, R., 1983, J. Phys. G. **9**, 847.
Izotov, Y. I., *et al.*, 2007, Astrophys. J. **662**, 15.
Jedamzik, K., and Pospelov, M., 2009, New J. Phys. **11**, 105028.
Kaboth, A., Formaggio, J. A., and Monreal, B., 2010, Phys. Rev. D **82**, 062001.
Kolb, E. W., and Turner, M. S., 1990, *The Early Universe* (Addison-Wesley, Redwood City).
Komatsu, E., *et al.* (WMAP Collaboration), 2009, Astrophys. J. Supp. **180**, 330.

Lazauskas, R., Vogel, P., and Volpe, C., 2008, J. Phys. G. **35**, 025001.
Li, Y. F., Xing, Z. Z., and Luo, S., 2010, Phys. Lett. B **692**, 261.
Mangano, G., *et al.*, 2002, Phys. Lett. B **534**, 8.
Mangano, G., *et al.*, 2005, Nucl. Phys. B **729**, 221.
Maor, I., *et al.*, 2002, Phys. Rev. D **65**, 123003.
Nakamura, K., *et al.* (Particle Data Group), 2010, J. Phys. G **37**, 075021.
Olive, K. A., and Skillman, E., 2004, Astrophys. J. **617**, 29.
Otten, E. W., and Weinheimer, C., 2008, Rept. Prog. Phys. **71**, 086201.
Peimbert, M., *et al.*, 2007, Astrophys. J. **667**, 636.
Perkins, D. H., 2009, *Particle Astrophysics* (Oxford University Press).
Perlmutter, S., Turner, M. S., and White, M. J., 1999, Phys. Rev. Lett. **83**, 670.
Ringwald, A., 2009, Nucl. Phys. A **827**, 501c.
Ringwald, A., and Wong, Y. Y. Y., 2004, JCAP **0412**, 005.
Roulet, E., 1993, Phys. Rev. D **47**, 5247.
Seljak, U., and Zaldarriaga, M., 1996, Astrophys. J. **469**, 437.
Shvartsman, B. F., *et al.*, 1982, JETP Lett. **36**, 277.
Smith, P. F., and Lewin, J. D., 1983, Phys. Lett. B **127**, 185.
Stodolsky, L., 1974, Phys. Rev. Lett. **34**, 110.
Strumia, A., and Vissani, F., 2006, arXiv:hep-ph/0606054.
Weiler, T. J., 1982, Phys. Rev. Lett. **49**, 234.
Weinberg, S., 1962, Phys. Rev. **128**, 1457.
Weinberg, S., 2008, *Cosmology* (Oxford University Press).
Yoshida, S., 1994, Astropart. Phys. **2**, 187.

10

Neutrinos and Cosmological Structures

As fairly stable and weakly interacting particles, relic neutrinos of the Big Bang must survive today and form a cosmic background similar to the cosmic microwave background (CMB) radiation. This cosmic neutrino background (CνB) played an important role in the evolution of the Universe. A measurement of the CMB anisotropies can tell us a lot of cosmological information, including the number of neutrino species and neutrino masses. Since massive neutrinos became non-relativistic when the temperature fell below their masses, they should have left an imprint on the clustering of galaxies. In this chapter we shall first describe how the CMB and large-scale structures (LSS) formed, and then discuss how to constrain neutrino masses from the measurements of the CMB and LSS. We shall also comment on sterile neutrinos as a possible candidate of warm dark matter in the Universe.

10.1 The Cosmic Microwave Background

The CMB radiation was first discovered by Arno Penzias and Robert Wilson in 1965 (Penzias and Wilson, 1965). The significance of this discovery was recognized with the Nobel Prize in Physics in 1978. Since then the CMB has become one of the most important pillars of the Big Bang model of cosmology. In 2006, John Mather and George Smoot received the Nobel Prize in Physics for their discovery of the blackbody form and anisotropy of the CMB radiation by means of the COBE satellite (Smoot *et al.*, 1992). It turns out that the CMB anisotropy measurements can place very precise constraints on a number of cosmological parameters, including the sum of neutrino masses, and thus have led us to the era of precision cosmology.

10.1.1 Matter-radiation Equality

As discussed in Section 9.2, the primordial nucleosynthesis started at about $t \approx 2$ s after the Big Bang. It was completed by about $t \approx 10^3$ s, after the tem-

perature had fallen to the level of $\mathcal{O}(10^{-2})$ MeV (Grupen *et al.*, 2005). Any neutrons that had not become bound into heavier nuclei by this time could no longer survive but would soon decay. Since then the early Universe evolved in a somewhat different way. The next remarkable event took place when the energy density of radiation (i.e., relativistic particles, including photons and neutrinos) became as low as the energy density of matter (i.e., non-relativistic particles, including nuclei and electrons). This matter-radiation equality signifies a transition of the Universe from its radiation-dominated era to its matter-dominated epoch. In the following let us work out the time of matter-radiation equality.

To estimate when the matter-radiation equality happened in the evolution of the early Universe, one needs some information on the energy densities of matter and radiation. It will be seen that a global analysis of current observational data on the CMB and LSS yields $\Omega_{\rm m}(t_0) \approx 0.26$ for non-relativistic matter and $\Omega_{\rm v}(t_0) \approx 0.74$ for vacuum energy if a flat Universe with $k = 0$ is assumed today at $t = t_0$ (Komatsu *et al.*, 2009; Nakamura *et al.*, 2010). In comparison, the energy density of photons $\rho_{\rm r}$ has a contribution $\Omega_{\rm r}(t_0) \approx 4.84 \times 10^{-5}$ as estimated below Eq. (9.25). Because the energy density of relativistic neutrinos ρ_ν is related to $\rho_{\rm r}$ through

$$\frac{\rho_\nu}{\rho_{\rm r}} = \frac{7}{8} \cdot \frac{g_\nu}{g_\gamma} \left(\frac{T_\nu}{T_\gamma} \right)^4 = \frac{21}{8} \left(\frac{4}{11} \right)^{4/3} \approx 0.681 \; , \tag{10.1}$$

we obtain $\Omega_\nu(t_0) = (\rho_\nu/\rho_\gamma)\Omega_{\rm r}(t_0) \approx 3.30 \times 10^{-5}$ for neutrinos [1]. The sum $\Omega_{\rm r}(t_0) + \Omega_\nu(t_0) \approx 8.14 \times 10^{-5}$ turns out to be about 3200 times smaller than $\Omega_{\rm m}(t_0)$. In addition, the energy density of non-relativistic baryons has a contribution $\Omega_{\rm B}(t_0) \approx 0.043$ as given below Eq. (9.51). Table 9.1 has provided us with the proportionality relations $\Omega_{\rm r} \propto \rho_{\rm r} \propto 1/R^4$ and $\Omega_{\rm m} \propto \rho_{\rm m} \propto 1/R^3$. Taking account of $R(t) = R(t_0)/(1+z)$, we find

$$\frac{\Omega_{\rm r}(t)}{\Omega_{\rm m}(t)} = \frac{\Omega_{\rm r}(t_0) R^4(t_0)}{R^4(t)} \cdot \frac{R^3(t)}{\Omega_{\rm m}(t_0) R^3(t_0)} = (1+z) \, \frac{\Omega_{\rm r}(t_0)}{\Omega_{\rm m}(t_0)} \; . \tag{10.2}$$

Then the redshift z for the *matter-photon* equality $\Omega_{\rm r}(t) = \Omega_{\rm m}(t)$ is given by

$$z = \frac{\Omega_{\rm m}(t_0)}{\Omega_{\rm r}(t_0)} - 1 \approx 5372 \; . \tag{10.3}$$

In a similar way, the redshift z for the *baryon-photon* equality $\Omega_{\rm r}(t) = \Omega_{\rm B}(t)$ is found to be

$$z = \frac{\Omega_{\rm B}(t_0)}{\Omega_{\rm r}(t_0)} - 1 \approx 887 \; ; \tag{10.4}$$

[1] Note that we have assumed neutrinos to be relativistic particles. When their masses are taken into account, at least two mass eigenstates of the relic neutrinos are already non-relativistic today. In this case $\Omega_\nu(t_0)$ should be estimated in a different way, as discussed in Section 10.2.

and the redshift z for the equality $\Omega_{\rm r}(t)+\Omega_{\nu}(t)=\Omega_{\rm m}(t)$ between the energy density of *matter* and that of *all relativistic particles* (i.e., both photons and neutrinos) is given by

$$z=\frac{\Omega_{\rm m}(t_0)}{\Omega_{\rm r}(t_0)+\Omega_{\nu}(t_0)}-1\approx 3193\,. \tag{10.5}$$

In order to figure out when the above equalities took place, one needs to establish the relations between t and t_0 via the redshift z. For illustration, we simply assume that the Universe has been matter-dominated since the matter-radiation equality. In this case $t\propto R^{3/2}$ holds as shown in Table 9.1, and therefore t is related to t_0 through

$$t=t_0\left[\frac{R(t)}{R(t_0)}\right]^{3/2}=\frac{t_0}{(1+z)^{3/2}}\,, \tag{10.6}$$

where $t_0\approx 13.7$ Gyr is the age of the Universe (Komatsu *et al.*, 2009). Then we obtain $t_{\rm mr}\approx 3.5\times 10^4$ yr for $z\approx 5372$ or $t_{\rm mr}\approx 7.6\times 10^4$ yr for $z\approx 3193$. Note that these numbers can only give us a ballpark feeling of the magnitude of $t_{\rm mr}$, because we know that the vacuum energy makes up an important portion of the total energy density of the Universe (i.e., $\Omega_{\rm v}(t_0)\approx 0.74$ today) and hence the assumption of matter dominance is more or less problematic.

When the energy density of matter exceeded that of radiation (i.e., for $z<3000$ as indicated by Eq. (10.5)), the gravitational clustering of matter could take place. Dark matter was vitally important here, because the dominance of baryons alone over radiation would not occur until very much later (e.g., at $z<900$ as indicated by Eq. (10.4) or after the decoupling of photons from matter) (Perkins, 2009).

10.1.2 Formation of the CMB

In the radiation-dominated epoch any protons and electrons that managed to bind into neutral hydrogen atoms via the reaction $p+e^-\rightarrow {\rm H}+\gamma$ would be immediately photodissociated via the inverse reaction ${\rm H}+\gamma\rightarrow p+e^-$. As the temperature T dropped significantly below the electron binding energy of hydrogen (i.e., $E_{\rm bind}=13.6$ eV), the formation of hydrogen became feasible and the Universe transformed from an ionized plasma into a gas of neutral atoms. This process is usually referred to as *recombination*. When the number density of free electrons in the cosmos was sufficiently small, the mean free path of a photon would be sufficiently long such that most photons have not scattered with matter since then. This phenomenon is usually called the decoupling of photons from matter.

Let us estimate the temperature and time of recombination. The process $p+e^-\leftrightarrow {\rm H}+\gamma$ should be in thermal equilibrium when the temperature T was above the ionization energy of hydrogen $E_{\rm bind}=13.6$ eV. We are interested

in what happened as the temperature fell. A naive expectation is that a significant amount of hydrogen could have been formed when T dropped below $E_{\rm bind}$. But the smallness of the baryon-to-photon ratio $\eta \equiv n_{\rm B}/n_\gamma \sim 6 \times 10^{-10}$ fixed during the Big Bang nucleosynthesis (BBN) implies that the number of photons with $E > E_{\rm bind}$ might be comparable with the number of baryons only at a much lower temperature. Note that the rate of the reaction $p + e^- \to {\rm H} + \gamma$ is proportional to the product of the number densities of protons and electrons $n_p n_e$, and the rate of the reaction ${\rm H} + \gamma \to p + e^-$ is proportional to the number density of hydrogen atoms $n_{\rm H}$ [2]. According to the Saha equation (Saha, 1921),

$$\frac{n_p n_e}{n_{\rm H}} = \left(\frac{m_e T}{2\pi}\right)^{3/2} \exp\left(-\frac{E_{\rm bind}}{T}\right) . \tag{10.7}$$

Here the total baryon number density is $n_{\rm B} = n_p + n_{\rm H}$. Using x to denote the fraction of hydrogen atoms which are ionized, we have $n_e = n_p = x n_{\rm B}$ and $n_{\rm H} = (1 - x) n_{\rm B}$. Then Eq. (10.7) can be rewritten as

$$\frac{x^2 n_{\rm B}}{1 - x} = \left(\frac{m_e T}{2\pi}\right)^{3/2} \exp\left(-\frac{E_{\rm bind}}{T}\right) . \tag{10.8}$$

One may numerically illustrate the changes of x with T by inputting the values of m_e and $E_{\rm bind}$. It is found that x catastrophically drops for T to vary from 0.35 eV to 0.25 eV (Perkins, 2009). This result implies that the Universe was transforming from an ionized plasma into an essentially neutral gas of hydrogen (and helium) at the recombination temperature $T_{\rm rec} \approx 0.3$ eV. A comparison between $T_{\rm rec}$ and today's CMB temperature $T_0 = 2.725\ {\rm K} = 2.348 \times 10^{-4}$ eV allows us to determine when recombination took place. Because of $T \propto 1/R$, the redshift at the time of recombination is

$$1 + z_{\rm rec} = \frac{R(t_0)}{R(t_{\rm rec})} = \frac{T_{\rm rec}}{T_0} . \tag{10.9}$$

Thus we obtain $z_{\rm rec} \approx 1277$. Assuming the Universe to be matter-dominated from this point up to today, we have $t \propto R^{3/2} \propto T^{-3/2}$ and thus

$$t_{\rm rec} = t_0 \left(\frac{T_0}{T_{\rm rec}}\right)^{3/2} = \frac{t_0}{(1 + z_{\rm rec})^{3/2}} . \tag{10.10}$$

Given $t_0 \approx 13.7$ Gyr as the age of the Universe, the time of recombination is then found to be $t_{\rm rec} \approx 3.0 \times 10^5$ yr.

Shortly after recombination, the mean free path of a photon became so long that radiation and matter were effectively decoupled. The decoupling

[2] Since the number density of photons n_γ is remarkably larger than n_p, n_e and $n_{\rm H}$, the reaction rate is essentially insensitive to n_γ (Perkins, 2009).

of photons from matter was of course not an instantaneous process, because a photon emitted upon recombination of one hydrogen atom could almost immediately ionize another hydrogen atom at $T \sim T_{\rm rec}$. While the Universe was an ionized plasma during this period, the photon scattering cross section was dominated by the Thomson scattering (i.e., the elastic scattering of electromagnetic radiation by a free charged particle). The mean free path of a photon was therefore determined by the decreasing number density of electrons as the Universe expanded. This path length became longer than the horizon distance (i.e., the radius of the observable Universe at a given time) at the decoupling temperature $T_{\rm dec} \approx 0.26$ eV, corresponding to a redshift $z_{\rm dec} \approx 1100$ (Grupen *et al.*, 2005). The decoupling time is determined by

$$t_{\rm dec} = t_0 \left(\frac{T_0}{T_{\rm dec}} \right)^{3/2} = \frac{t_0}{(1 + z_{\rm dec})^{3/2}} \, . \tag{10.11}$$

So we get $t_{\rm dec} \approx 3.8 \times 10^5$ yr, the approximate moment for the CMB to form.

After the decoupling of radiation from matter, the latter became transparent to the former and thus the formation of atoms and molecules could begin in earnest. We may define the "surface of last scattering" as the sphere centered about us with a radius equal to the mean distance to the last place where the CMB photons scattered (Grupen *et al.*, 2005). Such a distance is approximately equal to the one to where the matter-radiation decoupling took place, and the time of last scattering is essentially the same as $t_{\rm dec}$. In this sense, today's detection of the CMB is actually probing the conditions in the Universe at a time of roughly 3.8×10^5 years after the Big Bang.

10.1.3 Anisotropies of the CMB

The spectrum of the CMB measured initially by Penzias and Wilson could well be described by a blackbody function with a direction-independent temperature $T \sim 3$ K. In the 1970's it was found that the temperature was a bit higher in one particular direction of the microwave sky than in the opposite direction. This interesting anisotropy of the CMB, of $\mathcal{O}(10^{-3})$, was interpreted as being caused by the Earth's motion which should be equivalent to a peculiar velocity of the Milky Way (i.e., $v_{\rm MW} \sim 630$ km s^{-1}). In 1992, the COBE satellite discovered the temperature variations of $\mathcal{O}(10^{-5})$ in the CMB at smaller angular separations (Smoot *et al.*, 1992). These remarkable CMB anisotropies have been confirmed by a number of ground-based and ballon-borne measurements with much better sensitivities and angular resolutions (White *et al.*, 1994; Hu and Dodelson, 2002). In particular, the WMAP satellite has measured the CMB and its anisotropies to an unprecedentedly good degree of accuracy since 2003 (Bennett *et al.*, 2003; Jarosik *et al.*, 2007; Hinshaw *et al.*, 2009).

To describe the CMB anisotropies over a wide range of angular scales, one may consider the CMB temperature as a direction-dependent function

$T(\theta, \phi)$, where θ and ϕ stand respectively for the polar and azimuthal angles in the spherical coordinate system. This function can be expanded in terms of the spherical harmonic functions $Y_{\ell m}(\theta, \phi)$ as follows:

$$T(\theta, \phi) = \sum_{\ell=0}^{\infty} \sum_{m=-\ell}^{\ell} a_{\ell m} Y_{\ell m}(\theta, \phi) \; . \tag{10.12}$$

Such an expansion of the CMB sky is analogous to a Fourier series, in which the higher-order terms correspond to higher frequencies. Here the terms with higher ℓ values point to the structures of the CMB at smaller angular scales. A term in the series of Eq. (10.12) is usually referred to as a multipole moment: the $\ell = 0$ term is the monopole; the $\ell = 1$ term is the dipole; and so on. This language is borrowed from the multipole expansion used frequently in the study of electromagnetic and gravitational fields. Current theoretical models generally predict that the $a_{\ell m}$ modes are Gaussian random fields to a good degree of precision, and possible non-Gaussian effects are expected to be one or two orders of magnitude smaller than the present observational limits (Bartolo *et al.*, 2004). A statistically isotropic CMB sky means that all m values are equivalent; i.e., there is no preferred axis. Given this observation and the Gaussian statistics, the variance of the temperature field (or equivalently, the power spectrum in ℓ) can fully characterize the CMB anisotropies (Nakamura *et al.*, 2010). The power summed over all possible m values at each ℓ is $(2\ell + 1)C_\ell/(4\pi)$, where $C_\ell \equiv \langle |a_{\ell m}|^2 \rangle$ is defined. The set of C_ℓ (for $\ell = 0, 1, \cdots, \infty$) is called the angular power spectrum. The value of C_ℓ represents the level of the CMB structure measured at an angular separation $\Delta\theta \approx \pi/\ell$ (Grupen *et al.*, 2005). A measurement can only be able to resolve angles down to a minimum value, from which the maximal value of ℓ is then deducible.

(1) *The monopole.* The $\ell = 0$ term in the Laplace expansion of $T(\theta, \phi)$, which can be regarded as the monopole component of the CMB spectrum, signifies the temperature of the CMB averaged over all directions of the sky as shown in the left panel of Fig. 10.1. Its value with the 1σ error bar is $T_\gamma = 2.725 \pm 0.001$ K today (Mather *et al.*, 1999). The monopole distribution of the CMB is consistent with a blackbody function with $T = T_\gamma$, and the corresponding number density of relic photons is known as $n_\gamma \approx 411$ cm^{-3}.

(2) *The dipole.* The largest anisotropy of the CMB, with an amplitude of $\Delta T = 3.355 \pm 0.008$ mK (Hinshaw *et al.*, 2009) and a "yin-yang" pattern as shown in the middle panel of Fig. 10.1, is described by the $\ell = 1$ term in the Laplace expansion of $T(\theta, \phi)$. This dipole component of the CMB spectrum is characterized by the temperature variation $\Delta T/T_\gamma \approx 1.23 \times 10^{-3}$ and attributed to the Doppler shift caused by the Earth's motion relative to the nearly isotropic blackbody field, as confirmed by a measurement of the radial velocity of local galaxies (Courteau *et al.*, 2000). To be specific, the motion of an observer in the solar system with velocity v with respect to the rest frame of an isotropic Planckian radiation field of temperature T_0 produces a

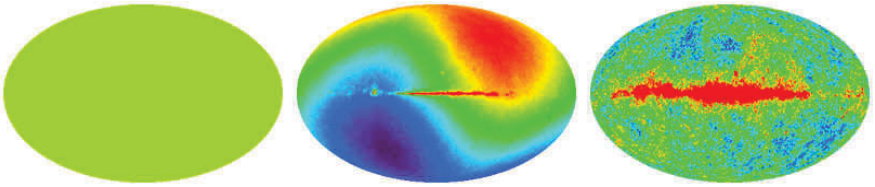

Fig. 10.1 The monopole (left), dipole (middle) and multipole (right) patterns in the cosmographic map of the CMB measured by the WMAP satellite (Courtesy of the WMAP Science Team, http://map.gsfc.nasa.gov/)

Doppler-shifted temperature pattern (Peebles and Wilkinson, 1968)

$$T(\theta) = T_0 \frac{\sqrt{1-\beta^2}}{1-\beta\cos\theta} \approx T_0 \left[1 + \beta\cos\theta + \mathcal{O}(\beta^2)\right] \ , \tag{10.13}$$

where θ is the angle between the line of sight and the direction of the motion of the observer, and $\beta \equiv v/c$ with c being the speed of light. The observed spectrum of the CMB as a function of θ is given by (Fixsen *et al.*, 1994)

$$S_\nu(\theta) = B_\nu(T) \approx B_\nu(T_0) + T_0 \beta \cos\theta \frac{\mathrm{d}B_\nu}{\mathrm{d}T}\bigg|_{T=T_0} \ , \tag{10.14}$$

where $B_\nu(T)$ denotes the Planck function. One observes a blackbody spectrum of the CMB at every point in the microwave sky with temperature $T(\theta)$. The monopole part of the spectrum is just described by $B_\nu(T_0)$, while the dipole part of the spectrum must have the shape of the derivative of $B_\nu(T)$ evaluated at the temperature $T = T_0$. Given $T_0 = T_\gamma$ together with $\Delta T = 3.355 \pm 0.008$ mK, the implied velocity for the solar system barycenter is $v = 369.0 \pm 0.9$ km s^{-1} towards $(\ell, b) = (263.99^\circ \pm 0.14^\circ, 48.26^\circ \pm 0.03^\circ)$ (Hinshaw *et al.*, 2009). The dipole anisotropy means that the CMB is blueshifted to a slightly higher temperature in the direction of motion and redshifted in the opposite direction. Because the dipole is a frame-dependent quantity, one may define a "local rest frame" of the Universe in which the CMB has no dipole anisotropy at all (Grupen *et al.*, 2005).

(3) *The multipoles.* The $\ell \geqslant 2$ terms in the Laplace expansion of $T(\theta, \phi)$ constitute the multipole part or small-angle anisotropies of the CMB spectrum characterized by the temperature variations $\Delta T/T_\gamma \sim 10^{-5}$. It was the COBE satellite that first discovered such small-angle CMB anisotropies, because it had an angular resolution $\Delta\theta \sim 7^\circ$ and could probe the angular power spectrum up to a multipole number $\ell \approx \pi/\Delta\theta \sim 20$ (Smoot *et al.*, 1992). An impressive multipole pattern in the cosmographic map of the CMB, as shown in the right panel of Fig. 10.1 (with the dipole component subtracted), has been established from the measurements of the WMAP satellite which has an angular resolution $\Delta\theta \sim 0.2^\circ$ and can therefore determine the angular

power spectrum up to $\ell \sim 1000$ (Bennett *et al.*, 2003; Jarosik *et al.*, 2007; Hinshaw *et al.*, 2009). The observed multipole effects can be interpreted as being mostly the result of small density fluctuations in the early Universe, manifesting themselves in the epoch of last scattering of the CMB photons. Such small density fluctuations could be amplified by gravity, with denser regions attracting more matter, until the non-relativistic matter of the Universe was separated into clumps. This picture is actually how the formation of galaxies is expected to have taken place (Grupen *et al.*, 2005). Given a certain amount of clumpiness observed today, it is possible to work out what density perturbations must have existed at the time of last scattering based on the Big Bang model of cosmology. Since these perturbations should correspond to regions of different temperatures, the observed LSS of the Universe would imply the existence of temperature variations at a level of about one part in 10^5 of T_γ in the microwave sky. Of course, this reasonable expectation was verified by the COBE and WMAP measurements.

Let us give a brief summary of the physics behind the CMB radiation. Before recombination, the baryons and photons were tightly coupled and the perturbations oscillated in the potential wells produced primarily by the dark matter perturbations (Nakamura *et al.*, 2010). After the decoupling of photons from baryons, the baryons were free to collapse into those potential wells. The CMB is expected to carry a record of conditions at the time of last scattering, often called the primary anisotropies. It may also be affected by a time-varying gravitational potential (i.e., the integrated Sachs-Wolfe effect or the so-called ISW rise), gravitational lensing and scattering from a homogeneous distribution of ionized gas at low redshifts. These effects can all be computed by using the CMBFAST (Seljak and Zaldarriaga, 1996) or CAMB (Lewis *et al.*, 2000) code based on the linear perturbation theory. The angular power spectrum of the CMB is usually plotted as $\ell(\ell+1)C_\ell/(2\pi)$ versus the multipole number ℓ, as shown in Fig. 10.2, in which a description of the physics underlying the CMB anisotropies can be separated into three main regions (Nakamura *et al.*, 2010):

- the ISW rise with $\ell \lesssim 10$ and the Sachs-Wolfe plateau with $10 \lesssim \ell \lesssim 100$ (Sachs and Wolfe, 1967) at large angular scales;
- the acoustic peaks with $100 \lesssim \ell \lesssim 1000$ at sub-degree angular scales;
- the damping tail with $\ell \gtrsim 1000$ at very tiny angular scales (Silk, 1968).

In particular, the acoustic peaks represent the oscillations of the photon-baryon fluid around the decoupling time of photons from matter. As mentioned above, the density fluctuations in the early Universe gave rise to gravitational instabilities. When a kind of matter fell into these gravitational potential wells, it was compressed and thereby heated up. This hot matter radiated photons causing the plasma of baryons to expand, and then it cooled down and hence produced less radiation. With decreasing radiation pressure the irregularities could reach a point at which gravity again took over and initiated another compression phase (Grupen *et al.*, 2005). A competition

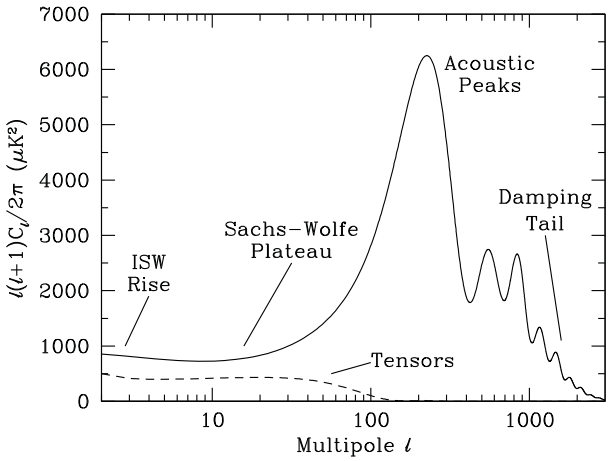

Fig. 10.2 A theoretical CMB anisotropy power spectrum computed from CMBFAST based on the standard ΛCDM model (Nakamura *et al.*, 2010. With permission from the Institute of Physics)

between the gravitational accretion and radiation pressure resulted in longitudinal acoustic oscillations in the photon-baryon fluid. After the decoupling of matter from radiation, the pattern of acoustic oscillations became frozen into the CMB. So the CMB anisotropies are actually a consequence of sound waves in the primordial baryon fluid. The first and most prominent acoustic peak appears at $\Delta\theta \sim 1^\circ$ or $\ell \sim 200$, as one can see from Fig. 10.2. Its position provides a measurement of the total energy density parameter Ω of the Universe. The fact that Ω is very close to unity implies that the early Universe should essentially be flat, as predicted by the inflation mechanism. The height of the first acoustic peak and the heights and positions of other peaks allow us to determine some other important cosmological parameters, such as the Hubble parameter, the baryon density and the amount of cold dark matter (Perkins, 2009).

10.1.4 Neutrino Species and Masses

An accurate measurement of the CMB anisotropy power spectrum may help determine or constrain the effective number of neutrino families and neutrino masses. Around the time of recombination (i.e., $t_{\rm rec} \sim 3\times10^5$ yr or $T_{\rm rec} \sim 0.3$ eV), the total energy density of relativistic particles (photons and neutrinos) can be expressed as follows:

$$\rho_{\rm r} + \rho_\nu = \rho_{\rm r}\left[1 + \frac{7}{8}\left(\frac{4}{11}\right)^{4/3} N_\nu^{\rm CMB}\right] , \tag{10.15}$$

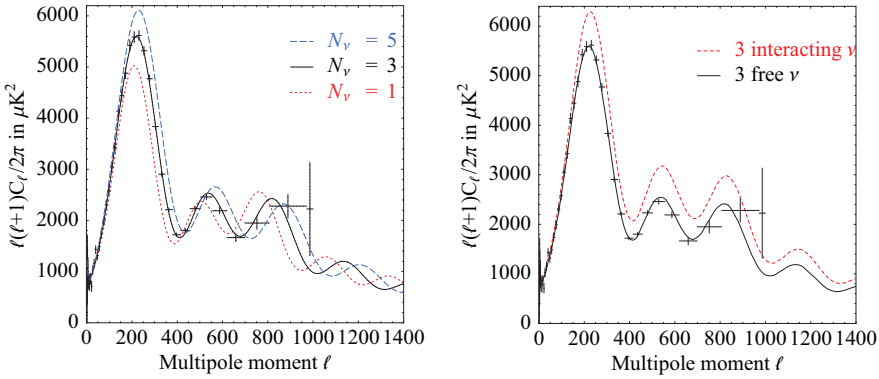

Fig. 10.3 How sensitive the power spectrum of CMB anisotropies is to the effective number of relativistic neutrino species (left) and to the fraction of free or interacting neutrinos (right), where the crosses denote the WMAP data and other parameters of the standard ΛCDM model have been fixed (Strumia and Vissani, 2006)

where $\rho_{\rm r}$ is the energy density of photons, $N_\nu^{\rm CMB}$ denotes the effective number of neutrino species relevant to the CMB, and Eq. (10.1) has been used by replacing "3" with $N_\nu^{\rm CMB}$. There are two different ways to reconstruct the value of $N_\nu^{\rm CMB}$ from the observational data on CMB anisotropies (Strumia and Vissani, 2006): (a) a determination of the energy density $\rho_{\rm r} + \rho_\nu$ which should significantly contribute to the measurable expansion rate of the Universe around recombination, because recombination took place slightly later than a transition from the radiation-dominated Universe to the matter-dominated one; (b) a determination of the energy density of freely-moving neutrinos which could slow down the growth of matter perturbations and the formation of galaxies and other structures (see Section 10.2 for more discussions). Fig. 10.3 illustrates how the power spectrum of CMB anisotropies changes with the effective number of relativistic neutrino species (left panel) and with the fraction of freely-moving or interacting neutrinos (right panel), where other cosmological parameters in the standard ΛCDM model have been fixed (Strumia and Vissani, 2006) [3]. Although current data on the CMB and its anisotropies are not precise enough to pin down the value of $N_\nu^{\rm CMB}$, it must not be far away from $N_\nu = 3$.

The WMAP Collaboration has recently reported $N_\nu^{\rm CMB} = 4.34^{+0.86}_{-0.88}$ at the 68% confidence level based on a careful analysis of the 7-year data (Komatsu *et al.*, 2010). A similar study including the SDSS data on the DR7 halo power spectrum has arrived at $N_\nu^{\rm CMB} = 4.78^{+1.86}_{-1.79}$ at the 95% confidence level (Hamann *et al.*, 2010a). These preliminary results seem to favor $N_\nu^{\rm CMB} > 3$,

[3] Note that the standard Big Bang model of cosmology is often referred to as the ΛCDM model, where the abbreviation ΛCDM means a combination of the cosmological constant Λ and cold dark matter.

implying that one or more sterile neutrinos with very small masses might exist and contribute to the total energy density of relativistic particles. If this is the case, such sterile neutrinos should mix with three active neutrinos and could be thermally excited by the interplay of oscillations and collisions (Kainulainen, 1990). Their mass scale is likely to lie in the sub-eV range and their family number might be one or two (Hamann *et al.*, 2010b). A mild conclusion is that the present cosmological constraints cannot be used as an argument against the existence of light sterile neutrinos.

The Planck spacecraft, which is taking data on the CMB with a much better degree of accuracy than the WMAP satellite, is expected to probe $N_\nu^{\rm CMB}$ up to the precision $\Delta N_\nu^{\rm CMB} = \pm 0.26$. Therefore, the ongoing Planck measurement has a good chance to confirm or rule out the hypothesis of light and cosmologically friendly sterile neutrinos (Hamann *et al.*, 2010b). If the CνB consists of both active and sterile neutrinos, how to directly detect them will be a great challenge. It is in principle possible to directly probe the active and sterile components of the CνB via the capture of relic electron neutrinos by means of radioactive beta-decaying nuclei (Li *et al.*, 2010), such as $\nu_e + {}^3{\rm H} \to {}^3{\rm He} + e^-$ (signal) against ${}^3{\rm H} \to {}^3{\rm He} + e^- + \overline{\nu}_e$ (background).

Note that a precision measurement of the CMB and its anisotropies can also help determine or constrain the sum of light neutrino masses m_i (for $i = 1, 2, \cdots$). When the temperature of the Universe was below m_i, the corresponding neutrino mass eigenstate would be non-relativistic. Hence neutrinos should be counted in the budget of non-relativistic matter when $T \lesssim m_i$, and be classified as radiation when $T \gtrsim m_i$. Such a "leak" from one category to the other is a rather specific effect of finite neutrino masses (Lesgourgues, 2010). By measuring the time of matter-radiation equality and other cosmological parameters, one may probe this leak and obtain a bound on the total mass of non-relativistic neutrinos $\sum m_i = 94 h^2 \Omega_\nu$ eV (see Eq. (10.21) for more discussions). The latter has been well constrained by means of current WMAP data combined with the distance information. Given the standard ΛCDM model with $k = 0$, an analysis of the 7-year WMAP data yields $\sum m_i < 1.3$ eV at the 95% confidence level (Komatsu *et al.*, 2010). After the latest distance measurements from the baryon acoustic oscillations in the distribution of galaxies (Percival *et al.*, 2010) and the Hubble constant measurement (Riess *et al.*, 2009) are also taken into account, one arrives at $\sum m_i < 0.58$ eV at the same confidence level (Komatsu *et al.*, 2010). This is currently the best upper limit on the sum of neutrino masses without information on the growth of structure.

10.2 Large-scale Structures and Dark Matter

The LSS in the Universe (e.g., galaxies, galactic clusters, superclusters, voids, etc.) should be seeded by some primordial density perturbations arising from quantum fluctuations during the period of inflation. The latter provides a

natural mechanism to solve the horizon problem, the flatness problem and the magnetic monopole problem in cosmology. Massive neutrinos must have played a role in the formation of the LSS, and they can leave a small imprint in the measurable amount of the gravitational clustering of galaxies. In this case it is possible to obtain a robust cosmological bound on the absolute mass scale of light active and sterile neutrinos.

10.2.1 Inflation and Density Fluctuations

The mechanism of inflation, which describes an exponentially accelerating phase in the very early Universe, was originally proposed by Alan Guth to solve the magnetic monopole problem (Guth, 1981). Magnetic monopoles were suggested by Paul Dirac a long time ago (Dirac, 1931), and their existence is definitely predicted in grand unified theories (GUTs). A magnetic monopole should be stable and its mass should be around the GUT scale $\Lambda_{\rm GUT} \sim 10^{16}$ GeV, but nobody has yet succeeded in observing it.

Model-independently, the elegant idea of inflation (Guth, 1981; Linde, 1982; Albrecht and Steinhardt, 1982) was motivated to resolve the cosmic horizon and flatness problems. The horizon problem arises on account of the observed isotropy of the CMB radiation out of the largest angles in the microwave sky. The horizon at the time of the decoupling between matter and radiation or equivalently the formation of the CMB (i.e., $t_{\rm dec} \approx 3.8 \times 10^5$ yr, corresponding to $T_{\rm dec} \approx 0.26$ eV and $z_{\rm dec} \approx 1100$) was of $\mathcal{O}(10^2)$ Mpc in size, subtending an angle of about 1° on the Earth today. It is therefore difficult to understand how the large-angle uniformity in temperature could have been achieved via some causal processes. In other words, the unexplained uniform temperature in regions that appear to be causally disconnected is referred to as the horizon problem (Grupen *et al.*, 2005; Perkins, 2009). The flatness problem is associated with today's observation that the total energy density of the Universe is very close to the critical energy density (i.e., $\Omega \equiv \rho/\rho_{\rm c} \approx 1$). With the help of Eq. (9.10), one has

$$\Omega - 1 = \frac{k}{\dot{R}^2} \sim \begin{cases} kt^{2/3} & (\text{matter-dominated era}, R \sim t^{2/3}) \,, \\ kt & (\text{radiation-dominated era}, R \sim t^{1/2}) \,. \end{cases} \tag{10.16}$$

Hence $\Omega(t_0) \approx 1$ at present (roughly matter-dominated) implies that $\Omega(t)$ must have been very much closer to unity at very early times of the Universe (essentially radiation-dominated), and the level of fine-tuning of $\Omega(t) \to 1$ at the Planck time would be of $\mathcal{O}(10^{-60})$ (Grupen *et al.*, 2005). This flatness problem implies that a Universe with non-vanishing curvature k today has to require very finely-tuned initial conditions, which seem to be very unnatural.

Let us take a look at how inflation works to solve the aforementioned problems. By definition, inflation means a short period of accelerating expansion in the very early Universe. If this period was dominated by the vacuum-energy term $\rho_{\rm v}$ in the Friedmann equation as given in Eq. (9.8), then the Universe

would undergo an exponential expansion described by $H = \dot{R}/R = \sqrt{\Lambda/3}$ with $\Lambda = 8\pi G_{\rm N}\rho_{\rm v}$ being the cosmological constant. Namely,

$$R(t) = R(t_{\rm i}) \exp\left[H\,(t - t_{\rm i})\right] \ , \tag{10.17}$$

where $t_{\rm i}$ denotes the initial time of inflation. In a specific inflation model it is possible to directly link $\rho_{\rm v}$ to the potential $V(\phi)$ of a scalar field $\phi(x)$ (Guth, 1981; Linde, 1982; Albrecht and Steinhardt, 1982). The form of $V(\phi)$ can be taken in such a way that the inflaton field first settles down into a metastable state or false vacuum near $\phi \approx 0$ and then effectively "rolls" down to the true vacuum (Grupen *et al.*, 2005). A combination of Eqs. (10.16) and (10.17) yields $\Omega(t) - 1 \propto \exp\left[-2H\,(t - t_{\rm i})\right]$, where H is a constant and t runs from the initial time $t_{\rm i}$ to the final time $t_{\rm f}$ of inflation. This result tells us that $\Omega(t)$ was exponentially driven towards unity during inflation. So one may easily obtain $\Omega(t_{\rm f}) \approx 1$ only if $H\,(t_{\rm f} - t_{\rm i})$ or $\rho_{\rm v}$ is sufficiently large. The flatness problem can therefore be resolved in this way, since $\Omega(t_0) \approx 1$ observed today must be intrinsically associated with $\Omega(t_{\rm f}) \approx 1$ as a consequence of the evolution of the Universe from $t_{\rm f}$ to t_0 through the radiation- and matter-dominated epochs. Note that a region of size $D(t)$ in the physical coordinate system would expand in proportion to the scale factor $R(t)$ during inflation. Hence the size $D(t_{\rm i})$ of a region, which was in causal contact at the beginning of inflation, would become $D(t_{\rm f}) = D(t_{\rm i}) \exp\left[H\,(t_{\rm f} - t_{\rm i})\right]$ at the end of inflation. The present size $D(t_0)$ of this region, in which everywhere has been causally connected, must be intrinsically related to $D(t_{\rm f})$ and thus can be sufficiently large (e.g., much larger than the current Hubble distance $ct_0 \approx c/H_0 \sim 10^{26}$ m) by adjusting the exponential factor $\exp\left[H\,(t_{\rm f} - t_{\rm i})\right]$. So the currently visible Universe, including the entire surface of last scattering, can easily fit into a much larger region which has been in causal contact and has been at the same temperature (Grupen *et al.*, 2005). This is just the solution to the horizon problem. In other words, inflation provides a natural mechanism to ensure the isotropy of the CMB radiation in the entire microwave sky to a high degree of accuracy. A solution to the magnetic monopole problem is also straightforward. One may simply assume that magnetic monopoles were produced before or during the period of inflation. In a GUT framework whose typical temperature and time scales were $T \sim 10^{16}$ GeV and $t \sim 10^{-39}$ s, for example, one expects that inflation should be taking place during the period from $t_{\rm i} \sim 10^{-38}$ s to $t_{\rm f} \sim 10^{-36}$ s. The number densities of magnetic monopoles at the beginning and end of inflation are related to each other via $n(t_{\rm f}) = n(t_{\rm i}) \exp\left[-3H\,(t_{\rm f} - t_{\rm i})\right]$, just because the volume containing a given number of magnetic monopoles increase in proportion to $R^3(t)$. Hence $n(t_{\rm f})$ must be vanishingly small if $H\,(t_{\rm f} - t_{\rm i})$ is sufficiently large as required to solve the flatness and horizon problems. Since today's number density of magnetic monopoles $n(t_0)$ must be intrinsically associated with $n(t_{\rm f})$, we expect that the inflationary expansion of the Universe made $n(t_0)$ so small that there might not even exist a single magnetic monopole in the observable Universe. That is why one has never seen a magnetic monopole.

After inflation the energy $\rho_{\rm v} \approx V(0)$ was transferred to particles such as photons, electrons and neutrinos, but their energy density turned to decrease as the Universe continued to expand in a relatively mild way. Because inflation itself might not simultaneously end everywhere [4], the commencement of this energy density decrease was somewhat delayed in regions where inflation went on a bit longer. As a result, the variation in the time of the end of inflation provides a natural mechanism to interpret spatial variations in the energy density. Such primordial density fluctuations were later on amplified by gravity and finally led to the LSS observed today, such as galaxies, galactic clusters and superclusters. As discussed in Section 10.1.3, quantum fluctuations at the very beginning of inflation were also responsible for the observed CMB anisotropies at the $\mathcal{O}(10^{-5})$ level in the microwave sky. They would become frozen density fluctuations when they were inflated beyond the causal horizon (Perkins, 2009).

The existence of the LSS is naturally attributed to the primordial density fluctuations. To be more explicit, let us consider the relative difference between the density at a given position and the average density:

$$\delta(\mathbf{x}) \equiv \frac{\rho(\mathbf{x}) - \langle\rho\rangle}{\langle\rho\rangle} \ . \tag{10.18}$$

Now that this density contrast inhabits a Universe which is isotropic and homogeneous on sufficiently large scales, its statistical nature should also be isotropic and homogeneous. One usually describes $\delta(\mathbf{x})$ as a Fourier series with periodic boundary conditions:

$$\delta(\mathbf{x}) = \sum \delta_{\mathbf{k}} \mathrm{e}^{\mathrm{i}\mathbf{k}\cdot\mathbf{x}} \ , \tag{10.19}$$

where the sum is taken over all values of $\mathbf{k} = (k_x, k_y, k_z)$ which fit into a cube of size L and volume $V = L^3$ (e.g., $k_x = 2\pi n_x/L$ with $n_x = 0, \pm1, \pm2, \cdots$; and similarly for k_y and k_z). Averaging over all directions yields the average magnitude of the Fourier coefficients as a function of $k = |\mathbf{k}|$ (Grupen *et al.*, 2005). So the matter power spectrum is defined as

$$P(k) \equiv \langle|\delta_k|^2\rangle = \langle|\delta_{\mathbf{k}}|^2\rangle \ , \tag{10.20}$$

which measures the level of structure at a wavelength $\lambda = 2\pi/k$. In most of the structure formation models one arrives at a primordial power law of the form $P(k) \sim k^n$, where $n = 1$ denotes the scalar spectral index and yields a scale-invariant Harrison-Zeldovich spectrum. Most of the inflationary models predict $|n-1| \lesssim 3\%$, and the exact value of n depends on the form of the potential $V(\phi)$ (Peacock, 1999; Liddle and Lyth, 2000). For example, an analysis of the 5-year WMAP data yields $n = 0.963^{+0.014}_{-0.015}$ based on the standard ΛCDM model (Nakamura *et al.*, 2010).

[4] Due to quantum fluctuations, the value of the inflaton field ϕ at the onset of inflation would not be exactly the same at all places (Grupen *et al.*, 2005).

In short, the main success of inflationary models is that they provide us with a simple but dynamical interpretation of specific initial conditions of the Universe such that the horizon, flatness and magnetic monopole problems can naturally be resolved. Moreover, inflation offers a natural mechanism to explain the primordial density fluctuations which finally grew into the LSS such as galaxies and clusters observed today. We shall proceed to discuss the indispensable role of dark matter in the formation of the LSS.

10.2.2 LSS and Dark Matter

The LSS observed today should most likely have evolved from gravitational instabilities which can be traced back to the primordial density fluctuations in the very early Universe. Such small perturbations in the energy density were amplified by gravity, and in the course of time they would collect more and more matter and lead to the formation of the LSS. The latter requires a sufficient amount of mass, otherwise the original density fluctuations could never have been transformed into distinct mass aggregations (Grupen *et al.*, 2005). However, the amount of visible matter itself has been found to be insufficient for the Universe to reach the critical energy density today (i.e., $\Omega \approx 1$). Non-baryonic dark matter is therefore needed in order to understand the dynamics of the Universe and its evolution.

In 1933, Fritz Zwicky found that luminous galaxies in the Coma cluster of galaxies moved faster than one would have expected if they had only felt the gravitational attraction from other visible objects (Zwicky, 1933, 1937). He was the first to infer the existence of dark matter by means of the virial theorem. In 1970 and 1980, Vera Rubin and her collaborators measured the rotation curves of individual galaxies and found further evidence for invisible matter (Rubin and Ford, 1970; Rubin *et al.*, 1980). Recent observations of clusters of galaxies yield $\Omega_{\rm DM} \approx 0.2$ as compared with $\Omega = 1$ for a flat Universe. They include measurements of the peculiar velocities of galaxies in the cluster; measurements of the X-ray temperature of hot gas in the cluster; and most directly, studies of (weak) gravitational lensing of background galaxies on the cluster (Nakamura *et al.*, 2010). A particularly compelling example is the bullet cluster (1E0657-558) which passed through another cluster recently. The hot gas forming most of the baryonic mass of these two clusters was shocked and decelerated, whereas the galaxies in them proceeded on ballistic trajectories. Gravitational lensing indicates that most of the total mass of the clusters also moved ballistically, implying that the self-interaction of dark matter should be quite weak (Clowe *et al.*, 2006; Nakamura *et al.*, 2010). In addition, current cosmological observations have clearly demonstrated the existence of a large quantity of cold dark matter and accurately determined the value of $\Omega_{\rm CDM}$. For example, an analysis of the 5-year WMAP data yields $\Omega_{\rm CDM}h^2 = 0.110 \pm 0.006$ with $h = 0.72 \pm 0.03$ (Dunkley *et al.*, 2009; Komatsu *et al.*, 2009). This result can be compared with the total matter density $\Omega_{\rm m}$ and the baryonic matter density $\Omega_{\rm B}$ obtained from the same

analysis based on the standard ΛCDM model, as shown in Table 10.1. We see $\Omega_{\rm CDM}/\Omega_{\rm m} \approx 83\%$ and $\Omega_{\rm B}/\Omega_{\rm m} \approx 17\%$; i.e., cold dark matter dominates today's matter content of the Universe. So somebody said, "If it's not *dark*, it doesn't *matter*" (Grupen *et al.*, 2005). Note that the average density of cold dark matter in the "neighborhood" of our solar system is roughly equal to that of luminous matter (stars, gas and dust): $\rho_{\rm CDM}^{\rm local} \approx 0.3$ GeV cm^{-3} (Kamionkowski and Kinkhabwala, 1998) and thus much larger than today's critical energy density of the Universe $\rho_{\rm c} \approx 5.4 \times 10^{-6}$ GeV cm^{-3}.

Table 10.1 Some important cosmological parameters determined from an analysis of the 5-year WMAP data based on the standard ΛCDM model (Nakamura *et al.*, 2010. With permission from the Institute of Physics). The cold dark matter density $\Omega_{\rm CDM}$ is given by $\Omega_{\rm CDM} = \Omega_{\rm m} - \Omega_{\rm B} - \Omega_{\nu}$

Parameter	Value
The Hubble parameter h	0.72 ± 0.03
The total matter density $\Omega_{\rm m}$	$\Omega_{\rm m}h^2 = 0.133 \pm 0.006$
The baryon density $\Omega_{\rm B}$	$\Omega_{\rm B}h^2 = 0.0227 \pm 0.0006$
The vacuum energy density $\Omega_{\rm v}$	$\Omega_{\rm v} = 0.74 \pm 0.03$
The radiation density $\Omega_{\rm r}$	$\Omega_{\rm r}h^2 = 2.47 \times 10^{-5}$
The neutrino density Ω_{ν}	$\Omega_{\nu}h^2 = \sum m_i/(94\ {\rm eV})$

The nature of dark matter remains a mystery in particle physics and cosmology. A candidate for non-baryonic dark matter must satisfy the following three conditions (Nakamura *et al.*, 2010): (a) it must be stable on cosmological time scales, otherwise it would have decayed by now; (b) it must interact very weakly with electromagnetic radiation, otherwise it would not be qualified as dark matter; and (c) it must have the right relic density. Possible candidates of cold dark matter include primordial black holes, axions and weakly interacting massive particles (WIMPs).

- Primordial black holes were proposed in a few cosmological models as a candidate for dark matter (Kohri *et al.*, 2008). They must have formed before the BBN epoch, otherwise they would have been counted as baryonic matter instead of cold dark matter.
- Axions were first postulated to resolve the strong CP problem in quantum chromodynamics (Peccei and Quinn, 1977). This kind of pseudo-Nambu-Goldstone bosons may result from the spontaneously broken Peccei-Quinn $U(1)$ symmetry at very high energies. Axions could constitute cold dark matter if they were non-thermally produced in the early Universe and their masses lie in the sub-eV range (e.g., from $\mathcal{O}(10^{-6})$ eV to $\mathcal{O}(1)$ eV).
- WIMPs are by definition a kind of particles whose interactions with ordinary matter are weak and whose masses lie in the range between 10 GeV

and a few TeV. WIMPs could constitute cold dark matter if they were thermally produced in the early Universe and then froze out after the temperature was below their masses. The lightest supersymmetric particle (e.g., neutralino) is currently the best motivated and widely studied WIMP candidate (Nakamura *et al.*, 2010).

These candidates for cold dark matter are all detectable by means of current experimental techniques, but no convincing evidence for any of them has so far been found. The present dark matter searches include direct searches, indirect searches and collider searches. Taking WIMPs for example, one may directly search for them by detecting their interactions with ordinary matter through elastic scattering on nuclei; or indirectly search for them by detecting their annihilation products such as neutrinos, gamma rays, positrons, antiprotons and antinuclei; or look for their signatures at high-energy colliders such as the Large Hadron Collider (LHC). A combination of all of them is necessary in order to pin down the nature of WIMPs on solid ground.

In general, candidates for dark matter are subdivided into three categories: "hot", "cold" and "warm" particles. Primordial black holes, axions and WIMPs belong to cold dark matter. The typical example of hot dark matter is light neutrinos. Sterile neutrinos with masses of $\mathcal{O}(1)$ keV are possible to constitute warm dark matter. A lot of more or less "exotic" candidates for dark matter have also been proposed in the literature. Although the nature of cold dark matter remains unclear, we believe that it dominates the matter content of the Universe and is primarily responsible for the formation of the observed LSS. The status and prospects of direct and indirect dark matter searches have recently been reviewed by the Particle Data Group (Nakamura *et al.*, 2010) and other authors (Feng, 2010).

10.2.3 Constraints on Neutrino Masses

Given the CνB temperature $T_\nu \approx 1.945$ K today, the average three-momentum of each relic neutrino is expected to be $\langle p_\nu \rangle = 3T_\nu \approx 5 \times 10^{-4}$ eV as given in Eq. (9.54). Hence neutrinos have become non-relativistic today if their masses are larger than $\langle p_\nu \rangle$. In this case the present CνB contribution to the total energy density of the Universe is [5]

[5] If one of the neutrinos has a mass much smaller than $\langle p_\nu \rangle$, it may remain relativistic today. But its contribution to the sum of all neutrino masses is insignificant, so Eq. (10.21) remains valid as a good approximation. On the other hand, light sterile neutrinos and antineutrinos should be most likely to stay in full thermal equilibrium in the early Universe provided their mixing with active neutrinos and antineutrinos is not strongly suppressed (Hannestad and Raffelt, 1999). In this case their number densities are expected to be equal to those of active neutrinos and antineutrinos, because the calculation of n_{ν_i} and $n_{\overline{\nu}_i}$ has nothing to do with the flavor properties. Therefore, the sum in Eq. (10.21) is over both active and sterile neutrinos only if they are sufficiently light.

$$\Omega_\nu \equiv \frac{\rho_\nu}{\rho_{\rm c}} = \frac{8\pi G_{\rm N}}{3H^2} \sum_i m_i \left(n_{\nu_i} + n_{\overline{\nu}_i} \right) \approx \frac{1}{94\ h^2\ {\rm eV}} \sum_i m_i \ , \tag{10.21}$$

where $n_{\nu_i} = n_{\overline{\nu}_i} \approx 56\ {\rm cm}^{-3}$ is today's number density of relic ν_i neutrinos or $\overline{\nu}_i$ antineutrinos as given in Eq. (8.27) or Eq. (9.40). The small values of m_i yield a small value of Ω_ν, typically of $\mathcal{O}(10^{-2})$ or smaller if the sum of m_i is of $\mathcal{O}(1)$ eV or smaller. But small effects of neutrino masses may still leave an imprint in the measurable amount of clustering of galaxies.

Table 10.1 lists today's energy densities of neutrinos, photons, baryons and total matter as compared with the vacuum energy density (or equivalently, the cosmological constant). In fact, ρ_ν, ρ_γ, $\rho_{\rm B}$ and $\rho_{\rm CDM}$ all decreased with the expansion of the Universe. The evolution of these energy densities is shown in Fig. 10.4 (Strumia and Vissani, 2006), from which one can clearly see the transition from the radiation-dominated epoch to the matter-dominated epoch around $T \sim \mathcal{O}(1)$ eV. As discussed before, gravity amplified the primordial density fluctuations of cold dark matter. This gravitational clustering process finally led to the formation of galaxies and other LSS that we have observed today. Relativistic particles with a mean free path larger than the horizon, such as relativistic neutrinos, could freely stream in the Universe and thus suppress the gravitational clustering process. However, neutrino masses should more or less hinder the free streaming of neutrinos because their velocities were smaller than the speed of light such that they could only travel in a fraction of the horizon within the Hubble time. On the other hand, the contribution of massive neutrinos to the total energy density of the Universe tended to increase the cosmological expansion which would weaken gravitational interactions and slow down the formation of structures. A careful study of the formation rate of structures in the recent past of the Universe should therefore provide us with a unique opportunity to measure the absolute neutrino mass scale.

Similar to Eq. (10.18), small fluctuations in the density of cold dark matter can be described by $\delta_{\rm CDM}(\mathbf{x}) \equiv [\rho_{\rm CDM}(\mathbf{x}) - \langle \rho_{\rm CDM} \rangle]/\langle \rho_{\rm CDM} \rangle$. The evolution of this parameter obeys (Bond *et al.*, 1980; Kolb and Turner, 1990)

$$\ddot{\delta}_{\rm CDM} + 2H\dot{\delta}_{\rm CDM} = 4\pi G_{\rm N} \Delta\rho \ , \tag{10.22}$$

where $\Delta\rho \equiv \rho(\mathbf{x}) - \langle \rho \rangle$ denotes the perturbations to the total energy density ρ. To examine the role of neutrinos with respect to that of cold dark matter in the LSS, we simply take $\rho \approx \rho_{\rm CDM} + \rho_\nu$ by neglecting other components of ρ. As long as $T \gg m_i$, neutrinos would be relativistic and have little chance to cluster. In this case we take $\Delta\rho_\nu = 0$ and rewrite Eq. (10.22) as

$$\ddot{\delta}_{\rm CDM} + 2H\dot{\delta}_{\rm CDM} = 4\pi G_{\rm N} \rho \, (1 - f_\nu) \, \delta_{\rm CDM} \ , \tag{10.23}$$

where $f_\nu \equiv \rho_\nu/\rho$. Given a spatially flat Universe with $k = 0$ or $\rho = \rho_{\rm c} = 3H^2/(8\pi G_{\rm N})$, an analytical solution to Eq. (10.23) can be found in the matter-dominated era with $H = 2/(3t)$. One obtains $\delta_{\rm CDM} \propto t^{2/3} \propto a(t) \propto$

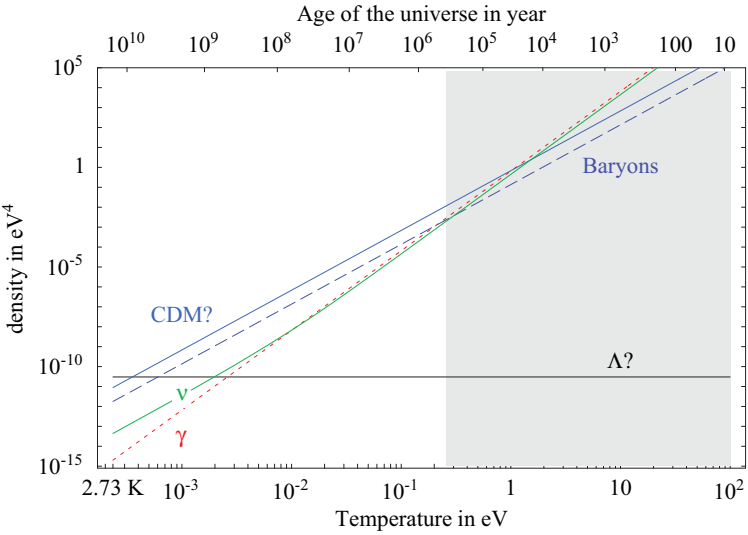

Fig. 10.4 Evolution of the energy densities of photons, neutrinos, baryons and cold dark matter (CDM) between $T \sim 10^2$ eV and $T_0 \approx 2.73$ K today, as compared with the cosmological constant Λ, based on the standard ΛCDM model (Strumia and Vissani, 2006). Note that neutrinos were relativistic at $T \gg m_i$ (where $\rho_\nu \propto T^4$) and non-relativistic at $T \lesssim m_i$ (where $\rho_\nu \propto m_i T^3$). For simplicity, different neutrino species are assumed to have the degenerate mass of $\mathcal{O}(0.1)$ eV. The shaded area covers the epoch before the decoupling of photons from matter

T^{-1} by taking $f_\nu = 0$, where $a(t) \equiv R(t)/R(t_0)$ is the dimensionless scale parameter and satisfies Hubble's law $\dot{a}(t) = Ha(t)$. During the period from $T \sim 1$ eV to $T_0 = 2.725$ K, the primordial fluctuations were enhanced by a large factor $T/T_0 \sim 4300$ and thus produced the LSS as one has observed today (Strumia and Vissani, 2006). Of course, $f_\nu \neq 0$ would somewhat suppress the growth of the dark matter fluctuations. One may obtain $\delta_{\rm CDM} \propto a^p(t)$ with $p = [\sqrt{1 + 24(1 - f_\nu)} - 1]/4$ in the assumption of a constant f_ν. It is obvious that the primordial fluctuations would have never grown (i.e., $p = 0$) if the Universe had been dominated by relativistic particles with $f_\nu = 1$ (i.e., $\rho = \rho_\nu$). That is why only the matter-dominated epoch was relevant to the formation of the LSS. Note that the cosmological constant (or vacuum energy) gradually dominated the energy density of the Universe after the temperature was below $T \lesssim 10^{-3}$ eV as shown in Fig. 10.4. It would reduce the late-time growth of the dark matter fluctuations by a factor $\sim 1/4$ (Strumia and Vissani, 2006; Lesgourgues and Pastor, 2006). Neutrinos became non-relativistic after $T \sim m_i$. One has $f_\nu = \Omega_\nu/\Omega \sim \Omega_\nu$ for non-relativistic neutrinos, as given in Eq. (10.21). Even such a small f_ν could make the growth of structure a bit slow from the time $T \sim m_i$ until today. Since the matter power spectrum $P(k)$ defined in Eq. (10.20) is proportional to $|\delta_{\rm CDM}|^2$, we find

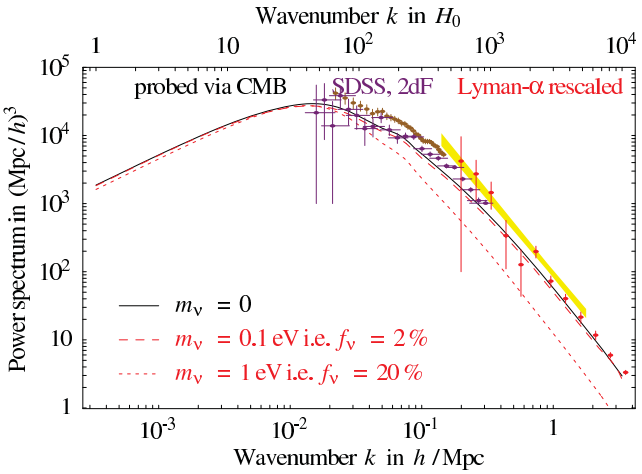

Fig. 10.5 The matter power spectrum $P(k)$ predicted by the standard ΛCDM model (solid curve) and its dependence on neutrino masses (dashed curves). Measurements at different cosmological scales are performed with different techniques, which slightly overlap. The data points do not show the overall uncertainty that plagues galaxy surveys (SDSS and 2dF) at intermediate scales and especially Lyman-α data at smaller scales with larger wavenumbers (Strumia and Vissani, 2006)

$$\frac{P(k)_{f_\nu \neq 0}}{P(k)_{f_\nu = 0}} \sim |a(t)|^{2(p-1)} \sim |a(t)|^{-6f_\nu/5} \tag{10.24}$$

during the aforementioned period. A simple numerical interpolation yields $P(k)_{f_\nu \neq 0}/P(k)_{f_\nu = 0} \sim \mathrm{e}^{-8f_\nu} \approx 1 - 8f_\nu$ (Strumia and Vissani, 2006; Lesgourgues and Pastor, 2006), and thus the matter power spectrum is modified up to $\Delta P(k)/P(k) \sim -8f_\nu$ on small cosmological scales.

A complete description of the effect of massive neutrinos on the matter power spectrum $P(k)$ is technically complicated (Lesgourgues and Pastor, 2006). For simplicity, here we only illustrate the shape of $P(k)$ and its dependence on neutrino masses in Fig. 10.5, where m_ν stands for nearly degenerate m_i (Strumia and Vissani, 2006). One can see that it is possible to probe neutrino masses via a precision measurement of $P(k)$, if $m_\nu \gtrsim 0.1$ eV holds. Future cosmological measurements of the LSS might even be sensitive to the mass splitting $\sqrt{\Delta m^2_{32}} \approx 0.05$ eV for atmospheric neutrino oscillations.

It is worth mentioning that a very tight upper bound on neutrino masses has recently been obtained from a new mapping of the matter density distribution of surrounding galaxies based on the standard ΛCDM model (Thomas *et al.*, 2010). In this analysis the authors used the SDSS data and photometric redshift estimates to reconstruct a three-dimensional map of galaxies on much larger cosmological scales than before, providing an important indication of

the distribution of structures not only in a recent past but also a few billion years ago when most remote galaxies in this map emitted the light that we have observed today (Lesgourgues, 2010). Such an approach is particularly suitable for probing the effect of neutrino masses on the rate of structure formation, on both smaller and larger cosmological scales as compared with the neutrino free-streaming scale. In combination with the WMAP data and other cosmological measurements, it yields $\sum m_i \lesssim 0.28$ eV at the 95% confidence level (Thomas *et al.*, 2010). Of course, this and other cosmological constraints on neutrino masses are strongly dependent upon specific model parameters and other theoretical assumptions. But they can always be complementary to the laboratory measurements of neutrino masses, which probe different quantities and have independent systematic errors.

10.2.4 Sterile Neutrinos as Dark Matter

The term "sterile neutrino" was coined by Bruno Pontecorvo in one of his seminal papers (Pontecorvo, 1968). A sterile neutrino is by definition a neutrino that does not take part in the standard weak interactions. In some literature the $SU(2)_{\rm L}$ singlet neutrinos or right-handed neutrinos are simply referred to as sterile neutrinos. Such hypothetical particles may not be completely "sterile" in the sense that they can slightly mix with ordinary neutrinos and thus indirectly take part in weak interactions (see, e.g., the type-I seesaw mechanism discussed in Section 3.2.3 and Section 4.1.2). The existence of completely or almost sterile neutrinos has not been experimentally established, although they are favored in some models to understand the origin of tiny masses of three active neutrinos, to interpret the cosmological matter-antimatter asymmetry and to describe dark matter. In this section we are going to briefly discuss warm dark matter in the form of keV sterile neutrinos.

To be specific, we assume the existence of a single sterile neutrino ν_s whose mass eigenstate $\tilde{\nu}_s$ has an eigenvalue m_s. Its mixing with active neutrinos can be described by an effective mixing angle θ as follows: $\nu_s \simeq \tilde{\nu}_s \cos\theta + \nu_{\rm L} \sin\theta$, where $|\theta| \ll 1$ holds and $\nu_{\rm L}$ denotes a linear combination of the mass eigenstates of three active neutrinos [6]. For this kind of sterile neutrinos to be a viable dark matter candidate, m_s should most likely lie in the keV range and θ must be extremely small. Such keV sterile neutrinos were never in thermal equilibrium at high temperatures in the early Universe, but they could be produced in several ways (Kusenko, 2009). For instance, light sterile neutrinos could be produced from neutrino oscillations at a temperature $T \sim 100$ MeV (Dodelson and Widrow, 1994). An estimate of the relic population of keV sterile neutrinos yields

[6] In a self-consistent parametrization of the four-neutrino mixing matrix (Guo and Xing, 2002), one approximately has $\nu_s \simeq \tilde{\nu}_s \cos\theta + (\nu_1 \hat{s}^*_{14} + \nu_2 \hat{s}^*_{24} + \nu_3 \hat{s}^*_{34})$ with $\hat{s}_{i4} \equiv {\rm e}^{{\rm i}\delta_{i4}} \sin\theta_{i4}$ (for $i = 1, 2, 3$). Hence $\sin^2\theta \simeq s^2_{14} + s^2_{24} + s^2_{34}$ (Li and Xing, 2010).

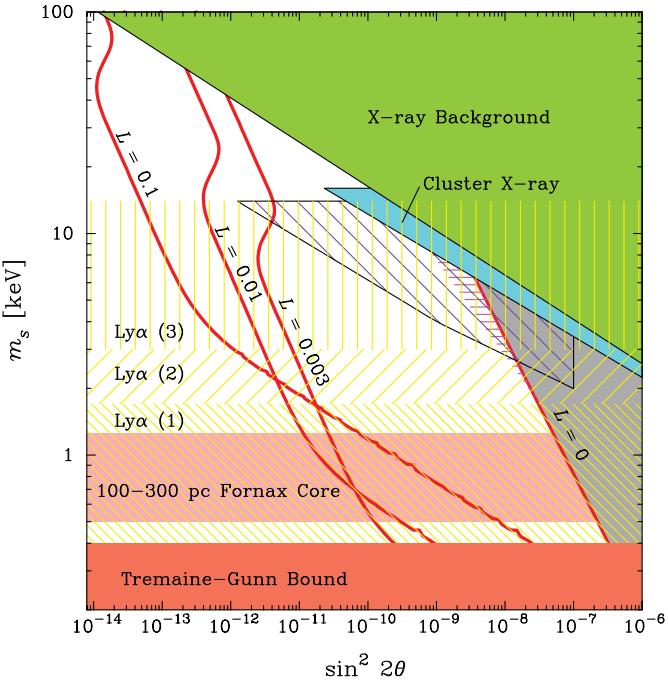

Fig. 10.6 Allowed regions of $\sin^2 2\theta$ and m_s for sterile neutrinos to be dark matter (Abazajian and Koushiappas, 2006). The contour labeled with $L = 0$ corresponds to the production scenario of sterile neutrinos with $\Omega_s \approx 0.24$, and those labeled with $L = 0.003$, 0.01 and 0.1 correspond to $\Omega_s \approx 0.3$. The grey region to the right of the $L = 0$ contour is excluded to avoid overproduction of sterile neutrinos as dark matter, and the "X-ray background" and "Cluster X-ray" regions are excluded because the X-ray signals arising from $\bar{\nu}_s \to \nu_i + \gamma$ decays (for $i = 1, 2, 3$) have never been seen. The diagonal wide-hatched region is the claimed potential constraint from future X-ray searches. The horizontal band with $m_s < 0.4$ keV is ruled out by a conservative application of the Tremaine-Gunn bound, whereas the one with $0.5 \text{ keV} \leqslant m_s \lesssim 1$ keV is consistent with the production of a core in the Fornax dwarf galaxy and pulsar kicks. The regions labeled with Lyα (1), (2) and (3) are constrained by the amplitude and slope of the matter power spectrum inferred from some high-resolution data on the SDSS Lyman-α forest

$$\Omega_s \sim 0.2 \times \left(\frac{\sin^2 2\theta}{10^{-8}}\right) \left(\frac{m_s}{3 \text{ keV}}\right)^{1.8} , \tag{10.25}$$

provided the Universe has a negligibly small lepton number asymmetry L (Feng, 2010). Here L is defined as $L \equiv (n_\nu - n_{\overline{\nu}})/n_\gamma$ with n_ν (or $n_{\overline{\nu}}$) being the number density of neutrinos (or antineutrinos) and n_γ being the number density of photons (Abazajian and Koushiappas, 2006). Fig. 10.6 shows the allowed parameter space of $\sin^2 2\theta$ and m_s for sterile neutrinos to be the

candidate of dark matter. Given a preexisting lepton number asymmetry $L \gtrsim 10^{-3}$, which remains small enough to be consistent with the current BBN data, sterile neutrinos with small masses and mixing angles may constitute all of dark matter in the Universe (Shi and Fuller, 1999; Asaka *et al.*, 2007; Feng, 2010). Sterile neutrinos could also be produced at much higher temperatures, for example, in the decays of heavy particles in the early Universe. Allowing a gauge-singlet scalar Φ to couple to right-handed neutrinos and their charge-conjugate fields, one may obtain a Majorana mass term similar to the M_μ term in Eq. (4.48) after Φ acquires its vacuum expectation value. The lepton-number-violating decay $\Phi \to \nu_s + \overline{\nu}_s$ might therefore produce sterile neutrinos as dark matter at a temperature $T \sim m_\Phi$ (Shaposhnikov and Tkachev, 2006; Kusenko, 2006, 2009; Feng, 2010).

Dark matter in the form of keV sterile neutrinos is referred to as warm dark matter, which should have little small-scale suppression in the matter power spectrum. In fact, both warm dark matter and cold dark matter can fit the observed structures on large scales, but their predictions on small scales are different. A potential problem associated with cold dark matter is the discrepancy between the number of satellites predicted in the N-body simulations and the one observed in galaxies such as the Milky Way (Kauffmann *et al.*, 1993; Moore *et al.*, 1999). This discrepancy can be ameliorated if dark matter is warm, because warm dark matter may suppress the formation of dwarf galaxies and other small-scale structures (Bode *et al.*, 2001; Kusenko, 2009). How warm sterile neutrinos could be depends on their production mechanism. Fig. 10.6 shows that m_s may vary from $\mathcal{O}(1)$ keV to $\mathcal{O}(10)$ keV.

Besides its impact on small-scale structures, dark matter in the form of sterile neutrinos may have some other astrophysical effects, for instance, on the X-ray spectrum, on the velocity distribution of pulsars and on the formation of the first stars (Kusenko, 2009; Feng, 2010). The search for an X-ray line from the radiative decay $\tilde{\nu}_s \to \nu_i + \gamma$ (for $i = 1, 2, 3$) is expected to offer the best chance to detect relic sterile neutrinos if they exist as warm dark matter. In view of Fig. 10.6 together with the widths of the dominant and subdominant decay modes of $\tilde{\nu}_s$ (Li and Xing, 2010)

$$\sum_{i,j=1}^{3} \Gamma(\tilde{\nu}_s \to \nu_i + \nu_j + \overline{\nu}_j) \simeq \frac{C_\nu G_{\rm F}^2}{192\pi^3} m_s^5 \sin^2\theta \simeq \frac{C_\nu \sin^2 2\theta}{1.2 \times 10^{20}\ {\rm s}} \left(\frac{m_s}{\rm keV}\right)^5 \tag{10.26}$$

and (Pal and Wolfenstein, 1982; Shrock, 1982; Li and Xing, 2010)

$$\sum_{i=1}^{3} \Gamma(\tilde{\nu}_s \to \nu_i + \gamma) \simeq \frac{9\alpha_{\rm em} C_\nu G_{\rm F}^2}{512\pi^4} m_s^5 \sin^2\theta \simeq \frac{C_\nu \sin^2 2\theta}{1.5 \times 10^{22}\ {\rm s}} \left(\frac{m_s}{\rm keV}\right)^5 \tag{10.27}$$

with $\alpha_{\rm em} \approx 1/137$ being the fine-structure constant and $C_\nu = 1$ (Dirac neutrinos) or $C_\nu = 2$ (Majorana neutrinos), one concludes that the lifetime of sterile neutrinos can be much longer than the age of the Universe (i.e., $t_0 \approx 13.7$ Gyr $\sim 10^{17}$ s) and thus satisfy one of the requirements for dark

matter candidates. The signature of the two-body radiative decay $\tilde{\nu}_s \to \nu_i + \gamma$ is a monoenergetic flux of X-rays with energy $E_\gamma \approx m_s/2$. It is in principle possible to observe this signature of sterile neutrinos in the XMN-Newton, Chandra X-ray and Suzaku observatories (Loewenstein and Kusenko, 2010; Prokhorov and Silk, 2010; Chan and Chu, 2010).

Finally, it is worth mentioning that a laboratory search for keV sterile neutrinos would require a careful analysis of kinematics of the beta decays of different isotopes (Trinczek *et al.*, 2003; Shaposhnikov, 2007). Because of the mixing between active and sterile neutrinos, one may study the details of kinematics of the tritium beta decay $^3\mathrm{H} \to {}^3\mathrm{He} + e^- + \overline{\nu}_e$ in which $\overline{\nu}_e$ contains a tiny contribution from sterile antineutrinos. On the other hand, one may probe the existence of keV sterile neutrinos by detecting the neutrino capture processes like $\tilde{\nu}_s + {}^3\mathrm{H} \to {}^3\mathrm{He} + e^-$ and $\tilde{\nu}_s + {}^{106}\mathrm{Ru} \to {}^{106}\mathrm{Rh} + e^-$ against the β-decay backgrounds (Li and Xing, 2010; Liao, 2010) in a way similar to the detection of the sterile component of the CνB (Li *et al.*, 2010). Although such direct laboratory searches for dark matter in the form of sterile neutrinos are extremely challenging, they might not be hopeless in the long term.

References

Abazajian, K., and Koushiappas, S. M., 2006, Phys. Rev. D **74**, 023527.
Albrecht, A., and Steinhardt, P. J., 1982, Phys. Rev. Lett. **48**, 1220.
Asaka, T., Laine, M., and Shaposhnikov, M., 2007, JHEP **0701**, 091.
Bartolo, N., *et al.*, 2004, Phys. Rept. **402**, 103.
Bennett, C. L., *et al.* (WMAP Collaboration), 2003, Astrophys. J. Supp. **148**, 1.
Bode, P., Ostriker, J. P., and Turok, N., 2001, Astrophys. J. **556**, 93.
Bond, J. R., Efstathiou, G., and Silk, J., 1980, Phys. Rev. Lett. **45**, 1980.
Chan, M. H., and Chu, M. C., 2010, arXiv:1009.5872.
Clowe, D., *et al.*, 2006, Astrophys. J. **648**, L109.
Courteau, S., *et al.*, 2000, Astrophys. J. **544**, 636.
Dirac, P. A. M., 1931, Proc. Roy. Soc. A **133**, 60.
Dodelson, S., and Widrow, L. M., 1994, Phys. Rev. Lett. **72**, 17.
Dunkley, J., *et al.* (WMAP Collaboration), 2009, Astrophys. J. Supp. **180**, 306.
Feng, J. L., 2010, arXiv:1003.0904.
Fixsen, D. J., *et al.*, 1994, Astrophys. J. **420**, 445.
Grupen, C., *et al.*, 2005, *Astroparticle Physics* (Springer-Verlag).
Guo, W. L., and Xing, Z. Z., 2002, Phys. Rev. D **65**, 073020.
Guth, A. H., 1981, Phys. Rev. D **23**, 347.
Hamann, J., *et al.*, 2010a, JCAP **1007**, 022.
Hamann, J., *et al.*, 2010b, Phys. Rev. Lett. **105**, 181301.
Hannestad, S., and Raffelt, G. G., 1999, Phys. Rev. D **59**, 043001.
Hinshaw, G., *et al.* (WMAP Collaboration), 2009, Astrophys. J. Supp. **180**, 225.
Hu, W., and Dodelson, S., 2002, Ann. Rev. Astron. Astrophys. **40**, 171.
Jarosik, N., *et al.* (WMAP Collaboration), 2007, Astrophys. J. Supp. **170**, 263.
Kainulainen, K., 1990, Phys. Lett. B **244**, 191.

Kamionkowski, M., and Kinkhabwala, A., 1998, Phys. Rev. D **57**, 3256.
Kauffmann, G., White, S. D. M., and Guiderdoni, B., 1993, Mon. Not. Roy. Astron. Soc. **264**, 201.
Kohri, K., Lyth, D. H., and Melchiorri, A., 2008, JCAP **0804**, 038.
Kolb, E. W., and Turner, M. S., 1990, *The Early Universe* (Addison-Wesley, Redwood City).
Komatsu, E., *et al.* (WMAP Collaboration), 2009, Astrophys. J. Supp. **180**, 330.
Komatsu, E., *et al.* (WMAP Collaboration), 2010, arXiv:1001.4538.
Kusenko, A., 2006, Phys. Rev. Lett. **97**, 241301.
Kusenko, A., 2009, Phys. Rept. **481**, 1.
Lesgourgues, J., 2010, Physics **3**, 57.
Lesgourgues, J., and Pastor, S., 2006, Phys. Rept. **429**, 307.
Lewis, A., Challinor, A., and Lasenby, A., 2000, Astrophys. J. **538**, 473.
Li, Y. F., and Xing, Z. Z., 2010, arXiv:1009.5870.
Li, Y. F., Xing, Z. Z., and Luo, S., 2010, Phys. Lett. B **692**, 261.
Liao, W., 2010, Phys. Rev. D **82**, 073001.
Liddle, A. R., and Lyth, D., 2000, *Cosmological Inflation and Large-Scale Structure* (Cambridge University Press).
Linde, A. D., 1982, Phys. Lett. B **108**, 389.
Loewenstein, M., and Kusenko, A., 2010, Astrophys. J. **714**, 652.
Mather, J. C., *et al.*, 1999, Astrophys. J. **512**, 511.
Moore, B., *et al.*, 1999, Astrophys. J. **524**, L19.
Nakamura, K., *et al.* (Particle Data Group), 2010, J. Phys. G **37**, 075021.
Pal, P., and Wolfenstein, L., 1982, Phys. Rev. D **25**, 766.
Peacock, J. A., 1999, *Cosmological Physics* (Cambridge University Press).
Peccei, R. D., and Quinn, H. R., 1977, Phys. Rev. Lett. **38**, 1440.
Peebles, P. J. E., and Wilkinson, D. T., 1968, Phys. Rev. **174**, 2168.
Penzias, A., and Wilson, R., 1965, Astrophys. J. **142**, 419.
Percival, W. J., *et al.*, 2010, Mon. Not. Roy. Astron. Soc. **401**, 2148.
Perkins, D. H., 2009, *Particle Astrophysics* (Oxford University Press).
Pontecorvo, B., 1968, Sov. Phys. JETP **26**, 984.
Prokhorov, D. A., and Silk, J., 2010, arXiv:1001.0215.
Riess, A. G., *et al.*, 2009, Astrophys. J. **699**, 539.
Rubin, V. C., and Ford, W. K., Jr., 1970, Astrophys. J. **159**, 379.
Rubin, V. C., Thonnard, N., and Ford, W. K., Jr., 1980, Astrophys. J. **238**, 471.
Sachs, R. K., and Wolfe, A. M., 1967, Astrophys. J. **147**, 73.
Saha, M. N., 1921, Proc. Roy. Soc. Lond. A **99**, 135.
Seljak, U., and Zaldarriaga, M., 1996, Astrophys. J. **469**, 437.
Shaposhnikov, M., 2007, arXiv:0706.1894.
Shaposhnikov, M., and Tkachev, I., 2006, Phys. Lett. B **639**, 414.
Shi, X. D., and Fuller, G. M., 1999, Phys. Rev. Lett. **82**, 2832.
Shrock, R. E., 1982, Nucl. Phys. B **206**, 359.
Silk, J., 1968, Astrophys. J. **151**, 459.
Smoot, G. F., *et al.*, 1992, Astrophys. J. **396**, L1.
Strumia, A., and Vissani, F., 2006, arXiv:hep-ph/0606054.

Thomas, S. A., Abdalla, F. B., and Lahav, O., 2010, Phys. Rev. Lett. **105**, 031301.
Trinczek, M., *et al.*, 2003, Phys. Rev. Lett. **90**, 012501.
White, M., Scott, D., and Silk, J., 1994, Ann. Rev. Astron. Astrophys. **32**, 319.
Zwicky, F., 1933, Helv. Phys. Acta **6**, 110.
Zwicky, F., 1937, Astrophys. J. **86**, 217.

11

Cosmological Matter-antimatter Asymmetry

The observed matter-antimatter asymmetry of the Universe is a big puzzle in particle physics and cosmology. Although the hot Big Bang model of cosmology is very successful in predicting the cosmic microwave background (CMB) radiation and the primordial abundances of light elements, it does not explain why the cosmic baryon-to-photon ratio $\eta \equiv n_{\rm B}/n_\gamma$ is about 6×10^{-10} and why the primordial number density of antibaryons $n_{\overline{\rm B}}$ is vanishing. In this chapter we shall first present some experimental evidence for such a baryon number asymmetry, and then outline a few interesting dynamic scenarios to account for it. Among the presently-proposed baryogenesis mechanisms, the leptogenesis mechanism is most promising because it is intrinsically related to the popular seesaw mechanisms of neutrino mass generation. So we shall pay particular attention to the details of this mechanism and give a broad overview of its recent developments.

11.1 Baryon Asymmetry of the Universe

Shortly after the discovery of the positron, the antiparticle of the electron, Paul Dirac made an intriguing conjecture in his Nobel lecture (Dirac, 1933): "If we accept the view of complete symmetry between positive and negative electric charge so far as concerns the fundamental laws of Nature, we must regard it rather as an accident that the Earth (and presumably the whole solar system), contains a preponderance of negative electrons and positive protons. It is quite possible that for some of the stars it is the other way about, these stars being built up mainly of positrons and negative protons. In fact, there may be half the stars of each kind. The two kinds of stars would both show exactly the same spectra, and there would be no way of distinguishing them by present astronomical methods." Unfortunately, current observational data indicate that there are no stars or galaxies made of antimatter at all in the visible Universe. If there existed a large region of antimatter, the matter and antimatter would have unavoidably annihilated with each other at their

common border. Such violent annihilations would have produced numerous energetic electrons and photons which must distort the CMB spectrum and contribute to the diffuse gamma rays with energies around 1 MeV. In this section we summarize the main astrophysical and cosmological observations against the presence of a large amount of antimatter in our Universe, and point out that there is no way to solve this baryon asymmetry problem within the standard model (SM) of particle physics.

11.1.1 Constraints from Antimatter Searches

It is well known that the fundamental interactions in nature are almost symmetric between particles and antiparticles. In particular, the CPT theorem states that a particle and its antiparticle must have the same mass (and the same lifetime if they are unstable). So it is rather reasonable to speculate that the Universe should be symmetric about matter and antimatter, just as Dirac did. However, it is unclear whether the symmetry between particles and antiparticles at the microscopic level definitely leads to a matter-antimatter symmetric Universe at the macroscopic scale (Steigman, 1976). But one may ask such a meaningful question: is our Universe symmetric between matter and antimatter based on the astrophysical and cosmological observations?

The searches for antimatter fall into two categories: one is the direct search (e.g., to search for antiprotons or antinuclei in the cosmic rays) and the other is the indirect search (e.g., to detect the products from matter-antimatter annihilations). The absence of antimatter on the Earth is obvious because we have not seen any proton-antiproton annihilations in our everyday lives. The largest amount of antimatter is stored in high-energy accelerators, where $p\bar{p}$ or e^+e^- collisions are used to produce new particles and reactions. Those successful activities of human beings in outer space demonstrate that the solar system is made of matter rather than antimatter. Another compelling evidence comes from the observation of cosmic rays. If there were a sizable region of antimatter in our galaxy or extragalaxies, we would have discovered antiprotons or antinuclei in the cosmic ray experiments. The ratio of the antiproton flux to the proton flux is found to be of $\mathcal{O}(10^{-4})$ in cosmic rays, and this small value can be explained by identifying antiprotons as the secondary products from the reaction $p + p \to \bar{p} + 3p$ initiated by the primary cosmic ray protons. Furthermore, current experimental constraints on the fluxes of antihelium and much heavier antielements are (Dolgov, 2001):

$$\frac{\Phi[\overline{\mathrm{He}}]}{\Phi[\mathrm{He}]} < 2 \times 10^{-6} , \qquad \frac{\Phi[\overline{A}(\overline{Z} > 2)]}{\Phi[A(Z > 2)]} < 2 \times 10^{-5} , \tag{11.1}$$

where $A(Z > 2)$ and $\overline{A}(\overline{Z} > 2)$ stand respectively for the nuclei with more than two protons and the antinuclei with more than two antiprotons. These constraints again indicate that stars or galaxies in the form of antimatter are actually absent in our Universe.

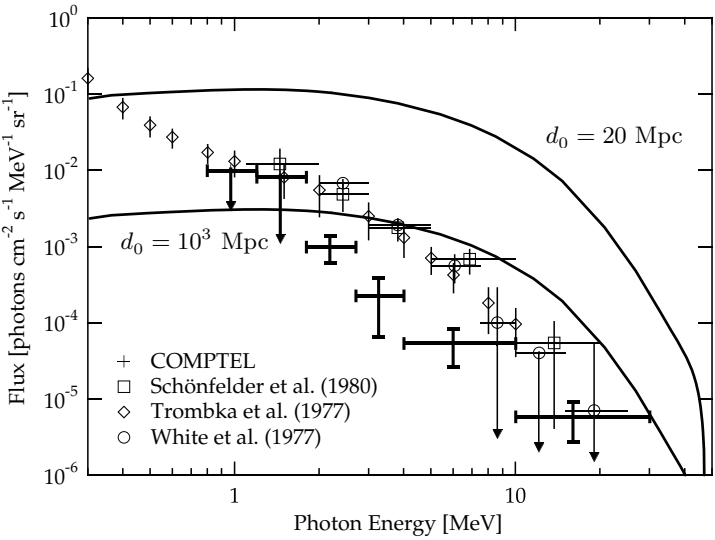

Fig. 11.1 The observed spectrum of the diffusive gamma rays (Kappadath *et al.*, 1995) as compared with the calculated one from the matter-antimatter annihilation (Cohen *et al.*, 1998), where $d_0 = 20$ Mpc (upper solid curve) and $d_0 = 10^3$ Mpc (lower solid curve) denote the typical sizes of matter domains

The indirect searches also indicate the absence of antimatter in the whole visible Universe. If there are large regions of antimatter, violent matter-antimatter annihilations are expected to occur at the borders [1]. In the matter-antimatter annihilation neutral and charged pions can be copiously generated. The decays of neutral pions via $\pi^0 \rightarrow 2\gamma$ give rise to a diffuse gamma-ray background. On the other hand, the decays of charged pions via $\pi^{\pm} \rightarrow \mu^{\pm} + \nu_{\mu}(\overline{\nu}_{\mu})$ together with $\mu^{\pm} \rightarrow e^{\pm} + \overline{\nu}_{\mu}(\nu_{\mu}) + \nu_e(\overline{\nu}_e)$ produce a lot of electrons, positrons and neutrinos. All these annihilation products have very similar energy spectra, and their number densities are peaked around $100 \sim 200$ MeV. The most useful component for probing matter-antimatter annihilation is the diffuse gamma rays (Steigman, 1976). But a measurement of the diffuse gamma rays can only impose an upper limit on the matter-antimatter annihilation, because the Compton scattering of the starlight and cosmic ray electrons may also contribute to the gamma rays. A careful analysis reveals that the size of matter domain should be as large as $d_0 = 10^3$ Mpc, which is just the typical scale of the visible Universe (Cohen *et al.*, 1998). The strategy of this analysis is to assume that the total baryon number of the Universe is zero, and the Universe is divided into domains of matter or

[1] The annihilation might not happen if matter and antimatter were well separated. In this case, however, one has to resort to very contrived mechanisms so as to make matter and antimatter far away from each other.

antimatter with the typical dimension d_0. Then the spectra of the diffuse gamma rays coming from the matter-antimatter annihilation in the epoch of recombination can be calculated, redshifted and compared with current observational data. The results are shown in Fig. 11.1, from which one can see that the case with $d_0 = 10^3$ Mpc is more consistent with data, implying that the visible Universe contains only matter and no sizable regions of antimatter (Cohen *et al.*, 1998).

11.1.2 Observations from the CMB and BBN

In the standard model of cosmology the anisotropies of the CMB and the primordial abundances of light elements from the Big Bang nucleosynthesis (BBN) can be computed with the baryon number density η as an important input parameter (Kolb and Turner, 1990; Dodelson, 2005; Weinberg, 1972, 2008). It is therefore possible to strictly determine or constrain the value of η from the precision measurements of the CMB and light element abundances.

The CMB formed shortly after the time of recombination, when protons and electrons combined to form neutral hydrogen atoms. From this moment on the cosmological thermal bath became transparent to relic photons, so they left the surface of last scattering and freely propagated until today. Hence the anisotropies of the CMB are mainly determined by the dynamics of the thermal bath before recombination. The value of η is actually extracted from the angular power spectrum of the CMB, in particular its acoustic peaks. An intuitive picture for the formation of acoustic peaks is as follows: (1) the density fluctuations in the early Universe induced the gravitational instabilities, and the baryon fluid falling into the gravitational potential wells were compressed and then heated up; (2) this hot baryon fluid expanded and radiated photons, and thus it gradually cooled down; (3) the gravity overtook the decreasing radiation pressure again and initiated another compressing phase. It was just the competition between the gravity and radiation pressure that induced the acoustic oscillations in the baryon fluid, which would be frozen in the CMB after the decoupling of photons from the baryon matter. The acoustic peaks in the angular power spectrum of the CMB serve as a consequence of the sound waves in the primordial baryon fluid (Grupen *et al.*, 2005). Given the five-year WMAP results, the ratio of cosmic baryon and photon number densities has been determined to a good degree of accuracy (Komatsu *et al.*, 2009) [2]

$$\eta \equiv \frac{n_{\rm B} - n_{\overline{\rm B}}}{n_\gamma} = (6.21 \pm 0.16) \times 10^{-10} \,, \tag{11.2}$$

where $n_{\overline{\rm B}} = 0$ holds today, as already discussed in Section 11.1.1.

[2] The WMAP Collaboration has recently released the seven-year data (Komatsu *et al.*, 2010), in which the central value of the baryon energy density is the same as that given in the five-year data.

The result obtained in Eq. (11.2) is in good agreement with the results extracted from the measurements of the primordial abundances of light elements based on the BBN theory. As shown in Fig. 9.1 and in Eqs. (9.48) and (9.49), the cosmic baryon-to-photon ratio η can be determined from both the measured ^{4}He mass fraction and the observed D and ^{7}Li number fractions. The BBN concordance range of η is consistent very well with the CMB measurement of η at the 95% confidence level (Nakamura *et al.*, 2010), pointing to $\eta \approx 6 \times 10^{-10}$. Because the time for the BBN to happen ($t \gtrsim 1$ s) is so different from that for the CMB to form ($t \sim 3.8 \times 10^5$ yr), an agreement between the values of η obtained from these two epochs is particularly striking. The dynamical origin of this baryon number asymmetry of the Universe (i.e., *baryogenesis*) is an important but unsolved problem in particle physics and cosmology. We shall briefly describe a few typical mechanisms of baryogenesis in the next section.

11.2 Typical Mechanisms of Baryogenesis

Even if the baryon number asymmetry were naively taken as one of the initial conditions of the Universe, it would unavoidably be erased in the inflation era. Hence a dynamical mechanism for baryogenesis is necessary, and it is among the most fundamental problems in modern particle physics and cosmology. In this section we first introduce Sakharov's three necessary conditions for baryogenesis, and then give an overview of a few intriguing mechanisms proposed so far to realize those conditions and explain the observed baryon number asymmetry of the Universe.

11.2.1 Sakharov Conditions

In 1967, Andrei Sakharov proposed three necessary conditions for baryogenesis (Sakharov, 1967). They are summarized as follows.

(1) *Baryon number violation.* If all the fundamental interactions preserved the baryon number B, it would be obvious that the Universe with an initial condition $B = 0$ could not gain any baryon number excess. In the SM both the lepton number L and the baryon number B are conserved at the classical level. But these two accidental symmetries are not as fundamental as the conservation of electric charges which is guaranteed by the local gauge symmetry. In fact, it has been found that only the combination $(B - L)$ is exactly conserved in the SM after taking into account the axial anomaly and the nontrivial vacuum structure of non-Abelian gauge theories ('t Hooft, 1976). Hence the baryon-number-violating interactions already exist in the minimal version of the SM, but at the non-perturbative level.

(2) *C and CP violation.* By definition, the baryon number of a given particle (B) is opposite to the baryon number of its antiparticle ($-B$). If the charge-conjugate symmetry (C) is conserved, the interaction rate for a

reaction generating an amount of B must be equal to that for its charge-conjugate process which produces the same amount of $-B$. In this case the net baryon number of the system remains vanishing. One usually encounters the chiral interactions which are relevant to both C and P properties of the fermion fields. For example, the left- and right-handed fermions have different interactions in the SM. Let us explain why the B- and C-violating interactions are not sufficient for the baryon number generation. Consider the B-violating decays $X \to \chi_{\rm L} + \psi_{\rm L}$ and $X \to \chi_{\rm R} + \psi_{\rm R}$ together with their CP-conjugate processes $\overline{X} \to \overline{\chi}_{\rm R} + \overline{\psi}_{\rm R}$ and $\overline{X} \to \overline{\chi}_{\rm L} + \overline{\psi}_{\rm L}$, where the baryon numbers of the involved particles are assigned to be $B(X) = B(\overline{X}) = 0$, $B(\chi_{\rm L,R}) = B(\psi_{\rm L,R}) = +1$ and $B(\overline{\chi}_{\rm L,R}) = B(\overline{\psi}_{\rm L,R}) = -1$. We further assume C violation; i.e., $\Gamma(X \to \chi_{\rm L}+\psi_{\rm L}) \neq \Gamma(\overline{X} \to \overline{\chi}_{\rm L}+\overline{\psi}_{\rm L})$ and $\Gamma(X \to \chi_{\rm R}+\psi_{\rm R}) \neq \Gamma(\overline{X} \to \overline{\chi}_{\rm R} + \overline{\psi}_{\rm R})$ hold for these four decay rates. If CP is a good symmetry, however, we must have

$$\begin{aligned} \Gamma(X \to \chi_{\rm L} + \psi_{\rm L}) &= \Gamma(\overline{X} \to \overline{\chi}_{\rm R} + \overline{\psi}_{\rm R}) \,, \\ \Gamma(X \to \chi_{\rm R} + \psi_{\rm R}) &= \Gamma(\overline{X} \to \overline{\chi}_{\rm L} + \overline{\psi}_{\rm L}) \,, \end{aligned} \tag{11.3}$$

implying that a net baryon number excess cannot be generated. Therefore, a successful baryogenesis mechanism requires both C and CP violation. Since the weak interactions violate both C and CP symmetries, the SM itself fulfills the second Sakharov condition too.

(3) *Departure from thermal equilibrium.* Given a baryon number asymmetry in the early Universe, its evolution with the temperature must be taken into account. If the whole system stays in thermal equilibrium, the ensemble average of the baryon number can be expressed as

$$\begin{aligned} \langle B \rangle &= \mathcal{N}^{-1} {\rm Tr}\left[B {\rm e}^{-\beta H}\right] \\ &= \mathcal{N}^{-1} {\rm Tr}\left[({\rm CPT}) B ({\rm CPT})^{-1} ({\rm CPT}) {\rm e}^{-\beta H} ({\rm CPT})^{-1}\right] \\ &= \mathcal{N}^{-1} {\rm Tr}\left[(-B) {\rm e}^{-\beta H}\right] = -\langle B \rangle \end{aligned} \tag{11.4}$$

with $\mathcal{N} \equiv {\rm Tr}\left[{\rm e}^{-\beta H}\right]$, where we have assumed the Hamiltonian H to be invariant under CPT (i.e., $({\rm CPT}) H ({\rm CPT})^{-1} = H$) and used the fact that the baryon number B is odd under C and CPT (i.e., $({\rm CPT}) B ({\rm CPT})^{-1} = -B$) (Bernreuther, 2002). Then we arrive at $\langle B \rangle = 0$ from Eq. (11.4). In practice, a process will depart from thermal equilibrium if its interaction rate is smaller than the expansion rate of the Universe.

CPT is a good symmetry in a local quantum field theory which is Lorentz-invariant and possesses a Hermitian Lagrangian. Most viable mechanisms of baryogenesis respect the above Sakharov conditions. But an exception can always be found, for instance, by discarding the CPT theorem (Dolgov, 1992).

11.2.2 Electroweak Baryogenesis

An immediate attempt to account for the cosmological baryon asymmetry should be made in the SM, where there exists baryon number violation to-

gether with C and CP violation. In addition, a departure from thermal equilibrium can be achieved to assure the generated baryon asymmetry to survive if the electroweak phase transition is of the first order. Such a baryogenesis mechanism is called the electroweak baryogenesis (Kuzmin *et al.*, 1985).

First, let us show how the baryon number is violated in the standard electroweak theory. The key point here is closely related to an important aspect of quantum field theories — the symmetry breaking induced by the quantum anomaly. For instance, the decay rate of $\pi^0 \to 2\gamma$ can be interpreted as a natural consequence of the chiral symmetry breaking caused by the anomaly. In a consistent quantum field theory one must make sure that the quantum anomaly arising from the triangle diagrams is absent, so as to guarantee the renormalizability of the theory itself (Adler, 1969; Bell and Jackiw, 1969). For illustration, we consider quantum electrodynamics with a massless fermion Ψ, for which the Lagrangian can be derived from Eq. (2.4) by setting $m = 0$. In this case one may verify that the Lagrangian is invariant under the transformations $\Psi \to \Psi' = \mathrm{e}^{-\mathrm{i}\alpha}\Psi$ and $\Psi \to \Psi' = \mathrm{e}^{-\mathrm{i}\alpha\gamma_5}\Psi$, where α is an arbitrary real constant. Then the Noether theorem leads us to the conserved axial current $J_5^\mu(x) \equiv \overline{\Psi}(x)\gamma^\mu\gamma_5\Psi(x)$ in addition to the conserved vector current $J^\mu(x) \equiv \overline{\Psi}(x)\gamma^\mu\Psi(x)$. Now we examine how the quantization of the theory violates the conservation of the axial current (i.e., $\partial_\mu J_5^\mu(x) \neq 0$). By means of the path-integral quantization, we should consider the functional integration over the gauge and fermion fields:

$$\mathcal{Z} = \int [\mathrm{d}A_\mu][\mathrm{d}\Psi][\mathrm{d}\overline{\Psi}] \exp\left\{ \mathrm{i} \int \mathrm{d}^4x \ \left[-\frac{1}{4} F^{\mu\nu} F_{\mu\nu} + \overline{\Psi} \mathrm{i} \not{D} \Psi \right] \right\} \tag{11.5}$$

with $\not{D} \equiv \gamma^\mu(\partial_\mu - \mathrm{i}eA_\mu)$ being the covariant derivative. Note that $\mathcal{Z}$ is independent of all the fields after integration, hence it should be invariant under the transformation $\Psi \to \Psi' = \mathrm{e}^{-\mathrm{i}\alpha(x)\gamma_5}\Psi$, where $\alpha(x)$ is an arbitrary real function of x. After applying such a local chiral transformation to the right-hand side of Eq. (11.5), we find two additional contributions to the total Lagrangian. The first one arises from the covariant-derivative term

$$\Delta\mathcal{L}_1 = \overline{\Psi'} \mathrm{i} \not{D} \Psi' - \overline{\Psi} \mathrm{i} \not{D} \Psi = -\alpha(x) \partial_\mu J_5^\mu(x) \ , \tag{11.6}$$

where the total-derivative term has been omitted. The other contribution comes from the measure of fermionic integration (Fujikawa, 1979)

$$[\mathrm{d}\Psi'] \left[\mathrm{d}\overline{\Psi'}\right] = \mathrm{Det} \left[\mathrm{e}^{2\mathrm{i}\alpha(x)\gamma_5} \right] [\mathrm{d}\Psi][\mathrm{d}\overline{\Psi}] \ , \tag{11.7}$$

where the determinant of the matrix is taken over the spin and space-time indices; i.e., $[\exp\{2\mathrm{i}\alpha(x)\gamma_5\}]_{mx,ny} \approx 1 + 2\mathrm{i}\alpha(x)[\gamma_5]_{mn}\delta^4(x-y)$ holds for the infinitesimal $\alpha(x)$. Using $\mathrm{Det}M = \exp[\mathrm{Tr}(M)]$, one can exponentialize the determinant in Eq. (11.7), which contributes to the total Lagrangian as

$$\Delta\mathcal{L}_2 = 2\alpha(x)\mathrm{Tr}[\gamma_5]\delta^4(x-x) \ . \tag{11.8}$$

Here the delta function yields infinity, while the trace is vanishing. In order to make Eq. (11.8) meaningful, we may introduce the gauge-invariant differential operator $\exp\{-(\mathrm{i}\not{D})^4/M^4\}$ to regularize the trace and delta function and then set $M \to +\infty$ (Fujikawa, 1979). The result is

$$\Delta\mathcal{L}_2 = \alpha(x)\frac{e^2}{8\pi^2}F_{\mu\nu}\tilde{F}^{\mu\nu} \ , \tag{11.9}$$

where $\tilde{F}_{\mu\nu} \equiv \varepsilon_{\mu\nu\rho\sigma}F^{\rho\sigma}/2$ is the dual of the field strength with $\varepsilon_{\mu\nu\rho\sigma}$ being a totally antisymmetric tensor. By requiring the generating functional in Eq. (11.5) to be invariant under the local chiral transformation, we have $\Delta\mathcal{L}_1 + \Delta\mathcal{L}_2 = 0$ for the arbitrary real function $\alpha(x)$, implying the anomaly of the axial current (Fujikawa, 1979, 1980)

$$\partial_\mu J_5^\mu(x) = \frac{e^2}{8\pi^2}F_{\mu\nu}\tilde{F}^{\mu\nu} \ . \tag{11.10}$$

Hence the symmetry at the classical level, which leads to $\partial_\mu J_5^\mu(x) = 0$, is violated at the quantum level. Due to the axial anomaly, the lepton and baryon numbers are not exactly conserved ('t Hooft, 1976). Consider the fermions in the SM, for which the Lagrangian has been given in Eq. (2.32). The baryon- and lepton-number currents can be defined as

$$\begin{aligned} J_{\rm B}^\mu &\equiv \sum_i \left(\overline{Q_{\rm L}^i}\gamma^\mu Q_{\rm L}^i + \overline{U_{\rm R}^i}\gamma^\mu U_{\rm R}^i + \overline{D_{\rm R}^i}\gamma^\mu D_{\rm R}^i\right) \ , \\ J_{\rm L}^\mu &\equiv \sum_\alpha \left(\overline{\ell_{\rm L}^\alpha}\gamma^\mu \ell_{\rm L}^\alpha + \overline{E_{\rm R}^\alpha}\gamma^\mu E_{\rm R}^\alpha\right) \ , \end{aligned} \tag{11.11}$$

where i $(= 1, 2, 3)$ and α $(= e, \mu, \tau)$ stand for the quark and lepton flavors, respectively. Note that the baryon number of each quark with a definite color is assigned to be $1/3$, which has been cancelled out by the summation over the color index of quark fields. Taking the divergences of baryon- and lepton-number currents, we obtain

$$\begin{aligned} \partial_\mu J_{\rm B}^\mu &= \frac{1}{2}\sum_i \partial_\mu \left(-\overline{Q^i}\gamma^\mu\gamma_5 Q^i + \overline{U^i}\gamma^\mu\gamma_5 U^i + \overline{D^i}\gamma^\mu\gamma_5 D^i\right) \ , \\ \partial_\mu J_{\rm L}^\mu &= \frac{1}{2}\sum_\alpha \partial_\mu \left(-\overline{\ell^\alpha}\gamma^\mu\gamma_5 \ell^\alpha + \overline{E^\alpha}\gamma^\mu\gamma_5 E^\alpha\right) \ , \end{aligned} \tag{11.12}$$

where we have used $P_{\rm L,R} = (1 \mp \gamma_5)/2$ and the conservation of vector currents. Along the same line in deriving Eq. (11.10) and making use of the covariant derivatives in Eq. (2.33), one may verify

$$\partial_\mu J_{\rm B}^\mu = \partial_\mu J_{\rm L}^\mu = \frac{N_f}{32\pi^2}\left(-g^2 W_{\mu\nu}^i \tilde{W}^{i\mu\nu} + g'^2 B_{\mu\nu}\tilde{B}^{\mu\nu}\right) \tag{11.13}$$

with $W_{\mu\nu}^i$ and $B_{\mu\nu}$ being the strengths of $SU(2)_{\rm L}$ and $U(1)_{\rm Y}$ gauge fields, respectively. Note that the number of fermion generations is $N_f = 3$ in the

SM. Now it becomes evident that both the baryon number $B \equiv \int \mathrm{d}^3\mathbf{x}\ J^0_{\mathrm{B}}(x)$ and the lepton number $L \equiv \int \mathrm{d}^3\mathbf{x}\ J^0_{\mathrm{L}}(x)$ are violated, but the combinations $(B-L)$ and $\Delta_\alpha \equiv B/3 - L_\alpha$ are conserved, where L_α (for $\alpha = e, \mu, \tau$) denotes the lepton flavor number. Furthermore, the $(B+L)$-violating interactions are uniquely determined by the gauge fields on the right-hand side of Eq. (11.13). As we shall show later on, such kinds of interactions are highly suppressed at the zero temperature but can be enhanced at a temperature higher than the electroweak scale.

Second, let us estimate the rates of B-violating interactions in the SM at both zero and finite temperatures. Note that the terms on the right-hand side of Eq. (11.13) can be written as a total divergence

$$\partial_\mu J^\mu_{\mathrm{B}} = \partial_\mu J^\mu_{\mathrm{L}} = \frac{N_f}{32\pi^2}\left(-g^2\partial_\mu \mathcal{K}^\mu + g'^2\partial_\mu K^\mu\right) , \tag{11.14}$$

where

$$\begin{aligned} \mathcal{K}^\mu &= 2\varepsilon^{\mu\nu\rho\sigma}\left[(\partial_\nu W^i_\rho)W^i_\sigma + \frac{1}{3}g\varepsilon^{ijk}W^i_\nu W^j_\rho W^k_\sigma\right] , \\ K^\mu &= 2\varepsilon^{\mu\nu\rho\sigma}\left[(\partial_\nu B_\rho)B_\sigma\right] . \end{aligned} \tag{11.15}$$

Integrating Eq. (11.15) over the three-space and using the definition of baryon and lepton numbers, one may then relate the changes of baryon and lepton numbers in a unit time to those of the Chern-Simons numbers:

$$\Delta B = \Delta L = N_f\left(\Delta N_{\mathrm{CS}} - \Delta n_{\mathrm{CS}}\right) , \tag{11.16}$$

where the Chern-Simons numbers are defined as

$$\begin{aligned} N_{\mathrm{CS}} &= -\frac{g^2}{16\pi^2}\int \mathrm{d}^3\mathbf{x}\ 2\varepsilon^{lmn}\mathrm{Tr}\left[(\partial_l W_m)W_n - \frac{2}{3}\mathrm{i}gW_l W_m W_n\right] , \\ n_{\mathrm{CS}} &= -\frac{g'^2}{16\pi^2}\int \mathrm{d}^3\mathbf{x}\ \varepsilon^{lmn}(\partial_l B_m)B_n . \end{aligned} \tag{11.17}$$

In Eq. (11.17) we have defined $W_l \equiv \tau^i W^i_l$ and used l, m and n to denote the spatial components. Now it is straightforward to verify that n_{CS} is gauge-invariant, but N_{CS} is not. Under the $SU(2)_{\mathrm{L}}$ gauge transformation

$$W'_m = U(\theta)W_m U^{-1}(\theta) - \frac{\mathrm{i}}{g}\left[\partial_m U(\theta)\right]U^{-1}(\theta) , \tag{11.18}$$

where $U(\theta) \equiv \exp\{-\mathrm{i}\theta^i(x)\tau^i\}$ is a unitary matrix, N_{CS} transforms as

$$\delta N_{\mathrm{CS}} = \frac{1}{24\pi^2}\int \mathrm{d}^3\mathbf{x}\varepsilon^{lmn}\mathrm{Tr}\left[(\partial_l U)U^{-1}(\partial_m U)U^{-1}(\partial_n U)U^{-1}\right] . \tag{11.19}$$

Although N_{CS} depends on the gauge, it is actually invariant under the infinitesimal transformations (Weinberg, 1996). As pointed out by Gerardus

't Hooft, the vacuum structure of the non-Abelian gauge theories is rather complicated in the sense that there exists an infinite number of topologically distinct vacua whose field configurations are just characterized by the Chern-Simons numbers ('t Hooft, 1976; Callan *et al.*, 1976; Jackiw and Rebbi, 1976). In this case the Chern-Simons numbers, and thus the baryon and lepton numbers, will be changed if a transition between two different vacua takes place. To be explicit, we consider a pure $SU(2)$ Yang-Mills theory, in which the field strength of the vacuum state should satisfy the condition $W_{\mu\nu} \equiv \tau^i W^i_{\mu\nu} = 0$ at any time. In the temporary gauge $W_0 = \tau^i W^i_0 = 0$, one can find that the gauge transformations in Eq. (11.18) now have to fulfill $\partial_0 U(x) = 0$ (i.e., $U(\mathbf{x})$ is time-independent). Hence the gauge fields $W_i(\mathbf{x}) = -\mathrm{i}g^{-1}[\partial_i U(\mathbf{x})]U^{-1}(\mathbf{x})$ obviously satisfy the vacuum condition. Furthermore, we restrict ourselves to a class of gauge transformation matrices which approach the identity matrix at infinity (i.e., $U(|\mathbf{x}| \to +\infty) = \mathbf{1}$). It is well known that a three-dimensional Euclidean space with all the points at infinity being identified as the same one is acutally the three-sphere S^3. On the other hand, the unitary matrix $U(\mathbf{x})$ defines the mapping from S^3 into the parameter space of the group $SU(2)$, which is also a three-sphere. According to the homotopy theory, the gauge transformation functions $U(\mathbf{x})$ fall into different homotopic classes, which are characterized by the integer numbers defined in Eq. (11.19). In a quantum theory there may exist transitions between two different vacuum states. To calculate the tunneling probability at the zero temperature, one should find out a solution to the field equations with finite energies (Belavin *et al.*, 1975; 't Hooft, 1976). For the transitions with $\Delta N_{\rm CS} = \pm 1$, the tunneling probability is approximately given by $\mathrm{e}^{-4\pi/\alpha_{\rm w}} \sim 10^{-161}$ with $\alpha_{\rm w} \equiv g^2/(4\pi)$, implying that the B-violating interactions are negligibly small.

Note that we have ignored two important issues in the above discussions. On the one hand, the baryon number asymmetry should be generated in the early Universe at extremely high temperatures, so one must take into account the finite-temperature effects. On the other hand, the field configurations of the vacua in the SM should include the Higgs boson field. In order for a transition between two different vacua to work, we have to examine whether there exists a static field configuration interpolating the two vacua (Manton, 1983). Such a solution, named *sphaleron* at the top of the potential barrier, has been found by solving the field equations in the limit of $\sin^2\theta_{\rm w} \to 0$ (Klinkhamer and Manton, 1984). The energy of the sphaleron is given by

$$E_{\rm sph} = \frac{4\pi v}{g}\mathcal{B}\left(\frac{\lambda}{g}\right) , \tag{11.20}$$

where v and λ are the vacuum expectation value and the self-coupling constant of the Higgs field, respectively. Note that the function $\mathcal{B}(x)$ is slowly varying; e.g., $\mathcal{B}(0) \simeq 1.52$ and $\mathcal{B}(\infty) \simeq 2.72$ (Klinkhamer and Manton, 1984). In the early Universe, when the temperature was higher than the potential barrier between the vacua, the transition should not be highly suppressed.

Including the finite-temperature corrections, the sphaleron energy turns out to be (Brihaye and Kunz, 1992)

$$E_{\rm sph}(T) = \frac{2M_W(T)}{\alpha_{\rm w}} \mathcal{B}\left(\frac{\lambda}{g}\right) , \tag{11.21}$$

where the W-boson mass $M_W(T) = gv(T)/2$ is temperature-dependent, so is the vacuum expectation value $v(T)$ of the Higgs field. It is worth mentioning that the gauge symmetry, which is spontaneously broken at the zero temperature, can be restored at much higher temperatures (Weinberg, 1974; Kirzhnits and Linde, 1974; Dolan and Jackiw, 1974; Bernard, 1974). Hence there must be a transition from the symmetric phase to the symmetry-breaking phase as the temperature T decreases. During and below the phase transition, the rate per unit volume for the sphaleron or B-violating processes is estimated to be (Carlson *et al.*, 1990; Dine *et al.*, 1992)

$$\gamma_{\rm sph} \sim 2.8 \times 10^5 \kappa T^4 \left(\frac{\alpha_{\rm w}}{4\pi}\right)^4 \left[\frac{E_{\rm sph}(T)}{\mathcal{B}(\lambda/g)T}\right]^7 \exp\{-E_{\rm sph}/T\} , \tag{11.22}$$

where $10^{-4} \lesssim \kappa \lesssim 10^{-1}$. Above the phase transition, one has $v(T) = 0$ and thus the rate per unit volume approximates to $\gamma_{\rm sph} \sim \kappa(\alpha_{\rm w}T)^4$. It can be shown that the sphaleron rate is in thermal equilibrium if the temperature T lies in the range 10^2 GeV $\lesssim T \lesssim 10^{12}$ GeV (Kuzmin *et al.*, 1985).

Finally, let us examine how CP violation in the SM comes into play and discuss possible implications of the departure from thermal equilibrium. A crucial period here is the electroweak phase transition, which is governed by the effective potential $V_{\rm eff}(H, T)$ of the system (Weinberg, 1974). At a high temperature the minimum of $V_{\rm eff}(H, T)$ is reached at $\langle H\rangle = 0$, indicating that the gauge symmetry is preserved. For the first-order phase transition, another local maximum and minimum of $V_{\rm eff}(H, T)$ appear at $\langle H\rangle_{\rm max}$ and $\langle H\rangle_{\rm min}$, as the temperature T decreases. Note that $\langle H\rangle_{\rm max} < \langle H\rangle_{\rm min}$, and the second minimum becomes degenerate with the original one at the critical temperature $T = T_c$ (i.e., $V_{\rm eff}(0, T_c) = V_{\rm eff}(\langle H\rangle_{\rm min}, T_c)$ holds). At this moment there are two degenerate vacua: one is at $\langle H\rangle = 0$, where the gauge symmetry is maintained; and the other is at $\langle H\rangle_{\rm min}$, where the gauge symmetry is broken. Therefore, a transition from the symmetric phase to the symmetry-breaking phase takes place by tunneling the potential barrier between them. If the temperature drops below T_c, the second local minimum of $V_{\rm eff}(H, T)$ becomes the global one. This first-order phase transition starts with the small bubbles inside which the symmetry is broken (i.e., $v(T) = \langle H\rangle \neq 0$), but outside is the symmetric phase with $v(T) = 0$. As T decreases, the bubbles expand and collide, and finally fill up the whole Universe. When the wall of the bubble expands outwards, the order parameter $v(T)$ changes dramatically from zero to a nonzero value which induces the departure from thermal equilibrium. On the other hand, the baryon numbers carried by quark and antiquark fields

transport from the outside into the inside of the bubbles, and vice versa. However, both quarks and antiquarks can be reflected by the bubble walls, and the reflection and transmission coefficients of quarks and antiquarks are different due to C and CP violation. The baryon number asymmetries are then generated in both the symmetric and symmetry-breaking phases, but the total baryon number is still vanishing. Because of the rapid rate of sphaleron processes in the symmetric phase, the corresponding baryon number stored in the left-handed quarks is finally washed out. Therefore, the net baryon number asymmetry only resides in the symmetry-breaking phase and can survive until today if the relevant sphaleron rate is far from thermal equilibrium. We conclude that it is possible to dynamically generate the cosmological baryon number asymmetry in the SM if the phase transition is strongly of the first order and the sphaleron processes are not very efficient. (Cohen *et al.*, 1993; Rubakov and Shaposhnikov, 1996).

One finds that the condition $E_{\rm sph}(T_c)/T_c > 45$ or $v(T_c)/T_c > 1$, which leads to a light Higgs boson with $M_h < 42$ GeV, should be satisfied in order to assure the sphaleron processes to be impotent. Current experimental bound on the Higgs mass is $M_h > 114$ GeV (Nakamura *et al.*, 2010). This contradiction, together with the fact that CP violation is badly suppressed due to the strong hierarchy of quark masses, excludes the possibility of explaining the observed baryon number asymmetry of the Universe within the SM. But a number of extensions of the SM with more sources of CP violation and more scalar fields, such as the minimal supersymmetric standard model (MSSM), can realize baryogenesis at the electroweak scale (Riotto, 1998; Riotto and Trodden, 1999).

11.2.3 GUT Baryogenesis

The unification of electromagnetic and weak interactions in the SM proves to be very successful. Including quantum chromodynamics, the SM as a $SU(3)_c \times SU(2)_{\rm L} \times U(1)_{\rm Y}$ gauge theory can well describe both strong and electroweak interactions. However, the direct product of these symmetry groups means that one has to introduce different gauge coupling constants for strong, weak and electromagnetic interactions. Howard Georgi and Sheldon Glashow made the first step in embedding these three fundamental forces into a gauge theory with the compact symmetry group $SU(5)$ (Georgi and Glashow, 1974). Subsequent developments along this line have taken advantage of other Lie groups, such as $SO(10)$ (Fritzsch and Minkowski, 1975; Georgi, 1975) and E_6 (Slansky, 1981). In such a grand unified theory (GUT), the SM quarks and leptons are usually grouped into one multiplet. Just like the W-boson which mediates charged-current weak interactions between a neutrino field $\nu_{\rm L}$ and the corresponding charged-lepton field $l_{\rm L}$ in the same $SU(2)_{\rm L}$ doublet, a new gauge boson X in the GUT may simultaneously interact with the quarks and leptons in the same multiplet. Thus the decays of this X boson must violate both baryon and lepton numbers. In the original Georgi-Glashow model, for

example, the left-handed fermions are embedded into the $\overline{\mathbf{5}}$ and **10** representations of the $SU(5)$ group:

$$\overline{\mathbf{5}} = \begin{pmatrix} D_1^c \\ D_2^c \\ D_3^c \\ \nu_e \\ e \end{pmatrix}_{\rm L} , \qquad \mathbf{10} = \begin{pmatrix} 0 & U_2^c & -U_1^c & u_1 & d_1 \\ -U_2^c & 0 & U_3^c & u_2 & d_2 \\ U_1^c & -U_3^c & 0 & u_3 & d_3 \\ -u_1 & -u_2 & -u_3 & 0 & E^c \\ -d_1 & -d_2 & -d_3 & -E^c & 0 \end{pmatrix}_{\rm L} , \tag{11.23}$$

where $U_{i\rm L}^c$, $D_{i\rm L}^c$ and $E_{\rm L}^c$ with i being the color index denote the antiparticles of the right-handed quark and charged-lepton singlets, $Q_{i\rm L} = (u_i, d_i)_{\rm L}^T$ and $\ell_{\rm L} = (\nu_e, e)_{\rm L}^T$ stand for the left-handed quark and lepton doublets. Since the $SU(5)$ gauge symmetry is not realized in nature, it must be spontaneously broken down to $SU(3)_c \times SU(2)_{\rm L} \times U(1)_{\rm Y}$ which can be further broken down to $U(1)_{\rm Q}$ as in the SM. The symmetry breaking is achievable by introducing a scalar multiplet in the adjoint representation, and its vacuum expectation value should be properly chosen such that the $SU(3)_c \times SU(2)_{\rm L} \times U(1)_{\rm Y}$ symmetry is preserved. After spontaneous symmetry breaking, the corresponding gauge boson X acquires a mass M_X and mediates the interactions between down-type quark singlets and lepton doublets (from the $\overline{\mathbf{5}}$ representation) and between charged-lepton singlets and quark doublets (from the **10** representation). This example illustrates that a GUT model may offer baryon number violation, which fulfills the first Sakharov condition. In addition, CP violation simply follows the Kobayashi-Maskawa mechanism as in the SM (Kobayashi and Maskawa, 1973). The rates of $X \to D + \ell$ and $X \to \overline{Q} + \overline{U}$ decays are equal to those of their CP-conjugate processes at the tree level, but the CP-violating asymmetries can arise at the loop level. The third Sakharov condition, or equivalently a departure from thermal equilibrium, will be satisfied if the decay rates of gauge bosons are smaller than the expansion rate of the Universe (Kolb and Turner, 1990).

The GUT baryogenesis seems to be promising in explaining the baryon number asymmetry, but this is not the case. The $(B+L)$-violating sphaleron processes, which must have been very efficient in the early Universe, are possible to erase all the preexisting baryon number asymmetry. One way out of this difficulty is to break the $(B-L)$ conservation in the GUT, then an asymmetry in the $(B-L)$ number should not be removed by the sphaleron interactions (Riotto and Trodden, 1999). This is in some sense similar to the leptogenesis mechanism, which will be discussed in detail in Section 11.2.5.

11.2.4 The Affleck-Dine Mechanism

We have seen that the minimal versions of electroweak and GUT baryogenesis mechanisms are not very successful in explaining the baryon number asymmetry. In this case more and more interest has recently been focused on baryogenesis via leptogenesis or via the Affleck-Dine mechanism. We shall

introduce the basic idea of the Affleck-Dine mechanism in this subsection, and then concentrate on leptogenesis in the remaining parts of this chapter.

Consider a theory of the complex scalar field, for which the Lagrangian can be written as (Dine and Kusenko, 2004)

$$\mathcal{L}_\phi = (\partial^\mu \phi^\dagger)(\partial_\mu \phi) - m^2 \phi^\dagger \phi \; . \tag{11.24}$$

It is obvious that $\mathcal{L}_\phi$ is invariant under the phase redefinition $\phi \to \phi' = \mathrm{e}^{\mathrm{i}\alpha}\phi$ with α being an arbitrary real constant. Thanks to the Noether theorem, we have the following conserved current:

$$J^\mu_{\rm B} = \mathrm{i}(\phi^\dagger \partial^\mu \phi - \phi \partial^\mu \phi^\dagger) \; , \tag{11.25}$$

where the global $U(1)$ symmetry has been identified with the baryon number. It is worth mentioning that the scalar fields with baryon and lepton numbers, such as the supersymmetric partners of quarks and leptons, are very common in a variety of supersymmetric theories (Affleck and Dine, 1985). Note that $\mathcal{L}_\phi$ is also invariant under the CP transformation $\phi \leftrightarrow \phi^\dagger$, and hence the theory is CP-invariant. Now we add the interaction terms described by (Dine and Kusenko, 2004)

$$\mathcal{L}_{\rm int} = \lambda(\phi^\dagger \phi)^2 + \left[\epsilon \phi^\dagger \phi^3 + \delta \phi^4 + \text{h.c.}\right] \; , \tag{11.26}$$

where ϵ and δ are in general complex constants. Then both the baryon number and CP invariance can be violated by the ϵ and δ terms in Eq. (11.26). The evolution of the scalar field $\phi(x)$ in the homogeneous Universe is governed by

$$\frac{\mathrm{d}^2\phi(t)}{\mathrm{d}t^2} + 3H\frac{\mathrm{d}\phi(t)}{\mathrm{d}t} + \frac{\partial V(\phi)}{\partial \phi} = 0 \; , \tag{11.27}$$

where H is the Hubble parameter, and $V(\phi)$ denotes the scalar potential. At early times the condition $H \gg m$ held, so the scalar field was frozen at $\phi = \phi_0$ with $\phi_0 \gg 0$ being the expectation value. Therefore, the initial baryon number must have been vanishing. When the Hubble parameter dropped far below m, the scalar field started to oscillate, as indicated in Eq. (11.27). Discarding the quartic term in the potential, we can get $\phi(t) = \phi_0 (mt)^{-3/2} \sin(mt)$ for the radiation-dominated epoch with $H = 1/(2t)$ or $\phi(t) = \phi_0 (mt)^{-1} \sin(mt)$ for the matter-dominated era with $H = 2/(3t)$. Taking ϕ_0 to be real and assuming ϵ and δ to be small coefficients, we solve Eq. (11.27) and obtain the imaginary part of ϕ as follows (Affleck and Dine, 1985):

$$\phi_{\rm I} = a_r \frac{\mathrm{Im}(\epsilon + \delta)\phi_0^3}{m^2 (mt)^{3/4}} \sin(mt + \delta_r) \tag{11.28}$$

with $a_r = 0.85$ and $\delta_r = -0.91$ in the radiation-dominated case; and

$$\phi_{\rm I} = a_m \frac{\mathrm{Im}(\epsilon + \delta)\phi_0^3}{m^3 t} \sin(mt + \delta_m) \tag{11.29}$$

with $a_m = 0.85$ and $\delta_m = 1.54$ in the matter-dominated case. Inserting either Eq. (11.28) or Eq. (11.29) into the baryon-number current in Eq. (11.25), we arrive at a nonzero baryon number at large times:

$$n_{\rm B} = 2a_r \frac{{\rm Im}(\epsilon+\delta)\phi_0^2}{m^3 t^2} \sin(\delta_r + \pi/8) \; , \quad \text{(radiation)} \; ,$$
$$n_{\rm B} = 2a_m \frac{{\rm Im}(\epsilon+\delta)\phi_0^2}{m^3 t^2} \sin(\delta_m) \; , \quad \text{(matter)} \; . \tag{11.30}$$

The baryon number stored in the scalar field will be converted to the baryon number of the SM particles through various decays of ϕ. If the squark plays the role of the dynamical scalar field, for instance, it can decay into the SM quarks. The final amount of the baryon number asymmetry depends on the details of the supersymmetric model and the inflation model (Affleck and Dine, 1985; Dine and Kusenko, 2004).

11.2.5 Leptogenesis

The leptogenesis mechanism (Fukugita and Yanagida, 1986) is the most popular mechanism of baryogenesis today, because it is closely related to the seesaw mechanism of neutrino mass generation. The fact that neutrinos are massive and lepton flavors are mixed implies that the minimal version of the SM must be incomplete. One of the most economical extensions of the SM is to introduce three right-handed neutrinos and allow lepton number violation (see Section 4.3.1). Such a canonical seesaw scenario can naturally accommodate baryogenesis via leptogenesis. Here we outline the basic idea of leptogenesis. A more detailed description of the leptogenesis mechanism will be presented in the subsequent sections.

The original leptogenesis mechanism works in the type-I seesaw model, which has the following gauge-invariant neutrino mass terms:

$$-\mathcal{L}_\nu = \overline{\ell_{\rm L}} Y_\nu \tilde{H} N_{\rm R} + \frac{1}{2} \overline{N_{\rm R}^c} M_{\rm R} N_{\rm R} + {\rm h.c.} \; . \tag{11.31}$$

After spontaneous gauge symmetry breaking, one obtains the Dirac mass matrix $M_{\rm D} = Y_\nu v/\sqrt{2}$ with $v \approx 246$ GeV. Provided the mass scale of $M_{\rm R}$ is significantly larger than that of $M_{\rm D}$, the seesaw mechanism works and leads to the effective Majorana mass matrix of three light neutrinos $M_\nu \approx -M_{\rm D} M_{\rm R}^{-1} M_{\rm D}^T$. Given $Y_\nu \sim \mathcal{O}(1)$, the sub-eV mass scale of M_ν requires $M_{\rm R} \sim \mathcal{O}(10^{14})$ GeV. Let us denote the mass eigenstates and eigenvalues of three heavy Majorana neutrinos to be N_i and M_i (for $i = 1, 2, 3$), respectively. Of course, the Majorana condition $N_i = N_i^c$ is fulfilled and lepton number is violated. In the very early Universe the temperature was so high that N_i could be thermally produced and then stayed in equilibrium with the thermal bath. As the temperature dropped below M_i, the lepton-number-violating decays $N_i \to \ell_\alpha + H$ and $N_i \to \bar{\ell}_\alpha + \overline{H}$ (for $\alpha = e, \mu, \tau$) would happen. The complex Yukawa coupling matrix Y_ν may result in the CP-violating asymmetries

$$\varepsilon_i \equiv \frac{\sum\limits_{\alpha} \left[\Gamma(N_i \to \ell_\alpha + H) - \Gamma(N_i \to \overline{\ell}_\alpha + \overline{H})\right]}{\sum\limits_{\alpha} \left[\Gamma(N_i \to \ell_\alpha + H) + \Gamma(N_i \to \overline{\ell}_\alpha + \overline{H})\right]} \tag{11.32}$$

via the interference between tree- and loop-level decay amplitudes. A net lepton number asymmetry can then be generated from ε_i if the decays of N_i are out of thermal equilibrium. The latter is satisfiable when the decay rates of N_i are smaller than the expansion rate of the Universe. For the decay of a heavier Majorana neutrino N_2 or N_3, the lepton-number-violating interactions of the lightest heavy Majorana neutrino N_1 may be rapid enough to wash out the lepton number asymmetry originating from ε_2 or ε_3. Hence only the CP-violating asymmetry ε_1 is survivable and relevant to leptogenesis. Once a net lepton number asymmetry is produced, the sphaleron interactions in thermal equilibrium will efficiently convert it into a baryon number asymmetry. This conversion can be expressed as (Kolb and Turner, 1990)

$$\left.\frac{n_{\rm B}}{s}\right|_{\rm equilibrium} = c \left.\frac{n_{\rm B} - n_{\rm L}}{s}\right|_{\rm equilibrium} = -c \left.\frac{n_{\rm L}}{s}\right|_{\rm initial} , \tag{11.33}$$

where $n_{\rm B}$ and $n_{\rm L}$ stand respectively for the baryon and lepton number densities, s denotes the entropy density of the Universe, and $c = 28/79$ in the SM. So the final baryon number asymmetry is determined by the initial lepton number asymmetry arising from the decays (and scattering processes) of heavy Majorana neutrinos. Fig. 11.2 illustrates the relation between B and L in the presence of rapid sphaleron interactions. Note that $n_{\rm L}$ should be negative so as to yield $n_{\rm B} > 0$. The evolution of $n_{\rm L}$ and $n_{\rm B}$ can be figured out by solving the relevant Boltzmann equations.

11.3 Baryogenesis via Leptogenesis

This section is devoted to a detailed description of baryogenesis via leptogenesis. First, we discuss the thermal or non-thermal production of heavy Majorana neutrinos N_i. Second, we calculate the CP-violating asymmetries ε_i in the decays of N_i. Third, we write out the full Boltzmann equations to describe how the produced lepton and baryon number asymmetries evolve. Finally, we make an analytical estimate of the net baryon number asymmetry.

11.3.1 Thermal or Non-thermal Production

Because of the Yukawa interactions, heavy Majorana neutrinos N_i with masses M_i could abundantly be produced via the inverse decays ($\ell_\alpha + H \to N_i$ and $\overline{\ell}_\alpha + \overline{H} \to N_i$) and scattering processes ($\ell_\alpha + U \to Q + N_i$ and

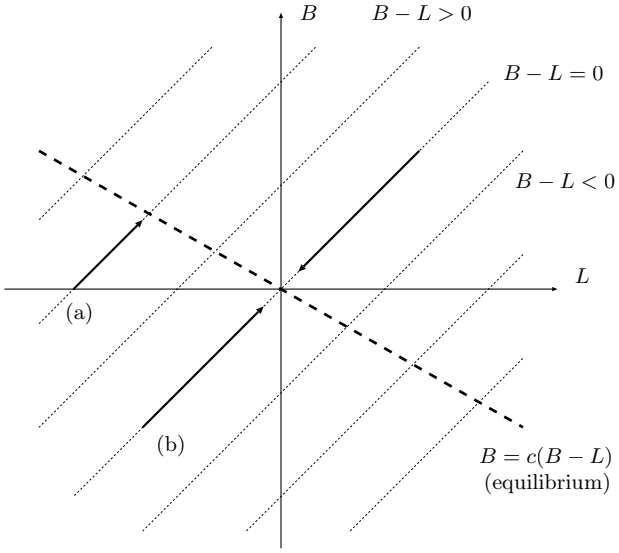

Fig. 11.2 The relationship between baryon (B) and lepton (L) numbers. The sphaleron processes change both B and L along the thin dotted lines with constant $(B - L)$. The thick dashed line represents $B = c(B - L)$, which should finally be reached if the sphaleron interactions are in thermal equilibrium. Arrows (a) and (b) correspond to successful and unsuccessful leptogenesis mechanisms, respectively (Hamaguchi, 2002)

$Q + \overline{U} \to \ell_\alpha + N_i$) when $T \gg M_i$ was satisfied in the early Universe [3]. It is usually assumed that the interaction rates of these processes are rapid enough to keep N_i in thermal equilibrium. Since the Yukawa interactions are responsible for both the thermal production of N_i and the out-of-equilibrium decays of N_i, whether the number density of N_i can reach the equilibrium value is determined by the Yukawa coupling matrix of neutrinos Y_ν and the evolution behavior of Boltzmann equations (Luty, 1992; Plümacher, 1997; Buchmüller *et al.*, 2005a).

In an inflation model the total energy of the early Universe was stored in the potential energy of an inflaton field ϕ, which would decay into the SM particles at the minimum of the potential energy and then reheat the Universe to the temperature $T_{\rm reh}$. The value of $T_{\rm reh}$ should be larger than the lightest heavy Majorana neutrino mass $M_1 \sim 10^{12}$ GeV. This requirement is free from any problems in those non-supersymmetric seesaw models. In some

[3]Here U and Q denote the $SU(2)_{\rm L}$ singlet of up-type quarks and the $SU(2)_{\rm L}$ doublet of quarks, respectively. Their Yukawa interactions with the Higgs doublet have been given in Eq. (2.46). Note that there are also the production processes involving the electroweak gauge bosons. We shall discuss such processes when we derive the Boltzmann equations in Section 11.3.3.

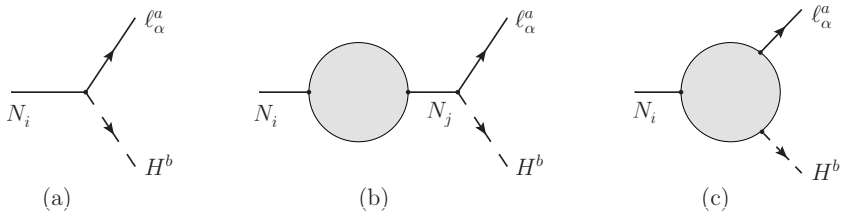

Fig. 11.3 The Feynman diagrams for the decays $N_i \to \ell^a_\alpha + H^b$ at the tree and one-loop levels, where $a, b = 1, 2$ are the $SU(2)$ indices of lepton and Higgs doublets

supersymmetric seesaw models, however, such a high reheating temperature may cause the overproduction of gravitinos — the supersymmetric partners of gravitons (Weinberg, 1982; Ellis *et al.*, 1982). A possible way out is to assume that heavy Majorana neutrinos were non-thermally generated in the supersymmetric case. If N_i and ϕ are coupled and the mass of ϕ satisfies $M_\phi > 2M_i$, then the decays $\phi \to N_i + N_i$ are allowed (Lazarides and Shafi, 1991; Kumekawa *et al.*, 1994). After the Hubble parameter H became comparable to or smaller than the decay width of ϕ (i.e., $H \lesssim \Gamma_\phi = \lambda_i^2 M_\phi / 4\pi$ with λ_i being the coupling constant between ϕ and N_i), the inflaton began to decay (Lazarides, 2002). Then the reheating temperature $T_{\rm reh}$ can be determined from $\Gamma_\phi = H$ together with Eqs. (9.30) and (9.31):

$$T_{\rm reh} = \left(\frac{45}{4\pi^3 g_*} \right)^{1/4} \sqrt{\Gamma_\phi M_{\rm Pl}} \,, \tag{11.34}$$

where $g_* = 106.75$ is the effective number of the relativistic degrees of freedom in the SM, and $M_{\rm Pl} \approx 1.22 \times 10^{19}$ GeV is the Planck mass. If $M_i \gg T_{\rm reh}$ holds, N_i must have decayed immediately after its production. The number density of N_i is roughly given by $n_{N_i} \approx 3 n^{\rm eq}_{N_i} T_{\rm reh} / (2M_i)$, where $n^{\rm eq}_{N_i}$ denotes the number density of N_i in thermal equilibrium (Kumekawa *et al.*, 1994).

Although the non-thermal production mechanism of heavy Majorana neutrinos is interesting, it depends on the details of an inflation model. In the following we shall only focus on the thermal leptogenesis.

11.3.2 CP-violating Asymmetries

The difference between the decay rates $\Gamma(N_i \to \ell_\alpha + H)$ and $\Gamma(N_i \to \overline{\ell}_\alpha + \overline{H})$ vanishes at the tree level, but it is nonzero at the one-loop level because direct CP violation may arise from the interference between tree- and loop-level decay amplitudes. The typical Feynman diagrams for $N_i \to \ell^a_\alpha + H^b$ decays are shown in Fig. 11.3, where the $SU(2)$ indices a and b refer to the components of lepton and Higgs doublets. One can see that the one-loop contributions to the decay amplitudes include the self-energy and vertex corrections. For

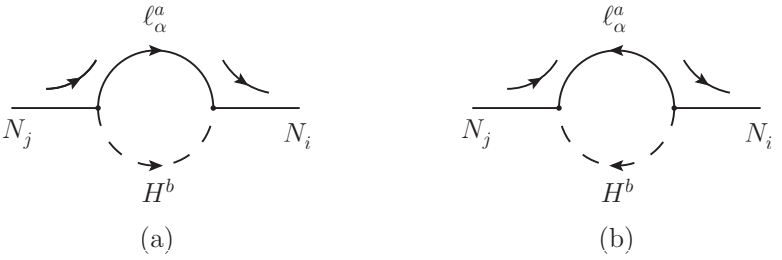

Fig. 11.4 The Feynman diagrams for the one-loop self-energies of heavy Majorana neutrinos N_i, where the arc arrows denote the direction of the fermion flow (Denner *et al.*, 1992. With permission from Elsevier; Dreiner *et al.*, 2010)

the decays of N_i with each lepton flavor in the final states, the corresponding CP-violating asymmetries are defined as

$$\varepsilon_{i\alpha} \equiv \frac{\Gamma(N_i \to \ell_\alpha + H) - \Gamma(N_i \to \overline{\ell}_\alpha + \overline{H})}{\sum\limits_\alpha \left[\Gamma(N_i \to \ell_\alpha + H) + \Gamma(N_i \to \overline{\ell}_\alpha + \overline{H})\right]} , \tag{11.35}$$

where the summation over the $SU(2)$ indices is implied. The total CP-violating asymmetry in N_i decays is therefore $\varepsilon_i = \varepsilon_{ie} + \varepsilon_{i\mu} + \varepsilon_{i\tau}$. It is easy to calculate the total decay rate of N_i at the tree level:

$$\Gamma_i \equiv \sum_\alpha \left[\Gamma(N_i \to \ell_\alpha + H) + \Gamma(N_i \to \overline{\ell}_\alpha + \overline{H})\right] = \frac{\left(Y^\dagger_\nu Y_\nu\right)_{ii}}{8\pi} M_i , \tag{11.36}$$

where $\Gamma(N_i \to \ell_\alpha + H) = \Gamma(N_i \to \overline{\ell}_\alpha + \overline{H})$ holds in the neglect of CP violation. Only the vertex corrections were considered in the early analysis of leptogenesis (Fukugita and Yanagida, 1986; Luty, 1992). The self-energy corrections were found to be important (Flanz *et al.*, 1995; Covi *et al.*, 1996) and even dominant if the masses of heavy Majorana neutrinos are nearly degenerate (Pilaftsis and Underwood, 2004). Note that CP violation requires at least two different weak phases and two different strong phases in the decay amplitudes. The weak phases come from the complex Yukawa coupling matrix Y_ν, while the strong phases can be generated if the lepton and Higgs doublets running in the loops are on their mass shells. This condition is always satisfied, because N_i are heavy enough as compared with the SM particles.

Let us begin to calculate the one-loop self-energies of heavy Majorana neutrinos N_i (see Fig. 11.4 for the Feynman diagrams). Because of $N^c_i = N_i$, it is straightforward to verify that the self-energies can be expressed as

$$\Sigma_{ij}(\not{p}) = \not{p} P_{\rm L} \Sigma^{\rm L}_{ij}(p^2) + \not{p} P_{\rm R} \Sigma^{\rm R}_{ij}(p^2) + P_{\rm L} \Sigma^{\rm M*}_{ij}(p^2) + P_{\rm R} \Sigma^{\rm M}_{ij}(p^2) , \tag{11.37}$$

where $\Sigma^{\rm R}_{ij}(p^2) = \Sigma^{\rm L*}_{ij}(p^2)$ and $P_{\rm L,R} \equiv (1 \mp \gamma_5)/2$. The contribution from the Feynman diagram in Fig. 11.4(a) is explicitly given by

$$
\begin{aligned}
-\mathrm{i}\Sigma_{ij}^{(a)}(\not{p}) &= \sum_{\alpha}\sum_{a,b}\left[-\mathrm{i}(Y_\nu^\dagger)_{i\alpha}(\epsilon^T)_{ba}\right]\left[-\mathrm{i}(Y_\nu)_{\alpha j}\epsilon_{ab}\right] \\
&\quad\times\int\frac{\mathrm{d}^4k}{(2\pi)^4}P_{\mathrm{L}}\frac{\mathrm{i}(\not{p}+\not{k})}{(k+p)^2+\mathrm{i}\epsilon^+}P_{\mathrm{R}}\frac{\mathrm{i}}{\not{k}+\mathrm{i}\epsilon^+} \\
&= \frac{\mathrm{i}}{16\pi^2}\left(Y_\nu^\dagger Y_\nu\right)_{ij}B_0(p^2,0,0)\not{p}P_{\mathrm{R}}\ , \qquad (11.38)
\end{aligned}
$$

where ϵ_{ab} is the totally antisymmetric tensor with $\epsilon_{12}=-\epsilon_{21}=1$, the positive infinitesimal ϵ^+ regularizes the propagators, and the masses of lepton and Higgs doublets have been omitted. The two-point scalar Passarino-Veltman function is defined as (Passarino and Veltman, 1979) [4]

$$
B_0(p^2,0,0)=\Delta_{\mathrm{E}}-\ln\left(\frac{|p^2|}{\mu^2}\right)+2+\mathrm{i}\pi\Theta(p^2)\ , \qquad (11.39)
$$

where $\Theta(p^2)$ denotes the step function, and $\Delta_{\mathrm{E}}\equiv 2/(4-D)-\gamma_{\mathrm{E}}+\ln(4\pi)$ with D being the space-time dimension and γ_{E} being the Euler constant. The Feynman diagram in Fig. 11.4(b) can similarly be calculated:

$$
\begin{aligned}
-\mathrm{i}\Sigma_{ij}^{(b)}(\not{p}) &= \sum_{\alpha}\sum_{a,b}\left[-\mathrm{i}(Y_\nu^T)_{i\alpha}(\epsilon^T)_{ba}\right]\left[-\mathrm{i}(Y_\nu^*)_{\alpha j}\epsilon_{ab}\right] \\
&\quad\times\int\frac{\mathrm{d}^4k}{(2\pi)^4}P_{\mathrm{R}}\frac{\mathrm{i}(\not{p}+\not{k})}{(k+p)^2+\mathrm{i}\epsilon^+}P_{\mathrm{L}}\frac{\mathrm{i}}{\not{k}+\mathrm{i}\epsilon^+} \\
&= \frac{\mathrm{i}}{16\pi^2}\left(Y_\nu^T Y_\nu^*\right)_{ij}B_0(p^2,0,0)\not{p}P_{\mathrm{L}}\ . \qquad (11.40)
\end{aligned}
$$

Although the divergence of the one-loop self-energies Δ_{E} is present, it may directly be removed as in the modified minimal subtraction scheme ($\overline{\mathrm{MS}}$). After the renormalization procedure, the finite self-energies turn out to be

$$
\Sigma_{ij}(\not{p})=\not{p}\left[K_{ji}P_{\mathrm{L}}+K_{ij}P_{\mathrm{R}}\right]\mathcal{A}(p^2)\ , \qquad (11.41)
$$

where $K\equiv Y_\nu^\dagger Y_\nu$ is a Hermitian matrix,

$$
\mathcal{A}(p^2)=\frac{1}{16\pi^2}\left[\ln\left(\frac{|p^2|}{\mu^2}\right)-2-\mathrm{i}\pi\Theta(p^2)\right]\ . \qquad (11.42)
$$

Note that the step function in Eq. (11.42) should be $\Theta(p^2-M_h^2-M_\ell^2)$ if the lepton and Higgs masses are taken into account, implying that an imaginary part in $\mathcal{A}(p^2)$ will appear if the particles in the loop are on their mass shells. Note also that the imaginary part of $\mathcal{A}(p^2)$ is independent of the renormalization scale μ.

[4] The Passarino-Veltman functions are frequently encountered in the loop calculations (Denner, 1993) if the dimensional regularization is implemented ('t Hooft, 1973). In this scheme the dimension of the space-time is assumed to be $D<4$ and the limit $D\to 4$ is taken for the final results.

Now we are ready to compute the CP-violating asymmetries arising from the interference between the tree-level amplitude and self-energy corrections. In this case the overall decay amplitude of $N_i \to \ell_\alpha^a + H^b$ is a sum of the contributions from Fig. 11.3(a) and Fig. 11.3(b):

$$\mathrm{i}\mathcal{M}_{\alpha i}^{\mathrm{s},ab} = -\mathrm{i}\epsilon_{ab} \sum_{j\neq i} \overline{u}(q) P_{\mathrm{R}} \left[(Y_\nu)_{\alpha i} + (Y_\nu)_{\alpha j} S(\not{p}, M_j) \Sigma_{ji}(\not{p}) \right] u(p) \; , \quad (11.43)$$

where $\mathrm{i}S(\not{p}, M_j)$ is the propagator of N_j. Note that only the truncated Green functions contribute to the relevant S-matrix elements, so the summation in Eq. (11.43) is over all N_j with $j \neq i$. The overall decay amplitude for the CP-conjugate process $N_i \to \overline{\ell}_\alpha + \overline{H}$ can be obtained in a similar way:

$$\mathrm{i}\overline{\mathcal{M}}_{\alpha i}^{\mathrm{s},ab} = -\mathrm{i}\epsilon_{ab} \sum_{j\neq i} \overline{v}(q) P_{\mathrm{L}} \left[(Y_\nu^*)_{\alpha i} + (Y_\nu^*)_{\alpha j} S(\not{p}, M_j) \Sigma_{ji}(\not{p}) \right] u(p) \; . \quad (11.44)$$

Integrating $|\mathcal{M}_{\alpha i}^{\mathrm{s},ab}|^2$ and $|\overline{\mathcal{M}}_{\alpha i}^{\mathrm{s},ab}|^2$ over the phase space of final states, we arrive at the CP-violating asymmetries induced by the self-energy corrections:

$$\begin{aligned} \varepsilon_{i\alpha}^{\mathrm{s}} &= \frac{\dfrac{1}{2M_i} \displaystyle\int \mathrm{d}\Pi_q \mathrm{d}\Pi_k (2\pi)^4 \delta^4(p - q - k) \sum_{a,b} \left[\left| \mathcal{M}_{\alpha i}^{\mathrm{s},ab} \right|^2 - \left| \overline{\mathcal{M}}_{\alpha i}^{\mathrm{s},ab} \right|^2 \right]}{\displaystyle\sum_\alpha \left[\Gamma(N_i \to \ell_\alpha + H) + \Gamma(N_i \to \overline{\ell}_\alpha + \overline{H}) \right]} \\ &= \frac{1}{8\pi K_{ii}} \sum_{j\neq i} \frac{M_i}{M_i^2 - M_j^2} \mathrm{Im} \left\{ (Y_\nu^*)_{\alpha i} (Y_\nu)_{\alpha j} \left[K_{ji} M_i + K_{ij} M_j \right] \right\} \; , \quad (11.45) \end{aligned}$$

where $\mathrm{d}\Pi_q \equiv \mathrm{d}^3\mathbf{q}/(2\pi)^3(2q^0)$ is the differential element of the phase space, and Eqs. (11.36), (11.41), (11.43) and (11.44) have been used. A sum of $\varepsilon_{i\alpha}^{\mathrm{s}}$ over the lepton flavors gives rise to the total CP-violating asymmetry

$$\varepsilon_i^{\mathrm{s}} \equiv \sum_\alpha \varepsilon_{i\alpha}^{\mathrm{s}} = \frac{1}{8\pi K_{ii}} \sum_{j\neq i} \frac{M_i M_j}{M_i^2 - M_j^2} \mathrm{Im} \left[(K_{ij})^2 \right] \; . \quad (11.46)$$

Note that $\varepsilon_{i\alpha}^{\mathrm{s}}$ and $\varepsilon_i^{\mathrm{s}}$ seem to be divergent provided the masses of two heavy Majorana neutrinos are degenerate (i.e., $M_i = M_j$). In this special case one has to take account of the finite decay widths of N_j in their propagators. The decay widths Γ_j actually serve as the regulator to make the CP-violating asymmetries well-behaved even in the $M_i = M_j$ limit. If the mass splits $|M_i - M_j|$ are comparable with Γ_i and Γ_j, then the magnitudes of $\varepsilon_{i\alpha}^{\mathrm{s}}$ and $\varepsilon_i^{\mathrm{s}}$ can be resonantly enhanced. This observation is a starting point of the *resonant* leptogenesis mechanism (Pilaftsis and Underwood, 2004, 2005).

We proceed to calculate the CP-violating asymmetries arising from the interference between the tree-level amplitude and one-loop vertex corrections in N_i decays (see Fig. 11.5 for the Feynman diagrams). The effective vertex in Fig. 11.5(a) can be written as

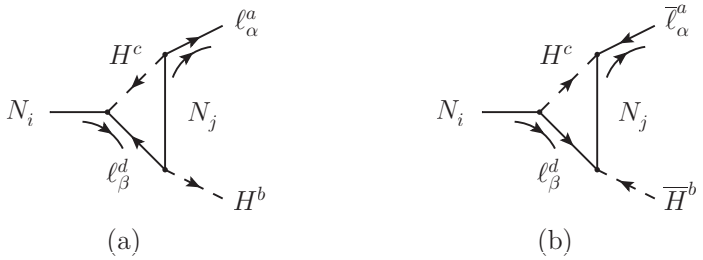

Fig. 11.5 The Feynman diagrams for the one-loop vertex corrections to the decays of heavy Majorana neutrinos N_i: (a) $N_i \to \ell_\alpha + H$ and (b) $N_i \to \overline{\ell}_\alpha + \overline{H}$, where the arc arrows denote the direction of the fermion flow (Denner *et al.*, 1992. With permission from Elsevier)

$$\begin{aligned} \mathrm{i}\Gamma^{ab}_{\alpha i} = & \sum_\beta \sum_{c,d} \sum_j \left[-\mathrm{i}(Y_\nu)_{\alpha j}\epsilon_{ac}\right]\left[-\mathrm{i}(Y^T_\nu)_{j\beta}(\epsilon^T)_{bd}\right]\left[-\mathrm{i}(Y^*_\nu)_{\beta i}\epsilon_{dc}\right] \\ & \times \int \frac{\mathrm{d}^4k}{(2\pi)^4} P_{\mathrm{R}}[\mathrm{i}S(\not{p}+\not{k}+\not{p}', M_j)]P_{\mathrm{R}}[\mathrm{i}S(\not{p}+\not{k})]P_{\mathrm{L}}[\mathrm{i}\Delta(k^2)] \ , \end{aligned} \tag{11.47}$$

where $\mathrm{i}S(\not{p}, M_j)$ is the propagator of N_j, $\mathrm{i}S(\not{p})$ denotes the propagator of the lepton doublet in the neglect of lepton masses, and $\mathrm{i}\Delta(k^2)$ represents the propagator of massless scalars. Using the dimensional regularization method, we explicitly work out this effective vertex:

$$\Gamma^{ab}_{\alpha i} = \sum_j \epsilon_{ab}(Y_\nu)_{\alpha j}\left[\left(\widehat{M}\mathcal{B}K^T\right)_{ji}\not{p} + \left(\widehat{M}\mathcal{C}K^T\right)_{ji}\not{p}'\right]P_{\mathrm{L}} \ , \tag{11.48}$$

where $\widehat{M}$, $\mathcal{B}$ and $\mathcal{C}$ are three diagonal matrices: $\widehat{M} = \mathrm{Diag}\{M_1, M_2, M_3\}$, and the diagonal elements of $\mathcal{B}$ and $\mathcal{C}$ are (for $k = 1, 2, 3$)

$$\begin{aligned} \mathcal{B}_k(p^2, p'^2) &= \frac{1}{16\pi^2}\left[C_{11}(p, p', 0, 0, M_k) + C_0(p, p', 0, 0, M_k)\right] \ , \\ \mathcal{C}_k(p^2, p'^2) &= \frac{1}{16\pi^2} C_{12}(p, p', 0, 0, M_k) \end{aligned} \tag{11.49}$$

with C_0, C_{11} and C_{12} being the three-point Passarino-Veltman functions (Denner, 1993). The Feynman diagram for the one-loop vertex corrections to the CP-conjugate decay $N_i \to \overline{\ell}_\alpha + \overline{H}$ is shown Fig. 11.5(b). Its effective vertex is similarly expressed as

$$\overline{\Gamma}^{ab}_{\alpha i} = \sum_j \epsilon_{ab}(Y^*_\nu)_{\alpha j}\left[\left(\widehat{M}\mathcal{B}K\right)_{ji}\not{p} + \left(\widehat{M}\mathcal{C}K\right)_{ji}\not{p}'\right]P_{\mathrm{R}} \ , \tag{11.50}$$

where $\mathcal{B}$ and $\mathcal{C}$ have been given in Eq. (11.49). After a sum of the contributions from Fig. 11.3(a) and Fig. 11.3(c), the overall decay amplitude of $N_i \to \ell_\alpha + H$ with the one-loop vertex corrections is then obtained:

$$\mathrm{i}\mathcal{M}^{\mathrm{v},ab}_{\alpha i} = -\mathrm{i}\overline{u}(q)\left[(Y_\nu)_{\alpha i}\epsilon_{ab}P_{\mathrm{R}} - \mathit{\Gamma}^{ab}_{\alpha i}\right]u(p)\ . \tag{11.51}$$

The overall decay amplitude of $N_i \to \overline{\ell}_\alpha + \overline{H}$ is similarly given by

$$\mathrm{i}\overline{\mathcal{M}}^{\mathrm{v},ab}_{\alpha i} = -\mathrm{i}\overline{v}(q)\left[(Y^*_\nu)_{\alpha i}\epsilon_{ab}P_{\mathrm{R}} - \overline{\mathit{\Gamma}}^{ab}_{\alpha i}\right]u(p)\ . \tag{11.52}$$

Integrating $|\mathcal{M}^{\mathrm{v},ab}_{\alpha i}|^2$ and $|\overline{\mathcal{M}}^{\mathrm{v},ab}_{\alpha i}|^2$ over the phase space of final states, we arrive at the CP-violating asymmetries induced by the vertex corrections:

$$\begin{aligned}\varepsilon^{\mathrm{v}}_{i\alpha} &= \frac{\dfrac{1}{2M_i}\displaystyle\int \mathrm{d}\mathit{\Pi}_q \mathrm{d}\mathit{\Pi}_k (2\pi)^4\delta^4(p-q-k)\sum_{a,b}\left[\left|\mathcal{M}^{\mathrm{v},ab}_{\alpha i}\right|^2 - \left|\overline{\mathcal{M}}^{\mathrm{v},ab}_{\alpha i}\right|^2\right]}{\displaystyle\sum_\alpha\left[\mathit{\Gamma}(N_i \to \ell_\alpha + H) + \mathit{\Gamma}(N_i \to \overline{\ell}_\alpha + \overline{H})\right]} \\ &= \frac{1}{8\pi K_{ii}}\sum_j \mathrm{Im}\left[(Y^*_\nu)_{\alpha i}(Y_\nu)_{\alpha j}K_{ij}\right] f_{\mathrm{v}}\left(\frac{M_j^2}{M_i^2}\right)\ ,\end{aligned} \tag{11.53}$$

where the vertex function $f_{\mathrm{v}}(M_j^2/M_i^2)$ is defined by

$$f_{\mathrm{v}}(x) \equiv \sqrt{x}\left[1 + (1+x)\ln\left(\frac{x}{1+x}\right)\right]\ . \tag{11.54}$$

Note that the term with $j = i$ on the right-hand side of Eq. (11.53) is actually vanishing. In the leading-order approximation the overall CP-violating asymmetry $\varepsilon_{i\alpha}$ is simply a sum of the CP-violating asymmetries induced by vertex and self-energy corrections (i.e., $\varepsilon_{i\alpha} = \varepsilon^{\mathrm{v}}_{i\alpha} + \varepsilon^{\mathrm{s}}_{i\alpha}$). Taking account of Eqs. (11.45) and (11.53), we obtain

$$\begin{aligned}\varepsilon_{i\alpha} = \frac{1}{8\pi(Y^\dagger_\nu Y_\nu)_{ii}}\sum_{j\neq i}\Bigg\{&\mathrm{Im}\left[(Y^*_\nu)_{\alpha i}(Y_\nu)_{\alpha j}(Y^\dagger_\nu Y_\nu)_{ij}\right]\mathcal{F}\left(\frac{M_j^2}{M_i^2}\right) \\ &+ \mathrm{Im}\left[(Y^*_\nu)_{\alpha i}(Y_\nu)_{\alpha j}(Y^\dagger_\nu Y_\nu)^*_{ij}\right]\mathcal{G}\left(\frac{M_j^2}{M_i^2}\right)\Bigg\}\ ,\end{aligned} \tag{11.55}$$

where we have introduced the loop functions $\mathcal{G}(x) \equiv 1/(1-x)$ and

$$\mathcal{F}(x) = \sqrt{x}\left[1 + \frac{1}{1-x} + (1+x)\ln\left(\frac{x}{1+x}\right)\right]\ . \tag{11.56}$$

If all the interactions in the era of leptogenesis were blind to lepton flavors, then only the total CP-violating asymmetry ε_i should be relevant:

$$\varepsilon_i = \sum_\alpha \varepsilon_{i\alpha} = \frac{1}{8\pi(Y^\dagger_\nu Y_\nu)_{ii}}\sum_{j\neq i}\mathrm{Im}\left[(Y^\dagger_\nu Y_\nu)^2_{ij}\right]\mathcal{F}\left(\frac{M_j^2}{M_i^2}\right)\ . \tag{11.57}$$

The above results are very useful for the study of flavor-dependent and flavor-independent leptogenesis scenarios in the type-I seesaw models.

The lepton number asymmetries can be generated from the CP-violating and out-of-equilibrium decays of heavy Majorana neutrinos N_i. Naively, a difference between the number densities of leptons (n_ℓ) and antileptons ($n_{\overline{\ell}}$) is determined by the CP-violating asymmetry ε_i and the number density of heavy Majorana neutrinos n_{N_i}; i.e., $n_\ell - n_{\overline{\ell}} \propto \varepsilon_i n_{N_i}$. But n_{N_i} may change due to the decay and inverse-decay processes. The values of n_ℓ and $n_{\overline{\ell}}$ may also be modified by both the decays and lepton-number-violating scattering processes. Hence an exact calculation of the lepton and baryon number asymmetries relies on the solution to the full set of Boltzmann equations (Kolb and Turner, 1990; Luty, 1992; Plümacher, 1997; Davidson *et al.*, 2008).

11.3.3 Boltzmann Equations

The Boltzmann equations are widely regarded as the standard tools for determining the particle number densities which may more or less be modified by decays and collisions in the expanding Universe (Kolb and Turner, 1990). Given the large mass scale of heavy Majorana neutrinos, the leptogenesis mechanism must have worked in the very early Universe where the total energy density was dominated by relativistic particles and all the SM particles were in thermal equilibrium. To be specific, the number density of the "x" particles in thermal equilibrium at the temperature T is described by

$$n_x = g_x \int \frac{\mathrm{d}^3\mathbf{p}}{(2\pi)^3} f_x(\mathbf{p}) = g_x \int \frac{\mathrm{d}^3\mathbf{p}}{(2\pi)^3} \frac{1}{\exp\left[\left(E_x - \mu_x\right)/T\right] \pm 1} \; , \tag{11.58}$$

where g_x represents the number of internal degrees of freedom, $f_x(\mathbf{p})$ is the distribution function in the phase space, m_x denotes the mass of the "x" particle, $T \gg m_x$ and $E_x = \sqrt{|\mathbf{p}|^2 + m_x^2} \to |\mathbf{p}|$ hold, μ_x stands for the chemical potential, and the "$\pm$" signs correspond to fermions ($+$) and bosons ($-$). Neglecting the tiny chemical potentials, one may calculate the energy densities of relativistic bosons and fermions (see Section 9.1.4):

$$\rho = \frac{g_* \pi^2}{30} T^4 \; , \tag{11.59}$$

where g_* is the effective number of degrees of freedom and its expression has been given in Eq. (9.29). In the SM of electroweak and strong interactions $g_* = 106.75$ holds when the temperature is much higher than the electroweak gauge symmetry breaking scale $v \approx 246$ GeV [5]. The Hubble parameter H

[5] At $T \sim v$ the Higgs boson, the photon and three massive gauge bosons totally contribute $1 + 2 + 3 \times 3 = 12$ to g_*. At $T \gg v$, however, the electroweak gauge symmetry is restored and all the gauge bosons are massless. In this case four real components of the Higgs doublet and two polarization states of each gauge boson should be taken into account. So they also contribute $4 + 2 \times 4 = 12$ to g_*.

in this radiation-dominated epoch can be expressed as $H \approx 1.66\sqrt{g_*}T^2/M_{\rm Pl}$ with $M_{\rm Pl}$ being the Planck mass, as already shown in Eq. (9.31). The entropy density of the Universe is defined as

$$s \equiv \frac{\rho + p}{T} = \frac{4\rho}{3T} = \frac{2\tilde{g}_* \pi^2}{45} T^3 \; , \tag{11.60}$$

where the equation of state $p = \rho/3$ is used for the relativistic gas, and

$$\tilde{g}_* \equiv \sum_{\rm b} g_{\rm b} \left(\frac{T^*_{\rm b}}{T} \right)^3 + \frac{7}{8} \sum_{\rm f} g_{\rm f} \left(\frac{T^*_{\rm f}}{T} \right)^3 \tag{11.61}$$

denotes the effective number of degrees of freedom for the entropy with $T^*_{\rm b}$ and $T^*_{\rm f}$ being the decoupling temperatures of the corresponding bosons and fermions. Since all the particles should be in thermal equilibrium at the temperature $T \gtrsim M_i$, where M_i are the masses of heavy Majorana neutrinos N_i, we have $T^*_{\rm b} = T^*_{\rm f} = T$ and therefore $\tilde{g}_* = g_*$ as given in Eq. (9.29). When $T < M_i$, however, non-relativistic N_i must have decayed and their number densities in thermal equilibrium are suppressed by the Boltzmann factors $e^{-M_i/T}$. To illustrate how a simple leptogenesis mechanism works, here we only consider the role of the lightest heavy Majorana neutrino N_1 and assume that the lepton number asymmetries produced previously from the decays of N_2 and N_3 have been completely washed out [6]. Furthermore, we neglect the Yukawa interactions of charged leptons and focus on the flavor-independent CP-violating asymmetries ε_i obtained in Eq. (11.57).

Now we present an intuitive derivation of the Boltzmann equations in the expanding Universe. The number density of the "a" particles is defined as $n_a \equiv N_a/V$, where N_a is the total number of the "a" particles in the physical volume $V = V_0 R^3(t)/R^3(t_0)$ with V_0 being the volume in the comoving coordinate system. In the absence of any interactions N_a should be conserved; i.e., $\dot{N}_a = 0$ or equivalently

$$\frac{{\rm d}(n_a V)}{{\rm d}t} = V(\dot{n}_a + 3Hn_a) = 0 \; , \tag{11.62}$$

where $H = \dot{R}(t)/R(t)$ is the Hubble parameter. If there exist collisions which change n_a, they should contribute to the right-hand side of Eq. (11.62). For instance, the reaction $a + X \to Y$ and its inverse process $Y \to a + X$ can modify the number of the "a" particles by one unit. Hence the change of the particle number in the physical volume V in the unit time can be written as

$$-V \sum_{X,Y} \int {\rm d}\Pi_a {\rm d}\Pi_X {\rm d}\Pi_Y (2\pi)^4 \delta^4(p_a + p_X - p_Y) \{ f_a f_X (1 \pm f_Y)$$

[6] The contributions of heavier Majorana neutrinos N_2 and N_3 to the lepton number asymmetries should in general be included, and the washout effects on these asymmetries can be evaluated by solving the relevant Boltzmann equations.

$$\times|\mathcal{M}(a+X\to Y)|^2 - f_Y(1\pm f_a)(1\pm f_Y)|\mathcal{M}(Y\to a+X)|^2\big\}\ , \quad (11.63)$$

where $\mathcal{M}(a+X\to Y)$ and $\mathcal{M}(Y\to a+X)$ are the Feynman amplitudes. Note that the amplitudes should be summed over all the internal degrees of freedom of initial and final states. Two reasonable approximations are usually made to simplify the collision integral: (a) the Maxwell-Boltzmann distribution function $f_x = n_x \mathrm{e}^{-E/T}/n_x^{\rm eq} = \mathrm{e}^{-(E-\mu_x)/T}$ is taken, where $n_x^{\rm eq} = g_x \int \mathrm{d}\Pi_x \mathrm{e}^{-E/T}$ stands for the number density in thermal equilibrium; and (b) $1\pm f_x \approx 1$ holds due to $f_x \approx \mathrm{e}^{-\langle E\rangle/T} \approx 0.05$, where $\langle E\rangle = 3T$ is the average energy. Then the Boltzmann equation can be derived from Eqs. (11.62) and (11.63) (Kolb and Turner, 1990; Luty, 1992). After a straightforward calculation, we arrive at

$$\dot{n}_a + 3Hn_a = \sum_{X,Y}\left[\frac{n_Y}{n_Y^{\rm eq}}\gamma(Y\to a+X) - \frac{n_a}{n_a^{\rm eq}}\cdot\frac{n_X}{n_X^{\rm eq}}\gamma(a+X\to Y)\right]\ , \quad (11.64)$$

where the interaction rate density is defined as

$$\gamma(a+X\to Y) \equiv \int \mathrm{d}\Pi_a \mathrm{d}\Pi_X \mathrm{d}\Pi_Y (2\pi)^4\delta^4(p_a+p_X-p_Y) \times \mathrm{e}^{-E_a/T}\mathrm{e}^{-E_X/T}|\mathcal{M}(a+X\to Y)|^2\ . \quad (11.65)$$

It is more convenient to express the Boltzmann equation in terms of the particle number per unit entropy $Y_a \equiv n_a/s$ and to replace the time t with the dimensionless variable $z \equiv M_a/T$. Note that

$$\frac{\mathrm{d}Y_a}{\mathrm{d}z} = \frac{\mathrm{d}t}{\mathrm{d}z}\cdot\frac{\mathrm{d}}{\mathrm{d}t}\left(\frac{Vn_a}{Vs}\right) = \frac{\mathrm{d}t}{\mathrm{d}z}\cdot\frac{\dot{n}_a+3Hn_a}{s} \quad (11.66)$$

holds, where the total entropy Vs is conserved. Because $H(t) = 1/(2t)$ and $T\propto 1/\sqrt{t}$ in the radiation-dominated epoch, it is easy to show $\dfrac{\mathrm{d}t}{\mathrm{d}z} = 1/(Hz)$. As a direct result, the Boltzmann equation in Eq. (11.64) can be rewritten as

$$\frac{\mathrm{d}Y_a}{\mathrm{d}z} = \frac{1}{sHz}\sum_{X,Y}\left[\frac{Y_Y}{Y_Y^{\rm eq}}\gamma(Y\to a+X) - \frac{Y_a}{Y_a^{\rm eq}}\cdot\frac{Y_X}{Y_X^{\rm eq}}\gamma(a+X\to Y)\right]\ . \quad (11.67)$$

The evolution of the number density of the heavy Majorana neutrino N_1 and that of the lepton number asymmetry produced from N_1 decays are governed by the corresponding Boltzmann equations. The latter can be fixed after a calculation of the interaction rate densities of the decays and lepton-number-violating scattering processes.

We first consider the lepton-number-violating decays $N_i\to \ell_\alpha + H$ and $N_i\to \overline{\ell}_\alpha + \overline{H}$ together with their inverse processes $\ell_\alpha + H\to N_i$ and $\overline{\ell}_\alpha + \overline{H}\to N_i$. The rates of these reactions have been given in Section 11.3.2. The

corresponding reaction rate density of $N_i \to \ell_\alpha + H$ can be calculated with the help of Eq. (11.65):

$$\begin{aligned}\gamma(N_i \to \ell_\alpha H) &= \int {\rm d}\Pi_{N_i} {\rm e}^{-E_{N_i}/T} \int {\rm d}\Pi_{\ell_\alpha} {\rm d}\Pi_H \\ &\quad \times (2\pi)^4 \delta^4(p_{N_i} - p_{\ell_\alpha} - p_H) |\mathcal{M}(N_i \to \ell_\alpha + H)|^2 \\ &= g_{N_i} \int {\rm d}\Pi_{N_i} {\rm e}^{-E_{N_i}/T} 2 M_i \Gamma(N_i \to \ell_\alpha + H) \\ &= n^{\rm eq}_{N_i} \frac{K_1(z)}{K_2(z)} \Gamma(N_i \to \ell_\alpha + H) \; , \end{aligned} \tag{11.68}$$

where $\Gamma(N_i \to \ell_\alpha + H)$ denotes the partial decay width of $N_i \to \ell_\alpha + H$ in the rest frame of N_i, and

$$\begin{aligned} K_1(z) &\equiv z^{-1} \int_z^{+\infty} {\rm e}^{-y} \sqrt{y^2 - z^2} \; {\rm d}y \; , \\ K_2(z) &\equiv z^{-2} \int_z^{+\infty} y {\rm e}^{-y} \sqrt{y^2 - z^2} \; {\rm d}y \end{aligned} \tag{11.69}$$

are the modified Bessel functions (Kolb and Turner, 1990). Concentrating on the lightest heavy Majorana neutrino N_1 and summing over the lepton flavors, we obtain the total decay rate density

$$\gamma_{\rm D} = \sum_\alpha \left[\gamma(N_1 \to \ell_\alpha + H) + \gamma(N_1 \to \overline{\ell}_\alpha + \overline{H}) \right] = n^{\rm eq}_{N_i} \frac{K_1(z)}{K_2(z)} \Gamma_1 \; , \tag{11.70}$$

where Γ_1 has been given in Eq. (11.36). When the one-loop corrections to $\Gamma(N_1 \to \ell + H)$ and $\Gamma(N_1 \to \overline{\ell} + \overline{H})$ are taken into account, their difference becomes nonzero and is characterized by the CP-violating asymmetry ε_1 given in Eq. (11.57). The CPT symmetry leads us to

$$\begin{aligned} \gamma(N_1 \to \ell + H) &= \gamma(\overline{\ell} + \overline{H} \to N_1) = \frac{1}{2}(1 + \varepsilon_1) \gamma_{\rm D} \; , \\ \gamma(N_1 \to \overline{\ell} + \overline{H}) &= \gamma(\ell + H \to N_1) = \frac{1}{2}(1 - \varepsilon_1) \gamma_{\rm D} \; . \end{aligned} \tag{11.71}$$

The important scattering processes include (a) the lepton-number-violating $\Delta L = 1$ processes involving the up-type quarks: $N_i + \ell_\alpha \to Q + \overline{U}$, $N_i + Q \to \ell_\alpha + U$ and $N_i + \overline{U} \to \ell_\alpha + \overline{Q}$ (Fig. 11.6), where the dominant contributions are induced by the top quark; (b) the $\Delta L = 1$ processes involving the electroweak gauge bosons: $N_i + \ell_\alpha \to \overline{H} + V_\mu$, $N_i + \ell_\alpha \to V_\mu + \overline{H}$ and $N_i + \overline{H} \to \ell_\alpha + V_\mu$ (Fig. 11.7), where V_μ stands for W^i_μ (for $i = 1, 2, 3$) and B_μ; (c) the $\Delta L = 2$ processes: $\ell_\alpha + H \to \overline{\ell}_\beta + \overline{H}$ and $\ell_\alpha + \ell_\beta \to \overline{H} + \overline{H}$ (Fig. 11.8). In general, one may define the reduced cross section for the process $a + X \to Y$ as follows (Davidson *et al.*, 2008):

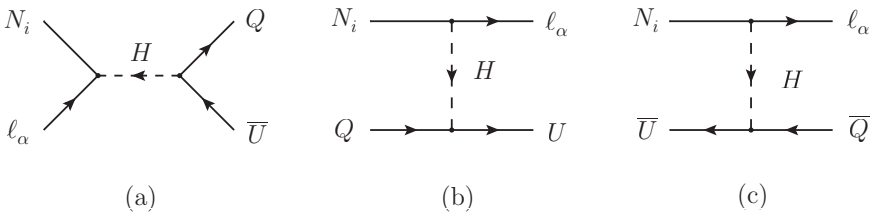

Fig. 11.6 The Feynman diagrams for the $\Delta L = 1$ scattering processes involving the top quark, whose Yukawa coupling constant $y_t = \sqrt{2}\, m_t/v$ is of $\mathcal{O}(1)$

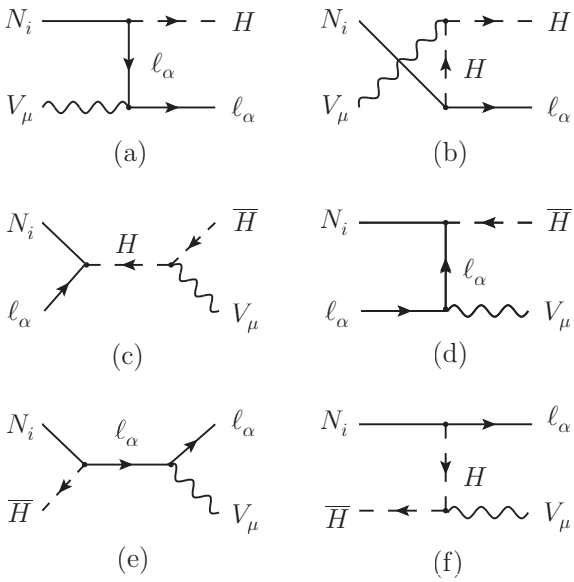

Fig. 11.7 The Feynman diagrams for the $\Delta L = 1$ scattering processes involving the electroweak gauge bosons V_μ, where $V_\mu = W^i_\mu$ and B_μ (for $i = 1, 2, 3$)

$$\hat{\sigma}(s') \equiv 8\pi\Phi_2(s') \int \mathrm{d}\Pi_Y (2\pi)^4 \delta^4(p_a + p_X - p_Y) |\mathcal{M}(a + X \to Y)|^2 \,, \quad (11.72)$$

where $\Phi_2(s')$ is the two-particle phase space integration

$$\Phi_2(s') \equiv \int \mathrm{d}\Pi_a \mathrm{d}\Pi_X (2\pi)^4 \delta^4(p_a + p_X - q) = \frac{\sqrt{\lambda(s', M_a^2, M_X^2)}}{8\pi s'} \quad (11.73)$$

with $s' = q^2$ and $\lambda(x, y, z) \equiv (x - y - z)^2 - 4yz$. Now Eq. (11.65) can be recast into the following form (Giudice *et al.*, 2004):

$$\gamma(a + X \to Y) = \int \mathrm{d}\Pi_a \mathrm{d}\Pi_X \mathrm{e}^{-E_a/T} \mathrm{e}^{-E_X/T} \frac{s'}{\sqrt{\lambda(s', M_a^2, M_X^2)}}\, \hat{\sigma}(s')$$

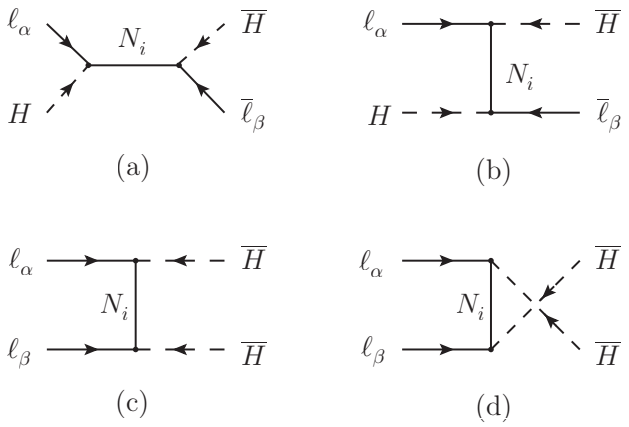

Fig. 11.8 The Feynman diagrams for the $\Delta L = 2$ scattering processes, and the on-shell contributions in the s-channel diagram should be subtracted for consistency

$$= \frac{M_a^4}{64\pi^4 z} \int_{x_{\rm thr}}^{\infty} {\rm d}x \, \sqrt{x} \, \hat{\sigma}(x) \, K_1(z\sqrt{x}) \, , \tag{11.74}$$

where $x \equiv s'/M_a^2$, and $x_{\rm thr}$ is the threshold value for the process $a + X \to Y$ to take place. Note that we have inserted the identity $\int \delta^4(p_a + p_X - q) \, {\rm d}^4 q = 1$ into the first line of Eq. (11.74) and changed the order of integration. To illustrate, we may explicitly work out the reduced cross section for the s-channel process $N_1(p) + \ell(p') \to Q(k) + \overline{U}(k')$ in Fig. 11.6(a). If only the top quark contribution is considered, we obtain

$$\sum |\mathcal{M}(N_1 + \ell \to Q + \overline{U})|^2 = \frac{8 y_t^2 \left(Y_\nu^\dagger Y_\nu\right)_{11}}{s'^2} (p \cdot p')(k \cdot k') \, , \tag{11.75}$$

where $s' = (p + p')^2$ and $y_t \equiv \sqrt{2} \, m_t/v$ with m_t being the top quark mass. Substituting Eq. (11.75) into Eq. (11.72), we arrive at

$$\begin{aligned} \hat{\sigma}(x) &= \left(\frac{s' - M_1^2}{s'} \right) \left(\frac{8 y_t^2 \left(Y_\nu^\dagger Y_\nu\right)_{11}}{s'^2} \right) \int \frac{{\rm d}^3 \mathbf{k}}{(2\pi)^3 2k^0} \cdot \frac{{\rm d}^3 \mathbf{k}'}{(2\pi)^3 2k'^0} \\ &\quad \times (2\pi)^4 \delta^4(p + p' - k - k') \left(\frac{s' - M_1^2}{2} \right) (k \cdot k') \\ &= \frac{y_t^2 \left(Y_\nu^\dagger Y_\nu\right)_{11}}{4\pi} \left(\frac{s' - M_1^2}{s'} \right)^2 = \frac{y_t^2 \left(Y_\nu^\dagger Y_\nu\right)_{11}}{4\pi} \left(\frac{x - 1}{x} \right)^2 \, , \end{aligned} \tag{11.76}$$

where $x \equiv s'/M_1^2$ and $p \cdot p' = (s' - M_1^2)/2$ have been used. Inserting Eq. (11.76) into Eq. (11.74), one may then obtain the reaction rate density $\gamma(N_1 + \ell \to Q + \overline{U})$ which appears in the Boltzmann equation. First, let us consider the

Boltzmann equation for the number density of heavy Majorana neutrinos (Giudice *et al.*, 2004; Buchmüller *et al.*, 2005a),

$$sHz\frac{\mathrm{d}Y_{N_1}}{\mathrm{d}z}=-\sum_{X,Y}\left[N_1+X\leftrightarrow Y\right]\ , \tag{11.77}$$

where the summation should be taken over both the decays and the scattering processes: (a) the decays and their inverse processes $D\equiv[N_1\leftrightarrow\ell+H]$; (b) the $\Delta L=1$ scattering $S_s\equiv H_s+V_s$ with $H_s\equiv\left[N_1+\ell\leftrightarrow Q+\overline{U}\right]$ and $V_s\equiv\left[N_1+\ell\leftrightarrow\overline{H}+V_\mu\right]$; (c) the $\Delta L=1$ scattering $S_t\equiv H_t+V_t$ with $2H_t\equiv\left[N_1+\overline{Q}\leftrightarrow\overline{\ell}+\overline{U}\right]+\left[N_1+U\leftrightarrow\overline{\ell}+\overline{Q}\right]$ and $2V_t\equiv\left[N_1+V_\mu\leftrightarrow\overline{\ell}+\overline{H}\right]+\left[N_1+H\leftrightarrow\overline{\ell}+V_\mu\right]$; (d) the $\Delta L=2$ scattering $N_s\equiv\left[\ell+H\leftrightarrow\overline{\ell}+\overline{H}\right]$ and $N_t\equiv\left[\ell+\ell\leftrightarrow\overline{H}+\overline{H}\right]$. Note that the terms D,S_s,S_t and their CP-conjugate terms $\overline{D},\overline{S}_s,\overline{S}_t$ change the number densities of both N_1 and the lepton doublets ℓ and $\overline{\ell}$, while the terms N_s,N_t and their CP-conjugate terms $\overline{N}_s,\overline{N}_t$ only modify the lepton number density. Hence the Boltzmann equations for the number densities of N_1, ℓ and $\overline{\ell}$ are given by

$$\begin{aligned}
sHz\frac{\mathrm{d}Y_{N_1}}{\mathrm{d}z}&=-D-\overline{D}-S_s-\overline{S}_s-S_t-\overline{S}_t\ ,\\
sHz\frac{\mathrm{d}Y_{\ell}}{\mathrm{d}z}&=D-N_s-N_t-S_s+\overline{S}_t\ ,\\
sHz\frac{\mathrm{d}Y_{\overline{\ell}}}{\mathrm{d}z}&=\overline{D}+N_s-\overline{N}_t-\overline{S}_s+S_t\ .
\end{aligned} \tag{11.78}$$

So it is straightforward to derive the Boltzmann equation for the lepton number asymmetry $Y_{\mathrm{L}}\equiv Y_\ell-Y_{\overline{\ell}}=(n_\ell-n_{\overline{\ell}})/s$ from Eq. (11.78). If only the decays and their inverse processes are taken into account, the Boltzmann equation for Y_{L} turns out to be

$$sHz\frac{\mathrm{d}Y_{\mathrm{L}}}{\mathrm{d}z}=D-\overline{D}=\left[\varepsilon_1\left(\frac{Y_{N_1}}{Y_{N_1}^{\mathrm{eq}}}+1\right)-\frac{Y_{\mathrm{L}}}{2Y_\ell^{\mathrm{eq}}}\right]\gamma_{\mathrm{D}}\ , \tag{11.79}$$

where Eq. (11.71) and the identity $Y_\ell+Y_{\overline{\ell}}=2Y_\ell^{\mathrm{eq}}$ have been used. In this case a net lepton number asymmetry seems to be producible even if the heavy Majorana neutrinos stay in thermal equilibrium (i.e., $Y_{N_1}=Y_{N_1}^{\mathrm{eq}}$), a result in conflict with the general argument that no particle number asymmetries can be generated in thermal equilibrium. The reason for this paradox is that the on-shell contributions from the s-channel process $\ell+H\leftrightarrow\overline{\ell}+\overline{H}$ should be subtracted, because they have been included in the decay and inverse decay terms (Kolb and Turner, 1990; Strumia, 2006). Such on-shell contributions are estimated to be

$$\gamma^{\mathrm{os}}(\ell+H\to\overline{\ell}+\overline{H})=\gamma(\ell+H\to N_1)\ \mathrm{Br}(N_1\to\overline{\ell}+\overline{H})\ , \tag{11.80}$$

where $\mathrm{Br}(N_1 \to \bar{\ell} + \overline{H}) = (1-\varepsilon_1)/2$ is the branching ratio of $N_1 \to \bar{\ell} + \overline{H}$. After a consistent subtraction, the reaction rate densities read

$$\gamma'(\ell + H \to \bar{\ell} + \overline{H}) = \gamma_{N_s} - \frac{(1-\varepsilon_1)^2}{4}\gamma_{\rm D} \; ,$$
$$\gamma'(\bar{\ell} + \overline{H} \to \ell + H) = \gamma_{N_s} - \frac{(1+\varepsilon_1)^2}{4}\gamma_{\rm D} \; , \tag{11.81}$$

where γ_{N_s} denotes the reaction rate density of the N_s process. Taking account of the decays and lepton-number-violating scattering processes, we finally arrive at the correct Boltzmann equations (Giudice *et al.*, 2004; Buchmüller *et al.*, 2005a, 2005b; Davidson *et al.*, 2008) as follows:

$$sHz\frac{{\rm d}Y_{N_1}}{{\rm d}z} = -\left(\frac{Y_{N_1}}{Y^{\rm eq}_{N_1}} - 1\right)\left(\gamma_{\rm D} + 2\gamma_{S_s} + 4\gamma_{S_t}\right) \; ,$$
$$sHz\frac{{\rm d}Y_{\rm L}}{{\rm d}z} = \left(\frac{Y_{N_1}}{Y^{\rm eq}_{N_1}} - 1\right)\varepsilon_1\gamma_{\rm D} - \frac{Y_{\rm L}}{Y^{\rm eq}_{\ell}}\left(2\gamma_N + 2\gamma_{S_t} + \gamma_{S_s}\frac{Y_{N_1}}{Y^{\rm eq}_{N_1}}\right) \; , \tag{11.82}$$

where $\gamma_N \equiv \gamma_{N_s} + \gamma_{N_t}$, and a subtraction of the on-shell contributions from γ_{N_s} has been done as in Eq. (11.81). The final lepton number asymmetry $Y_{\rm L}$ can then be obtained by solving the above Boltzmann equations.

11.3.4 Baryon Number Asymmetry

So far another important lepton-number-violating reaction, the sphaleron process, has not been considered. In the epoch of leptogenesis the sphaleron interactions were in thermal equilibrium, so they were very efficient in converting the lepton number asymmetry into the baryon number asymmetry. Since the sphaleron interactions conserve $(B-L)$, we shall derive the relation between B and $(B-L)$.

The number density of the "x" particles has been given in Eq. (11.58), from which one may also write out the number density of their antiparticles by flipping the sign of the chemical potential μ_x (Kolb and Turner, 1990). In the very early Universe the conditions $\mu_x/T \ll 1$ and $m_x/T \ll 1$ are both satisfied for the SM particles, and hence the particle number asymmetry $\Delta n_x \equiv n_x - n_{\overline{x}}$ can approximate to $\Delta n_x = (\mu_x/T)g_x T^3/6$ for fermions or $\Delta n_x = (\mu_x/T)g_x T^3/3$ for bosons. Let us consider the SM with N_f generations of fermions and N_H Higgs doublets. It consists of the quark doublets Q_i, right-handed up-type quarks U_i and down-type quarks D_i, the lepton doublets ℓ_i and right-handed charged leptons E_i (for $i = 1, 2, \cdots, N_f$), and the Higgs doublets H_j (for $j = 1, 2, \cdots, N_H$). At a sufficiently high temperature the electroweak gauge symmetry is restored and the gauge interactions are in thermal equilibrium. In this case the chemical potentials of gauge bosons are vanishing, and those of the components in the same quark, lepton or Higgs doublet should be equal. So the baryon and lepton numbers are given by

$$n_{\rm B} = \frac{1}{6}T^2 \sum_{i=1}^{N_f} (2\mu_{Q_i} + \mu_{U_i} + \mu_{D_i}) \ ,$$
$$n_{\rm L} = \frac{1}{6}T^2 \sum_{i=1}^{N_f} (2\mu_{\ell_i} + \mu_{E_i}) \ , \tag{11.83}$$

where the summation over the color quantum number of quarks is implied. On the other hand, the reactions in chemical equilibrium allow the chemical potentials to relate to one another. First, all the Yukawa interactions at a temperature below TeV are fast enough to guarantee

$$\begin{aligned} \mu_{Q_i} + \mu_H - \mu_{U_i} &= 0 \ , \\ \mu_{Q_i} - \mu_H - \mu_{D_i} &= 0 \ , \\ \mu_{\ell_i} - \mu_H - \mu_{E_i} &= 0 \ , \end{aligned} \tag{11.84}$$

where we have assumed the Higgs doublets to have a common chemical potential (i.e., $\mu_{H_i} = \mu_H$). Furthermore, the mixing of quark flavors arising from the non-diagonal Yukawa couplings can make the chemical potentials of quarks flavor-independent (i.e., $\mu_{Q_i} = \mu_Q$, $\mu_{U_i} = \mu_U$ and $\mu_{D_i} = \mu_D$). Second, the hypercharge conservation requires

$$N_f(\mu_Q - 2\mu_U - \mu_D) - \sum_i (\mu_{\ell_i} + \mu_{E_i}) + 2N_H \mu_H = 0 \ . \tag{11.85}$$

Finally, the sphaleron processes turn all the left-handed fermions into the vacuum state. As a consequence,

$$3N_f \mu_Q + \sum_i \mu_{\ell_i} = 0 \ . \tag{11.86}$$

With the help of Eqs. (11.84), (11.85) and (11.86), all the chemical potentials can be expressed in terms of the N_f-independent ones. It is then easy to rewrite the lepton and baryon numbers as (Harvey and Turner, 1990)

$$n_{\rm B} = +\frac{1}{6}T^2 \frac{8N_f + 4N_H}{2N_f + 3N_H} \sum_i \mu_{E_i} \ ,$$
$$n_{\rm L} = -\frac{1}{6}T^2 \frac{14N_f + 9N_H}{2N_f + 3N_H} \sum_i \mu_{E_i} \ . \tag{11.87}$$

This result leads to the following relation between B and $(B - L)$:

$$n_{\rm B} = \frac{8N_f + 4N_H}{22N_f + 13N_H} (n_{\rm B} - n_{\rm L}) \equiv c\,(n_{\rm B} - n_{\rm L}) \ . \tag{11.88}$$

In the SM we obtain $c = 28/79$ from $N_f = 3$ and $N_H = 1$. Eq. (11.88) implies that the $(B - L)$ number was first generated in the leptogenesis era

and then reprocessed into the baryon number by the sphaleron interactions. The above relation depends on the assumption that the electroweak gauge symmetry is restored and the chemical potentials of gauge bosons are vanishing. If this assumption is relaxed during or below the electroweak phase transition and only the electric charge neutrality is imposed, then $c = 12/37$ can be obtained (Harvey and Turner, 1990). After the sphaleron processes go out of equilibrium, there are no more interactions that can change the baryon number asymmetry $Y_{\rm B} \equiv (n_{\rm B} - n_{\overline{\rm B}})/s$. Hence $Y_{\rm B}$ generated at the temperature $T^* \sim \mathcal{O}(10^2)$ GeV keeps unchanged until today. On the other hand, the baryon-to-photon ratio η is related to $Y_{\rm B}$ through

$$\eta \equiv \frac{n_{\rm B} - n_{\overline{\rm B}}}{n_\gamma} = \frac{s}{n_\gamma} Y_{\rm B} = \frac{\tilde{g}_* \pi^4}{45\zeta(3)} Y_{\rm B} \approx 1.8 \tilde{g}_* Y_{\rm B} \; , \tag{11.89}$$

where Eqs. (9.24) and (11.60) are used. The effective number of relativistic degrees of freedom $\tilde{g}_*$ can be computed by means of Eq. (11.61). The present-day value of $\tilde{g}_*$ gets contributions only from the photons with $T_{\rm b}^* = T_\gamma = T$ and the neutrinos with $T_{\rm f}^* = T_\nu = (4/11)^{1/3} T_\gamma$; namely, $\tilde{g}_*(T) = 2 + 7/8 \times 3 \times 2 \times 4/11 \approx 3.91$. So we have $\eta \approx 7.04 Y_{\rm B}$ (and $n_{\overline{\rm B}} = 0$) today. The value of η at $T^* \sim \mathcal{O}(10^2)$ GeV can be given in terms of today's value of η at T; i.e., $\eta(T^*)/\eta(T) = \tilde{g}_*(T^*)/\tilde{g}_*(T) \approx 27.3$, where $\tilde{g}_*(T^*) = g_*(T^*) = 106.75$ in the SM has been input.

To assure the N_1 decay to be out of thermal equilibrium, we require that its decay rate Γ_1 be smaller than the Hubble parameter H at the temperature $T = M_1$. With the help of Eqs. (9.31) and (11.36), one may express the requirement $\Gamma_1 < H(T = M_1)$ as

$$\frac{(M_{\rm D}^\dagger M_{\rm D})_{11}}{M_1} \equiv \tilde{m}_1 < m^* \equiv \sqrt{\frac{64 g_* \pi^5}{45}} \cdot \frac{v^2}{M_{\rm Pl}} \approx 1.08 \times 10^{-3} \text{ eV} \; . \tag{11.90}$$

where $\tilde{m}_1$ and m^* are referred to as the effective neutrino mass and the equilibrium neutrino mass (Buchmüller *et al.*, 2005a), respectively. Note that the value of $\tilde{m}_1$ determines not only the rates of the N_1 decay and its inverse decay but also the rates of the $\Delta L = 1$ scattering processes, as indicated in Eqs. (11.70) and (11.76).

Let us briefly reiterate the spirit of baryogenesis via leptogenesis in the type-I seesaw mechanism with $M_1 \ll M_2$ and $M_1 \ll M_3$. First, the lepton number asymmetry $Y_{\rm L}$ can be produced by the CP-violating and out-of-equilibrium decays of the lightest heavy Majorana neutrino N_1. The evolution of $Y_{\rm L}$ is governed by the Boltzmann equations in Eq. (11.82). Second, the efficient sphaleron interactions convert $Y_{\rm L}$ into the baryon number asymmetry $Y_{\rm B}$, and the efficiency of this conversion is essentially determined by $c = 28/79$ in Eq. (11.88). Third, the baryon-to-photon ratio η can be diluted by the decreasing number of relativistic degrees of freedom $\tilde{g}_*$ from $T^* \sim \mathcal{O}(10^2)$ GeV to today, as shown in Eq. (11.89). Finally, today's baryon number asymmetry is approximately given by (Buchmüller *et al.*, 2005a)

$$\eta \approx -0.96 \times 10^{-2} \varepsilon_1 \kappa_f \ , \tag{11.91}$$

where ε_1 denotes the CP-violating asymmetry in the N_1 decays and κ_f is an efficiency factor measuring the washout effects on $Y_{\rm L}$. In the weak washout regime $\tilde{m}_1 < m^*$, the final baryon number asymmetry sensitively depends on the initial number density of heavy Majorana neutrinos. In the strong washout regime $\tilde{m}_1 > m^*$, the final result of η is independent of the initial conditions and the efficiency factor κ_f can be expressed as (Buchmüller *et al.*, 2004; Giudice *et al.*, 2004)

$$\kappa_f \approx (2 \pm 1) \times 10^{-2} \left(\frac{0.01 \text{ eV}}{\tilde{m}_1} \right)^{1.1 \pm 0.1} \ . \tag{11.92}$$

This empirical result is a good approximation to the solution to the full set of Boltzmann equations. By assuming a successful leptogenesis mechanism and using current experimental data on neutrino oscillations, one may set a lower bound on the magnitude of M_1 (Davidson and Ibarra, 2002; Buchmüller *et al.*, 2004). However, such a bound will be modified if the contributions from heavier Majorana neutrinos and different lepton flavors are taken into account (Davidson *et al.*, 2008).

11.4 Recent Developments in Leptogenesis

The leptogenesis mechanism has been extensively studied since it was first proposed by Masataka Fukugita and Tsutomu Yanagida in 1986, and now its content has become very sophisticated. In Fukugita and Yanagida's original paper, the one-loop vertex corrections to heavy Majorana neutrino decays were calculated and the baryon number asymmetry was estimated (Fukugita and Yanagida, 1986). Later on, the Boltzmann equations for the evolution of the lepton number asymmetry were derived (Luty, 1992), and the importance of the self-energy corrections to heavy Majorana neutrinos was realized (Liu and Segre, 1994; Flanz *et al.*, 1995; Covi *et al.*, 1996). The latter contribution to CP violation may even dominate in some cases (Pilaftsis, 1997a, 1997b). In this section we shall introduce some recent developments in leptogenesis: (a) the leptogenesis mechanism in the type-II or type-III seesaw model, where heavy triplet scalars or fermions are introduced; (b) the resonant leptogenesis mechanism, in which CP violation can be resonantly enhanced if there are two nearly degenerate heavy Majorana neutrinos; (c) the soft leptogenesis mechanism, which works in a supersymmetric version of the type-I seesaw model; and (d) the flavor-dependent leptogenesis mechanism.

11.4.1 Triplet Leptogenesis

It is known that the unique dimension-5 Weinberg operator for neutrino masses can be derived at the tree-level from an extension of the SM by

adding heavy $SU(2)_{\rm L}$ singlet neutrinos, $SU(2)_{\rm L}$ triplet scalars or $SU(2)_{\rm L}$ triplet fermions and allowing lepton number violation. The first option is just the type-I seesaw mechanism and corresponds to the conventional Fukugita-Yanagida scenario of leptogeneis. Here we discuss the main features of leptogenesis induced by the triplet scalars. The leptogenesis mechanism associated with the triplet fermions may similarly work (Hambye, 2004; Strumia, 2006).

In the type-II seesaw mechanism the Lagrangian of neutrino mass terms associated with an $SU(2)_{\rm L}$ scalar triplet Δ has been given in Eq. (4.7), where the last two terms determine the lepton-number-violating decay modes of Δ and $\overline{\Delta}$ (i.e., $\Delta \to \ell + \ell$, $\Delta \to \overline{H} + \overline{H}$ and $\overline{\Delta} \to \overline{\ell} + \overline{\ell}$, $\overline{\Delta} \to H + H$). Note that there are no one-loop vertex corrections to the above decays, in contrast with the decays of heavy Majorana neutrinos. Hence at least two triplet scalars Δ_1 and Δ_2 are needed to generate CP violation via the self-energy corrections (Ma and Sarkar, 1998). The relevant Lagrangian can be written as

$$-\mathcal{L} = \frac{1}{2} \sum_{a=1}^{2} \overline{\ell_{\rm L}} Y_{\Delta_a} \Delta_a {\rm i}\sigma_2 \ell_{\rm L}^c - \sum_{a=1}^{2} \lambda_{\Delta_a} M_{\Delta_a} H^T {\rm i}\sigma_2 \Delta_a H + {\rm h.c.} \,, \qquad (11.93)$$

where Y_{Δ_a} are the Yukawa coupling matrices, λ_{Δ_a} denote the doublet-triplet Higgs coupling constants, and M_{Δ_a} are the tree-level masses of Δ_a (for $a = 1, 2$). At the one-loop level Δ_1 and Δ_2 mix with each other via the lepton and Higgs doublets, so their mass matrices are given by (Ma and Sarkar, 1998)

$$\mathcal{M}^2 = \begin{pmatrix} M_{\Delta_1}^2 - {\rm i}\Gamma_{11} M_{\Delta_1} & -{\rm i}\Gamma_{12} M_{\Delta_2} \\ -{\rm i}\Gamma_{21} M_{\Delta_1} & M_{\Delta_2}^2 - {\rm i}\Gamma_{22} M_{\Delta_2} \end{pmatrix} \,, \qquad (11.94)$$

where Γ_{11} and Γ_{22} stand respectively for the tree-level decay rates of Δ_1 and Δ_2, and Γ_{ab} (for $a, b = 1, 2$) can be obtained by calculating the imaginary parts of the $\Delta_b \to \Delta_a$ transition amplitudes:

$$\Gamma_{ab} = \frac{M_{\Delta_a}}{16\pi} \left[4\lambda_{\Delta_a} \lambda_{\Delta_b}^* + {\rm Tr}\left(Y_{\Delta_a}^\dagger Y_{\Delta_b} \right) \right] \,. \qquad (11.95)$$

It is straightforward to obtain the decay rates Γ_{11} and Γ_{22} by setting $a = b$ in Eq. (11.95). After diagonalizing the mass matrix in Eq. (11.94), one can find the corresponding mass eigenstates Φ_1 and Φ_2, which are the linear superpositions of Δ_1 and Δ_2. One may similarly consider the mass matrix for $\overline{\Delta}_1$ and $\overline{\Delta}_2$, and define the mass eigenstates $\overline{\Phi}_1$ and $\overline{\Phi}_2$. Although Φ_a and $\overline{\Phi}_a$ have the same masses, they are not CP eigenstates. The quantity Γ_{12} is in general complex. The asymmetries between the decays $\Phi_a \to \ell + \ell$ and their CP-conjugate processes $\overline{\Phi}_a \to \overline{\ell} + \overline{\ell}$ are given by (Ma and Sarkar, 1998)

$$\begin{aligned} \varepsilon_a &\equiv 2 \frac{\Gamma(\Phi_a \to \ell + \ell) - \Gamma(\overline{\Phi}_a \to \overline{\ell} + \overline{\ell})}{\Gamma(\Phi_a \to \ell + \ell) + \Gamma(\Phi_a \to \overline{H} + \overline{H})} \\ &= \frac{M_{\Delta_1} M_{\Delta_2} M_{\Delta_a}}{2\pi^2 (M_{\Delta_1}^2 - M_{\Delta_2}^2) \Gamma_{aa}} {\rm Im}\left[\lambda_{\Delta_1} \lambda_{\Delta_2}^* {\rm Tr}\left(Y_{\Delta_2}^\dagger Y_{\Delta_1} \right) \right] \,, \end{aligned} \qquad (11.96)$$

where $|M^2_{\Delta_1} - M^2_{\Delta_2}| \gg 2|\Gamma_{12}| M_{\Delta_2}$ has been assumed and the summation over the lepton-flavor index is implied. Note that the factor "2" in the definition of ε_a takes into account the fact that each $\Phi_a \to \ell + \ell$ decay mode violates the lepton number by two units. The CP-violating and out-of-equilibrium decays of Φ_a generate a net lepton number asymmetry, which can partly be converted into the baryon number asymmetry via the sphaleron processes. Although the basic ingredients of this leptogenesis mechanism follow the standard picture, the interactions of triplet scalars are quite different from those of heavy Majorana neutrinos. In particular, the triplet scalars charged under the $SU(2)_{\rm L}$ group may be involved with rapid gauge interactions. One can also use the Boltzmann equations to describe how the number densities of the triplet scalars and the lepton number asymmetry evolve (Ma and Sarkar, 1998).

In the type-(I+II) seesaw scenario both the scalar triplet Δ and heavy Majorana neutrinos N_i contribute to the light neutrino masses and the lepton number asymmetry. The Lagrangian relevant to the decays of Δ and N_1 reads

$$-\mathcal{L} = \overline{\ell_{\rm L}} Y_\nu \tilde{H} N_{\rm R} + \frac{1}{2} \overline{\ell_{\rm L}} Y_\Delta \Delta {\rm i}\sigma_2 \ell^c_{\rm L} - \lambda_\Delta M_\Delta H^T {\rm i}\sigma_2 \Delta H + {\rm h.c.}\,, \qquad (11.97)$$

from which one may immediately work out the total decay rates of heavy Majorana neutrinos $\Gamma_i = (Y^\dagger_\nu Y_\nu)_{ii} M_i/(8\pi)$ and that of the triplet scalar

$$\Gamma_\Delta = \frac{M_\Delta}{16\pi} \left[{\rm Tr}\left(Y^\dagger_\Delta Y_\Delta \right) + 4\lambda^2_\Delta \right]\,, \qquad (11.98)$$

where a specific phase convention has been chosen to assure λ_Δ to be real. As a consequence of the CPT invariance, the total decay rates of Δ and $\overline{\Delta}$ are equal (i.e., $\Gamma_\Delta = \Gamma_{\overline{\Delta}}$). It is worth pointing out that the presence of $\Delta \to \overline{H} + \overline{H}$ and $\overline{\Delta} \to H + H$ decays is necessary for generating a CP-violating asymmetry between $\Delta \to \ell + \ell$ and $\overline{\Delta} \to \overline{\ell} + \overline{\ell}$ decays. The type-(I+II) seesaw scenario yields the effective neutrino mass matrix $M_\nu \approx M_{\rm L} - M_{\rm D} M^{-1}_{\rm R} M^T_{\rm D}$, as shown in Chapter 4. One may rewrite this mass formula as $M_\nu \approx M_{\rm I} + M_{\rm II}$ with $M_{\rm I} \equiv -M_{\rm D} M^{-1}_{\rm R} M^T_{\rm D}$ and $M_{\rm II} \equiv M_{\rm L}$, so as to emphasize that it consists of a pure type-I seesaw term and a pure type-II seesaw term. Note that $M_{\rm D} = Y_\nu v/\sqrt{2}$ and $M_{\rm L} = Y_\Delta v_\Delta$ with $v_\Delta = \lambda_\Delta v^2/M_\Delta$ and $v \approx 246$ GeV.

For simplicity, let us consider the limit $M_1 \gg M_\Delta$ or $M_1 \ll M_\Delta$, where M_1 and M_Δ stand respectively for the mass of the lightest heavy Majorana neutrino N_1 and that of the triplet scalar Δ. In the $M_1 \gg M_\Delta$ case only the CP-violating asymmetry arising from the leptonic Δ and $\overline{\Delta}$ decays is relevant to the bargogenesis via leptogenesis, since a CP-violating asymmetry induced by the N_1 decays can be erased by the Δ-induced lepton-number-violating processes. Unlike the pure triplet leptogenesis scenario discussed above, here there exist the N_i-mediated one-loop vertex corrections to the leptonic $\Delta \to \ell + \ell$ decay (see Fig. 11.9). A straightforward calculation leads us to (Hambye and Senjanovic, 2004; Hambye *et al.*, 2006)

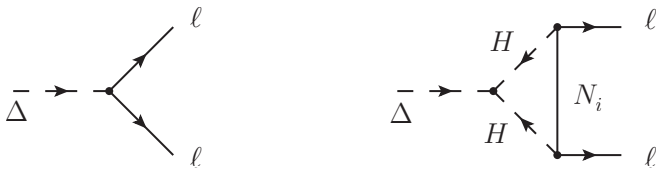

Fig. 11.9 The Feynman diagrams for the leptonic $\Delta \to \ell + \ell$ decay at the tree- and one-loop levels, where N_i $(i = 1, 2, 3)$ are heavy Majorana neutrinos

$$\begin{aligned}\varepsilon_{\Delta} &\equiv 2\frac{\Gamma(\Delta \to \ell + \ell) - \Gamma(\overline{\Delta} \to \overline{\ell} + \overline{\ell})}{\Gamma_{\Delta} + \Gamma_{\overline{\Delta}}} \\ &= \frac{1}{2\pi} \sum_j \frac{\lambda_{\Delta} M_j}{M_{\Delta}} \frac{\mathrm{Im}\left[\left(Y_{\nu}^{\dagger} Y_{\Delta} Y_{\nu}^{*}\right)_{jj}\right]}{\mathrm{Tr}\left[Y_{\Delta}^{\dagger} Y_{\Delta}\right] + 4\lambda_{\Delta}^2} \ln\left(1 + \frac{M_{\Delta}^2}{M_j^2}\right) . \end{aligned} \tag{11.99}$$

Given $M_i \gg M_{\Delta}$, Eq. (11.99) can approximate to (Hambye *et al.*, 2006)

$$\varepsilon_{\Delta} \approx \frac{M_{\Delta}}{2\pi v^2} \sqrt{B_{\ell} B_H} \frac{\mathrm{Im}\left[\mathrm{Tr}\left(M_{\mathrm{II}}^{\dagger} M_{\mathrm{I}}\right)\right]}{\sqrt{\mathrm{Tr}\left(M_{\mathrm{II}}^{\dagger} M_{\mathrm{II}}\right)}} , \tag{11.100}$$

where $M_{\mathrm{I}} \equiv -M_{\mathrm{D}} M_{\mathrm{R}}^{-1} M_{\mathrm{D}}^{T}$, $M_{\mathrm{II}} \equiv M_{\mathrm{L}}$, B_{ℓ} and B_H stand respectively for the branching ratios of $\Delta \to \ell + \ell$ and $\Delta \to \overline{H} + \overline{H}$ decays. It is now evident that the CP-violating asymmetry ε_{Δ} will vanish if $B_H = 0$ holds.

In the $M_1 \ll M_{\Delta}$ case, we focus on CP violation in the N_1 decays instead of the Δ decays. The Feynman diagrams for the one-loop corrections to the decay $N_1 \to \ell + H$ are shown in Fig. 11.10. Note that the contributions from Fig. 11.10(a) and Fig. 11.10(b) have been evaluated in Eq. (11.57), and the corresponding CP-violating asymmetry can be recast into the following form:

$$\varepsilon_1^{\mathrm{N}} = \frac{3M_1}{8\pi v^2} \cdot \frac{\mathrm{Im}\left[\left(Y_{\nu}^{\dagger} M_{\mathrm{I}} Y_{\nu}^{*}\right)_{11}\right]}{\left(Y_{\nu}^{\dagger} Y_{\nu}\right)_{11}} , \tag{11.101}$$

where $\mathcal{F}(x) \to -3/(2x)$ has been taken for $x \to +\infty$ (i.e., $M_1 \ll M_2, M_3$). In comparison, the CP-violating asymmetry induced by Δ via Fig. 11.10(c) is found to be (Hambye and Senjanovic, 2004; Antusch and King, 2004)

$$\varepsilon_1^{\Delta} = \frac{3M_1}{8\pi v^2} \cdot \frac{\mathrm{Im}\left[\left(Y_{\nu}^{\dagger} M_{\mathrm{II}} Y_{\nu}^{*}\right)_{11}\right]}{\left(Y_{\nu}^{\dagger} Y_{\nu}\right)_{11}} . \tag{11.102}$$

The total CP-violating asymmetry is $\varepsilon_1 = \varepsilon_1^{\mathrm{N}} + \varepsilon_1^{\Delta}$. Note that $\varepsilon_1^{\mathrm{N}}$ and ε_1^{Δ} are proportional to M_{I} and M_{II}, respectively. Note also that the minimal type-(I+II) seesaw model with only one heavy Majorana neutrino and one triplet

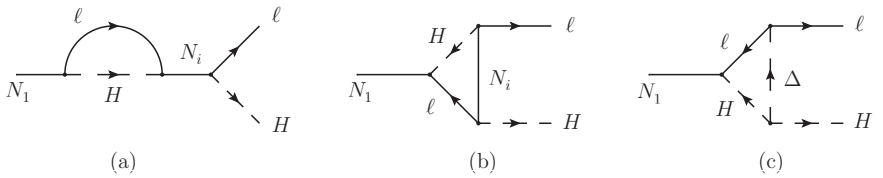

Fig. 11.10 The Feynman diagrams for $N_1 \to \ell + H$ at the one-loop level: (a) the self-energy correction; (b) the vertex correction mediated by heavy Majorana neutrinos N_i; (c) the vertex correction mediated by the triplet scalar Δ

scalar can account for both the mass spectrum of three light neutrinos and the observed baryon number asymmetry (Gu *et al.*, 2006). Since Δ and $\overline{\Delta}$ are involved with rapid gauge interactions, their number densities may follow the thermal equilibrium distribution such that the lepton number asymmetry is essentially independent of the initial conditions (Hambye *et al.*, 2006).

11.4.2 Resonant Leptogenesis

So far we have assumed that three heavy Majorana neutrinos have a strong mass hierarchy (i.e., $M_1 \ll M_2, M_3$). It has been pointed out that the CP-violating asymmetry arising from the one-loop self-energy corrections can be resonantly enhanced provided the masses of two or three heavy Majorana neutrinos are nearly degenerate (Pilaftsis, 1997a, 1997b; Pilaftsis and Underwood, 2004). If the difference between M_i and M_j is comparable with the decay widths of N_i and N_j (i.e., $|M_i - M_j| \sim \Gamma_i, \Gamma_j$), then the conventional perturbation field theory should not work here. For instance, the CP-violating asymmetry $\varepsilon_i^{\rm s}$ obtained in Eq. (11.46) is apparently divergent at $M_i = M_j$. A proper way to deal with this problem is as follows (Flanz *et al.*, 1995; Buchmüller and Plümacher, 1998; Plümacher, 1998): (a) we first calculate the amplitude of $\ell + H \leftrightarrow \overline{\ell} + \overline{H}$ scattering mediated by N_i in the s-channel; (b) the resummed propagators of N_i can be written in the matrix form as $S_{ij}(\not{p})$, whose non-diagonal elements come from the transition amplitudes of $N_j \to N_i$; (c) expanding $S_{ij}(\not{p})$ around the complex poles $\sqrt{s}_i = M_i^{\rm pole} - {\rm i}\Gamma_i^{\rm pole}/2$ with $M_i^{\rm pole}$ and $\Gamma_i^{\rm pole}$ being the physical masses and decay widths, one can define the effective couplings of the interaction vertices of $N_i \to \ell + H$ and $N_i \to \overline{\ell} + \overline{H}$. Then the CP-violating asymmetry can be directly figured out by using these effective couplings (Pilaftsis, 1997b; Pilaftsis and Underwood, 2004):

$$\varepsilon_i = \frac{{\rm Im}\left[(Y_\nu^\dagger Y_\nu)_{ij}^2\right]}{(Y_\nu^\dagger Y_\nu)_{ii}(Y_\nu^\dagger Y_\nu)_{jj}} \cdot \frac{(M_i^2 - M_j^2) M_i \Gamma_j}{(M_i^2 - M_j^2)^2 + M_i^2 \Gamma_j^2} \; , \tag{11.103}$$

where $i \neq j$. Note that this result is only applicable to the case of two nearly degenerate heavy Majorana neutrinos. It is worth remarking that two heavy

Majorana neutrinos are sufficient for generating the light neutrino masses and explaining the baryon number asymmetry in the minimal type-I seesaw model (Frampton *et al.*, 2002; Guo and Xing, 2004; Guo *et al.*, 2007). The decay width Γ_j appearing in Eq. (11.103) serves as a regulator, which makes the CP-violating asymmetry ε_i well-behaved in the $M_i = M_j$ limit. It is obvious that $\varepsilon_i \sim \mathcal{O}(1)$ can be obtained when the conditions

$$\frac{\mathrm{Im}\left[(Y_\nu^\dagger Y_\nu)_{ij}^2\right]}{(Y_\nu^\dagger Y_\nu)_{ii}(Y_\nu^\dagger Y_\nu)_{jj}} \sim \mathcal{O}(1) \; , \quad \left|M_i - M_j\right| = \frac{1}{2}\Gamma_j \tag{11.104}$$

are satisfied. This resonant leptogenesis mechanism provides us with an interesting possibility to lower the masses of N_i down to the TeV scale or even the electroweak scale (Pilaftsis, 2005; Pilaftsis and Underwood, 2005).

In a viable resonant leptogenesis scenario, the required mass degeneracy $|M_i - M_j|/M_j$ is usually of $\mathcal{O}(10^{-7})$ (Xing and Zhou, 2007). Such a high degree of degeneracy may arise from the flavor symmetry breaking or radiative corrections, if $M_i = M_j$ holds in the symmetry limit or at a superhigh energy scale (Pilaftsis and Underwood, 2004, 2005; Turzynski, 2004; Gonzalez Felipe *et al.*, 2004; Joaquim, 2005; Branco *et al.*, 2006).

11.4.3 Soft Leptogenesis

The idea of leptogenesis can be directly applied to the supersymmetric seesaw models (Giudice *et al.*, 2004). In this case one has to take into account the CP-violating asymmetries arising from the decays of supersymmetric partners of heavy Majorana neutrinos, denoted as $\tilde{N}_i$, and from some new decay modes with supersymmetric particles in the final states and running in the loops. The overall CP-violating asymmetry from the N_i (or $\tilde{N}_i$) decays is approximately twice as large as that in a conventional seesaw model. However, the effective number of relativistic degrees of freedom is now doubled (i.e., $g_* = 228.75$ as compared with $g_* = 106.75$ in the SM-like case), leading to a dilution factor of two for the N_i-induced (or $\tilde{N}_i$-induced) lepton number asymmetry. In the strong washout regime the inverse decays double the washout rates and hence the total lepton number asymmetry is suppressed by another factor of two. All in all, the final baryon number asymmetry is more or less the same in a supersymmetric seesaw model as that in a conventional seesaw scenario (Davidson *et al.*, 2008).

It has been shown that new sources of CP violation may exist in a supersymmetric seesaw model: indirect CP violation is possible to arise from the mixing between $\tilde{N}_i$ and $\tilde{N}_i^*$ and in the interference of decays with and without mixing (Grossman *et al.*, 2003; D'Ambrosio *et al.*, 2003). For illustration, we consider a one-generation toy model whose superpotential reads

$$\mathcal{W} = Y\mathbb{L}\mathbb{N}\mathbb{H}_{\rm u} + \frac{1}{2}M\mathbb{N}\mathbb{N} \; , \tag{11.105}$$

where $\mathbb{N}$, $\mathbb{L}$ and $\mathbb{H}_{\rm u}$ stand for the singlet neutrino, lepton doublet and up-type Higgs doublet chiral superfields, respectively. Note that Y is the Yukawa coupling constant, and M is the Majorana mass of the neutrino singlet. The supersymmetry-breaking terms involving the singlet sneutrino are

$$-\mathcal{L}_{\rm soft} = \tilde{m}^2 \tilde{N}^* \tilde{N} + \left(AY \tilde{\ell} H \tilde{N} + \frac{1}{2} BM \tilde{N} \tilde{N} + \text{h.c.} \right) , \qquad (11.106)$$

where $\tilde{m}^2$ is the soft mass of the sneutrino, A and B denote the trilinear and bilinear scalar couplings. So the heavy Majorana neutrino has a mass M, and the sneutrino $\tilde{N}$ mixes with the anti-sneutrino $\tilde{N}^*$ via the mass matrix which can directly be read off from Eqs. (11.105) and (11.106). In the basis $\Phi \equiv (\tilde{N}^*, \tilde{N})^T$, we write out the mass term as follows:

$$-\mathcal{L}_{\rm m} = \frac{1}{2} \Phi^\dagger \mathcal{M}^2 \Phi = \frac{1}{2} \begin{pmatrix} \tilde{N} & \tilde{N}^* \end{pmatrix} \begin{pmatrix} M^2 + \tilde{m}^2 & BM \\ B^* M & M^2 + \tilde{m}^2 \end{pmatrix} \begin{pmatrix} \tilde{N}^* \\ \tilde{N} \end{pmatrix} . \qquad (11.107)$$

In analogy with the K^0-$\overline{K}^0$ mixing system, the evolution of the $\tilde{N}$-$\tilde{N}^*$ mixing system is governed by the effective Hamiltonian $H = \widehat{M} - {\rm i}\widehat{\Gamma}/2$, where Hermitian $\widehat{M}$ and $\widehat{\Gamma}$ can be expressed as (D'Ambrosio *et al.*, 2003)

$$\widehat{M} = M \begin{pmatrix} 1 & B/(2M) \\ B/(2M) & 1 \end{pmatrix} , \qquad \widehat{\Gamma} = \Gamma \begin{pmatrix} 1 & A^*/M \\ A/M & 1 \end{pmatrix} \qquad (11.108)$$

to the lowest order of the soft terms. Note that the total decay rate of $\tilde{N}$ is given by $\Gamma = Y^2 M/(4\pi)$. Note also that we have chosen a specific phase convention in which only A is complex. The eigenstates of H are defined as

$$\tilde{N}_{\rm L} = p\tilde{N} + q\tilde{N}^* , \qquad \tilde{N}_{\rm H} = p\tilde{N} - q\tilde{N}^* , \qquad (11.109)$$

where the subscript "L" (or "H") means "light" (or "heavy"), p and q are the mixing parameters which are commonly used in the phenomenology of neutral meson-antimeson mixing and CP violation (Xing, 1997). The proper-time evolution of the initial sneutrino states $|\tilde{N}\rangle$ and $|\tilde{N}^*\rangle$ reads

$$\begin{aligned} |\tilde{N}(t)\rangle &= g_+(t) |\tilde{N}\rangle + \frac{q}{p} g_-(t) |\tilde{N}^*\rangle , \\ |\tilde{N}^*(t)\rangle &= g_+(t) |\tilde{N}^*\rangle + \frac{p}{q} g_-(t) |\tilde{N}\rangle , \end{aligned} \qquad (11.110)$$

where

$$\begin{aligned} g_+(t) &= \exp\left[-\left({\rm i}M + \frac{\Gamma}{2} \right) \right] \cosh\left[\left({\rm i}\Delta M - \frac{\Delta\Gamma}{2} \right) \frac{t}{2} \right] , \\ g_-(t) &= \exp\left[-\left({\rm i}M + \frac{\Gamma}{2} \right) \right] \sinh\left[\left({\rm i}\Delta M - \frac{\Delta\Gamma}{2} \right) \frac{t}{2} \right] , \end{aligned} \qquad (11.111)$$

with $M = (M_{\rm L} + M_{\rm H})/2$, $\Delta M \equiv M_{\rm H} - M_{\rm L}$, $\Gamma \equiv (\Gamma_{\rm L} + \Gamma_{\rm H})/2$ and $\Delta\Gamma \equiv \Gamma_{\rm L} - \Gamma_{\rm H}$. Here $M_{\rm L,H}$ and $\Gamma_{\rm L,H}$ are the mass and width of $\tilde{N}_{\rm L,H}$, respectively. The time-integrated CP-violating asymmetry, defined in the standard way (Xing, 1997), turns out to be (D'Ambrosio *et al.*, 2003)

$$\begin{aligned}\varepsilon &= \frac{1}{2}\left(\left|\frac{q}{p}\right|^2 - \left|\frac{p}{q}\right|^2\right)\left(\frac{c_{\rm B} - c_{\rm F}}{c_{\rm B} + c_{\rm F}}\right)\frac{\int_0^\infty {\rm d}t|g_-(t)|^2}{\int_0^\infty {\rm d}t(|g_-(t)|^2 + |g_+(t)|^2)} \\ &\approx \frac{{\rm Im}A}{M}\left(\frac{c_{\rm B} - c_{\rm F}}{c_{\rm B} + c_{\rm F}}\right)\frac{\Gamma B}{\Gamma^2 + B^2}\,, \end{aligned} \tag{11.112}$$

where $c_{\rm B}$ and $c_{\rm F}$ parametrize the phase-space contributions of the bosonic and fermionic final states. Note that $|q/p| \neq 1$ implies the mixing-induced CP violation. This soft leptogenesis mechanism may even offer the dominant source of CP violation to produce the observed baryon number asymmetry of the Universe (Grossman *et al.*, 2003; D'Ambrosio *et al.*, 2003).

11.4.4 Flavor Effects

So far we have assumed that the Yukawa interactions of charged leptons are negligible in leptogenesis, and thus there are no interactions which can distinguish one lepton flavor from another. In this case it is convenient to define the lepton and antilepton states from the decays of heavy Majorana neutrinos $N_i \to \ell_\alpha + H$ and $N_i \to \overline{\ell}_\alpha + \overline{H}$:

$$\begin{aligned}|\ell_i\rangle &\equiv \frac{1}{\sqrt{(Y_\nu^\dagger Y_\nu)_{ii}}}\sum_\alpha (Y_\nu)_{\alpha i}|\ell_\alpha\rangle\,, \\ |\overline{\ell}_i'\rangle &\equiv \frac{1}{\sqrt{(Y_\nu^\dagger Y_\nu)_{ii}}}\sum_\alpha (Y_\nu^*)_{\alpha i}|\overline{\ell}_\alpha\rangle\,, \end{aligned} \tag{11.113}$$

which are also the states involved in the subsequent inverse decays and scattering processes. However, the Yukawa interactions of charged leptons are possible to be faster than the (inverse) decays of N_i and destroy the coherent absorption or scattering of the states $|\ell_i\rangle$ and $|\overline{\ell}_i'\rangle$. Note that $|\ell_i\rangle$ and $\overline{\ell}_i'\rangle$ are not CP-conjugate states, although $|\overline{\ell}_\alpha\rangle$ itself is the CP conjugate of $|\ell_\alpha\rangle$. Let us estimate the interactions involving the tau leptons, such as $\ell_{\tau{\rm L}} + Q_{3{\rm L}} \to t_{\rm R} + \tau_{\rm R}$ with $Q_{3{\rm L}} = (t_{\rm L}, b_{\rm L})^T$ and $\ell_{\tau{\rm L}} = (\nu_{\tau{\rm L}}, \tau_{\rm L})^T$ being the third-family quark and lepton doublets. Neglecting all the relevant masses, one may immediately obtain the cross section (Davidson *et al.*, 2008)

$$\sigma(\ell_{\tau{\rm L}} + Q_{3{\rm L}} \to t_{\rm R} + \tau_{\rm R}) = \frac{y_t^2 y_\tau^2}{16\pi s'}\,, \tag{11.114}$$

where $y_t = \sqrt{2}\, m_t/v$ and $y_\tau = \sqrt{2}\, m_\tau/v$. With the help of Eq. (11.114), one can further compute the corresponding interaction rate density γ_τ introduced

in Eq. (11.74). After the summation over all the processes involving the tau leptons, the interaction rate is given by

$$\Gamma_\tau \equiv \frac{\gamma_\tau}{n_\ell^{\rm eq}} \approx 10^{-3} y_\tau^2 T \; . \tag{11.115}$$

Comparing Γ_τ with the Hubble parameter $H \approx 1.66\sqrt{g_*}T^2/M_{\rm pl}$, one finds that $\Gamma_\tau > H$ holds when $T < 10^{12}$ GeV. In a similar way one may find that the Yukawa interactions of the muon leptons can be in thermal equilibrium around $T \sim 10^9$ GeV. When the temperature drops below $T \sim 10^5$ GeV, all the charged-lepton Yukawa interactions are faster than the expansion rate of the Universe (Barbieri *et al.*, 2000; Endoh *et al.*, 2004; Vives, 2006).

In the temperature range 10^{12} GeV $> T > 10^9$ GeV, the tau flavor is distinguishable but the electron and muon flavors are indistinguishable. As a consequence, the tau-flavor component of the lepton state $|\ell_i\rangle$ from the N_i decays should be singled out and then the inverse decays may take place as $\ell_\tau + H \to N_i$ and $\ell_o + H \to N_i$, where $|\ell_o\rangle$ denotes the non-tau flavor component orthogonal to $|\ell_\tau\rangle$. Both the CP-violating asymmetry and washout effects associated with the tau flavor should be treated separately, so it is necessary to have two Boltzmann equations for the lepton number asymmetries $Y_{\rm L}^{(\tau)}$ and $Y_{\rm L}^{(o)}$. To see the flavor effects in a clear way, we consider the N_1-dominated leptogensis in the full flavor regime with $T \lesssim 10^9$ GeV and all the lepton flavors being distinguishable. First, the flavor-dependent CP-violating asymmetries $\varepsilon_{1\alpha}$ (for $\alpha = e, \mu, \tau$) should be calculated. A particular case is that the successful leptogenesis might be achieved from $\varepsilon_{1\alpha} \neq 0$ even though the total CP-violating asymmetry ε_1 is vanishing or vanishingly small (i.e., $\varepsilon_1 = \varepsilon_{1e} + \varepsilon_{1\mu} + \varepsilon_{1\tau} \approx 0$) (Nardi *et al.*, 2006; Abada *et al.*, 2006). Second, the efficiency factors $\kappa_{1\alpha}$ can be computed via the effective neutrino masses

$$\tilde{m}_{1\alpha} \equiv \frac{|(Y_\nu)_{\alpha 1}|^2}{(Y_\nu^\dagger Y_\nu)_{11}} \tilde{m}_1 \; . \tag{11.116}$$

The values of $\tilde{m}_{1\alpha}$ characterize the washout effects of different flavors. Finally, the sphaleron processes conserve the quantum number $\Delta_\alpha = B/3 - L_\alpha$, as indicated below Eq. (11.13). In the temperature range under consideration, the processes in thermal and chemical equilibrium include all the gauge interactions, strong and electroweak sphaleron interactions, (t, b, c)-quark and (τ, μ)-lepton Yukawa interactions. After imposing the hypercharge conservation and the equilibrium conditions of chemical potentials, one can obtain (Abada *et al.*, 2006; Nardi *et al.*, 2006; Davidson *et al.*, 2008)

$$\begin{pmatrix} Y_{\rm L_e} \\ Y_{\rm L_\mu} \\ Y_{\rm L_\tau} \end{pmatrix} = \begin{pmatrix} -151/179 & 20/179 & 20/179 \\ 25/358 & -344/537 & 14/537 \\ 25/358 & 14/537 & -344/537 \end{pmatrix} \begin{pmatrix} Y_{\Delta_e} \\ Y_{\Delta_\mu} \\ Y_{\Delta_\tau} \end{pmatrix} \; . \tag{11.117}$$

This result, together with $Y_{\rm B} = 28/79 \times (Y_{\Delta_e} + Y_{\Delta_\mu} + Y_{\Delta_\tau})$, measures the efficiency in converting the lepton number asymmetries into the baryon number

asymmetry. Since $\varepsilon_{1\alpha}$ and $\tilde{m}_{1\alpha}$ are sensitive to the flavor structure of Y_ν, the prediction for the final value of $Y_{\rm B}$ is strongly model-dependent. This actually signifies the importance of flavor effects in a specific leptogenesis scenario.

It is worth mentioning that the thermal corrections, spectator processes and quantum effects in leptogenesis have also been considered (Buchmüller and Fredenhagen, 2000; Buchmüller and Plümacher, 2001; Giudice *et al.*, 2004). In addition, CP violation in the decays of heavy Majorana neutrinos has recently been calculated in the non-equilibrium quantum field theories (Garny *et al.*, 2009, 2010a, 2010b; Beneke *et al.*, 2010; Kießig *et al.*, 2010). A full quantum-mechanical calculation of the lepton number asymmetry based on the Kadanoff-Baym equations has also been done (Anisimov *et al.*, 2010). It has been found that these improvements are likely to modify the previous results by one order of magnitude in some cases (Anisimov *et al.*, 2010; Garny *et al.*, 2010a).

References

Abada, A., *et al.*, 2006, JCAP **0604**, 004.
Adler, S. L., 1969, Phys. Rev. **177**, 2426.
Affleck, I., and Dine, M., 1985, Nucl. Phys. B **249**, 361.
Anisimov, A., *et al.*, 2010, Phys. Rev. Lett. **104**, 121102.
Antusch, S., and King, S. F., 2004, Phys. Lett. B **582**, 73.
Barbieri, R., *et al.*, 2000, Nucl. Phys. B **575**, 61.
Belavin, A. A., *et al.*, 1975, Phys. Lett. B **59**, 85.
Bell, J. S., and Jackiw, R., 1969, Nuovo Cim. A **60**, 47.
Beneke, M., *et al.*, 2010, Nucl. Phys. B **838**, 1.
Bernard, C. W., 1974, Phys. Rev. D **9**, 3312.
Bernreuther, W., 2002, Lect. Notes Phys. **591**, 237.
Branco, G. C., *et al.*, 2006, Phys. Lett. B **633**, 336.
Brihaye, Y., and Kunz, J., 1992, Phys. Rev. D **46**, 3587.
Buchmüller, W., and Fredenhagen, S., 2000, Phys. Lett. B **483**, 217.
Buchmüller, W., and Plümacher, M., 1998, Phys. Lett. B **431**, 354.
Buchmüller, W., and Plümacher, M., 2001, Phys. Lett. B **511**, 74.
Buchmüller, W., Di Bari, P., and Plümacher, M., 2004, New J. Phys. **6**, 105.
Buchmüller, W., Di Bari, P., and Plümacher, M., 2005a, Ann. Phys. **315**, 305.
Buchmüller, W., Peccei, R. D., and Yanagida, T., 2005b, Annu. Rev. Nucl. Part. Sci. **55**, 311.
Callan, C. G., Dashen, R. F., and Gross, D. J., 1976, Phys. Lett. B **63**, 334.
Carlson, L., *et al.*, 1990, Phys. Rev. D **42**, 2127.
Cohen, A. G., De Rújula, A., and Glashow, S. L., 1998, Astrophys. J. **495**, 539.
Cohen, A. G., Kaplan, D. B., and Nelson, A. E., 1993, Annu. Rev. Nucl. Part. Sci. **43**, 27.
Covi, L., Roulet, E., and Vissani, F., 1996, Phys. Lett. B **384**, 169.
D'Ambrosio, G., Giudice, G. F., and Raidal, M., 2003, Phys. Lett. B **575**, 75.
Davidson, S., and Ibarra, A., 2002, Phys. Lett. B **535**, 25.
Davidson, S., Nardi, E., and Nir, Y., 2008, Phys. Rept. **466**, 105.
Denner, A., 1993, Fortsch. Phys. **41**, 307.

Denner, A., *et al.*, 1992, Nucl. Phys. B **387**, 467.
Dine, M., and Kusenko, A., 2004, Rev. Mod. Phys. **76**, 1.
Dine, M., Huet, P., and Singleton, R., 1992, Nucl. Phys. B **375**, 625.
Dirac, P. A. M., 1933, in *Nobel Lecture*, Physics 1922-1941 (Elsevier Publishing Company, Amsterdam, 1965).
Dodelson, S., 2005, *Modern Cosmology* (Academic Press).
Dolan, L., and Jackiw, R., 1974, Phys. Rev. D **9**, 3320.
Dolgov, A. D., 1992, Phys. Rept. **222**, 309.
Dolgov, A., 2001, Nucl. Phys. B (Proc. Suppl.) **95**, 42.
Dreiner, H. K., Haber, H. E., and Martin, S. P., 2010, Phys. Rept. **494**, 1.
Ellis, J., Linde, A. D., and Nanopoulos, D. V., 1982, Phys. Lett. B **118**, 519.
Endoh, T., Morozumi, T., and Xiong, Z. H., 2004, Prog. Theor. Phys. **111**, 123.
Flanz, M., Paschos, E. A., and Sarkar, U., 1995, Phys. Lett. B **345**, 248.
Frampton, P. H., Glashow, S. L., and Yanagida, T., 2002, Phys. Lett. B **548**, 119.
Fritzsch, H., and Minkowski, P., 1975, Annals Phys. **93**, 193.
Fujikawa, K., 1979, Phys. Rev. Lett. **42**, 1195.
Fujikawa, K., 1980, Phys. Rev. D **21**, 2848.
Fukugita, M., and Yanagida, T., 1986, Phys. Lett. B **174**, 45.
Garny, M., Hoheneggera, A., and Kartavtsev, A., 2010a, Phys. Rev. D **81**, 085028.
Garny, M., *et al.*, 2009, Phys. Rev. D **80**, 125027.
Garny, M., *et al.*, 2010b, Phys. Rev. D **81**, 085027.
Georgi, H., 1975, AIP Conf. Proc. **23**, 575.
Georgi, H., and Glashow, S. L., 1974, Phys. Rev. Lett. **32**, 438.
Giudice, G. F., *et al.*, 2004, Nucl. Phys. B **685**, 89.
Gonzalez Felipe, R., Joaquim, F. R., and Nobre, B. M., 2004, Phys. Rev. D **70**, 085009.
Grossmann, Y., *et al.*, 2003, Phys. Rev. Lett. **91**, 251801.
Grupen, C., *et al.*, 2005, *Astroparticle Physics* (Springer-Verlag).
Gu, P. H., Zhang, H., and Zhou, S., 2006, Phys. Rev. D **74**, 076002.
Guo, W. L., and Xing, Z. Z., 2004, Phys. Lett. B **583**, 163.
Guo, W. L., Xing, Z. Z., and Zhou, S., 2007, Int. J. Mod. Phys. E **16**, 1.
Hamaguchi, K., 2002, arXiv:hep-ph/0212305.
Hambye, T., 2004, arXiv:hep-ph/0412053.
Hambye, T., and Senjanovic, G., 2004, Phys. Lett. B **582**, 73.
Hambye, T., *et al.*, 2004, Nucl. Phys. B **695**, 169.
Hambye, T., Raidal, M., and Strumia, A., 2006, Phys. Lett. B **632**, 667.
Harvey, J. A., and Turner, M. S., 1990, Phys. Rev. D **42**, 3344.
Jackiw, R., and Rebbi, C., 1976, Phys. Rev. Lett. **37**, 172.
Joaquim, F. R., 2005, Nucl. Phys. B (Proc. Suppl.) **145**, 276.
Kappadath, S. C., *et al.*, 1995, Proc. 24th Int. Cosmic Ray Conf. **2**, 230.
Kießig, C. P., Plümacher, M., and Thoma, M. H., 2010, Phys. Rev. D **82**, 036007.
Kirzhnits, D. A., and Linde, A. D., 1974, Zh. Eksp. Teor. Fiz. **67**, 1263.
Klinkhamer, R. F., and Manton, N. S., 1984, Phys. Rev. D **30**, 2212.
Kobayashi, M., and Maskawa, T., 1973, Prog. Theor. Phys. **49**, 652.
Kolb, E. W., and Turner, M. S., 1990, *The Early Universe* (Addison-Wesley Publishing Company).

Komatsu, E., *et al.*, 2009, Astrophys. J. Suppl. **180**, 330.
Komatsu, E., *et al.*, 2010, arXiv:1001.4538.
Kumekawa, K., Moroi, T., and Yanagida, T., 1994, Prog. Theor. Phys. **92**, 437.
Kuzmin, V. A., Rubakov, V. A., and Shaposhnikov, M. E., 1985, Phys. Lett. B **155**, 36.
Lazarides, G., 2002, Lect. Notes Phys. **592**, 351.
Lazarides, G., and Shafi, Q., 1991, Phys. Lett. B **258**, 305.
Liu, J., and Segre, G., 1993, Phys. Rev. D **48**, 4609.
Luty, M. A., 1992, Phys. Rev. D **45**, 455.
Ma, E., and Sarkar, U., 1998, Phys. Rev. Lett. **80**, 5716.
Manton, N. S., 1983, Phys. Rev. D **28**, 2019.
Nakamura, K., *et al.* (Particle Data Group), 2010, J. Phys. G **37**, 075021.
Nardi, E., *et al.*, 2006, JHEP **0601**, 164.
O'Donnell, P. J., and Sarkar, U., 1994, Phys. Rev. D **49**, 2118.
Passarino, G., and Veltman, M. J. G., 1979, Nucl. Phys. B **160**, 151.
Pilaftsis, A., 1997a, Nucl. Phys. B **504**, 61.
Pilaftsis, A., 1997b, Phys. Rev. D **56**, 5431.
Pilaftsis, A., 2005, Phys. Rev. Lett. **95**, 081602.
Pilaftsis, A., and Underwood, T. E. J., 2004, Nucl. Phys. B **692**, 303.
Pilaftsis, A., and Underwood, T. E. J., 2005, Phys. Rev. D **72**, 113001.
Plümacher, M., 1997, Z. Phys. C **74**, 549.
Plümacher, M., 1998, arXiv:hep-ph/9807557.
Riotto, A., 1998, arXiv:hep-ph/9807454.
Riotto, A., and Trodden, M., 1999, Annu. Rev. Nucl. Part. Sci. **49**, 35.
Rubakov, V. A., and Shaposhnikov, M. E., 1996, Phys. Usp. **39**, 461.
Sakharov, A. D., 1967, JETP Lett. **5**, 24.
Slansky, R., 1981, Phys. Rept. **79**, 1.
Steigman, G., 1976, Annu. Rev. Astron. Astrophys. **14**, 339.
Strumia, A., 2006, arXiv:hep-ph/0608347.
't Hooft, G., 1973, Nucl. Phys. B **61**, 455.
't Hooft, G., 1976, Phys. Rev. Lett. **37**, 8.
't Hooft, G., and Veltman, M. J. G., 1979, Nucl. Phys. B **153**, 365.
Turzynski, K., 2004, Phys. Lett. B **589**, 135.
Vives, O., 2006, Phys. Rev. D **73**, 073006.
Weinberg, S., 1972, *Gravitation and Cosmology: Principles and Applications of the General Theory of Relativity* (John Wiley & Son).
Weinberg, S., 1974, Phys. Rev. D **9**, 3357.
Weinberg, S., 1982, Phys. Rev. Lett. **48**, 1303.
Weinberg, S., 1996, *The Quantum Theory of Fields: Modern Applications* (Cambridge University Press).
Weinberg, S., 2008, *Cosmology* (Oxford University Press).
Xing, Z. Z., 1997, Phys. Rev. D **55**, 196.
Xing, Z. Z., and Zhou, S., 2007, Phys. Lett. B **653**, 278.

Index

D

E

S